THE IDENTIFICATION OF NOVEL THERAPY OPTIONS IN DIFFICULT TO TREAT NON-SMALL CELL LUNG CANCER

BY HELEN LOUISE ROBBINS

A thesis submitted to the
University of Birmingham
for the degree of
DOCTOR PHILOSOPHY

Institute of immunology and immunotherapy
College of Medical and Dental Sciences
University of Birmingham
February 2024

Abstract

Overview

There is a lack of treatment options for smoking related lung cancer. It is important to explore reasons for failure of apparently rational targeted therapies and to identify new avenues for treatment. This thesis focuses on three common subsets of smoking related lung cancer: *STK11*-mutant lung adenocarcinoma, *KRAS*-mutant lung adenocarcinoma and 3q amplified squamous cell lung cancer. In *STK11*-mutant lung cancer, this thesis seeks to explore resistance to mTORC1/2 inhibition. In *KRAS*-mutant lung cancer, this thesis seeks to identify predictors of sensitivity to CDK4/6 inhibition. In 3q-amplified squamous cell lung cancer, this thesis seeks to identify key driver (or drivers) within the 3q amplicon, and to identify potential targeting options for this driver through both supervised and unsupervised approaches.

Methods

Serial ctDNA samples were analysed from patients treated in the National Lung Matrix Trial from *STK11*-mutant lung adenocarcinoma patients treated with vistusertib (mTORC1/2 inhibition) and *KRAS*-mutant lung adenocarcinoma treated with palbociclib (CDK4/6 inhibition). Reactivation of PI3K/Akt signalling following prolonged treatment with mTORC1/2 inhibition *in vitro* was assessed using western blotting. Critical drivers on the 3q amplicon were identified using genome-wide CRISPR knockout data from DepMap, with validation using siRNA. Western blotting was used to assess the impact of drugs on SOX2 protein expression in squamous cell lung cancer cells, with parallel assessment of the impact on drugs viability. Finally, novel strategies to modulate SOX2 expression in 3q amplified squamous cell lung cancer was explored using a FACS assisted genome wide CRISPR knockout screen.

Key Results

SMARCA4 and *FOXP1* mutations become enriched following treatment with vistusertib in patients with *STK11*-mutant lung adenocarcinoma, potentially reflecting a novel resistance mechanism. Analysis of *KRAS*-mutant lung adenocarcinoma treated with palbociclib suggests that absence of

KDR variants, and presence of *MTOR* or *CHEK2* mutations may predict better prognosis, potentially reflecting a new cohort of patients who may benefit from CDK4/6 inhibitor therapy. In 3q amplified squamous cell lung cancer, *SOX2* was identified as a critical driver within 3q. BRD4 inhibition and CDK7 inhibition represent potential strategies to modulate SOX2 protein expression in the context of 3q amplification. The FACS-assisted genome wide CRISPR knockout screen identifies PCNA as an important regulator of SOX2, therefore targeting PCNA is a potential additional strategy for indirect targeting of SOX2.

Conclusions

Smoking related lung cancer remains a challenge for personalised medicine. SOX2 is a crucial component of the 3q amplicon and represents a candidate for targeted therapies. Identification of co-mutations that may drive resistance and sensitivity to CDK4/6 and mTORC1/2 inhibition may allow better selection of patients who may benefit from these targeted therapies.

Dedication

This thesis is dedicated to my colleague at medical school who informed me that female brains were not suitable for academia. Whilst you will never read this thesis, your feedback has been a constant source of motivation when academic challenges seem unsurmountable, and for that I am eternally grateful.

Acknowledgements

I would like to sincerely thank my supervisors Professor Gary Middleton and Professor Andrew Beggs. I would like to highlight Gary's endless optimism and enthusiasm, and Andrew's endless patience with my questions.

There are so many people without whom the project would have floundered. Firstly, I would like to thank the Beggs group. In particular: Jo Stockton, Vicky Simms, Elena Efstathiou, and Luke Ames for their support with the ctDNA work; Louise Tee for her good humour and support with the CRISPR screen; Genomics Birmingham for support with sequencing; and Oliver Pickles for his words of wisdom. Thanks must also go out to the wider University and academic community. Firstly, the Clinical Trials Unit: I would like to thank Joshua Savage, Professor Lucinda Billingham and Peter Fletcher for their support and collaboration for the work involving the National Lung Matrix Trial. I would like to thank HBRC for their support with samples. Thanks also goes out to the Flow Cytometry Team, in particular Guillaume Desanti, Ferdus Sheik and Shahram Golbabapour for their expertise and dedication when performing the massive cell sort required for the CRISPR screen. I would also like to sincerely thank Illumina, and in particular David McBride, Uma Maheswari and Maya Bajracharya for all their support with TSO500 sequencing and their technical expertise and guidance. Finally, I would like to thank patients for donating samples for research, without whom much of this work would not be possible.

Funding from Cancer Research UK is gratefully acknowledged. Without such support I would not have had the opportunity to pursue my passion for academic research. It is with the dedication of funders such as Cancer Research UK that we can hope to improve outcomes for our patients for the future.

Contents

List of Illustrations

List of tables

List of abbreviations

ADC	Antibody Drug Conjugate
BSA	Bovine serum albumin
Cas9	CRISPR-associated protein 9
cfDNA	Cell Free Deoxyribonucleic acid
ChIP-seq	Chromatin Immunoprecipitation Sequencing
COPD	Chronic Obstructive Pulmonary Disease
CCLE	Cancer Cell Line Encyclopaedia
COSMIC	The Catalogue of Somatic Mutations In Cancer
CRISPR	Clustered Regularly Interspaced Short Palindromic Repeats
CRUK	Cancer Research UK
ctDNA	Circulating Tumour Deoxyribonucleic acid
DCR	Disease Control Rate
DepMap	The Cancer Dependency Map Project
D-PBS	Dulbecco's Phosphate Buffered Saline
DNA	Deoxyribonucleic acid
E-cigarettes	Electronic cigarettes
ECL	Enhanced chemiluminescence
FACS	Fluorescence-activated Cell Sorting
FCS	Foetal calf Serum
FDA	The United States Food and Drug Administration
GAP	GTPase-activating Proteins
GCP	Good Clinical Practice
GEF	Guanine Nucleotide Exchange Factor
GeCKO	Genome-Scale CRISPR-Cas9 Knockout
GISTIC	Genomic Identification of Significant Targets in Cancer
GWAS	Genome-Wide Association Study
HBRC	Human Biomaterials Resource Centre
HDR	Homology Directed Repair
HIV	Human Immunodeficiency Virus
HMG	High Mobility Group
HPV	Human Papillomavirus
HRAS	Harvey rat sarcoma viral oncogene homolog
IASCLC	International Association for the Study of Lung Cancer
ICI	Immune Checkpoint Inhibitor
iPSCs	Induced pluripotent stem cells
LCC	Large Cell Carcinoma
LUAD	Lung adenocarcinoma
LUSC	Lung squamous cell carcinoma
mAb	Monoclonal Antibody
mNSCLC	Metastatic Non-Small Cell Lung Cancer
MOI	Moiety of Infection
mRNA	Messenger RNA
MuSyc	Multi-dimensional Synergy of Combinations
MUT	Mutant
nAChR	Nicotinic acetylcholine receptor
N/A	Not Applicable
NE	Not Estimable
NGS	Next Generation Sequencing
NHEJ	Non-Homologous End Joining

NICE	National Institute for Health and Care Excellence
NLMT	National Lung Matrix Trial
NSCLC	Non-small cell lung cancer
ORR	Overall Response Rate
OS	Overall Survival
PBS	Phosphate Buffered saline
PET-CT	Positron Emission Tomography – Computed Tomography
PFS	Progression Free Survival
PCR	Polymerase Chain Reaction
PFS	Progression Free Survival
PVDF	Polyvinylidene Fluoride
qPCR	Quantitative Polymerase Chain Reaction
RIPA	Radioimmunoprecipitation assay
RTK	Receptor Tyrosine Kinase
RPMI	Roswell Park Memorial Institute Media
SCC	Squamous Cell Carcinoma
SCLC	Small Cell Lung Cancer
SDS	Sodium Dodecyl Sulphate
SDS-PAGE	Sodium Dodecyl Sulphate – Polyacrylamide Gel Electrophoresis
sgRNA	Single Guide RNA
shRNA	Short hairpin RNA
siRNA	Small interfering RNA
STR	Short Tandem Repeat
TBS	Tris-buffered saline
TBST	1 x Tris-buffered saline, 0.1% Tween 20
TCGA	The Cancer Genome Atlas Program
TKI	Tyrosine Kinase Inhibitor
UCSC	University of Santa Cruz California
UK	United Kingdom
USA	United States of America
TKI	Tyrosine Kinase Inhibitor
WGBS	Whole Genome Bisulphite Sequencing
WT	Wild-type

Chapter 1: Introduction

1.1 Overview

Despite the era of personalised medicine, targeted therapies are available for only a minority of lung cancer patients. The National Lung Matrix Trial (NLMT) sought to address the unmet need: matching patients based on their tumour genotype to 25 drug-biomarker cohorts. However, responses were predominantly restricted to never- or light-smokers, and no squamous cell lung cancer patients had a confirmed objective response (4). There is an urgent need to identify novel therapy options in smoking-related lung cancer, and to understand why rational treatments fail.

This thesis focusses on genetic subtypes common in smoking-related lung cancer: *STK11*-mutant lung adenocarcinoma, *KRAS*-mutant lung adenocarcinoma, and 3q amplified squamous cell carcinoma. In the National Lung Matrix trial, *STK11* (± *KRAS*) mutant lung adenocarcinomas were treated with vistusertib (mTORC1/2 inhibition), *KRAS* (± *STK11*) mutant lung adenocarcinomas were treated with palbociclib (CDK4/6 inhibition), and 3q amplified (*PIK3CA* amplified) squamous cell lung cancers were treated with capivasertib (Akt inhibition). The mechanisms of resistance to vistusertib in *STK11*-mutant lung cancer will be explored *in vitro*, and mutations that may drive resistance will be identified using serial circulating tumour DNA (ctDNA) samples taken from *STK11*-mutant lung cancer patients treated with vistusertib in the NLMT. Mutations that may predict sensitivity to palbociclib will be identified using ctDNA taken from *KRAS*-mutant lung cancer patients treated within the National Lung Matrix Trial. Finally, this thesis identifies SOX2 as a crucial driver within the 3q amplicon in squamous cell lung cancer. Potential therapeutic approaches to target SOX2 will be investigated. Firstly, drugs known to modulate SOX2 expression in other contexts are screened. Secondly, potential novel approaches are identified using Fluorescence-Activated Cell Sorting (FACS)-assisted genome wide Clustered Regularly Interspaced Short Palindromic Repeats (CRISPR) screening. Overall, it is hoped that a better

understanding of these challenging genetic subtypes of lung cancer will support development of therapeutic options for the future.

1.2 Lung Cancer

1.2.1 Non-Small Cell Lung Cancer

Primary lung cancers are divided into non-small cell lung cancer (NSCLC) and small cell lung cancer (SCLC), NSCLC accounting for 80 - 90% of diagnoses (5-7). NSCLC is further divided by histological subtypes. Lung adenocarcinoma (LUAD), squamous cell lung cancer (SCC) and large cell carcinoma (LCC) are the most common subsets of NSCLC, accounting for around 38%, 20% and 3% of all lung cancer cases, respectively (7). All types of NSCLC are more common in smokers. LUAD is the most common histology in never-smokers (7).

1.2.2 Epidemiology and Risk

Lung cancer has evolved from being a rare malignancy in the 1800s and early 1900s (8-10) to being the most common cause of cancer death today (11, 12). 80 to 90% of lung cancer is attributed to cigarette smoking, with the tobacco pandemic driving the precipitous rise in lung cancer mortality (9). Historical falls in tobacco smoking in the United Kingdom (UK) and United States of America (USA) are now reflected by declining lung cancer mortality (13-15). However, rates of tobacco smoking remain high in much of the world, including in China, South-East Asia, and Eastern Europe (9, 16). It is therefore expected that the global incidence of smoking-related lung cancer will continue to rise.

Whilst tobacco smoking is a major contributor to lung cancer, not all heavy smokers develop the disease, and approximately 10 - 25% of lung cancers occur in never smokers (9, 17, 18). There is increasing evidence that air pollution plays a role in lung carcinogenesis in never-smokers (9, 19-21). Additional environmental risk is conferred by exposure to second-hand smoke (22-25), asbestos, radon gas, heavy metals (9), and ionizing radiation (26, 27). Further risk may be

conferred by respiratory diseases, including: asthma, tuberculosis, pneumonia, and chronic obstructive pulmonary disease (COPD) (28-30). It has been suggested that viral infections including Human Immunodeficiency Virus (HIV) (31-33), and Human Papillomavirus (HPV) may contribute to lung carcinogenesis (5, 34), but this remains controversial. The impact of cannabis on lung cancer risk remains unclear: epidemiological data is limited by under-reporting of cannabis use, small sample sizes, and dual use of tobacco and cannabis (35-37). Cannabis and tobacco smoke contain similar carcinogens, with cannabis smoking resulting in greater deposition of tar than cigarettes (38). Cannabis smokers' lungs reveals similar histological changes those seen in tobacco smokers (35, 37). However, cannabinoids may inhibit oncogenesis, potentially providing protective effects (39).

An area of evolving concern is use of electronic cigarettes (e-cigarettes). E-cigarettes are useful tools in smoking cessation. However, the prevalence of vaping in adolescents is rapidly rising in the UK: around 10% of 11 - 15 year olds used e-cigarettes in 2021 (40). E-cigarettes deliver nicotine, flavourings and heavy metals, all of which are potentially carcinogenic, or are metabolised to carcinogens (41). Aerosolised e-cigarette liquid is inflammatory and oncogenic in mice (42), e-cigarette aerosols transform bronchial epithelial cells in vitro (43), and e-cigarette liquid promotes stemness by upregulating SOX2 in NSCLC cell lines (44). Epidemiological evidence linking e-cigarettes to lung cancer risk in humans is lacking. Nonetheless, due to the lag between carcinogen exposure and detection of malignancy, it is premature to be conclude that e-cigarettes are risk-free.

1.2.3 Genetic Predisposition

Familial clustering of lung cancer has long been recognised (45-49). Shared environmental exposures and smoking habits play a substantial role in determining familial aggregation of lung cancers (9). Around 8% of lung cancers are attributed to genetic predisposition (49-52), with

complex interactions between the genome and the environment. Studies have consistently found associations between lung cancer and variants at 15q24-25.1 (53-60). 15q25 encodes a cluster of nicotinic acetylcholine receptor (nAChR) subunits, with variants associated with tobacco use, nicotine dependence, and lung cancer predisposition (53-60). Lung cancer susceptibility loci have also been identified at 5p15 (*TERT/CLPTM1L*) (54, 59, 61-63), 6p21-22 (54, 58, 64, 65), 9p21 (*CDKN2A/CDKN2B/ANRIL*) (54, 58, 66) and 22q12 (*CHEK2*) (54, 65, 67, 68). Familial lung cancers have been associated with germline *EGFR* mutations, with germline *EGFR* T790M being the most recognised (69). A third of non-smoking women with germline *EGFR* T790M develop NSCLC, with a further somatic *EGFR* mutation seemingly required for oncogenesis (69). Lung cancers are a rare feature of other familial cancer syndromes. Peutz-Jegher syndrome, caused by germline *STK11* mutations, confers a 13% risk of lung cancer is in men (70). Li Fraumeni syndrome, caused by germline *TP53* mutations, confers a 2 – 7% risk of lung cancer (71, 72).

1.3 Overview of Systemic Treatment Modalities in Non-Small Cell Lung Cancer

Treatment can be broadly divided into surgery, radiotherapy, and systemic anti-cancer therapy (SACT). Systemic therapies in lung cancer include cytotoxic chemotherapy, immunotherapy, and targeted therapies.

1.3.1 Chemotherapy

Cytotoxic chemotherapy is the longest standing systemic treatment modality for NSCLC. Controversy surrounding the potential role for chemotherapy in metastatic NSCLC was largely settled by a meta-analysis published in 1995, which reported that platinum-based treatment improved one-year survival by 10% (73).

1.3.2 Immunotherapy

The immune system plays an essential role in detecting pre-malignant and malignant cells. Immunotherapy refers to agents that activate the immune response, facilitating recognition and

destruction of cancer cells. All immunotherapies currently licensed for use in NSCLC by the United States Food and Drug Administration (FDA) are immune checkpoint inhibitors (ICI). Immune checkpoints are receptors and their ligands that modulate the immune response. Antibodies targeting CTLA-4 (Cytotoxic T-lymphocyte-associated Protein 4), PD-1 (Programmed cell death protein 1) and PD-L1 (Programmed death-ligand 1) are in current therapeutic use across multiple cancer types (74). Anti-PD-1 and anti-PD-L1 antibodies have well-established roles in NSCLC. Drug development and clinical trials for drugs targeting other immune checkpoint molecules (including LAG3) are ongoing (75).

PD-1 is expressed on the surface of activated T-cells and recognises two ligands: PD-L1 and PD-L2. Binding of PD-1 to its ligands provides a co-inhibitory signal, negatively regulating T-cell activation (Figure 1). Pro-inflammatory cytokines upregulate expression of PD-L1, acting as a negative feedback loop to prevent overactivation of the T-cell response and limit autoimmunity. However, these pathways are hijacked by cancer cells: multiple oncogenic and inflammatory pathways drive PD-L1 overexpression, promoting immune escape (76). Inhibiting PD-1 or PD-L1 with monoclonal antibodies (mAbs) reverses the negative regulation of the immune system, stimulating immune-mediated killing of cancer cells (Figure 1) (74). PD-L1 is a well validated, but imperfect, predictor of response to single-agent checkpoint blockade in lung cancer. PD-L2 is less well understood. PD-L2 expression is classically reported to be restricted to professional antigen presenting cells, such as dendritic cells and macrophages. However, recent evidence suggests that PD-L2 is more widely expressed (77, 78). PD-L2 is overexpressed in a proportion of lung adenocarcinomas (79) and squamous cell lung cancers (80), potentially driving resistance to PD-L1 blockade.

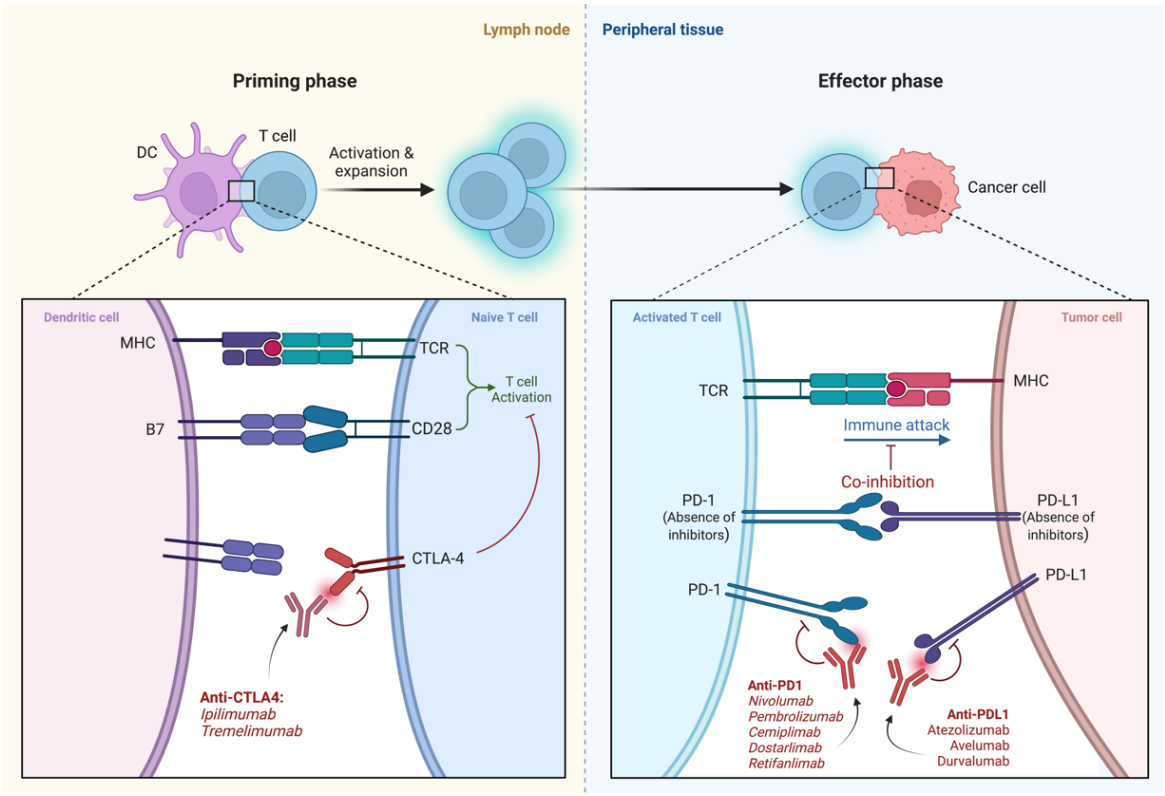

Figure 1: Mechanisms of action of PD1, PDL1 and CTLA4 inhibitors. Adapted from 'Blockade of CTLA-4 or PD-1 Signaling in Tumor Immunotherapy' by Biorender.com (2023). *Retrieved from https://app.biorender.com/biorender-templates, printed with permission.*

1.3.3 Targeted Therapies

Stratified medicine, or personalised medicine, is the approach of matching tumour genotype to targeted therapy (4). Epidermal growth factor receptor (EGFR) tyrosine kinase inhibitors (TKIs) were the first targeted therapies approved for use in NSCLC. However, whilst dramatic responses were seen, response rates were only 10% in unselected patients (81-84). The era of personalised medicine was heralded by the findings that activating mutations in *EGFR* underpin these dramatic responses, allowing for selection of patients likely to benefit from treatment (85, 86). Successful targeted therapies rely on oncogene addiction: the dependency of cancer cells on a single gene (oncogenic driver) (87). However, targeting oncogene addiction imposes substantial selection pressure, driving selection for resistance mutations. A classic example is development of the *EGFR* T790M mutation during treatment with 1st or 2nd generation EGFR inhibitors (88). Newer agents may target resistance mechanisms, for example the 3rd generation EGFR TKI Osimertinib is active against EGFR T790M (89, 90). However, the resultant "arms race" between cancer and available therapies presents ongoing therapeutic challenges.

Union for International Cancer Control. TNM Classification for lung cancer. 8th Edition

Primary tumour (T)

TX	Primary tumour cannot be assessed, or tumour proven by presence of malignant cells in sputum or bronchial washings, but not visualised by imaging or bronchoscopy
T0	No evidence of primary tumour
Tis	Carcinoma in situ
T1	Tumour 3cm or less in greatest dimension, surrounded by lung or visceral pleura, without bronchoscopic evidence of invasion more proximal than the lobar bronchus (i.e. not in the main bronchus)
T1mi	Minimally invasive adenocarcinoma
T1a	Tumour 1 cm or less in greatest dimension
T1b	Tumour more than 1 cm but no more than 2 cm
T1c	Tumour more than 2 cm but not more than 3 cm
T2	Tumour more than 3 cm but no more than 5 cm, or any of the following: - Involves main bronchus, regardless of distance to the carina, but without involvement of the carina - Invades visceral pleura - Associated with atelectasis or obstructive pneumonitis that extends to the hilar region either involving part of or the entire lung
T2a	Tumour more than 3 cm but not more than 4 cm in the greatest dimension
T2b	Tumour more than 4 cm, but no more than 5 cm in the greatest dimension
T3	Tumour more than 5 cm but no more than 7 cm in the greatest dimension or one that directly invades any of the following: parietal pleura, chest wall (including superior sulcus tumours), phrenic nerve, parietal pericardium; or separate tumour nodule(s) in the same lobe as the primary
T4	Tumour more than 7 cm or of any size that invades any of the following: diaphragm, mediastinum, heart, great vessels, trachea, recurrent laryngeal nerve, oesophagus, vertebral body, carina; separate tumour nodule(s) in a different ipsilateral lobe to that of the primary

Regional Lymph Nodes (N)

NX	Regional lymph nodes cannot be assessed
N0	No regional lymph node metastases
N1	Metastasis in ipsilateral peribronchial and/or ipsilateral hilar lymph nodes and intrapulmonary nodes, including involvement by direct extension
N2	Metastasis mediastinal and/or subcarinal lymph nodes
N3	Metastasis in contralateral mediastinal, contralateral hilar, ipsilateral, or contralateral scalene, or supraclavicular lymph nodes

Distant metastasis (M)

M0	No distant metastasis
M1	Distant metastasis
M1a	Separate tumour nodule(s) in a contralateral lobe; tumour with pleural or pericardial nodules or malignant pleural or pericardial effusion
M1b	Single extrathoracic metastasis in a single organ
M1c	Multiple extrathoracic metastasis in a single or multiple organs

	N0	N1	N2	N3
T1	IA	IIB	IIIA	IIIB
T2a	IB	IIB	IIIA	IIIB
T2b	IIA	IIB	IIIA	IIIB
T2b	IIA	IIB	IIIA	IIIB
T3	IIB	IIIA	IIIB	IIIC
T4	IIIA	IIIA	IIIB	IIIC
M1a	IVA	IVA	IVA	IVA
M1b	IVA	IVA	IVA	IVA
M1c	IVB	IVB	IVB	IVB

Table 1: Staging for Lung Cancer According to the Union for International Cancer Control, TNM Classification for Lung Cancer, 8th Edition *(reproduced from (1, 4))*

1.4 Treatment Approach for Non-Small Cell Lung Cancer

Management of Non-Small Cell Lung Cancer is divided into treatment of early-stage disease (Stage I – II), locally advanced disease (Stage III) and metastatic disease (Stage IV). An outline of NSCLC staging, according to the TNM Classification of Lung Cancers 8th edition, is provided in Table 1. Organised screening programmes using low-dose computed tomography (CT) in high-risk populations offer an opportunity for early diagnosis and reduced lung cancer mortality (5-7).

1.4.1 Treatment of Early-stage Disease

Surgery is the only potentially curative treatment of NSCLC, and is the optimal approach for localised disease, and for selected patients with locally advanced disease (8). Stereotactic radiotherapy offers an alternative for patients not suitable for surgery (8). However, even after curative-intent surgical resection, recurrence rates are between 30 – 50% (9-14).

Adjuvant platinum-based doublet chemotherapy is standard practice in patients with stage IIB – III disease (and selected patients with IIA) (8), improving absolute 5-year survival by approximately 5% (15-19). In the IMpower010 study, the addition of adjuvant atezolizumab provided significant disease-free survival (DFS) benefits in patients with completely resected stage IB-IIIA disease with PD-L1 expression ≥ 1% (HR 0·66; 95% CI 0·50–0·88) (20), leading to the first FDA approval of adjuvant immunotherapy in NSCLC. In KEYNOTE-091, adjuvant pembrolizumab improved median disease-free survival by 11.6 months in patients with completely resected stage IB - IIIA NSCLC of any histology and any PD-L1 status (21). Whilst chemotherapy was not required for trial entry into KEYNOTE-091, 86% of patients had received some chemotherapy, with 80% completing at least 3 cycles (21). Overall Survival data is not yet mature for either KEYNOTE-091 or IMpower-010.

Until recently, neoadjuvant treatment has been reserved for NSCLC patients with borderline resectable disease with view to downstaging. Whilst neoadjuvant chemotherapy offers potential

advantages over adjuvant chemotherapy (22, 23), these must be balanced against risking delaying curative surgery due to chemotherapy toxicity. In the NATCH trial, which compared neoadjuvant and adjuvant chemotherapy, more patients receiving chemotherapy in the neoadjuvant arm did not translate to significant improvements in DFS or overall survival (OS) (24). Similar results have been reported in paired retrospective analysis of over 300 patients (25). However, practise is shifting with the introduction of neoadjuvant chemoimmunotherapy. In CheckMate-816 neoadjuvant nivolumab plus platinum-doublet chemotherapy resulted in a pathological complete response rate of 24%, with a prolonged event free survival versus adjuvant chemotherapy (26). Whilst overall survival data is awaited, the results of CheckMate-816 led to the first FDA-approval of neoadjuvant chemoimmunotherapy in NSCLC.

Studies of adjuvant EGFR-directed therapies have reported impressive disease-free survival outcomes versus adjuvant chemotherapy in resected *EGFR*-mutant disease (27-30). In the ADAURA study, adjuvant Osimertinib reduced disease recurrence or death at 24 months by 80% when compared with placebo in *EGFR*-mutant NSCLC (27). These impressive DFS outcomes have recently been shown to translate to a significant overall survival benefit, with a median OS of 56.2 vs 49.9 months (31). However, analysis alongside the ADJUVANT trial suggests that the optimal choice of adjuvant chemotherapy versus EGFR-targeted agents may depend on an cancer's genetic landscape (32).

1.4.2 Treatment of Metastatic Non-Small Cell Lung Cancer

Over 40% of NSCLC present with distant metastatic disease (33). Empirical platinum-based chemotherapy has historically been the standard treatment for patients with metastatic NSCLC (mNSCLC). However, treatment has been revolutionised through introduction of immunotherapy and targeted therapies.

1.4.2.1 Oncogene-Addicted Metastatic Non-Small Cell Lung Cancer

As discussed earlier, *EGFR*-mutant mNSCLC displays oncogene addiction, conferring sensitivity to tyrosine kinase inhibition. Similar targetable dependencies are seen in mNSCLC with translocations involving *ALK*, *ROS1*, *RET* and *NTRK*; overexpression of MET or ALK; *BRAF* V600E mutation; or *MET* Exon 14 skipping mutations (34). Selected clinical trials for each of these targets are summarised in Tables 2 – 8. Overall, response rates to inhibitors in these contexts is high, with prolonged overall survival and better tolerability versus conventional chemotherapy regimens. As a result, comprehensive molecular profiling of mNSCLC is essential to identify oncogene-addicted cancers likely to benefit from targeted therapies (34). First-line treatment with targeted agents is recommended in NSCLC with sensitising *EGFR* mutations, *ALK*-rearrangement, *ROS1*-rearrangement, *BRAF* mutation, or *RET* fusions (34).

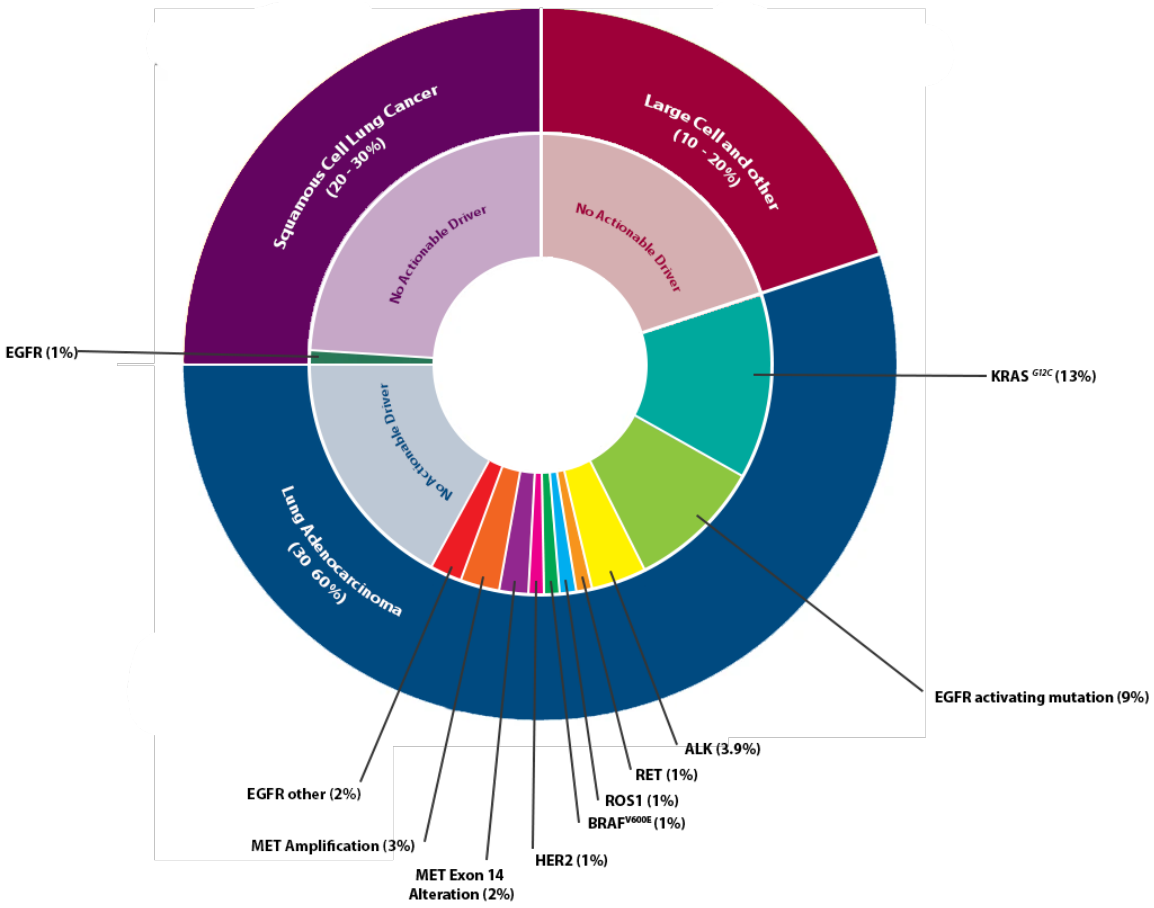

Figure 2: Frequency of actionable oncogenic drivers in NSCLC *Adapted with permission from: Wang M et al. Towards Personalized Treatment Approaches for non-small-cell lung cancer. Nature medicine 27.8 (2021): 1345-1356 (35). Printed with permission.*

Not all genetic alterations are as easily targeted. *HER2* aberrations are found in approximately 4% of NSCLC (most commonly amplification and in-frame exon 20 insertions) (123). However, whilst HER2 is a well-established target in breast cancer, TKIs or mAbs targeting HER2 show at best modest activity in NSCLC (123). Antibody-drug conjugates (ADCs) (trastuzumab deruxtecan and trastusumab emtansine) show more promise (Table 9). Antibody drug conjugates comprise a monoclonal antibody covalently bound to a cytotoxic drug, harnessing the overexpression of HER2 to deliver a concentrated cytotoxic payload to cancer cells. In the Destiny-Lung02 study, Trastuzumab Deruxtecan resulted in a confirmed objective response rate of 49% at 5.4 mg/kg and 56% at 6.4mg/kg (36), resulting in the first FDA-approved HER2-directed therapy in NSCLC.

KRAS is one of the most common mutated gene in smoking-related lung adenocarcinomas, with *KRAS* G12C being the most frequent variant. KRAS was classically viewed to be 'undruggable'. However, KRAS G12C can be inhibited by agents that covalently bind the altered cysteine 12, which sits within the switch II pocket, locking KRAS G12C in its inactive (GDP-bound) conformation (125). This discovery has led to development of specific KRAS G12C inhibitors. Key clinical trials targeting KRAS G12C in NSCLC are outlined in Table 10. However, whilst these agents exhibit clinical activity, KRAS G12C inhibitors have not yet replicated the dramatic and durable responses seen in oncogene-addicted cancers treated with TKIs. In an open-label phase III trial of sotorasib vs docetaxel, median progression-free survival (PFS) was improved by 1.1 months with no difference in OS (126). There are suggestions adagrasib may have more activity, with an objective response rate of 45% in NSCLC in a phase I/II trial (127).

Specific inhibitors for other *KRAS* alterations are in development. However, due to the lack of a targetable cysteine residue, discovery of specific inhibitors is more challenging in the absence of KRAS G12C (128). The first in-human data of HRS-4642, a KRAS G12D inhibitor, has recently been reported: in a Phase I trial across multiple cancer types, one partial response was reported out of 13 evaluable patients (129). pan-KRAS inhibitors are also under active development. In one "molecular-glue based" approach, RMC-6236 sequesters KRAS by promoting formation of a ternary complex with CYPA, preventing activation of downstream KRAS targets. Clinical development is still in early stages, but early data suggests there is some clinical activity, with an overall response rate (ORR) of 38% and disease control rate of 85% in *KRAS*-mutant NSCLC and pancreatic ductal adenocarcinoma (130).

Drug (Generation)	Trial (Phase)	Comparator	Molecular testing	Treatment Line	Population (Intervention arm)			Results (Intervention arm)			
					N	% ADC	Never Smoker (%)	ORR (%)	Median PFS (months)	Median OS (months)	
Gefitinib	IFUM (IV)	None	*EGFR*-mutant	1st	106	97.2	64.2	69.8	9.7	19.2	(37)
	IPASS (III)	Carboplatin/Paclitaxel	No selection	1st	609	95.4	93.8	43	5.7	18.8	(38, 39)
	First-SIGNAL (III)	Cisplatin/Gemcitabine	No selection	1st	159	100	100	55.4	5.8	22.3	(40)
	WJTOG 3405 (III)	Cisplatin/Docetaxel	*EGFR*-mutant	1st	86	96.5	70.9	62.1	9.2	34.9	(41, 42)
	NEJSG (III)	Carboplatin/Paclitaxel	*EGFR*-mutant	1st	114	90.4	75	84	10.8	30.5	(43)
Erotinib	EURTAC (III)	Cisplatin/docetaxel Carboplatin/Gemcitabine	*EGFR*-mutant	1st	86	95	66	64	9.7	19.3	(44)
	OPTIMAL (III)	Carboplatin/Gemcitabine	*EGFR*-mutant	1st	83	88	72	82	13.1	22.8	(45, 46)
Afatinib	LUX-Lung 3 (III)	Cisplatin/Pemetrexed	*EGFR*-mutant	1st	230	100	67	56	11.1	31.6	(47-49)
	LUX-Lung 6 (III)	Gemcitabine/Cisplatin	*EGFR*-mutant	1st	242	100	75	66.9	11	23.6	(47, 50)
	LUX-Lung 7 (IIb)	Gefitinib	*EGFR*-mutant	1st	160	99	66	70	11	27.9	(51, 52)
Osimertinib	AURA2 (II)	None	*EGFR* T790M	After 1st line TKI	210	95	76	70	9.9	-	(53)
	AURA3 (III)	Platinum/Pemetrexed	*EGFR* T790M	After 1st line TKI	279	83	68	71	10.1	26.8	(54, 55)
	FLAURA (III)	Gefitinib or Erlotinib	*EGFR*-mutant	1st	279	99	65	80	18.9	38.6	(56, 57)

Table 2: Summary of Key Clinical Trials using TKI in *EGFR*-mutant metastatic or locally advanced NSCLC . (Abbreviations: - no data). Note that for IPASS and First-SIGNAL no selection based EGFR status was performed

Drug	Trial (Phase)	Comparator	Molecular testing	Line	Cohort	Population (Intervention arm)			Results (Intervention arm)			
						N	% ADC	Never Smoker (%)	ORR (%)	Median PFS (months)	Median OS (months)	
Crizotinib	PROFILE-1001 (I)	None	ALK-positive (FISH)	Any	N/A	149	97	71	60.8	9.7	-	(58, 59)
	PROFILE-1005 (II)	None	ALK-positive (FISH, PCR or IHC)	≥ 2nd	N/A	1069	96	67	54	8.4	21.8	(60)
	PROFILE-1007 (III)	Pemetrexed or Docetaxel	ALK-positive (FISH)	1st	N/A	173	95	62	65	7.7	21.	(61)
Ceritinib	ASCEND-1 (I)	None	ALK-positive (FISH)	Post all standard lines	TKI Naïve TKI Pre-treated	246	93	98	72 56	18.4 6.9	NE 16.7	(62)
	ASCEND-3 (II)	None	ALK-positive (FISH)	≤ 4	N/A	124	96.8	-	67.7	16.6	51.3	(63-65)
	ASCEND-4 (III)	Platinum/Pemetrexed	ALK-positive (IHC)	1st	N/A	189	95%	57%	72.5	16.6	NE	(66)
Alectinib	NP28673 (II)	None	ALK-positive (FISH)	Post crizotinib	N/A	138	96	70	49	8.9	26	(67, 68)
	AF-001JP (I/II)	None	ALK-positive (IHC and FISH or RT-PCR)	ALK inhibitor naïve	N/A	46[1]	100	59	93.5	-	-	(69, 70)
	ALEX (III)	Crizotinib	ALK-positive (IHC)	1st	N/A	152	90	65	82.9	34.8	-	(71, 72)
	J-ALEX (III)	Crizotinib	ALK-positive (IHC and FISH or RT-PCR)	1st or 2nd ALK inhibitor naive	N/A	103	97	54	93.5	34.1	68	(73-75)
Brigatinib	NCT01449461	None	ALK-positive (FISH)	Any (previous crizotinib allowed)	N/A	79[2]	94	66	75	13.2	-	(76)
	ALTA-1L (III)	Crizotinib	ALK-positive (locally determined)	≤ 2nd ALK inhibitor naive	N/A	137	92	61	71	24	-	(77)
	ALTA (II)	None	ALK-positive	Post-crizotinib	90 mg OD	112	96	63	45	9.2	29.5	(78, 79)
		None			180 mg OD	110	98	57	54	16.7	34.1	(78, 79)
Lorlatinib	CROWN (III)	Crizotinib	ALK-positive (IHC)	1st	N/A	149	94	54	76	-	-	(80, 81)
	French Expanded Access Program	None	ALK positive	Any	N/A	208	94	31	49	9.9	32.9	(82)

Table 3: Summary of Key Clinical Trials using selective TKI in ALK-positive or altered metastatic or locally advanced NSCLC [1]Only phase II data presented [2]Only data from ALK-rearranged NSCLC population is presented. (- no data; N/A, Not Applicable; NE, Not estimable)

Drug (Generation)	Trial (Phase)	Comparator	Molecular testing	Treatment Line	Cohort	Population (Intervention arm)			Results (Intervention arm)			
						N	% ADC	Never Smoker (%)	ORR (%)	Median PFS (months)	Median OS (months)	
Crizotinib	PROFILE 1001 (I)	None	*ROS1* fusion (FISH ± PCR)	Any	N/A	53	96	75	72	19.3	51.4	(83, 84)
	Shen et al	Platinum/ Pemetrexed	*ROS1* fusion	1st	N/A	30	100	83.3	86.7	18.4	-	(85)
	OO1201 (II)	None	*ROS1* fusion (RT-PCR)	≤ 4th	N/A	127	97.6	71.7	71.7	15.9	44.2	(86, 87)
	AcSe (I/II)	None	*ROS1* fusion (IHC + FISH)	After all standard treatment	N/A	78	89	-	47.2	5.5	17.2	(88)
	METROS (II)	None	*ROS1* fusion (FISH)	≥ 2nd (at least one chemotherapy line)	N/A	26	100	54	65	22.8	-	(89)
Entrectinib	NCT01970865 (I/II)	None	*ROS1* fusion	Varied by phase	N/A	69	-	-	41	21	-	(90)
	STARTRK-1 (I) STARTRK-2 (I) ALKA-372-001 (I)	None	*ROS1* fusion	Varied by trial	N/A	54[1]	9	59	77	11.2	20.9	(91, 92)
Ceritinib	NCT01964157	None	*ROS1* fusion (FISH)	≥ 2nd (at least one platinum doublet)	N/A	32	100	84	62	9.3	24	(93)
Reprotrectiib	TRIDENT-1 (I/II)	None	*ROS1* fusion	Any	No Previous ROS1 TKI Previous ROS1 TKI	71 56	97 95	63 64	79 39	35.7 9.0	NE 25.1	(94, 95)

Table 4: Summary of Key Clinical Trials using selective TKI in *ROS1*-fusion metastatic or locally advanced NSCLC. [1]Combined analysis of three Phase I trials in solid tumours, of which 10 patients had NSCLC. (Abbreviations: - no data; N/A not applicable; NE not estimable).

Drug	Trial (Phase)	Comparator	Molecular testing	Treatment Line	Subgroup	Population (Intervention arm)			Results (Intervention arm)			
						N	% ADC	% Never Smoker	ORR (%)	Median PFS (months)	Median OS (months)	
Selpercatinib	LIBRETTO-001 (II)	None	*RET* Fusion	≥ 1st	Pre-treated Treatment naïve	247 69	89.5 89.9	66.8 69.6	61 88	24.9 22.0	NE NE	(96-98)
Pralsetinib	ARROW (I/II)	None	*RET* fusion	≥ 1st	Pre-treated (Platinum) Pre-treated (Non-Platinum) Treatment naïve	136 22 75	-	63 82 55	69 73 72	16.5 12.8 13.0	NE NE NE	(99, 100)

Table 5: Summary of Clinical Trials using selective RET-TKI in RET-positive metastatic or locally advanced NSCLC. Studies utilising unselective multityrosine kinase inhibitors not shown. (Abbreviations: - no data; NE not estimable).

Drug	Trial (Phase)	Comparator	Molecular testing	Line	Cohort	Population (Intervention arm) N	% ADC	Never Smoker (%)	Results (Intervention arm) ORR (%)	Median PFS (months)	Median OS (months)	
Crizotinib	AcSe (II)	None	*MET* Amp (≥ 6) or Mutant	No standard treatment available	*MET* Amp (≥ 6)	25	84	24	16	3.2	7.7	(88)
					MET-mutant	28	82	48	10.7	2.4	8.1	
	PROFILE-1001 (I)	None	*MET* Amplification (FISH) or *MET* Exon 14 alteration	≥ 1st	≥ 4 *MET:CEP7*	21	90.5	9.5	38.1	6.7	11.4	(101, 102) (101)
					> 2.2 TO < 4 *MET:CEP7*	14	85.7	14.3	14.3	1.9	9.2	
					≥ 1.8 to ≤ 2.2 *MET: CEP7*	3	66.7	0	33.3	1.8	5.6	
					MET Exon 14 alteration	68	84	38	32	7.3	-	
	METROS (II)	None	*MET* exon 14 alteration and/or Amplification (FISH) (*MET:CEP7* > 2.2)	≥ 2nd	N/A	26	89	23	27	4.4	5.4	(89)
Capmatinib	GEOMETRY Mono-1 (II)	None	*MET* Amplification or *MET* Exon 14 Skipping		CN ≥ 10 Pre-treated	69	83	7	40	4.1	-	(103)
					CN ≥ 10 Treatment-naive	15	73	13	29	4.2	-	
					CN 6-9	54	83	13	12	2.7	-	
					CN 4 -5	20	89	20	9	2.7	-	
					CN < 4	23	73	30	7	3.6	-	
					MET Exon 14 Treatment-naive	28	89	64	68	12.4	-	
					MET Exon 14 Pre-treated	69	77	58	41	5.4	-	
	NCT01324479 (I)	None	MET IHC 2+ or 3+, or *MET*/Centromere ratio ≥2, or CN ≥ 5	Treatment refractory / no effective treatment available	N/A	55	81	-	20	3.7	-	(104)
	NCT02750215 (II)	None	*MET* amplification (*MET:CEP7* ≥1.8) or *MET* Exon 14 skipping (NGS)	Post-crizotinib	N/A	20	80	40	10	5.5	11.3	(105)
Tepotinib	VISION (II)	None	*MET* Exon 14 Skipping	≤ 3rd	N/A	99	90	45	46	8.5	-	(106)

Table 6: Summary of Key Clinical Trials using TKI in MET-positive or altered metastatic or locally advanced NSCLC
(Abbreviations: - no data, N/A not applicable)

Drug	Trial (Phase)	Comparator	Molecular testing	Treatment Line	Subgroup	Population			Results			
						N	% ADC	% Never Smoker	ORR (%)	Median PFS (months)	Median OS (months)	
Dabrafenib	BRF113928 (II)	None	*BRAF* V600E	≥ 1st	Pre-treated Treatment-naïve	78 6	96	37	33 66	5.5	12.7	(107)
Dabrafenib + Trametinib	BRF113928 (II)	None	*BRAF* V600E	≥ 1st	Treatment-naïve Pre-treated	36 57	89 93	28 28	63.9 68.4	10.8 10.2	17.3 18.2	(108, 109)
Vemurafenib	VE-BAKSET (II)	None	*BRAF* V600E	Refractory to standard therapy	N/A	62	94	58	37	6.5	15.4	(110)
	AcSe Basket(II)	None	*BRAF*-mutant	≥ 2nd	BRAF V600E BRAF V600 Non-E	101 17	98 100	39.0 14.3	44.8 0	5.2 1.8	10 5.2	(111, 112)

Table 7: Key prospective trials targeting BRAF in metastatic or locally advanced NSCLC (Abbreviations: N/A not applicable)

Drug	Trial (Phase)	Comparator	Molecular testing	Line	Population			Results			
					N	% ADC	% Never Smoker	ORR (%)	Median PFS (months)	Median OS (months)	
Larotrectinib	NCT02576431 (II) NCT02637687 (I) NCT02122913 (I)	None	NTRK fusion	Varied by trial	20	95	-	73%	35.4	40.7	(113)
Entrectinib	STARTRK-1 STARTRK-2 ALKA-372-001	None	NTRK fusion	Varied by trial	10	-	-	70%	-	-	(91)

Table 8: Summary of Prospective Clinical Trials using NTRK TKI in metastatic or locally advanced NSCLC
For both Larotrectinib and Entrectinib, data is pooled from multiple trials (as reported by trialist). Only lung-cancer specific data is presented. (Abbreviations: - no data)

Drug	Trial (Phase)	Comparator	Molecular testing	Line	Cohort	Population (Intervention arm) N	% ADC	Never Smoker (%)	Results (Intervention arm) ORR (%)	Median PFS (months)	Median OS (months)	
Trastuzumab Deruxtecan	DESTINY-Lung01 (II)	None	*HER2*-mutant or Overexpression	Relapsed or refractory	N/A	91	100	57	55	8.2	17.8	(114)
	DESTINY-Lung02 (II)	None	*HER2*-mutant	≥ 2nd	5.4 mg/kg 6.4 mg/kg	10 2 50	98 100	53.9 58	49 56	9.9 15.4	19.5 NE	(36)
	NCT02564900 (I)	None	*HER2*-mutant or Expression	-	N/A	18	-	-	55.6	11.3	-	(115)
Trastuzumab Emtansine	NCT02675829 (II)	None	*HER2*-mutant or Amplified	Any	*HER2*-mutant	18	100	39	44	5	-	(116, 117)
					HER2 Amplified	6	-	-	50	-	-	(118)
	UMIN000017709 (II)	None	HER2 Positive	≥ 2nd	N/A	15	100	67	6.7	2.0	10.9	(119)
	NCT02289833 (II)	None	HER2 Positive	≥ 2nd	All IHC 2+ IHC 3+	49 29 20	75.5 85 68.9	20.4 24.1 15.0	8.16 0.0 20.0	2.6 2.6 2.7	12.2 12.2 15.3	(120, 121)

Table 9: Summary of Clinical Trials using Antibody Drug Conjugates in *HER2* altered metastatic or locally advanced Non-Small Cell Lung Cancer
(Abbreviations: - no data, N/A not applicable, NE not estimable)

Drug	Trial (Phase)	Comparator	Molecular testing	Line	Cohort	Population (Intervention arm) N	% ADC	Never Smoker (%)	Results (Intervention arm) ORR (%)	Median PFS (months)	Median OS (months)	
Sotorasib	CodeBreaK100 (I/II)	None	*KRAS* G12C	≥ 2nd	N/A	126	95.2	4.8	37.1	6.8	12.5	(122, 123)
	CodeBreaK200 (III)	Docetaxel	*KRAS* G12C	≥ 2nd	N/A	171	98.8[1]	2.9	28.1	5.6	10.6	(124)
Adagrasib	KRYSTAL-1 (I/II)	None	*KRAS* G12C	≥ 2nd	N/A	116	97.4	4.3	42.9	6.5	12.6	(125, 126)

Table 10: Summary of Clinical Trials using KRAS G12C inhibitors in *KRAS* G12C mutant metastatic or locally advanced Non-Small Cell Lung Cancer ([1]Non-Squamous)

1.4.2.2 Metastatic Non-Small Cell Lung Cancer with no actionable drivers

A simplified schema for first-line treatment of mNSCLC in the absence of actionable mutations is shown in Figure 3. PD-L1 expression ≥ 50% predicts good response to pembrolizumab monotherapy, with a median survival of 30 months in KEYNOTE-024 (218). Chemotherapy remains a cornerstone of treatment in the absence of high PD-L1. Treatment of non-squamous mNSCLC was refined by findings that platinum/pemetrexed significantly improves survival when compared with other platinum doublet chemotherapies (219). More recently, combination chemo-immunotherapy has been shown to improve overall survival versus chemotherapy alone, and is now the preferred option in suitable patients, various regimens are available (Figure 3) (220).

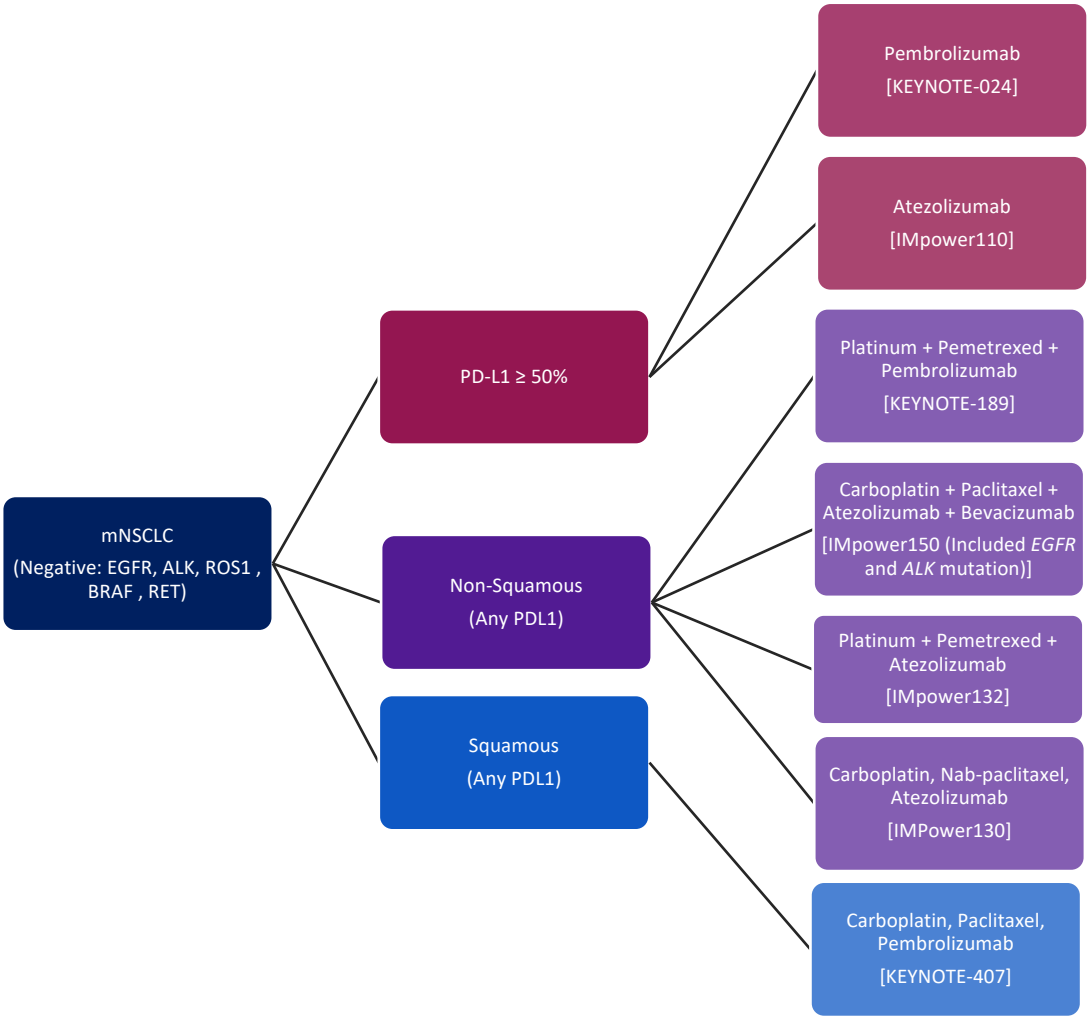

Figure 3: Simplified schema for first-line treatment of metastatic NSCLC in patients of good performance status with no contraindication to immunotherapy or chemotherapy. Summarised from (1), only showing regimens approved for use within the UK by NICE (National Institute for Health and Care Excellence) (correct as of September 2023)

Second-line options remain limited. Second-line immunotherapy may be considered where immunotherapy was not given first-line (220). After platinum-based therapy, response rates to docetaxel are around 15 – 20% (221). Second-line pemetrexed demonstrates comparable overall survival to docetaxel in non-squamous NSCLC (222). Addition of angiogenesis inhibitors to docetaxel provides a modest benefit. Docetaxel plus nintedanib (VEGFR1-3, FGFR1-3, PDGFR inhibitor) improves overall survival versus docetaxel monotherapy in lung adenocarcinoma after first-line chemotherapy (12.6 months versus 10.3 months)) (223). Addition of ramucirumab (VEGFR2 inhibition) to docetaxel improves overall survival (10.5 months vs. 9.1 months (docetaxel/ramucirumab versus docetaxel/placebo)) (224). Overall, second-line treatments have suboptimal clinical activity, and further treatment options are needed in this setting.

1.5 The National Lung Matrix Trial

Whilst treatment options for lung cancer have expanded in recent years, the most rapid progress is restricted to patients with well-defined oncogene addiction. A significant proportion of patients are still faced with few treatment options and poor outcomes. The National Lung Matrix Trial (NLMT) sought to address this disparity and is the largest stratified medicine trial in NSCLC, matching rationally chosen targeted agents to tumour genotype (Figure 4).

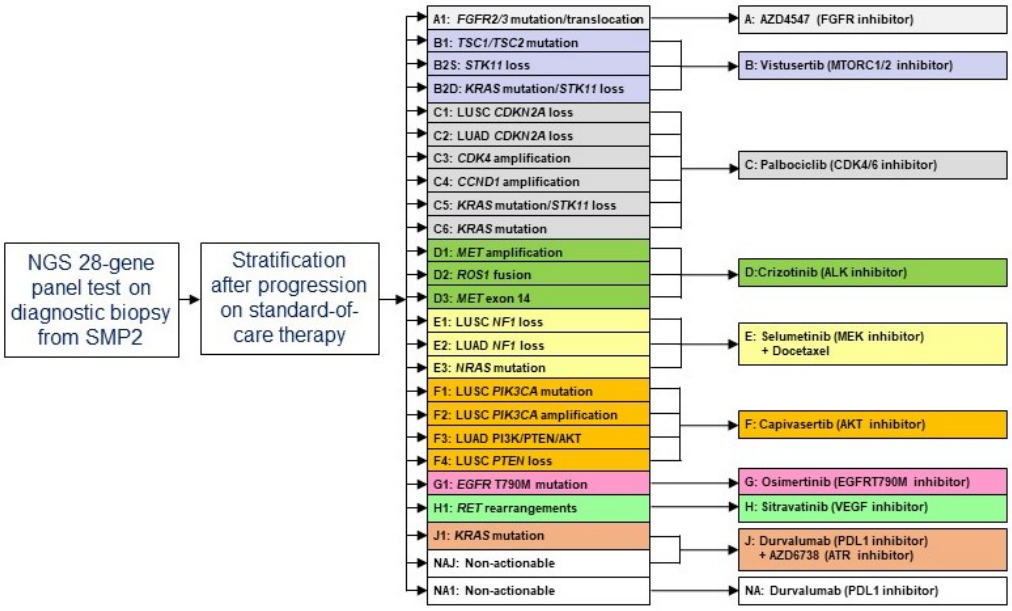

Figure 4: Schematic of National Lung Matrix Trial Study Design. Patients with locally advanced or metastatic NSCLC were stratified using *SMP2* (28-gene next generation sequencing panel) into arms matching genotype to targeted therapy. From (127), printed with permission

However, results from the NLMT have been relatively disappointing (4, 225). Whilst 30 out of 187 non-squamous NSCLC patients had confirmed objective response to therapy, no confirmed responses were seen in patients with squamous cell lung cancer (Figure 6) (4). Furthermore, treatment responses were predominantly seen in non-smokers or light smokers (Figure 5) (4). These results are mirrored in LUNG-MAP, an American umbrella trial with a focus on squamous lung cancer, where none of the published arms have reached their primary endpoint (226). This thesis seeks to address this issue, focussing on three genetic subtypes common in smoking-related lung cancer: *STK11*-mutant lung adenocarcinoma, *KRAS*-mutant lung adenocarcinoma and 3q-amplified squamous cell lung cancer.

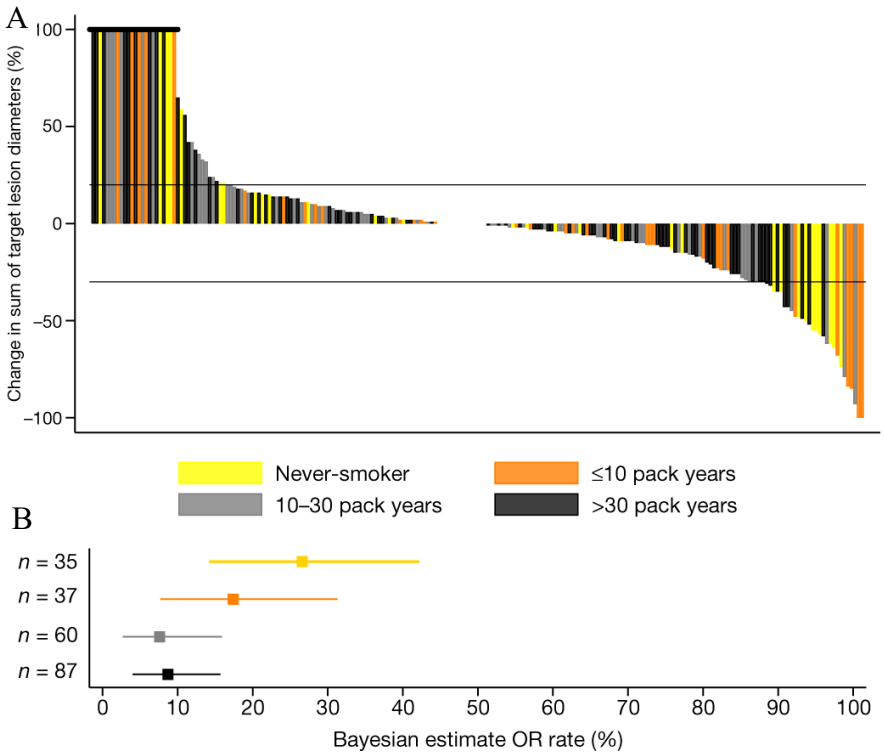

Figure 5: Waterfall plot (A) and Bayesian Estimate for Objective Response Rates (B) according to smoking status in the National Lung Matrix Trial. Adapted with from (127), printed with permission

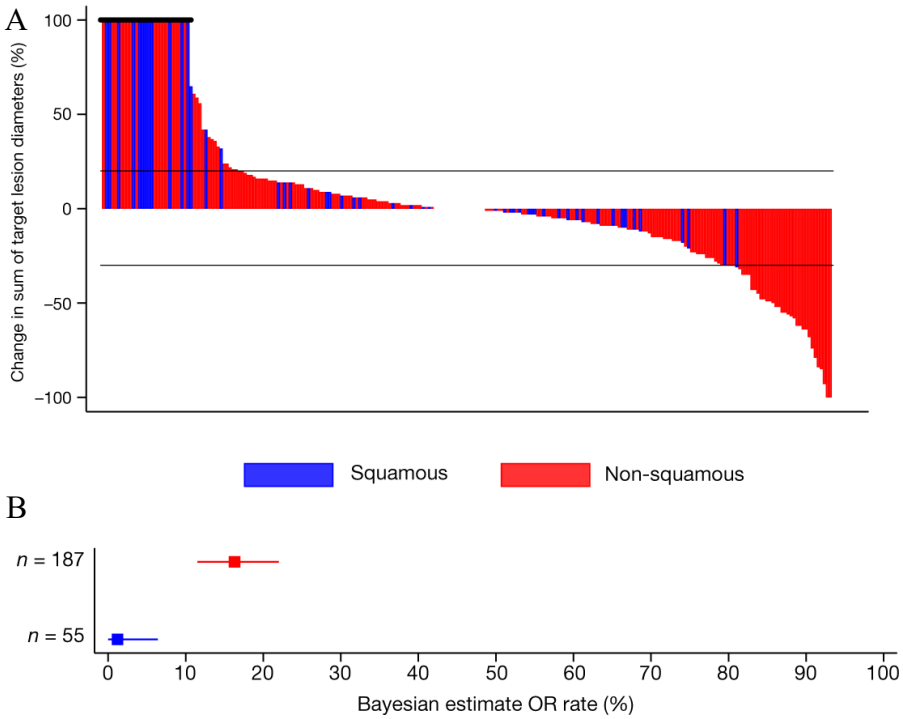

Figure 6: Waterfall plot (A) and Bayesian Estimate for Objective Response Rates (B) according to histology in the National Lung Matrix Trial. Adapted from (127), printed with permission

1.6 *KRAS*-Mutant Non-Small Cell Lung Cancer

1.6.1 KRAS

RAS (Rat Sarcoma Virus) are a family of GTPases: hydrolysing guanosine triphosphate (GTP) to guanosine diphosphate (GDP) (227). Three highly homologous family members are present in humans: HRAS, KRAS, NRAS. Activating mutations in RAS are amongst the most common events in human malignancy. *KRAS* mutations occur in around a third of lung adenocarcinoma, with hotspots in codons 12 and 13 (228, 229). *KRAS* mutations (and particularly *KRAS* G12C) are strongly associated with smoking and are more common in Western populations (229, 230). In general, *KRAS* mutations have been associated with high tumour mutational burden, high levels of PD-L1 and an inflammatory tumour microenvironment (231-233). However, *KRAS*-mutant NSCLC is highly heterogeneous. Concomitant mutations are commonly seen in *STK11*, *TP53* and *CDKN2A*, with each co-mutation driving different phenotypes (234, 235).

1.6.2 KRAS Signalling

KRAS serves as a molecular switch, integrating signals from an array of receptor tyrosine kinases (RTKs) (Figure 7). KRAS is active when bound to GTP and is inactive when bound to GDP. Activation of RTKs results in recruitment of adaptor proteins (such as Grb2), which in turn recruit guanine nucleotide exchange factors (GEFs), such as SOS-1. GEFs encourage KRAS to exchange GDP for GTP, promoting KRAS activity. The action of GEFs is opposed by GTPase activating proteins (GAPs), which support intrinsic KRAS GTPase activity, promoting hydrolysis of GTP to GDP, hence inactivating KRAS (227, 236). Active KRAS activates several downstream signalling pathways, including Raf/MEK/Erk and PI3K/Akt/mTOR and PLCε, promoting cell survival and migration (227, 236).

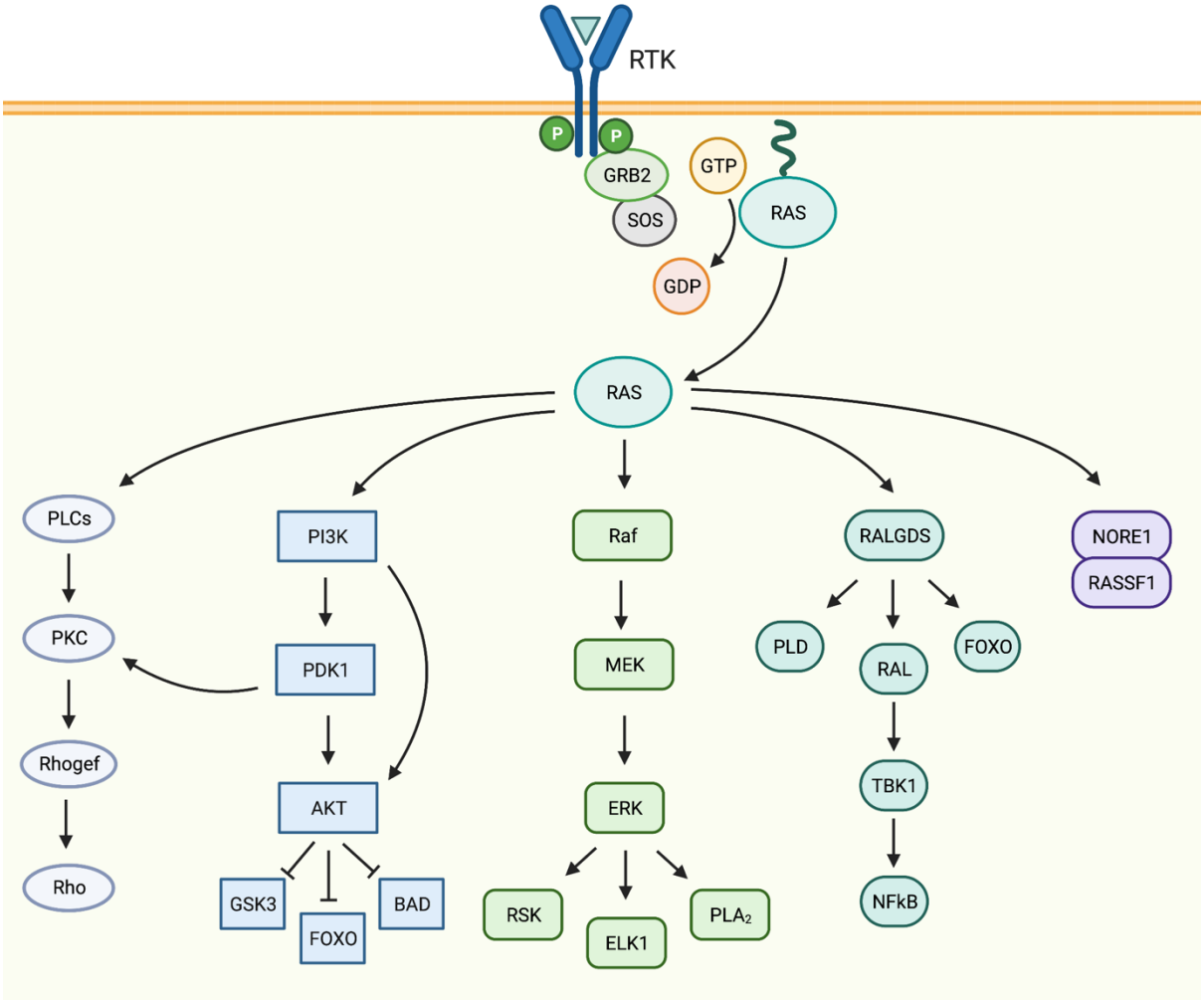

Figure 7: RAS Signalling. RAS is in an inactive state when bound to GDP and in an active state when bound GTP. Ligand binding to Receptor Tyrosine Kinases (RTKs) promotes recruitment of guanine nucleotide exchange factors (GEFs), such as SOS-1. GEFs promote the exchange of GDP for GTP, activating RAS. In turn, RAS activates an array of downstream signalling pathways, such as PI3K/Akt and Raf/Mek/Erk. *Adapted from 'Ras Pathway' by Biorender.com (2023). Retrieved from https://app.biorender.com/biorender-templates. Printed with permission*

1.6.3 CDK4/6 inhibition as a candidate in *KRAS*-mutant Non-Small Cell Lung Cancer

KRAS mutations are common in lung adenocarcinoma and KRAS G12C inhibitors are now licensed, however responses rates with sotorasib are relatively modest and often short-lived (124, 128, 129). Furthermore, around 60% of *KRAS*-mutant lung adenocarcinoma are non-G12C (130, 131), and for these patients no currently licensed targeted therapies are available. Whilst clinical trials for non-G12C inhibitors and pan-KRAS inhibitors are ongoing (132, 133), it is clearly important to expand the clinical arsenal for this common subset of lung adenocarcinoma. CDK4/6 inhibition has been proposed as a therapeutic option in *KRAS*-mutant NSCLC (134-136). CDK4/6 inhibitors are well-established therapies in breast cancer (137), therefore retooling these agents for *KRAS*-mutant NSCLC is a highly attractive option. Use of the palbociclib (CDK4/6i) in *KRAS*-mutant NSCLC was explored within the arms C5 and C6 of National Lung Matrix Trial (Figure 4, page 41).

1.6.3.1 Overview of Cyclin D and CDK4/6 Signalling

Cyclin D and CDK4/6 are central regulators of cell cycle progression. The classical model of G1/S progression requires cells to pass a single critical decision point: the Restriction Point. Cyclin D binds and activates CDK4 and CDK6, activating CDK4/6, which in turn phosphorylates Rb. Phosphorylated Rb releases E2F, promoting transcription of Cyclin E, which activates CDK2. Active CDK2 hyperphosphorylates Rb, fully releasing E2F, driving increased E2F-dependent transcription and committing cells to S phase (138). More recent research suggest that the regulation of G1/S transition is more nuanced (138, 139). Nonetheless, Cyclin D and CDK4/6 remain critical regulators of cell cycle progression.

Whilst CDK4 and CDK6 levels remain static, cyclin Ds have a short half-life, are closely regulated, and act as nutrient sensors. Cyclin D1 transcription is upregulated by multiple pro-mitogenic pathways including: PI3K/Akt; Mek/Erk; and NFκB (140). Active PI3K/Akt signalling also increases translation of Cyclin D (140), whilst GSK3β-mediated phosphorylation of Cyclin D

promotes its nuclear export and degradation (141). A further level of regulation is provided by $p16^{INK4A}$, $p57^{KIP2}$ and $p21^{CIP1}$, which regulate the formation of cyclin D/CDK4 and cyclin D/CDK6 complexes (140).

1.6.3.2 KRAS and CDK4/6

As a key effector of pro-mitogenic signalling, multiple pathways downstream of KRAS converge to drive Cyclin D upregulation. *KRAS*-mutation is associated with increased Cyclin D1 expression in advanced and early-stage NSCLC (142, 143), with high cyclin D1 correlating with worse prognosis in advanced *KRAS*-mutant disease (142). Preclinical evidence suggests CDK4/6 inhibition may be a tractable target in *KRAS*-mutant lung cancer. Knockdown of CDK4 or CDK6 is synthetically lethal to *KRAS*-mutant NSCLC cells (134). Absence of CDK4 impairs cancer development and induces cell senescence in a *KRAS*-mutant model of NSCLC, and treatment with the CDK4/6 inhibitor palbociclib reduces tumour burden in xenograft mice (134). Abemaciclib shows preferential toxicity to *KRAS*-mutant versus *KRAS* wild-type (wt) NSCLC cells (135), and is synergistic with paclitaxel treatment (136). In the Phase I/II setting, abemaciclib achieved a 55% disease control rate in *KRAS*-mutant NSCLC patients (compared to 39% DCR in KRAS wild-type NSCLC), with progression-free survival exceeding 24 weeks in 31% of the KRAS-mutant subgroup (135). However, the Phase III JUNIPER trial (Abemaciclib versus erlotinib in pre-treated metastatic *KRAS*-mutant NSCLC) failed to meet its primary endpoint: median PFS was 3.6 months vs. 1.9 months (abemaciclib vs. erlotinib), DCR 54.4% vs 31.7%, with no improvement in overall survival (144).

1.6.3.3 Mechanisms and Predictors of resistance and sensitivity to CDK4/6 inhibitors in KRAS-mutant NSCLC

Resistance to CDK4/6 inhibition in *KRAS*-mutant NSCLC is poorly understood. Acquired resistance to Palbociclib in *KRAS*-mutant NSCLC models was associated with: increased levels of cyclin D1, cyclin D3, cyclin E, $p27^{Kip1}$ and CDK6; increased Erk1/2 phosphorylation; and increased mTOR activation (145). Palbociclib resistant NSCLC cells increase secretion of FGF, driving increased

FGFR1 activation, resulting in Erk-dependent mTOR activation. In keeping with this, resistant cells are sensitive to MEK and mTOR inhibition (145). Mechanisms of resistance and predictors for sensitivity have not been characterised in human *KRAS*-mutant NSCLC. In breast cancer, detection of *KRAS* mutations in baseline ctDNA predict resistance to combination treatment with Palbociclib and fulvestrant. Likewise, detection of a de novo *KRAS* mutation on treatment was associated with worse outcomes (146). Whilst this may seem conflicting, these results may reflect KRAS hyperactivation bypassing dependence on oestrogen receptor signalling, rather than true Palbociclib resistance.

1.7 *STK11*-Mutant Non-Small Cell Lung Cancer

1.7.1 STK11

STK11 (LKB1) is a serine/threonine kinase involved in regulation of cell metabolism, growth, polarity, proliferation, and p53-dependent apoptosis (147-149). Germline mutations in *STK11* cause Peutz-Jeghers syndrome, an autosomal dominant disorder characterised by gastrointestinal hamartomatous polyps, mucocutaneous pigmentation, and high risk of malignancy (150). Loss or inactivation of *STK11* is relatively rare in most sporadic cancers (150). In contrast, *STK11* mutation is one of the most common genetic aberrations in lung adenocarcinoma (131, 151, 152). STK11 loss/inactivation is more common in smokers (153), and commonly occurs in combination with *KRAS* mutation (131, 154-156). NSCLCs with both *STK11* mutation and *KRAS* mutation have poor prognosis (157-161), present with a higher metastatic burden (153), and are more likely to develop brain metastasis (153). In addition, *STK11*/*KRAS* co-mutant NSCLC is associated with a cold tumour microenvironment, reduced tumour infiltrating lymphocytes (TILs), increased suppressive neutrophils (162, 163), and poor response to immunotherapy (161, 164, 165). Overall, *STK11* mutant lung cancer (and *STK11*/*KRAS* co-mutant lung cancer in particular) represents a subset of disease, with a particularly poor prognosis, primary resistance to immunotherapy, and no current targeted therapy options. Expanding therapeutic options for these patients is of crucial importance.

1.7.2 STK11 Signalling

STK11 phosphorylates AMP-activated protein kinase (AMPK) and thirteen AMPK-related kinases (166). AMPK regulates cellular response to energetic stress (Figure 8). Phosphorylation by STK11 activates AMPK, which in turn activates TSC1/2. The TSC1/2 heterodimer repress Rheb, a key activator of mTORC1 (156). In addition, AMPK directly inhibits mTORC1 through phosphorylation of RAPTOR (167). As a result, *STK11*-mutant NSCLCs have reduced AMPK activity and increased mTORC1 activation (131). However, deletion of AMPK fails to reproduce the effects of STK11 loss, but instead inhibits tumorigenesis (168), suggesting that an alternate

target is the main mediator of STK11's tumour suppressive effects. CRISPR knockout data suggests that Salt Inducible Kinase 1 (SIK1) and Salt Inducible Kinase 3 (SIK3), both AMP-related kinases, may be key mediators of the tumour-suppressive actions of STK11 (169).

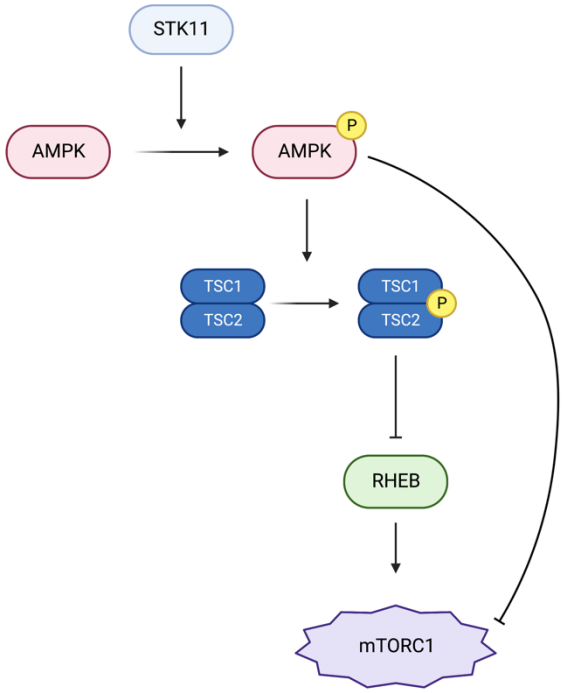

Figure 8: Canonical STK11 Signalling: STK11 phosphorylates and activates AMPK, which in turn activates TSC1/2. TSC1/2 repressess Rheb, a key activator of mTORC1. AMPK also directly inhibits mTORC1. In tact STK11 signalling therefore serves to restrict mTORC1 activation. *Created using Biorender.com, printed with permission.*

1.7.3 *STK11* mutation and *KRAS* mutation as concomitant drivers of oncogenesis

Concurrent *STK11* and *KRAS* mutation drive a pro-tumorigenic, pro-metastatic phenotype in mouse models of lung cancer, pancreatic cancer, and melanoma (170-172). Re-expression of STK11 in *STK11*/*KRAS* co-mutant NSCLC cells suppresses anchorage independent growth and impairs metastatic potential when injected into immunocompromised mice (172). STK11 knockdown promotes migration of NSCLC cells in vitro (173). In a conditionally activatable mouse model, concomitant KRAS activation and STK11 deficiency leads to aggressive lung tumours with an increased burden of metastatic disease (172). In the same model, loss of STK11 alone is insufficient to initiate tumorigenesis, and KRAS activation results in indolent tumours with infrequent metastases, suggesting that mutation of both STK11 and KRAS are required for the

aggressive phenotype (172). In mice, *STK11/KRAS* co-mutant tumours show upregulation of genes associated with metastasis and angiogenesis, and are more resistant to docetaxel (172). However, it is important to note that mouse models of *STK11/KRAS* co-mutant NSCLC are imperfect mimics of human disease: loss of STK11 in the context of KRAS activation drives a squamous phenotype in mice (172), which contrasts with the adenocarcinoma-predominant picture seen in human *STK11/KRAS* co-mutant NSCLC.

1.7.4 Concurrent mutations in *STK11* and *KRAS* as drivers of metabolic reprogramming

STK11 and *KRAS* mutations synergise in driving metabolic and epigenetic re-programming of cancer cells: driving GLUT1 up-regulation and increased glucose uptake (170); increasing flux through the hexosamine biosynthesis pathway (174); and altering nitrogen metabolism with increased serine biosynthesis (170). These metabolic perturbations are potentially targetable. *STK11/KRAS* co-mutant cells are more sensitive to glucose deprivation and glycolysis inhibition, (170). Likewise, *STK11/KRAS* co-mutant cells are dependent on serine metabolism (170), and are sensitive to inhibition of Glutamine-Fructose-6-Phosphate Transaminase (a key enzyme in the hexosamine biosynthesis pathway) (174). Altered serine metabolism in *STK11/KRAS* co-mutant cells drives DNA methylation, and *STK11/KRAS* co-mutant cells are also sensitive to inhibition of DNA methyltransferases (170). In addition, human *STK11/KRAS* co-mutant NSCLC cell lines have been reported to be more sensitive to MEK inhibition with CI-1040 (156), however these results were not replicated in a *STK11/KRAS* co-mutant mouse models with selumetinib (175).

1.7.5 mTORC1/2 Inhibition as a target in *STK11/KRAS* co-mutant NSCLC

Combined inhibition of mTORC1 and mTORC2 is a potential therapeutic option in *STK11/KRAS* co-mutant NSCLC. mTORC1/2 inhibition reverses the metabolic reprogramming seen in *STK11/KRAS* co-mutant murine pancreatic ductal epithelial cells, reducing glucose uptake and reversing the glycolytic phenotype (170). mTORC2 is a crucial driver of glycolysis in A549, an *STK11/KRAS* co-mutant human NSCLC cell line (176). Likewise, mTORC1/2 inhibition reverses

the metabolic reprogramming seen in *STK11*/*KRAS* co-mutant pancreatic ductal epithelial cells in vitro, with significantly increased sensitivity to Torin 1 (mTORC1/2 inhibition) in *STK11*/*KRAS* co-mutant cells (170). mTORC1/2 inhibition with MLN0128 (sapanisertib) inhibits GLUT1 and potentiates apoptosis in A549, with synergy between MLN0128 and phenformin (177).

Clinical outcomes of mTORC1/2 inhibition in other cancer sites has been disappointing: progression free survival (PFS) was shorter with vistusertib (mTORC1/2 inhibition) than with everolimus (mTORC1-only inhibition) in renal clear cell cancer (178). PFS was also shorter with vistusertib/fulvestrant than with everolimus/fulvestrant in ER+ breast cancer (179). These treatment failures may be attributable to reactivation of pro-proliferative signalling following mTORC1/2 inhibition. In breast cancer cells, phosphorylation of Akt-T308 and FOXO1/3 rebound after treatment with vistusertib (at 4 hours and 24 hours, respectively), and this reactivation of mitogenic signalling likely dampens the toxicity of mTORC1/2 inhibition (180, 181). However, evidence suggests that STK11 is required for phosphorylation of FOXO by Akt (28), therefore this resistance pathway may be less relevant in *STK11*/*KRAS* co-mutant cells. It is therefore possible that *STK11*/*KRAS* co-mutant cells are uniquely vulnerable to mTORC1/2 inhibition: inhibition targets a metabolic vulnerability, whilst cells may lack a key resistance mechanism. Considering the strong pre-clinical rationale for mTORC1/2 inhibition in this context, *STK11* mutant lung adenocarcinoma was treated with vistusertib (AZD2014) in the National Lung Matrix Trial: $STK11^{MUT}KRAS^{MUT}$ lung adenocarcinoma were treated with vistusertib in arm B2D; $STK11^{MUT}KRAS^{WT}$ lung adenocarcinoma was treated with vistusertib in arm B2S. This represents the first trial of mTORC1/2 inhibition in *STK11*-mutant lung adenocarcinoma in the clinic.

1.8 3q-Amplified Squamous Cell Lung Cancer

There are no current stratified medicine options for squamous cell lung cancer (LUSC). The biology of LUSC is less well understood than that of lung adenocarcinoma, and druggable targets are less well characterised. Actionable drivers that commonly occur in lung adenocarcinoma, such as *EGFR* mutation or *ALK* fusions, are absent in squamous cell lung cancer (182, 183). As a result, first-line treatment for advanced squamous cell lung cancer is either single-agent pembrolizumab, combination chemotherapy, or combination chemoimmunotherapy, depending on patient fitness, co-morbidities and tumour PD-L1 expression (1). However, even with chemoimmunotherapy, prognosis remains poor: in KEYNOTE-407, overall survival was 17.2 months in treatment-naïve patients treated with pembrolizumab plus platinum doublet chemotherapy (184, 185).

There is a clear need to expand therapeutic options for these patients by identifying novel targets in squamous cell lung cancer. NRF2 (encoded by *NFE2L2*) and KEAP1 are potential emerging targets in squamous cell lung cancer (186, 187). Combination treatment of Telaglenastat (CB-839), a glutaminase inhibitor and sapanisertib, an mTORC1/2 inhibitor are synergistic, and this combination therapy shows early suggestions of efficacy in a Phase I trial in NRF2 or KEAP1 -altered NSCLC (187). Another proposed target in squamous cell lung cancer is FGFR1. *FGFR1* is commonly amplified in squamous cell lung cancer as part of the 8p amplicon (183). However, clinical results with targeting FGFR1 in this context have proved disappointing (188, 189). Crucially, recent data suggests that *FGFR1* is not the true oncogenic driver within the 8p amplicon; instead, the nearby H3K36 methyltransferase *NSD3* may be the more critical oncogene. (190). Overall, these data highlight the importance of empirically defining driver genes within any amplicon.

Amplification of distal 3q is one of the most common genomic aberrations in LUSC (183, 191), head and neck cancer (192) and oesophageal squamous cell cancer (191). 3q-amplification occurs frequently in high-grade dysplasia, but is absent in low-grade dysplasia (193). In addition, progressive 3q copy number increase has been observed during progression from high-grade dysplasia to invasive malignancy (193). *PIK3CA* is a well characterised oncogene in this region, and therefore the distal 3q amplicon is commonly referred to as the '*PIK3CA* amplicon'. As a result, targeting PI3K/Akt signalling downstream of PIK3CA has been extensively explored in 3q amplified squamous cell lung cancer, including in the National Lung Matrix Trial (127). However, the amplified region encompasses multiple other oncogenes, including *SOX2*, *DCUN1D1*, *PRKCI*, *TP63*, and *BCL6*. One analysis has shown 3q amplification centres around *SOX2*, *ATP11B*, *DCUN1D1* and *MCCC1* in squamous cell lung cancer (191). A separate analysis identified a 4.3 Mb minimal amplified region, spanning 17 genes, including *PIK3CA* and *SOX2* (193). It is important not to assume that *PIK3CA* is the oncogenic driver within the 3q amplicon, but instead to empirically define the relative importance of drivers in 3q to allow rational therapeutic targeting of 3q amplified squamous cell lung cancer.

1.8.1 PIK3CA and PI3K/Akt Signalling

The PI3K family is subdivided into three classes (Class I, II and III). Class I PI3Ks are best characterised, and are subdivided into Class IA and Class IB (299). Class IA PI3K, is a heterodimer, comprising a regulatory subunit (p85α, p85β or p85γ, encoded by *PIK3R1*, *PIK3R2* and *PIK3R3*, respectively) and a catalytic subunit (p110α, p110β or p110δ, encoded by *PIK3CA*, *PIK3CB* and *PIK3CD*, respectively) (299). Binding of the p85 subunit to receptor tyrosine kinases or G-protein coupled receptors results in activation of the catalytic subunit, which acts to phosphorylate phosphatidylinositol-4,5-bisphosphate (PIP2) to phosphatidylinositol-3,4,5-triphosphate (PIP3) (300, 301). The action of PI3K is counteracted by PTEN, which dephosphorylates PIP3 back to PIP2. PIP3 promotes recruitment of proteins bearing a pleckstrin-homology (PH) domain to the

plasma membrane, including Akt, PDK1 and mTORC2 (300, 301). Akt is a family of homologous serine-threonine kinases (Akt1, Akt2 and Akt3), which are activated by phosphorylation at equivalent threonine residues (Thr308/309/305) by PDK1 (300-302). Full activation of Akt requires further phosphorylation at Ser473/474/472 by mTORC2 (300-302). Akt is deactivated via dephosphorylation by PHLPP1, PHLPP2 and PP2A (300, 301). Akt serves as a central node in cell signalling, modulating the activation of multiple downstream targets (Figure 9).

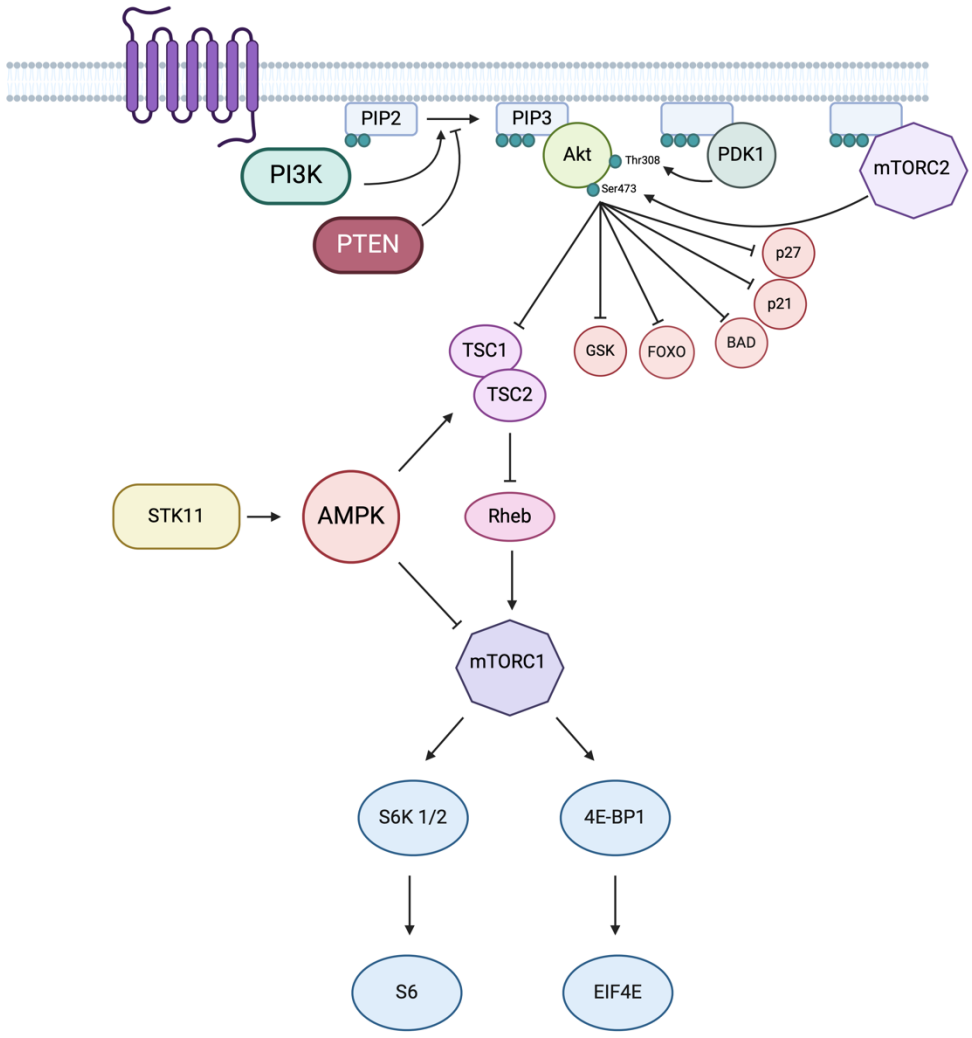

Figure 9: The PI3K/Akt signalling pathway. Phosphorylation of PIP2 to PIP3 by PI3K recruits Akt to the plasma membrane, where it is co-localised with and phosphorylated by PDK1 and mTORC2. Akt phosphorylates numerous downstream targets, with important targets shown, including GSK3β, FOXO and TSC2. Phosphorylation of TSC2 relieves repression of Rheb, allowing mTORC1 activation. Convergent points with STK11 signalling are also shown (Adapted from (194)). *Created using Biorender.com, printed with permission.*

The Phosphatidylinositol 3-kinase (PI3K)/Akt pathway is a well-recognised pathway in carcinogenesis, playing a key role in regulating cell survival, cell cycle progression, protein metabolism, glucose metabolism, cellular differentiation, angiogenesis, DNA repair and migration (302). This pathway is particularly relevant in squamous malignancies. Hyperactivation of PI3K/Akt signalling is detected in a significant proportion of squamous cell cancers (303-307): *PIK3CA* amplification occurs in around 30% (308-310), *PIK3CA* mutation occurs in 4 – 10 % (288, 308, 311) and loss of expression of *PTEN* occurs in 20 – 40% (299). PI3K/Akt signalling plays a role in early tumorigenesis (304, 312), however, active PI3K/Akt signalling (typically measured by Akt phosphorylation) has also been associated with higher tumour stage and grade (307). Whilst some studies have reported an association between Akt phosphorylation and prognosis (303, 306), data remains conflicting (304, 305). In addition, alterations in the PI3K/Akt pathway have been demonstrated in squamous transformation following treatment of lung adenocarcinomas with tyrosine kinase inhibitors, suggesting a role of PI3K/Akt signalling in driving squamous differentiation (313, 314).

Preclinical data for targeting the PI3K/Akt in NSCLC is compelling. Inhibition of the PI3K/Akt pathway reduces cellular proliferation, induces apoptosis and reduces invasiveness in squamous cell lung cancer cells *in vitro* (315). Likewise, dual PI3K/mTOR inhibition leads to marked regression of PIK3CA-driven lung tumours in a mouse model (316) (although in this mouse model PIK3CA led to development of lung adenocarcinomas, rather than squamous cell carcinomas). In addition, the Akt pathway modulates sensitivity to chemotherapy and radiotherapy in NSCLC lung cancer cells *in vitro* (317), with inhibition of the PI3K/Akt pathway increasing chemosensitivity and radiosensitivity (317).

However, the BASALT-1 trial, a phase II trial of the pan-class I PI3K inhibitor buparlisib (BKM120) in relapsed NSCLC with *PIK3CA* mutation, *PTEN* mutation or *PTEN* loss, failed to meet its primary objective (318). Likewise, in the National Lung Matrix Trial, no patients with *PIK3CA* mutation, *PIK3CA* amplification or *PTEN* loss responded the Akt inhibitor capivasertib (4). However, it is perhaps premature to conclude that targeting the PI3K/Akt pathway in squamous cell lung cancer is futile. In oestrogen receptor positive (ER+) breast cancer, combining alpelisib (alpha-specific class I protein kinase inhibitor) with fulvestrant prolongs progression free survival (319), leading to FDA approval of alpelisib in this setting. It is therefore possible that the optimal combinatorial strategy remains undefined in squamous cell lung cancer.

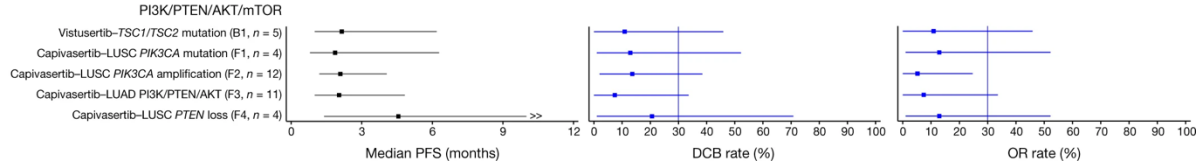

Figure 10: Outcomes of Targeting the PI3K/Akt Signalling Pathway in the National Lung Matrix Trial across multiple arms. Bayesian Estimates and 95% credible intervals for true values of median PFS, DCB rate and OR Rate in arms targeting the PI3K/Akt signalling pathway in the National Lung Matrix Trial. Arm B1: vistusertib, mTORC1/2 inhibition, was used in TSC1/TSC2 mutant NSCLC. Arm F1: capivasertib, Akt inhibition, was used in PIK3CA mutant squamous cell lung cancer. Arm F2: capivasertib in PIK3CA amplified squamous cell lung cancer. Arm F3: capivasertib in lung adenocarcinoma with aberrations in PI3K, PTEN or Akt. Arm F4: capivasertib in squamous cell lung cancer with PTEN loss (adapted with from (127), printed with permission)

1.8.2 SOX2

SOX2 is commonly co-amplified with *PIK3CA* in 3q amplified squamous cell lung cancer, and has been identified as an important component of the amplicon (296, 298). SOX2 is a member of the SRY-related high mobility group (HMG) box (SOX) transcription factors. SOX2 plays a key role in pluripotency and stemness and is one of the four Yamanaka factors required for creation of induced pluripotent stem cells (iPSCs) (320). Germline SOX2 mutations have been associated with autosomal dominant anophthalmia-oesophageal-genital syndrome (320), anophthalmia or microphthalmia (321, 322), hypogonadotrophic hypogonadism (321) and pituitary hypoplasia (323).

SOX2 plays a critical role in embryogenesis, and homozygous deletion results in peri-implantation lethality (324). SOX2 expression is first detectable within morula, later becoming restricted to the inner cell mass (325), where expression maintains pluripotency (326). Following gastrulation, SOX2 expression is restricted to gut endoderm, neuroectoderm, pharyngeal arches, sensory placodes and primordial germ cells (320). SOX2 dictates development of multiple lineages, including playing a role in regulating lung development. During lung morphogenesis, SOX2 expression levels are dynamic: downregulated during lung bud formation, followed by upregulation once lung bud formation is established, and then downregulated during bronchial tree branching (327). Later in embryogenesis, SOX2 is expressed in proximal airways, whilst being suppressed in alveoli (320), a pattern that persists in adulthood (328). During lung development, SOX2 suppresses epithelial differentiation, limits bronchial branching, and promotes multipotent progenitor cells through increasing p63 expression (327). In the adult lung SOX2 maintains Clara cells and Basal cells (both of which serve as progenitor cells) (328). SOX2 is also essential for maintaining bronchial epithelial proliferation and ciliated morphology, and is required for goblet cell differentiation in response to allergens (328).

SOX2 overexpression promotes proliferation, invasion, stemness, metastatic potential and drug resistance *in vitro* (320, 329). However, effects of SOX2 overexpression appear to depend on mutational landscape and are dose dependent: in some contexts SOX2 overexpression promotes quiescence and reduced proliferation (330). Data regarding association between SOX2 and prognosis are conflicting, and differ with cancer type (329). In squamous cell lung cancer, SOX2 expression has been associated with longer overall survival, lower T and M stage, absence of angiolymphatic invasion, and younger age at diagnosis (331). In the same study, SOX2 amplification (assessed by FISH) was associated with lower tumour grade (331).

A role of SOX2 in lung oncogenesis is supported by findings that overexpression of SOX2 in basal cells induces squamous metaplasia in a PI3K-signalling dependent manner (312). Overall, mouse models of squamous cell lung cancer support a role for SOX2 in squamous cell lung cancer development. Overexpression of SOX2 in epithelial cells in the murine adult lung results in bronchial epithelial hyperplasia and development of p63 positive lung tumours (332). Lentiviral-driven overexpression of SOX2 promotes squamous cell lung carcinogenesis in a LKB1-loss model of mouse squamous cell lung cancer (333). Likewise, SOX2 overexpression in mice with conditional PTEN and CDKN2AB loss drives development of squamous lung cancers with high penetrance (334). Overexpression of PRKCI, SOX2 and ECT2 in the context of TP53 loss transforms mouse lung basal cells into tumours with similar characteristics to human lung squamous cell lung cancer (335), in keeping with a cassette of genes on 3q driving squamous lung carcinogenesis. However, it must be acknowledged that mouse models do not fully recapitulate the broad 3q amplicon or the genomic complexity seen in human squamous cell lung cancer.

In vivo evidence for a role of SOX2 in the maintenance of squamous cell lung cancer is more limited (336). However, deletion of SOX2 results in tumour regression in a chemical carcinogenesis model of cutaneous squamous cell carcinoma in mice (337). Knockdown of SOX2 with siRNA and shRNA in human squamous cell lung cancer cell lines reduces viability and impairs colony formation (296, 338), with greatest effect in 3q amplified squamous cell lung cancer cell lines (296). SOX2 downregulates CDKN1A in squamous cell lung cancer cells, whilst SOX2 knockdown induces G1 growth arrest through relieving SOX2-mediated inhibition of CDKN1A (338).

1.9 Circulating Tumour DNA

1.9.1. Overview of circulating Tumour DNA

Cell-free DNA (cfDNA) is fragmented DNA released by cells into plasma and other body fluids. Circulating tumour DNA (ctDNA) is the fraction of cfDNA released by cancer cells, and was first described in 1989 (339). cfDNA levels correlate with cancer burden. However, high cfDNA levels are also driven by other disease states including inflammation and tissue injury, therefore cfDNA quantification in isolation has poor sensitivity as a cancer biomarker (340, 341). The utility of ctDNA was unlocked by advances in sequencing and bioinformatics (reviewed in (342)). Tissue biopsies may be technically challenging or impossible in some lung cancer patients, therefore ctDNA sequencing allows genetic characterisation of cancers where sequencing data may be otherwise unavailable. Furthermore, ctDNA better represents disease heterogeneity, is less invasive, carries less clinical risk, requires fewer resources, and may be arranged more quickly than conventional biopsies (342, 343). ctDNA analysis may therefore improve time to molecular characterisation, whilst being less burdensome to patients. In addition, serial ctDNA sampling allows longitudinal of assessment of cancer evolution, genetic drift and development of resistance to treatment (344). However, ctDNA is less sensitive than tissue sequencing, particularly in tumours with low disease burdens or in tumours with low levels of ctDNA shedding (343). An additional complication of ctDNA analysis is detection of non-ctDNA mutations from clonal haematopoiesis of indeterminate potential (ChiP) (343), which may complicate analysis

1.9.2 Circulating Tumour DNA in Cancer Screening

ctDNA has the potential to revolutionise cancer screening. Current cancer screening techniques are cancer-site specific, whilst ctDNA offers the opportunity for multi- or pan-cancer screening. CancerSEEK™, Galleri™ and PanSEER™ are all in development as screening platforms. CancerSEEK™ uses a combined 61 amplicon (16 gene) and 39 protein biomarker panel (345). GALLERI and PanSEER assess ctDNA methylation, using whole genome bisulphite sequencing and semi-targeted bisulphite polymerase chain reaction (PCR), respectively (346, 347).

CancerSEEK™ demonstrated a median sensitivity of 70% in 1005 patients with stage I – III cancer, with sensitivity ranging from 33% in breast cancer to 98% in ovarian cancer (345). In DETECT-A, a prospective study of 10,000 women who underwent Cancer-SEEK™ followed by confirmatory Positron Emission Tomography – Computed Tomography (PET-CT), 26 cancers were detected by the test (348). PanSEER was tested as part of the Taizhou Longitudinal Study, with a sensitivity of 91% in pre-diagnosis samples in asymptomatic patients who developed gastric, oesophaeal, colorectal, lung or liver cancer; PanSEER was able to detect cancer up to 4 years prior to diagnosis (346). The Circulating Cell-Free Genome Atlas study (CCGA) is a prospective observational trial for the development, testing and validation of GALLERI™. In the initial discovery sub-study, whole genome bisulphite sequencing (WGBS) outperformed whole genome sequencing (WGS) and panel-based approaches (349). In the validation sub-study, sensitivity of GALLERI™ for cancer detection was 51.5% in patients with known or highly suspected malignancy, with a cancer-site prediction accuracy of 88.7% (347). As may be expected, GALLERI sensitivity was cancer and stage-dependent, with a sensitivity of 16.8% for stage I disease and 90.1% for stage IV (347). Prospective trials of GALLERI are ongoing in high-risk populations: STRIVE in women undergoing mammography screening and SUMMIT in individuals at high risk of lung cancer.

1.9.3 Circulating Tumour DNA in Lung Cancer

1.9.3.1 Current Clinical Practice

Three FDA-approved ctDNA tests are in current clinical use in NSCLC: the Cobas *EGFR* Mutation Test, Guardant360 and FoundationOne Liquid CDx (343). The Cobas *EGFR* Mutation Test v2 uses real-time PCR of exons 18 – 21 of *EGFR*. Guardant 360 and FoundationOne are NGS-based assays, with Guardant 360 testing 83 genes and FoundationOne testing 324 genes. Plasma-first *EGFR* testing to detect T790M mutations in patients progressing on 1st or 2nd generation EGFR tyrosine kinase inhibitors has been standard of care for several years. However, the practice of

plasma-first sequencing to establish mechanisms of resistance to targeted therapies is now expanding to all oncogene addicted NSCLC (343). Likewise, recent guidelines support use of ctDNA analysis at time of diagnosis, either as a supplement to tissue-based sequencing, or in a plasma-first approach (343).

1.9.3.2 ctDNA for tumour genotyping at diagnosis

Around 20 – 30% of patients do not have molecular results available before initiation of first-line treatment (350, 351). Lack of molecular testing hampers effective treatment of non-squamous NSCLC, and is associated with shorter overall survival (195). ctDNA next-generation sequencing (NGS) provides an opportunity for genotyping when tissue is inadequate, and several trials have evaluated the utility of Guardant360 in genotyping NSCLC at diagnosis. In one multi-centre study of 93 patients with inadequate or insufficient tissue for *EGFR*, *ALK* or *ROS1* genotyping, Guardant360 identified actionable genomic variants in 60% with a median turnaround of 13 days (196). In the Spanish Lung Liquid versus Invasive Biopsy Program (SLLIP), 186 treatment-naïve stage IIIB-IV lung adenocarcinoma patients underwent ctDNA analysis (Guardant360) alongside standard-of-care tissue biopsy (197). ctDNA identified comparable numbers of actionable mutations as tissue analysis, and was reported faster with a higher success rate (198). Formal analysis of sensitivity of ctDNA in this Spanish Lung Liquid versus Invasive biopsy Programme is limited by lack of availability of comprehensive molecular testing of tissue: no patients had complete genotype of all 8 genes in tissue (*EGFR*, *ALK*, *ROS1*, *BRAF*, *MET*, *RET*, *ERBB2*) (197).

In the Korean Lung Liquid vs Invasive Biopsy Program, 421 NSCLC patients underwent concurrent tumour biopsy NGS and plasma ctDNA analysis using Guardant360. Sensitivity of ctDNA was 67.7%, specificity 88.8%, and concordance 77.6% (355). Sensitivity for individual genetic mutations on ctDNA ranged from 81.3% for *EGFR* del 19 to 18.8% for *ROS1* fusion (355). Of note, 84 patients with no ctDNA results were excluded from sensitivity and specificity analysis.

Reasons for ctDNA results being unavailable included: no detection of somatic mutations, possible sample contamination, failure of sample enrichment, and low diversity of samples (355). It is therefore likely that the reported sensitivity is an overestimate of the real-world performance. In the NILE study (Non-invasive versus invasive lung Evaluation), 303 patients with biopsy-proven, treatment-naïve, non-squamous mNSCLC (Stage IIIB/IV) underwent physician-choice standard-of-care tissue typing alongside Guardant360 ctDNA testing. ctDNA was non-inferior to tissue with a sensitivity of 80% (356). Notably however, complete tissue genotyping (*EGFR* mutation, *ALK* fusion, *ROS1* fusion, *BRAF* V600E, *RET* fusion, *MET* Amp/Exon 14 skipping, *HER2* mutation) was only completed in 18.1% of participants (356).

The actionability of mutations detected on ctDNA in NSCLC is confirmed in the Blood-first Assay Screening Trial, an open-label multicohort study screening patients for targeted therapies using Foundation Medicine ctDNA testing. Tissue results were not required for trial entry. In the ALK-positive cohort, patients with an *ALK* rearrangement on ctDNA were treated with alectinib, with an overall response rate (ORR) of 87.4% (357). Likewise, in the VISION trial response rates to tepotinib are similar in *MET* Exon-14 skipping mutations identified on ctDNA and tissue biopsy (358).

1.9.3.3 Risk Stratification in early-stage disease

Whilst lung cancer surgery or radical radiotherapy is potentially curative, recurrence rates are high. ctDNA may assist with detection of residual disease and in prognostication (359-362). In a study of patients with stage I – III NSCLC planned for curative-intent treatment, detection of ctDNA using personalised assays predicted poor prognosis (359). Both pre-treatment and post-treatment ctDNA detection were associated with poor prognosis, however, the association was strongest for patients who failed to clear ctDNA after treatment. Furthermore, ctDNA detection preceded clinical detection of disease recurrence by a median of 212.5 days (359). DNA could

therefore be useful to identify patients may benefit from treatment intensification, or to give more accurate prognostic information.

1.9.3.4 ctDNA and prognosis in targeted therapies

ctDNA detection has been shown to be associated with prognosis in clinical trials. In the FLAURA trial patients were enrolled based on *EGFR* mutations detected from tissue biopsy. Detection of *EGFR* mutation on ctDNA at baseline was associated with worse prognosis: PFS was 23.5 months in the ctDNA negative population treated with Osimertinib versus 15.2 months in the ctDNA positive population treated with Osimertinib (363). These differences may reflect disease burden: in FLAURA ctDNA positive patients had significantly larger median target lesions (363). ctDNA shedding could also reflect more aggressive disease, for example due to higher cell turnover and/or necrosis. It is therefore possible that ctDNA-only recruitment to clinical trials may bias recruited populations towards those with a worse prognosis. Serial monitoring of ctDNA may provide additional prognostic data: in AURA3 clearance of detectable *EGFR* mutations on ctDNA was associated with better prognosis (364).

1.9.3.5 ctDNA and cancer evolution / resistance to therapy

Serial ctDNA sampling provides opportunities to define mechanisms of resistance to therapies. In AURA3, 41% of patients had acquired resistance mutations at discontinuation of treatment or disease progression, including *EGFR* C797X (18%) and *MET* amplification (18%) (365). TRACERx has provided invaluable insights into evolution of early-stage and metastatic lung cancer (344, 362). Phylogenetic tracking of ctDNA can detect changes in subclones, reflecting response to treatment and selection pressure, and may predict subclones predominant in future metastatic disease (362). In the future, evolving resistance may therefore be predicted and anticipated, with modulation of therapy depending on evolving subclones.

1.10 Genome Wide CRISPR Cas9 Screening

1.10.1 CRISPR-Cas9

The clustered regularly interspaced short palindromic repeat (CRISPR)/CRISPR-associated protein (Cas9) system forms part of the microbial adaptive immune system (366). CRISPR/Cas9 requires two components: Cas9 (an RNA-guided endonuclease) and sgRNA (single guide RNA). sgRNA directs Cas9 to a target site, where Cas9 forms double-strand breaks (366). Double-strand breaks may be repaired through non-homologous end-joining (NHEJ), or, less commonly, homology-directed repair (HDR). NHEJ is error-prone, and frequently introduces loss-of-function mutations (367) (Figure 11). Changing the guide RNA sequence allows selection of different targets, therefore CRISPR-Cas9 can be harnessed to produce targeted loss-of-function in a gene (or genes) of interest. CRISPR-Cas9 carries is more specific than RNA knockdown approaches, with greater knockdown, and reduced off-targets effects (367-369).

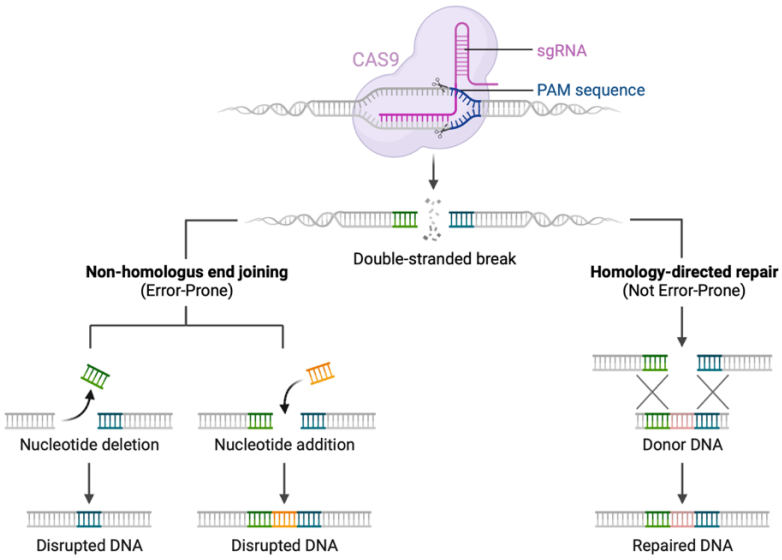

Figure 11 CRISPR/Cas9 Gene Editing. CAS9 is guided to specific DNA sequences by sgRNA and produces a double strand break. Repairs may be completed by Non-homologous End Joining or Homology-Directed repair. Whilst Homology-Directed Repair is generally not error-prone, Non-Homologous End Joining is error prone and commonly disrupts DNA by insertions or deletion. *Adapted from 'CRISPR/Cas9 Gene Editing' by Biorender.com (2023). Retrieved from https://app.biorender.com/biorender-templates/.* Printed with permission

1.10.2 Genome-wide CRISPR Screening

Forward genetic screens seek to identify genes that drive a phenotype of interest. CRISPR-Cas9 is of great use in this context, as the phenotype of many genes of interest can be examined concurrently with great specificity. Genome-wide CRISPR-Cas9 screens using libraries of sgRNA that target every gene in the genome, typically using multiple sgRNAs per gene. CRISPR-Cas9 screens require both Cas9 and sgRNAs to be introduced into cells. In the two-vector approach, Cas9 is first stably expressed using lentiviral transduction, and the sgRNA library is later introduced to these Cas9-expressing cells. In the one-plasmid approach, both Cas9 and sgRNAs are introduced using a single vector (369). Due to the scale of genome-wide screens, pooled approaches are generally used: introducing large number of cells to sgRNA at a low multiplicity of infection (MOI), such that most cells receive at most one sgRNA, and non-transduced cells are be removed with antibiotic selection (367, 369). The selection pressure of interest is then applied. After selection is complete, nucleic acids are extracted, and sequencing of sgRNAs is used to identify sgRNA with altered representation in populations of interest (367, 369). In general, pooled screens can be classified as 'positive' or 'negative'. Positive screens look for enrichment of sgRNAs in the selected population. Negative screens look for sgRNAs under-represented in the selected population. Negative screens often have a lower signal-to-noise ratio, therefore requiring larger number of cells (367).

1.11 Aims and Objectives

There is an urgent need to identify new treatment options in smoking-related lung cancer, and to understand why rational treatments fail. This thesis focusses on three common genetic subtypes in smoking-related lung cancer: *STK11*-mutant lung adenocarcinoma, *KRAS*-mutant lung adenocarcinoma, and 3q amplified squamous cell lung cancer.

1.11.1 Aims

1. To identify predictors of response to treatment, and better define resistance to mTORC1/2 inhibition in *STK11*-mutant NSCLC.
2. To identify predictors for response to treatment, and better define resistance to CDK4/6 inhibition in *KRAS*-mutant NSCLC.
3. To identify a key oncogenic driver (or drivers) on the 3q amplicon in squamous cell lung cancer, and to identify therapeutic strategies to target this driver (or drivers)

1.11.2 Objectives

1. Examine whether *STK11*-mutant cell lines are exempt from reactivation of PI3K/Akt signalling following treatment with mTORC1/2 inhibition.
2. Assess sensitivity of *STK11*-mutant cell lines to mTORC1-only (everolimus) and mTORC1/2 inhibition (vistusertib) *in vitro*.
3. Identify mutations associated with sensitivity and resistance to mTORC1/2 inhibition using serial ctDNA samples from STK11-deficient NSCLC patients treated with vistusertib in the National Lung Matrix Trial.
4. Identify mutations associated with sensitivity and resistance to CDK4/6 inhibition using serial ctDNA samples from *KRAS*-mutant NSCLC patients treated with palbociclib in the National Lung Matrix Trial.
5. Define the frequency of amplification of genes within 3q in the TCGA squamous cell lung cancer dataset, and explore the relationship between amplification and mRNA expression
6. To identify genes within 3q with differential sensitivity to CRISPR knockout in 3q amplified versus non amplified lines using genome-wide CRISPR knockout data from DepMap, and to validate candidate(s).
7. To identify therapeutic strategies to target the key oncogenic driver (or drivers) on 3q. Firstly, screening drugs known to downregulate the expression of this protein in other contexts. Secondly, using an unsupervised approach by application of a FACS-assisted genome wide CRISPR screen

Chapter 2: Methods

2.1 Cell Culture

2.1.1 Cell Line Authentication and Sources

MCF-7, NCI-H460, A549, A-427, CAL-12T, Chago-K-1 and NCI-H1755 were gifted by Richard Buchanan (University of Birmingham). NCI-H1703, NCI-H520 and SKMES-1 were purchased from American Type Culture Collection (ATCC, USA). RERF-LC-SQ1 and LC-1-SQ were purchased from Japanese Collection of Research Biosources Cell Bank (JCRB) (Tokyo, Japan). HCC1897, HCC2450 and HCC2814 (generated by Adi Gazdar and John Minna) were kindly shared from the UT Southwestern Cell Bank with thanks to the lab of John Minna (UT Southwestern, USA). All cell lines that were not directly obtained from ATCC were authenticated by Short Tandem Repeat (STR) typing by ATCC. Cell lines were banked at low passage, and experiments were performed at a maximum of passage 20 after thawing. Cell lines were routinely tested (and confirmed negative) for mycoplasma using EZ-PCR Mycoplasma Test Kit (Biological Industries, Israel).

2.1.2 Routine Cell Line Maintenance

Cell culture was conducted under sterile conditions in a laminar flow hood. Cell culture media was changed when required, at least every three days. Composition of complete growth media for each cell line is given in Table 11. Cells were passaged when approaching 70% confluence (usually twice a week). In brief, cells were washed twice with D-PBS, sufficient TrypLE (Thermofisher, USA) was added to cover the cell monolayer, and cells were incubated at 37°C until dissociation was achieved. Complete growth media was added, and cells were transferred to 10 ml centrifuge tubes. Cells were pelted by centrifugation at 200g for 5 minutes. Media was discarded, the cell pellet was disaggregated and then diluted in fresh complete growth media. An appropriate volume of the cell mixture was added to a fresh cell culture flask, and volume of media

was made up to a final volume of 12 mls (for T75 flask). Cells were returned to the incubator, with all cell lines being maintained in a humidified incubator at 37°C with 5% CO_2.

Cell Line	Complete Growth Media	Supplier (Catalogue number)
MCF-7	90% RPMI-1640 with L-glutamine 10% FBS 1% Penicillin/Streptomycin	Thermofisher (#21875034) Sigma (F7524) Thermofisher (15140122)
NCI-H460	90% RPMI-1640 with L-glutamine 10% FBS 1% Penicillin/Streptomycin	Thermofisher (#21875034) Sigma (F7524) Thermofisher (15140122)
A569	90% RPMI-1640 with L-glutamine 10% FBS 1% Penicillin/Streptomycin	Thermofisher (#21875034) Sigma (F7524) Thermofisher (15140122)
A-427	90% RPMI-1640 with L-glutamine 10% FBS 1% Penicillin/Streptomycin	Thermofisher (#21875034) Sigma (F7524) Thermofisher (15140122)
CAL-12T	90% RPMI-1640 with L-glutamine 10% FBS 1% Penicillin/Streptomycin	Thermofisher (#21875034) Sigma (F7524) Thermofisher (15140122)
ChaGo-K-1	90% RPMI-1640 with L-glutamine 10% FBS 1% Penicillin/Streptomycin	Thermofisher (#21875034) Sigma (F7524) Thermofisher (15140122)
NCI-H1755	90% RPMI-1640 with L-glutamine 10% FBS 1% Penicillin/Streptomycin	Thermofisher (#21875034) Sigma (F7524) Thermofisher (15140122)
NCI-H1703	90% RPMI-1640 with L-glutamine 10% FBS 1% Penicillin/Streptomycin	Thermofisher (#21875034) Sigma (F7524) Thermofisher (15140122)
NCI-H520	90% RPMI-1640 with L-glutamine 10% FBS 1% Penicillin/Streptomycin	Thermofisher (#21875034) Sigma (F7524) Thermofisher (15140122)
RERF-LC-SQ1	90% RPMI-1640 with L-glutamine 10% FBS 1% Penicillin/Streptomycin	Thermofisher (#21875034) Sigma (F7524) Thermofisher (15140122)
SKMES-1	90% EMEM with Earles salts 10% FBS 1% Non-Essential Amino Acids 2 mM L-Glutamine 1% Penicillin/Streptomycin	Sigma (M2279) Sigma (F7524) Thermofisher (11140050) Thermofisher (25030024) Thermofisher (15140122)
HCC1897	90% RPMI-1640 with L-glutamine 10% FBS 1% Penicillin/Streptomycin	Thermofisher (#21875034) Sigma (F7524) Thermofisher (15140122)
HCC2450	90% RPMI-1640 with L-glutamine 10% FBS 1% Penicillin/Streptomycin	Thermofisher (#21875034) Sigma (F7524) Thermofisher (15140122)
HCC2814	90% RPMI-1640 with L-glutamine 10% FBS 1% Penicillin/Streptomycin	Thermofisher (#21875034) Sigma (F7524) Thermofisher (15140122)
LC-1-SQ	90% DMEM/F12 10% FBS 1% Penicillin/Streptomycin	Thermofisher (11330032) Sigma (F7524) Thermofisher (15140122)

Table 11: Composition of Complete Growth Media for Cell Lines. (RPMI-1640 – Roswell Park Memorial Institute Medium 1640; FBS – foetal bovine serum; DMEM F12 – Dulbecco's Modified Eagle Medium / Nutrient Mixture F-12 EMEM: Eagle's Minimum Essential Media)

2.1.3 CellTiter Glo 2.0 Assay (Single Drug)

Cells were seeded in white 96 well plates at 500 – 1000 cells per well in 100 μL complete growth media (Table 11). Seeding density was pre-determined for each cell line and timepoint of interest, ensuring cell growth remained within the linear range of the assay. After 6 hours, 100μL of the drug of interest was added. DMSO concentration was normalised for all conditions, maintaining DMSO concentrations < 0.5 %. For extended drug incubations, media and drug was refreshed at 4 days. After incubation for the indicated time, cell viability was assessed using CellTiter-Glo 2.0 Luminescent Cell Viability Assay: plates and reagents were equilibrated to room temperature; 100 μL of growth medium was removed from the well; 75μL CellTiter-Glo 2.0 (Promega, USA) was added; plates were sealed and gently agitated on an orbital shaker for 2 minutes; plates were incubated at room temperature for 15 minutes and luminescence was read using a FLUOstar Omega Platereader (BMG LabTech, Germany). Background luminescence (media with CellTiter-Glo 2.0 with no cells, averaged across at least three wells) was subtracted from each reading. Cell Viability was expressed relative to control conditions (no drug), as follows:

$$\%\ \text{Viability} = \frac{\text{Luminescence Sample}}{\text{Luminesence Control}} \times 100$$

2.1.4 CellTiter Glo 2.0 Assay (Combination Drug)

Cells were seeded in white 96 well plates at 1000 cells per well in 100 µL complete growth media. After 6 hours, 50 µL drug 1 and 50 µL drug 2 were added to achieve the desired final drug concentrations as per Figure 12. DMSO concentrations were normalised across the plate. Plates were seeded in triplicate, with experiments repeated four times for each drug combination. After incubation for the indicated time, cell viability was assessed using CellTiter-Glo 2.0 Luminescent Cell Viability Assay as per section 2.1.3.

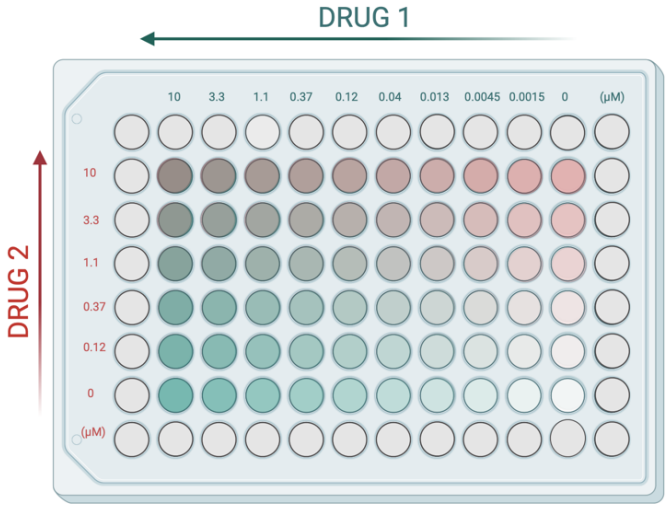

Figure 12: Plate map used for combination drug experiments. 50 µL drug 1 and 50 µL were added to achieve the final drug concentrations indicated, with drug dilutions performed in the appropriate DMSO concentration to ensure DMSO concentration was normalised across the plate, Outside wells were not used for experimentation, and instead filled with plain media. Plates seeded in triplicate for each biological replicate. Experiment performed in quadruplicate on separate passages for each drug combination

Potential synergy was assessed using Multi-dimensional Synergy of Combinations (MuSyC) (2, 3) using Synergy Finder 2.0 (370) (https://synergyfinder.fimm.fi). MuSyc permits an interpretation of drug synergy along multiple axes: Efficacy, Potency and Co-operativity. Potency is the amount of drug required to produce a defined effect (2, 3). Synergistic potency is the magnitude of the shift in potency from addition of a second drug (2, 3). Efficacy is the magnitude drug of effect (2, 3). Synergistic efficacy is the alteration in maximal efficacy of the combination versus the most efficacious single drug (2, 3). Co-operativity is measured by the hill coefficient, i.e. the steepness of the response curve (Figure 13) (2, 3).

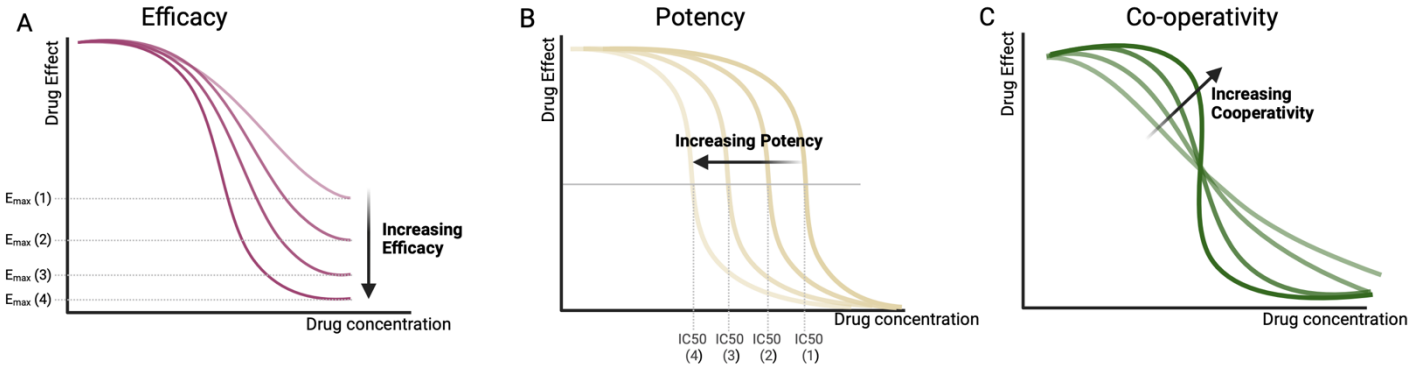

Figure 13: Illustration of Efficacy, Potency and Co-operativity. Efficacy is a measure of measure of maximum rug effect, with shifts in efficacy leading to alterations in E_{max}. Potency is the amount of drug required to produce an effect and can be measured by the concentration of drug required to produce 50% of the maximum drug effect (Relative IC50). Co-operativity is measured by the hill coefficient, i.e. the steepness of the response curve. Adapted from (2, 3), created using Biorender.com, printed with permissions

2.1.5 Drugs

A list of drugs used is provided in cell experiments is provided in Table 12

Drug	Solvent	Catalogue Number	Supplier
Vistusertib (AZD2014)	DMSO	S2783	Selleck Chemicals, USA
Everolimus (RAD001)	DMSO	S1120	Selleck Chemicals, USA
Iadedemstat Dihydrochloride (ORY1001)	H_2O	HY-12782T	MedchemExpress.com
Pevonedistat (MLN4924)	DMSO	S7109	Selleck Chemicals, USA
THZ1	DMSO	HY-80013	MedchemExpress.com
Samuraciclib hydrochloride (ICEC0942 / CT7001)	H_2O	S8722	Selleck Chemicals, USA
SY-5609	DMSO	HY-138293	MedchemExpress.com
AZD5153	DMSO	S8344	Selleck Chemicals, USA
Napabucasin (BB1608)	DMSO	S7977	Selleck Chemicals, USA

Table 12: List of Drugs used for Cell Culture Experiments

2.1.6 SiRNA Transfection

Both forward and reverse transfection were attempted, however, reverse transfection was found to be the most efficient strategy for all tested cell lines. Full details of siRNA optimisation are provided in Section 5.3.3.1 Optimisation of SOX2 knockdown. The general method used for reverse transfection in a 6 well plate format is outlined here. siRNA duplexes were diluted in 500 µL Opti-MEM I Reduced Serum Media (Thermofisher Scientific, USA). Lipofectamine RNAiMAX (Thermofisher Scientific, USA) was added to Opti-MEM/RNAi mixture, mixed by pipetting, and the mixture was incubated for 30 minutes at room temperature. After incubation, the Opti-MEM/RNAi/Lipofectamine mixture was added to 6 well plates. 0.3 – 0.5 x 10^6 cells per well in antibiotic-free complete growth medium were added, and cells were returned to the incubator (incubation overnight at 37°C). The next morning, media was removed and replaced with antibiotic-containing complete growth media. Where transfected cells were used for growth curves, cells were seeded 24 hours post transfection in flat-bottomed 96 well plates at 500 cells per well. Lysates were collected 48 hours post transfection and assessed for protein levels using western blotting. All transfection experiments utilised scrambled siRNA as a negative control (Silencer select negative Control no 1). BLOCK-iT Alexa Fluor Red Fluorescent Control was used

as a positiec control and to ensure transfection efficiency, ensuring transfection efficiency > 90% for each experimental replicate (assessed on the Cytation5 microscope). Full details of controls are provided in Table 14. Individual siRNAs used for experiments are listed in Table 13

Target		ID	Product
SOX2	SOX2 siRNA #1	S13294	Silencer Select Pre-designed
	SOX2 siRNA #2	S13295	Silencer Select Pre-designed
	SOX2 siRNA #3	S13296	Silencer Select Pre-designed
VCP	VCP siRNA #1	S14765	Silencer Select Validated
	VCP siRNA #2	S14767	Silencer Select Validated
PCNA	PCNA siRNA #1	S10133	Silencer Select Validated
	PCNA siRNA #2	S10134	Silencer Select Validated
TTI1	TTI1 siRNA #1	S18620	Silencer Select Pre-designed
	TTI1 siRNA #2	S18621	Silencer Select Pre-designed
EIF4G1	EIF4G1 siRNA #1	S4585	Silencer Select Pre-designed
	EIF4G1 siRNA #2	S4586	Silencer Select Pre-designed
PGM3	PGM3 siRNA #1	S10409	Silencer Select Pre-designed
	PGM3 siRNA #2	S10411	Silencer Select Pre-designed

Table 13: List of siRNA used in Transfection Experiments (All from Thermofisher Scientific, USA)

Control	ID
Negative Control	Silencer select negative control no.1 siRNA
Positive Control	Silencer Select GAPDH Positive Control siRNA
Red Fluorescent Control	BLOCK-iT Alexa Fluor Red Fluorescent Control

Table 14: Positive and negative controls used for Transfection experiments (All items from Thermofisher Scientific, USA)

2.1.7. Colony Formation Assay

Cells were seeded at 500 cells per well in a 6 well plate in 3 ml of complete growth media. After 7 days of incubation, plates were placed on ice, media was removed, and plates were gently washed twice with ice cold D-PBS. Cells were fixed with ice-cold 400 μL methanol per well for 10 minutes. Methanol was aspirated, 0.5% crystal violet was added, and plates were incubated for 10 minutes. Excess crystal violet was removed, and wells were rinsed thoroughly with distilled water. Plates were air-dried overnight and imaged using the Cytation 5 microscope (Agilent, USA). Colonies were counted manually, with > 50 cells being considered a countable colony.

2.1.8 Real-time imaging and cell counting

Real-time cell imaging was conducted using the Cytation 5 microscope and Agilent Biospa 8 (Agilent, USA), maintaining temperatures at 37°C and 5% CO_2. Experiments were conducted in a 96-well plate format, using a single 4x Bright Field:High Contrast image to capture the entire well at 12 hourly intervals. For each individual experimental replicate, each condition was plated in at least 15 wells. Experiments continued until confluency or images became uncountable. Image pre-processing and cell counting utilised the Gen5 software (Agilent). Images were first processed with background flattening (rolling ball diameter of 10 µm and an image smoothing strength of 7 cycles of 3 x 3 average filter, prioritising fast speed). The periphery of the plate was removed from image counting to prevent edge effects (utilising an 'image plug' of the central 4000 µm diameter circle). Counting thresholds were set for individual cell lines to maximise counting accuracy. Images were visually checked to ensure counting accuracy. Images were excluded where counting was inaccurate (for example due to debris). No experimental replicate required more than two wells to be excluded.

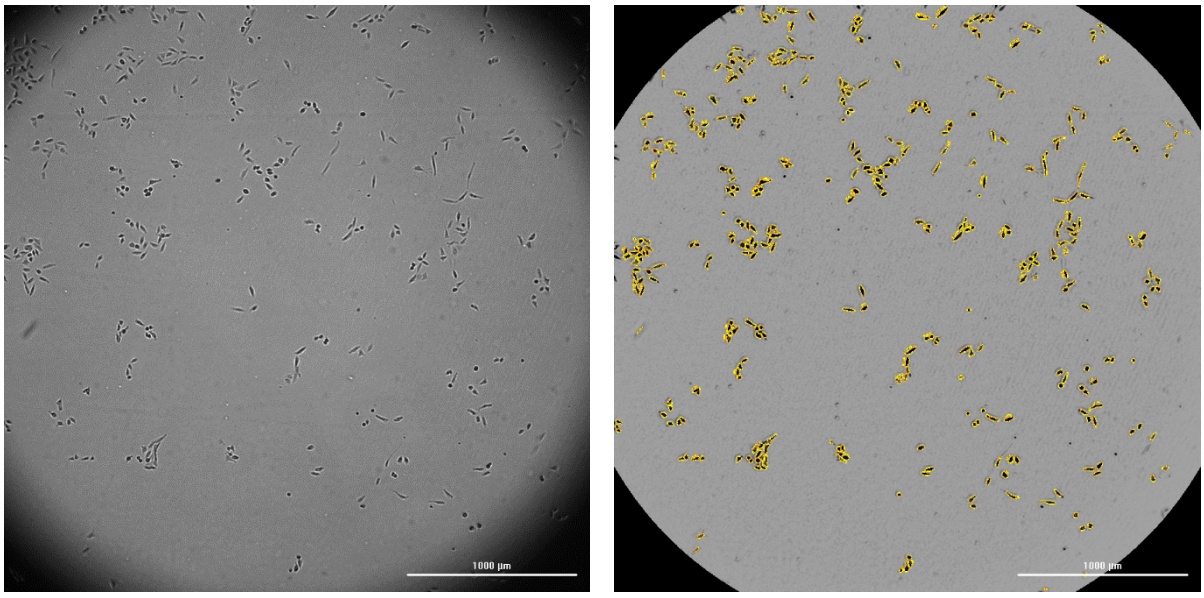

Figure 14: Example of image processing and cell counting. Images were captured using 4 x bright field on the Cytation 5 microscope. Image processing was applied to reduce background and to remove the penumbra from shadowing from well edges. Automated cell counting was optimised for each cell line, and visually checked for accuracy.

To account for variations in seeding density, normalised cell count was calculated as follows:

$$\text{Normalised cell count} = \frac{\text{Cell count at indicated time point}}{\text{Cell count at T} = 0}$$

Proliferation was expressed relative to negative control (cells transfected with negative control 'scramble' siRNA) as follows:

$$Relative\ proliferation = \frac{Normalised\ cell\ count}{Normalised\ cell\ count\ negative\ control\ (scramble)}$$

2.2 Western Blotting

2.2.1 Cell Culture

Cells were seeded at an appropriate cell density in 6 well plates (typically 0.1 – 0.5 x 10^6 cells per well, depending on timepoint of interest), and allowed to adhere overnight. Drug at the appropriate concentration was added, and cells were incubated for the required time.

2.2.2 Protein Lysis

All steps performed on ice. Cells monolayer was rinsed twice with ice-cold PBS. Radioimmunoprecipitation assay buffer (RIPA buffer, Thermoscientific, USA) with 2 x Protease/Phosphatase inhibitor cocktail (Cell Signalling Technology, USA) was added to each well, and wells were scraped into sterile Eppendorf tubes. Lysates were heated to 100°C for five minutes, sonicated three times for ten seconds, and centrifuged at 130000 g for five minutes. Supernatant was transferred into fresh Eppendorf tubes, and then vortexed twice for 10 seconds.

2.2.3 Protein Quantification

Protein quantification was performed using the Pierce Bovine Serum Albumin (BSA) Protein Assay Kit (Thermo scientific, USA) according to the manufacturer's instructions, comparing samples with a 0 – 2000 µg/ml standard curve of BSA using a spectrophotometer at 540 nm (FLUOstar Omega Plate Reader). Where concentrated protein samples were obtained, samples were diluted (typically 1:4 in RIPA buffer) to ensure that quantification was within the linear portion of the standard BSA curve.

2.2.4 SDS-PAGE

Samples were normalised for protein quantity with 1:6 loading buffer (Lane Marker Reducing Sample Buffer, Thermo Scientific USA). Volume was equalised using nuclease free water. Samples were denatured by boiling for five minutes, briefly centrifuged, and loaded onto gels (10 – 12%, Mini-protean Precast Gel, Bio-rad, USA). PageRuler Plus Prestained Protein Ladder (Thermofisher, USA) was used to confirm molecular weight. Electrophoresis was performed at 80V for ten

minutes and then 140V until the dye front approached the end of the gel. Solutions used for SDS-PAGE are given in Table 15.

2.2.5 Transfer

Transfer to polyvinylidene fluoride (PVDF) membranes was performed using wet transfer for all western blots performed in chapter 3. For all other chapters, transfer was conducted using dry transfer using the Invitrogen iBlot2 Transfer Device

Wet Transfer

PVDF membranes (GE Healthcare, Germany) were activated in 100% methanol for 10 seconds, followed by equilibration of all transfer apparatus in transfer buffer (Table 15). Transfer sandwich was assembled as per Figure 15, with transfer performed in a transfer tank (Bio-rad, USA) in Transfer Buffer as 90V for 90 minutes at 4°C.

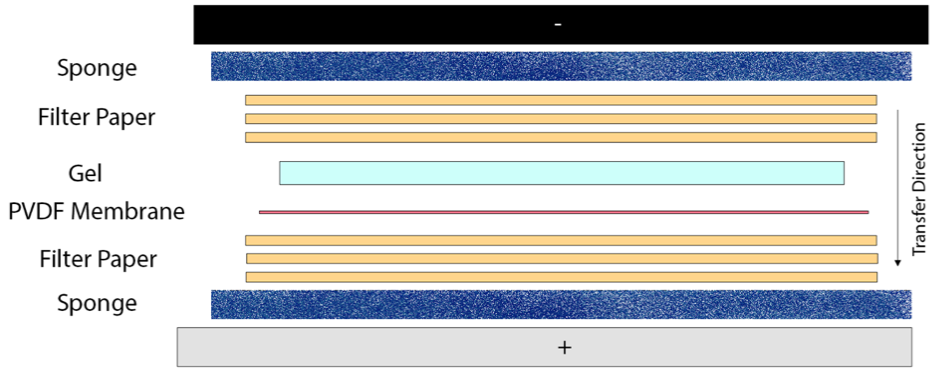

Figure 15: Assembly of Transfer Sandwich for Wet Transfer. Created using Biorender.com, printed with permission.

Dry Transfer

Dry transfer was performed using the Invitrogen iBlot 2 Gel Transfer Device (Invitrogen). Transfer was conducted as per manufacturer's instructions using the iBlot2 PVDF Transfer Stacks (Invitrogen) (regular size for 2 blots, mini for 1 blot). Transfer conditions were optimised for the transfer of SOX2: 20V for 1 minute, 23 V for 4 minutes, and 25 V for 1.5 minutes. These transfer conditions prevented over-transfer of smaller proteins (such as SOX2), whilst maintaining adequate transfer of larger proteins.

Solution	Constituents	Preparation	Manufacturer
10 x TBS	200 mM Tris 1500 mM NaCl	24 g Tris-HCl 5.6g Tris base 88g NaCl Final volume 1L in diH20 pH 7.6	Sigma-Aldrich, USA Sigma-Aldrich, USA Sigma-Aldrich, USA -
1 x TBST	20 mM Tris 150 mM NaCl 0.1% v/v Tween20	100 ml 10 x TBS 899 ml diH20 1 ml Tween20	- - VWR Chemicals, France
Stripping buffer	1.5% w/v glycine 0.1% SDS 1% v/v Tween20	15 g glycine 1g SDS 10ml Tween20 Final volume 1L in diH20 pH 2.2	Sigma-Aldrich, USA Sigma-Aldrich, Japan VWR Chemicals, France -
Transfer buffer	25 mM Tris 192 mM Glycine (pH 8.3)	100 ml 10x Tris/Glycine Buffer 200 ml methanol 700 ml diH20	Bio-Rad, Germany VWR Chemicals, France
Running buffer	25 mM Tris 192 mM Glycine 0.1% w/v SDS (pH 8.3)	100 ml 10x Tris/Glycine/SDS Buffer 900 ml diH20	Bio-Rad, Germany

Table 15: Solutions used for western blotting

2.2.6 Primary and Secondary antibodies

Membrane blocking was performed for one hour at room temperature, using 5% dried skimmed milk powder (Marvel) in 1 x Tris-buffered saline, 0.1% Tween 20 (TBST) (Table 15) for one hour on a rocking platform at room temperature. After rinsing briefly with TBST, membranes were incubated with primary antibodies (diluted in 5% BSA/TBST) overnight at 4°C. Antibodies used are listed in Table 16.

Target	Clone	Catalogue number	Species	Clonality	Molecular Weight (Kda)	Dilution	Supplier
PFOXO1 (Thr24)/ FOXO3a (Thr32)	-	9464	Rabbit	Polyclonal	78 – 82, 95	1:1000	Cell Signalling Technology, USA
pAkt (Ser473)	D9E	4060	Rabbit	Monoclonal	60	1:1000	Cell Signalling Technology, USA
pErk 1/2 (Thr202/Tyr204)	-	9101	Rabbit	Polyclonal	42, 44	1:1000	Cell Signalling Technology, USA
Phospho-S6 Ribosomal Protein (Ser235/236)	-	2211	Rabbit	Polyclonal	32	1:1000	Cell Signalling Technology, USA
pEBP1 (Thr37/56)	-	9459	Rabbit	Polyclonal	15-20	1:1000	Cell Signalling Technology, USA
TTI1	H-1	sc-271638	Mouse	Monoclonal	122	1:500	Santa-Cruz, USA
VCP	-	2648	Rabbit	Polyclonal	89	1:1000	Cell Signalling Technology, USA
PCNA	PC10	2586	Mouse	Monoclonal	36	1:1000	Cell Signalling Technology, USA
EIF4G1	-	2858	Rabbit	Polyclonal	220	1:1000	Cell Signalling Technology, USA
PGM3	-	PA522353	Rabbit	Monoclonal	60	1:500	Invitrogen, USA
SOX2	D6D9	3579	Rabbit	Monoclonal	35	1:1000	Cell Signalling Technology, USA
β-Actin	-	4970	Rabbit	Polyclonal	45	1:1000	Cell Signalling Technology, USA
α-Tubulin	-	2144	Rabbit	Polyclonal	52	1:1000	Cell Signalling Technology, USA

Table 16: Primary Antibodies used for Western Blotting. All primary antibodies were diluted in 5% bovine serum albumin (BSA) at the indicated concentration.

Following incubation with primary antibody, membranes were washed in 1 x TBST (4 x 10 minutes) on a rocking platform at room temperature. Membranes were then incubated with goat anti-rabbit antibody in 5% skimmed milk/TBST for one hour at room temperature, followed by further washes in 1 x TBST (4 x 10 minutes). Enhanced chemiluminescence (ECL) was used to measure peroxidase activity as per the manufacturer's instructions. Blots were imaged using a Fuxion FX6XT digital imaging system (Vilber Lourmat, Germany) for chapter 3, and the Bio-rad ChemiDoc imaging system for all other chapters.

2.2.7 Stripping and re-probing

Stripping of membranes was performed by incubation with mild stripping buffer (Table 15) at room temperature on a rocking platform (2 x 10 minutes), followed by washing with PBS washes (2 x 10 minutes), and washing with TBST (2 x 5 minutes). Repeated blocking, incubation with secondary antibody, and ECL detection was performed to ensure completeness of stripping. Membranes were then blocked in 5% skimmed milk/TBST, followed by re-probing as described above.

2.3 Genome-wide CRISPR Screen

2.3.1 Overview and GeCKO lentivirus

Genome wide CRISPR screening using GeCKO (Genome-scale CRISPR-Cas9 knockout) pooled library A and B were performed according to methods outlined by Joung et al (367). GeCKO A + B lentivirus was obtained from Louise Tee (Beggs' Group, University of Birmingham), which had been previously purchased from Addgene, and prepared as per methods reported elsewhere (367). Optimisation experiments were performed in two 3q amplified cell lines: RERF-LC-SQ1 and HCC2814. RERF-LC-SQ1 was selected for the genome-wide CRISPR screen, due to better performance in FACS sorting on SOX2 expression.

2.3.2 Puromycin Kill Curve

The minimum puromycin concentration to kill each cell line was determined. Cells were seeded in white-walled, clear bottomed 96 well plates at density of 2000 cells/well in 100µL media. 100 µL puromycin (Thermofisher), diluted in complete media to achieve a final concentration of 0 – 3 µg/ml, was added 24 hours post seeding. After 96 hours, wells were observed to determine the lowest puromycin concentration that was lethal to all cells in the well. Cell viability was also quantitatively assessed using CellTiter-Glo 2.0 (Promega) (as per methods described in 2.1.3 CellTiter Glo 2.0 Assay). The lowest puromycin concentration to achieve less than 1 % cell viability relative to untreated cells was selected for puromycin selection for ongoing experiments.

2.3.3 Determination of Moiety of Infection

Volume of lentivirus supernatant required to achieve a moiety of infection (MOI) of 0.3 was determined for each cell line. Cells were seeded in 6 well plates to achieve 80 – 90% confluence 24 hours post-seeding (0.3×10^6 per well for RERF-LC-SQ1 and 0.5×10^6 per well for HCC2814). 24 hours post-seeding, media was removed and replaced with complete media without antibiotics, containing 8 µg/ml polybrene. 0 – 800 µL lentivirus was then added (Figure 16). Plates were gently agitated, and transduced using spinfection by centrifugation for 1.5 hours, at 1000g, at 33°C in sealed buckets, and returned to the incubator overnight at 37°C.

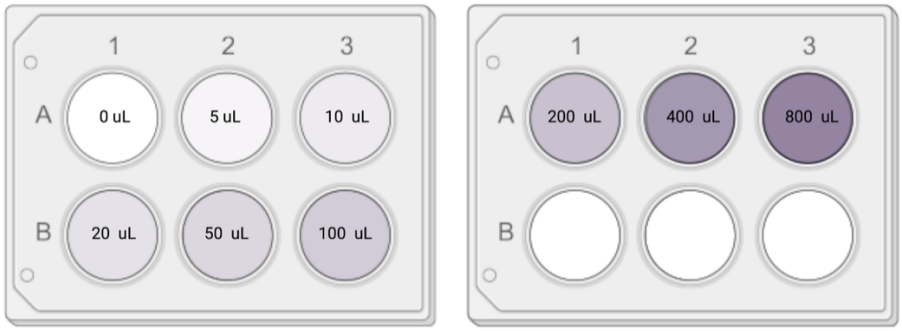

Figure 16: Plate Layout for Determining Moiety of Infection. *Created using Biorender.com, printed with permission.*

After overnight incubation, wells were washed twice with D-PBS, and cells were detached using 500 µL TrypleE per well (10 minute incubation, 37°C). 1 ml complete media was added and mixed gently to form a cell suspension. For each virus concentration, cells were plated in quadruplicate in an opaque-walled 96 well plate in 100 µL of complete media. After overnight incubation at 37°C, 100 µL puromycin diluted in complete media was added to achieve a final puromycin concentration as determined in section 2.3.2 Puromycin Kill Curve. An additional four wells were included as 'unselected controls', with 100 µL complete growth media without puromycin added.

After 96 hours of puromycin selection, CellTiter Glo 2.0 was used to determine viability as described in Section 2.1.3 CellTiter Glo 2.0 Assay. For each condition, MOI was calculated as follows:

$$MOI = \frac{Average\ luminescence\ with\ antibiotic\ selection}{Average\ luminescence\ with\ no\ antibiotic\ selection}$$

MOI for each condition was plotted using Prism 9, and the lentivirus volume required for MOI of 0.3 was interpolated from the curve.

2.3.4 Lentiviral Transduction and Puromycin Selection

RERF-LC-SQ1 cells were expanded to achieve sufficient cells for the genome-wide CRISPR screen. Numbers of cells required was calculated as follows:

$$Number\ of\ cells = \frac{Required\ coverage\ \times\ sgRNA\ in\ GeCKO\ Library}{MOI}$$

As the GeCKO library has 122,000 sgRNA, it was determined that a minimum of 2.03 x 10^8 cells would be required to maintain a coverage of 500 x and an MOI of 0.3. To allow for anticipated loses of cells during cell sorting, 2.80 x 10^8 cells were transduced at the start of the experiment. Cells were seeded and transduced as described in section 2.3.3 Determination of Moiety of Infection. A further 6 well plate was not transduced with sgRNA, to provide a 'no-transfected control' condition, allowing monitoring for complete puromycin selection. After overnight incubation, wells were washed with D-PBS, 500 µL of TrypLE Express was added to each well, and plates were returned to the incubator for 10 minutes to allow cells to detach. Cells were transferred to T150 cm^2 flasks (pooling 4 wells into one flask, in 30 ml complete media). 24 hours after seeding in T150 flasks (48 hours after transduction), media was removed from flasks, and was replaced by media containing puromycin at the concentration determined in section 2.3.2 Puromycin Kill Curve. Non-transfected control cells were treated with the same concentration of puromycin.

2.3.5 Pooling of cells

After 4 days of puromycin selection, it was confirmed that all non-transfected cells had died. All transfected T150 cm^2 flasks were pooled: cells were washed twice with D-PBS, detached with of TrypLE Express, resuspended in media, pelleted by centrifugation, supernatant discarded, and resuspended in complete growth media, and pooled in a T150 cm^2 flask in suspension at 37°C. Cells were mixed thoroughly, and re-seeded into T150 cm^2 flasks with ongoing puromycin

selection. After a total of 7 days of puromycin selection, cells were re-pooled, and portioned as follows:

1. At least 6.2 x 10^7 cells pelleted and snap frozen (unsorted control)
2. At least 22.4 x 10^7 cells for FACS (12.4 X 10^7 for sorting + additional for controls)

2.3.6 Fluorescence-activated Cell Sorting (FACS): Sample Preparation

There is an absence of well validated FACS sorting strategies for SOX2 expression, SOX2 staining for flow cytometry was therefore optimised, with full details of optimisation provided in Section 7.3.1.3 (Optimisation of sort strategy for SOX2). The finalised protocol used during the CRISPR screen is described here. Fixation/Permeabilisation was performed using an the eBioscience™ Foxp3/Transcription Factor Staining Buffer Set (Thermofisher, USA), using an adapted protocol to allow processing of the large numbers of cells required for the genome-wide CRISPR screen. Details of buffers used for Fixation/Permeabilization are provided in Table 17. Stains and antibodies used are outlined in Table 18. Preparation of controls is outlined in Table 19.

A single cell suspension was prepared by passing pooled cells through 50 µM cell strainer (Greiner). Cells were separated into 15 ml centrifuge tubes, with 2 x 10^7 cells in each tube. Cells were washed twice with D-PBS and resuspended in 2 ml D-PBS. 2 µL of Fixable Viability Dye eFluor 450 (Thermofisher, USA) was added, and the resulting mixture was thoroughly vortexed. Tubes were incubated for 30 minutes at 4°C, with a vortex midway through incubation. Samples were washed twice with FACS buffer and supernatant was discarded. Pellets were thoroughly dissociated by pulse vortexing, and then resuspended in 400 µL FACS buffer. 4 ml FOXP3 Fixation/Permeabilization working solution was added to each tube, samples were vortexed and incubated for 45 minutes at 4°C and protected from light (samples were vortexed half-way through the incubation). 6 ml of 1 x FOXP3 Fixation/Permeabilization buffer was added to each tube, and samples were centrifuged at 500 g for 5 minutes at room temperature, supernatant

was then discarded. Samples were washed for a second time with 6 ml 1 x permeabilization buffer, supernatant was once again discarded. Samples were resuspended in 1 ml 1:50 antibody (dissolved in 1 x FOXP3 Fixation/Permeabilization buffer), or the equivalent concentration of isotype control (corrected for lot concentration of PE anti-SOX2 antibody). Samples were incubated for 45 minutes at room temperature. 6 ml of 1 x FOXP3 Fixation/Permeabilization buffer was added, samples were centrifuged at 500 g for 5 minutes at room temperature. Samples were washed for a second time, and cells were resuspended in 1 ml of FACS buffer. Samples were stored in the fridge overnight, with sorting by FACS was completed the next day.

Solution	Constituents
FACS Buffer	2.5 ml FBS 97.5 ml D-PBS 100 µL EDTA Filter Sterilised
FOXP3 Fixation/Permeabilization working solution	1 part FOXP3 Fixation/Permeabilization Concentrate 3 parts FOXP3 Fixation/permeabilization Diluent
FOXP3 Fixation/Permeabilization buffer	1 part FOXP3 10x permeabilization buffer 9 parts distilled water

Table 17: Buffers used for Fixation/permeabilization. FOXP3 Fixation/Permeabilization Concentrate and FOXP3 Fixation/Permeabilization Diluent are components of the eBioscience FOXP3/Transcription Factor Staining Buffer Set (Thermofisher Scientific). FBS was purchased from Sigma. EDTA and D-PBS were also from Thermofisher Scientific

Antibody / Stain	Clone	Isotype	Fluorochrome (laser)	Concentration	Supplier
PE anti-SOX2	14A6A34	Mouse IgG1, κ	PE (561 [Yellow])	1:50	Biolegend, USA
PE mouse IgG1 Isotype Control	MOPC-21	Mouse IgG1, κ	PE (561 [Yellow])		Biolegend, USA
Fixable Viability Dye eFluor 450	-	-	eFluor 450 (355 [UV])	1:1000	Thermofisher, USA

Table 18: Antibodies and stains used during flow cytometry. Note that concentration of isotype control was corrected for individual lot concentrations of PE anti-SOX2 antibody as per the data-sheets provided by Biolegend. Where more than one aliquot of antibody was required for staining the entire batch of cells, aliquots were pooled to ensure consistency of staining across tubes.

		Viability Dye	Fix/Perm	SOX2	Isotype Control
	Sample	☑	☑	☑	
Controls	Unstained/No Perm/No Fix				
	Unstained, Fixed and Permeabilized		☑		
	SOX2 Staining Only		☑	☑	
	Isotype Control Only		☑		☑
	Viability Dye Only	☑	☑		

Table 19: Summary of Preparation of Controls for Flow Cytometry / FACS experiments. Indicated are steps or stains that are included or excluded from each control population. Controls were prepared in synchrony with samples, and where fixation/permeabilization was excluded, this step was replaced with addition of equivalent volumes of D-PBS. Viability dye is Fixable Viability Dye eFluor 450, SOX2 is PE anti-SOX2, Isotype Control is PE Mouse IgG1 Isotype Control. Fixation/Permeabilization is eBioscience™ Foxp3/Transcription Factor Staining Buffer Set. For the 'viability dye only' sample, half of the sample was heated to 80°C for 1 minute before being placed on ice for 5 minutes, to ensure a proportion of cells were dead for the live/dead staining control.

2.3.7 Fluorescence-activated Cell Sorting

Fluorescence-activated Cell Sorting (FACS) was conducted on the BD FACSAria Fusion Flow Cytometer by the University of Birmingham Flow Cytometry Facility, with thanks to Dr Guillaume Desanti, Dr Shahram Golbabapour and Ferdus Sheik. To ensure two clean populations of $SOX2^{LOW}$ and $SOX2^{HIGH}$, a double sort strategy was adopted. Sorting was performed with the 85 µm nozzle using Precision Yield, sorting cells into $SOX2^{LOW}$ (bottom 10% of stained cells + negative cells) and $SOX2^{HIGH}$ (top 10% of stained cells). Resulting tubes were centrifuged at 500g for 5 minutes, resuspended in an appropriate volume of FACS buffer, and re-enriched for the target population (either $SOX2^{LOW}$ or $SOX2^{HIGH}$) by performing a further sort using Purity 16-32-0. Purity checks were performed for each tube, ensuring purity of >95% for the target population. Sorted cells were pelleted by centrifugation at 500g for 5 minutes, supernatant was discarded, and cell pellets were frozen at -80°C.

2.3.8 DNA Extraction

Commercial kits performed poorly when attempting DNA extraction from fixed cells. DNA extraction was therefore performed using Proteinase K / salt out extraction (methodology adapted from (199)). On validation, this methodology produced slightly lower yields in fixed than unfixed cells, but this difference was relatively small (Figure 17). Overall, this strategy was felt to be preferable to pursuing phenol/chloroform extraction, which would pose greater experimental hazard.

The following methodology applies to inputs of $3 \times 10^7 - 5 \times 10^7$ cells, volumes of reagents was adjusted accordingly for higher or lower inputs. A list of solutions and reagents used for DNA extraction is provided in Table 20. Pelleted cells were thawed, and 6 ml of NK lysis buffer and 60 µL 20 mg/ml Proteinase K were added. Samples were vortexed and incubated at 55°C for 18 hours. 30 µL RNAse A (10 mg/ml in NK lysis buffer) was added to lysates, followed by incubation at 37°C for 30 minutes. Samples were placed on ice, and 2 ml chilled 7.5 M ammonium acetate was added to precipitate proteins. Samples were vortexed for 30 seconds and centrifuged at 5000 g for 10 minutes. Supernatant was decanted into fresh conical tubes and 6 ml 100% isopropanol was added. Tubes were inverted 50 times and centrifuged at 5000g for 10 minutes. Supernatant was discarded, 6 ml 70% ethanol was added, and tubes were inverted 10 times and centrifuged at 5000g for 1 minute. Supernatant was discarded, and residual ethanol was removed. DNA pellets were air dried for 20 minutes. 500 µL of 1 x TE buffer was added and the tube was incubated at 65°C for 1 hour, and then at room temperature overnight. DNA was vortexed, and concentration was measured using the Qubit BR DNA kit, and visualised using Tapestation with a D1000 DNA tape.

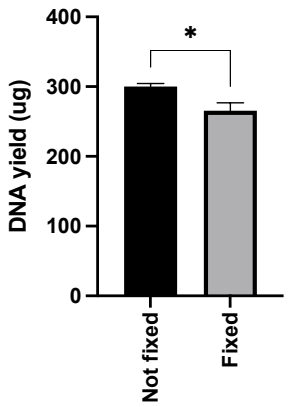

Figure 17:Validation of DNA Extracted using proteinase K, saltout extraction. 3 x 10^7 cells cells were fixed and permeabilised with eBioscience™ Foxp3/Transcription Factor Staining Buffer Set (Fixed), 3 x 10^7 cells processed as per FOXP3 fixation/permeabilization kit but using D-PBS for all steps. DNA extraction for both samples using Proteinase K / Salt out extraction. DNA quantified with dsDNA QuBit broad range. Quality of DNA confirmed in tapestation. Results from single validation experiment, QuBit performed in quadruplicate. Whilst Fixed Cells did have a significantly lower yield that non-fixed cells. Overall this method was judged to perform adequately for use for DNA extraction following FACS sorting.

Solution	Components	Supplier
NK Lysis Buffer	50 mM Tris 50 mM EDTA 1% w/v SDS Dissolved/diluted H_2O pH 8	Sigma, USA Corning, USA ThermoFisher Scientific, USA
Proteinase K	20 mg/ml	QIAGEN, Germany
RNAse A	10 mg/ml Diluted in NK Lysis buffer	QIAGEN, Germay
Ammonium Acetate	7.5 M Ammonium Acetate	Sigma, USA

Table 20: Solutions used for DNA Extraction during GeCKO screen. All components used were DNase free, RNase free and/or molecular grade

2.3.9 Library Preparation

To ensure maximum coverage, all harvested DNA was taken through to Polymerase Chain Reaction (PCR), with multiple reactions set up per condition. Each condition was barcoded using different reverse primer sequences, allowing pooling of multiple conditions on a single flow cell. Multiplexed, staggered forward primers were used to increase library diversity. Primer sequences for reverse and forward primers are provided in the Appendix (Supplementary Table 1 and 2). PCR Master mix components are outlined in Table 21, with sufficient reactions set-up to process all harvested DNA (1µg DNA per reaction). PCR cycle number was determined such that the lowest number of cycles were used for the PCR product to be visualised on a 1% agarose gel (22 cycles). PCR conditions are outlined in Table 22.

Reagent	1 reaction	Supplier
2 x NEB Q5 HiFi master mix	25 µL	New England Biolabs, USA
Harvested DNA	1 µg DNA	-
GeCKO forward primer (10 µM)	1.25 µL	Merck, USA
GeCKO reverse primer (10 µM)	1.25 µL	Merck, USA
Nuclease free water	To make up total volume to 50 µL	-

Table 21: Master Mix for Polymerase chain Reactions. Quantities for single reaction shown, with volumes upscaled to requirements. 10 forward primers were pooled at equal concentraitons to reach final 10 µM of multiplexed forward primers. Primer sequences available from (199) and Appendix (Supplementary Table 1 and 2).

Cycle	Denature	Anneal	Extend
Cycle 1	95°C (300 seconds)		
Cycle 2 – 22	98°C (20 seconds)	60°C (15 seconds)	72°C (15 seconds)
Cycle 23			72°C (60 seconds)

Table 22: Polymerase Chain Reaction (PCR) Conditions. PCR performed on MJ Research DNA Tetrad

For each condition, PCR products were pooled. Where input was > 1 x 10^7 cells, products were purified using Zymo-Spin™ V Columns with reservoir (ZYMO Research, USA) according to manufacturer's instructions. For lower inputs, PCR products were purified using the QIAquick PCR Purification Kit (QIAGEN, Germany). Products were quantified using the Qubit Broad Range DNA kit (Thermofisher Scientific, USA) and visualised on TapeStation (Agilent). PCR products were run on a 1.5% agarose gel, and the band corresponding to the purified PCR product (size range 260 – 270 bp) was cut from the gel. DNA was extracted from the gel using the NEB Monarch gel extraction kit (New England Biolabs, USA) according to manufacturer's instructions. The final purified DNA was quantified using the Qubit BR DNA kit, and visualised using Tapestation with a D1000 DNA tape, allowing molarity to be calculated. Concentration was checked with the Kapa qPCR kit.

$$\text{Concentration (nM)} = \frac{\text{Concentration (ng/ul)}}{660\ \text{(g/mol)} \times\ \text{average library size (bp)}}$$

Libraries were diluted to 4 nM. Sequencing was performed by Genomics Birmingham (University of Birmingham, UK) on Illumina Nextseq (Illumina, USA) using a Nextseq High 75 cycle kit with 80 cycles of read 1 and 8 cycles of index 1.

2.4 Circulating Tumour DNA

2.4.1 cfDNA Extraction

Stored plasma samples from patients treated in the National Lung Matrix Trial were received from the Human Biomaterials Resource Centre (HBRC), University of Birmingham. Samples were received as anonymised plasma aliquots. Where possible, cfDNA was extracted at baseline and at progression or treatment discontinuation. Where no discontinuation sample was available, the last available sample was extracted. All samples were historic samples that had been collected according to the Declaration of Helsinki and Good Clinical Practice (GCP) guidelines as part of the clinical trial.

For each timepoint for each patient, total volume of plasma was pooled, measured, made up to 5 ml with D-PBS and transferred to a 50 ml centrifuge tube. cfDNA was extracted using the QIAamp Circulating Nucleic Acid kit (QIAGEN, Germany) according to manufacturer instructions. In brief: 500 µL Proteinase K was added to samples, followed by 4 ml Buffer ACL (containing 1 µg carrier RNA). Samples were pulse vortexed for 30 seconds and incubated at 60°C for 30 minutes. 9 ml ACB Buffer was added to lysate, the mixture was pulse-vortexed for 30 seconds and incubated on ice for 5 minutes. Samples were passed through QIAamp Mini Columns using the QIAvac 24 plus vacuum system (QIAGEN, Germany). 600 µL Buffer ACW1 was passed through QIAamp Mini columns, followed by 750 µL Buffer ACW2, followed by 750 µL 100% ethanol. QIAamp mini columns were placed into 2 ml collection tubes and incubated for 10 minutes at 56°C to evaporate residual ethanol. QIAamp Mini columns were placed in microcentrifuge tubes, 53 µL Buffer AVE was added to the membrane and incubated at room temperature for 5 minutes. DNA was eluted by centrifugation at 17000g for 1 minute. The eluted nucleic acids in AVE were added back onto the membrane for a second elution to ensure maximal DNA yields were obtained. cfDNA samples were stored at -20°C.

2.4.2 cfDNA Quantification

The 96 – 270 bp region of DNA was quantified using Tapestation, using Agilent High sensitivity D5000 Screen Tape and Reagents (Agilent Technologies, USA). Quantification was not performed with Qubit as per advice of Illumina, as Qubit would include non-target high molecular weight DNA, and therefore would over-estimate input.

2.4.3 Library Preparation

Library preparation was completed using TruSight Oncology 500 (TSO500) ctDNA kit (Illumina, USA) according to manufacturer's instructions and using cfDNA inputs of 9 – 75 ng. Where quantified DNA was < 9 ng, input was judged to be insufficient, and samples were not library prepped. A simplified summary of library preparation is provided in Figure 18.

2.4.4 Sequencing

Sequencing was performed by Illumina. Normalised libraries were shipped to the Illumina (Cambridge) on dry ice. Samples were pooled 24-plex onto an S4 flowcell and sequenced on a Novaseq 6000 instrument to a median of 35000x normalized read depth coverage.

2.4.5 cfDNA Analysis

Generated FASTQ files were processed using DRAGEN Pipeline for Trusight Oncology 500 ctDNA, generating a final set of BAM, variant VCF, TMB, MSI and copy number variants aligned to the hg38 genome. VCF files were converted to MAF file format using vcf2maf (201), merged and then imported into maftools v2.16 (202) via R/Bioconductor v. 4.20/3.17 (203) for analysis. All processing was carried out on the University of Birmingham BEAR PC service (http://www.birmingham.ac.uk/bear).

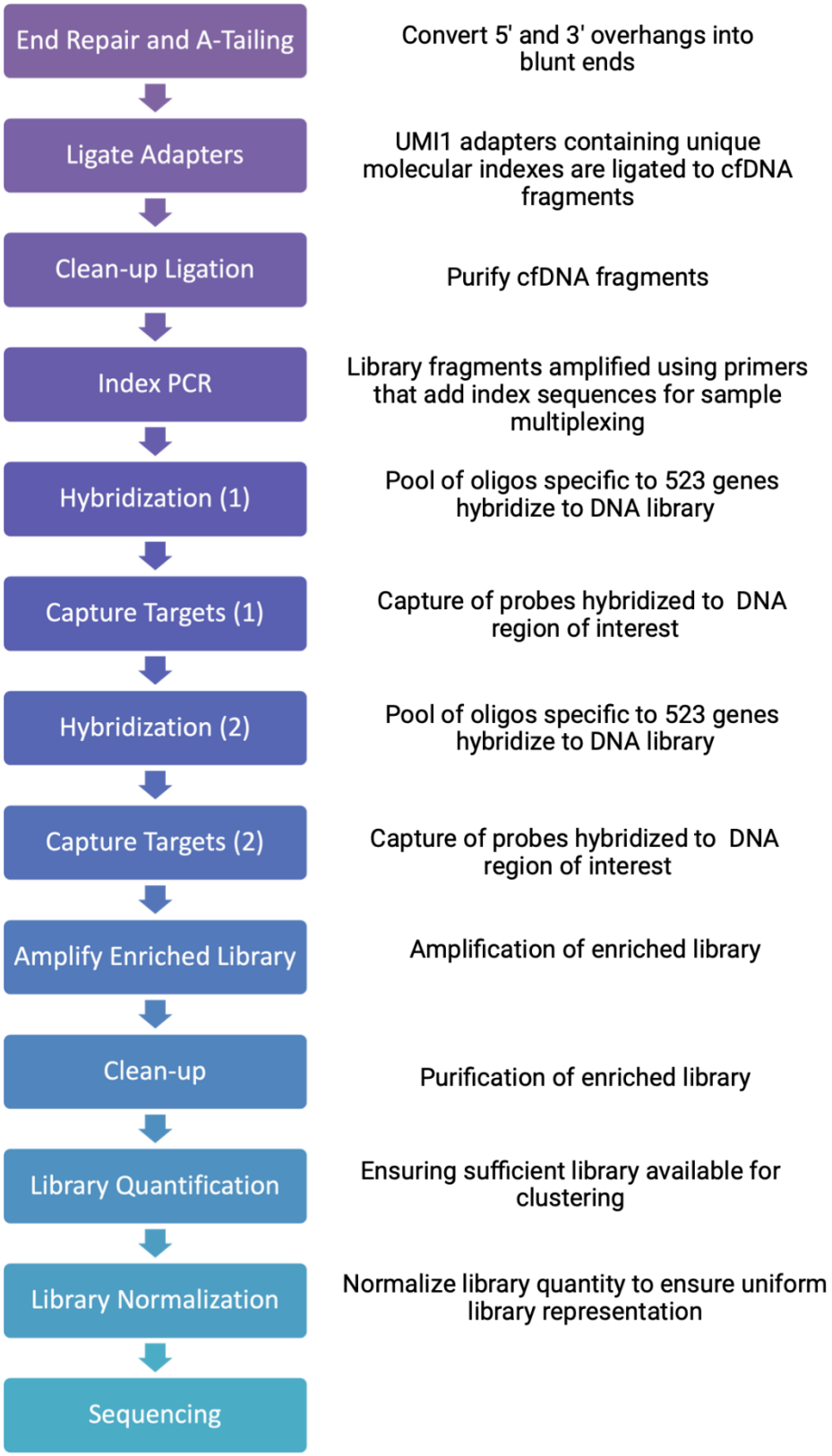

Figure 18: Simplified schema for TSO500 ctDNA Library Preparation. Summarised from manufacturer's support documentation (Illumina). Created using Biorender.com, printed with permission.

2.4.5 Sensitivity, Specificity and Concordance

Sensitivity, specificity and concordance of ctDNA were calculated using tissue mutation status as gold standard. Cases where quality control failed on tissue were excluded from the analysis.

Definitions are as follows:

- True Positives: defined as detection of mutation on ctDNA and tissue
- True Negatives: defined detection of mutation on neither tissue nor on ctDNA
- False Negatives: defined as detection of mutation on tissue but not on ctDNA
- False Positives: defined as detection of mutation on ctDNA but not on tissue.

Calculations for sensitivity, specificity and concordance are as follows:

$$Sensitivity = \frac{Number\ of\ True\ Positives}{Number\ of\ True\ Positives + Number\ of\ False\ Negatives} \times 100$$

$$Specificity = \frac{Number\ of\ True\ Negatives}{Number\ of\ True\ Negatives + Number\ of\ False\ Positives} \times 100$$

$$Concordance = \frac{Number\ of\ True\ Positives\ + True\ Negatives}{Total\ number\ of\ tests} \times 100$$

2.5 Analysis of 3q amplicon

2.5.1 Incidence of amplification of genes within 31 26-20

A list of all genes within 3q 26 – 29 was generated from the University of California Santa-Cruz (UCSC) Genome Brower (chr3:161,000,001 – 198,295,559 (HGNC)), GRCh38/h38) (204-206). Frequency of amplification for all genes within this region was examined in the TCGA Lung Squamous Cell Lung Cancer Cohort (207), accessed via cBioPortal (208, 209), and expressed as a percentage. Within this data-set, putative copy number is generated by GISTIC (Genomic Identification of Significant Targets in Cancer) (Table 23), with amplification defined as ≥ +2 (high-level amplification).

Score	Interpretation
-2	Deep Deletion
-1	Shallow Loss
0	Diploid
+1	Low-level gain
+2	High-level Amplification

Table 23: Thresholds used for interpretation of copy number data from TCGA datasets (200, 201)

2.5.2 RNA Expression

The association between amplification and mRNA expression for genes in 3q26-29 was reviewed, using data from the TCGA Pan-cancer Lung Squamous Cell Lung Cancer Cohort (207), accessed via cBioPortal (208, 209). Analysis was restricted to samples with complete data (mutation, copy number and expression data). Correlation between gene copy number (Log2 copy number values) and mRNA expression (expressed as Z score relative to all samples) for each gene within 3q 26-29 was assessed using Spearman rank correlation co-efficient.

2.5.3 Dependency

CERES-corrected dependency scores were obtained from DepMap (21Q2 release) (210). CERES is a computational method that allows estimation of dependency from essentiality screens (such as CRISPR screens) whilst correcting for copy number (211). Analysis was conducted using R (4.1.0) within R studio (1.4.1717) utilising the tidyverse (212, 213). 3q amplification was defined pragmatically as log2 (copyratio +1) ≥ 1.8 in both *PIK3CA* and *SOX2*. Only 21 squamous

cell lung cancer cell lines have available DepMap dependency data, of which 3 meet criteria for high-level 3q amplification, therefore analysis was extended to include all squamous cell lines. To assess the difference in dependency of genes, a differential dependency score was calculated:

$$\text{Differential dependency} = \text{Mean Dependency Amplified} - \text{Mean Dependency Not Amplified}$$

Statistical analysis between non-amplified and amplified lines was performed using unpaired two-tailed t test with Bonferroni correction. Assessment of linear relationship between copy relative number and dependency were assessed with Pearson correlation co-efficient.

Chapter 3: STK11-mutant lung adenocarcinoma
mTORC1/2 inhibition in STK11-mutant lung adenocarcinoma

3.1 Introduction

Mutations in *KRAS* and *STK11* are common in lung adenocarcinoma and frequently co-exist: around 30% of lung adenocarcinomas are *KRAS*-mutant, 15% are *STK11*-mutant, and 8.5% are *STK11* / *KRAS* co-mutant (131, 208). NSCLCs with concurrent mutations in *STK11* and *KRAS* have poor prognosis (157-161), and respond poorly to immunotherapy (161, 164, 165). This chapter contains work that was conducted alongside the National Lung Matrix Trial, seeking to identify potential predictors of sensitivity and mechanisms of resistance in *STK11*-mutant (± *KRAS*-mutant) lung adenocarcinoma treated with mTORC1/2 inhibition.

3.1.1 Targeting *STK11*-mutant adenocarcinoma with mTORC1/2 inhibition

STK11 (LKB1) is a serine/threonine kinase that plays roles in regulating multiple processes including cell metabolism, proliferation, and apoptosis (147-149). NSCLC with STK11 loss/inactivation have reduced AMPK activity and increased mTORC1 activation (131). Furthermore, *STK11* and *KRAS* mutations synergise in driving metabolic and epigenetic re-programming of cancer cells (170), a phenomenon reversed by mTORC1/2 inhibition (170, 176). mTORC1/2 inhibition is therefore a potential promising therapeutic strategy for *STK11* ± *KRAS* mutant lung adenocarcinoma.

Clinical outcomes of mTORC1/2 inhibition in other cancer sites have been disappointing: progression free survival (PFS) was shorter with vistusertib (mTORC1/2 inhibition) than with everolimus (mTORC1-only inhibition) in renal and breast cancers (178, 179). A key resistance pathway driven by mTORC1/2 inhibition is relief of feedback inhibition of receptor tyrosine kinase signalling, driving reactivation of PI3K/Akt signalling and consequent phosphorylation of targets including FOXO (180, 181). However, this feedback loop may be less relevant in the context of

loss-of-function of STK11, as STK11 is required for phosphorylation of FOXO by Akt (28). Therefore, it is hypothesised that STK11 deficient cells are uniquely sensitive to mTORC1/2 inhibition. In light of this strong pre-clinical rationale, patients with *STK11*-mutant lung adenocarcinoma were treated with vistusertib (AZD2014) in the National Lung Matrix Trial: *STK11*^{MUT}*KRAS*^{MUT} lung adenocarcinoma were treated with vistusertib in arm B2D; *STK11*^{MUT}*KRAS*^{WT} lung adenocarcinoma was treated with vistusertib in arm B2S. This represents the first trial of mTORC1/2 inhibition in *STK11*-mutant lung adenocarcinoma in the clinic.

3.1.2 ctDNA: opportunities within the National Lung Matrix Trial

Patients were enrolled into the NLMT based on tissue SMP2 sequencing, which used a 28-gene NGS panel. Analysis of ctDNA provides an opportunity to assess clonal evolution and identify development of novel mutations on treatment. ctDNA analysis will also facilitate more comprehensive molecular profiling of NLMT patients: evolution in technology has allowed for large panel sequencing on ctDNA, and this present work will use the TSO500 ctDNA panel which sequences 523 genes. In addition, it has been demonstrated that detection of mutations on ctDNA may have additional prognostic value (214). Overall, it is hoped that this ctDNA analysis will identify novel markers of sensitivity and resistance to mTORC1/2 inhibition in *STK11*-mutant disease.

3.2 Aims and Objectives

3.2.1 Aim

mTORC1/2 would seem to be a promising strategy in STK11-deficient lung adenocarcinoma. The work presented in this chapter is the preclinical and ctDNA-based analyses that ran alongside arms B2 of the National Lung Matrix Trial, seeking to explore predictors for response to treatment, and better define resistance to mTORC1/2 inhibition in this common genetic subset of NSCLC.

3.2.2 Objectives

1. Examine whether STK11-deficient cell lines are exempt from reactivation of PI3K/Akt signalling following treatment with mTORC1/2 inhibition.
2. Compare sensitivity of STK11-deficient cell lines to mTORC1-only (everolimus) and mTORC1/2 inhibition (vistusertib).
3. Identify mutations associated with sensitivity and resistance to mTORC1/2 inhibition using serial ctDNA samples of STK11-deficient NSCLC patients treated with vistusertib in the National Lung Matrix Trial.

3.2.3 Note

The clinical outcomes for the relevant arms of the National Lung Matrix Trial are provided for context in section 3.3.1. Please note that analysis of clinical outcomes was not performed as part of this PhD work. Conduct and management of the clinical trial and analysis of clinical outcomes was performed by the University of Birmingham Clinical Trials Unit (including Professor Lucinda Billingham, Dr Peter Fletcher, Dr Joshua Savage, Professor Gary Middleton).

3.3 Results

3.3.1 Summary of Clinical Outcomes for *STK11*-mutant NSCLC treated with vistusertib in arm B2 of the National Lung Matrix Trial

In arm B2 of the National Lung Matrix Trial, cancers with STK11 loss were treated with vistusertib (mTORC1/2 inhibition): arm B2S being comprised of *STK11*-mutant *KRAS* wild-type cancers; B2D being comprised of *STK11*/*KRAS* co-mutant cancers. 49 patients were recruited to arm B2: 19 patients into B2S (17 per-protocol); 30 patients into B2D (26 per-protocol). However, there were only 2 per-protocol objective responses (OR) in arm B2 (Figure 19). Both objective responses were in patients with *STK11*/*KRAS* co-mutant cancers. The probability of a clinically relevant true DCB rate was low (PP = 0.26) (unpublished data, National Lung Matrix Trial, Middleton et al). It is therefore important to explore why a rational targeted therapy did not have the anticipated benefit in this patient population.

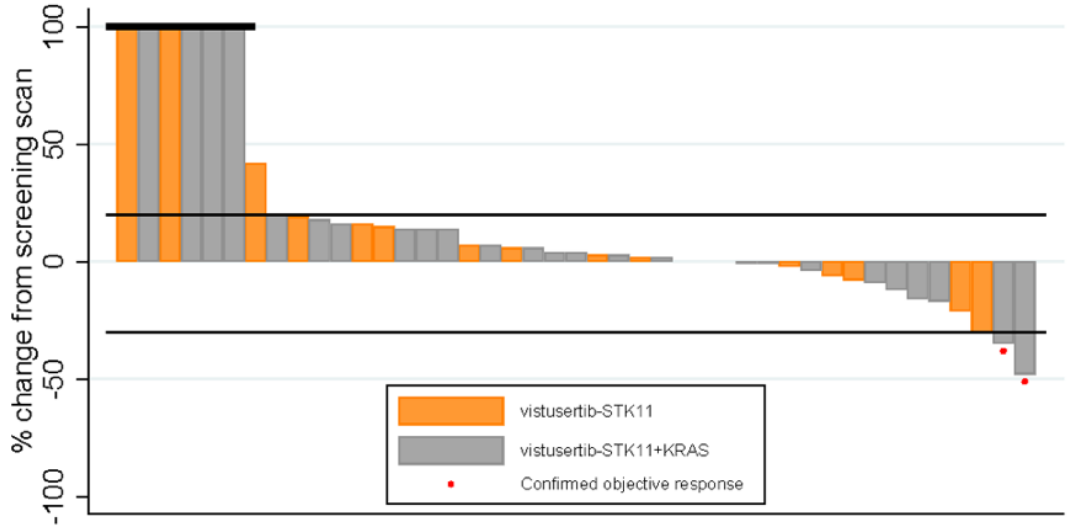

Figure 19: Waterfall plots for patients with STK11 loss NSCLC treated with vistusertib (mTORC1/2 inhibition) in cohort B2 of the National Lung Matrix Trial. Best percentage change in sum of target lesion diameters is plotted, with confirmed objective response indicated. Patients coded according to presence or absence of concomitant KRAS mutation. Per-protocol patients who discontinued are included with default measurement of 100% (unpublished data, National Lung Matrix Trial, Middleton et al)

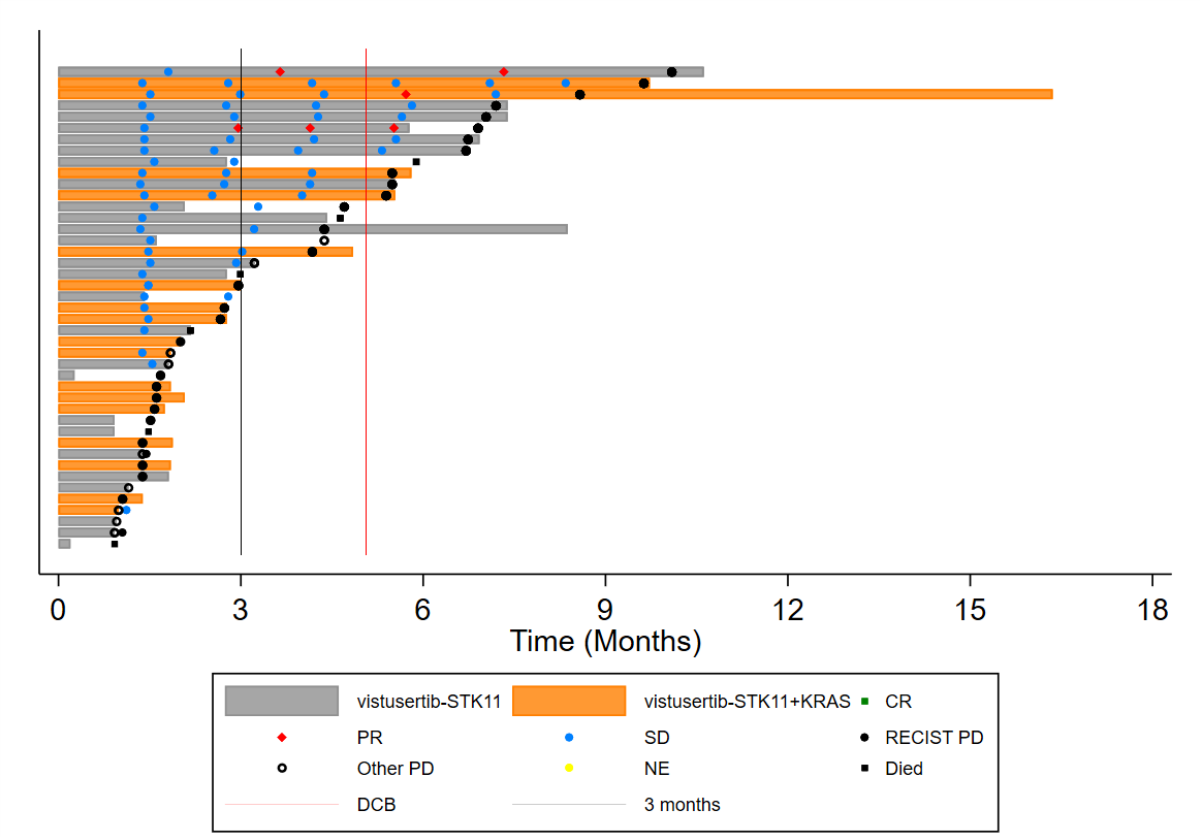

Figure 20: Swimmer plot for patients with STK11 loss NSCLC treated with vistusertib (mTORC1/2 inhibition) in cohort B2 of the National Lung Matrix Trial (NLMT). Assessments with CT-imaging are indicated and coded for response (complete or partial), stable disease or progressive disease (according to RECIST v1.1). (unpublished data, National Lung Matrix Trial, Middleton et al)

3.3.2 STK11-deficient NSCLC cells are not exempt from relief of feedback inhibition of receptor tyrosine kinase signalling

A key resistance mechanism to mTORC1/2 inhibition is relief of feedback inhibition of receptor tyrosine kinase signalling, driving reactivation of PI3K/Akt signalling and phosphorylation of downstream targets including FOXO transcription factors (180, 181). To explore whether this resistance pathway is relevant in STK11-deficient cells, a panel of *STK11*-mutant cell lines were treated with 2μM vistusertib. Whole-cell protein lysates were collected at baseline, and after 1 and 24 hours of vistusertib treatment. MCF7 cells were used as a positive control across all experiments and blots, as reactivation of PI3K/Akt signalling has been well characterised in MCF7 following treatment with AZD8055, a close analogue of AZD2014 (181).

Treatment with vistusertib reduced phosphorylation of P-S6 Ribosomal protein and P-4E-BP1 in all tested cell lines, as would be expected with mTOR inhibition (Figure 21). Whilst Akt phosphorylation at Ser473 was reduced after 1 hour of treatment, re-phosphorylation of Akt was observed at 24 hours in all lines. In control MCF7 breast cancer cells, FOXO3A phosphorylation was reduced after 1 hour of vistusertib treatment, with rebound hyper-phosphorylation at 24 hours, mirroring previously reported results (181). In all tested STK11-deficient cell lines, FOXO1/3a phosphorylation levels were low at baseline, and further reduced at 1 hours. However, all lines demonstrated rebound FOXO1/3a phosphorylation at 24 hours. *STK11*-mutant cell lines also demonstrated increased Erk phosphorylation following vistusertib treatment, most marked at 1 hour, and particularly pronounced in CAL-12T ($STK11^{MUT}KRAS^{WT}$). Overall, STK11-deficient cells are not exempt from reactivation of pro-survival signalling following treatment with the mTORC1/2 inhibitor vistusertib, potentially contributing to therapy resistance, and hampering effective treatment.

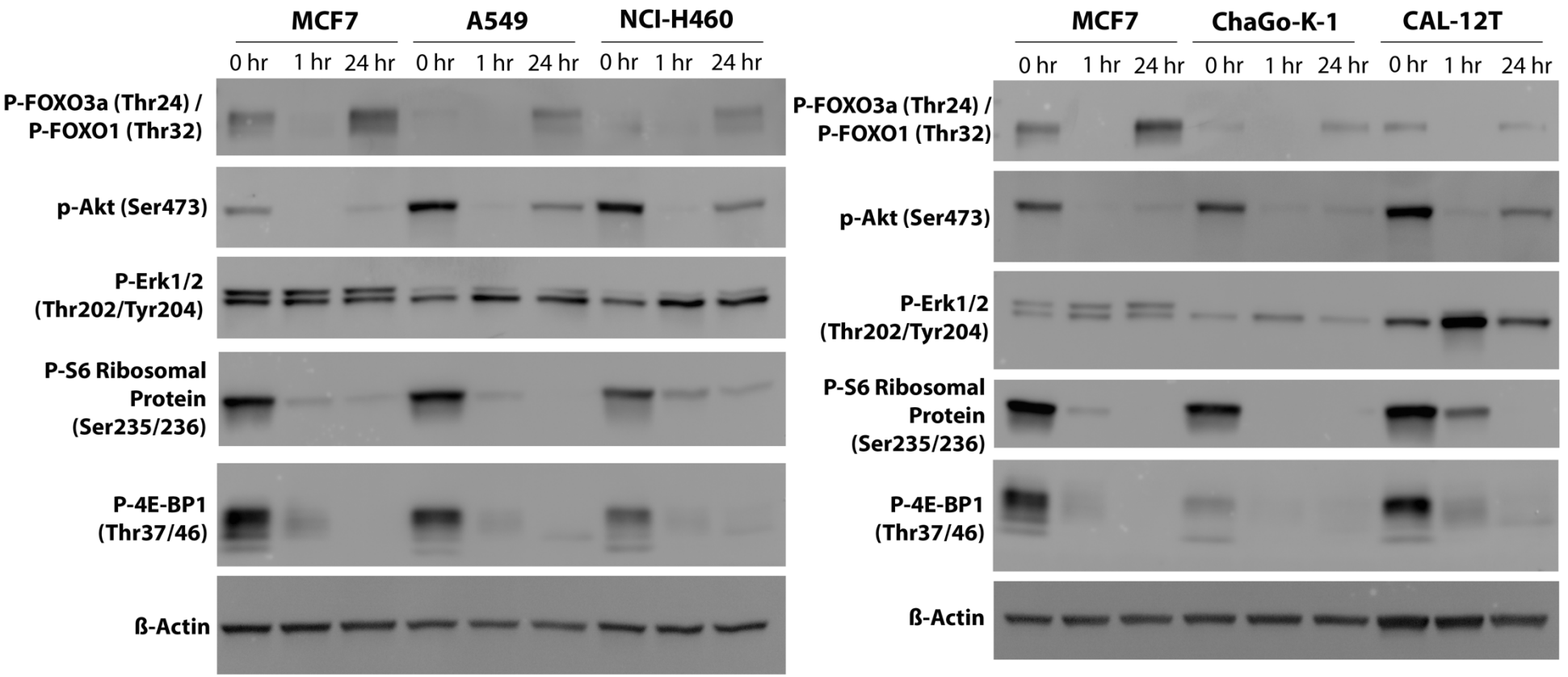

Figure 21: Effect of Visutsertib (AZD2014) on PI3K/Akt/mTOR signalling in *STK11*-mutant NSCLC cell lines. MCF7 (control breast cancer cell line), NCI-A549 (*STK11*^{MUT}*KRAS*^{MUT}) and NCI-H460 (*STK11*^{MUT}*KRAS*^{MUT}) (left) and MCF7 (control breast cancer cell line), ChaGo-K-1 (*STK11*^{MUT}*KRAS*^{WT}) and CAL-12T (*STK11*^{MUT}*KRAS*^{WT}) (right) were treated with 2μM vistusertib. Whole cell lysates were collected at baseline and after 1 and 24 hours of treatment. Phosphorylation of components PI3K/Akt pathway and phosphorylation Erk was assessed using western blotting. β-Actin was included as a loading control. Experiment repeated three times using independently collected biological replicates at least 1 week apart, with similar results on each replicate. Representative blots are shown.

3.3.3 In vitro response of STK11 deficient NSCLC cells to Everolimus (mTORC1 inhibition) and Vistusertib (mTORC1/2 inhibition)

Clinical development of vistusertib has been halted, reflecting inferior clinical results versus everolimus (mTORC1-only inhibition) in renal and breast cancer (178, 179). It is important to evaluate whether mTORC1-only inhibition may be a better candidate drug in the setting of *STK11*-mutant NSCLC.

A panel of STK11-deficient cells were treated with 0 – 10 μM vistusertib or everolimus, and cell viability was measured at 48 hours (Figure 22, Table 24). Pharmacologically achievable doses for vistusertib and everolimus were estimated from previously published data, extracting data from steady-state C_{min} and C_{max} from human pharmacokinetic studies [1, 2]. Viability curves confirm sensitivity of cell lines to vistusertib: all tested cell lines show sigmoidal dose-dependent reduction in viability, achieving IC50 at pharmacologically relevant doses (215, 216). In contrast, all tested cell lines show poor sensitivity to everolimus. IC50 was not reached for everolimus in any *STK11*^{MUT}*KRAS*^{WT} cell line. IC50 was reached for *STK11*^{MUT}*KRAS*^{MUT} co-mutant cell lines, however, this was only achieved at doses far exceeding clinically achievable doses. For 5 out of 6 tested cell lines, 1 μM vistusertib achieved significantly greater reduction in viability when compared to 1 μM everolimus.

Overall, everolimus is unlikely to be a be a more promising candidate than vistusertib in STK11-deficient NSCLC. This approach was therefore not taken forward for further testing in organoid or mouse models.

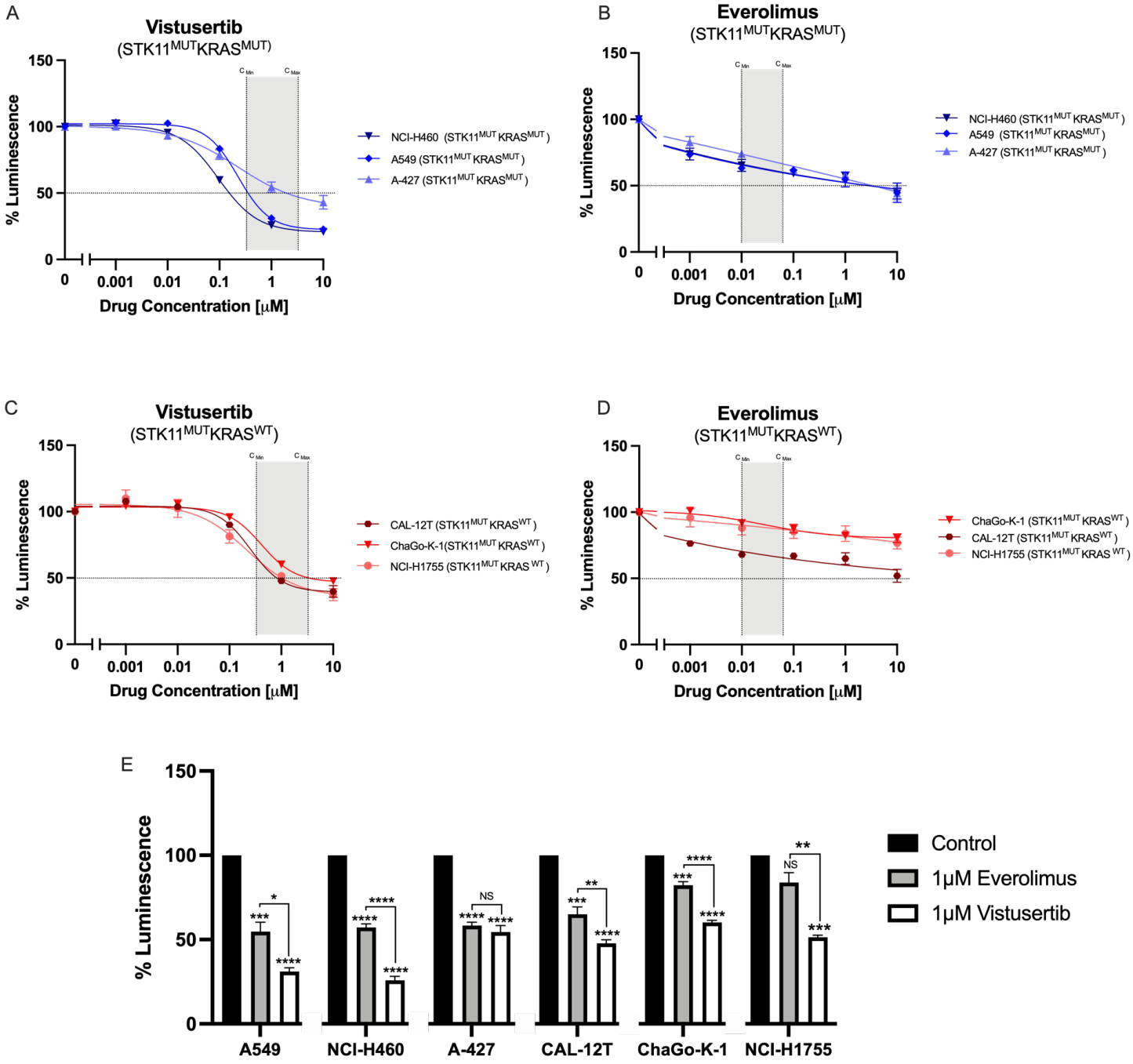

Figure 22: Viability curves of *STK11*^{MUT}*KRAS*^{MUT} and *STK11*^{MUT}*KRAS*^{WT} lung cancer cell lines treated with Vistusertib (mTORC1/2 inhibition) or Everolimus (mTORC1-only inhibition). A-D: NCI-H460, A-427, NCI-A549 (*STK11*^{MUT}*KRAS*^{MUT}) and ChaGoK1, NCI-H1755, CAL-12T (*STK11*^{MUT}*KRAS*^{WT}) were treated with 0 – 10 μM vistusertib or everolimus for 48 hours, cell viability was measured using Cell Titer Glo 2.0. Background luminescence (media with no cells) was subtracted from each reading. Luminescence was then expressed relative to untreated cells. Values expressed as mean ± SEM from at least 3 independent experiments. Pharmacologically relevant concentrations are indicated in shaded areas, calculated from previous published in-human data (202, 203). (E) Relative luminescence for cells treated with 1 μM everolimus vs 1 μM vistusertib (data presented from same experiments as described in A-D. Statistical analysis using one-way ANOVA with Tukey's post-test for multiple comparisons – stars above columns demonstrate comparison of indicates treatment versus control. Comparison of vistusertib vs everolimus indicated separately (* P <0.05, ** P<0.01, *** P <0.001, **** p<0.0001)

		IC50 Vistusertib (µM)	IC50 Everolimus (µM)
STK11^{MUT}*KRAS*^{MUT}	NCI-A549	0.356	8.497
	NCI-H460	0.153	6.360
	A-427	1.912	2.950
STK11^{MUT}*KRAS*^{WT}	ChaGo-K-1	2.971	Not Estimable
	NCI-H1755	0.992	Not Estimable
	CAL-12T	0.818	Not Estimable

Table 24: Calculated IC50 for Everolimus and Vistusertib in *STK11*-mutant lines. Absolute IC50 values were calculated from curves shown in Figure 22. Curves were plotted using non-linear regression using Prism. Absolute IC50 is defined as the concentration achieving 50% reduction in luminescence compared to no treatment. IC50 was not estimable if 50% reduction in luminescence was not reached.

3.3.4 ctDNA Sample Processing

Samples were retrieved from the Human Biomaterial Resource Centre (HBRC), University of Birmingham. Sample processing is summarised in Figure 23. 11 samples were retrieved as pre-extracted ctDNA. ctDNA was extracted from 72 samples in-house using the QIAmp Circulating Nucleic Acid Kit. Of the 83 combined samples, 71 underwent library preparation using the TSO500 ctDNA kit (Illumina) (7 samples had insufficient cfDNA for library preparation, 6 were not prioritised for library preparation due to being mid-treatment samples). 1 sample failed quality control during library preparation.

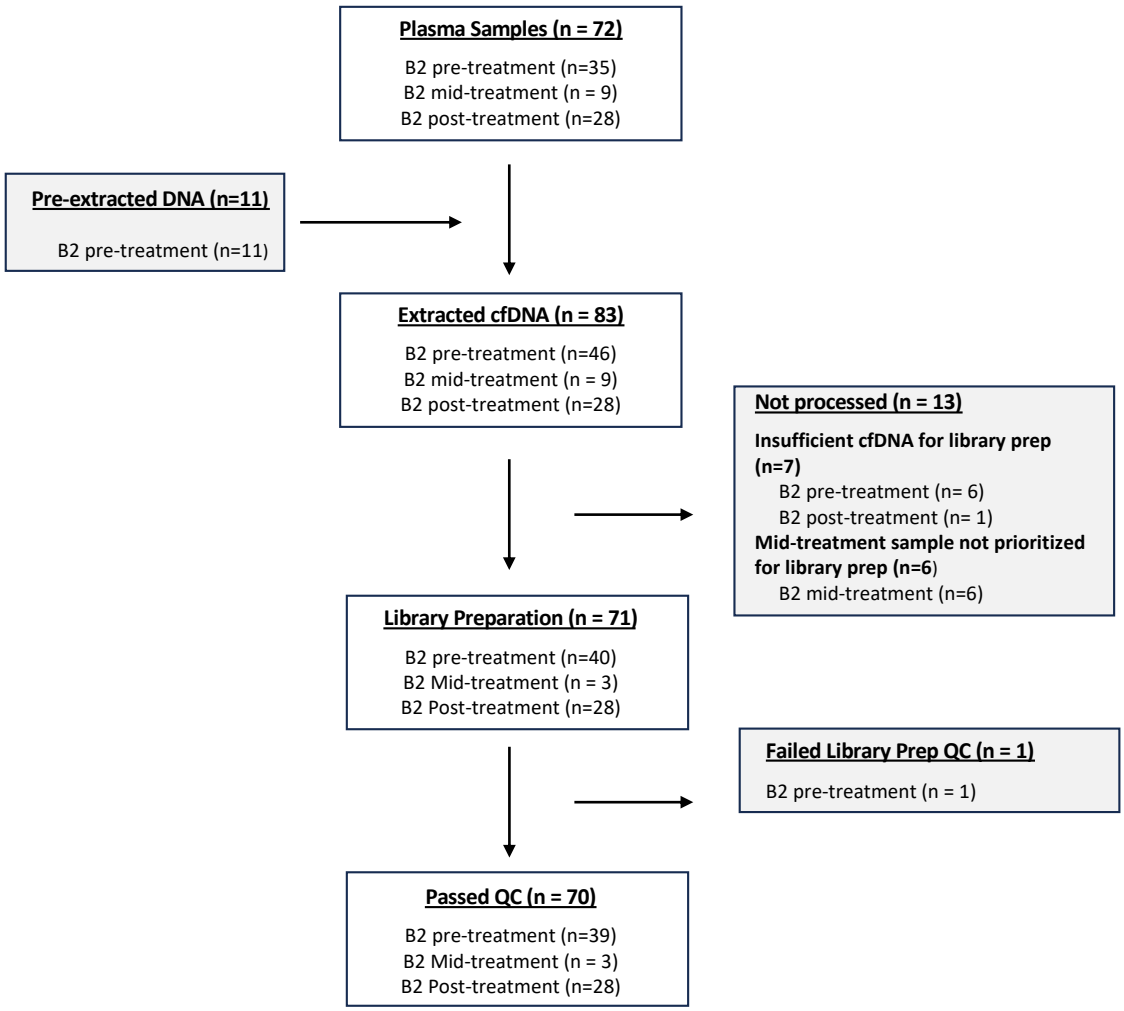

Figure 23: Flow Chart summarising ctDNA Sample processing for Arm B2 of the National Lung Matrix Trial

3.3.5 Sensitivity and Specificity of ctDNA

Tissue *KRAS* status was available for 90% of samples (n=63) (data was unavailable for 7 samples due to SMP2 failure). *KRAS* mutation status was concordant between ctDNA and tissue in 81.0% of samples (51/63), with a sensitivity of 75.6% (34/45) and a specificity of 94.4% (17/18). The single 'false positive' ctDNA KRAS mutation developed on treatment, and was not present in the baseline sample, so may represent clonal evolution or *de novo* mutation. When analysis was restricted to the first available ctDNA sample for each patient (n=38), concordance was 84.2% (32/38), sensitivity was 76.9% (20/26) and specificity was 100% (12/12).

Tissue *STK11* status was available for all samples. *STK11* mutation was concordant between ctDNA and tissue in 54.3% of samples (38/70), with a sensitivity of 54.3% (38/70). Specificity cannot be calculated, as all samples were STK11 mutant on tissue analysis. When analysis was restricted to the first available ctDNA sample for each patient, concordance was 50.0% (21/42), sensitivity was 50.0% (21/42).

The lower sensitivity of ctDNA for *STK11* mutation likely reflects different mutation profiles between *STK11* and *KRAS*. Nucleotide transversions/transitions in well-characeterised hotspots are common in *KRAS* (131), whereas more complex mutations are whole gene deletions are seen in *STK11* (131), which may be more challenging to identify on ctDNA-based sequencing.

3.3.6 Analysis of ctDNA in Arm B2 of the National Lung Matrix Trial: STK11-deficient NSCLC patients treated with vistusertib

ctDNA Predictors of Prognosis to in STK11-deficient lung adenocarcinoma treated with Vistusertib as part of the National Lung Matrix Trial

To identify ctDNA predictors of 'good' prognosis on vistusertib, the mutational profile of pre-treatment samples from *STK11*-mutant lung adenocarcinoma patients who had a PFS greater than 154 days was compared with those that had a PFS less than 90 days. These cut-offs were chosen in collaboration with the clinical trials team: 154 days reflects the minimum time for a patient within the trial to reach the fourth monitoring CT scan on treatment, and therefore be considered for Durable Clinical Benefit (DCB).

Pathogenic *TP53* mutations were enriched in pre-treatment samples from patients who went on to have a poor prognosis (P=0.0436). Pathogenic *TET2* and *DNMT3A* mutations were non-significantly enriched in pre-treatment samples who went on to have a poor prognosis. *TP53* mutations are a biologically plausible driver of resistance to targeted therapies (217). However, it must also be noted that mutations in *TP53*, *TET2* and *DNMT3A* are commonly detected in clonal haematopoiesis of indeterminate potential (CHIP). These results may therefore reflect a greater burden of CHIP in patients who responded poorly to treatment, which may in turn be driven by smoking status, age, and heavy chemotherapy pre-treatment.

Detection of *KRAS* mutations did not significantly differ between pre-treatment samples who went onto have a PFS of < 90 days versus those who had a PFS > 154 days (47.4% 9/19, vs 50.0%, 5/10 respectively). However, detection of *STK11* mutations was enriched in pre-treatment samples who went onto have poor prognosis (68.4% 13/19 vs 30.0% 3/10, p=0.048). Interpretation is hampered by poor sensitivity of ctDNA *STK11* mutations, however this could reflect a greater ctDNA levels in patients with poor prognosis.

Overall, detection of *TP53* mutations in pre-treatment plasma may predict a worse prognosis in *STK11*-mutant lung cancer treated with vistusertib. However, in the absence of sequencing of paired buffy coat samples to rule-out CHIP, it is not possible to conclude whether this reflects tumour *TP53* mutation status, or a higher burden of clonal haematopoiesis (or a mixed picture), or a greater sensitivity of ctDNA sequencing in patients with poor prognosis (for example due to higher cell turnover or altered cell metabolism).

Gene	Bad (%) [n=19]	Good (%) [n=10]	Odds Ratio (CI)	P-value
TP53	10 (52.6316)	1 (10.0000)	9.2842 (0.9515 - 479.7666)	0.0436
TET2	10 (52.6316)	2 (20.0000)	4.2226 (0.6071 - 51.1897)	0.1261
DNMT3A	7 (36.8421)	1 (10.0000)	4.9954 (0.4884 - 262.0244)	0.2008
NOTCH4	1 (5.2632)	2 (20.0000)	0.2354 (0.0036 - 5.1287)	0.2668
ATM	4 (21.0526)	0 (0.0000)	Inf (0.3564 - Inf)	0.2680
FANCA	4 (21.0526)	0 (0.0000)	Inf (0.3564 - Inf)	0.2680
NOTCH3	4 (21.0526)	0 (0.0000)	Inf (0.3564 - Inf)	0.2680

Table 25: Analysis of predictors of prognosis in pre-treatment plasma cfDNA samples from STK11-deficient lung adenocarcinoma patients treated with vistusertib as part of Arm B2 of the National Lung Matrix Trial. Patients who went onto have a PFS > 154 days versus those who went on to have PFS < 90 days were categorised as having 'good' or 'bad' prognosis, respectively. CfDNA was extracted from baseline plasma samples, library preparation using Illumina TSO500 cfDNA kit, with sequencing performed by Illumina. Generated FASTQ files were processed using DRAGEN Pipeline for Trusight Oncology 500 ctDNA, with downstream analysis using MafTools. Mutations filtered with only those passing the quality threshold and only likely pathogenic mutations are analysed. Presented data represents number of patients in each group with detectable mutations in the indicated genes. *KRAS* mutations were not significantly different between patients with a 'good' vs 'bad' prognosis, *STK11* mutations were enriched in patients with 'poor' prognosis (p=0.048), however this lost significance when filtered only for pathogenic mutations (and therefore does not appear on this table).

Pre-treatment versus post-treatment ctDNA in STK11-deficient lung adenocarcinoma treated with Vistusertib as part of the National Lung Matrix Trial

To assess for mutations that may confer on-treatment resistance to vistusertib, mutations in post-treatment samples (n=27) were compared with baseline samples (n=36). 2 genes were enriched in post-treatment samples (using a conventional $p<0.05$ cut-off for significance). *SMARCA4* mutations were detectable in 11 patients post-therapy (41% of post-treatment samples), whilst being detected in only 3 patients at baseline (8%) (P=0.004). All detected *SMARCA4* mutations were predicted to be pathogenic (frameshift, trinucleotide indel, pathogenic splice or CADD > 20). *FOXP1* mutations were detectable in 4 patients post-treatment (15%) (p=0.029), but were not detectable in any patients at baseline (p=0.029).

Detection of *KRAS* or *STK11* mutations on ctDNA did not significantly change with treatment. *STK11* mutations were detectable in 50.0% pre-treatment (18/36) and 55.6% post-treatment (15/27) (p=0.662, ns). *KRAS* mutation was detectable in 47.2% pre-treatment (17/36) and 51.9% post-treatment (14/27) (p=0.7161, ns). The lack of change of detection rates for *KRAS* or *STK11* mutations with treatment suggests that enrichment of *SMARCA4* and *FOXP1* mutation is unlikely to reflect increased overall ctDNA detection.

Overall, these results suggest that *SMARCA4* and *FOXP1* mutations may be selected for in patients with *STK11*-mutant NSCLC on vistusertib treatment, potentially reflecting more resistant subclones that are selected for on therapy.

Gene	Baseline (n=36) (%)		Post treatment (n=27) (%)		Odds Ratio (CI)		P-Value
SMARCA4	3	(8.3333)	11	(40.7407)	7.3028	(1.6285 - 46.4474)	0.0046
FOXP1	0	(0.0000)	4	(14.8148)	Inf	(0.9316 - Inf)	0.0295
TRAF2	1	(2.7778)	5	(18.5185)	7.7123	(0.7886 - 385.8754)	0.0758
ZFHX3	29	(80.5556)	26	(96.2963)	6.1288	(0.7097 - 293.0756)	0.1230
CTCF	1	(2.7778)	4	(14.8148)	5.9231	(0.5415 - 307.5889)	0.1550
DAXX	1	(2.7778)	4	(14.8148)	5.9231	(0.5415 - 307.5889)	0.1550
FLI1	1	(2.7778)	4	(14.8148)	5.9231	(0.5415 - 307.5889)	0.1550
RUNX1T1	1	(2.7778)	4	(14.8148)	5.9231	(0.5415 - 307.5889)	0.1550
KMT2A	3	(8.3333)	6	(22.2222)	3.0847	(0.583 - 21.1375)	0.1550
ACVR1	0	(0.0000)	2	(7.4074)	Inf	(0.2529 - Inf)	0.1797
CHD4	0	(0.0000)	2	(7.4074)	Inf	(0.2529 - Inf)	0.1797
GATA3	0	(0.0000)	2	(7.4074)	Inf	(0.2529 - Inf)	0.1797
IGF1R	0	(0.0000)	2	(7.4074)	Inf	(0.2529 - Inf)	0.1797
MAX	0	(0.0000)	2	(7.4074)	Inf	(0.2529 - Inf)	0.1797
ARID1A	4	(11.1111)	7	(25.9259)	2.753	(0.608 - 14.537)	0.1818

Table 26: Analysis of post-treatment vs pre-treatment cfDNA samples from STK11-deficient lung adenocarcinoma patients treated with vistusertib as part of Arm B2 of the National Lung Matrix Trial. CfDNA was extracted from baseline and post-treatment plasma samples, library preparation using Illumina TSO500 cfDNA kit, with sequencing performed by Illumina. Generated FASTQ files were processed using DRAGEN Pipeline for Trusight Oncology 500 ctDNA, with downstream analysis using MafTools using MafCompare. Mutations filtered with only those passing the quality threshold. Presented data represents number of patients in each group with detectable mutations in the indicated genes.

3.4 Summary

Despite convincing preclinical evidence, outcomes for treating *STK11*-mutant lung adenocarcinoma with mTORC1/2 inhibition were disappointing in the National Lung Matrix Trial. This chapter sought to explore potential reasons for vistusertib treatment failure in *STK11*-mutant lung adenocarcinoma.

The key results are as follows:

1. STK11-deficient cells are not exempt from reactivation of pro-survival signalling following prolonged treatment with mTORC1/2 inhibition.
2. mTORC1 inhibition with everolimus shows limited activity *in vitro*, and is unlikely to be a be a more promising candidate than vistusertib.
3. *SMARCA4* and *FOXP1* mutations become enriched in ctDNA in patients *STK11*-mutant NSCLC following treatment with vistusertib.
4. Detection of *TP53* mutations in pre-treatment plasma may predict a worse prognosis in *STK11*-mutant lung cancer treated with vistusertib (although without paired buffy coat sequencing it is unclear if this reflects CHIP or tumour mutations).

3.5 Discussion

This work has identified potential contributors to failure of vistusertib treatment in *STK11*-mutant lung adenocarcinoma. In other contexts it has been hypothesized that the underperformance of vistusertib is partly driven by reactivation of PI3K/Akt signalling through de-repression of receptor tyrosine kinases (180, 181). Whilst STK11 has been shown to be required for Akt-driven FOXO phosphorylation in some contexts (28), the current work demonstrates that this pathway remains relevant even in the context of STK11 loss. This reactivation of PI3K/Akt/FOXO signalling may reduce the anti-mitogenic impact of mTORC1/2 inhibition, limiting the clinical tractability of treatment. Therefore, the reasons for failure of vistusertib treatment may mirror those that are reported in other contexts. mTORC1 inhibition presents an alternate therapeutic approach and has proven useful in breast and renal cancers (178, 179). However, this current work confirms that *STK11*-mutant NSCLC cells do not demonstrate meaningful sensitivity to mTORC1-only inhibition with everolimus *in vitro*, therefore this not a promising route for further development.

The present analysis also adds serial ctDNA analysis, and this is the first of its kind in the context of mTORC1/2 inhibition. *SMARCA4* mutations were significantly enriched in post-treatment samples, whilst *STK11* and *KRAS* mutations were detectable at comparable levels in pre- and post-treatment samples. *SMARCA4* encodes BRG1, a component of SWI/SNF complexes, which regulates chromatin remodelling and hence gene transcription (218). Due to the relatively short time interval between pre- and post-treatment samples, it seems likely that the *SMARCA4* mutation represents a subclonal mutation that becomes rapidly dominant on vistusertib treatment driving ongoing disease. In keeping with this, *SMARCA4* mutation commonly co-occurs with mutations in *KRAS* and/or *STK11* in lung adenocarcinoma, and is associated with worse prognosis (219). However, we are unable to exclude the possibility of SMARCA4 mutations developing *de novo* without further experiments. Crucially, *SMARCA4* is emerging as a potential driver of resistance to targeted therapies in lung adenocarcinoma. Baseline *SMARCA4* mutation is

associated with inferior PFS and OS in *KRAS* G12C lung adenocarcinoma treated with Sotorasib (220). Likewise, *SMARCA4* mutation is associated with resistance to Osimertinib in *EGFR*-mutant lung adenocarcinoma (221). It is therefore possible that vistusertib treatment is selecting for more resistant *SMARCA4*-mutant subclones in STK11-deficient lung adenocarcinoma.

FOXP1 was the second mutation enriched in post-treatment ctDNA samples compared with baseline samples. Loss of FOXP1 promotes A549 ($STK11^{MUT}KRAS^{MUT}$) lung adenocarcinoma cell proliferation and migration (222). FOXP1 loss drives mTORC1 hyperactivation in prostate cancer cells (223) and drives PI3K/Akt/mTOR activity in CD8 T cells (224). It is therefore feasible that FOXP1 may drive resistance to mTORC1/2 inhibition through driving overactivation of mTORC signalling. However, it must be acknowledged that this data is limited by the lack of tissue-based sequencing of *SMARCA4* or *FOXP1*, as well as a lack of in vitro confirmation that SMARCA4 or FOXP1 modulates mTORC1/2i sensitivity.

Work exploring the role of *SMARCA4* mutations as mediator of resistance to targeted therapies is of great interest for further development. As SMARCA4 regulates epigenetic programming, short-term knockdown with siRNA is unlikely to replicate the full phenotype, and therefore shRNA or genome editing represent more promising approaches. The simplest experiment would be to assess whether mutation or knockout of *SMARCA4* alters sensitivity to targeted therapy agents. A more nuanced approach would be to challenge mixed cultures, spheres, or xenografts of differentially fluorescently tagged genetically engineered *SMARCA4* mutant and *SMARCA4* wild-type cells to therapeutic agents, allowing for assessment for clonal selection of the *SMARCA4* mutant population. More complex models would better represent the cell-cell interactions and clonal selection seen in human malignancy, and would provide a better model of the sub-clonal nature of *SMARCA4* mutations in smoking related lung adenocarcinoma. In addition, it will be

important to formally assess whether *SMARCA4* or *FOXP1* mutation drives altered activation of PI3K/Akt or mTOR signalling in lung cancer cell lines.

ctDNA better represents disease heterogeneity, is less invasive, carries less clinical risk, requires fewer resources, and may be arranged more quickly than conventional biopsies (225, 226). In addition, serial ctDNA sampling allows longitudinal of assessment of cancer evolution, genetic drift and development of resistance to treatment (227). However, ctDNA is less sensitive than tissue sequencing, particularly in tumours with low disease burdens or in tumours with low levels of ctDNA shedding (226). The present analysis may therefore miss some mutations that would have been identified on repeat biopsy, particularly where VAF is low.

Sensitivity for detection of *KRAS* mutations on ctDNA was 75.6%, which is fully in line with previously reported sensitivity of ctDNA (214, 228, 229). In the Korean Lung Liquid vs Invasive Biopsy Program, overall sensitivity of ctDNA using Guardant360 was 67.7%, specificity was 88.8%, and concordance was 77.6% (229). Sensitivity for individual genetic mutations on ctDNA ranged from 81.3% for *EGFR* del 19 to 18.8% for *ROS1* fusion, with sensitivity for *KRAS* mutation being 67.6% (229). Sensitivity for EGFR mutation in the FLAURA study was 68% using the cobas *EGFR* mutation test (214). In the present work, sensitivity for detection of *STK11* mutations was lower than for *KRAS* (54.3%). However, this likely reflects the nature of *STK11* mutations, with ctDNA more likely to miss whole gene deletions or complex mutations due to analysis of fragmented DNA. To the best of our knowledge there is currently no published data reporting the sensitivity of ctDNA for identification of *STK11* mutations, so it is not possible to comment on whether alternative assays would perform better in this context.

It is interesting to note that identification of *STK11* mutations may be more common in patients with poor prognosis, mirroring results of the FLAURA study where detection of *EGFR* mutation on ctDNA was associated with poor prognosis in patients treated with TKIs (214). However, the difference in ctDNA positivity for *STK11* mutations between patients who had a PFS < 90 days versus those who had a PFS of > 154 days means that any data around other prognostic markers on ctDNA must be interpreted with caution.

A further limitation of the present analysis is that sequencing data is not available from peripheral blood lymphocytes to confirm whether mutations are derived from clonal haematopoiesis (CHIP). It is therefore difficult to draw conclusions regarding the prognostic role of *TP53* mutations in pre-treatment samples of *STK11*-mutant lung adenocarcinoma treated with vistusertib. Whilst the rate of *TP53* mutation far exceeds what would be expected on CHIP (230), this population of lung cancer patients have been heavily pre-treated and/or have a heavy smoking history. It is therefore not possible to conclude definitively that *TP53* co-mutation is a driver of primary resistance to vistusertib.

3.6 Conclusions

The work in this chapter sought to explore potential reasons for vistusertib treatment failure in *STK11*-mutant lung adenocarcinoma. Firstly, it is demonstrated that STK11-deficient cells are not exempt from reactivation of pro-survival signalling following prolonged treatment with mTORC1/2 inhibition. Secondly, mTORC1 inhibition with everolimus shows limited activity in vitro, and is unlikely to be a be a more promising candidate than vistusertib. Thirdly, *SMARCA4* and *FOXP1* mutations become enriched on ctDNA in patients *STK11*-mutant NSCLC following treatment with vistusertib.

Chapter 4: *KRAS*-Mutant Lung Adenocarcinoma

CDK4/6 inhibition in KRAS-mutant lung cancer

4.1 Introduction

KRAS is one of the most commonly mutated gene in smoking-related lung adenocarcinoma (131). Development of KRAS G12C inhibitors has made direct targeting possible in around 40% of *KRAS*-mutant lung adenocarcinoma (122, 124, 125). However, these agents have not yet replicated the dramatic response seen with classic oncogene addiction such as *EGFR*: in a phase III trial of sotorasib versus docetaxel, median progression-free survival (PFS) was improved by 1.1 months, with no difference in OS (124). Furthermore, no currently licensed KRAS-targeting agents are available for the 60% of *KRAS*-mutant lung adenocarcinoma patients with non-G12C *KRAS*-mutations (130, 131). It is therefore important to look for alternate targeted therapy approaches for *KRAS*-mutant lung adenocarcinoma.

Preclinical evidence suggests that CDK4/6 inhibition is a potential approach in KRAS-mutant lung adenocarcinoma (142, 143). Overactivation of KRAS drives cyclin D upregulation (142, 143), and *KRAS*-mutant NSCLC is sensitive to CDK4/6 inhibition *in vitro* and in mouse models (134-136). Initial clinical data was promising: abemaciclib achieved a 55% disease control rate in *KRAS*-mutant NSCLC patients in a Phase I/II trial (135). However, the Phase III JUNIPER trial of abemaciclib versus erlotinib failed to meet its primary endpoint (144). In arm C5 and C6 of National Lung Matrix Trial, *KRAS*-mutant lung adenocarcinomas were treated with palbociclib. Crucially, the NLMT provides an opportunity to better understand predictors of sensitivity and resistance to CDK4/6 inhibition in *KRAS*-mutant NSCLC, as analysis of ctDNA samples in the NLMT may help define subgroups who benefit from therapy.

This chapter contains work that was conducted alongside the National Lung Matrix Trial, seeking to identify potential predictors of sensitivity and mechanisms of resistance in *KRAS*-mutant (± *STK11*-mutant) lung adenocarcinoma treated with CDK4/6 inhibition.

4.2 Aims and Objectives

4.2.1 Aim

CDK4/6 inhibition would seem to be a promising strategy in *KRAS*-mutant lung adenocarcinoma. The work presented in this chapter is ctDNA-based analysis that ran alongside arms C5 and C6 of the NLMT, seeking to explore predictors for response to treatment, and better define resistance to CDK4/6 inhibition in this common genetic subset of NSCLC.

4.2.2 Objectives

1. Identify mutations in baseline ctDNA associated with sensitivity to CDK4/6 inhibition in *KRAS*-mutant NSCLC patients treated with palbociclib
2. Identify mutations that develop on treatment that may drive secondary resistance to CDK4/6 inhibition in *KRAS*-mutant NSCLC patients treated with palbociclib

4.2.3 Note

The clinical outcomes for the relevant arms of the National Lung Matrix Trial are provided for context in section 4.3.1. This analysis was not performed as part of this PhD work. Conduct and management of the clinical trial and analysis of clinical outcomes was performed by the University of Birmingham Clinical Trials Unit (including Professor Lucinda Billingham, Dr Peter Fletcher, Dr Joshua Savage, Professor Gary Middleton).

4.3 Results

4.3.1 Summary of Clinical Outcomes for *KRAS*-mutant NSCLC treated with Palbociclib

In arms C5 and C6 of the National Lung Matrix trial, patients with *KRAS*-mutant lung adenocarcinoma were treated with Palbociclib (CDK4/6 inhibition): arm C5 consisting of *STK11*/*KRAS* co-mutant cancers, and arm C6 consisting of $KRAS^{MUT}$ $STK11^{WT}$ cancers. 18 patients were treated in arm C5, 30 patients were treated in arm C6 (127). In arm C6, PFS was 5.3 months (95% credible interval: 3.8 – 7.9 months), with a DCB rate of 40% (95% credible interval: 25 – 58%). In C5, PFS was 2.6 months (95% credible interval: 1.5 – 5 months) (127). However, it must be noted that a small population of patients in C6 had durable disease control. It is important to determine potential predictors of durable response to CDK4/6 inhibitors to better define *KRAS*-mutant lung adenocarcinomas that may benefit from treatment.

4.3.2 ctDNA Sample Processing

Samples were retrieved from the Human Biomaterial Resource Centre (HBRC), University of Birmingham. Sample processing is summarised in Figure 24. 8 samples were retrieved as pre-extracted ctDNA. ctDNA was extracted from 103 plasma samples in-house using the QIAmp Circulating Nucleic Acid Kit. Of the 111 combined samples, 97 underwent library preparation with the TSO500 ctDNA kit (Illumina) (3 samples had insufficient cfDNA for library preparation, 11 were not prioritised for library preparation due to being mid-treatment samples). 8 samples failed quality control during library preparation.

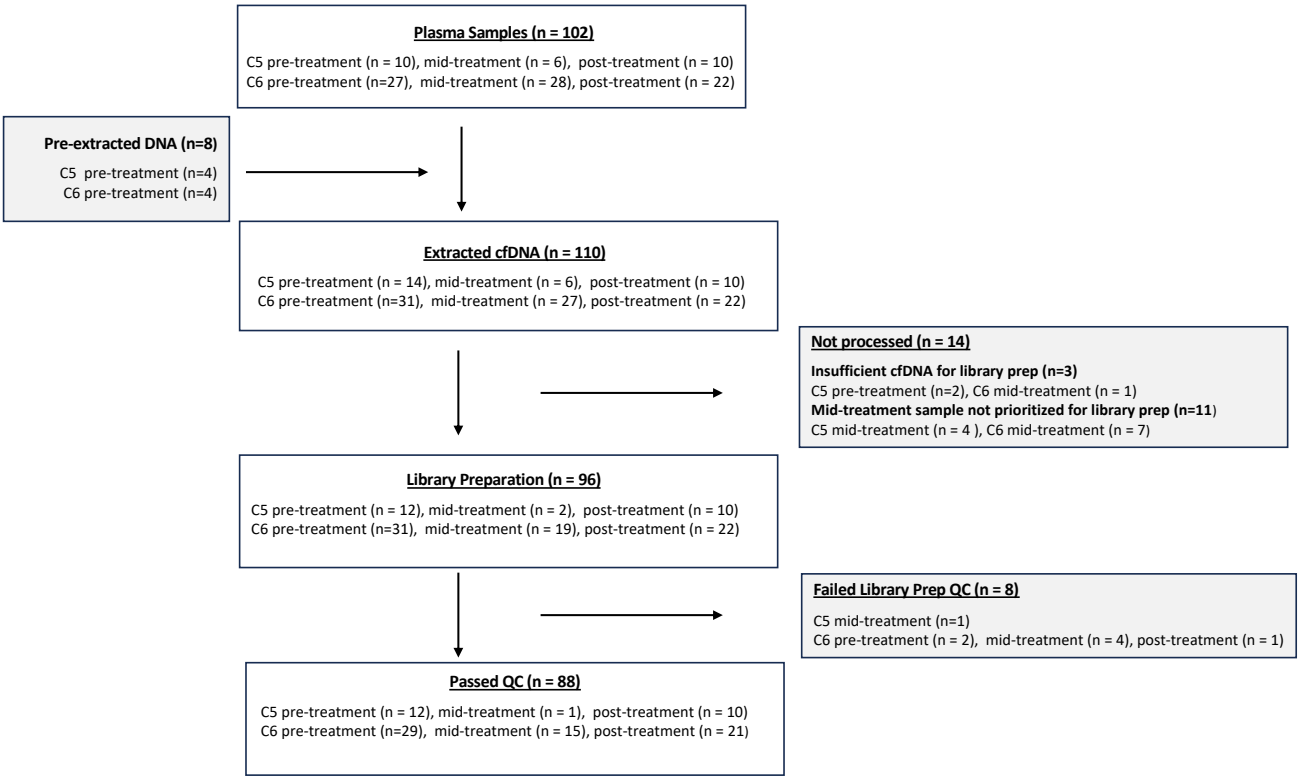

Figure 24: Flow Chart summarising ctDNA Sample processing for Arm C5/C6 of the National Lung Matrix Trial

4.3.3 Sensitivity and Specificity of ctDNA

Historical tissue *KRAS* mutation status was available from SMP2 for 100% of patients. 8 ctDNA samples failed quality control after library preparation, therefore 88 samples had evaluable *KRAS* ctDNA and tissue status. 1 patient (C5-06) was negative for *KRAS* mutation on SMP2, with the corresponding ctDNA sample being negative for *KRAS* mutation. *KRAS* mutation status was concordant between ctDNA and tissue in 61.4% of samples (54/88), with a sensitivity of 62.0% (54/87). When analysis was restricted to the first available ctDNA sample for each patient (n=43), concordance was 65.1% (28/43) and sensitivity was 64.3% (27/42).

4.3.4 Analysis of ctDNA in Arm C5/C6 of the National Lung Matrix Trial: *KRAS*-mutant NSCLC patients treated with palbociclib

ctDNA Predictors of Prognosis in *KRAS*-deficient lung adenocarcinoma treated with palbociclib as part of the National Lung Matrix Trial

The mutational profile of baseline cfDNA samples from patients with a PFS less than 90 days versus baseline samples from patients with a PFS greater than 154 days was assessed (Table 27). The PFS groups were chosen in collaboration with the clinical trials team: 154 days reflects the minimum time for a patient within the trial to reach the fourth monitoring CT scan on treatment, and therefore be considered for Durable Clinical Benefit (DCB). *KDR* variants were significantly enriched in patients with poor prognosis (P = 0.00932). *MTOR*, *MDC1*, *CHEK2* and *ETV1* mutations were significantly enriched in patients with good prognosis (P = 0.01310, P = 0.02376, P = 0.03492, P = 0.03768). *KDR*, *MTOR* and *CHEK2* provided the cleanest differential between groups, therefore these mutations were examined in greater depth.

KDR

KDR variants were significantly enriched in patients with poor prognosis (P = 0.00932). For the majority of patients, *KDR* variants were detected at a VAF of 40 – 60%, implying that these variants are germline single nucleotide polymorphisms (SNPs) (231). An annotated swimmer plot of the distribution of *KDR* mutations is displayed in Figure 25. The most commonly detected *KDR* variant was p.Q472H (19 pre-treatment samples, mean VAF 52.79%, median VAF 48.40%), followed by p.V297I (6 samples, mean VAF 57.27%, median VAF 49.77%) and pC482R (2 samples, VAF of 44.6% and 49.38%). Q472H, V297I and C482R are well-characterised germline polymorphisms (232), supporting the assertion that these variants are likely germline in origin. N1300K and A1166T were detected in one patient each, with VAF < 1% in both cases. Whilst the significance of N1300K and A1166T is unclear, both cases co-occurred with likely germline variants.

MTOR

Detection of *MTOR* mutations at baseline was associated with prolonged disease-free survival (>154 days). Of the missense mutations, G1508R, R1080C, D1109A are all expected to be pathogenic activating mutations in *MTOR* (CADD > 27) (233). A329T is likely pathogenic (CADD 21.6) (233). An annotated swimmer plot is given in Figure 26. It is notable that pathogenic *MTOR* mutations appear to cluster in the patients with a PFS > 12 months. Of 7 patients with a PFS > 12 months, 6 had available pre-treatment plasma samples; of these 6 patients, 50% had pathogenic *MTOR* mutation detectable in baseline ctDNA. This data suggests that activating mutations in *MTOR* may sensitise to Palbociclib treatment in *KRAS*-mutant lung cancer.

CHEK2

Detection of *CHEK2* mutations at baseline was associated with prolonged disease-free survival (>154 days). An annotated swimmer plot is displayed in Figure 26. All detected missense mutations are expected to be pathogenic (CADD > 25) (233). Of the six patients who went on to have PFS > 12 months with available plasma for cfDNA analysis, 50% had a *CHEK2* mutation at baseline. One patient had both CHEK2 and MTOR mutations, suggesting that *CHEK2* and MTOR mutations are not mutually exclusive. Overall, these data suggest that inactivating mutations in CHEK2 may sensitise to Palbociclib treatment in KRAS-mutant lung cancer.

KRAS

It must be noted that *KRAS* mutations are non-significantly enriched in ctDNA of patients who went onto have a poor prognosis, with *KRAS* mutations detectable in 4/13 (30.8%) patients who went on to have a PFS of > 154 days versus 11/15 (73.3%) of those who went onto have a PFS of <90 days, although this did not reach significance ($p = 0.05571$) (Table 27). This may reflect higher disease burden or more aggressive disease, for example due to higher cell turnover and/or necrosis.

Summary

Analysis of *KRAS*-mutant lung adenocarcinoma patients who have durable benefit on palbociclib suggests that absence of KDR variants, and presence of *MTOR* or *CHEK2* mutations on ctDNA may predict better prognosis on treatment. This population may reflect a new cohort of patients who may particularly benefit from CDK4/6 inhibitor therapy. This is therefore an important area for further research and validation.

Gene	Good (n=13) (%)		Bad (n=15) (%)		Odds Ratio (CI)		P-Value
KDR	2	(15.3846)	10	(66.6667)	0.10059	(0.7209 - 0.0079)	0.00932
MTOR	5	(38.4615)	0	(0)	Inf	(Inf - 1.2894)	0.01310
MDC1	11	(84.6154)	6	(40)	7.58732	(95.014 - 1.0725)	0.02376
CHEK2	4	(30.7692)	0	(0)	Inf	(Inf - 0.8596)	0.03492
ETV1	12	(92.3077)	8	(53.3333)	9.67196	(510.03 - 0.9489)	0.03768
KRAS	4	(30.7692)	11	(73.3333)	0.17415	(1.0571 - 0.0228)	0.05571
IRS2	10	(76.9231)	6	(40)	4.69720	(38.377 - 0.7639)	0.06707
FGF23	1	(7.6923)	6	(40)	0.13410	(1.4111 - 0.0025)	0.08357
GATA2	1	(7.6923)	6	(40)	0.13410	(1.4111 - 0.0025)	0.08357
MST1	12	(92.3077)	9	(60)	7.45703	(396.96 - 0.7087)	0.08357
FANCI	10	(76.9231)	15	(100)	0.00000	(1.9761 - 0)	0.08730
ARID1A	0	(0)	4	(26.6667)	0.00000	(1.6071 - 0)	0.10159
FANCA	13	(100)	11	(73.333)	Inf	(Inf - 0.6222)	0.10159
STK11	0	(0)	4	(26.6667)	0.00000	(1.6071 - 0)	0.10159
CSF1R	7	(53.8462)	3	(20)	4.39452	(36.471 - 0.6906)	0.11407
ROS1	11	(84.6154)	8	(53.3333)	4.54442	(56.2834- 0.6309)	0.11449
MUTYH	10	(76.9231)	7	(46.6667)	3.62376	(29.137 - 0.5890)	0.13673
ADGRA2	4	(30.7692)	1	(6.6667)	5.83494	(327.11 - 0.4762)	0.15278
SETBP1	9	(69.2308)	14	(93.3333)	0.17138	(2.0998 - 0.0031)	0.15278
GABRA6	1	(7.6923)	5	(33.3333)	0.17687	(1.9661 - 0.0033)	0.17271

Table 27: Analysis of predictors of prognosis in pre-treatment plasma cfDNA samples from *KRAS*-mutant adenocarcinoma patients treated with palbociclib as part of Arm C5/C6 of the National Lung Matrix Trial. Patients who went onto have a PFS > 154 days versus those who went on to have PFS < 90 days were categorised as having 'good' or 'bad' prognosis, respectively. CfDNA was extracted from baseline plasma samples, library preparation using Illumina TSO500 cfDNA kit, with sequencing performed by Illumina. Generated FASTQ files were processed using DRAGEN Pipeline for Trusight Oncology 500 ctDNA, with downstream analysis using MafTools. Mutations filtered with only those passing the quality threashold. Presented data represents number of patients in each group with detectable mutations in the indicated genes.

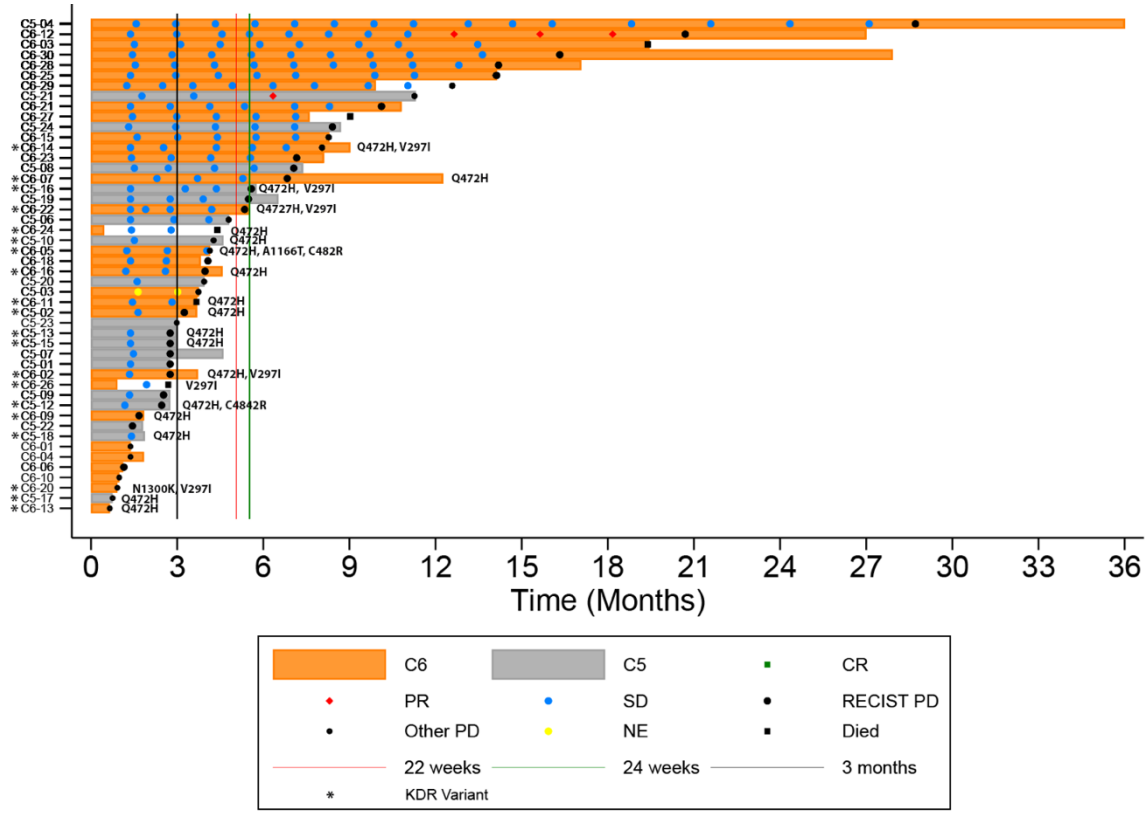

Figure 25: Annotated Swimmer highlighting detected *KDR* variants in participants with *KRAS* ± *STK11*-mutant lung adenocarcinoma treated with Palbociclib. Participants ordered by progression-free survival time. CT assessments are indicated and coded for complete response (CR), partial response (PR), stable disease (SD), or progressive disease (PD) or not evaluable (NE) according to RECIST v1.1. Follow-up time after treatment discontinuation and death are also indicated. *CHEK2* and *MTOR* variants detected on pre-treatment cfDNA are indicated, with annotation detailing variant (or variants) detected (adapted from unpublished data, Middleton et al)

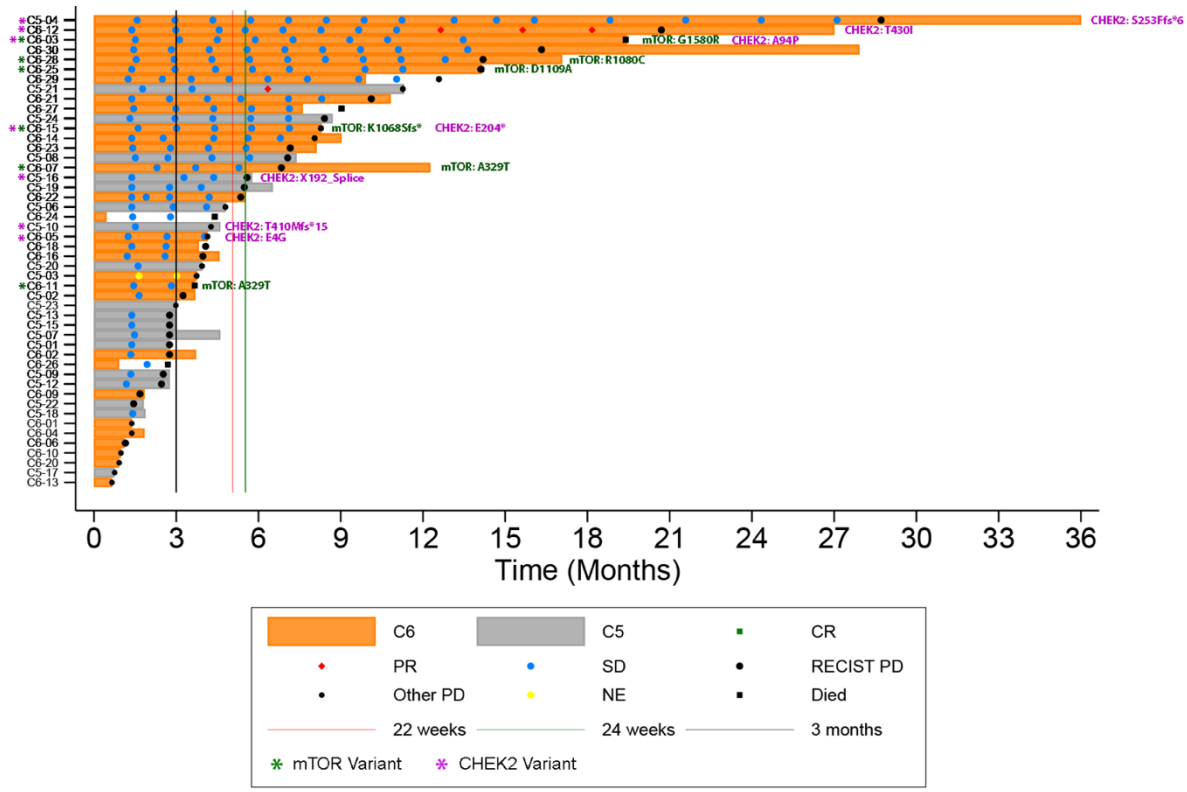

Figure 26: Annotated Swimmer highlighting detected *MTOR and CHEK2* variants in participants with *KRAS* ± *STK11*-mutant lung adenocarcinoma treated with Palbociclib. Participants ordered by progression-free survival time. CT assessments are indicated and coded for complete response (CR), partial response (PR), stable disease (SD), or progressive disease (PD) or not evaluable (NE) according to RECIST v1.1. Follow-up time after treatment discontinuation and death are also indicated. *KDR* variants detected on pre-treatment cfDNA are indicated, with annotation detailing variant (or variants) detected (adapted from unpublished data, Middleton et al)

Pre-treatment versus post-treatment ctDNA in *KRAS*-mutant lung adenocarcinoma treated with palbocicilib as part of the National Lung Matrix Trial

To assess for mutations that may confer on-treatment resistance to palbociclib, mutations in post-treatment samples (n=31) were compared with baseline samples (n=41) (using a conventional p<0.05 cut-off for significance). *SMC3* mutations were detectable in 4 patients post-therapy (12.9% of post-treatment samples), whilst being detected in no baseline samples (P=0.0306). *FRS2* mutations were detectable in 3 patients post-treatment (9.7 %), but were not detectable in any patients at baseline (p=0.0754).

Gene	Baseline (n=41) (%)		Post Treatment (n=31) (%)		Odds Ratio (CI)		P-Value
SMC3	0	0	4	12.9032	0	(0 - 1.0909)	0.0306
FRS2	0	0	3	9.6774	0	(0 - 1.7833)	0.0754
SMARCA4	7	17.0732	11	35.4839	0.3797	(0.1056 - 1.2742)	0.1006
SMAD4	4	9.7561	0	0	Inf	(0.511 - Inf)	0.1290
TAF1	1	2.4390	4	12.9032	0.1727	(0.0034 - 1.8693)	0.1579
BLM	8	19.5122	2	6.4516	3.4606	(0.6203 - 36.0178)	0.1712
KIF5B	0	0	2	6.4516	0	(0 - 3.9912)	0.1819
TRAF2	0	0	2	6.4516	0	(0 - 3.9912)	0.1819
ZBTB2	0	0	2	6.4516	0	(0 - 3.9912)	0.1819
RUNX1T1	5	12.1951	8	25.8065	0.4046	(0.092 - 1.6048)	0.2154

Table 28: Analysis of post-treatment vs pre-treatment cfDNA samples from *KRAS*-mutant lung adenocarcinoma patients treated with palbociclib as part of Arms C5 and C6 of the National Lung Matrix Trial. CfDNA was extracted from baseline and post-treatment plasma samples, library preparation using Illumina TSO500 cfDNA kit, with sequencing performed by Illumina. Generated FASTQ files were processed using DRAGEN Pipeline for Trusight Oncology 500 ctDNA, with downstream analysis using MafTools using MafCompare. Mutations filtered with only those passing the quality threshold. Presented data represents number of patients in each group with detectable mutations in the indicated genes.

4.4 Summary

Despite convincing preclinical evidence, outcomes for treating patients with *KRAS*-mutant lung adenocarcinoma with palbociclib were disappointing overall. However, a small number of patients appear to have durable benefit. The work in this chapter sought to identify potential predictors of sensitivity to palbociclib treatment in *KRAS*-mutant lung adenocarcinoma. The key results were that an absence of *KDR* variants, and presence of *MTOR* or *CHEK2* mutations on ctDNA may predict better prognosis in *KRAS*-mutant NSCLC treated with palbociclib. This population may reflect a new cohort of patients who may particularly benefit from CDK4/6 inhibitor therapy.

4.5 Discussion

Whilst the JUNIPER trial failed to meet its primary endpoint, it is important to note that clinical benefit rate at 9 months was 21.1% for abemaciclib (144). Likewise, in the National Lung Matrix Trial, a proportion of *KRAS*-mutant lung adenocarcinomas appear to have durable clinical benefit from palbociclib treatment. It is therefore important to assess whether it is possible to identify new biomarkers that may predict benefit from CDK4/6 inhibitor therapy in *KRAS*-mutant lung adenocarcinoma.

Analysis identified the unexpected finding that germline variants in *KDR* may be associated with worse prognosis in *KRAS*-mutant lung adenocarcinoma treated with Palbociclib. *KDR* encodes VEGFR-2, a VEGF receptor. Germline variants in *KDR* may drive poor prognosis by altering angiogenesis. Indeed, Q472H (rs1870377), V297I (rs2305948), C482R (rs34231037) have all been associated with altered cancer behaviour, worse prognosis, or altered treatment response in malignancy (232, 234-238). *KDR* Q472H has been associated with increased microvascular density in NSCLC, melanoma, and astrocytic glioma (232, 236, 239). Melanoma patients with germline *KDR* Q472H have lower response rates to immunotherapy, and shorter PFS following treatment with MAPKi (237). Likewise, *KDR* Q472H is associated with shorter overall survival in glioblastoma (236). In contrast, Q472H and V297I have been associated with prolonged overall survival in head and neck cancers treated with chemoradiotherapy, potentially reflecting enhanced radiosensitivity driven by increased tumour oxygenation (240). In lung cancer, published associations between *KDR* polymorphisms and prognosis have been restricted to patients treated with angiogenesis inhibitors in Chinese populations (241, 242): rs2305948 was associated with worse prognosis in patients treated with chemotherapy and bevacizumab (242).

Based on present data it is not possible to conclude whether *KDR* variants are a general marker of poor prognosis in *KRAS*-mutant lung adenocarcinoma, or whether there is an interaction

between *KDR* variants and palbociclib treatment. However, VEGFR2 hyperactivation has been suggested to drive CDK4/6 resistance in bladder cancer cells (243), making it possible that this is a predictive biomarker. Work is ongoing in this area and will help to bring clarity. Firstly, work is ongoing to sequence cfDNA from the remaining arms of the NLMT: if *KDR* variants are a prognostic but not predictive biomarker, it would be expected that an association between *KDR* variants and prognosis will be seen in multiple arms. Secondly, wet lab work is planned to genetically engineer *KDR* variants into NSCLC cell lines, allowing assessment of whether *KDR* variants alter sensitivity to CDK4/6 inhibitors *in vitro*. If this is confirmed in NSCLC, it would be important to expand experimentation to breast cancer cell lines, as CDK4/6 inhibitors are in active use in the clinic in breast cancer patients. More advanced work may require 3D angiogenesis or mouse modelling to recapitulate the impact of *KDR* on angiogenesis and the wider tumour microenvironment.

MTOR mutations were enriched in pre-treatment samples of *KRAS*-mutant lung adenocarcinoma patients who went onto have a prolonged PFS on palbociclib. mTOR is a crucial mediator of senescence (244, 245). The relevance of mTOR activity in driving a senescent phenotype has been demonstrated in breast cancer cells *in vitro*. In most contexts, CDK4/6 inhibition leads to reversible G1-arrest, however, in the context of persistent MTOR activation, breast cancer cells are driven to complete senescence, a phenomenon prevented by inhibiting MTORC1 (246). It is therefore possible that the prolonged responses seen in the lung cancer patients with activating *MTOR* mutations could reflect CDK4/6 inhibition driving irreversible senescence. The pivotal role of mTOR activity in modulating CDK4/6 response is also supported by findings that two out of seven patients in the JUNIPER trial who achieved a partial response harboured a *RICTOR* amplification, which would also be expected to hyperactivate mTOR signalling (144). Activating mutations in *MTOR* may therefore be a novel biomarker for sensitivity to CDK4/6 inhibition in

KRAS-mutant lung adenocarcinoma. Experiments are planned that will genetically engineer *KRAS*-mutant lung adenocarcinoma cells with the observed *MTOR* variants to assess the impact on CDK4/6 inhibitor sensitivity, and to assess whether these variants are associated with a senescent phenotype.

CHEK2 mutations were also enriched in *KRAS*-mutant lung cancer patients who achieved prolonged progression free survival with palbociclib. *CHEK2* encodes CHK2, which plays roles in DNA repair, DNA damage response and cell cycle arrest. Data surrounding *CHEK2* and CDK4/6 response is conflicting. In a Phase I/II study of Palbociclib and vemurafenib combination therapy in *BRAF*^{V600E} metastatic melanoma, elevated levels of CHEK2 mRNA were associated with response to therapy (247). Germline mutations in DNA Damage Response (DDR) genes *(BRCA1, BRCA2, ATM, CHEK2)* have been associated with resistance to CDK4/6 inhibitor therapy plus endocrine therapy in a real-world study of ER+ breast cancer (247). However, knockdown of CHEK2 causes substantial increases in sensitivity to CDK4/6 inhibition in ER+ breast cancer cells (248). It is possible that the impact of *CHEK2* mutations on CDK4/6 sensitivity is context dependent. Clearly this is an area that needs further clarification. Experiments are planned that will genetically engineer *KRAS*-mutant lung adenocarcinoma cells, either with *CHEK2* knock-out, or knock-in of the observed *CHEK2* mutations. This work will allow an empirical assessment of the impact of *CHEK2* on CDK4/6i sensitivity.

As discussed in chapter 3, analysis of ctDNA offers key advantages over tissue sequencing: ctDNA better represents disease heterogeneity, is less invasive, carries less clinical risk, requires fewer resources, and may be arranged more quickly than conventional biopsies (225, 226). It is therefore highly suitable for exploratory analyses alongside clinical trials, particularly where repeated tissue sampling may be a barrier to entry. However, ctDNA is less sensitive than tissue

sequencing, particularly in tumours with low disease burdens or in tumours with low levels of ctDNA shedding (226). Sensitivity for detection of *KRAS* mutations on ctDNA was 62.0%, which, although lower than that in Chapter 3, remains in line with previously reported sensitivity of ctDNA (214, 228, 229). In the Korean Lung Liquid vs Invasive Biopsy Program, sensitivity for *KRAS* mutation was 67.6% using Guardant360 (229). However, it is acknowledged that ctDNA sequencing may miss mutations that would have been detected on tissue sampling.

It is important to note that detection of *KRAS* mutations were non-significantly enriched in patients who went onto have poor prognosis. This may represent differences in disease burden, cell metabolism or cell death, and mirrors reports that detection of *EGFR* mutation on ctDNA was associated with poor prognosis in patients treated with TKIs (214). As a result, any data around markers of poor prognosis ctDNA should be interpreted with caution and require further validation. However, this is perhaps less of an issue in the context of *KDR* variants. The majority of *KDR* variants appear to be germline variants, and are therefore detected at high VAF, with ctDNA sensitivity unlikely to be playing a role in identification rates. Findings that *KDR* variants confer a poor prognosis will be validated on germline sequencing of banked blood samples in future work.

4.6 Conclusions

The work in this chapter sought to identify potential predictors of sensitivity to palbociclib treatment in *KRAS*-mutant lung adenocarcinoma. Absence of *KDR* variants, and presence of *MTOR* or *CHEK2* mutations on ctDNA may predict better prognosis in *KRAS*-mutant NSCLC treated with palbociclib. This population may reflect a new cohort of patients who may particularly benefit from CDK4/6 inhibitor therapy, and this work represents an area of active area of ongoing work for validation.

Chapter 5: 3q Amplified Squamous Cell Lung Cancer Part 1: *Defining SOX2 as a key target on 3q*

5.1 Introduction

Chapter 3 and Chapter 4 explore potential resistance mechanisms to single-agent targeted therapies in *KRAS*-mutant and *STK11*-mutant lung adenocarcinoma. Whilst introducing effective targeted therapies in smoking-related lung adenocarcinoma remains challenging, an even greater challenge is identifying successful targeted therapies in squamous cell lung cancer (LUSC). Actionable drivers that commonly occur in lung adenocarcinoma are largely absent in LUSC (182, 183). Current first-line treatment for advanced LUSC is either single-agent immunotherapy, cytotoxic chemotherapy, or combination chemoimmunotherapy, dependent on PD-L1 expression, patient fitness and co-morbidities (1). Prognosis remains poor: in KEYNOTE-407, overall survival was 17.2 months in treatment-naïve patients treated with pembrolizumab plus platinum doublet chemotherapy (184, 185). There are no current stratified medicine options for squamous cell lung cancer (LUSC), although potential emerging targets include NRF2/KEAP1 and ATR (186).

In the National Lung Matrix Trial no confirmed responses were seen in patients with squamous cell lung cancer (Figure 6) (127). In arm F2 of the National Lung Matrix Trial, squamous cell lung cancers with PIK3CA amplification were treated with capivasertib (Akt1/2/3 inhibition). PIK3CA sits within the 3q amplicon. 3q amplification is one of the most common genetic changes in LUSC (183, 191), and is also commonly seen in other squamous malignancies, including head and neck cancer (192) and oesophageal squamous cell cancer (191). 3q amplification is absent in low-grade bronchial dysplasia, but commonly observed in high-grade dysplasia, with progressive increases in 3q copy number during progression to malignancy (193). However, 3q amplification is relatively poorly characterised in squamous cell lung cancer. *PIK3CA* is a well-known oncogene within the amplicon, however, clinical outcomes of targeting PI3K/Akt signalling in 3q amplified squamous cell lung cancer have been disappointing (127, 249). 3q encompasses hundreds of

potential oncogenes in addition to *PIK3CA*, including: *DCUN1D1*, *PRKCI*, *TP63*, *BCL6* and *SOX2*. However, it is likely that many genes within the amplicon will be passengers, having little or no impact on oncogenicity. Due to the underwhelming outcomes with inhibition of the PI3K/Akt axis in 3q amplified lung cancer, it is important to take a step back and re-assess potential drivers within 3q.

One approach to determining critical genes within 3q is to define the minimally amplified region. In one analysis, the peak of amplification as determined by GISTIC (Genomic Identification of Significant Targets in Cancer) contained the genes *SOX2*, *ATP11B*, *DCUN1D1* and *MCC1* in squamous cell lung cancer, and only contained *SOX2* in oesophageal squamous cancers (191). However, patients numbers were relatively small: this analysis included 40 oesophageal squamous cancers and 47 squamous cell lung cancers, of which 23% oesophageal and 15% lung cancers had 3q amplification (191). A separate study identified a 4.3 Mb amplified region, spanning 17 genes, including *PIK3CA* and *SOX2* in 10 high grade bronchial dysplasias (193). In an arrayed shRNA approach examining knockdown of 14 genes within 3q, *SOX2* had the greatest anti-proliferative effect in four 3q amplified cell lines (two squamous lung and two oesophageal squamous). *SOX2* knockdown also reduces anchorage independent growth in 3q amplified cell lines (191). These results are fully in keeping with the established role of *SOX2* in squamous carcinogenesis in mouse models (250-253). It is therefore likely that *SOX2* plays an important role within this amplicon. However, published knockdown data are limited by small sample sizes, and by assessment of only a limited number of genes within a broad amplicon.

5.2 Aims and Objectives

3q amplification is a common aberration in squamous cell lung cancer. It is important to determine the relative importance of genes within the amplicon to prioritise candidates for therapeutic targeting. The aim of this chapter is to provide a complete assessment of the 3q amplicon to identify a target (or targets) to take forward as candidates for ongoing development. This chapter will explore the TCGA squamous cell lung cancer cohort dataset, examining amplifications and mRNA expression of genes across 3q in 469 squamous cell lung cancer patients. In addition, Cancer Dependency Map (DepMap) data has made available genome-wide CRISPR-Cas9 knockout data for many well-characterised cell lines. DepMap data will be examined to identify genes within 3q with differential sensitivity in amplified vs non-amplified cell lines. This approach will be used to triage genes within 3q as candidates for targeted therapy approaches in 3q amplified squamous cell lung cancer, allowing prioritisation of promising candidates for further research and development.

Objectives:

1. Define the frequency of amplification of individual genes within 3q in the TCGA squamous cell lung cancer dataset.
2. Explore the relationship between amplification of genes within 3q and mRNA expression in the TCGA squamous cell lung cancer dataset to understand the relevance of these genes to squamous cell lung cancer.
3. To identify genes within 3q with differential sensitivity to CRISPR knockout in 3q amplified versus non amplified lines using genome-wide CRISPR knockout data from DepMap.
4. To validate candidate(s) identified from DepMap using siRNA.

5.3 Results

5.3.1 Analysis of TCGA Squamous Cell Lung Cancer Data of Amplified Genes within 3q26-29

5.3.1.1 Frequency of amplification for genes within 3q26-29 in squamous cell lung cancer

A list of all protein-coding genes within 3q26-29 was generated using the UCSC Genome Browser (chr3:161,000,001 – 198,295,559 (HGNC)), GRCh38/h38) (204-206), producing a list of 191 genes of interest. Frequency of amplification of these genes was examined in the TCGA Pan-cancer Lung Squamous Cell Lung Cancer Cohort (207), accessed via cBioPortal (208, 209). Analysis was restricted to samples with available copy number data (n=487). No data was available for 5 novel protein coding genes (ENSG00000285218, ENSG00000275163, ENSG00000288698, ENSG00000283765, ENSG0000028974), leaving 186 genes with available data (Table 29). The most commonly amplified region centred around 3q26.33 – 3q27.1 (Table 29). The most commonly amplified genes were *ATP11B*, *DCUN1D1*, *MCCC1* and *MCF2L2* (amplified in 195 of 487 cases, 40.04%, 95% CI 35.66 – 44.55%), followed by *SOX2* and *B3GNT5* (amplified in 194 of 487 cases, 38.84%, 95% CI 35.46 to 44.34%) and *LAMP3* in 39.63% (193 of 487 cases, 95% CI 35.26% to 44.13%). Whilst the top 6 amplified genes were all contained within Chr3:181,711,925 – 183,298,504, the amplicon was broad containing numerous oncogenes including *PIK3CA* (37.7%, 184 of 487, 95% CI 33.46 to 42.26), BCL6 (31%, 151 of 487, 95% CI 26.92 to 35.32) and *TP63* (31.62%, 154 of 487, 95% CI 27.51 to 35.96%). Oncoplot of key cancer-related genes in this region is displayed in Figure 27 (list of genes adapted from (127)).

Gene	Band	Location	Pt	%
PPM1L	3q25.33-q26.1	chr3:160,755,602-161,078,902	112	23.00
B3GALNT1	3q26.1	chr3:161,083,883-161,105,411	111	22.79
NMD3		chr3:161,104,696-161,253,532	111	22.79
SPTSSB		chr3:161,344,798-161,372,880	113	23.20
OTOL1		chr3:161,496,808-161,503,942	115	23.61
SI		chr3:164,978,898-165,157,921	143	29.36
SLITRK3		chr3:165,186,720-165,197,109	144	29.57
BCHE		chr3:165,772,904-165,837,462	150	30.80
ZBBX		chr3:167,178,402-167,407,886	159	32.65
SERPINI2		chr3:167,441,914-167,478,972	159	32.65
SERPINI1		chr3:167,453,031-167,543,356	163	33.47
WDR49		chr3:167,478,684-167,657,923	162	33.26
PDCD10		chr3:167,683,298-167,734,939	162	33.26
GOLIM4	3q26.2	chr3:168,008,689-168,095,924	165	33.88
MECOM		chr3:169,083,499-169,663,775	174	35.73
ACTRT3		chr3:169,766,921-169,769,561	173	35.52
MYNN		chr3:169,773,396-169,789,716	173	35.52
LRRC34		chr3:169,793,003-169,812,986	173	35.52
LRRIQ4		chr3:169,812,870-169,837,773	173	35.52
LRRC31		chr3:169,839,172-169,869,935	173	35.52
SAMD7		chr3:169,911,572-169,939,175	174	35.73
SEC62		chr3:169,966,635-169,998,373	174	35.73
GPR160		chr3:170,037,995-170,085,392	174	35.73
PHC3		chr3:170,086,732-170,181,749	174	35.73
PRKCI		chr3:170,222,424-170,305,977	175	35.93
SKIL		chr3:170,357,342-170,396,849	175	35.93
CLDN11		chr3:170,418,868-170,454,733	174	35.73
SLC7A14		chr3:170,459,548-170,586,075	176	36.14
RPL22L1		chr3:170,864,875-170,870,208	175	35.93
Eif5A2		chr3:170,888,418-170,908,644	175	35.93
SLC2A2		chr3:170,996,347-171,026,743	175	35.93
TNIK	3q26.2-q26.31	chr3:171,058,414-171,460,408	177	36.34
PLD1	3q26.31	chr3:171,600,404-171,810,950	179	36.76
TMEM212		chr3:171,843,349-171,938,715	179	36.76
FNDC3B		chr3:172,039,578-172,401,669	179	36.76
GHSR		chr3:172,443,291-172,448,456	179	36.76
TNFSF10		chr3:172,505,508-172,523,475	179	36.76
NCEH1		chr3:172,630,249-172,711,218	179	36.76
ECT2		chr3:172,750,682-172,829,265	178	36.55
SPATA16		chr3:172,889,357-173,141,235	176	36.14
NLGN1		chr3:173,395,952-174,294,372	175	35.93
NAALADL2		chr3:174,438,573-175,810,548	180	36.96
TBL1XR1	3q26.32	chr3:177,019,340-177,228,000	179	36.76
KCNMB2		chr3:178,272,932-178,844,429	183	37.58
ZMAT3		chr3:178,960,121-179,072,513	183	37.58
PIK3CA		chr3:179,148,114-179,240,093	184	37.78
KCNMB3		chr3:179,236,691-179,267,050	184	37.78
ZNF639	3q26.33	chr3:179,322,876-179,338,583	184	37.78
MFN1		chr3:179,347,709-179,394,936	183	37.58
GNB4		chr3:179,396,088-179,527,798	183	37.58
ACTL6A		chr3:179,562,886-179,588,407	182	37.37
MRPL47		chr3:179,588,285-179,604,649	182	37.37
NDUFB5		chr3:179,604,690-179,627,647	182	37.37
USP13		chr3:179,653,032-179,804,366	183	37.58
PEX5L		chr3:179,794,958-180,037,053	184	37.78
TTC14		chr3:180,602,163-180,618,329	183	37.58
CCDC39		chr3:180,602,858-180,684,942	183	37.58
FXR1		chr3:180,868,141-180,982,753	188	38.60
DNAJC19		chr3:180,983,697-180,989,838	187	38.40
SOX2		chr3:181,711,925-181,714,436	194	39.84
ATP11B		chr3:182,793,503-182,921,629	195	40.04
DCUN1D1		chr3:182,938,074-182,985,953	195	40.04
MCCC1	3q27.1	chr3:183,015,218-183,116,196	195	40.04
LAMP3		chr3:183,122,215-183,163,839	193	39.63
MCF2L2		chr3:183,178,041-183,428,778	195	40.04
B3GNT5		chr3:183,253,253-183,298,504	194	39.84
KLHL6		chr3:183,487,551-183,555,706	190	39.01
KLHL24		chr3:183,635,610-183,684,519	190	39.01
YEATS2		chr3:183,697,797-183,812,624	190	39.01
MAP6D1		chr3:183,815,922-183,825,594	190	39.01
PARL		chr3:183,826,489-183,884,933	190	39.01
ABCC5		chr3:183,919,934-184,017,939	190	39.01
HTR3D		chr3:184,031,544-184,039,369	190	39.01
HTR3C		chr3:184,053,047-184,060,673	190	39.01
HTR3E		chr3:184,097,064-184,106,995	190	39.01
EIF2B5		chr3:184,135,038-184,146,127	190	39.01
DVL3		chr3:184,155,377-184,173,614	190	39.01
AP2M1		chr3:184,174,689-184,184,214	190	39.01
ABCF3		chr3:184,186,095-184,194,012	180	36.96
VWA5B2		chr3:184,229,585-184,242,329	178	36.55
ALG3		chr3:184,242,301-184,249,548	178	36.55
CAMK2N2		chr3:184,259,213-184,261,553	178	36.55
ECE2		chr3:184,276,011-184,293,031	178	36.55
PSMD2		chr3:184,299,198-184,309,050	178	36.55
EIF4G1		chr3:184,314,495-184,335,358	178	36.55
FAM131A		chr3:184,335,926-184,348,421	178	36.55
CLCN2		chr3:184,346,185-184,361,650	178	36.55
POLR2H		chr3:184,361,710-184,368,596	178	36.55
THPO		chr3:184,371,935-184,381,968	178	36.55
CHRD		chr3:184,380,054-184,390,739	178	36.55
EPHB3		chr3:184,561,785-184,582,408	179	36.76
MAGEF1		chr3:184,710,364-184,712,064	179	36.76
VPs8	3q27.2	chr3:184,812,143-185,052,614	179	36.76
C3ORF70		chr3:185,076,838-185,153,060	175	35.93
EHHADH		chr3:185,190,624-185,281,990	173	35.52
MAP3K13		chr3:185,282,941-185,489,094	173	35.52
TMEM41A		chr3:185,476,496-185,499,057	171	35.11
LIPH		chr3:185,506,262-185,552,588	170	34.91
SENP2		chr3:185,582,496-185,633,551	168	34.50
IGF2BP2		chr3:185,643,130-185,825,042	168	34.50
TRA2B		chr3:185,914,558-185,938,103	164	33.68
ETV5		chr3:186,046,314-186,110,318	163	33.47
DGKG	3q27.2-q27.3	chr3:186,105,668-186,362,234	161	33.06
CRYGS	3q27.3	chr3:186,538,441-186,546,702	158	32.44
TBCCD1		chr3:186,546,067-186,570,543	158	32.44
DNAJB11		chr3:186,567,403-186,585,800	158	32.44
AHSG		chr3:186,613,060-186,621,318	155	31.83
FETUB		chr3:186,635,969-186,653,141	155	31.83
HRG		chr3:186,660,216-186,678,234	155	31.83
KNG1		chr3:186,717,348-186,744,410	156	32.03
EIF4A2		chr3:186,783,205-186,789,897	155	31.83
RFC4		chr3:186,789,880-186,807,058	155	31.83
ADIPOQ		chr3:186,842,704-186,858,463	155	31.83
ST6GAL1		chr3:186,930,325-187,078,553	154	31.62
RPL39L		chr3:187,120,948-187,180,908	153	31.42
RTP1		chr3:187,197,486-187,201,462	153	31.42
MASP1		chr3:187,217,282-187,291,980	152	31.21
RTP4		chr3:187,368,385-187,372,076	151	31.01
SST		chr3:187,668,912-187,670,394	150	30.80
RTP2		chr3:187,698,259-187,715,691	150	30.80
BCL6		chr3:187,721,377-187,745,725	151	31.01
LPP	3q27.3-q28	chr3:188,153,021-188,890,671	155	31.83
TPRG1	3q28	chr3:188,947,214-189,325,304	150	30.80
TP63		chr3:189,596,746-189,897,276	154	31.62
P3H2		chr3:189,956,728-190,122,437	151	31.01
CLDN16		chr3:190,290,361-190,412,138	146	29.98
CLDN1		chr3:190,305,707-190,322,446	146	29.98
TMEM207		chr3:190,428,655-190,449,901	146	29.98
IL1RAP		chr3:190,514,051-190,659,750	148	30.39
GMNC		chr3:190,843,271-190,892,429	146	29.98
OSTN		chr3:191,199,241-191,265,615	145	29.77
UTS2B		chr3:191,267,168-191,346,182	145	29.77
CCDC50		chr3:191,329,085-191,398,659	146	29.98
PYDC2		chr3:191,461,163-191,461,456	146	29.98
FGF12	3q28-q29	chr3:192,139,390-192,767,764	146	29.98
MB21D2	3q29	chr3:192,796,815-192,917,856	146	29.98
PLAAT1		chr3:193,240,606-193,281,426	145	29.77
ATP13A5		chr3:193,274,789-193,378,820	145	29.77
ATP13A4		chr3:193,398,967-193,593,119	144	29.57
OPA1		chr3:193,593,144-193,697,811	144	29.57
HES1		chr3:194,136,148-194,138,732	143	29.36
CPN2		chr3:194,339,768-194,351,328	142	29.16
LRRC15		chr3:194,355,249-194,369,743	142	29.16
GP5		chr3:194,394,821-194,399,266	142	29.16
ATP13A3		chr3:194,402,672-194,498,364	143	29.36
TMEM44		chr3:194,587,673-194,633,689	143	29.36
LSG1		chr3:194,640,791-194,672,463	143	29.36
FAM43A		chr3:194,685,883-194,689,037	143	29.36
XXYLT1		chr3:195,068,284-195,271,159	143	29.36
ACAP2		chr3:195,274,745-195,443,044	145	29.77
PPP1R2		chr3:195,514,428-195,543,386	145	29.77
APOD		chr3:195,568,705-195,584,033	145	29.77
MUC20		chr3:195,720,884-195,741,123	145	29.77
MUC4		chr3:195,746,765-195,811,973	145	29.77
TNK2		chr3:195,863,364-195,911,945	145	29.77
TFRC		chr3:196,012,511-196,082,153	146	29.98
ZDHHC19		chr3:196,197,452-196,211,437	147	30.18
SLC51A		chr3:196,211,487-196,243,178	147	30.18
PCYT1A		chr3:196,214,222-196,287,957	147	30.18
DYNLT2B		chr3:196,291,219-196,318,299	147	30.18
TM4SF19-DYNLT2B		chr3:196,316,082-196,338,420	147	30.18
TM4SF19		chr3:196,319,342-196,338,503	147	30.18
UBXN7		chr3:196,347,662-196,432,430	147	30.18
RNF168		chr3:196,468,783-196,503,768	147	30.18
SMCO1		chr3:196,506,879-196,520,955	147	30.18
WDR53		chr3:196,554,177-196,568,674	146	29.98
FBXO45		chr3:196,568,611-196,589,059	146	29.98
NRROS		chr3:196,639,694-196,662,004	151	31.01
PIGX		chr3:196,639,775-196,736,007	151	31.01
CEP19		chr3:196,706,277-196,712,250	151	31.01
MELTF		chr3:196,728,611-196,756,688	151	31.01
PAK2		chr3:196,739,857-196,832,647	151	31.01
SENP5		chr3:196,867,856-196,934,714	151	31.01
NCBP2		chr3:196,935,402-196,942,594	151	31.01
NCBP2AS2		chr3:196,942,674-196,943,543	151	31.01
PIGZ		chr3:196,946,356-196,969,060	151	31.01
DLG1		chr3:197,042,560-197,299,330	151	31.01
BDH1		chr3:197,509,783-197,573,343	150	30.80
RUBCN		chr3:197,668,867-197,749,820	149	30.60
FYTTD1		chr3:197,737,179-197,787,596	149	30.60
LRCH3		chr3:197,791,226-197,888,436	149	30.60
IQCG		chr3:197,889,077-197,960,177	149	30.60
RPL35A		chr3:197,950,190-197,956,610	149	30.60
LMLN		chr3:197,960,200-198,043,720	149	30.60

Table 29. Frequency of Amplification of genes within 3q26-29 in the TCGA Squamous Cell Lung Cancer Cohort. List of genes within 3q26-29 was generated from the UCSC Genome Browser. Frequency of amplification for each genes is shown. Amplification was defined as +2, high level amplification (GISTIC). Genes are ordered by position within the amplicon. Analysis restricted to squamous cell lung cancer patients with copy number data available (n=487).

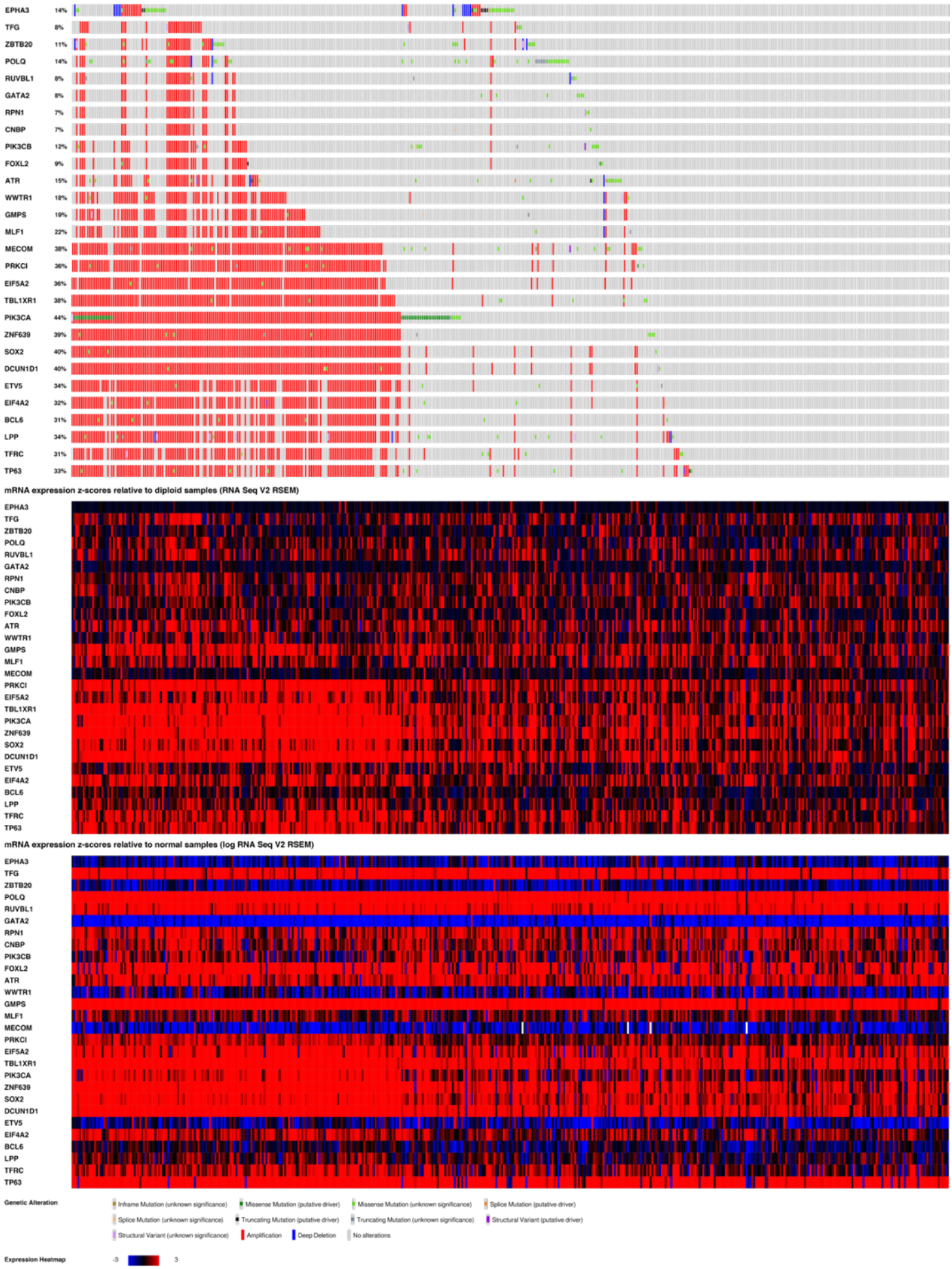

Figure 27. Oncoplot of known cancer-related genes in 3q, showing: amplification (and other aberrations) (top), mRNA expression relative to diploid samples (middle) and mRNA expression relative to normal samples (bottom) in patients with squamous cell lung cancer (TCGA Pan Cancer Atlas). Data obtained using cBioPortal, with analysis restricted to samples with complete data (n = 466)

5.3.1.2 Association between copy number and mRNA expression for genes in 3q26-29 in squamous cell lung cancer

Amplification of a gene is more likely to be functionally relevant if increased copy number is associated with increased mRNA expression. The association between copy number and mRNA expression for genes in 3q26-29 was reviewed, using data from the TCGA Pan-cancer Lung Squamous Cell Lung Cancer Cohort (207), accessed via cBioPortal (208, 209). Analysis was restricted to samples with complete data (mutation, copy number and expression data) (n=466). Correlation between gene copy number (Log2 copy number values) and mRNA expression (expressed as Z score relative to all samples) are outlined in Table 30 – Table 32, listing genes by strength of association according to Spearman rank correlation co-efficient. Many genes within 3q show a strong correlation between copy number and mRNA expression (Table 30), including key cancer-related genes such as *PRKCI* (Spearman $\rho = 0.83$, corrected $p<0.0001$). However, this was not the case for all genes within the region (Table 32). The relationship between copy number and mRNA expression for the six most commonly amplified genes within the amplicon is shown in Figure 28 and Figure 29: all six genes show at least moderate correlation between copy number and mRNA expression (*APT11B*: Spearman $\rho = 0.81$, $p<0.0001$; *DCUN1D1*: $\rho = 0.81$, $p<0.0001$; *MCCC1*: $\rho = 0.71$, $p<0.0001$; *MCF2L2*: $\rho = 0.46$, $p<0.0001$; *SOX2*: $\rho = 0.73$ $p<0.0001$; *B3GNT5*: $\rho = 0.73$, $p<0.0001$ (P-values corrected for all measures)). In contrast, *LAMP3* (the seventh most commonly amplified gene) shows marginal correlation between *LAMP3* copy number and *LAMP3* mRNA expression (Spearman $\rho = 0.15$, corrected $p= 0.027$).

	Spearman			Pearson		
	ρ	P-value (uncorrected)	P-value (corrected)	ρ	P-value (uncorrected)	P-value (corrected)
ZNF639	0.87	5.12E-144	9.42E-142	0.85	1.12E-129	2.06E-127
SENP2	0.86	2.33E-137	4.29E-135	0.85	5.44E-129	1.00E-126
FXR1	0.83	3.96E-120	7.29E-118	0.83	9.91E-122	1.82E-119
PRKCI	0.83	8.08E-118	1.49E-115	0.81	2.92E-110	5.37E-108
ACTL6A	0.83	2.09E-117	3.85E-115	0.80	2.47E-103	4.54E-101
DVL3	0.82	1.30E-114	2.39E-112	0.78	4.22E-96	7.76E-94
SENP5	0.82	6.06E-116	1.12E-113	0.78	1.83E-97	3.37E-95
DCUN1D1	0.81	8.38E-111	1.54E-108	0.80	5.25E-104	9.66E-102
ATP11B	0.81	2.24E-107	4.12E-105	0.79	4.18E-100	7.69E-98
OPA1	0.81	1.18E-111	2.17E-109	0.79	6.76E-100	1.24E-97
LSG1	0.81	8.68E-112	1.60E-109	0.78	2.54E-95	4.67E-93
DNAJC19	0.80	4.17E-107	7.67E-105	0.80	8.72E-106	1.60E-103
MFN1	0.80	6.58E-106	1.21E-103	0.79	1.08E-98	1.99E-96
PSMD2	0.80	2.26E-103	4.16E-101	0.78	3.48E-98	6.40E-96
RFC4	0.80	6.09E-103	1.12E-100	0.78	1.06E-97	1.95E-95
TBCCD1	0.80	1.07E-103	1.97E-101	0.77	1.09E-92	2.01E-90
ABCF3	0.79	4.78E-101	8.80E-99	0.78	4.41E-97	8.11E-95
ALG3	0.79	2.44E-100	4.49E-98	0.78	1.98E-98	3.64E-96
WDR53	0.79	2.89E-100	5.32E-98	0.78	4.58E-95	8.43E-93
ACAP2	0.78	8.74E-98	1.61E-95	0.76	4.97E-88	9.14E-86
PARL	0.78	1.37E-95	2.52E-93	0.75	1.75E-85	3.22E-83
EIF2B5	0.77	2.43E-94	4.47E-92	0.76	1.35E-88	2.48E-86
PIK3CA	0.77	1.02E-93	1.88E-91	0.76	2.70E-90	4.97E-88
POLR2H	0.77	4.73E-92	8.70E-90	0.76	6.85E-90	1.26E-87
TRA2B	0.77	9.24E-92	1.70E-89	0.74	3.15E-83	5.80E-81
NCBP2	0.77	1.28E-91	2.36E-89	0.74	5.27E-82	9.70E-80
FYTTD1	0.77	1.15E-92	2.12E-90	0.73	1.69E-78	3.11E-76
NCBP2AS2	0.77	7.39E-91	1.36E-88	0.72	1.03E-76	1.90E-74
FAM131A	0.76	1.43E-89	2.63E-87	0.77	1.82E-91	3.35E-89
VPS8	0.76	2.59E-88	4.77E-86	0.76	1.71E-90	3.15E-88
MAGEF1	0.76	1.71E-90	3.15E-88	0.75	2.40E-84	4.42E-82
PAK2	0.76	1.04E-88	1.91E-86	0.74	3.66E-83	6.73E-81
ECT2	0.76	1.86E-87	3.42E-85	0.71	3.58E-72	6.59E-70
ABCC5	0.76	2.43E-87	4.47E-85	0.70	1.28E-70	2.36E-68
TBL1XR1	0.75	3.65E-86	6.72E-84	0.75	1.54E-85	2.83E-83
PHC3	0.74	1.11E-82	2.04E-80	0.74	1.20E-80	2.21E-78
YEATS2	0.74	1.70E-82	3.13E-80	0.72	1.99E-74	3.66E-72
MRPL47	0.74	2.33E-82	4.29E-80	0.72	3.43E-76	6.31E-74
PIGX	0.74	1.87E-80	3.44E-78	0.69	1.87E-68	3.44E-66
PPP1R2	0.73	1.90E-78	3.50E-76	0.71	2.36E-73	4.34E-71
B3GNT5	0.73	4.99E-78	9.18E-76	0.66	3.10E-60	5.70E-58
SOX2	0.73	1.90E-78	3.50E-76	0.62	4.88E-51	8.98E-49
TMEM41A	0.72	3.38E-75	6.22E-73	0.72	2.15E-76	3.96E-74
FBXO45	0.72	3.21E-75	5.91E-73	0.71	4.15E-72	7.64E-70
CLCN2	0.72	8.00E-77	1.47E-74	0.70	9.62E-69	1.77E-66
MYNN	0.72	5.86E-76	1.08E-73	0.68	1.51E-64	2.78E-62
XXYLT1	0.72	9.28E-76	1.71E-73	0.68	1.04E-63	1.91E-61
PDCD10	0.72	1.12E-74	2.06E-72	0.67	8.89E-62	1.64E-59
DNAJB11	0.71	2.25E-73	4.14E-71	0.73	1.60E-79	2.94E-77
MCCC1	0.71	1.37E-71	2.52E-69	0.70	5.03E-70	9.26E-68
UBXN7	0.71	1.13E-72	2.08E-70	0.69	2.08E-67	3.83E-65
DLG1	0.71	1.58E-73	2.91E-71	0.68	1.82E-63	3.35E-61
NDUFB5	0.70	3.64E-69	6.70E-67	0.66	1.09E-60	2.01E-58
ECE2	0.68	1.27E-63	2.34E-61	0.66	2.35E-60	4.32E-58
EIF4A2	0.68	1.37E-64	2.52E-62	0.66	2.26E-60	4.16E-58
KLHL24	0.67	6.21E-62	1.14E-59	0.65	1.63E-56	3.00E-54
SEC62	0.66	1.81E-58	3.33E-56	0.70	4.23E-69	7.78E-67
EIF4G1	0.66	9.39E-59	1.73E-56	0.63	1.39E-52	2.56E-50
EHHADH	0.66	3.39E-59	6.24E-57	0.63	3.63E-53	6.68E-51
PCYT1A	0.65	4.74E-58	8.72E-56	0.64	1.48E-55	2.72E-53
RNF168	0.65	4.87E-58	8.96E-56	0.62	4.20E-51	7.73E-49
ATP13A3	0.64	4.26E-54	7.84E-52	0.64	3.01E-54	5.54E-52
TFRC	0.64	8.74E-56	1.61E-53	0.63	3.78E-52	6.96E-50
MAP6D1	0.63	4.57E-52	8.41E-50	0.63	1.11E-53	2.04E-51
NMD3	0.63	4.45E-52	8.19E-50	0.60	3.59E-46	6.61E-44
RPL35A	0.62	2.40E-51	4.42E-49	0.62	7.87E-50	1.45E-47
LRCH3	0.62	8.51E-52	1.57E-49	0.60	2.40E-47	4.42E-45
BDH1	0.62	7.75E-51	1.43E-48	0.57	1.96E-41	3.61E-39
KCNMB3	0.61	4.30E-48	7.91E-46	0.60	4.39E-47	8.08E-45

Table 30: Genes within 3q26-29 with strong correlation between copy number and mRNA expression in patients with squamous cell lung cancer (TCGA Pan Cancer Atlas). Correlation between gene copy number (Log2 copy number values) and mRNA expression (expressed as Z score relative to all samples), listing genes by strength of association according to Spearman rank correlation co-efficient. Cut-off of Spearman $\rho \geq 0.6$ for strong correlation. Data obtained using cBioPortal, with analysis restricted to samples with complete data (n = 466)

	Spearman			Pearson		
	ρ	P-value (uncorrected)	P-value (corrected)	ρ	P-value (uncorrected)	P-value (corrected)
AP2M1	0.59	2.78E-44	5.12E-42	0.57	3.58E-41	6.59E-39
PLD1	0.57	4.45E-41	8.19E-39	0.54	4.80E-36	8.83E-34
USP13	0.56	3.29E-39	6.05E-37	0.58	2.78E-43	5.12E-41
EIF5A2	0.56	4.23E-40	7.78E-38	0.54	2.66E-36	4.89E-34
RPL22L1	0.55	7.49E-38	1.38E-35	0.58	1.54E-43	2.83E-41
CEP19	0.55	1.19E-37	2.19E-35	0.55	1.01E-37	1.86E-35
VWA5B2	0.54	1.54E-36	2.83E-34	0.53	2.01E-34	3.70E-32
EPHB3	0.54	3.01E-37	5.54E-35	0.49	5.56E-30	1.02E-27
RPL39L	0.54	3.17E-37	5.83E-35	0.49	2.39E-29	4.40E-27
IGF2BP2	0.54	4.27E-37	7.86E-35	0.47	4.14E-27	7.62E-25
TP63	0.54	2.64E-36	4.86E-34	0.40	4.24E-19	7.80E-17
GOLIM4	0.53	1.47E-34	2.70E-32	0.52	3.04E-33	5.59E-31
KCNMB2	0.53	2.37E-35	4.36E-33	0.50	1.50E-30	2.76E-28
HRG	0.52	3.85E-34	7.08E-32	0.55	1.52E-38	2.80E-36
TMEM44	0.52	4.76E-34	8.76E-32	0.52	7.12E-34	1.31E-31
FETUB	0.50	2.38E-31	4.38E-29	0.49	4.24E-30	7.80E-28
MELTF	0.49	1.27E-29	2.34E-27	0.49	4.80E-30	8.83E-28
ZMAT3	0.48	1.18E-27	2.17E-25	0.48	7.77E-29	1.43E-26
TPRG1	0.48	6.49E-28	1.19E-25	0.48	8.35E-29	1.54E-26
LMLN	0.48	2.82E-02	5.19E+00	0.45	4.11E-25	7.56E-23
DYNLT2B	0.47	7.90E-27	1.45E-24	0.46	2.78E-25	5.12E-23
MCF2L2	0.46	1.81E-25	3.33E-23	0.50	2.67E-30	4.91E-28
AHSG	0.46	7.21E-26	1.33E-23	0.44	1.05E-23	1.93E-21
FGF12	0.46	1.52E-25	2.80E-23	0.42	7.32E-22	1.35E-19
TTC14	0.45	4.51E-24	8.30E-22	0.49	2.79E-29	5.13E-27
ACTRT3	0.45	1.42E-24	2.61E-22	0.48	1.74E-28	3.20E-26
TNK2	0.45	9.21E-25	1.69E-22	0.44	7.68E-24	1.41E-21
LPP	0.43	6.07E-22	1.12E-19	0.43	1.69E-22	3.11E-20
DGKG	0.42	2.51E-21	4.62E-19	0.37	2.00E-16	3.68E-14
RUBCN	0.41	3.53E-20	6.50E-18	0.43	1.72E-22	3.16E-20
GPR160	0.41	1.34E-20	2.47E-18	0.41	4.86E-20	8.94E-18
FAM43A	0.41	2.08E-20	3.83E-18	0.40	8.68E-20	1.60E-17
NLGN1	0.40	4.67E-19	8.59E-17	0.41	4.62E-20	8.50E-18
PIGZ	0.40	6.54E-19	1.20E-16	0.41	1.78E-20	3.28E-18

Table 31: Genes within 3q26-29 with moderate correlation between copy number and mRNA expression in patients with squamous cell lung cancer (TCGA Pan Cancer Atlas). Correlation between gene copy number (Log2 copy number values) and mRNA expression (expressed as Z score relative to all samples), listing genes by strength of association according to Spearman rank correlation co-efficient. This table shows Spearman $\rho \geq 0.4$ and < 0.6. Data obtained using cBioPortal, with analysis restricted to samples with complete data (n = 466)

	Spearman			Pearson		
	ρ	P-value (uncorrected)	P-value (corrected)	ρ	P-value (uncorrected)	P-value (corrected)
P3H2	0.19	4.04E-05	7.42E-03	0.19	4.71E-05	8.66E-03
MUC20	0.19	3.01E-05	5.54E-03	0.19	3.35E-05	6.16E-03
GNB4	0.17	2.70E-04	4.97E-02	0.21	6.72E-06	1.24E-03
IL1RAP	0.17	1.95E-04	3.60E-02	0.18	1.16E-04	2.14E-02
HTR3D	0.17	2.96E-04	5.45E-02	0.14	3.23E-03	5.95E-01
SLC7A14	0.17	2.75E-04	5.06E-02	0.13	6.28E-03	1.16E+00
HES1	0.16	5.34E-04	9.83E-02	0.17	1.54E-04	2.83E-02
GHSR	0.16	4.22E-04	7.76E-02	0.11	1.38E-02	2.54E+00
LAMP3	0.15	1.47E-03	2.70E-01	0.23	5.65E-07	1.04E-04
FNDC3B	0.15	1.02E-03	1.88E-01	0.23	4.87E-07	8.96E-05
THPO	0.15	1.13E-03	2.07E-01	0.22	1.13E-06	2.08E-04
LRRIQ4	0.15	1.08E-03	1.98E-01	0.19	3.78E-05	6.95E-03
C3ORF70	0.15	1.18E-03	2.18E-01	0.18	1.06E-04	1.96E-02
PEX5L	0.14	1.80E-03	3.32E-01	0.11	1.61E-02	2.96E+00
HTR3E	0.14	2.62E-03	4.82E-01	0.09	4.44E-02	8.17E+00
IQCG	0.14	3.00E-03	5.51E-01	0.09	6.07E-02	1.12E+01
TNIK	0.13	5.18E-03	9.53E-01	0.13	4.14E-03	7.62E-01
LIPH	0.12	0.0109	2.01E+00	0.14	2.22E-03	4.09E-01
TMEM207	0.12	9.15E-03	1.68E+00	0.08	1.05E-01	1.93E+01
SAMD7	0.10	0.0276	5.08E+00	0.15	1.05E-03	1.94E-01
RTP4	0.10	0.0387	7.12E+00	0.09	4.17E-02	7.67E+00
PYDC2	0.10	0.0258	4.75E+00	0.09	6.67E-02	1.23E+01
MUC4	0.07	0.121	2.23E+01	0.09	6.59E-02	1.21E+01
SLC2A2	0.07	0.158	2.91E+01	0.03	5.71E-01	1.05E+02
TM4SF19	0.06	0.184	3.39E+01	0.05	2.61E-01	4.80E+01
NRROS	0.05	0.276	5.08E+01	0.11	1.84E-02	3.39E+00
MASP1	0.05	0.3	5.52E+01	0.04	3.72E-01	6.84E+01
UTS2B	0.05	0.288	5.30E+01	0.04	3.45E-01	6.35E+01
ADIPOQ	0.05	0.29	5.34E+01	0.03	5.28E-01	9.72E+01
SPATA16	0.04	0.371	6.83E+01	0.06	2.34E-01	4.31E+01
ATP13A4	0.04	0.36	6.62E+01	0.03	4.97E-01	9.14E+01
CHRD	0.03	0.528	9.72E+01	0.10	2.97E-02	5.46E+00
SI	0.03	0.504	9.27E+01	0.00	9.91E-01	1.82E+02
CLDN11	0.02	0.705	1.30E+02	0.05	2.53E-01	4.66E+01
OSTN	0.02	0.66	1.21E+02	0.04	3.42E-01	6.29E+01
SST	0.01	0.88	1.62E+02	0.06	1.61E-01	2.96E+01
MECOM	0.01	0.795	1.46E+02	0.03	4.99E-01	9.18E+01
WDR49	0.00	0.957	1.76E+02	0.01	8.38E-01	1.54E+02
OTOL1	-0.02	0.722	1.33E+02	-0.01	8.43E-01	1.55E+02
SERPINI2	-0.03	0.56	1.03E+02	-0.02	5.95E-01	1.09E+02
HTR3C	-0.04	0.377	6.94E+01	0.07	1.15E-01	2.12E+01
GMNC	-0.04	0.396	7.29E+01	-0.03	5.09E-01	9.37E+01
ZBBX	-0.06	0.183	3.37E+01	-0.07	1.06E-01	1.95E+01
GP5	-0.11	0.0149	2.74E+00	-0.10	3.06E-02	5.63E+00
TMEM212	-0.11	0.0226	4.16E+00	-0.12	7.98E-03	1.47E+00
CPN2	-0.13	3.66E-03	6.73E-01	-0.10	2.83E-02	5.21E+00
APOD	-0.13	3.90E-03	7.17E-01	-0.13	5.80E-03	1.07E+00
KLHL6	-0.15	1.34E-03	2.46E-01	-0.10	2.60E-02	4.78E+00
LRRC31	-0.17	2.76E-04	5.07E-02	-0.16	4.12E-04	7.58E-02
LRRC15	-0.23	7.75E-07	1.43E-04	-0.18	1.08E-04	1.99E-02
ST6GAL1	-0.26	9.10E-09	1.67E-06	-0.22	1.60E-06	2.95E-04

Table 32: Genes within 3q26-29 with weak, no or negative correlation between copy number and mRNA expression in patients with squamous cell lung cancer (TCGA Pan Cancer Atlas). Correlation between gene copy number (Log2 copy number values) and mRNA expression (expressed as Z score relative to all samples), listing genes by strength of association according to Spearman rank correlation co-efficient. This table shows Spearman $\rho < 0.4$. Data obtained using cBioPortal, with analysis restricted to samples with complete data (n = 466)

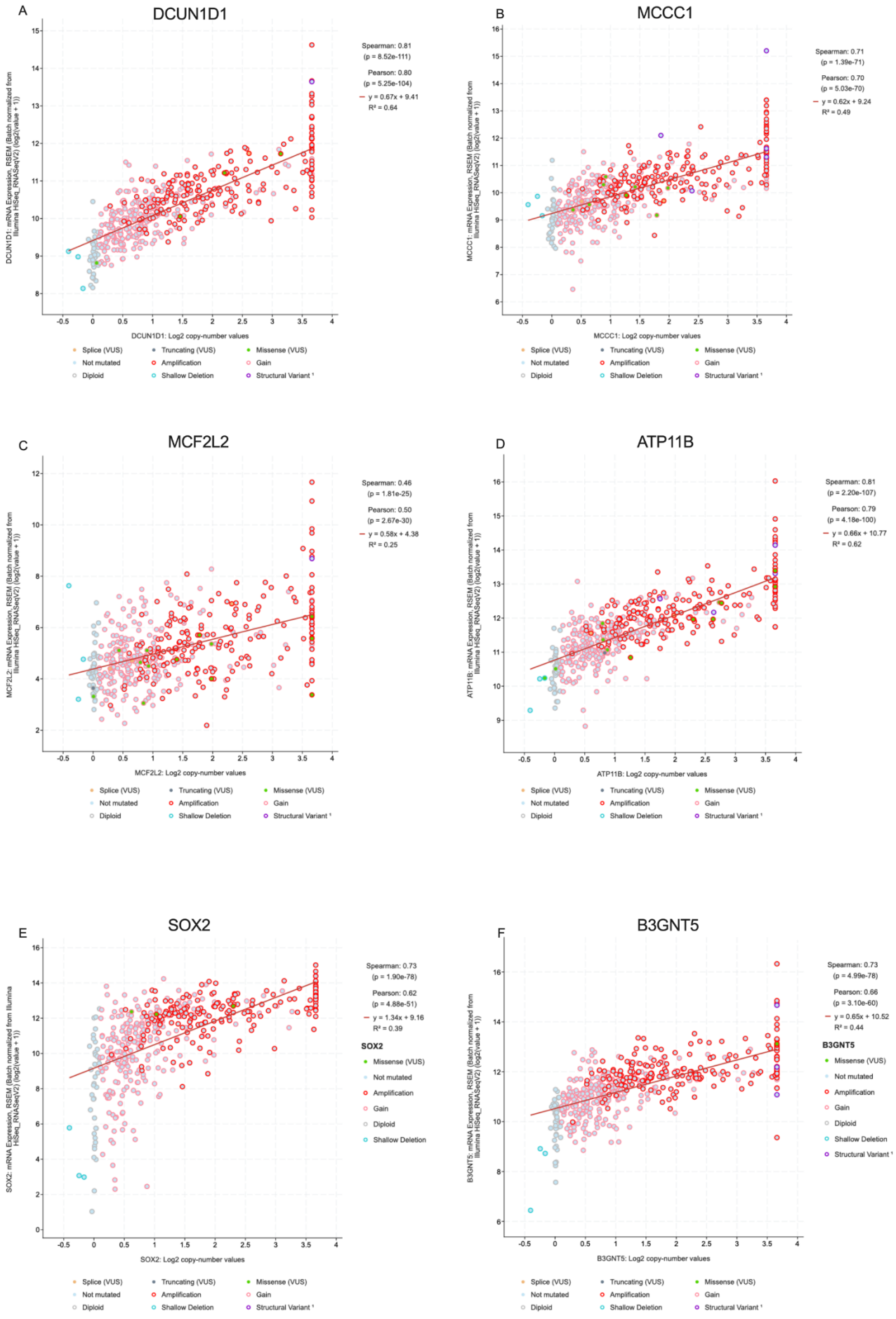

Figure 28: Relationship between copy number and mRNA expression for most commonly amplified genes within the 3q 26-29 in patients with squamous cell lung cancer (TCGA Pan Cancer Atlas). Genetic alterations are also displayed. Data obtained and plotted using cBioPortal, with analysis restricted to samples with complete data (n = 466)

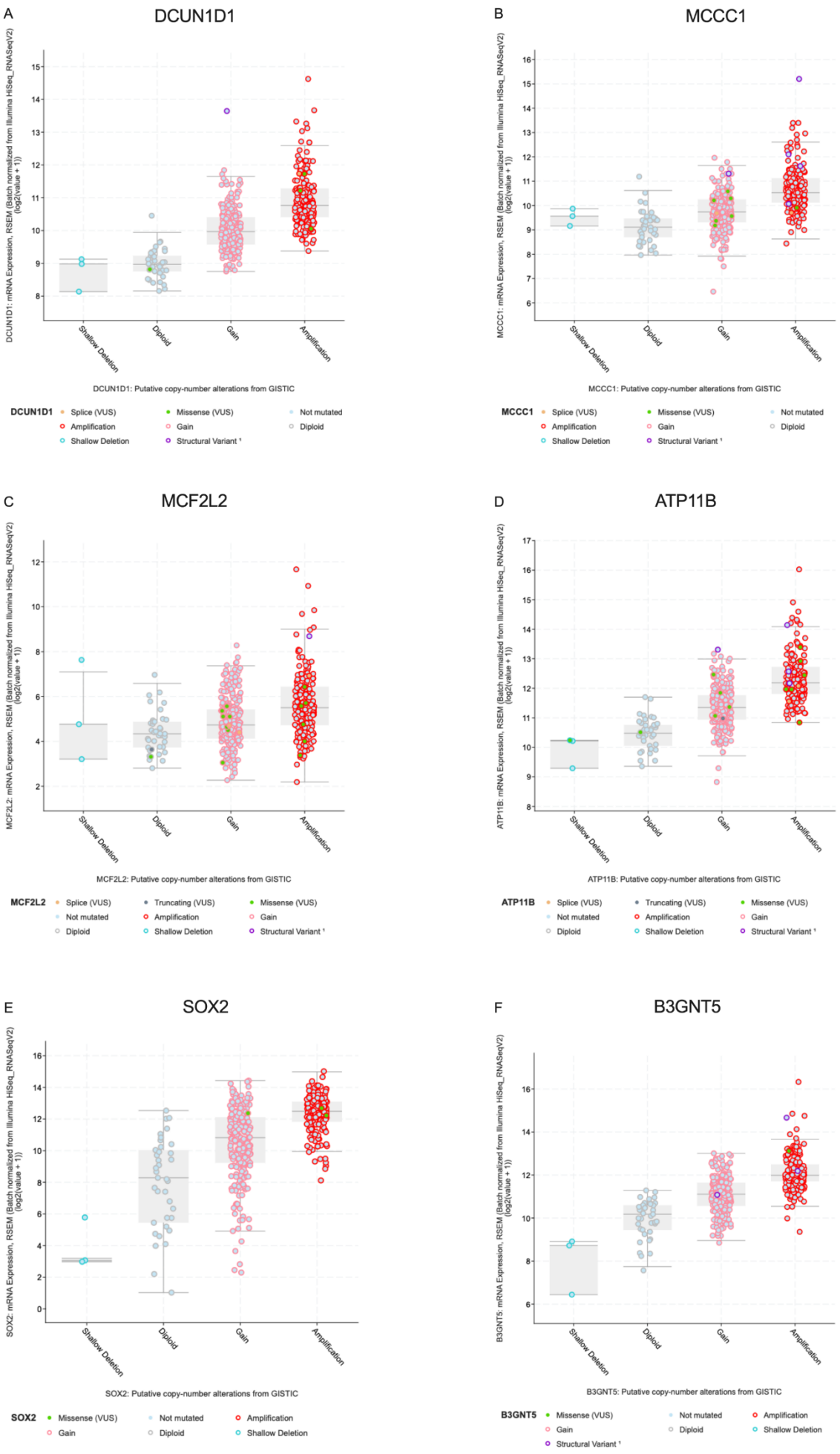

Figure 29: Relationship between copy number and mRNA expression for most commonly amplified genes within the 3q 26-29 in patients with squamous cell lung cancer (TCGA Pan Cancer Atlas). Genetic alterations are also displayed. Data obtained and plotted using cBioPortal, with analysis restricted to samples with complete data (n = 466)

5.3.2 Analysis of Cancer Dependency Map (Depmap) data

The Cancer Dependency Map (DepMap) Project from the Broad Institute has made available genome-wide CRISPR loss-of-function data for thousands of well characterised cancer cell line models (210). Dependency scores are a measure of essentiality of genes to individual cell lines, with a more negative score demonstrating greater dependency, -1 reflects the mean of common essential genes (210). This data was used to assess the relationship between 3q amplification and dependency on genes within 3q26-29. CERES-corrected dependency scores and copy number (log2(copyratio +1)) were obtained from DepMap. CERES is a computational method that allows estimation of dependency from essentiality screens (such as CRISPR screens) whilst correcting for copy number (211).

5.3.2.1 Assessment of dependency scores for 3q genes in 3q amplified vs. non 3q amplified squamous cell lung cancer

3q amplification was defined pragmatically as log2(copyratio +1) $\geq$ 1.8 in both *PIK3CA* and *SOX2*. *SOX2* and *PIK3CA* were chosen as two well characterised and recognised components of the 3q amplicon that span the most commonly amplified region. Visual analysis of the data confirmed that cell lines classified as 'amplified' demonstrated broad amplification across distal 3q mirroring the human TCGA datasets shown in section 3.2.1. All cell lines classified as amplified for either *SOX2* or *PIK3CA* were also amplified for second gene, and it was therefore judged this was a robust strategy for classification of amplification in this setting. To assess the difference in dependency of genes, a differential dependency score was calculated:

$$\text{Differential dependency} = \text{Mean Dependency Amplified} - \text{Mean Dependency Not Amplified}$$

Initial intent was to restrict analysis to LUSC cell lines only. However, only 21 squamous cell lung cancer cell lines had available DepMap CRISPR dependency data, of which 3 met criteria for 3q amplification. Analysis was therefore completed three times: all squamous cell lines; all non-haematological cell lines; only squamous cell lung cancer cell lines. Haematological cell lines were excluded to avoid skewing results in either 'amplified' or 'non-amplified' groups by inclusion of

lymphoid or myeloid lineage cells which may have distinct dependencies and behaviour: for example diffuse large B-cell lymphoma commonly displays trisomy 3 or 3q gain (254), but is likely to have very distinct biological behaviour from smoking-driven squamous cell cancers.

When genes within 3q26-29 were ranked on differential dependency in amplified vs non-amplified lines, the highest ranked gene was *SOX2* (Table 33, Table 34). *SOX2* was the top ranked candidate in both analysis of all non-haematological cell lines (Table 33) and when analysis was restricted to squamous cell lines only (Table 34). Across all non-haematological cell lines, mean *SOX2* dependency was -0.721 (SEM ± 0.158) in amplified lines versus -0.142 (SEM ± 0.00636) in non-amplified lines ($P<0.0001$), remaining significant after Bonferroni correction. Likewise, when analysis was restricted to squamous lines, mean *SOX2* dependency was -0.721 (SEM ± 0.158) in amplified lines versus -0.167 (SEM ± 0.222) in non-amplified lines ($P<0.0001$), again remaining significant after Bonferroni correction.

Amplified lines showed a greater dependency on *TP63*. Across all non-haematological cell lines, mean *TP63* dependency was -0.445 (SEM ± 0.0773) in amplified lines versus -0.0356 (SEM ± 0.00810) in non-amplified lines ($P<0.0001$), remaining significant after Bonferroni correction. However, this difference was not significant when analysis was restricted to squamous lines: mean *TP63* dependency -0.445 (SEM ± 0.0773) in amplified lines versus -0.26 (SEM ± 0.0366) in non-amplified lines ($P = 0.154$).

Amplified lines showed a greater dependency on *MUC20*. Across all non-haematological cell lines, mean *MUC20* dependency was -0.424 (SEM ± 0.105) in amplified lines and -0.185 (SEM ± 0.00539) in non-amplified lines ($P<0.0001$). When analysis was restricted to squamous cell lines mean dependency was -0.424 (SEM ± 0.105) in amplified lines and -0.216 (SEM ±

0.0148) in non-amplified lines (P = 0.001), although this was not significant after Bonferonni correction.

For the top seven most commonly amplified genes (excluding SOX2), significant increases in dependency in amplified lines were seen for B3GNT5, MCCC1, LAMP3, MCF2L2. However, these increases were either modest or unlikely to be therapeutically meaningful due to low level of dependency in either context (differential dependency -0.272 for B3GNT5 (P<0.0001), (differential dependency -0.139 for MCCC1 (p = 0.006)) (differential dependency -0.061 for LAMP3 (P = 0.0018)) (differential dependency -0.111 for MCF2L2 (p = 0.0189)). There was no increased dependency in amplified lines for DCUN1D1 (differential dependency -0.024, p = 0.7479). For most genes within the 3q26-29 amplicon, amplification status was not associated with dependency, including key oncogenes within the amplicon such as *PIK3CA*, *PRKCI* and *BCL6*. These results may suggest that these genes are less relevant in the context of 3q amplification. However, it is acknowledged that CRISPR screens are designed to target diploid genomes, and therefore high copy number genes may not have their function overcome by a CRISPR screen. Nonetheless, these genes do not seem promising targets to prioritise for therapeutic targeting based on this data.

Gene	Dependency 3q Amplified Cell lines		Dependency Not 3q Amplified		Differential Dependency	P-Value	
	Mean (n=9)	SD	Mean (N=972)	SD	(Mean Amp - Mean No Amp)	(uncorrected)	
SOX2	-0.721	0.475	-0.142	0.198	-0.580	<0.0001	****
TP63	-0.445	0.232	0.036	0.253	-0.481	<0.0001	****
MUC20	-0.424	0.317	-0.185	0.168	-0.239	<0.0001	****
B3GNT5	-0.272	0.124	-0.063	0.133	-0.208	<0.0001	****
CRYGS	-0.242	0.153	-0.059	0.113	-0.184	<0.0001	****
FAM131A	-0.169	0.124	-0.002	0.107	-0.167	<0.0001	****
THPO	-0.175	0.162	-0.012	0.107	-0.163	<0.0001	****
XXYLT1	-0.314	0.156	-0.160	0.125	-0.155	0.0002	***
MAP6D1	-0.225	0.103	-0.079	0.119	-0.146	0.0002	***
FNDC3B	-0.175	0.189	-0.029	0.176	-0.146	0.0133	*
USP13	-0.106	0.107	0.029	0.106	-0.135	0.0001	***
MAGEF1	-0.110	0.170	0.024	0.107	-0.135	0.0002	***
CAMK2N2	-0.127	0.129	0.003	0.098	-0.130	<0.0001	****
MCCC1	-0.139	0.110	-0.016	0.107	-0.123	0.0006	***
CHRD	-0.082	0.139	0.031	0.102	-0.112	0.0011	**
MELTF	-0.129	0.148	-0.023	0.100	-0.106	0.0016	**
TNFSF10	-0.054	0.220	0.052	0.158	-0.106	0.0476	*
LAMP3	-0.061	0.133	0.043	0.099	-0.104	0.0018	**
RTP2	-0.112	0.184	-0.011	0.112	-0.101	0.0075	**
NRROS	-0.129	0.116	-0.031	0.107	-0.098	0.0068	**
SLC51A	-0.057	0.169	0.038	0.089	-0.095	0.0017	**
APOD	-0.130	0.162	-0.036	0.104	-0.095	0.0071	**
MCF2L2	-0.111	0.131	-0.020	0.116	-0.092	0.0189	*
FBXO45	0.019	0.093	0.108	0.113	-0.089	0.0185	*
CCDC39	-0.115	0.158	-0.026	0.120	-0.089	0.027	*
FXR1	-0.011	0.172	0.077	0.141	-0.088	0.0637	NS
DLG1	-0.100	0.132	-0.013	0.115	-0.087	0.0235	*
HTR3C	-0.073	0.131	0.009	0.115	-0.082	0.0347	*
BCL6	-0.139	0.122	-0.059	0.180	-0.080	0.1818	NS
IGF2BP2	-0.372	0.144	-0.292	0.115	-0.080	0.0391	*
BDH1	-0.104	0.134	-0.024	0.101	-0.080	0.0193	*
EPHB3	-0.153	0.195	-0.075	0.112	-0.078	0.0392	*
RUBCN	-0.008	0.095	0.070	0.112	-0.077	0.0384	*
FYTTD1	-0.108	0.107	-0.031	0.110	-0.077	0.0384	*
VPS8	-0.238	0.128	-0.162	0.176	-0.076	0.1972	NS
ABCC5	-0.024	0.098	0.052	0.107	-0.076	0.0342	*
LMLN	-0.244	0.159	-0.168	0.104	-0.076	0.0302	*
WDR53	-0.153	0.150	-0.078	0.105	-0.075	0.034	*
LRCH3	-0.130	0.129	-0.056	0.121	-0.074	0.0696	NS
MUC4	-0.046	0.147	0.027	0.104	-0.073	0.0361	*
GOLIM4	-0.041	0.181	0.031	0.110	-0.071	0.0545	NS
EIF5A2	0.043	0.155	0.113	0.113	-0.070	0.0636	NS
KLHL6	-0.036	0.110	0.033	0.109	-0.069	0.0566	NS
PIK3CA	-0.547	0.231	-0.478	0.288	-0.069	0.4733	NS
VWA5B2	-0.259	0.135	-0.191	0.103	-0.068	0.0515	NS
DVL3	-0.199	0.132	-0.132	0.115	-0.067	0.0819	NS
LIPH	-0.045	0.155	0.022	0.099	-0.067	0.0446	*
SAMD7	0.099	0.148	0.165	0.102	-0.066	0.0532	NS
DGKG	-0.022	0.163	0.044	0.103	-0.065	0.0595	NS
GP5	0.045	0.096	0.109	0.100	-0.064	0.0556	NS
PIGZ	0.018	0.144	0.081	0.105	-0.064	0.0722	NS
CLCN2	-0.043	0.136	0.020	0.096	-0.063	0.0529	NS
IQCG	-0.058	0.109	0.004	0.105	-0.062	0.0803	NS
RPL22L1	-0.281	0.194	-0.221	0.175	-0.060	0.3037	NS
LRRC31	0.035	0.162	0.094	0.099	-0.060	0.0753	NS
KNG1	-0.160	0.088	-0.100	0.108	-0.059	0.1008	NS
LRRC34	-0.058	0.102	0.000	0.111	-0.058	0.1183	NS
PARL	-0.388	0.123	-0.331	0.137	-0.056	0.2204	NS
PIGX	-0.116	0.104	-0.060	0.125	-0.056	0.1813	NS
C3ORF70	-0.132	0.144	-0.077	0.101	-0.055	0.1045	NS
P3H2	0.030	0.170	0.085	0.095	-0.055	0.0877	NS
MASP1	-0.016	0.143	0.037	0.101	-0.053	0.1157	NS
MAP3K13	-0.087	0.123	-0.034	0.096	-0.053	0.982	NS
GHSR	0.088	0.171	0.140	0.113	-0.052	0.1703	NS
MYNN	-0.068	0.150	-0.016	0.116	-0.052	0.184	NS
CCDC50	0.003	0.101	0.053	0.110	-0.051	0.1666	NS
GPR160	-0.012	0.124	0.038	0.113	-0.050	0.1851	NS
DNAJB11	-0.313	0.151	-0.263	0.184	-0.050	0.4196	NS
ATP11B	-0.138	0.088	-0.092	0.112	-0.046	0.2175	NS
SST	0.113	0.171	0.159	0.106	-0.046	0.1979	NS
TPRG1	0.005	0.169	0.050	0.112	-0.045	0.236	NS
SLITRK3	0.034	0.127	0.079	0.107	-0.045	0.2152	NS
HES1	-0.239	0.093	-0.195	0.154	-0.044	0.394	NS
LRRC15	-0.235	0.143	-0.192	0.120	-0.043	0.2874	NS
SLC7A14	-0.023	0.186	0.020	0.103	-0.043	0.2199	NS
CLDN1	-0.093	0.127	-0.051	0.099	-0.042	0.2115	NS
BCHE	0.009	0.041	0.051	0.110	-0.042	0.2581	NS
OSTN	0.130	0.092	0.169	0.102	-0.040	0.2445	NS
TBCCD1	0.066	0.126	0.105	0.106	-0.038	0.2812	NS
HTR3E	-0.046	0.169	-0.009	0.102	-0.037	0.2796	NS
CLDN11	-0.113	0.157	-0.075	0.102	-0.037	0.2783	NS
FETUB	-0.176	0.116	-0.140	0.102	-0.037	0.2864	NS
CLDN16	0.056	0.167	0.092	0.105	-0.035	0.3209	NS
HRG	-0.025	0.099	0.010	0.110	-0.034	0.3664	ns
EHHADH	-0.002	0.153	0.032	0.088	-0.034	0.2613	NS
ACTRT3	-0.147	0.179	-0.118	0.111	-0.029	0.437	NS
TMEM212	-0.021	0.081	0.006	0.095	-0.028	0.3815	NS

Gene	Dependency 3q Amplified Cell lines		Dependency Not 3q Amplied		Differential Dependency	P-Value	
	Mean (n=9)	SD	Mean (N=972)	SD	(Mean Amp - Mean No Amp)	(uncorrected)	
TMEM44	-0.265	0.091	-0.239	0.119	-0.026	0.512	NS
ZNF639	-0.012	0.142	0.012	0.127	-0.024	0.5734	NS
TTC14	-0.248	0.129	-0.224	0.166	-0.024	0.6673	NS
SENP2	-0.089	0.164	-0.066	0.135	-0.023	0.6111	NS
TM4SF19	0.052	0.112	0.071	0.088	-0.019	0.514	NS
GMNC	-0.033	0.127	-0.014	0.104	-0.019	0.5919	NS
ATP13A3	-0.067	0.070	-0.049	0.121	-0.018	0.6643	NS
SKIL	-0.028	0.071	-0.011	0.115	-0.018	0.6471	NS
AHSG	0.048	0.126	0.064	0.107	-0.016	0.6648	NS
ZMAT3	0.113	0.086	0.126	0.115	-0.014	0.7189	NS
SMCO1	0.072	0.111	0.085	0.091	-0.013	0.677	NS
LRRIQ4	-0.012	0.185	0.001	0.109	-0.012	0.735	NS
ST6GAL1	0.160	0.196	0.172	0.099	-0.012	0.7212	NS
MB21D2	-0.031	0.116	-0.022	0.102	-0.008	0.8059	NS
KLHL24	0.015	0.083	0.022	0.096	-0.007	0.8255	NS
ZDHHC19	-0.090	0.128	-0.084	0.107	-0.006	0.862	NS
PHC3	0.125	0.103	0.130	0.112	-0.005	0.8859	NS
ACAP2	-0.038	0.100	-0.034	0.134	-0.004	0.9204	NS
ATP13A5	0.144	0.112	0.148	0.087	-0.003	0.9064	NS
TNIK	0.004	0.063	0.007	0.106	-0.003	0.9274	NS
HTR3D	-0.018	0.086	-0.015	0.102	-0.003	0.9271	NS
SPATA16	-0.005	0.061	-0.003	0.090	-0.002	0.9537	NS
CPN2	-0.037	0.120	-0.036	0.115	-0.001	0.981	NS
TMEM41A	-0.051	0.147	-0.051	0.146	-0.001	0.9892	NS
RTP1	-0.114	0.139	-0.113	0.098	-0.001	0.9864	NS
PLD1	-0.001	0.120	0.000	0.114	0.000	0.9942	NS
KCNMB2	0.132	0.116	0.130	0.101	0.002	0.9569	NS
PEX5L	0.041	0.152	0.038	0.116	0.004	0.9259	NS
FGF12	0.091	0.122	0.087	0.095	0.004	0.9003	NS
NCBP2	-1.657	0.200	-1.662	0.196	0.005	0.9449	NS
NLGN1	-0.038	0.071	-0.043	0.106	0.005	0.8906	NS
TNK2	0.154	0.123	0.146	0.106	0.008	0.8286	NS
SLC2A2	0.044	0.134	0.035	0.103	0.009	0.7999	NS
RPL39L	0.038	0.090	0.028	0.112	0.010	0.7908	NS
ADIPOQ	0.114	0.109	0.104	0.106	0.010	0.7766	NS
ABCF3	0.071	0.109	0.060	0.109	0.011	0.7571	NS
RTP4	0.139	0.128	0.128	0.085	0.011	0.687	NS
SERPINI2	0.075	0.075	0.063	0.094	0.012	0.7013	NS
ETV5	-0.031	0.130	-0.044	0.150	0.013	0.7943	NS
IL1RAP	0.008	0.136	-0.006	0.123	0.014	0.7384	NS
DCUN1D1	-0.024	0.168	-0.039	0.139	0.015	0.7479	NS
KCNMB3	0.193	0.091	0.176	0.092	0.017	0.5788	NS
MFN1	-0.040	0.110	-0.059	0.127	0.019	0.6561	NS
NDUFB5	-0.347	0.134	-0.366	0.158	0.019	0.7207	NS
SENP5	0.101	0.124	0.072	0.097	0.029	0.3762	NS
SEC62	-0.401	0.117	-0.430	0.192	0.029	0.6525	NS
CEP19	-0.049	0.148	-0.078	0.103	0.029	0.3982	NS
EIF4A2	-0.073	0.105	-0.102	0.122	0.030	0.4658	NS
OTOL1	0.023	0.074	-0.008	0.110	0.031	0.4025	NS
SI	0.043	0.118	0.012	0.101	0.031	0.3628	NS
UBXN7	-0.009	0.103	-0.041	0.128	0.031	0.4625	NS
NCEH1	0.011	0.141	-0.023	0.118	0.033	0.4049	NS
FAM43A	0.076	0.122	0.043	0.098	0.033	0.3105	NS
LPP	0.080	0.121	0.046	0.098	0.034	0.3081	NS
UTS2B	0.089	0.080	0.052	0.107	0.037	0.3033	NS
SERPINI1	0.082	0.074	0.043	0.097	0.039	0.2316	NS
DNAJC19	-0.135	0.179	-0.175	0.252	0.040	0.635	NS
ATP13A4	0.100	0.131	0.052	0.106	0.047	0.1862	NS
PRKCI	-0.050	0.112	-0.097	0.179	0.048	0.4282	NS
MECOM	0.060	0.133	0.010	0.173	0.049	0.3952	NS
NAALADL2	0.295	0.130	0.246	0.105	0.050	0.1609	NS
PPP1R2	-0.825	0.205	-0.881	0.250	0.056	0.5019	NS
ALG3	0.075	0.070	0.012	0.156	0.062	0.2337	NS
PAK2	-0.189	0.262	-0.257	0.211	0.068	0.3385	NS
GNB4	0.076	0.130	0.005	0.125	0.071	0.0901	NS
TRA2B	-0.572	0.212	-0.653	0.275	0.081	0.3792	NS
RPL35A	-0.785	0.107	-0.867	0.177	0.082	0.1656	NS
YEATS2	-0.474	0.087	-0.557	0.164	0.083	0.1288	NS
ZBBX	0.173	0.091	0.086	0.120	0.087	0.0307	*
TFRC	-0.797	0.283	-0.890	0.365	0.093	0.4474	NS
OPA1	-0.502	0.129	-0.596	0.170	0.093	0.1022	NS
MRPL47	-0.358	0.124	-0.457	0.170	0.099	0.0833	NS
NMD3	-0.930	0.174	-1.032	0.155	0.102	0.0495	*
LSG1	-0.890	0.135	-1.001	0.172	0.111	0.0536	NS
RNF168	-0.436	0.197	-0.555	0.234	0.118	0.1312	NS
TBL1XR1	-0.240	0.216	-0.376	0.264	0.136	0.1227	NS
AP2M1	-0.663	0.212	-0.823	0.280	0.161	0.0859	NS
RFC4	-0.735	0.103	-0.913	0.158	0.178	0.0008	***
PSMD2	-1.077	0.169	-1.262	0.186	0.185	0.003	**
EIF4G1	-0.660	0.161	-0.850	0.193	0.189	0.0034	**
EIF2B5	-0.806	0.163	-1.012	0.162	0.206	0.0002	***
PDCD10	0.499	0.356	0.280	0.257	0.219	0.0112	*
ACTL6A	-1.146	0.163	-1.374	0.191	0.227	0.0004	***
PCYT1A	-0.462	0.195	-0.694	0.333	0.232	0.0371	*
ECT2	-0.801	0.195	-1.039	0.224	0.238	0.0016	**
POLR2H	-0.961	0.222	-1.207	0.190	0.246	0.0001	***

Table 33: 3q amplification status and dependency on genes in 3q26-29, analysis for all non-haematological cell lines. Differential CERES-corrected dependency scores for 3q amplified cell lines versus (n=9) non-3q-amplified cell lines (n=972). Data obtained from DepMap (204), with analysis on R using R Studio. Statistical analysis using unpaired two-tailed T-test, with uncorrected p values displayed. * P <0.05, ** P<0.01, *** P <0.001, **** p<0.0001)

Gene	Dependency 3q Amplified Cell lines		Dependency Not 3q Amplified		Differential Dependency	P-Value	
	Mean (n=9)	SD	Mean (N=109)	SD	(Mean Amp - Mean No Amp)	(uncorrected)	
SOX2	**-0.721**	**0.475**	**-0.167**	**0.231**	**-0.555**	**<0.0001**	****
MUC20	-0.424	0.317	-0.216	0.155	-0.208	0.001	***
TP63	-0.445	0.232	-0.26	0.382	-0.186	0.154	NS
CRYGS	-0.242	0.153	-0.074	0.102	-0.168	<0.0001	****
THPO	-0.175	0.162	-0.021	0.087	-0.154	<0.0001	****
B3GNT5	-0.272	0.124	-0.123	0.151	-0.149	0.005	**
FAM131A	-0.169	0.124	-0.023	0.089	-0.146	<0.0001	***
MAGEF1	-0.110	0.17	0.030	0.102	-0.140	0.000	***
USP13	-0.106	0.107	0.032	0.097	-0.139	<0.0001	****
XXYLT1	-0.314	0.156	-0.181	0.125	-0.134	0.003	**
MAP6D1	-0.225	0.103	-0.097	0.109	-0.128	0.001	***
FNDC3B	-0.175	0.189	-0.051	0.159	-0.124	0.028	*
BCL6	-0.139	0.122	-0.025	0.114	-0.114	0.005	**
MCCC1	-0.139	0.110	-0.025	0.103	-0.114	0.002	**
DLG1	-0.100	0.132	0.006	0.116	-0.106	0.01	*
CAMK2N2	-0.127	0.129	-0.024	0.08	-0.103	0.001	***
NRROS	-0.129	0.116	-0.026	0.097	-0.103	0.003	**
FXR1	-0.011	0.172	0.090	0.131	-0.101	0.033	*
ABCC5	-0.024	0.098	0.070	0.099	-0.095	0.007	**
CHRD	-0.082	0.139	0.013	0.09	-0.094	0.005	**
LAMP3	-0.061	0.133	0.029	0.084	-0.090	0.004	**
MCF2L2	-0.111	0.131	-0.022	0.095	-0.089	0.01	*
MELTF	-0.129	0.148	-0.041	0.087	-0.088	0.007	**
RTP2	-0.112	0.184	-0.025	0.086	-0.088	0.009	***
CCDC39	-0.115	0.158	-0.028	0.099	-0.087	0.018	*
APOD	-0.13	0.162	-0.044	0.105	-0.087	0.025	*
RUBCN	-0.008	0.095	0.078	0.102	-0.086	0.016	*
HTR3C	-0.073	0.131	0.012	0.104	-0.084	0.024	*
TNFSF10	-0.054	0.22	0.029	0.187	-0.082	0.213	NS
FBXO45	0.019	0.093	0.098	0.101	-0.079	0.026	*
RPL22L1	-0.281	0.194	-0.204	0.124	-0.077	0.09	NS
LRCH3	-0.130	0.129	-0.054	0.116	-0.076	0.064	NS
GOLIM4	-0.041	0.181	0.031	0.12	-0.072	0.101	NS
KLHL6	-0.036	0.11	0.035	0.105	-0.071	0.054	NS
LIPH	-0.045	0.155	0.025	0.086	-0.070	0.031	*
DGKG	-0.022	0.163	0.048	0.099	-0.069	0.059	NS
SLC51A	-0.057	0.169	0.012	0.094	-0.069	0.05	NS
CCDC50	0.003	0.101	0.071	0.083	-0.069	0.02	NS
TTC14	-0.248	0.129	-0.179	0.127	-0.069	0.124	NS
EPHB3	-0.153	0.195	-0.085	0.109	-0.068	0.095	NS
FYTTD1	-0.108	0.107	-0.04	0.101	-0.068	0.056	NS
PIGX	-0.116	0.104	-0.048	0.111	-0.067	0.082	NS
IGF2BP2	-0.372	0.144	-0.306	0.093	-0.066	0.052	NS
MUC4	-0.046	0.147	0.02	0.101	-0.066	0.074	NS
WDR53	-0.153	0.15	-0.087	0.089	-0.066	0.047	*
EIF5A2	0.043	0.155	0.108	0.11	-0.065	0.101	NS
BDH1	-0.104	0.134	-0.038	0.087	-0.065	0.041	*
SAMD7	0.099	0.148	0.163	0.1	-0.065	0.076	NS
KNG1	-0.16	0.088	-0.097	0.098	-0.063	0.066	NS
LMLN	-0.244	0.159	-0.185	0.096	-0.059	0.095	NS
IQCG	-0.058	0.109	0	0.093	-0.058	0.077	NS
LRRC31	0.035	0.162	0.093	0.09	-0.058	0.088	NS
C3ORF70	-0.132	0.144	-0.075	0.088	-0.058	0.076	NS
DVL3	-0.199	0.132	-0.144	0.093	-0.055	0.1	NS
CLCN2	-0.043	0.136	0.012	0.076	-0.055	0.056	NS
SST	0.113	0.171	0.167	0.091	-0.053	0.122	NS
LRRC34	-0.058	0.102	-0.005	0.104	-0.053	0.143	NS
BCHE	0.009	0.041	0.061	0.098	-0.052	0.119	NS
VPS8	-0.238	0.128	-0.187	0.167	-0.051	0.37	NS
MASP1	-0.016	0.143	0.036	0.094	-0.051	0.136	NS
GP5	0.045	0.096	0.095	0.092	-0.05	0.12	NS
HTR3E	-0.046	0.169	0.002	0.105	-0.048	0.212	NS
MYNN	-0.068	0.150	-0.02	0.103	-0.048	0.203	NS
OSTN	0.130	0.092	0.177	0.096	-0.047	0.16	NS
PIGZ	0.018	0.144	0.064	0.098	-0.046	0.197	NS
SLITRK3	0.034	0.127	0.077	0.111	-0.042	0.278	NS
PARL	-0.388	0.123	-0.346	0.132	-0.041	0.367	NS
VWA5B2	-0.259	0.135	-0.218	0.106	-0.041	0.283	NS
GHSR	0.088	0.171	0.128	0.12	-0.04	0.35	NS
TBCCD1	0.066	0.126	0.106	0.087	-0.04	0.21	NS
ZNF639	-0.012	0.142	0.027	0.107	-0.038	0.804	NS
DNAJB11	-0.313	0.151	-0.275	0.148	-0.038	0.459	NS
TFRC	-0.797	0.283	-0.759	0.301	-0.038	0.713	NS
ATP13A3	-0.067	0.07	-0.032	0.108	-0.035	0.345	NS
MAP3K13	-0.087	0.123	-0.055	0.089	-0.033	0.307	NS
NCBP2	-1.657	0.200	-1.625	0.189	-0.032	0.624	NS
CLDN1	-0.093	0.127	-0.062	0.090	-0.031	0.337	NS
TM4SF19	0.052	0.112	0.082	0.081	-0.030	0.301	NS
NDUFB5	-0.347	0.134	-0.317	0.156	-0.030	0.577	NS
EHHADH	-0.002	0.153	0.027	0.074	-0.029	0.307	NS
LRRC15	-0.235	0.143	-0.207	0.108	-0.028	0.461	NS
HES1	-0.239	0.093	-0.211	0.121	-0.028	0.497	NS
ATP11B	-0.138	0.088	-0.11	0.108	-0.028	0.453	NS
SLC7A14	-0.023	0.186	0.004	0.094	-0.027	0.449	NS
GPR160	-0.012	0.124	0.014	0.098	-0.026	0.446	NS
HRG	-0.025	0.099	0.002	0.099	-0.026	0.444	NS
FETUB	-0.176	0.116	-0.150	0.09	-0.026	0.41	NS

Gene	Dependency 3q Amplified Cell lines		Dependency Not 3q Amplified		Differential Dependency	P-Value	
	Mean (n=9)	SD	Mean (N=109)	SD	(Mean Amp - Mean No Amp)	(uncorrected)	
P3H2	0.03	0.170	0.055	0.086	-0.025	0.442	NS
SPATA16	-0.005	0.061	0.015	0.089	-0.020	0.505	NS
DNAJC19	-0.135	0.179	-0.115	0.231	-0.020	0.154	NS
ZMAT3	0.113	0.086	0.132	0.101	-0.020	0.575	NS
CLDN11	-0.113	0.157	-0.093	0.109	-0.020	0.619	NS
KLHL24	0.015	0.083	0.033	0.082	-0.018	0.523	NS
TMEM212	-0.021	0.081	-0.004	0.093	-0.018	0.581	NS
SMCO1	0.072	0.111	0.09	0.083	-0.018	0.549	NS
UBXN7	-0.009	0.103	0.006	0.103	-0.016	0.662	NS
SENP2	-0.089	0.164	-0.073	0.117	-0.015	0.72	NS
ATP13A5	0.144	0.112	0.159	0.089	-0.015	0.638	NS
SKIL	-0.028	0.071	-0.013	0.104	-0.015	0.676	NS
GMNC	-0.033	0.127	-0.018	0.097	-0.014	0.676	NS
TPRG1	0.005	0.169	0.016	0.111	-0.011	0.79	NS
TRA2B	-0.572	0.212	-0.562	0.180	-0.01	0.871	NS
ST6GAL1	0.16	0.196	0.17	0.086	-0.01	0.765	NS
CPN2	-0.037	0.12	-0.028	0.091	-0.009	0.791	NS
AHSG	0.048	0.126	0.057	0.099	-0.009	0.807	NS
CLDN16	0.056	0.167	0.065	0.110	-0.008	0.837	NS
KCNMB2	0.132	0.116	0.14	0.098	-0.008	0.911	NS
TMEM44	-0.265	0.091	-0.258	0.106	-0.007	0.854	NS
PHC3	0.125	0.103	0.13	0.093	-0.005	0.868	NS
LRRIQ4	-0.012	0.185	-0.007	0.120	-0.004	0.918	NS
ACTRT3	-0.147	0.179	-0.143	0.106	-0.004	0.92	NS
TNK2	0.154	0.123	0.155	0.093	-0.001	0.965	NS
TMEM41A	-0.051	0.147	-0.051	0.143	0.000	0.992	NS
MB21D2	-0.031	0.116	-0.031	0.097	0.000	0.996	NS
FGF12	0.091	0.122	0.088	0.084	0.002	0.939	NS
RTP4	0.139	0.128	0.137	0.091	0.002	0.94	NS
SEC62	-0.401	0.117	-0.405	0.144	0.004	0.933	NS
RTP1	-0.114	0.139	-0.118	0.094	0.004	0.898	NS
MFN1	-0.04	0.11	-0.045	0.124	0.005	0.802	NS
TNIK	0.004	0.063	-0.003	0.093	0.007	0.823	NS
PLD1	-0.001	0.12	-0.008	0.092	0.007	0.82	NS
ETV5	-0.031	0.13	-0.039	0.106	0.008	0.841	NS
HTR3D	-0.018	0.086	-0.026	0.102	0.008	0.826	NS
KCNMB3	0.193	0.091	0.185	0.091	0.008	0.463	NS
IL1RAP	0.008	0.136	-0.001	0.111	0.009	0.826	NS
PEX5L	0.041	0.152	0.032	0.110	0.01	0.316	NS
ZDHHC19	-0.09	0.128	-0.101	0.100	0.011	0.766	NS
RPL39L	0.038	0.09	0.027	0.100	0.011	0.75	NS
ADIPOQ	0.114	0.109	0.102	0.102	0.012	0.745	NS
ACAP2	-0.038	0.1	-0.05	0.151	0.012	0.817	NS
NLGN1	-0.038	0.071	-0.05	0.094	0.012	0.71	NS
SERPINI1	0.082	0.074	0.067	0.089	0.015	0.617	NS
CEP19	-0.049	0.148	-0.064	0.087	0.015	0.631	NS
SERPINI2	0.075	0.075	0.057	0.091	0.017	0.579	NS
ABCF3	0.071	0.109	0.052	0.106	0.019	0.6	NS
SENP5	0.101	0.124	0.08	0.079	0.02	0.479	NS
PRKCI	-0.050	0.112	-0.071	0.128	0.022	0.625	NS
EIF4A2	-0.073	0.105	-0.099	0.11	0.026	0.496	NS
SLC2A2	0.044	0.134	0.017	0.096	0.026	0.446	NS
OTOL1	0.023	0.074	-0.01	0.108	0.033	0.375	NS
NAALADL2	0.295	0.13	0.263	0.107	0.033	0.386	NS
DCUN1D1	-0.024	0.168	-0.059	0.132	0.035	0.46	NS
UTS2B	0.089	0.08	0.048	0.101	0.041	0.24	NS
LPP	0.080	0.121	0.037	0.083	0.042	0.157	NS
FAM43A	0.076	0.122	0.03	0.112	0.046	0.242	NS
RPL35A	-0.785	0.107	-0.834	0.149	0.048	0.341	NS
ATP13A4	0.100	0.131	0.05	0.093	0.049	0.141	NS
LSG1	-0.890	0.135	-0.941	0.146	0.051	0.311	NS
SI	0.043	0.118	-0.009	0.099	0.052	0.143	NS
GNB4	0.076	0.130	0.022	0.118	0.054	0.194	NS
NCEH1	0.011	0.141	-0.046	0.119	0.056	0.184	NS
MECOM	0.06	0.133	0	0.161	0.059	0.285	NS
PIK3CA	-0.547	0.231	-0.609	0.24	0.061	0.804	NS
NMD3	-0.93	0.174	-0.997	0.149	0.067	0.204	NS
OPA1	-0.502	0.129	-0.572	0.131	0.069	0.13	NS
MRPL47	-0.358	0.124	-0.433	0.152	0.074	0.158	NS
ALG3	0.075	0.07	-0.001	0.147	0.076	0.129	NS
YEATS2	-0.474	0.087	-0.552	0.151	0.078	0.13	NS
PSMD2	-1.077	0.169	-1.158	0.148	0.081	0.119	NS
ZBBX	0.173	0.091	0.091	0.105	0.082	0.025	*
AP2M1	-0.663	0.212	-0.746	0.213	0.083	0.262	NS
PAK2	-0.189	0.262	-0.273	0.179	0.083	0.198	NS
PPP1R2	-0.825	0.205	-0.912	0.175	0.087	0.16	NS
EIF4G1	-0.66	0.161	-0.792	0.140	0.131	0.009	**
RNF168	-0.436	0.197	-0.576	0.188	0.14	0.035	*
RFC4	-0.735	0.103	-0.877	0.139	0.142	0.003	**
PDCD10	0.499	0.356	0.341	0.273	0.158	0.106	NS
EIF2B5	-0.806	0.163	-0.972	0.159	0.166	0.003	**
ACTL6A	-1.146	0.163	-1.317	0.144	0.171	0.001	***
PCYT1A	-0.462	0.195	-0.637	0.301	0.176	0.089	NS
TBL1XR1	-0.24	0.216	-0.453	0.250	0.213	0.015	*
POLR2H	-0.961	0.222	-1.200	0.182	0.239	0.0001	***
ECT2	-0.801	0.195	-1.076	0.225	0.275	0.0016	***

Table 34: 3q amplification status and dependency on genes in 3q26-29, analysis for all squamous cell lines. Differential CERES-corrected dependency scores for 3q amplified cell lines versus (n=9) non-3q-amplified cell lines (n=109). Data obtained from DepMap (204), with analysis on R using R Studio. Statistical analysis using unpaired two-tailed T-test, with uncorrected p values displayed. * P <0.05, ** P<0.01, *** P <0.001, **** p<0.0001)

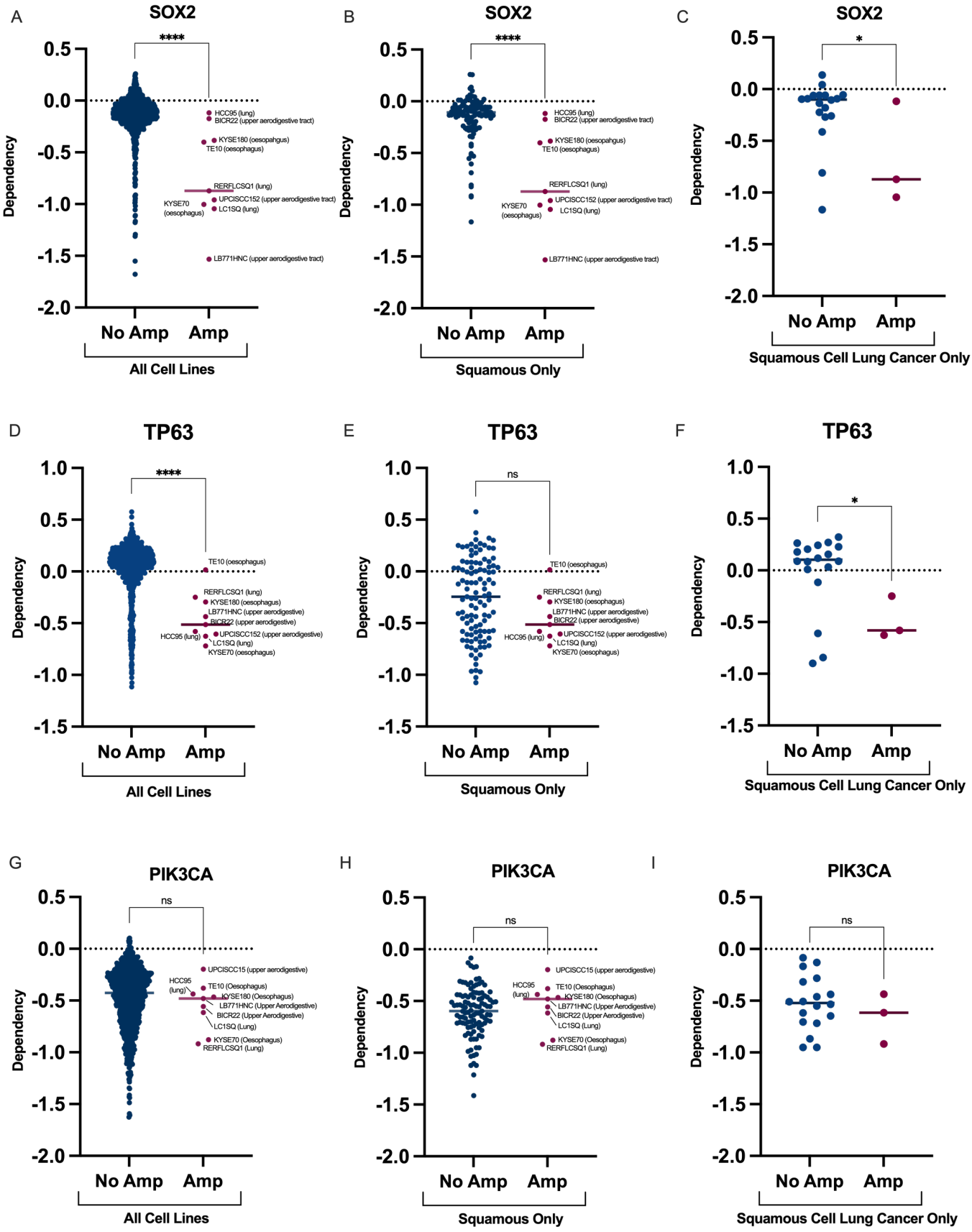

Figure 30: 3q amplification status and dependency on SOX2 (A-C), TP63 (D-F) and PIK3CA (G-I) in 3q amplified vs non-amplified lines. 3q amplified cell lines (n=9), non-3q-amplified squamous cell lines (n=109) non-3q-amplified all non-haematological cell lines (n=972) Data obtained from DepMap (204). Statistical analysis using unpaired two-tailed T-test, with uncorrected p values displayed. * P <0.05, ** P<0.01, *** P <0.001, **** p<0.0001)

5.3.2.2 Association Between Squamous Histology and SOX2 and TP63 Dependency

TP63, *PIK3CA* and *SOX2* are drivers of squamous histology (255-258). It is therefore important to assess whether dependency on *SOX2*, *PIK3CA* and *TP63* is a wider characteristic of squamous origin cell lines, rather than being a specific feature of 3q amplification (Figure 31). Squamous cancer cell lines showed significantly higher *SOX2* and *PIK3CA* dependency than non-squamous cancer cell lines, although this effect was relatively modest. Mean *SOX2* dependency in squamous and non-squamous solid cancer lines were -0.2318 (SEM ± 0.0250) and -0.1649 (SEM ± 0.00619), respectively.

Squamous solid cancer cell lines showed substantial increased dependency on *TP63* versus non-squamous solid cancer cell lines: mean *TP63* dependency was -0.3474 (SEM ± 0.0263) in squamous and -0.04482 (SEM ± 0.00506) in non-squamous solid cancer lines (P<0.0001). Therefore, the apparent increase in dependency of amplified cell lines on *TP63* may be at least partially explained by an overall increase in dependency across all squamous lines, potentially explaining the loss of significant relationship when analysis was restricted to squamous lines.

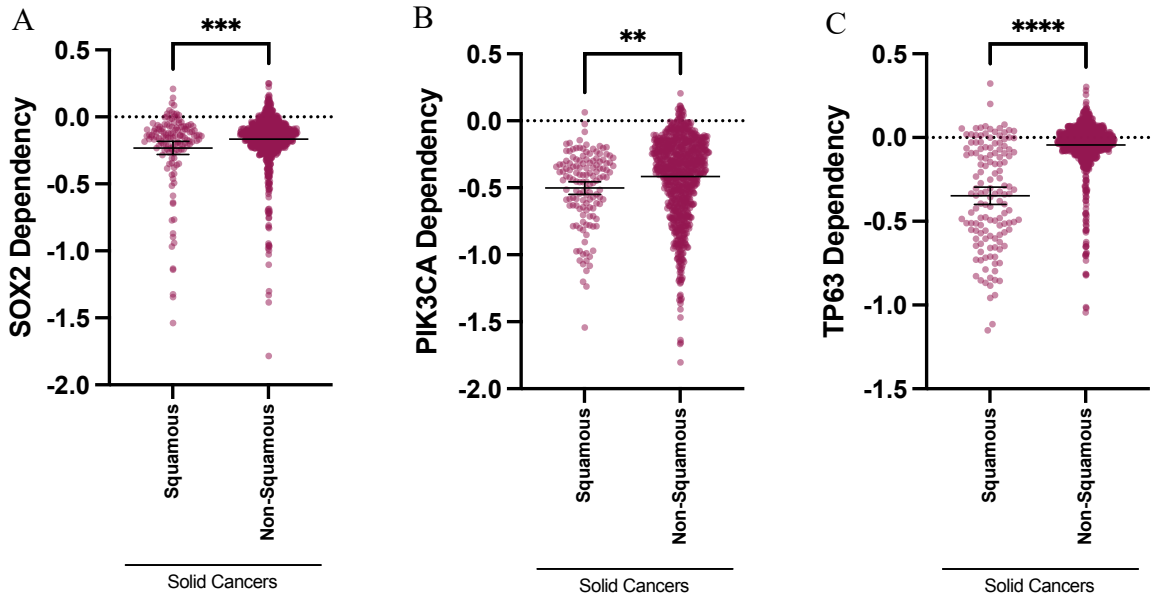

Figure 31: Relationship between squamous/non-squamous lineage of non-haematological cell lines and dependency of SOX2 (A), PIK3CA (B) and TP63 (C). Data obtained from DepMap. Individual values for SOX2 dependency are plotted, squamous cell lines, n=136; non-squamous cell lines = 853. Horizontal line indicates mean. 95% CI indicated. Statistical analysis with two-tailed unpaired t-test (Uncorrected P values displayed, * P <0.05, ** P<0.01, *** P <0.001, **** p<0.0001)

5.3.2.3 SOX2 Dependency Exhibits a Linear Relationship with SOX2 Copy Number in Squamous Cancer Cell Lines

The nature of the relationship between *SOX2* copy number and *SOX2* dependency was assessed in greater depth. Increasing relative *SOX2* copy number correlates with an increasing in *SOX2* dependency (Figure 32). When analysis was conducted across all solid cancer cell lines the strength of the association was weak (R^2 = 0.05588, P <0.0001). This correlation was stronger when analysis was restricted to squamous cell lines (R^2 = 0.2668, P<0.001), and was further strengthened by restriction to analysis of lung squamous (R^2 = 0.4018, P=0.0027) or oesophageal squamous lines (R^2 = 0.4225, P=0.006). The association was weaker in upper aerodigestive squamous lines (R^2 = 0.1256, P=0.0035), although proportion of *SOX2* amplified cell lines was much lower in this subpopulation. No other gene within the amplicon displayed as convincing a dose-response relationship, Similar analyses for *TP63* and *PIK3CA* are displayed for comparison in Figure 33 and Figure 34.

Overall, these results suggest that increasing *SOX2* copy number is strongly related to *SOX2* dependency in squamous lung and squamous oesophageal cancer cell lines. *SOX2* could therefore be a therapeutic target in 3q amplified squamous cell lung and oesophageal cancer, with the greatest benefit likely being in patients with high-level 3q amplification.

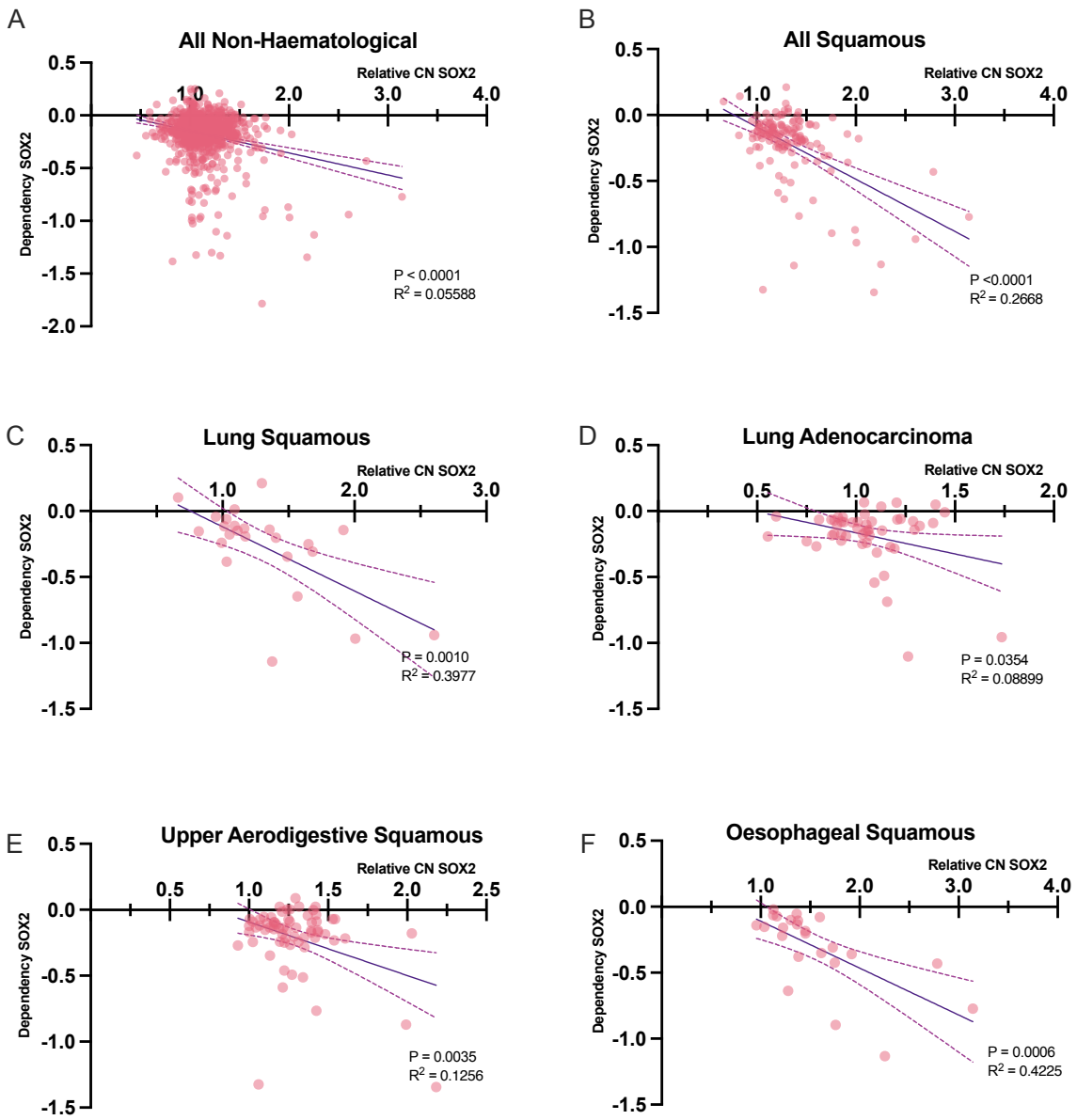

Figure 32: Relationship between relative *SOX2* copy number and *SOX2* Dependency in cancer cell lines. Relative *SOX2* copy number and *SOX2* dependency for cancer cell lines were extracted from DepMap. (A) Analysis across all non-haematological cell lines (n=981) (B) all squamous cell lines (n=135) (C) squamous cell lung cancer cell lines (n=24) (D) lung adenocarcinoma cell lines (n=50) upper aerodigestive squamous cell lines (n=65). Line plotted with simple linear regression; Correlation assessed using Pearson correlation co-efficient

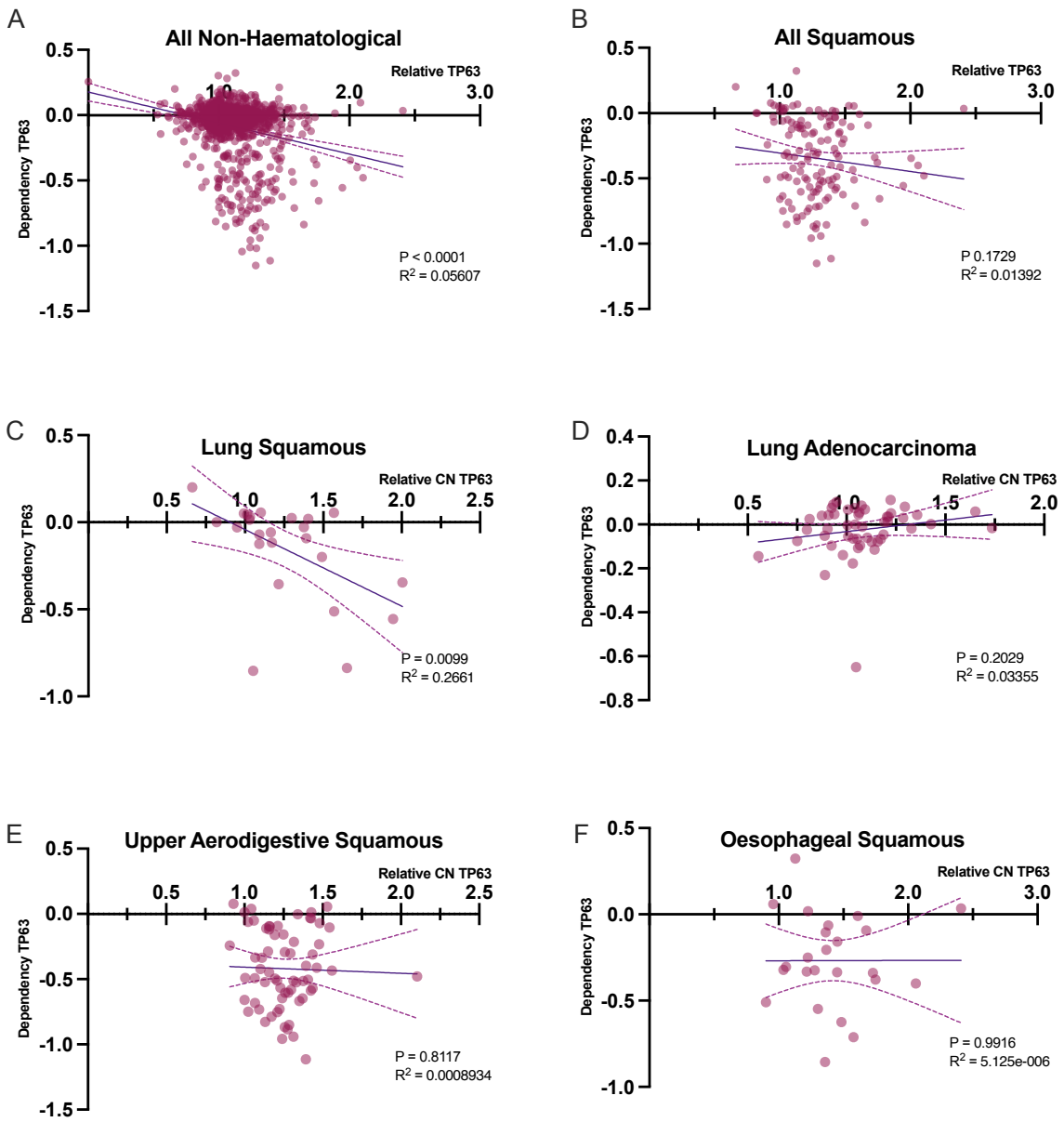

Figure 33: Relationship between *TP63* Copy Number and *TP63* Dependency. Relative TP63 copy number and TP63 dependency for cancer cell lines were extracted from DepMap. (A) Analysis across all non-haematological cell lines (n=981) (B) all squamous cell lines (n=135) (C) squamous cell lung cancer cell lines (n=24) (D) lung adenocarcinoma cell lines (n=50) upper aerodigestive squamous cell lines (n=65). Line plotted with simple linear regression; Correlation assessed using Pearson correlation co-efficient

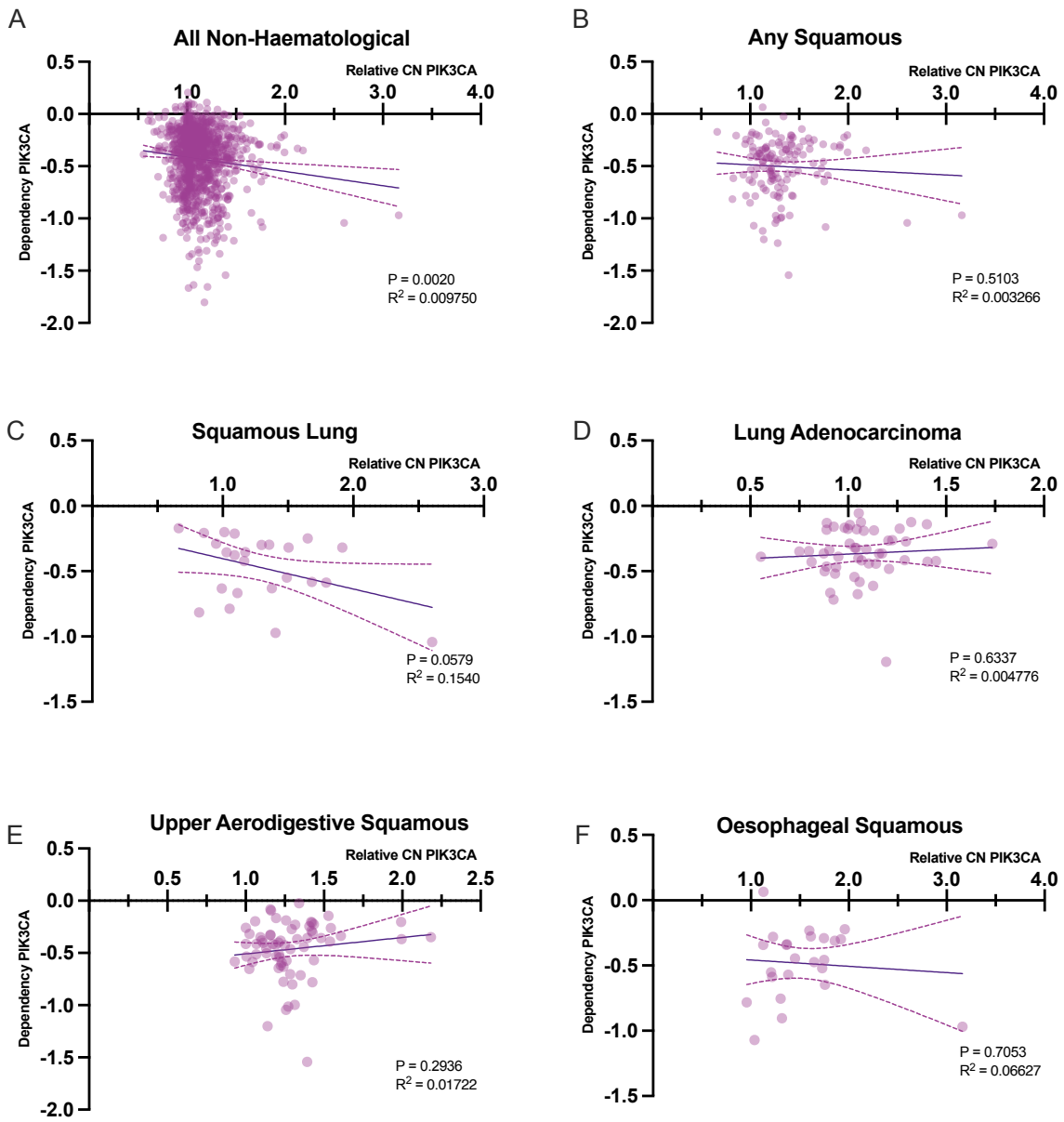

Figure 34: Relationship between *PIK3CA* Copy Number and *PIK3CA*. Dependency Relative *PIK3CA* copy number and *PIK3CA* dependency was extracted from DepMap. (A) Analysis across all non-haematological cell lines (n=981) (B) all squamous cell lines (n=135) (C) squamous cell lung cancer cell lines (n=24) (D) lung adenocarcinoma cell lines (n=50) upper aerodigestive squamous cell lines (n=65). Line plotted with simple linear regression; Correlation assessed using Pearson correlation co-efficient

5.3.3 Validation of SOX2 as a Target in 3q amplified squamous cell lung cancer

In section 3.4.2 it is demonstrated that *SOX2* is amongst the most frequently amplified genes within 3q26-29. In addition, 3q amplification is associated with increased dependency on *SOX2* in the analysis of a genome-wide CRISPR data from Depmap. Further analysis demonstrates a linear relationship between *SOX2* copy number and *SOX2* dependency. Overall, these results suggest that SOX2 could be a candidate for therapeutic targeting in 3q-amplified squamous cell lung cancer. SOX2 knockdown was therefore undertaken to validate and quantify this effect. siRNA was selected over CRISPR for these experiments to ensure that results from DepMap was validated with a second modality of SOX2 depletion.

5.3.3.1 Optimisation of SOX2 knockdown

Initial Optimisation: BLOCK-iT Alexa Fluor Red Fluorescent Control

Initial optimisation of transfection was performed using BLOCK-iT Alexa Fluor Red Fluorescent Control (Figure 35). Forward transfection with 20 nM BLOCK-iT achieved close to 100% transfection efficiency across a panel of cell lines.

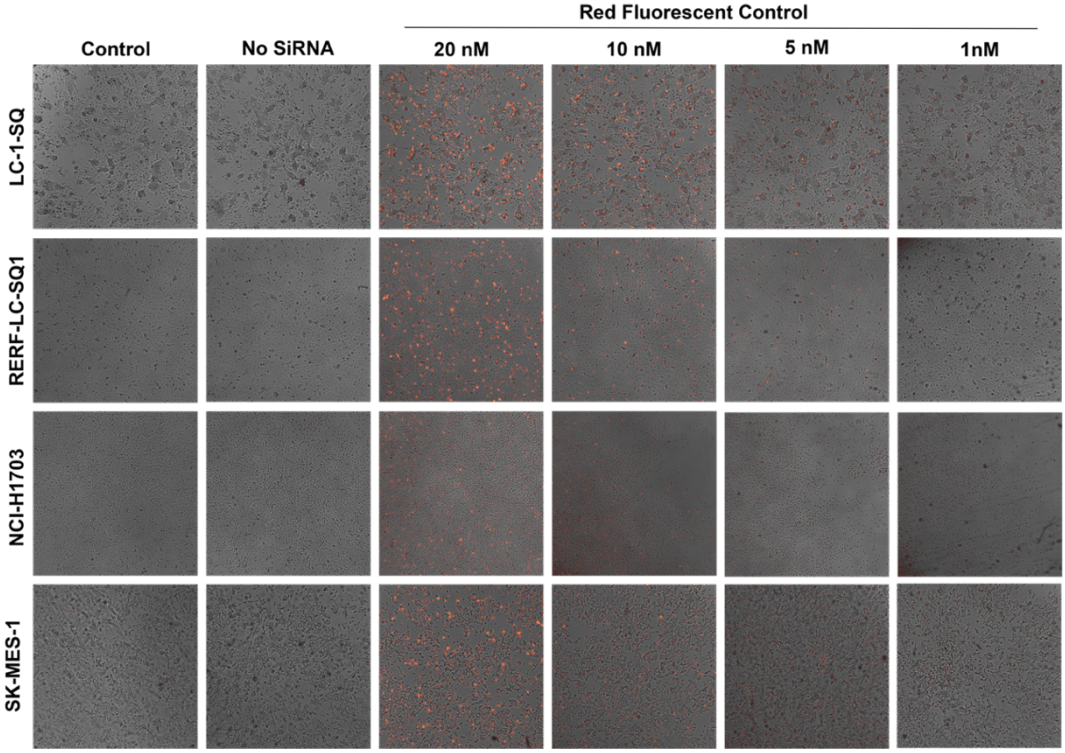

Figure 35: Optimisation of transfection using BLOCK-IT Alexa Fluorescent Control using forward transfection. Cells were seeded at 1 x 10^5 cells per well in a 24-well plate in antibiotic-free complete growth media. 24 hours after seeding BLOCK-IT Alexa Fluorescent Control/Lipofectamine duplexes were prepared according to manufacturer's instructions, at final concentrations of 0 – 20 nM. Untreated cells are also included as an additional negative control. After overnight incubation, media was changed and wells were imaged on the Cytation microscope using Gen5 to assess transfection efficiency

Forward Transfection

As 20 nM BLOCK-iT Alexa Fluorescent control achieved > 95% transfection efficiency across a panel of cell lines, this concentration of siRNA chosen for optimisation of SOX2 knockdown. Experiments were scaled up to a 6-well format to ensure sufficient protein extraction for western blotting for SOX2 expression. Transfection of RERF-LC-SQ1 with the S13294, S13295 and S13926 siRNAs achieved partial knockdown of SOX2, with greatest knockdown with S13294 and S13295 (Figure 36).

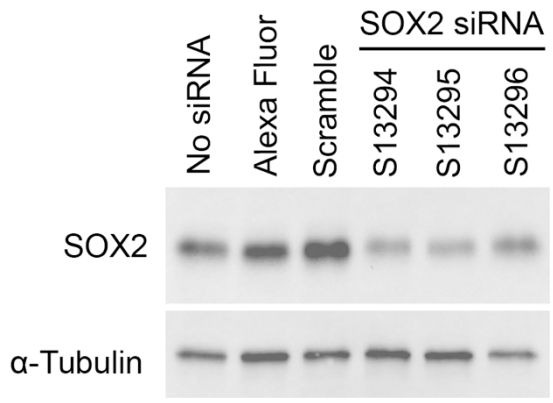

Figure 36: Selection of siRNA for ongoing optimisation of SOX2 knockdown (forward transfection). RERF-LC-SQ1 were seeded at 3 x 10^5 cells per well in a 6-well plate in antibiotic-free complete growth media. siRNA/Lipofectamine duplexes were prepared according to manufacturer's instructions, at final concentrations 20 nM. BLOCK-IT Alexa Fluorescent Control was used as a visual positive control to ensure maintained transfection efficiency. Mock transfection (lipofectamine without siRNA) and transfection with negative control siRNA (Scramble) were included as negative controls. Whole cell lysates were collected 24 hours post transfection, and SOX2 expression was assessed with Western blotting. α-Tubulin is included as a loading control.

Reverse transfection

Greatest knockdown was seen with S13294 and S13295, therefore these two siRNAs were selected for ongoing optimisation (Figure 37). SOX2 knockdown was optimised by use of reverse transfection, maintaining siRNA concentration of 20 nM. Timepoint of cell lysates collection was also extended to 48 hours. This approach achieved reliable and substantial reductions in SOX2 protein expression in 3q amplified cell lines (HCC2814 and RERF-LC-SQ1) and non-amplified cells (NCI-H1703) (Figure 37), and this approach was therefore used for ongoing knockdown experiments. These results also provide validation for both the D6D9 SOX2 antibody (Cell Signalling Technology, #3579) and SOX2 siRNAs (S13294 and S13295) for further experiments.

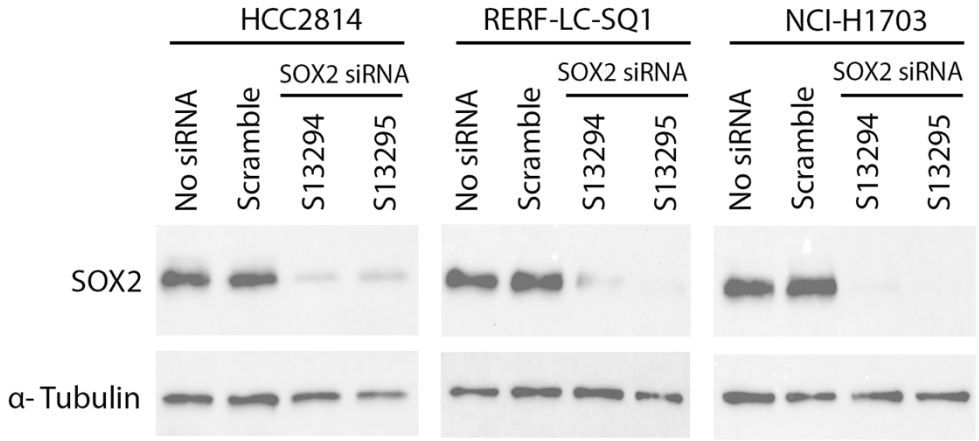

Figure 37: Optimised knockdown of SOX2 in squamous cell lung cancer cell lines (reverse transfection). siRNA/Lipofectamine duplexes were prepared according to manufacturer's instructions (to achieve final concentration of 20 nM in 6 well plate format). 3 x 10^5 cells in antibiotic-free media were added to the siRNA/Lipofectamine duplexes. Cells were incubated overnight, and antibiotic-free media was replaced with antibiotic-containing media. BLOCK-IT Alexa Fluorescent Control was used as a visual positive control to ensure maintained transfection efficiency. Mock transfection (lipofectamine without siRNA [no siRNA]) and transfection with negative control siRNA [Scramble] were included as negative controls. Whole cell lysates were collected 48 hours post transfection, and SOX2 expression was assessed with Western blotting. α-Tubulin is included as a loading control. Representative images from at least three independent replicates are shown.

5.3.3.2 Effect of siRNA knockdown on cell growth in squamous cell lung cancer cell lines

3q amplified squamous cell lung cancer cells

Impact of SOX2 knockdown using siRNA on cell growth was assessed in two 3q amplified cell lines: RERF-LC-SQ1 and HCC2814. HCC2814 and RERF-LC-SQ1 were selected as two cell lines with high-level amplification of 3q: relative and absolute copy number for *SOX2*, *ECT2*, *PIK3CA* and *PRKCI* was obtained from DepMap (210). Amplification was defined as relative copy number ≥ 1.8. High levels of SOX2 expression were confirmed on western blotting and immunofluorescence (not shown).

SOX2 knockdown with siRNA resulted in time-dependent reduction in proliferation for both cell lines, with greatest effect seen at extended time points. At 96 hours, SOX2 knockdown with S13295 in RERF-LC-SQ1 reduced proliferation by an average of 37.5% ($P < 0.0001$), and S13294 reduced proliferation by an average of 35.1% ($P < 0.0001$) (Figure 38). Likewise, at 96 hours, SOX2 knockdown with S13295 in HCC2814 reduced proliferation by 36.9% versus scramble ($P < 0.0001$), whilst S13294 reduced proliferation by 49.37% ($P < 0.0001$) (Figure 39). These results are consistent with analysis of the DepMap genome-wide CRISPR data, and suggest that SOX2 promotes cell survival and/or proliferation in 3q amplified cell lines.

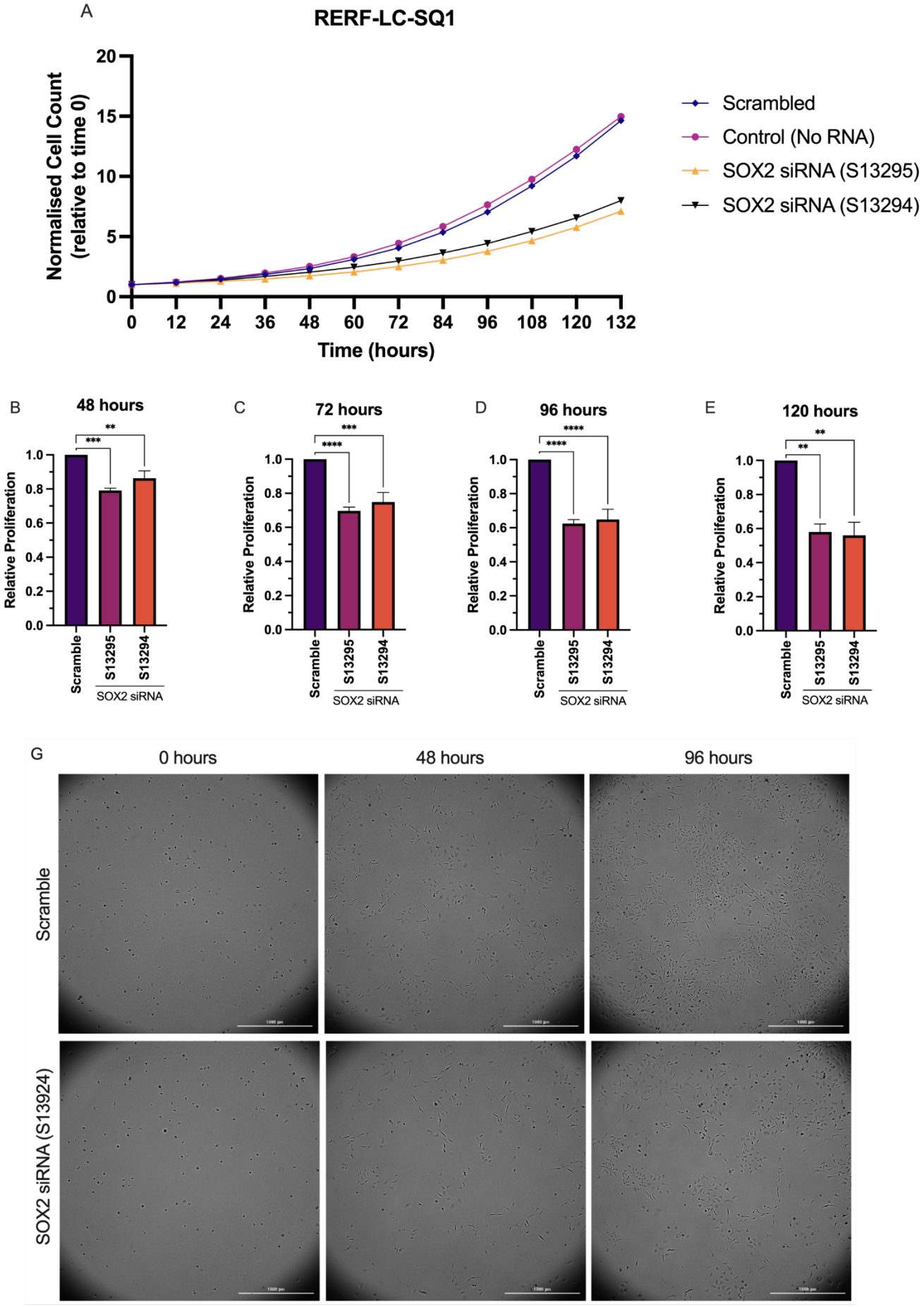
A
RERF-LC-SQ1
Normalised Cell Count (relative to time 0)
Time (hours)
Scrambled
Control (No RNA)
SOX2 siRNA (S13295)
SOX2 siRNA (S13294)
B
48 hours
C
72 hours
D
96 hours
E
120 hours
Relative Proliferation
Scramble
S13295
S13294
SOX2 siRNA
G
0 hours
48 hours
96 hours
Scramble
SOX2 siRNA (S13924)

Figure 38: Impact of SOX2 knockdown on cell proliferation in 3q amplified RERF-LC-SQ1 cell line (Overleaf). RERF-LC-SQ1 cells were transfected with negative control siRNA ('scramble'), SOX2 siRNA (S13925 or S13924) or mock transfected with no siRNA (Control). 24 hours post-transfection, cells were seeded at 500 cells per well in a 96 well plate and imaged 12 hourly on the Cytation 5 microscope. Automated cell counts were performed using Gen5. Experiment was performed five times, and for each biological replicate measurements were taken from at least 15 wells. Reads were stopped when confluency was reached, or images were no longer countable. (A) Representative cell growth curve from single experimental replicate, plotted as cell count relative to time 0, mean ± SEM. (B-E). Proliferation relative to scramble at indicated time points (mean ± SEM) (n=5 for all timepoints shown, average of independent replicates). Statistical analysis: one-way ANOVA with Dunnett's multiple comparisons test (* P <0.05, ** P<0.01, *** P <0.001, **** p<0.0001) (F) Representative raw images

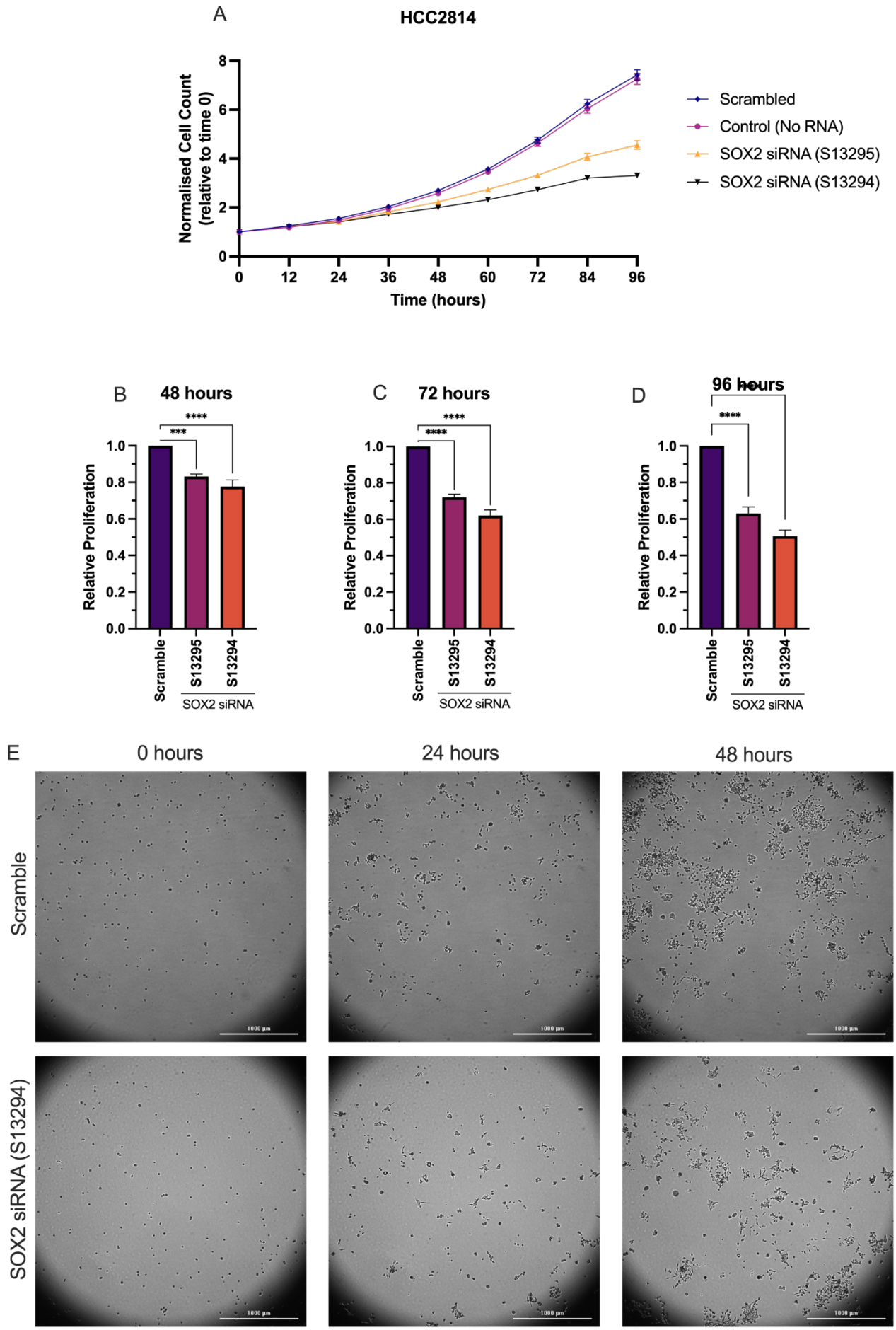
A
HCC2814
Normalised Cell Count (relative to time 0)
Time (hours)
Scrambled
Control (No RNA)
SOX2 siRNA (S13295)
SOX2 siRNA (S13294)
B
48 hours
C
72 hours
D
96 hours
Relative Proliferation
Scramble
S13295
S13294
SOX2 siRNA
E
0 hours
24 hours
48 hours
Scramble
SOX2 siRNA (S13294)

Figure 39: Impact of SOX2 knockdown on cell proliferation in 3q amplified HCC2814 cell line (Overleaf). HCC2814 cells were transfected with negative control siRNA ('scramble'), SOX2 siRNA (S13925 or S13924) or mock transfected with no siRNA (Control). 24 hours post-transfection, cells were seeded at 500 cells per well in a 96 well plate and imaged 12 hourly on the Cytation 5 microscope. Automated cell counts were performed using Gen5. For each biological replicate measurements were taken from at least 15 wells. Experiment was performed five times. Reads were stopped when confluency was reached, or images were no longer countable. (A) Representative cell growth curve from single experimental replicate, plotted as cell count relative to time 0, mean ± SEM. (B-D) Relative proliferation for scramble, S13925 and S13924 at indicated time points (mean ± SEM) (n=5, average of independent replicates, proliferation expressed relative to scramble). Statistical analysis: Sone-way ANOVA with Dunnett's multiple comparisons test (* $P < 0.05$, ** $P < 0.01$, *** $P < 0.001$, **** $p < 0.0001$) (F) Representative raw images (E) Representative raw images

Non 3q amplified squamous lung cancer cells

Impact of SOX2 knockdown using siRNA on cell growth was assessed in non-amplified cells. NCI-H1703 was selected due to absence of high-level amplification (relative copy number for *SOX2* and *PIK3CA* being 1.112 for both genes). It must be noted that low level copy number gain in 3q is almost universal in squamous cell lung cancer: in the TCGA Squamous Cell Lung Cancer dataset, 37 out of 466 tumours were diploid for *SOX2*, 241 of had CN gain, 185 had Amplification (207) (accessed via C-Bioportal (208, 209)). Therefore restricting 'non-amplified' status to only diploid or sub-diploid lines would not be representative of the clinical picture seen in squamous lung cancers.

In NCI-H1703, minimal inhibition of cell growth was seen with siRNA S13295 despite effective SOX2 knockdown (Figure 40). In comparison, with siRNA S13294, substantial growth inhibition was observed. Notably, in NCI-H1703, degree of SOX2 knockdown was consistently comparable between S13294 and S13295 (Figure 37). Overall, this suggests that the growth inhibition seen with S13294 in NCI-H1703 was not explainable solely by reduced SOX2 protein levels and may be due to off-target effects. When combined with the data from DepMap and results from Bass et al (191), these results are in keeping with SOX2 knockdown being less toxic in the cells without 3q amplification.

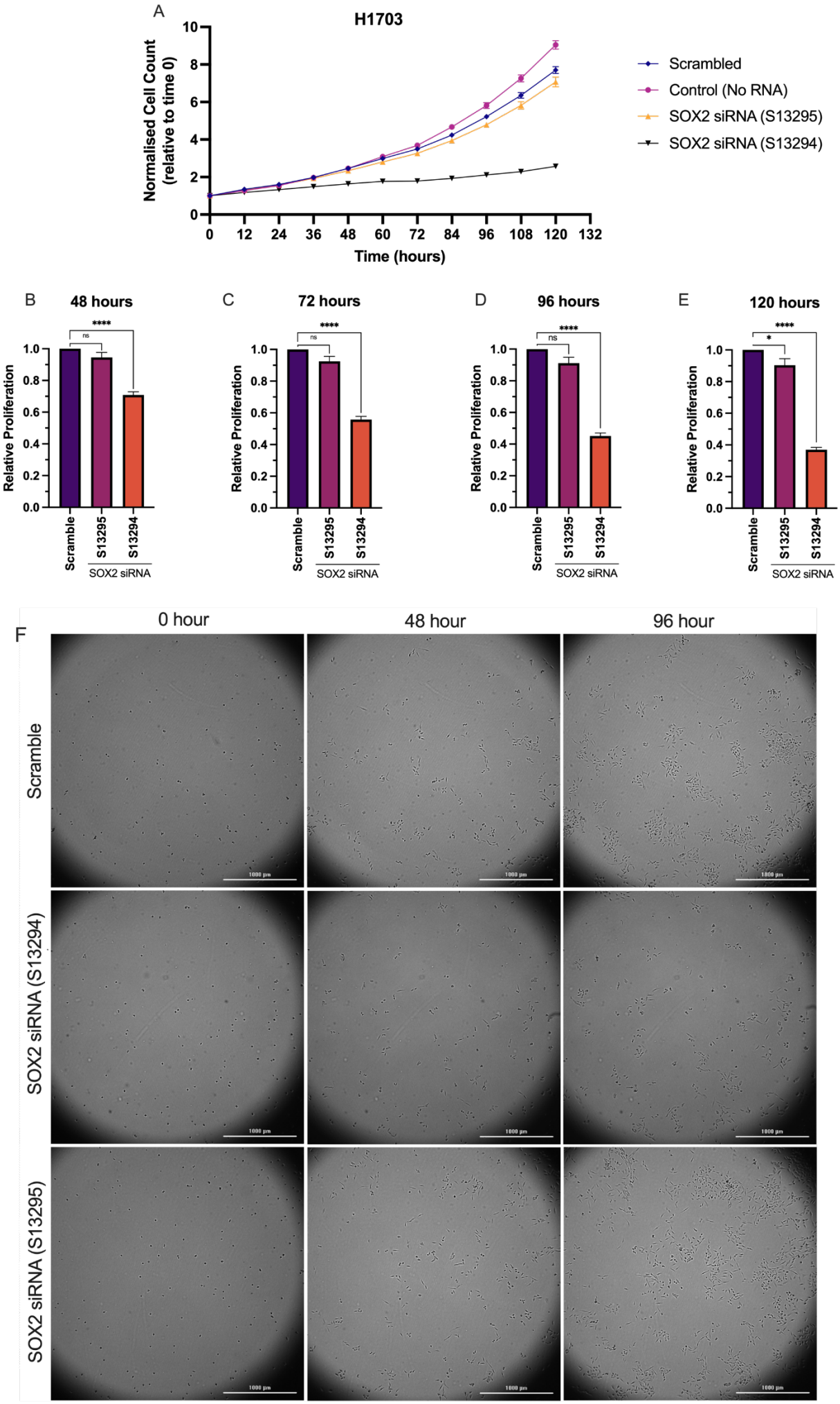
A
H1703
Normalised Cell Count (relative to time 0)
Time (hours)
Scrambled
Control (No RNA)
SOX2 siRNA (S13295)
SOX2 siRNA (S13294)
B
48 hours
C
72 hours
D
96 hours
E
120 hours
Relative Proliferation
Scramble
S13295
S13294
SOX2 siRNA
ns
****
*
F
0 hour
48 hour
96 hour
Scramble
SOX2 siRNA (S13294)
SOX2 siRNA (S13295)

Figure 40: Impact of SOX2 knockdown on cell proliferation in non 3q amplified NCI-H1703 cell line (Overleaf). NCI-H1703 cells were transfected with negative control siRNA ('scramble'), SOX2 siRNA (S13925 or S13924) or mock transfected with no siRNA (Control). 24 hours post-transfection, cells were seeded at 500 cells per well in a 96 well plate and imaged 12 hourly on the Cytation 5 microscope. Automated cell counts were performed using Gen5. For each biological replicate measurements were taken from at least 15 wells. Experiment was performed five times. Reads were stopped when confluency was reached, or images were no longer countable. (A) Representative cell growth curve from single experimental replicate, plotted as cell count relative to time 0, mean ± SEM. (B-D) Relative proliferation for scramble, S13925 and S13924 at indicated time points (mean ± SEM) (n=4 for 48 hour, 72 hour, 120 hour; n=3 for 96 hour), average of independent replicates, proliferation expressed relative to scramble). Statistical analysis: Sone-way ANOVA with Dunnett's multiple comparisons test (* P <0.05, ** P<0.01, *** P <0.001, **** p<0.0001) (F) Representative raw images

5.3.3.3 Effect of SOX2 knockdown on colony formation in squamous cell lung cancer cell lines

The impact of SOX2 knockdown on colony formation was assessed. Due to the transient nature of siRNA knockdown, 7 days was chosen as the timepoint for analysis. SOX2 knockdown with both S13294 and S13295 profoundly inhibited colony formation of 3q amplified RERF-LC-SQ1 cells. When compared with cells transfected with non-targeting control siRNA, S13294 reduced colony formation by 84.79% (95% CI -84.79 to -97.62%, P <0.0001), whilst S13295 reduced colony formation by 91.46% (95% CI -85.91 to -97.00%, P <0.0001) (Figure 38, Figure 41). Attempts to assess impact of colony formation on 3q amplified HCC2814 were unsuccessful: cells were only loosely adherent, particularly after transfection, resulting in clumping of cells and disturbance of colonies. Attempts to assess impact of colony formation on non-amplified NCI-H1703 were also unsuccessful, as NCI-H1703 did not reliably form countable colonies, even with extended incubation. However, even though these results are only from a single cell line, they are fully supported by published results with shRNA in two further 3q amplified squamous cell lung cancer cell lines: SOX2 shRNA significantly reduces colony formation in HCC95 and NCI-H520 (191).

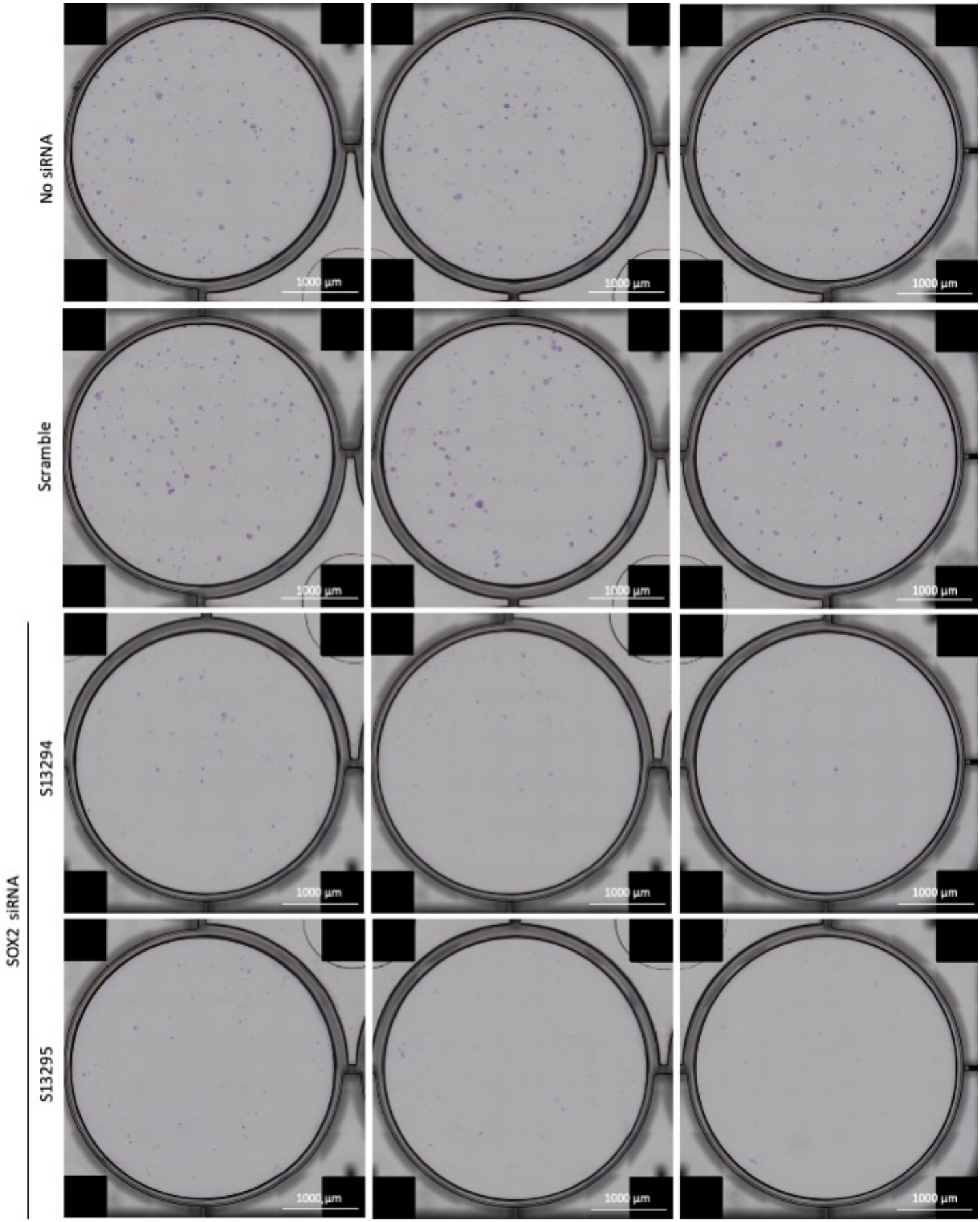

Figure 41: Impact of SOX2 knockdown on colony formation in RERF-LC-SQ1 (example of raw data). RERF-L-CSQ1 cells were transfected with 20 nM siRNA targeting SOX2 (S13295 or S13294), negative control siRNA (Scramble), or mock transfected with no lipofectamine and no siRNA (no siRNA). 24 hours post-transfected, cells were harvested and seeded in triplicate at 750 cells per well in 6 well plates. After 7 days, colonies were fixed with methanol and stained with 0.5% crystal violet. Wells were imaged at x4 magnification on the Cytation microscope running Gen5.). Experiment performed 4 times at least 1 week apart, with each biological replicate seeded in triplicate, representative images shown.

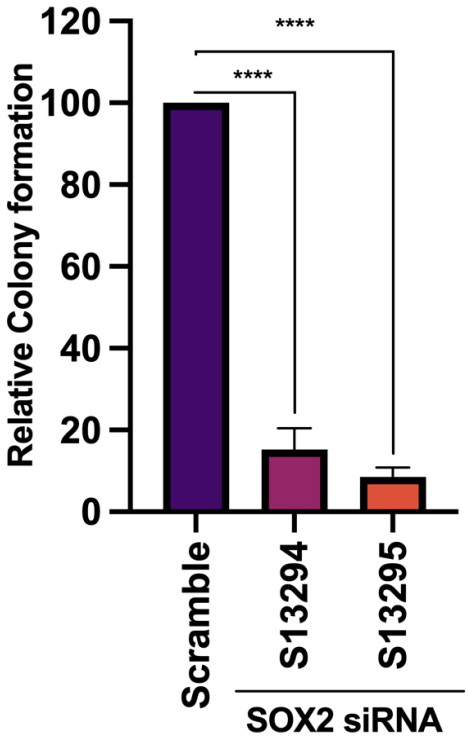

Figure 42: Impact of SOX2 knockdown on colony formation in RERF-LC-SQ1 (data analysis). RERF-L-CSQ1 cells were transfected with 20 nM siRNA targeting SOX2 (S13295 or S13294), negative control siRNA (Scramble), or mock transfected (no siRNA). After 7 days colonies were fixed and stained, imaged, and manually counted (>50 cells considered a countable colony). Experiment performed 4 times at least 1 week apart, with each biological replicate seeded in triplicate. For each biological replicate, the mean colony count for SOX2 knockdown (S13294 or S13295) was expressed relative to the mean colony count for negative control siRNA (scramble). Presented is the mean (+/- SEM) across the four biological replicates. Statistics: one-way ANOVA with Dunnett's multiple comparisons test (* P <0.05, ** P<0.01, *** P <0.001, **** p<0.0001)

5.4 Key Findings

This work confirms that *SOX2* appears to be the key component of the 3q amplicon, and is therefore an important potential target in 3q amplified squamous cell lung cancer:

1. *SOX2* was one of the most commonly amplified genes within 3q in the TCGA squamous cell lung cancer cohort.
2. *SOX2* amplification status strongly correlates with overexpression of *SOX2* mRNA in the TCGA squamous cell lung cancer cohort.
3. When genes within 3q26-29 were ranked based on differential dependency in amplified versus non-amplified cell lines, *SOX2* was the highest ranked gene (based on DepMap genome wide CRISPR knockout data).
4. *SOX2* Dependency Exhibits a Linear Relationship with *SOX2* Copy Number in Squamous Cancer Cell Lines (based on DepMap genome wide CRISPR knockout data)
5. SOX2 knockdown with siRNA significantly impairs proliferation and colony formation of 3q amplified squamous lung cancer cell lines in vitro

5.5 Discussion

This chapter sought to identify key drivers within the 3q26-29 amplicon in 3q amplified squamous cell lung cancer. By harnessing publicly available DepMap genome wide CRISPR knockout data, this analysis represents the most complete analysis of this amplicon in the largest panel of cell lines. In addition, to the best of our knowledge this is the first analysis of genes within the 3q amplicon in 3q amplified cells based on CRISPR data.

The present analysis supports previous reports that *SOX2* is a key oncogene in 3q (191, 193). *SOX2* is one of a limited number of genes within 3q where amplification is associated with increased dependency, with an apparently linear relationship between *SOX2* copy number and *SOX2* dependency. The importance of SOX2 in 3q amplified cells was confirmed with siRNA in two 3q amplified squamous cell lines, with a significant reduction in proliferation in both cell lines. Further, SOX2 knockdown obliterated colony formation in RERF-LC-SQ1, in keeping with the known function of SOX2 in regulation of stemness (259). Unfortunately, analysis of the impact of SOX2 knockdown on the non-amplified squamous cell NCI-H1703 was complicated by discordant results between two tested siRNA. However, overall, when taken with the available published data (191), these results would seem to support the assertion that SOX2 knockdown is less toxic in the absence of 3q amplification.

The present analysis does have some weaknesses. Firstly, the number of SOX2 amplified lines available for analysis on Depmap remains small, and therefore data from different squamous malignancies were pooled. It is acknowledged that the impact of SOX2 siRNA on colony formation only produced analysable results in a single cell line. However, these results are fully supported by published results with shRNA in a further two 3q amplified squamous cell lung cancer lines (NCI-H520 and HCC95) (191). Therefore, when this data is considered as a whole, we can be reasonably confident that SOX2 depletion does reduced colony formation in the context of 3q

amplification. Nonetheless, future work will be undertaken in a larger panel of squamous cell lung cancer cell lines. Colony forming assays will be repeated in a further two amplified cell lines. The impact of SOX2 knockdown on viability and colony formation will be assessed in at least one additional non-amplified line.

A second weakness in the present analysis is that 3q26-29 is a complex region and encompasses many pseudogenes encoding long non-coding RNAs (lncRNA) and miRNAs. For example, SOX2-OT is a high-conserved multi-exon lncRNA that bridges the *SOX2* gene, and is transcribed in the same orientation (260, 261). At present, DepMap has limited evaluable data on non-protein coding genes. This analysis therefore cannot comment on the contribution of these pseudogenes. However, the focus of this work is on the evaluation of potential targetable pathways. At present, there is limited therapeutic tractability for targeting non-coding genes in clinical practice, although this remains an active area for research and development (262). Therefore, in the current therapeutic landscape, these would be unlikely to be prioritised for further exploration.

A further disadvantage of the present approach is that we are unable to evaluate gene-gene interactions. It is likely that a cassette of genes within the amplicon co-operate to drive oncogenicity. Furthermore, genome-wide CRISPR screens are poorly placed to assess dependency on closely related genes where there is significant redundancy. Therefore, whilst *SOX2* is clearly a key gene within the amplicon, additional genes likely collaborate to drive phenotype. Further analysis examining the interaction between genes within the region would be of great value, with potential approaches including combinatorial CRISPR screening (263). Finally, it is acknowledged that CRISPR screens are designed to target diploid genomes. CERES-correction reduces false positive results and estimates for dependency by computationally correcting for copy number (211). However, impacts of copy number effects cannot be excluded entirely. However, the

purpose of this approach was to triage candidate genes within 3q for further work and development, and overall when combined with siRNA validation and work of others (191, 193), it was felt that there was sufficient evidence to prioritise SOX2 as a target in the context of 3q amplification.

A final drawback of the current work is the limited number of models available for squamous cell lung cancer research. HCC2814, RERF-LC-SQ1 and NCI-H7103 are well-characterised models of squamous cell lung cancer (210, 264-267), and were therefore chosen for the present work. Cell line identity was confirmed with STR-typing. However, it is acknowledged that the squamous lung cancer phenotype (e.g. TTF1 negative, CK5/6 positive, p63 (p40) positive (268, 269)) of these cell lines was not confirmed in the present work. It is therefore possible that the results described are more representative of 3q amplification, rather than specifically representing 3q amplified squamous cell lung cancer. Full phenotyping of these cell lines will be completed in further work.

5.6 Conclusions

SOX2 is amongst the most commonly amplified genes in the 3q amplicon and is amongst a small number of candidates where gene amplification is associated with increased dependency on genome-wide CRISPR knockout based on publicly available DepMap data. siRNA validates that *SOX2* knockdown impairs cell growth and colony formation in 3q amplified cell lines. SOX2 is therefore a potential target of interest in 3q amplified squamous cell lung cancer. Subsequent chapters will therefore explore potential to target SOX2 in squamous cell lung cancer. In Chapter 5, literature is reviewed to identify drugs that have been reported to knockdown SOX2 in other contexts, and these drugs will be tested in 3q amplified squamous cell lung cancer. In Chapter 6, an unsupervised approach will be applied to identify potential other pathways to target SOX2 in 3q amplified squamous cell lung cancer.

Chapter 6: 3q Amplified Squamous Cell Lung Cancer Part 2 - *Prioritisation of drug candidates to target SOX2 in 3q amplification*

6.1 Introduction

In Chapter 4 it is demonstrated that *SOX2* is a central oncogene within the 3q amplicon in squamous cell lung cancer. *SOX2* is amongst the most commonly amplified genes in 3q, and 3q amplified cell lines demonstrate dependency on *SOX2*. As a result, SOX2 is an attractive candidate target in this context. However, transcription factors remain challenging drug targets. Several drugs have been reported to modulate SOX2 levels (270), however, these approaches are poorly explored in the setting of 3q amplification as they have reported targeting of SOX2 in isolation. This chapter will present a review of drugs that have been reported to modulate SOX2 expression levels in other contexts. These drugs will then be screened for their potential utility in 3q amplified squamous cell lung cancer.

6.1.1 Literature Review

An extensive review was undertaken to identify therapeutic strategies that have been reported to modulate SOX2 expression, with the search strategy outlined in Appendix 2. Strategies using drugs or drug classes in active clinical development were prioritised. Therapeutic strategies which are currently challenging to translate to clinical practice (such as miRNA, siRNA or PROTAC) were deprioritised. Five approaches were selected for exploration: KDM1A (LSD1) inhibition, NAE Inhibition, BRD4 inhibition, STAT3 inhibition and CDK7 Inhibition, The biological rationales for these approaches and the existing evidence bases are outlined in Section 6.1.2 to 6.1.6. It is hoped that this approach may identify drug candidates for ongoing development as therapeutic strategies for 3q amplified squamous cell lung cancer.

6.1.2 KDM1A (LSD1) Inhibition (ORY-1001)

KDM1A (LSD1) is a flavin adenine dinucleotide (FAD)-dependent lysine-specific demethylase. KDM1A regulates gene expression through demethylation of mono- and dimethylated H3K9. H3K9 methylation represses gene expression, therefore demethylation promotes genes expression (Figure 43)(271). KDM1A has additional non-histone substrates including STAT3, E2F1 and p53 (271). A number of KDM1A inhibitors have entered clinical trials, including covalent inhibitors (phenylzine, tranylcypromide, iadademstat (ORY-1001), bomedemstat (IMG-7289), GSK-2879552, JBI-802, INCB05987), non-covalent inhibitors (pulrodemstat (CC-90011) and seclidemstat (SP-2577) and a combined LSD/MAO-B inhibitor (vafidemstat (ORY-2001)) (272).

LSD-1 play a role in regulating *SOX2* transcription (Figure 43). Iadedemstat (ORY-1001) is a potent LSD-1 inhibitor, which has demonstrated safety and suggestions of clinical efficacy in Acute Myeloid Leukemia (AML) in a Phase I trial (273). Iadedemstat reduces mammosphere formation in breast cancer stem cell models, and suppresses SOX2 transcriptional activation in mammosphere culture (274). CBB1007, a competitive inhibitor of KDM1A, has been reported to suppress growth of SOX2-expressing squamous cell lung cancer cells (275). CBB1007, and the closely related compound CBB1003, reduce SOX2 expression in NCI-H520 squamous cell lung cancer cells (SOX2 CN 4) (275). However the dose used (50 μM) is unlikely to be clinically achievable: Cmax on Day 26 is 55 pg/mL at the recommended phase II dose of 140 μg/m^2/day (273).

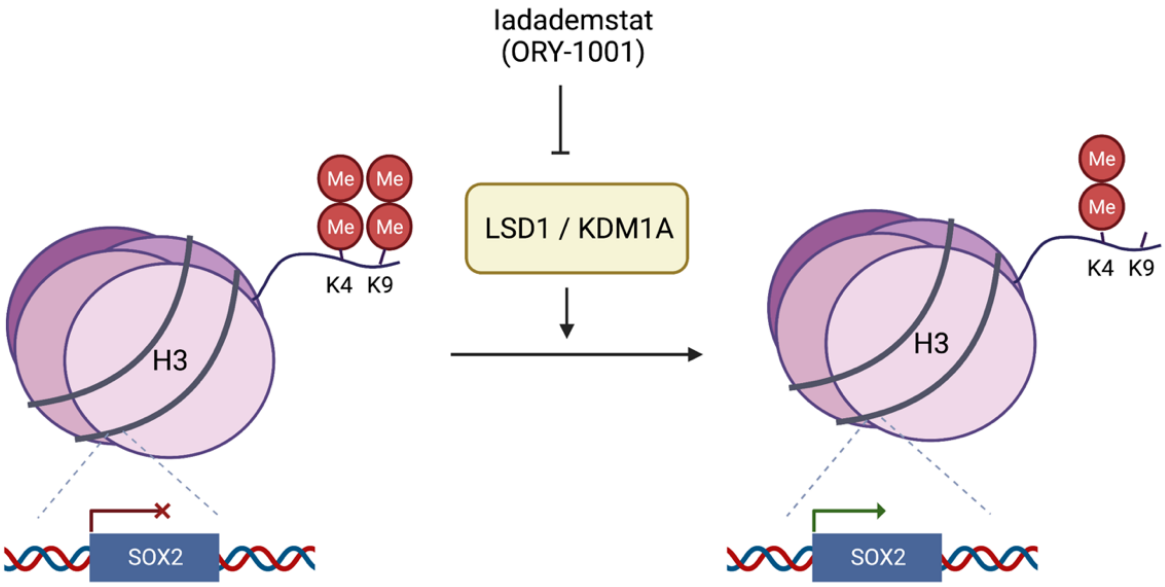

Figure 43: Proposed Role of KDM1A (LSD1) in SOX2 regulation. KDM1A demethylates di- or mono-methylated H3K4. As a result, KDM1A regulates transcription, including that of key stemness genes including SOX2. Inhibition of KDM1A prevents demethylation of di/mono-methylated H3K4 and hence reduces SOX2 transcription. *Created using Biorender.com, printed with permission.*

6.1.3 NAE Inhibition (Pevonedistat (MLN4924/TAK-924))

Pevonedistat (MLN4924/TAK-294) is a potent inhibitor of NEDD8-activating enzyme (NAE). Neddylation is the process of by which NEDD8 (an 81-amino acid ubiquitin-like protein) is added to target proteins (276). NEDD8-activating enzyme (NAE), a heterodimer comprised of AppBp1 and Uba3, is an important regulator of Neddylaton. Neddylation, in turn, is essential for activity of cullin-RING E3 ubiquitin ligase (CRL). Which targets proteins for degradation through ubiquitination. Pevonedistat (MLN4924/TAK-294) is a potent inhibitor of NAE, preventing neddylation of CRL, and therefore maintaining CRL in an inactive state. Pevonedistat has demonstrated preclinical activity in many settings, including neuroblastoma (277), colorectal cancer (278) and pancreatic cancer (279). In haematological malignancies, combination treatment of pevonedistat and azacitidine has shown a good safety profile with evidence of efficacy in Phase I and II trials (280, 281). Furthermore, in heavily pre-treated solid malignancies, treatment with pevonedistat, carboplatin and paclitaxel was tolerable, with a response rate of 28% (9/32) (282). Pevonedistat has been shown to reduce SOX2 expression in NSCLC cell lines (A549, H1299, H2170, H358) and breast cancer (MCF7) cell lines, with the proposed mechanism of action displayed in Figure 44 (283). However, no studies have examined whether pevonedistat effectively modulates SOX2 protein levels in the context of 3q amplification.

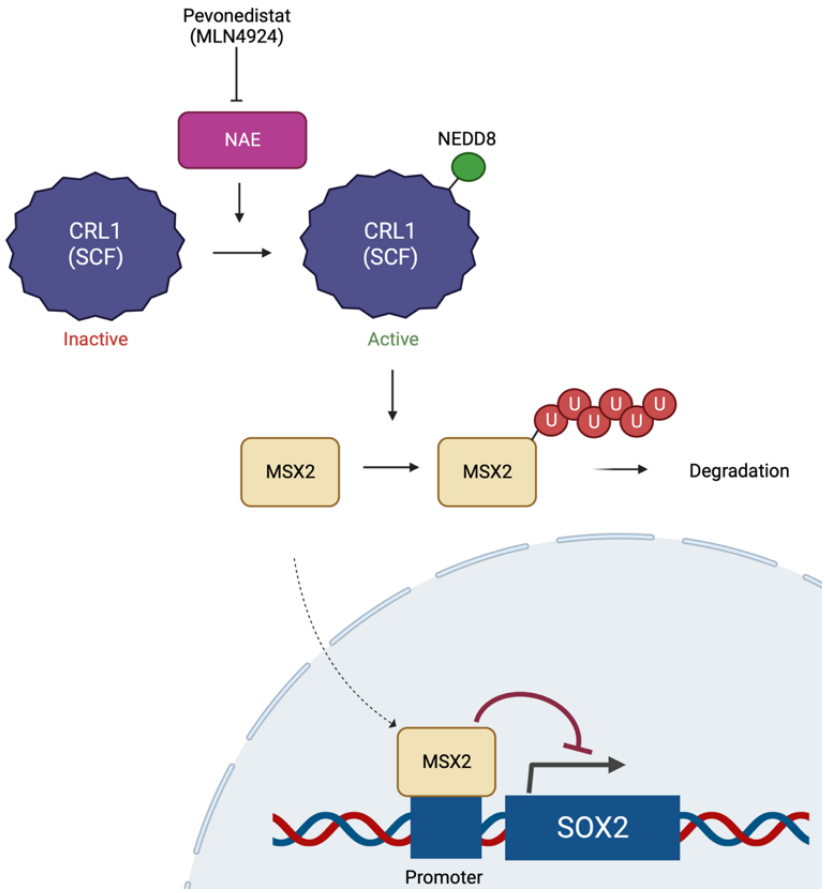

Figure 44: Proposed regulation of SOX2 by the NAE/CRL1/MSX2 axis. CRL1 is a complex comprised of cullin-1, SKP1, RBX1 or RBX2 and F-box proteins. CRL1 activity requires neddylation, catalysed by NEDD8-activating enzyme (NAE). Active CRL1 acts as an E3 ubiquitin ligase, targeting proteins for proteasomal degradation by ubiquitination. By inhibiting NAE, Pevonedistat (MLN4924) maintains CRL1 in the inactive state, preventing ubiquitination of MSX2, and allowing MSX2 to accumulate. MSX2 is a transcriptional repressor of SOX2, and therefore pevonedistat reduces SOX2 expression (205). *Created using Biorender.com, printed with permission.*

6.1.4 CDK7 Inhibition (THZ1, ICEC0942, SY-5609)

CDK7 regulates the cell cycle through phosphorylation of CDK1, CDK2, CDK4 and CDK6. In addition, CDK7 regulates transcription through phosphorylation of RNA polymerase II as part of the Transcription factor II H complex (TFIIH), and through phosphorylation of transcription factors (284) (Figure 45).

A role of CDK7 in modulating SOX2 expression was first suggested by research using THZ1. THZ1 is an ATP-competitive covalent inhibitor of CDK7 (284), which also inhibits CDK12 and CDK13 (284, 285). In NSCLC cells, THZ1 induces G_2/M arrest and apoptosis (286, 287) impairs glycolysis (286), inhibits MYC transcriptional activity (287), and suppresses PDL1 expression (287). THZ1 also modulates antitumour immunity in a mouse model of NSCLC (287). THZ1 reduces SOX2 protein expression in squamous cell lung cancer cell lines (288). Hur et al also reported that SOX2-amplified cells are more sensitive to THZ1 [434], however, it must be noted that according to publically available DepMap data, two of the three tested 'amplified' cells have relatively low-level copy number gain (H520 has a *SOX2* copy number of 4, H1703 has a *SOX2* copy number of CN 3) (210). THZ1 is not a candidate for clinical drug development. Its derivative SY-1365 entered phase I clinical trials, but its clinical development has also been discontinued (284). However, alternate CDK7 inhibitors with greater potency and selectivity for CDK7 have been developed (284). ICEC0942 (Samuraciclib, CT7001) and SY-5609 are two highly potent and specific CDK7 inhibitors that have entered clinical trials (289, 290). Both ICEC0942 and SY-5609 are tolerable with early evidence of clinical activity (289-291). No studies have examined whether next generation selective CDK7 inhibitors modulate SOX2 expression.

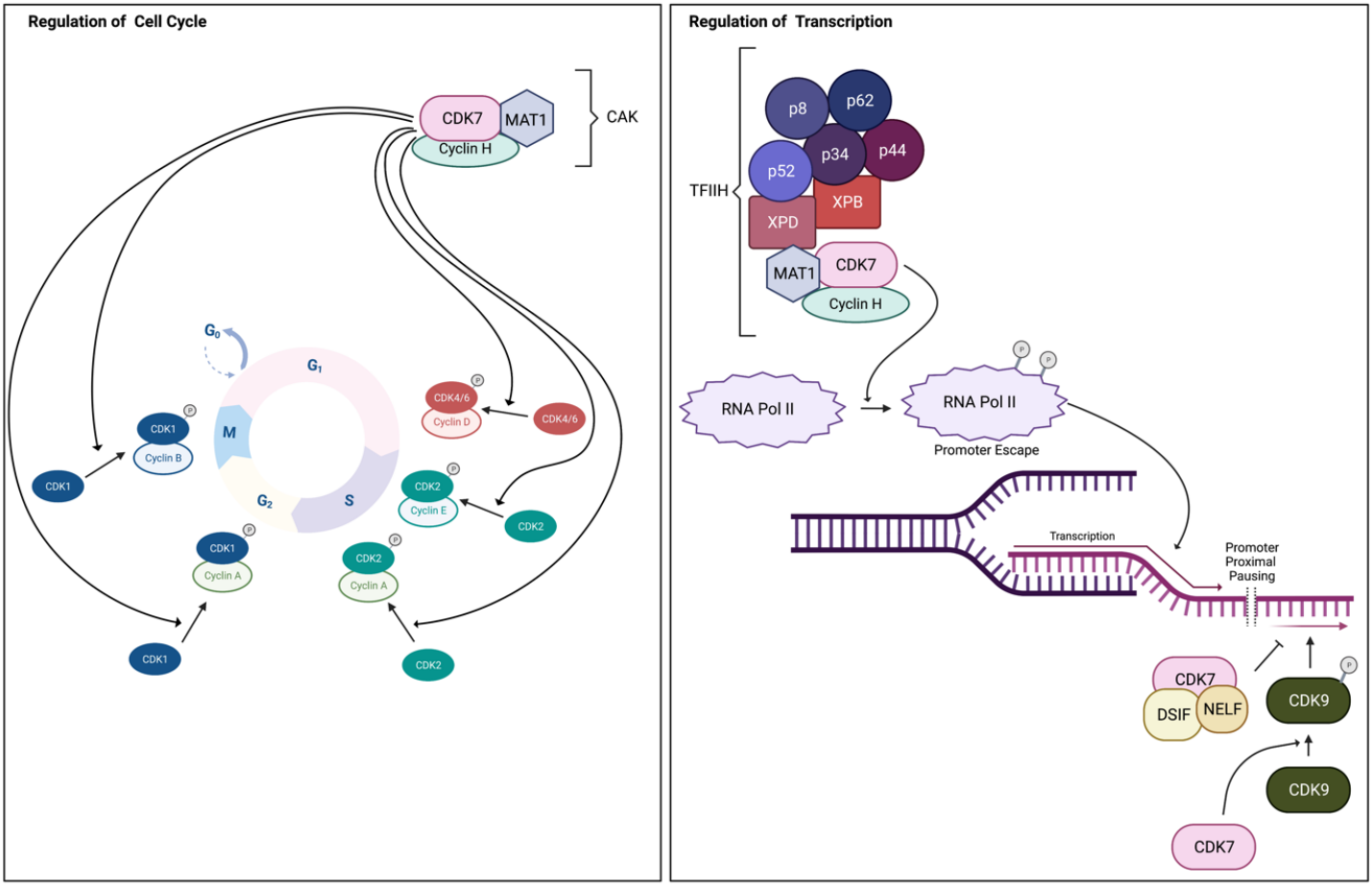

Figure 45: Regulation of the cell cycle and transcription by CDK7. CDK7, MAT1 and Cylin H form the CDK-activating kinase (CAK) complex, which regulates the cell cycle through phosphorylation of CDKs 1, 2, 4 and 6. In addition, CAK forms part of the TFIIH complex. TFIIH plays a crucial role in regulating gene transcription: TFIIH is recruited to active gene promoters where it forms part of the preinitiation complex alongside RNA Pol II. CDK7 (as part of the TFIIH) phosphorylates RNA Pol II at Ser5 and Ser7, allowing it to leave the preinitiation complex and start transcription. After transcription of a short run of bases, RNA Pol II pauses transcription (promoter-proximal pausing). This pause is directed by CDK7, which recruits DSIF and NELF. However, CDK7 also plays a role in releasing RNA Pol II from the pause through phosphorylating CDK9. *Adapted from Sava et al, CDK7 Inhibitors as anticancer drugs. Cancer Metastasis Rev, 2020, 39(3): 805-823(206). Created using Biorender.com, printed with permission.*

6.1.5 BRD4 Inhibition (AZD5153)

BRD4 is a member of the Bromodomain and Extraterminal (BET) protein family. BET proteins contain two bromodomains that bind acetylated lysine residues (292). Acetylated histones are key binding targets for BET proteins, recruiting BET proteins to open chromatin, where they promote transcription (292). BRD4 plays a role in maintaining stemness of embryonic stem cells, supporting transcription of *NANOG*, *OCT4* and *SOX2* (293, 294). BET inhibition with JQ1 may suppress SOX2 in embryonic stem cells and mesenchymal stem cells (295, 296), although data in embryonic stem cells is conflicting (293, 294, 297). BRD4 binds the e1 *SOX2* enhancer, which is commonly amplified in squamous cancers, driving SOX2 overexpression (298). PROTAC-mediated degradation of BRD4 suppresses SOX2 expression in squamous cancer cells (298). Finally, in NUT midline carcinoma, a rare but aggressive malignancy commonly driven by t(15;19) translocations, resulting in in a BRD4-NUT fusion protein, BRD4-NUT binds the SOX2 promoter and enhancers, driving SOX2 overexpression, an effect reversed by BET inhibition (299). Therefore, there is strong evidence for BRD4 directly driving SOX2 overexpression.

BRD4 may also indirectly regulate SOX2 via GLI1. GLI1 is a transcription facto, which is overexpressed in a non-canonical, hedgehog-independent, PI3K-dependent manner in squamous cell lung cancer (300). GLI1, BRD4 and SOX2 signalling interact at multiple points. SOX2 is a transcriptional target of GLI1 (301). BRD4 and SOX2 form a transcriptional complex, which drives non-canonical GLI1 transcription in melanoma (302). SOX2 and GLI1 also form a transcriptional complex, which promotes invasive behaviour in melanoma and prostate cancer (303, 304). One potential strategy for targeting GLI1 is the use of arsenic trioxide (ATO) (300, 305, 306). Arsenic trioxide reduces GLI1 expression in squamous cell lung cancer cells, suppressing colony formation and proliferation (300). Furthermore, combinations of ATO and PI3K inhibition synergistically suppressing squamous cell lung cancer xenograft growth (300), suggesting that combined targeting of GLI1 and PI3K/Akt may be valuable. Whilst arsenic trioxide is no longer in clinical

development, BRD4 inhibitors have been identified as an alternate strategy for targeting GLI1 (307), therefore BRD4 inhibition may inhibit GLI1 and SOX2 signalling at multiple points, potentially enhancing any therapeutic vulnerability.

Despite strong evidence for BRD4 playing a critical role in regulating SOX2 expression, no studies have investigated whether BRD4 inhibitors suppress SOX2 in 3q amplified squamous cell lung cancer. Multiple BRD4 inhibitors have been developed (308). AZD5153 is an innovative, potent BRD4 inhibitor which binds both bromodomains of BRD4, showing activity in a variety of preclinical settings (309-311), and tolerability in a Phase I Trial (312). It is also of interest to explore whether combining AZD5153 with PI3K/Akt inhibition is synergistic, as it is possible that this combination could mirror results seen with ATO and PI3K/Akt inhibition (300).

6.1.6 STAT3 Inhibition (Napabucasin)

SOX2 is a transcriptional target of STAT3 (313, 314). STAT3 overexpression drives SOX2 upregulation in cervical cancer stem cells (315), whilst STAT3 knockdown suppresses SOX2 expression in HER2-positive breast cancer stem cells and abolishes tumour sphere formation (316). Napabucasin is a STAT3 inhibitor, which has been shown to reduce expression of SOX2 in glioblastoma (317) and breast cancer (318). 1 μM napabucasin reduces SOX2 mRNA expression in lung adenocarcinoma cell lines and non-amplified squamous cell lung cancer cells (SKMES1) at 72 hours (319). Furthermore, SOX2 and STAT3 co-operate in inducing transformation of oesophageal basal cells, and double knockdown of SOX2 and STAT3 substantially reduces squamous oesophageal cancer cell proliferation (320). No studies have examined whether inhibiting STAT3 suppresses SOX2 expression in 3q amplified squamous cell lung cancer.

6.2 Aims and Objectives

Aim:

This chapter seeks to screen a panel of drug candidates in squamous cell lung cancer, with a particular focus on whether these agents modulate SOX2 expression in 3q amplified cell lines.

Drug Candidates:

Drug candidates were selected based on published data suggestive of a potential role in regulation of SOX2. Drug candidates in active clinical development, particularly those with available safety data, were prioritised wherever possible. The drug candidates chosen are:

1. CDK7 Inhibition: THZ1, SY-5609 and ICEC0942
2. BRD4 Inhibition: AZD5153
3. NAE Inhibition: Pevonedistat (MLN4924)
4. KDM1A (LSD1) Inhibition: Iadademstat (ORY-1001)
5. STAT3 Inhibition: Napabucasin (BB1608)

Due to reports of synergy between Arsenic Trioxide and inhibition of the PI3K/Akt pathway, it was hypothesised that drugs that successfully target SOX2 may have synergy with targeting the PI3K/Akt pathway, therefore combination strategies were also explored.

Objectives:

1. To assess the impact of drug candidates on cell viability in a panel of squamous cell lung cancer cell lines
2. To assess whether 3q amplified cell lines show increased sensitivity to drug candidates by assessing impact of drugs on viability in squamous cell lung cancer cell lines with and without high level 3q amplification
3. To assess whether drug candidates modulate SOX2 protein expression in a panel of lung cancer cell lines
4. To assess whether selected drug candidates show synergy with inhibition of the PI3K/Akt pathway

6.3 Results

6.3.1 Cell Line Characterisation and Categorisation

A panel of squamous cell lung cancer cell lines was assembled. Relative and absolute copy number for *SOX2*, *ECT2*, *PIK3CA* and *PRKCI* was obtained from DepMap (summarised in Table 35) (210). Cell line identity was confirmed with STR typing. Amplification was defined as relative copy number ≥ 1.8. This cut-off was intentionally chosen to allow focus on high-level amplification, which, as shown in Chapter 4, is likely to be the most clinically significant when targeting SOX2. It must also be noted that low level copy number gain in 3q is almost universal in squamous cell lung cancer: in the TCGA Squamous Cell Lung Cancer dataset, 37 out of 466 tumours were diploid for *SOX2*, 241 of had CN gain, 185 had Amplification (207) (accessed via C-Bioportal (208, 209)). Therefore restricting 'non-amplified' status to only diploid or sub-diploid lines would not be representative of clinical picture seen in squamous lung cancers. All cell lines classified as 3q amplified either demonstrate *SOX2* dependency in DepMap datasets (LC1SQ or RERF-LC-SQ1) and/or have been demonstrated to show sensitivity to SOX2 knockdown in Chapter 4 (RERF-LC-SQ1 and HCC2814). Three out of the four non-amplified lines have available SOX2 dependency data from Depmap, all showing low levels of *SOX2* dependency.

		Absolute Copy Number		Relative Copy Number		*SOX2* Dependency
		SOX2	*PIK3CA*	*SOX2*	*PIK3CA*	
Amp	LC-1/sq	7	7	1.97	1.805	-1.045
	RERF-LC-SQ1	7	7	3.240	2.777	-0.872
	HCC2814	6	6	2.319	2.282	-
Not Amp	HCC1897	4	4	1.667	1.667	-
	HCC2450	-	-	1.404	1.404	-0.225
	NCI-H1703	3	3	1.112	1.112	-0.137
	SK-MES-1	3	3	1.165	1.165	-0.060

Table 35: Cell Line Panel used for Drug Screening. Absolute copy number, relative copy number and SOX2 Dependency obtained from DepMap (All data from Depmap 21Q4 release). No data available for absolute copy number for HCC2450 or for *SOX2* dependency for HCC1897 or HCC2814

6.3.2 CDK7 Inhibition (THZ1, SY-5609, ICEC0942)

CDK7 regulates the cell cycle and gene transcription (284). THZ1 has been reported to reduce SOX2 expression in squamous cell lung cancer cell lines (288). However, THZ1 is relatively non-specific and is not in clinical development. ICEC0942 (Samuraciclib, CT7001) and SY-5609 are two highly potent and specific CDK7 inhibitors in active clinical trials (289, 290). Three CDK7 inhibitors were therefore assessed in this work. Firstly, it was explored whether previously reported results with THZ1 could be replicated. Secondly, SY-5609 and ICEC0942 were explored as candidates with potential clinical applicability.

6.3.2.1 Impact of CDK7 Inhibition (THZ1, SY-5609, ICEC0942) on cell viability at 72 hours

THZ1

All three tested 3q amplified lines demonstrated sensitivity to THZ1. In amplified cell lines, absolute IC50 ranged from 0.0764 μM to 0.1156 μM (Figure 46B, Table 36). Almost complete suppression of cell viability was seen (Emax 1.30% - 18.33% (percentage of viable cells remaining at bottom of cell viability curve)). The efficacy of THZ1 was lower in two non-amplified lines: E_{max} was 39.26% in HCC2450 and 47.37% in HCC1897. However, whilst reduced efficacy is seen in a proportion of tested non-amplified cells, these findings cannot be entirely attributed to 3q amplification cells: cell lines with lowest *SOX2* amplification status (NCI-H1703 and SK-MES-1) show sensitivity to THZ1 comparable to cell lines with high-level 3q amplification (RERF-LC-SQ1, HCC2814, LC-1/SQ).

SY-5609

Efficacy of SY-5609 was low in all tested cell lines at 72 hours. (Figure 46C, D). Absolute IC50 was not estimable in six out of seven tested cell lines, as reduction in viability was less than 50% in sigmoid portion of the viability curves (Table 36). Above 1 μM, greater reductions in viability were seen, but this was judged to be non-specific toxicity: reported EC50 in HCC70 is 1nM, with a Kd for CDK7 of 0.07 nM (321)

ICEC0942

All three tested 3q amplified lines demonstrated dose-dependent reductions in viability, with absolute IC50 ranging from 0.0126 μM to 0.4695 μM (Figure 46F, Table 36), with 19.36% to 0.58% viable cells remaining at Emax. Absolute IC50 in the four tested non-amplified lines was comparable to those seen in amplified lines (0.0549 μM to 0.2615 μM). However, HCC1897 and HCC2450 demonstrated lower levels of maximal growth inhibition with ICEC0942, mirroring results with THZ1 in the same cell lines (Figure 46E, Table 36). However, as was seen with THZ1, 3q amplification is not a clear determinant of sensitivity to ICEC0942: the two lines with the lowest levels of 3q amplification display comparable sensitivity to cell lines with high-level 3q amplification.

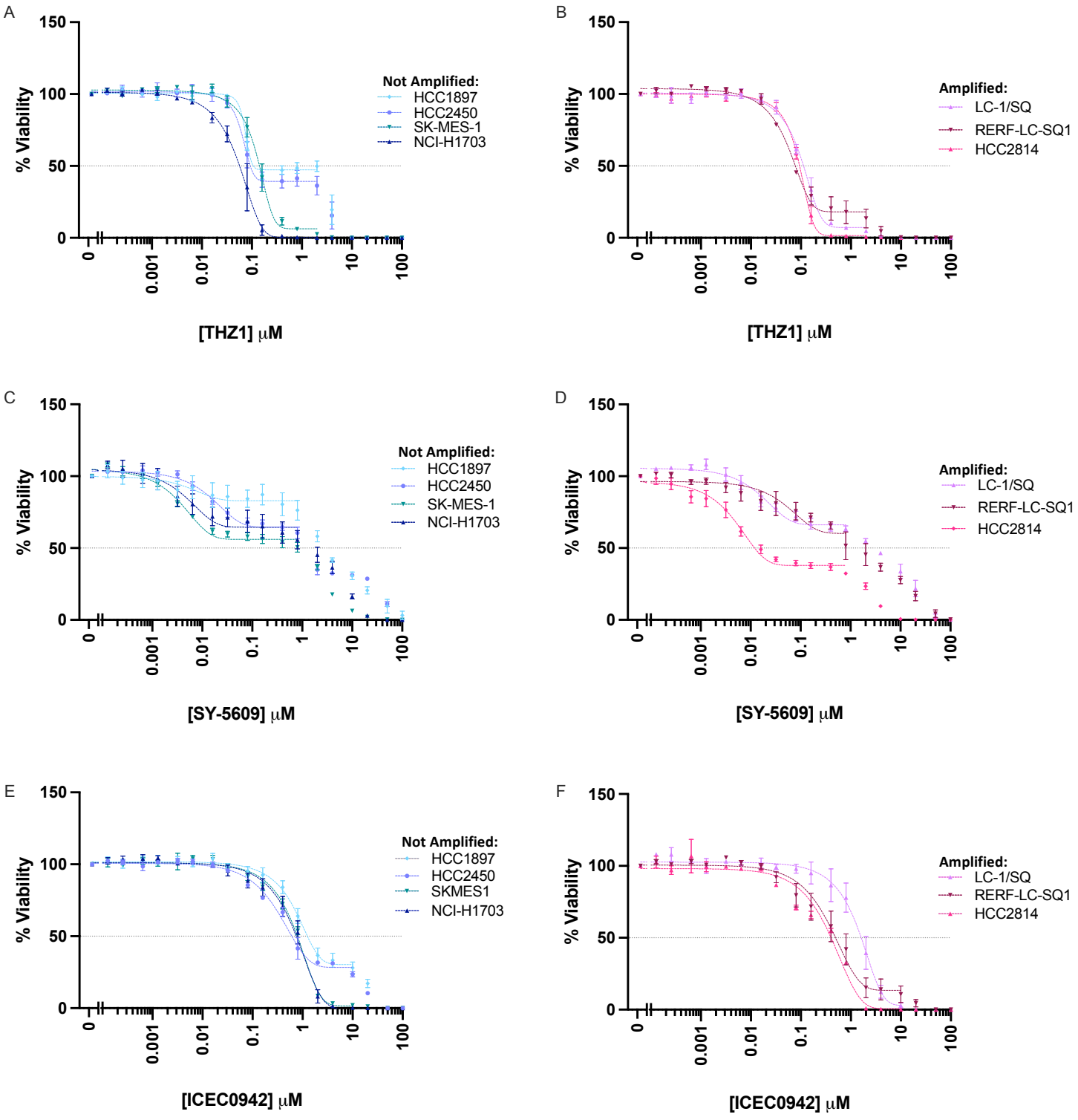

Figure 46: Impact of CDK7 inhibitors on cell viability at 72 hours. Non-amplified squamous cell lung cancer cell lines (A, C, E) and 3q amplified cell lines (B, D, F) were treated with 0 – 100 μM THZ1 (A, B), SY-5609 (C, D) or ICEC0942 (E, F). Cell viability was assessed at 72 hours using cell titer-glo 2.0, subtracting background luminescence, and expressed relative to 0 μM drug. Curves plotted using Prism using non-linear regression. Experiment repeated at least three times for each cell line. Mean and SEM displayed. 50% reduction in viability indicated by horizontal line.

Cell Line (relative *SOX2* CN)	THZ1 (72 hours)			
	IC50 (µM)	(SEM)	Emax (%)	(SEM)
RERF-LC-SQ1 (3.24)	0.0764	0.0022	18.33	7.80
HCC2814 (2.319)	0.0954	0.0079	1.30	0.79
LC-1/SQ (1.97)	0.1156	0.0132	6.87	0.72
HCC1897 (1.667)	NE	-	47.37	3.40
HCC2450 (1.404)	0.1157	0.0334	39.26	5.20
SK-MES-1 (1.165)	0.1456	0.0204	5.69	0.85
NCI-H1703 (1.11)	0.0617	0.0158	0.07	0.43

Cell Line (relative *SOX2* CN)	ICEC0942 (72 hours)			
	IC50 (µM)	(SEM)	Emax (%)	(SEM)
RERF-LC-SQ1 (3.24)	0.7398	0.2787	19.36	5.82
HCC2814 (2.319)	0.4015	0.0126	0.58	0.21
LC-1/SQ (1.97)	1.6236	0.4695	4.70	1.82
HCC1897 (1.667)	1.3451	0.2615	32.88	5.83
HCC2450 (1.404)	0.6892	0.1689	27.74	1.19
SK-MES-1 (1.165)	0.7344	0.0549	1.56	0.55
NCI-H1703 (1.11)	0.7155	0.1715	0.59	0.98

Cell Line (relative *SOX2* CN)	SY-5609 (72 hours)			
	IC50 (µM)	(SEM)	Emax (%)	(SEM)
RERF-LC-SQ1 (3.24)	NE	-	54.29	13.44
HCC2814 (2.319)	0.0124	(0.0026)	37.92	1.71
LC-1/SQ (1.97)	NE	-	67.31	2.04
HCC1897 (1.667)	NE	-	79.70	7.19
HCC2450 (1.404)	NE	-	67.88	1.58
SK-MES-1 (1.165)	NE	-	55.97	2.63
NCI-H1703 (1.11)	NE	-	64.58	6.67

Table 36: Absolute IC50 and Emax for THZ1, ICEC0942 and SY-5609 at 72 hours. Squamous cell lung cancer cell lines were treated with 0 – 100 µM THZ1, ICEC0942 or SY-5609. Cell viability was assessed at 72 hours using cell titer-glo 2.0, with viability curves displayed in Figure 46. Absolute IC50 and Emax are interpolated from curve using Prism for each experimental replicate. IC50 is defined as the concentration required to reduce viability by 50% relative to no treatment control. Emax is defined as the maximum drug effect observed within the sigmoidal curve ('bottom of the curve') (non-specific death beyond this point is disregarded), and is presented as percent viability relative to no treatment control. IC50 and Emax was calculated for each experimental replicate, with mean and SEM displayed. IC50 judged to be non-estimable (NE) where IC50 could not be interpolated from one or more experimental replicates.

6.3.2.2 Impact of CDK7 Inhibition (THZ1, SY-5609, ICEC0942) on cell viability at 7 days

CDK7 plays a central role in regulating the cell cycle. In addition, the effects of SOX2 knockdown were highly time dependent (Chapter 4). It is possible that 72 hours is insufficient to observe the full effects of CDK7 inhibition on cell cycle arrest, and/or any secondary effects from modulation of SOX2 levels. Therefore, selected cell lines (NCI-H1703, RERF-LC-SQ1 and HCC2814) were incubated with CDK7 inhibitors for 7 days, with drug refreshed after 4 days. 7 days of treatment with SY-5609 was highly toxic even low doses, contrasting strikingly with the modest reductions in viability seen after only 72 hours of treatment. Absolute IC50 with 7 days of SY-5609 was below 0.003 µM in all tested cell lines (Table 37, Figure 47), which appears to be within pharmacologically achievable concentrations in humans (290) (data extracted from figure). Absolute IC50 for ICEC0942 was around 0.03 µM in all tested lines (Table 37, Figure 47), which is also pharmacologically achievable (geometric mean trough plasma concentration 39.22 ng/mL, 0.091 µM (289).

Cell Line (Relative SOX2 CN)	**THZ1 (7 days)**			
	IC50 (µM)	(SEM)	Emax (%)	(SEM)
RERF-LC-SQ1 (3.24)	0.0305	0.0005	0.80	0.24
HCC2814 (2.319)	0.0619	0.0119	-0.05	0.08
NCI-H1703 (1.11)	0.0112	0.0005	0.68	0.15

Cell Line (Relative SOX2 CN)	**SY-5609 (7 days)**			
	IC50 (µM)	(SEM)	Emax (%)	(SEM)
RERF-LC-SQ1 (3.24)	0.0016	0.0008	13.66	3.57
HCC2814 (2.319)	0.0027	0.0004	6.23	1.95
NCI-H1703 (1.11)	0.0010	0.0002	4.74	2.03

Cell Line (Relative SOX2 CN)	**ICEC0942 (7 days)**			
	IC50 (µM)	(SEM)	Emax (%)	(SEM)
RERF-LC-SQ1 (3.24)	0.0303	0.0078	12.13	2.11
HCC2814 (2.319)	0.0314	0.0039	6.02	2.08
NCI-H1703 (1.11)	0.0247	0.0018	4.91	2.05

Table 37: Absolute IC50 and Emax for THZ1, ICEC0942 and SY-5609 at 7 days. Squamous cell lung cancer cell lines were treated with 0 – 100 µM THZ1, ICEC0942 or SY-5609. Cell viability was assessed at 7 days using cell titer-glo 2.0, plots of cell viability are displayed in Figure 47. Absolute IC50 and Emax are interpolated from curve using Prism for each experimental replicate. IC50 is defined as the concentration required to reduce viability by 50% relative to no treatment control. Emax is defined as the maximum drug effect observed within the sigmoidal curve ('bottom of the curve') (non-specific death beyond this point is disregarded), and is presented as percent viability relative to no treatment control. IC50 and Emax was calculated for each experimental replicate, with mean and SEM displayed. IC50 judged to be non-estimable (NE) where IC50 could not be interpolated from one or more experimental replicates.

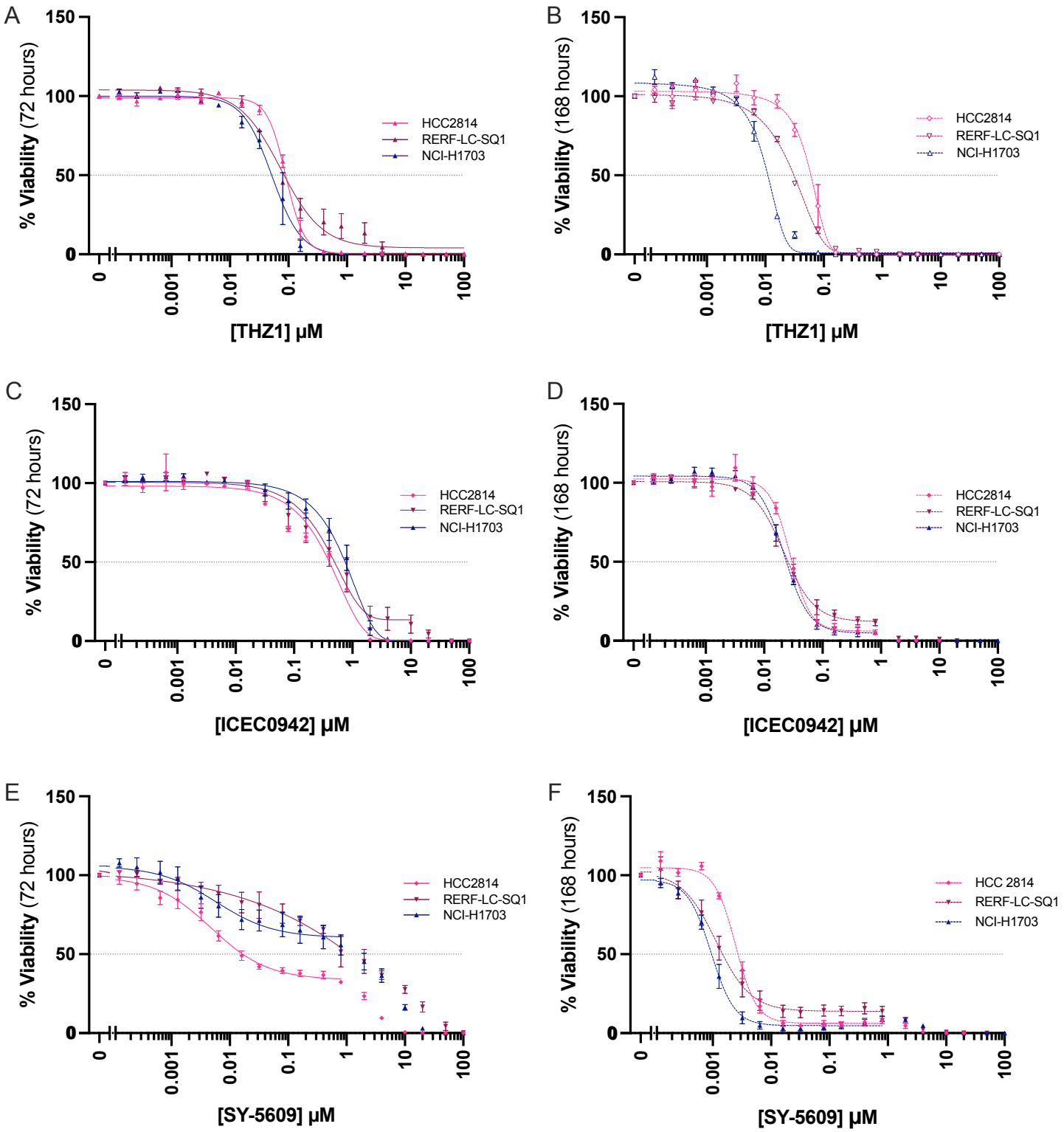

Figure 47: Impact of CDK7 Inhibition on cell viability at 72 hours and 7 days. Squamous cell lung cancers cell lines cell lines (RERF-LC-SQ1 relative SOX2 CN 3.24, HCC2814 relative SOX2 CN 2.319, NCI-H1703 relative SOX2CN 1.11) were treated with 0 – 100 µM THZ1 (A, B), ICEC0942 (C, D) or SY-5609 (E, F). Cell viability was assessed at 72 hours (A, C, E) and 7 days (B, D, F) using CellTiter-glo 2.0, subtracting background luminescence, and expressed relative to 0 µM drug. Curves plotted using Prism using non-linear regression. Experiment repeated at least three times for each cell line, with the exception of RERF-LC-SQ1 treated with THZ1 for 7 days (which was repeated twice). Mean and SEM displayed. 50% reduction in viability indicated by horizontal line. Note data displayed in A is the same as displayed in Figure 41 for the selected cell lines, but is presented to allow comparison of 72 hours and 7 days.

6.3.2.3 Impact of CDK7 inhibition (THZ1) on SOX2 expression at 48 hours

The impact of THZ1 treatment on SOX2 protein expression in RERF-LC-SQ1 cells was assessed (Figure 48). Treatment of RERF-LC-SQ1 with 1μM and 10 μM THZ1 markedly reduced SOX2 protein expression. These results corroborate previously published results that THZ1 treatment modulates SOX2 expression in squamous cell lung cancer cell lines (287), and confirms that this effect is also seen in high-level 3q amplification. As THZ1 is not a candidate for clinical development the impact of THZ1 on SOX2 expression was not assessed in additional squamous cell lines.

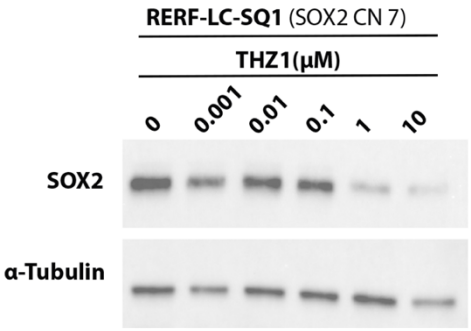

Figure 48: Impact of THZ1 treatment on SOX2 expression in 3q amplified squamous cell lung cancer cell lines. RERF-LC-SQ1 was treated with 0 – 10 μM THZ1 for 48 hours, and whole cell lysates were collected. SOX2 protein expression was assessed by western blotting. Experiment repeated twice, representative blot shown.

6.3.2.4 Impact of CDK7 inhibition (SY-5609) on SOX2 expression at 48 hours

Of the two options (ICEC0942 and SY-5609), SY-5609 was prioritised due to the remarkable potency in reducing viability at 7 days (321). SY-5609 treatment resulted in dose-dependent reduction in SOX2 protein levels in all tested lung cancer cell lines (Figure 49). 0.1 μM SY-5609 significantly reduced SOX2 expression in all cell lines: reducing SOX2 expression on densitometry by 58.2% in A549 ($P = 0.0039$), 53.6% in NCI-H1703 ($P = 0.00480$), 37.6% in HCC2814 ($P=0.0344$) and 48.3% in RERF-LC-SQ1 ($P = 0.0005$). Notably, the doses at which SY-5609 reduce SOX2 protein expression in squamous cell lines are within the dose ranges seen to have an impact on cell viability at 7 days (section 5.3.2.2). Future work will assess the impact of ICEC0942 on SOX2 protein expression.

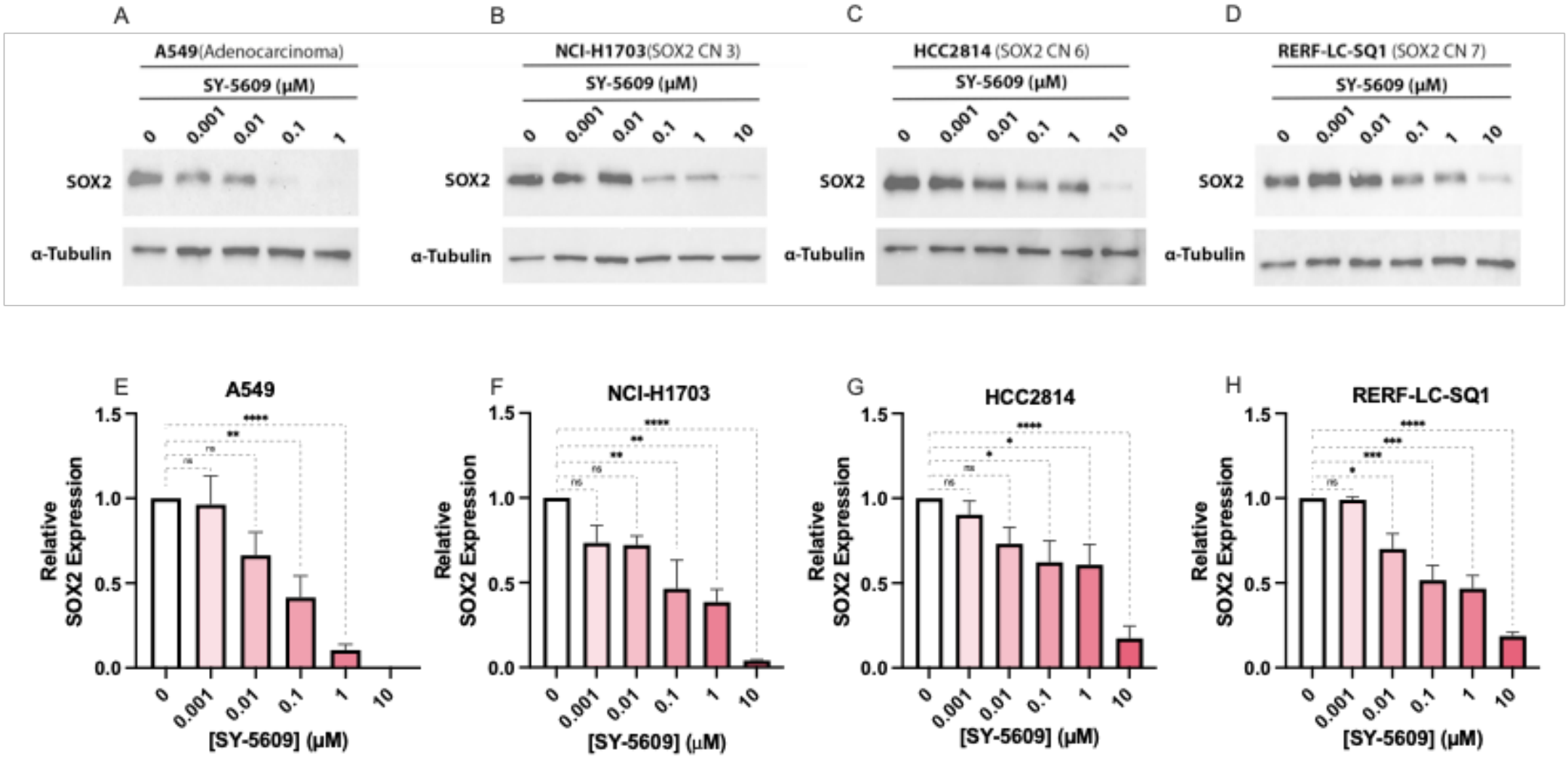

Figure 49: Impact of SY5609 treatment on SOX2 expression in panel of lung cancer cell lines. Lung cancer cell lines were treated with 0 – 10 μM SY-5609 for 48 hours, and whole cell lysates were collected. SOX2 protein expression was assessed by western blotting. For each cell line, experiment performed on three independent occasions, with representative blots shown are shown in A – D. No data available for 10 μM SY-5609 in A549, as cellular toxicity prohibited collection of sufficient protein at this dose. Densitometry plots are shown in E – H, with mean SOX2 expression (relative to 0 μM SY-5609) and SEM displayed. Statistical analysis performed using Prism, using ordinary one-way ANOVA with Dunett's multiple comparisons test (Adjusted P-values displayed: ns not significant, * P <0.05, ** P<0.01, *** P <0.001, **** p<0.0001)

6.3.2.5 CDK7 Inhibitors: summary

CDK7 inhibitors show *in vitro* activity in squamous cell lung cancer cell lines. However, for the SY-5609 and ICEC0942 reductions in viability were more mostly seen at 7 days. CDK7 inhibition reduces SOX2 expression in squamous cell lung cancer cell lines, including those with 3q amplification. Notably, this effect appears to be present at pharmacologically relevant concentrations in SY-5609. CDK7 inhibition is therefore a potential approach to modulate SOX2 expression in 3q amplified squamous cell lung cancer. CDK7 inhibition is therefore prioritised for ongoing work as a potential strategy to target SOX2 in 3q amplified squamous cell lung cancer.

6.3.3 AZD5153

AZD5153 is a potent BRD4 inhibitor (207-209). BRD4 and SOX2 signalling interact at multiple levels, including through promoting transcription of SOX2 (210, 211). PROTAC-mediated degradation of BRD4 suppresses SOX2 expression in squamous cancer cells (212). Likewise, BET inhibition (less specific than BRD4 inhibiton) has been shown to reduce SOX2 in some contexts (213, 214). However, no studies have investigated whether BRD4 inhibitors reduce SOX2 expression in squamous cell lung cancer.

6.3.3.1 Impact of AZD5153 on cell viability at 72 hours

Impact of 72 hours of AZD5153 treatment on viability of a panel of squamous cell lung cancer cell lines was assessed. All tested squamous cell lung cancer lines displayed dose-dependent reductions in viability (Figure 50, Table 38). Absolute IC50 was less than 0.3 µM in all three amplified cell lines, although suppression of viability was incomplete (Emax 15 – 35%). Three out of four non-amplified lines had an IC50 exceeding 1 µM (HCC1897, HCC2450 and H1703). Overall, these results suggest that 3q amplified cell lines are sensitive to treatment with AZD5153. However, 3q amplification status is not a strict criterion for sensitivity to AZD5153 in squamous cell lung cancer cell lines (IC50 for SKMES1 0.1148 µM).

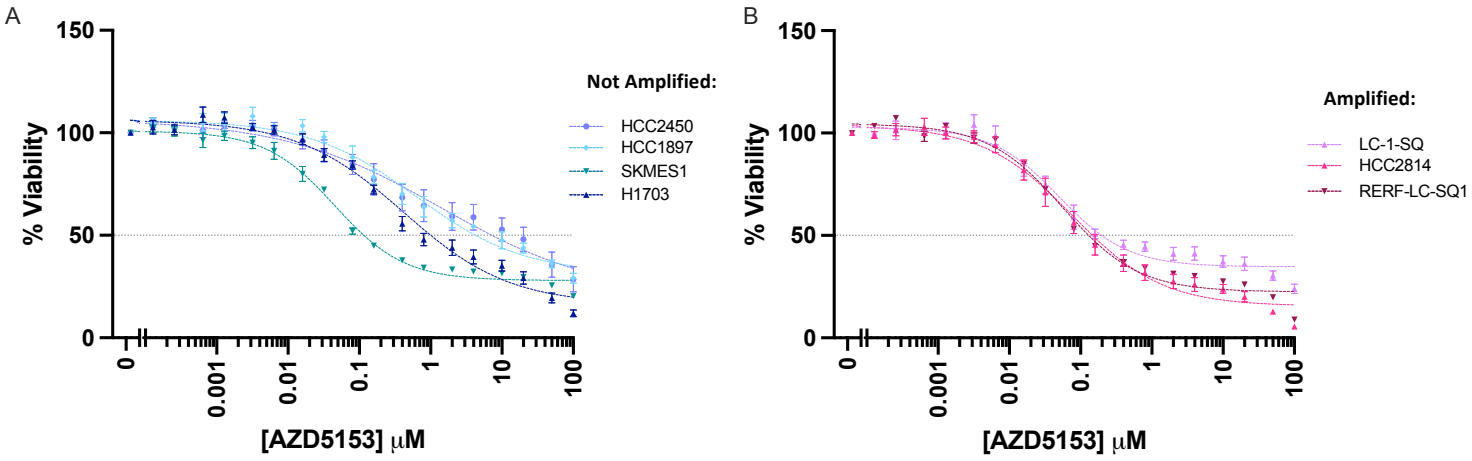

Figure 50: Impact of AZD5153 on cell viability at 72 hours. Non-amplified squamous cell lung cancer cell lines (A) and 3q amplified cell lines (B) were treated with 0 – 100 µM AZD5153. Cell viability was assessed at 72 hours using cell titer-glo 2.0, subtracting background luminescence, and expressed relative to 0 µM drug. Curves plotted using Prism using non-linear regression. Experiment repeated at least three times for each cell line, with mean and SEM displayed. 50% reduction in viability indicated by horizontal line.

Cell Line (relative SOX2)	**AZD5153 (72 hour)**			
	IC50 (µM)	(SEM)	Emax (%)	SEM
RERF-LC-SQ1 (3.24)	0.1286	0.0111	22.31	0.26
HCC2814 (2.319)	0.1952	0.0965	15.27	1.34
LC-1/SQ (1.97)	0.2019	0.0444	32.38	1.45
HCC1897 (1.667)	4.5755	1.8270	31.31	1.43
HCC2450 (1.404)	14.7838	11.7131	NE	-
SK-MES-1 (1.165)	0.1148	0.0021	27.81	0.94
NCI-H1703 (1.11)	1.1152	0.2778	15.77	0.95

Table 38: Absolute IC50 and Emax for AZD5153 at 72 hours. Squamous cell lung cancer cell lines were treated with 0–100 µM AZD5153. Cell viability was assessed at 72 hours using cell titer-glo 2.0, graphs displayed in Figure 53. Absolute IC50 and Emax are interpolated from curve using Prism for each experimental replicate. IC50 is defined as the concentration required to reduce viability by 50% relative to no treatment control. Emax is defined as the maximum drug effect observed within the sigmoidal curve ('bottom of the curve') (non-specific death beyond this point is disregarded), and is presented as percent viability relative to no treatment control. IC50 and Emax was calculated for each experimental replicate, with mean and SEM displayed. Emax judged to be non-estimable (NE) where plateau of sigmoid curve not reached for at least one replicate

6.3.3.2 Impact of AZD5153 on cell viability at 7 days

Impact of 7 days of AZD5153 treatment was assessed in three squamous cell lung cancer cell lines. IC50 was 0.0606 µM and 0.0355 µM for RERF-LC-SQ1 and HCC2814, which was significantly lower than IC50 at 72 hours for both lines (P = 0.0036, P = 0.0004). IC50 was 0.1920 µM for NCI-H1703, which was also significantly lower than at 72 hours (P = 0.0299) (Figure 51, Table 39). Emax was less than 5% in all three tested squamous lines at 7 days. In humans, C_{max} for AZD5153 is 272.4 nmol/L, at the recommended phase II dose of 30 mg once daily dosing (multiple-dose parameter) (322). Therefore, AZD5153 reduces viability of 3q amplified cell lines at clinically meaningful concentrations.

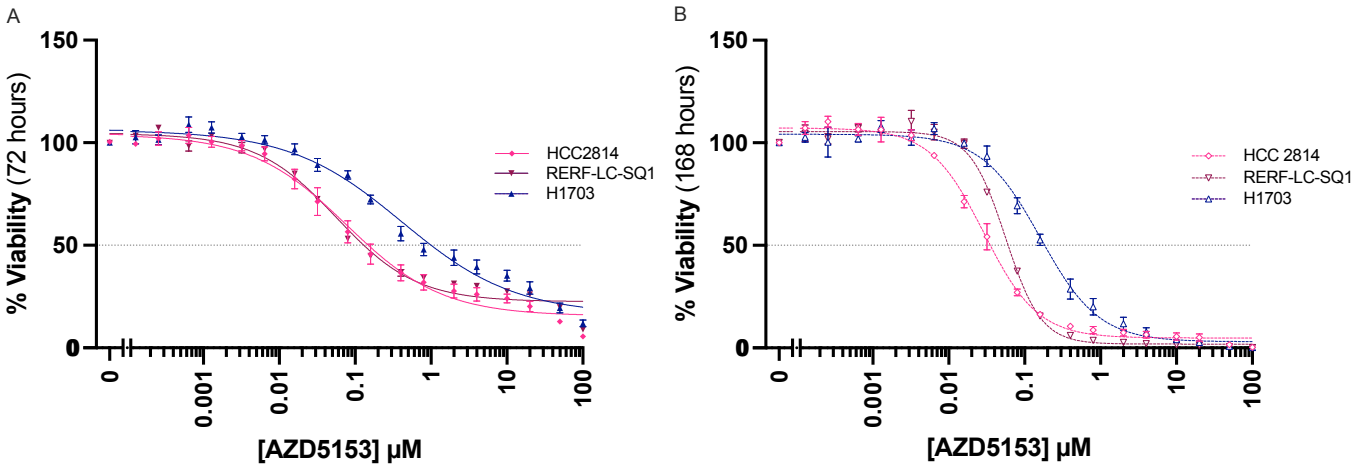

Figure 51: Impact of AZD513 on cell viability at 72 hours and 7 days. Squamous cell lung cancer cell lines (RERF-LC-SQ1 relative SOX2 CN 3.24, HCC2814 relative SOX2 CN 2.319, NCI-H1703 relative SOX2 CN 1.11) treated with 0 – 100 µM AZD5153. Cell viability was assessed at 72 hours (A) and 7 days (B) using CellTiter-glo 2.0, subtracting background luminescence, and expressed relative to 0 µM ORY-1001. Curves plotted using Prism using non-linear regression. Experiment repeated at least three times for each cell line, with mean and SEM displayed. 50% reduction in viability indicated by horizontal line. *Note data displayed in A is the same as displayed in Figure 45 for the selected cell lines, but is presented to allow comparison of 72 hours*

Cell Line (Relative SOX2 CN)	**AZD5153 (7 day)**			
	IC50 (µM)	(SEM)	Emax (%)	(SEM)
RERF-LC-SQ1 (3.24)	0.0606	0.0006	1.88	0.20
HCC2814 (2.319)	0.0355	0.0040	4.93	1.35
NCI-H1703 (1.11)	0.1920	0.0323	2.62	0.18

Table 39: Absolute IC50 and Emax for AZD5153 at 7 days. Squamous cell lung cancer cell lines treated with 0 – 100 µM AZD5153 Cell viability was assessed at 7 days using cell titer-glo 2.0 (Graphs displayed in Figure 51B). Absolute IC50 and Emax are interpolated from curve using Prism for each experimental replicate. IC50 is defined as the concentration required to reduce viability by 50% relative to no treatment control. Emax is defined as the maximum drug effect observed within the sigmoidal curve ('bottom of the curve') (non-specific death beyond this point is disregarded), and is presented as percent viability relative to no treatment control. IC50 and Emax was calculated for each experimental replicate, with mean and SEM displayed. IC50 judged to be non-estimable (NE) where IC50 could not be interpolated from one or more experimental replicates

6.3.3.3 Impact of AZD5153 on SOX2 expression at 48 hours

Treatment with AZD5153 resulted in a dose dependent reduction in SOX2 protein expression in all tested squamous cell lung cancer cell lines (Figure 52). This reduction in SOX2 protein expression was apparent in both 3q amplified lines (HCC2814 and RERF-LC-SQ1) and in cells without 3q amplification (NCI-H1703). The doses at which AZD5153 reduce SOX2 protein expression in squamous cell lines are within the dose ranges seen to have an impact on cell viability.

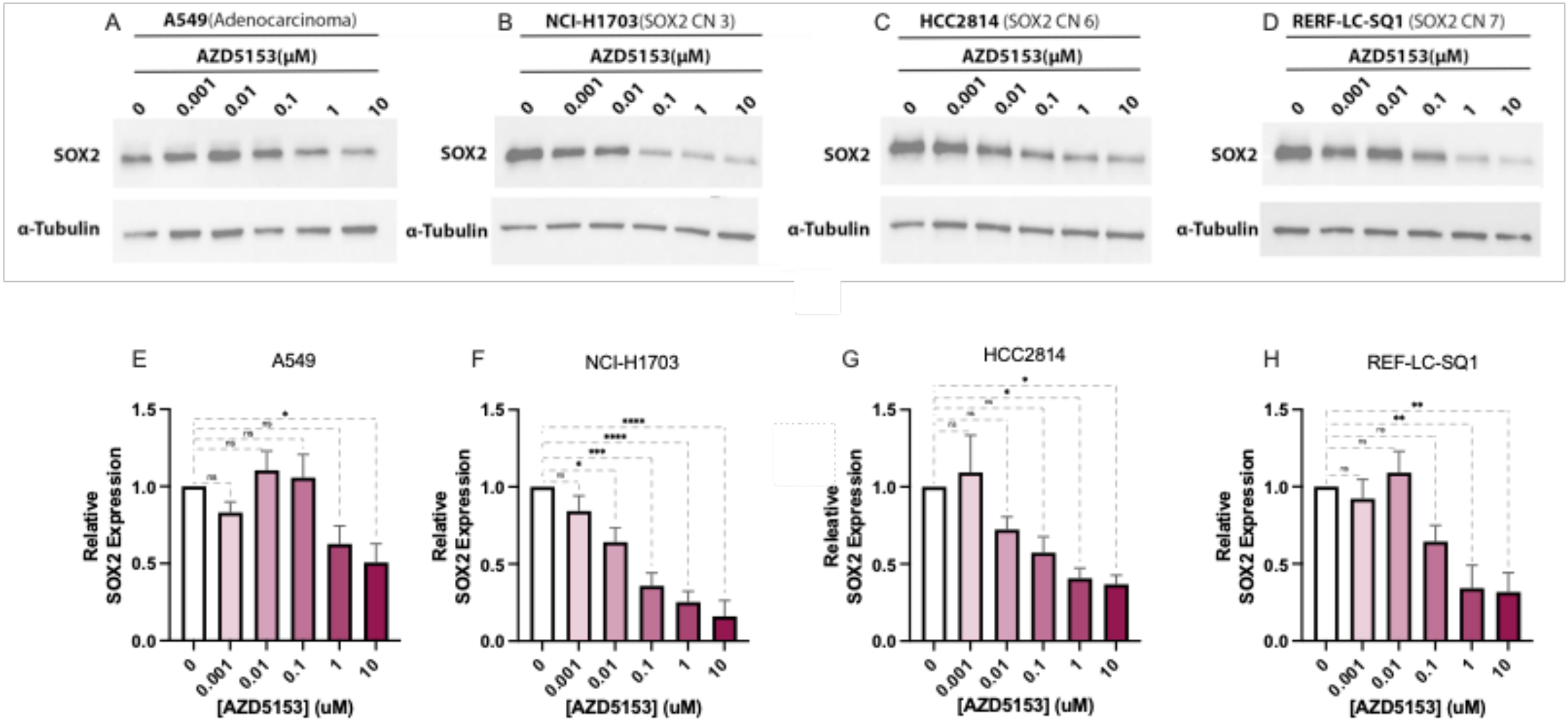

Figure 52: Impact of AZD5153 treatment on SOX2 expression in panel of lung cancer cell lines. Lung cancer cell lines were treated with 0 – 10 μM AZD5153 for 48 hours, and whole cell lysates were collected. SOX2 protein expression was assessed by western blotting. For each cell line, experiment repeated at least three times with collection, processing and running of independently drugged and collected lysates. Representative blot shown are shown in A – D.. Densitometry plots are shown in E – H, with mean SOX2 expression (relative to 0 μM AZD5153) and SEM displayed. Statistical analysis performed using Prism, using ordinary one-way ANOVA with Dunett's multiple comparisons test (Adjusted P-values displayed: ns not significant, * P <0.05, ** P<0.01, *** P <0.001, **** p<0.0001)

6.3.3.4 Combination Drug Experiments with AZD5153

It was hypothesised that a strategy of targeting SOX2 with AZD5153 may synergise with inhibition of the PI3K/Akt axis. AZD5153 in combination with alpelisib (PI3Kα inhibition) (323) or capivasertib (Akt1/2/3 inhibition) (324) in RERF-LC-SQ1. Cell viability was assessed at 72 hours and synergy was assessed using MuSyc (2, 3), accessed via SynergyFinder 2.0 (325). Synergistic efficacy was observed when AZD5153 was combined with Capivasertib treatment, although this was relatively modest (15% increase in maximum effect when combination of both drugs compared to most efficacious single drug) and there was no synergistic potency observed (Figure 53). No synergistic effects were observed when AZD5153 was combined with Alpelisib treatment (Figure 54).

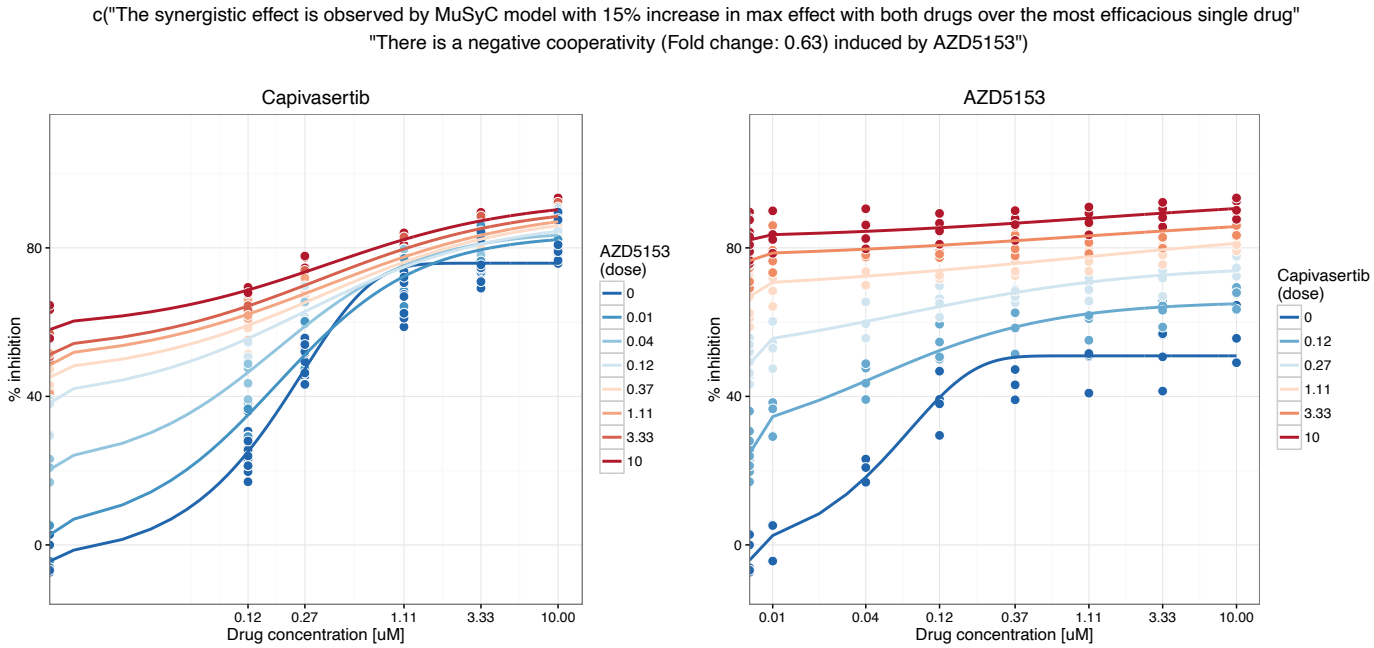

Figure 53: MuSyc plot of combination treatment with Capivasertib and AZD5153. RERF-LC-SQ1 cells were seeded in 96 well plates and treated with 0 – 10 μM Capivasertib in combination with 0 - 10 μM AZD5153. For each biological replicate, plates were seeded and treated in triplicate. Experiment repeated four times on independent passages. Analysis using MuSyc which was accessed via Synergy Finder (https://synergyfinder.fimm.fi). Interpretation of the drug interactions is outlined at the top of the plot (as generated by MuSyC)

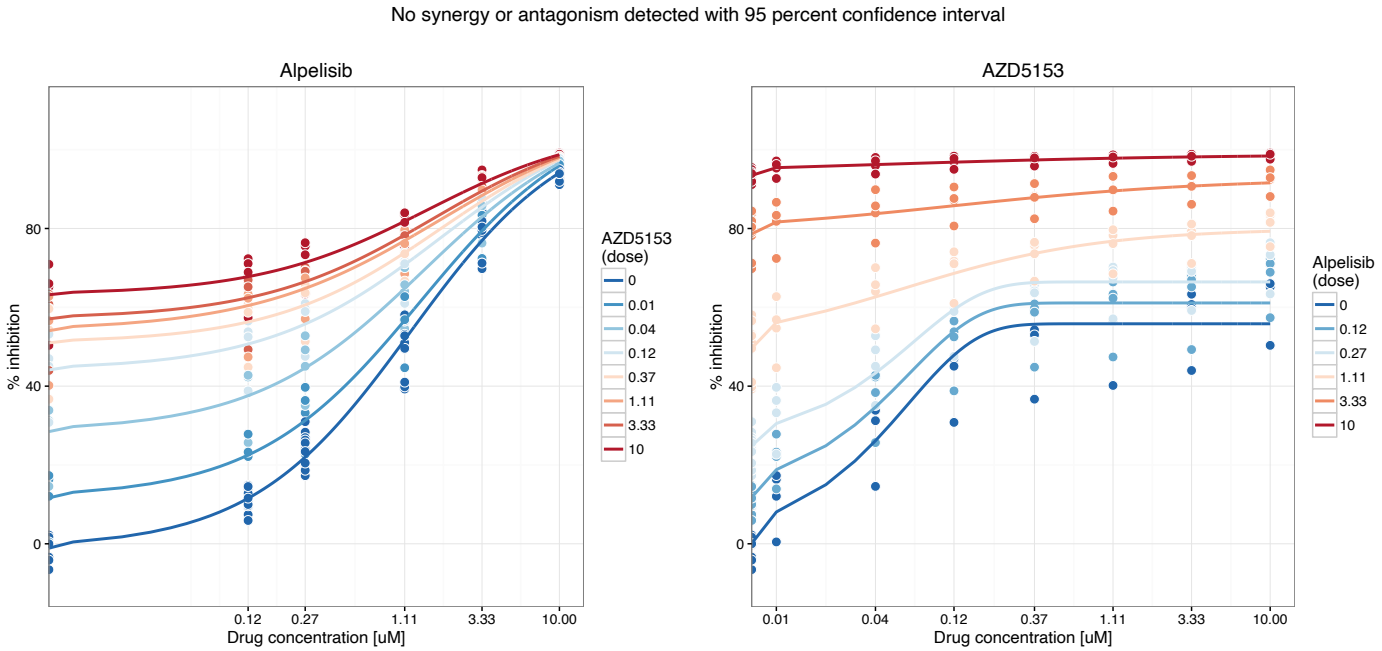

Figure 54: MuSyc plot of combination treatment with Alpelisib and AZD5153. RERF-LC-SQ1 cells were seeded in 96 well plates and treated with 0 – 10 µM Alpelisib in combination with 0 - 10 µM AZD5153. For each biological replicate, plates were seeded and treated in triplicate. Experiment repeated four times on independent passages. Analysis using MuSyc which was accessed via Synergy Finder (https://synergyfinder.fimm.fi). Interpretation of the drug interactions is outlined at the top of the plot (as generated by MuSyC)

6.3.3.5 AZD5153: Summary

AZD5153 suppresses viability of 3q amplified cell lines at pharmacologically meaningful concentrations and reduces SOX2 expression in vitro. Therefore, BRD4 inhibition with AZD5153 represents a potential approach to modulate SOX2 expression in squamous cell lung cancer. AZD5153 is therefore prioritised for ongoing work.

6.3.4 Pevonedistat (MLN4924)

Pevonedistat is an inhibitor of NEDD8-activating enzyme (NAE, which leads to a reduction in NEDDlyation). Pevonedistat has been shown to reduce SOX2 expression in non 3q amplified NSCLC cell lines, however no studies have examined whether pevonedistat exerts this effect in the context of 3q amplification.

6.3.4.1 Impact of Pevonedistat (MLN4924) on cell viability at 72 hours

Impact of 72 hours of pevonedistat (MLN4924) treatment on viability of a panel of squamous cell lung cancer cell lines was assessed. All cell lines displayed a dose-dependent reduction in viability with increasing concentrations of pevonedistat (Figure 55), IC50 ranging from 0.035–1.700 μM (Table 40). There was no clear relationship between 3q amplification status and sensitivity to pevonedistat.

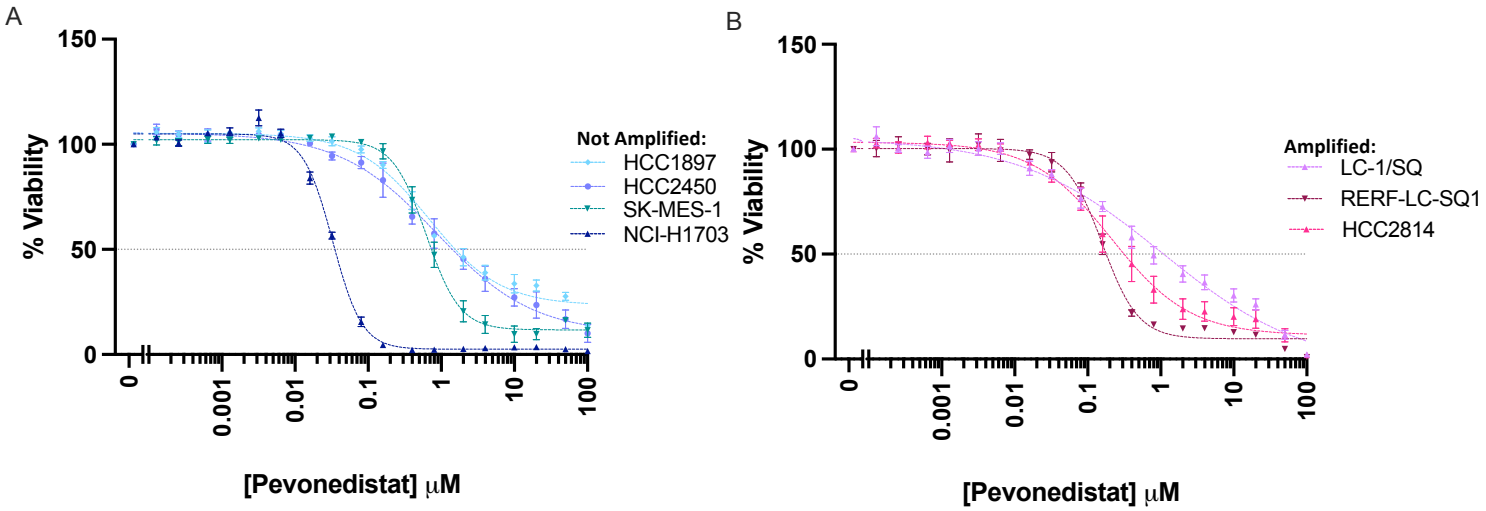

Figure 55: Impact of Pevonedistat on cell viability at 72 hours. Non-amplified squamous cell lung cancer cell lines (A) and 3q amplified cell lines (B) were treated with 0 – 100 μM Pevonedistat (A, B). Cell viability was assessed at 72 hours using cell titer-glo 2.0, subtracting background luminescence, and expressed relative to 0 μM drug. Curves plotted using Prism using non-linear regression. Experiment repeated at least three times for each cell line. Mean and SEM displayed. 50% reduction in viability indicated by horizontal line.

Cell Line (relative SOX2 CN)	Pevonedistat (72 hour)			
	IC50 (μM)	(SEM)	Emax (%)	(SEM)
RERF-LC-SQ1 (3.24)	0.180	0.016	9.85	0.58
HCC2814 (2.319)	0.383	0.125	11.04	1.83
LC-1/SQ (1.97)	1.363	0.548	NE	NE
HCC1897 (1.667)	1.700	0.425	22.98	1.06
HCC2450 (1.404)	1.691	0.722	10.54	3.99
SK-MES-1 (1.165)	0.763	0.118	11.57	2.37
NCI-H1703 (1.11)	0.035	0.001	2.52	0.23

Table 40: Absolute IC50 and Emax for Pevonedistat at 72 hours. Squamous cell lung cancers treated with 0–100 μM Pevonedistat. Cell viability was assessed at 72 hours using cell titer-glo 2.0, graphs displayed in (Figure 55), Absolute IC50 and Emax are interpolated from curve using Prism for each experimental replicate. IC50 is defined as the concentration required to reduce viability by 50% relative to no treatment control. Emax is defined as the maximum drug effect observed within the sigmoidal curve ('bottom of the curve') (non-specific death beyond this point is disregarded), and is presented as percent viability relative to no treatment control. IC50 and Emax was calculated for each experimental replicate, with mean and SEM displayed. IC50 judged to be non-estimable (NE) where IC50 could not be interpolated from one or more experimental replicates

6.3.4.2 Impact of Pevonedistat (MLN4924) on cell viability at 7 days

Impact of 7 days of pevonedistat treatment on viability on squamous cell lung cancer cell lines was assessed. IC50 ranged from 0.0064 μM for NCI-H1703 (non-amplified) to 0.0791 μM for RERF-LC-SQ1 (3q amplified) (Figure 56, Table 41). As may be expected, IC50 shifted leftwards with longer treatment, but this did not seem to be more marked in the amplified vs non-amplified cell line (although it is acknowledged only a small number of lines were tested)

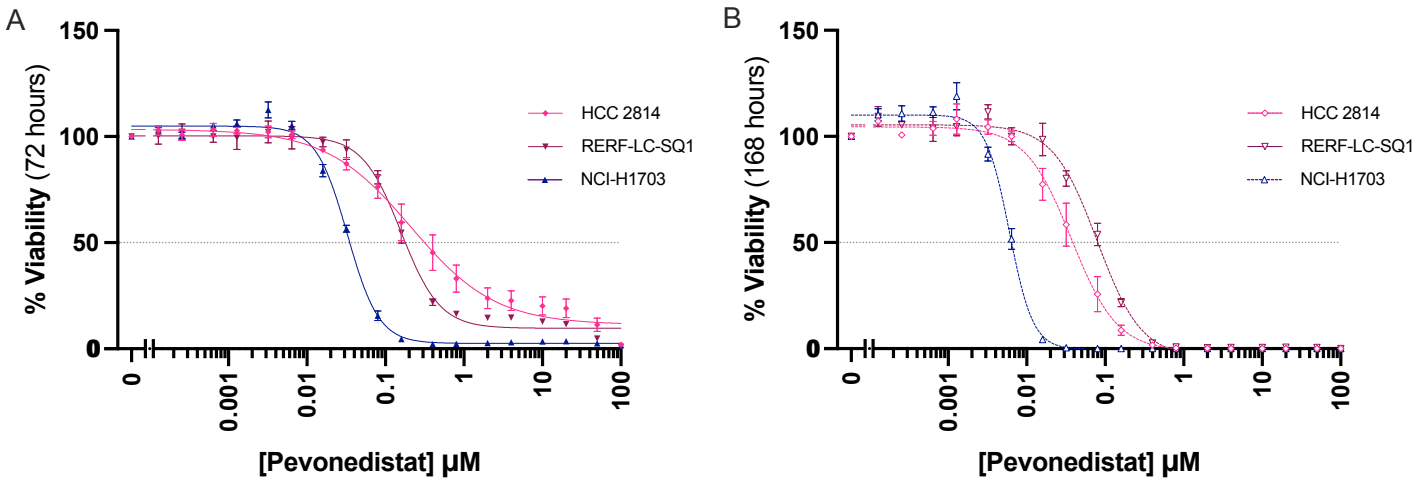

Figure 56: Impact of Pevonedistat on cell viability at 72 hours and 7 days. Squamous cell lung cancer cell lines (RERF-LC-SQ1 relative SOX2 CN 3.24, HCC2814 relative SOX2 CN 2.319, NCI-H1703 relative SOX2CN 1.11) were treated with 0 – 100 μM Pevonedistat. Cell viability was assessed at 72 hours (A) and 7 days (B) using CellTiter-glo 2.0, subtracting background luminescence, and expressed relative to 0 μM ORY-1001. Curves plotted using Prism using non-linear regression. Experiment repeated at least three times for each cell line, with mean and SEM displayed. 50% reduction in viability indicated by horizontal line. Note data displayed in A is the same as displayed in Figure 45 for the selected cell lines, but is presented to allow comparison of 72 hours and 7 days

Cell Line (Relative SOX2 CN)	Pevonedistat (7 day)			
	IC50 (μM)	(SEM)	Emax (%)	(SEM)
RERF-LC-SQ1 (3.24)	0.0791	0.0078	-4.08	0.87
HCC2814 (2.319)	0.0407	0.0106	-0.68	0.68
NCI-H1703 (1.11)	0.0064	0.0004	-0.30	0.06

Table 41: Absolute IC50 and Emax for Pevonedistat at 7 days. Squamous cell lung cancer cell lines were treated with 0–100 μM Pevonedistat. Cell viability was assessed at 7 days using cell titer-glo 2.0, graphs displayed in (Figure 56)). Absolute IC50 and Emax are interpolated from curve using Prism for each experimental replicate. IC50 is defined as the concentration required to reduce viability by 50% relative to no treatment control. Emax is defined as the maximum drug effect observed within the sigmoidal curve ('bottom of the curve') (non-specific death beyond this point is disregarded), and is presented as percent viability relative to no treatment control. IC50 and Emax was calculated for each experimental replicate, with mean and SEM displayed. IC50 judged to be non-estimable (NE) where IC50 could not be interpolated from one or more experimental replicates

6.3.4.3 Impact of Pevonedistat (MLN4924) on SOX2 Expression at 48 hours

Treatment of A549 lung adenocarcinoma cells and non-amplified squamous cell lung cancer cells (NCI-H1703) resulted in substantial reductions in SOX2 protein expression. Non-amplified NCI-H1703 cells were particularly sensitive: 0.01 μM Pevonedistat reduced SOX2 by 69.5% (P =0.0003). The reductions in SOX2 protein expression were less apparent in 3q amplified RERF-LC-SQ1 cells, and were only significant at high concentrations which are suprapharmacological (281). In 3q amplified HCC2814, there was no clear reduction in SOX2 protein expression even with 10 μM Pevonedistat. Although it is acknowledged that the number of 3q amplified cell lines that are tested is small, these results are not supportive for ongoing work in using pevonedistat to modulate SOX2 in the context of 3q amplification.

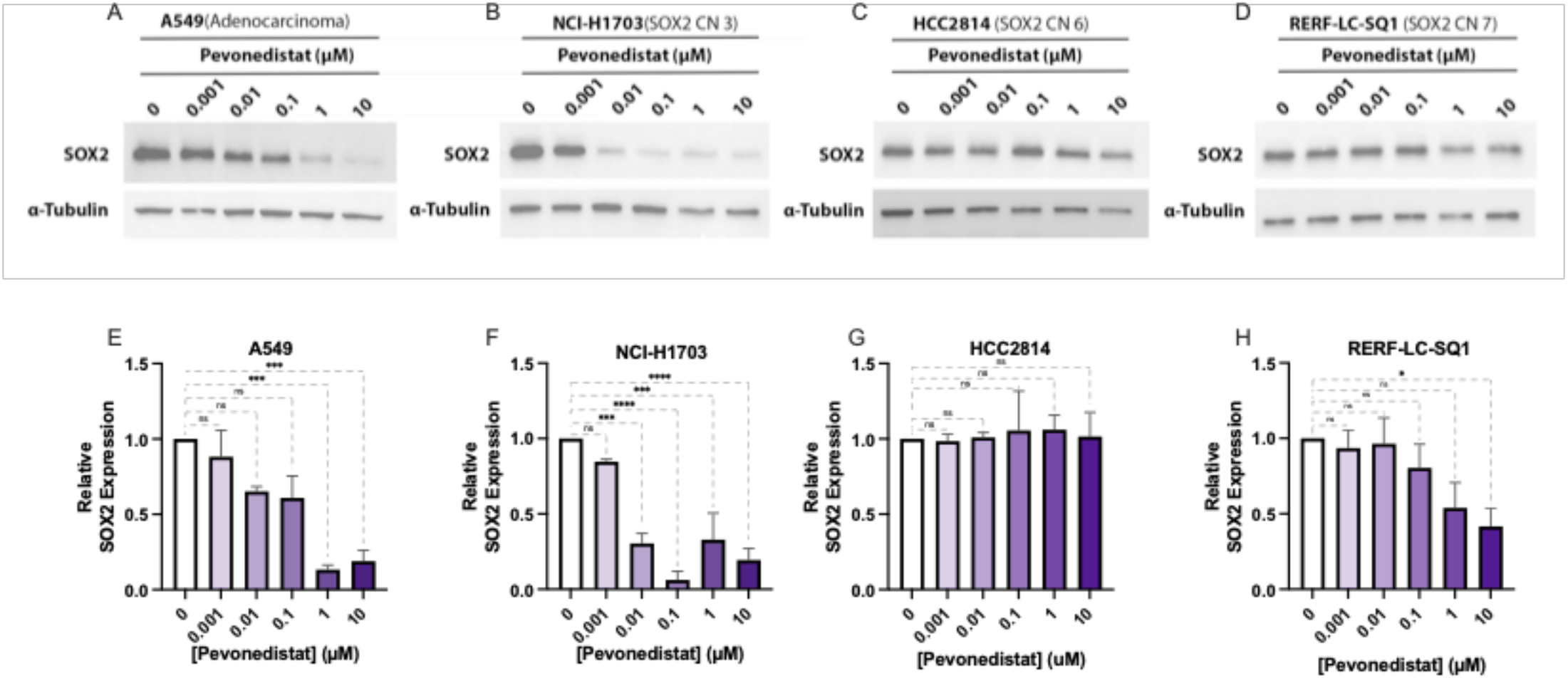

Figure 57: Impact of Pevonedistat treatment on SOX2 expression in panel of lung cancer cell lines. Lung cancer cell lines were treated with 0 – 10 μM Pevonedistat for 48 hours, and whole cell lysates were collected. SOX2 protein expression was assessed by western blotting. For each cell line, experiment repeated at least three times with collection, processing and running of independently drugged and collected lysates. Representative blot shown are shown in A – D.. Densitometry plots are shown in E – H, with mean SOX2 expression (relative to 0 μM Pevonedistat) and SEM displayed. Statistical analysis performed using Prism, using ordinary one-way ANOVA with Dunett's multiple comparisons test (Adjusted P-values displayed: ns not significant, * P <0.05, ** P<0.01, *** P <0.001, **** p<0.0001)

6.3.4.4 Combination Drug Experiments with Pevonedistat

It was hypothesised that a strategy of targeting SOX2 with pevonedistat may synergise with inhibition of the PI3K/Akt axis. Combination treatments of Pevonedistat/Gefitnib, Pevonedistat/Alpelisib and Pevonedistat/Capivasertib were assessed in RERF-LC-SQ1. Cell viability was assessed at 72 hours and synergy was assessed using MuSyc (2, 3), accessed via SynergyFinder 2.0 (2) (Figure 58 - Figure 60). Antagonistic potency shifts were observed with all drug combinations, meaning that relative IC50 for a drug was higher in combination than when in used as monotherapy. Therefore there was no evidence of synergy, and Pevonedistat/Gefitnib, Pevonedistat/Alpelisib and Pevonedistat/Capivasertib are not promising drug combinations in 3q amplified squamous cell lung cancer cell lines.

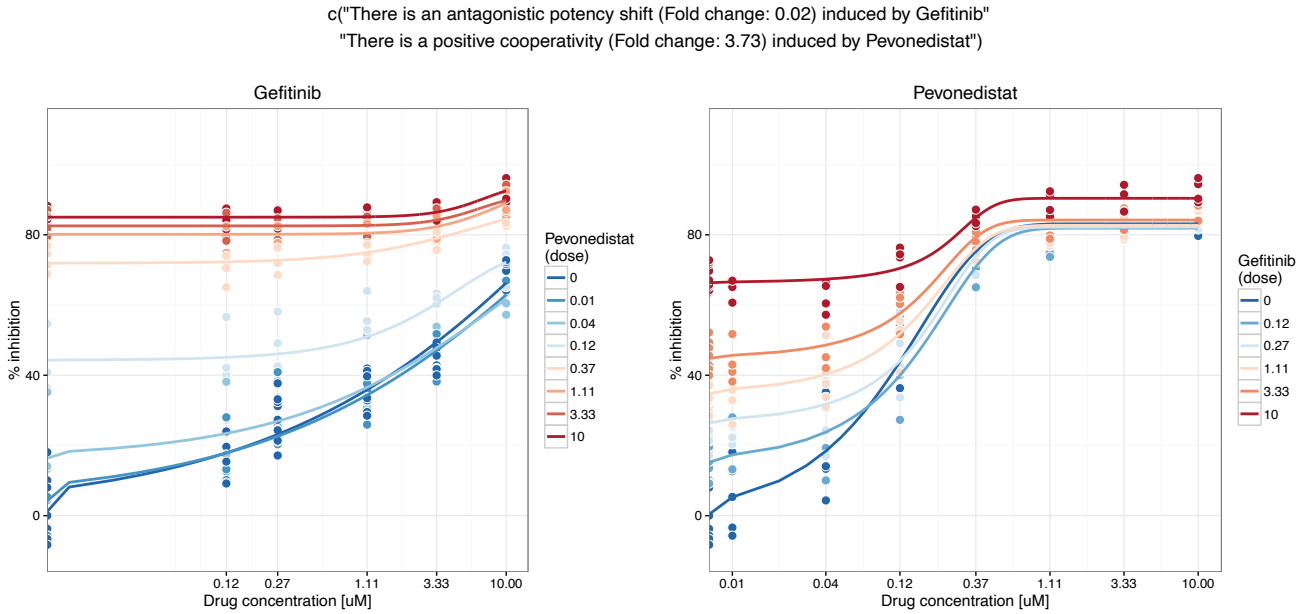

Figure 58: MuSyc plot of combination treatment with Gefitinib and Pevonedistat. RERF-LC-SQ1 cells were seeded in 96 well plates and treated with 0 – 10 µM Gefinib in combination with 0 - 10 µM Pevonedistat. For each biological replicate, plates were seeded and treated in triplicate. Experiment repeated four times on independent passages. Analysis using MuSyc which was accessed via Synergy Finder (https://synergyfinder.fimm.fi). Interpretation of the drug interactions is outlined at the top of the plot (as generated by MuSyC)

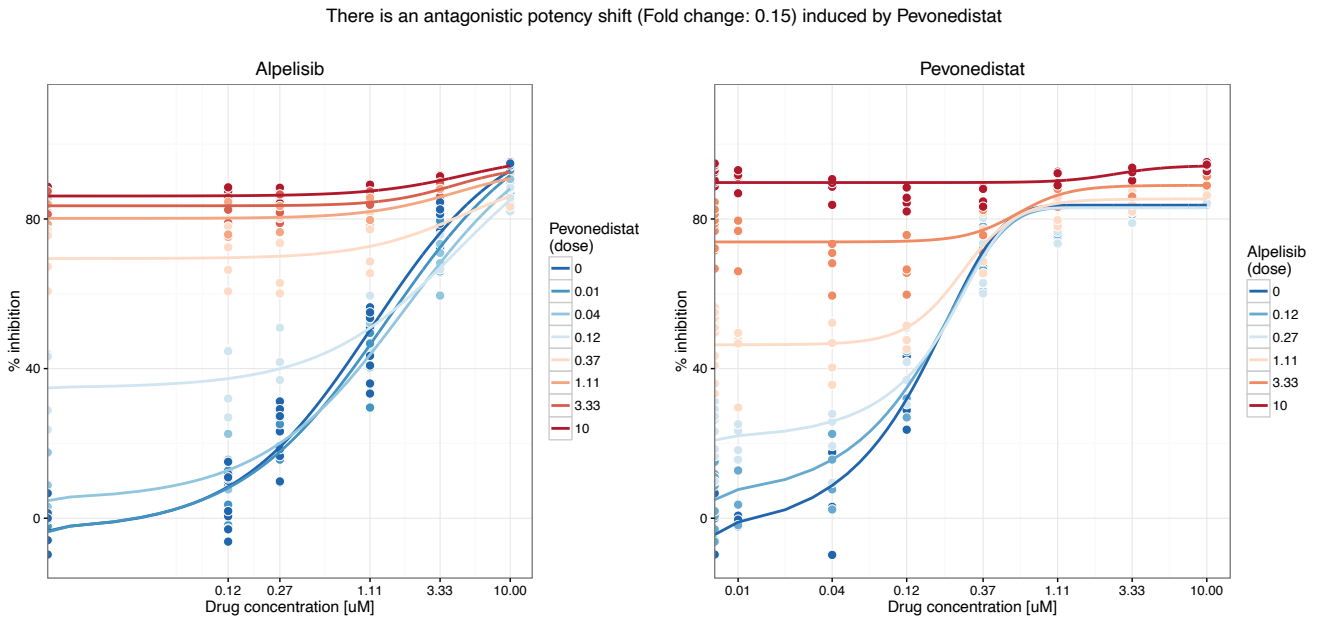

Figure 59: MuSyc plot of combination treatment with Alpelisib and Pevonedistat. RERF-LC-SQ1 cells were seeded in 96 well plates and treated with 0 – 10 µM Alpelisib in combination with 0 - 10 µM Pevonedistat. For each biological replicate, plates were seeded and treated in triplicate. Experiment repeated four times on independent passages. Analysis using MuSyc which was accessed via Synergy Finder (https://synergyfinder.fimm.fi). Interpretation of the drug interactions is outlined at the top of the plot (as generated by MuSyC)

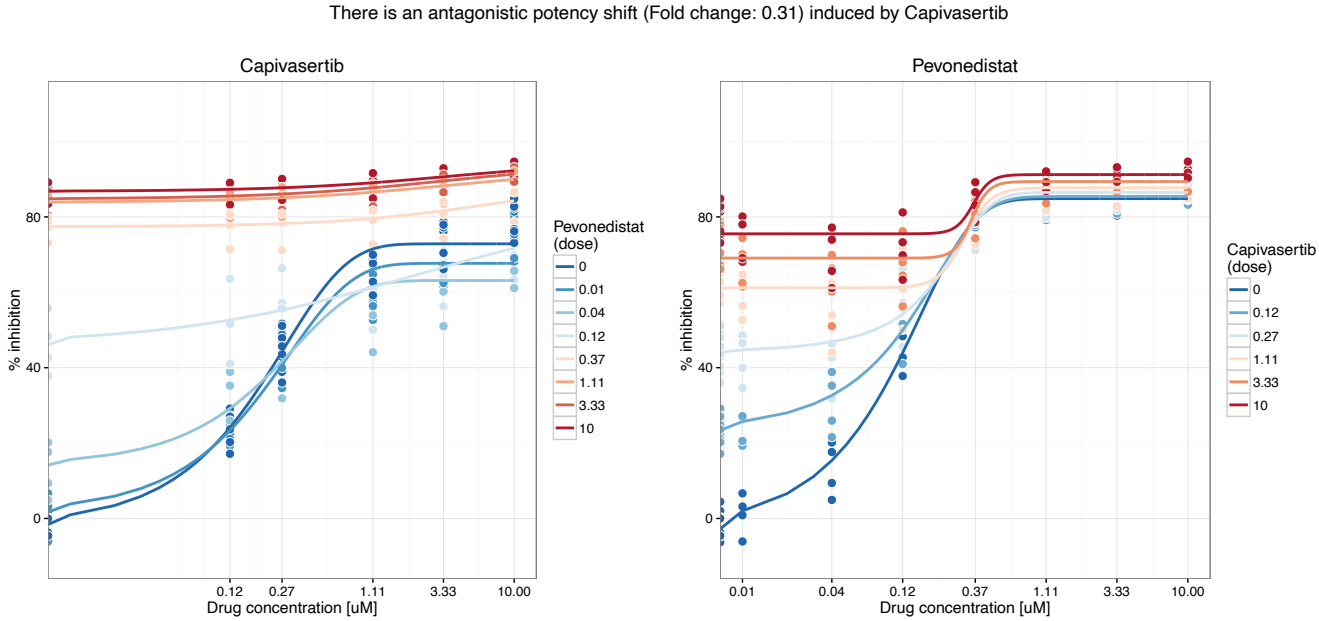

Figure 60: MuSyc plot of combination treatment with Capivasertib and Pevonedistat. RERF-LC-SQ1 cells were seeded in 96 well plates and treated with 0 – 10 µM Alpelisib in combination with 0 - 10 µM Pevonedistat. For each biological replicate, plates were seeded and treated in triplicate. Experiment repeated four times on independent passages. Analysis using MuSyc which was accessed via Synergy Finder (https://synergyfinder.fimm.fi). Interpretation of the drug interactions is outlined at the top of the plot (as generated by MuSyC)

6.3.4.5 Pevonedistat: Summary

There was no convincing evidence of an increase in sensitivity of 3q amplified lines versus non-amplified lines to pevonedistat. Whilst pevonedistat treatment reduced SOX2 expression in non-amplified cell lines, this effect was either muted or absent in the tested 3q amplified lines. No synergy was demonstrated between pevonedistat and either PI3Ki or Akti. Overall, pevonedistat does not seem a promising candidate for further work as a strategy to target SOX2 in 3q amplified squamous cell lung cancer

6.3.5 KDM1A (LSD1) Inhibition: ORY-1001 (Iadedemstat)

KDM1A (LSD1) regulates gene expression through demethylation of mono- and dimethylated H3K9 (271). Iadedemstat (ORY-1001) is a potent KDM1A inhibitor (273). Iadedemstat suppresses SOX2 transcriptional activation in breast cancer mammosphere culture (274). CBB1007 and CBB1003, closely related competitive inhibitors of KDM1A, reduce SOX2 expression in squamous cell lung cancer cells (275). However the dose used (50 μM) is unlikely to be clinically achievable: at a dose of 140 μg/m^2/day, Cmax on Day 26 is 55 pg/mL (0.18 nM) (273).(273). No other studies have investigated with KDM1A inhibition impacts SOX2 protein expression in 3q amplified cell lines.

6.3.5.1 Impact of ORY-1001 on cell viability at 72 hours

Impact of 72 hours of ORY-1001 treatment on viability of a panel of squamous cell lung cancer cell lines was assessed. IC50 exceeded 40 μM in all tested cell lines (Figure 61, Table 42). In four cell lines (HCC2814, LC-1/SQ, HCC1897, H1703) IC50 exceeded 100 μM. There was no apparent increased sensitivity with increasing SOX2 copy number. Similar results were achieved in serum-containing and serum-free conditions (not shown). Similar results were achieved with ORY-1001 obtained from two separate suppliers (Generon and Stratech) in two different solvents (DMSO or H_2O) (not shown). Emax could not be estimated for any cell lines.

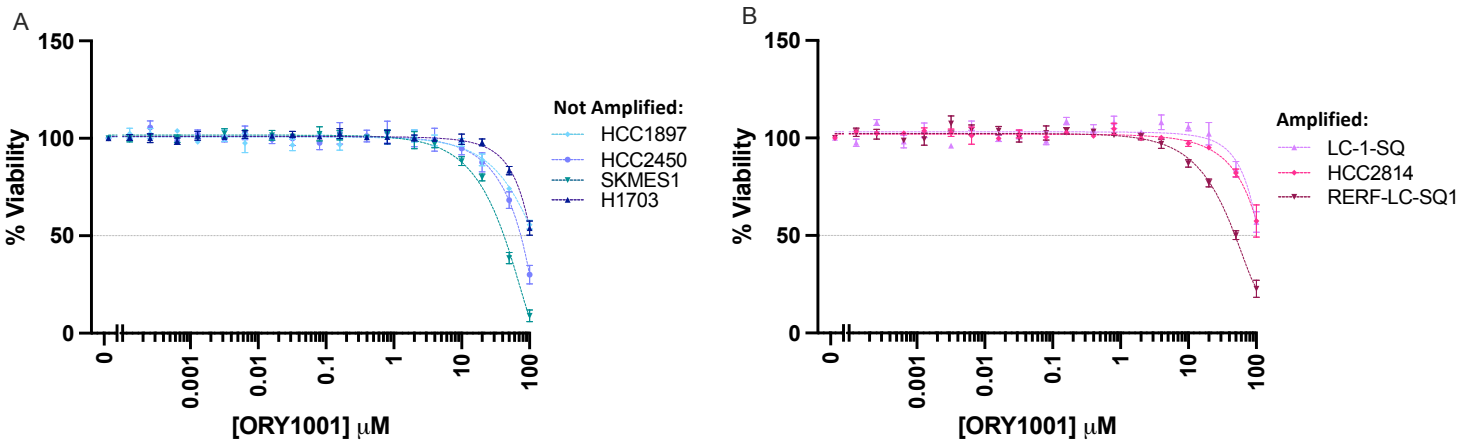

Figure 61: Impact of ORY-1001 on cell viability at 72 hours. Non-amplified squamous cell lung cancer cell lines (A) and 3q amplified cell lines (B) were treated with 0 – 100 μM ORY-1001 (ladedemstat). Cell viability was assessed at 72 hours using cell titer-glo 2.0, subtracting background luminescence, and expressed relative to 0 μM ORY-1001. Curves plotted using Prism using non-linear regression (second order polynomial, quadratic). Experiment repeated at least three times for each cell line, with mean and SEM displayed. 50% reduction in viability indicated by horizontal line.

	ORY-1001 (72 hour)			
Cell Line (relative SOX2 CN)	IC50 (μM)	(SEM)	Emax (%)	(SEM)
RERF-LC-SQ1 (3.24)	49.44	(3.46)	NE	-
HCC2814 (2.319)	NE	-	NE	-
LC-1-SQ (1.97)	105.60	(5.71)	NE	-
HCC1897 (1.667)	NE	-	NE	-
HCC2450 (1.404)	73.90	(6.26)	NE	-
SKMES1 (1.165)	42.07	(0.69)	NE	-
H1703 (1.11)	105.08	(5.09)	NE	-

Table 42: Absolute IC50 and Emax for ORY-1001 at 72 hours. Squamous cell lung cancers treated with 0 – 100 μM ORY-1001 (ladedemstat). Cell viability was assessed at 72 hours using cell titer-glo 2.0, graphs displayed in Figure 61. Absolute IC50 and Emax are interpolated from curve using Prism for each experimental replicate. IC50 is defined as the concentration required to reduce viability by 50% relative to no treatment control. Emax is defined as the maximum drug effect observed within the sigmoidal curve ('bottom of the curve') (non-specific death beyond this point is disregarded), and is presented as percent viability relative to no treatment control. IC50 and Emax was calculated for each experimental replicate, with mean and SEM displayed. IC50 judged to be non-estimable (NE) where IC50 could not be interpolated from one or more experimental replicates

6.3.5.2 Impact of ORY-1001 on viability at 7 days

Even after 7 days of drug incubation, ORY-1001 showed limited toxicity at pharmacologically meaningful concentrations. IC50 at 7 days was not estimable in HCC2814, and exceeded 20 µM in RERF-LC-SQ1 and NCI-H1703 (Figure 62, Table 43). Emax could not be estimated for any cell lines. Achievable concentrations of ORY-1001 are in the pg/ml range (273), therefore the reductions in cell viability at very high doses are not clinically translatable or meaningful.

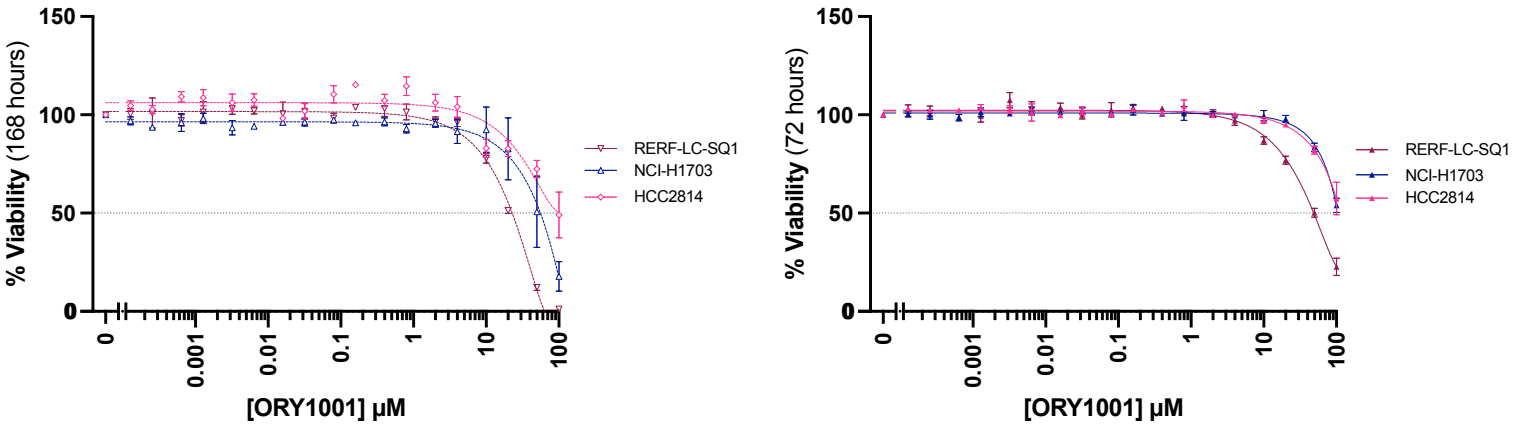

Figure 62: Impact of ORY-1001 on cell viability at 72 hours and 7 days. Squamous cell lung cancer cell lines cell lines (RERF-LC-SQ1 relative SOX2 CN 3.24, HCC2814 relative SOX2 CN 2.319, NCI-H1703 relative SOX2CN 1.11) were treated with 0 – 100 µM ORY-1001 (ladedemstat). Cell viability was assessed at 72 hours (A) and 7 days (B) using CellTiter-glo 2.0, subtracting background luminescence, and expressed relative to 0 µM ORY-1001. Curves plotted using Prism using non-linear regression (second order polynomial, quadratic). Experiment repeated at least three times for each cell line, with mean and SEM displayed. 50% reduction in viability indicated by horizontal line. *Note data displayed in A is the same as displayed in Figure 45 for the selected cell lines, but is presented to allow comparison of 72 hours and 7 days*

Cell Line (Relative SOX2 CN)	**ORY1001 (7 day)**			
	IC50 (µM)	(SEM)	Emax (%)	(SEM)
RERF-LC-SQ1 (3.24)	22.81	(0.21)	NE	-
HCC2814 (2.319)	NE	-	NE	-
H1703 (1.11)	59.87	(19.14)	NE	-

Table 43: Absolute IC50 and Emax for ORY-1001 at 7 days. Squamous cell lung cancers treated with 0 – 100 µM ORY-1001 (ladedemstat). Cell viability was assessed at 7 days using cell titer-glo 2.0 (Graphs displayed in Figure 62). Absolute IC50 and Emax are interpolated from curve using Prism for each experimental replicate. IC50 is defined as the concentration required to reduce viability by 50% relative to no treatment control. Emax is defined as the maximum drug effect observed within the sigmoidal curve ('bottom of the curve') (non-specific death beyond this point is disregarded), and is presented as percent viability relative to no treatment control. IC50 and Emax was calculated for each experimental replicate, with mean and SEM displayed. IC50 judged to be non-estimable (NE) where IC50 could not be interpolated from one or more experimental replicates. Emax judged to be non-estimable (NE) where plateau of sigmoid curve not reached for at least one replicate

6.3.5.3 Impact of ORY-1001 on SOX2 expression at 48 hours

No evidence of a reduction in SOX2 expression levels was seen in lung cancer cell lines treated with 0 – 1 μM ORY-1001 at 48 hours. (Figure 63). Apparent reductions in SOX2 expression at 10 μM in H1703 and HCC2814 were interpreted as non-specific, as reduced SOX2 was accompanied by reductions in α-Tubulin (Figure 63B, D). Experiments to assess the impact on prolonged incubation with ORY-1001 on SOX2 protein expression were not pursued. If ORY-1001 is operating at the level of SOX2, some level of toxicity would be expected by 7 days (as is seen in Chapter 4 with SOX2 knockdown), but ORY-1001 has no impact on viability at pharmacologically meaningful concentrations (273). It was therefore judged that this approach was not a promising therapeutic strategy and was not pursued further.

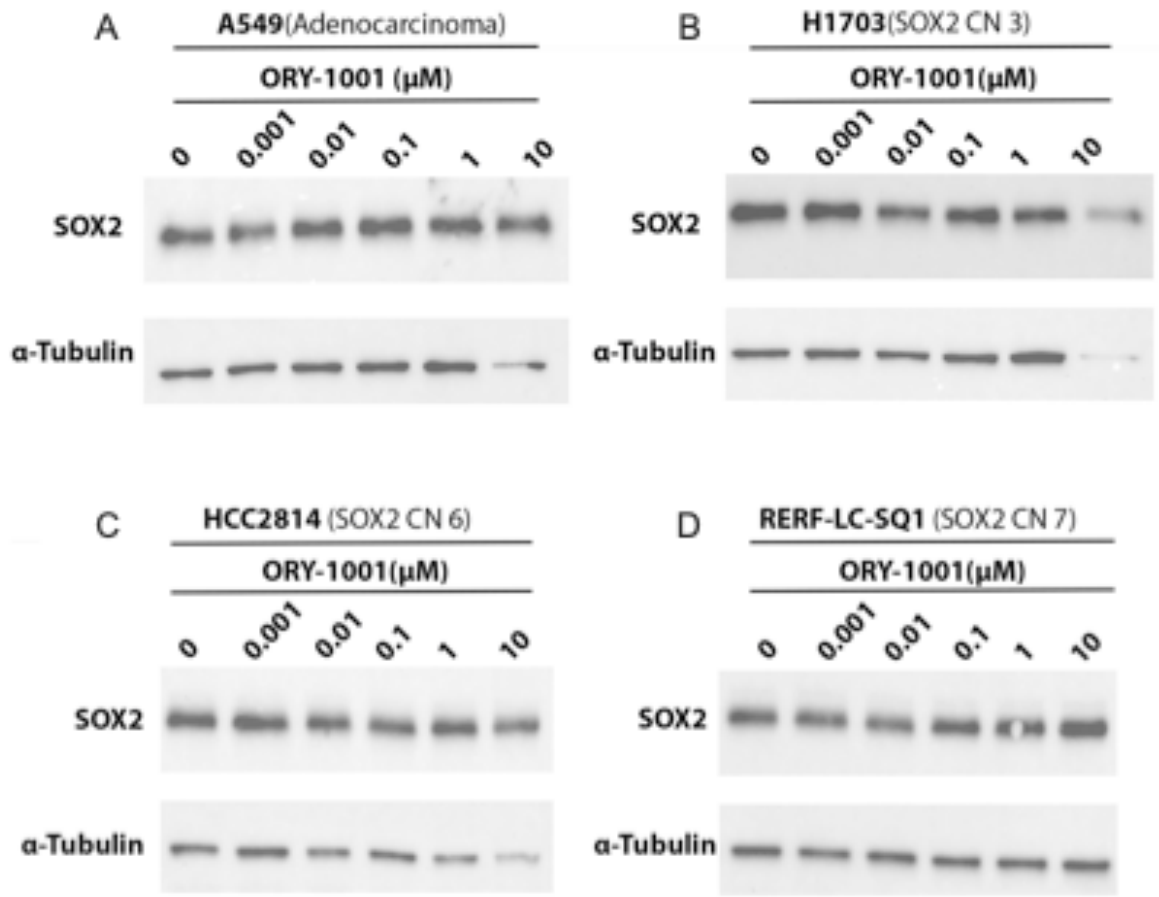

Figure 63: Impact of ladademstat (ORY-1001) on SOX2 protein expression in lung cancer cell lines. Lung adenocarcinoma (A549) (A), non-3q-amplified squamous cell lung cancer (H1703) (B), 3q amplified squamous cell lung cancer (HCC2814 and RERF-LC-SQ1 (C,D) were treated with 0 – 10 μM ORY-1001 for 48 hours. Whole cell lysates were collected, and SOX2 expression was assessed using western blotting. α-Tubulin is used as a loading control (housekeeping protein). Western blots repeated at least twice for all cell lines, with representative blots shown.

6.3.5.4 ORY-1001 Summary

ORY-1001 showed no activity at pharmacologically meaningful concentrations at either 72 hours or 7 days, with no convincing evidence found for reductions in SOX2 expression. ORY-1001 is not a promising therapy for modulating SOX2 expression in this context in 3q amplified squamous cell lung cancer.

6.3.6 Napabucasin

Napabucasin is a STAT3 inhibitor, and has been reported to reduce SOX2 expression in glioblastoma (317) and breast cancer (318). In addition, 1 μM napabucasin reduces SOX2 mRNA expression in lung adenocarcinoma cell lines and non-amplified squamous cell lung cancer cells (SKMES1) at 72 hours (319). No studies have examined whether STAT3 inhibition reduces SOX2 in 3q amplified squamous cell lung cancer cells.

6.3.6.1 Impact of Napabucasin on cell viability at 72 hours

All tested squamous cell lung cancer cell lines displayed dose-dependent reductions in viability with increasing doses of napabucasin treatment (Figure 64, Figure 44). There was no clear difference in sensitivity between amplified and non-amplified squamous cell lung cancer cell lines. Absolute IC50 was 0.1 – 3.5 μM, with almost complete suppression of viability at Emax (Table 44). Reductions in cell viability are seen at concentrations pharmacologically achievable in humans (mean Cmax at day 29 is 643.3 ng/ml in unresectable hepatocellular carcinoma (2.68 μM)) (326), suggesting that napabucasin may be a drug of interest in squamous cell lung cancer, irrespective of 3q amplification status .

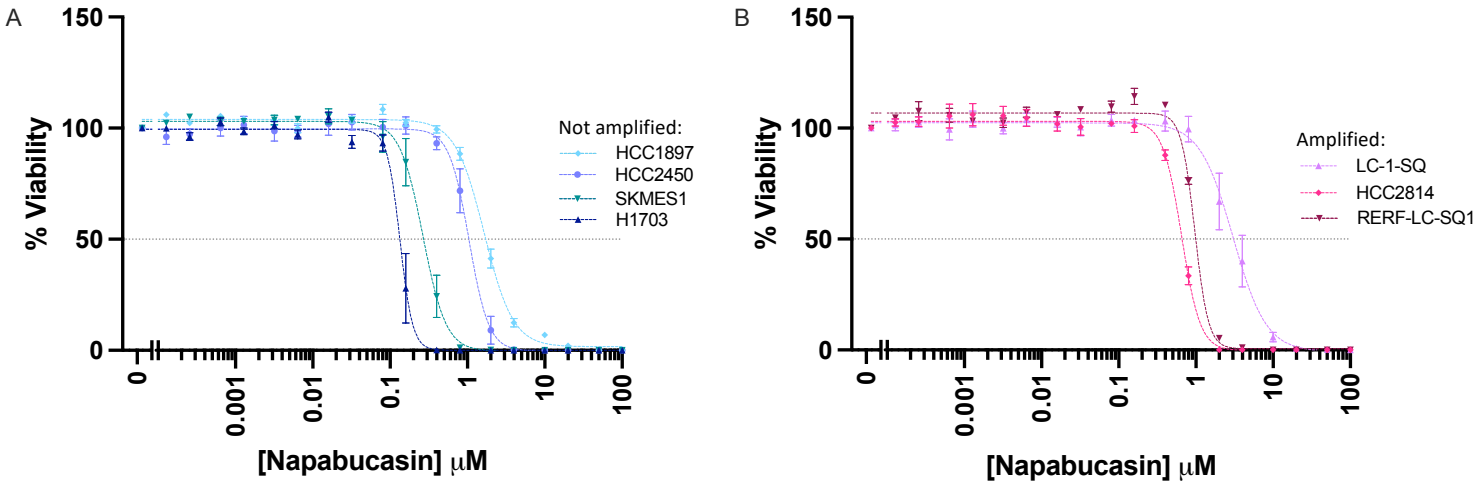

Figure 64: Impact of Napabucasin on cell viability at 72 hours. Non-amplified squamous cell lung cancer cell lines (A) and 3q amplified cell lines (B) were treated with 0 – 100 μM Napabucasin. Cell viability was assessed at 72 hours using cell titer-glo 2.0, subtracting background luminescence, and expressed relative to 0 μM Napabucasin. Curves plotted using Prism using non-linear regression (second order polynomial, quadratic). Experiment repeated at least three times for each cell line, with mean and SEM displayed. 50% reduction in viability indicated by horizontal line.

	Napabucasin (72 hour)			
Cell Line (relative SOX2 CN)	IC50 (μM)	(SEM)	Emax (%)	(SEM)
RERF-LC-SQ1 (3.24)	0.9649	(0.0622)	0.51	0.03
HCC2814 (2.319)	0.6893	(0.0251)	-0.30	0.10
LC-1-SQ (1.97)	3.5128	(0.4057)	-0.70	0.96
HCC1897 (1.667)	1.7341	(0.1347)	1.67	0.27
HCC2450 (1.404)	1.0978	(0.2058)	-0.22	0.17
SKMES1 (1.165)	0.2804	(0.0493)	-0.23	0.22
H1703 (1.11)	0.1360	(0.0186)	0.02	0.08

Table 44: Absolute IC50 and Emax for Napabucasin at 72 hours. Squamous cell lung cancers treated with 0 – 100 μM Napabucasin. Cell viability was assessed at 72 hours using cell titer-glo 2.0, graphs displayed in Figure 61. Absolute IC50 and Emax are interpolated from curve using Prism for each experimental replicate. IC50 is defined as the concentration required to reduce viability by 50% relative to no treatment control. Emax is defined as the maximum drug effect observed within the sigmoidal curve ('bottom of the curve') (non-specific death beyond this point is disregarded), and is presented as percent viability relative to no treatment control. IC50 and Emax was calculated for each experimental replicate, with mean and SEM displayed. IC50 judged to be non-estimable (NE) where IC50 could not be interpolated from one or more experimental replicates

6.3.6.2 Impact of Napabucasin on cell viability at 7 days

After 7 days of napabucasin treatment, IC50 ranged from 0.1360 µM to 0.9649 µM (Figure 65, Table 45). As may be expected, IC50 shifted leftwards with longer treatment, but this did not seem to be more marked in the amplified vs non-amplified cell line (although it is acknowledged only a small number of lines were tested)

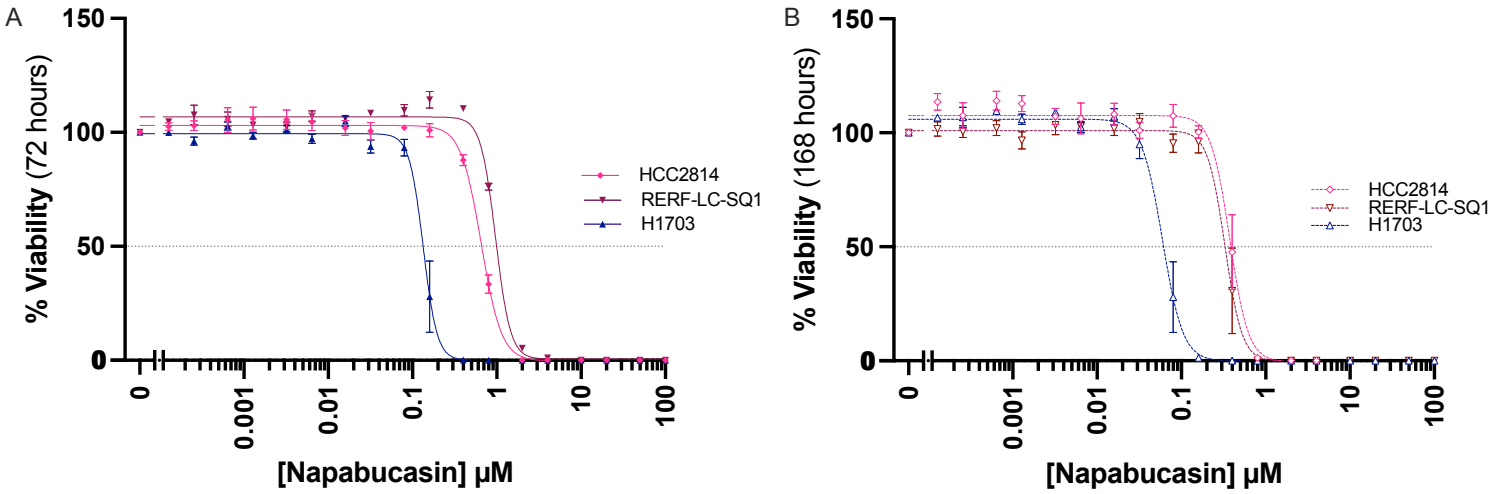

Figure 65: Impact of Napabucasin on cell viability at 72 hours and 7 days. Squamous cell lung cancer cell lines cell lines (RERF-LC-SQ1 relative SOX2 CN 3.24, HCC2814 relative SOX2 CN 2.319, NCI-H1703 relative SOX2CN 1.11) were treated with 0 – 100 µM Napabucasin. Cell viability was assessed at 72 hours (A) and 7 days (B) using CellTiter-glo 2.0, subtracting background luminescence, and expressed relative to 0 µM Napabucasin. Curves plotted using Prism using non-linear regression. Experiment repeated at least three times for each cell line, with mean and SEM displayed. 50% reduction in viability indicated by horizontal line. *Note data displayed in A is the same as displayed in Figure 45 for the selected cell lines, but is presented to allow comparison of 72 hours and 7 days*

Cell Line (Relative SOX2 CN).	**Napabucasin (7 day)**			
	IC50 (µM)	(SEM)	Emax (%)	(SEM)
RERF-LC-SQ1 (3.24)	0.3246	0.0546	-0.12	0.12
HCC2814 (2.319)	0.3914	0.0476	-0.16	0.06
H1703 (1.11)	0.0629	0.0124	-0.05	0.09

Table 45: Absolute IC50 and Emax for Napabucasin at 7 days. Squamous cell lung cancers treated with 0 – 100 µM Napabucasin. Cell viability was assessed at 7 days using cell titer-glo 2.0 (Graphs displayed in Figure 62). Absolute IC50 and Emax are interpolated from curve using Prism for each experimental replicate. IC50 is defined as the concentration required to reduce viability by 50% relative to no treatment control. Emax is defined as the maximum drug effect observed within the sigmoidal curve ('bottom of the curve') (non-specific death beyond this point is disregarded), and is presented as percent viability relative to no treatment control. IC50 and Emax was calculated for each experimental replicate, with mean and SEM displayed. IC50 judged to be non-estimable (NE) where IC50 could not be interpolated from one or more experimental replicates

6.3.6.3 Impact of Napabucasin on SOX2 Expression

Treatment with 0 – 1 μM napabucasin had no detectable impact on SOX2 protein expression at 48 hours in HCC2814 or RERF-LC-SQ1 (Figure 66). Reductions in SOX2 protein with 10 μM of Napabucasin were interpreted to be non-specific as this was accompanied by comparable reduction in α-Tubulin (Figure 66) and β-actin (not shown).

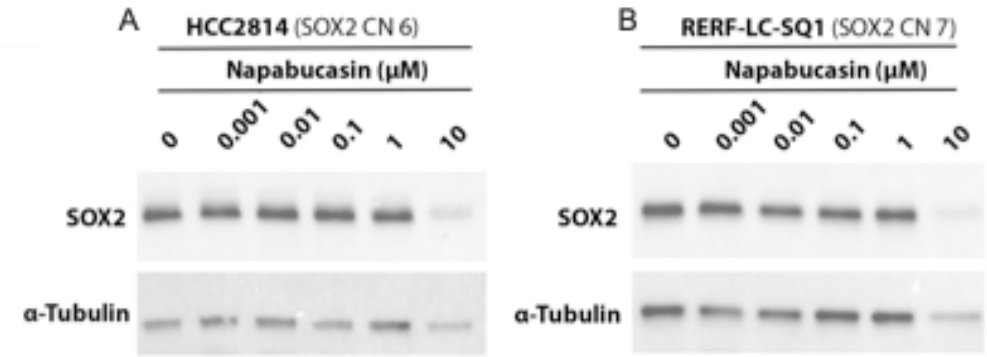

Figure 66: Impact of Napabucasin (ORY-1001) on SOX2 protein expression in lung cancer cell lines at 48 hours. HCC2814 and RERF-LC-SQ1 were treated with 0 – 10 μM Napabucasin for 48 hours. Whole cell lysates were collected, and SOX2 expression was assessed using western blotting. α-Tubulin is used as a loading control (housekeeping protein). Western blots repeated at least twice, with representative blots shown. No data for NCI-H1703 and A549 as napabucasin toxicity prevented collection of sufficient protein

Toxicity of napabucasin at 48 hours precluded collection of sufficient protein for analysis in NCI-H1703 and A549 despite repeated attempts. Impact of napabucasin on SOX2 expression was therefore assessed at 24 hours, with no convincing reduction in SOX2 protein expression in any tested cell line (Figure 67). Overall, no evidence was found to support napabucasin modulating SOX2 protein expression in lung cancer cell lines. This may suggest that STAT3 does not play a role in regulation of SOX2 in lung cancer cell lines, but this will need to be confirmed with assessment of STAT3 expression in these samples.

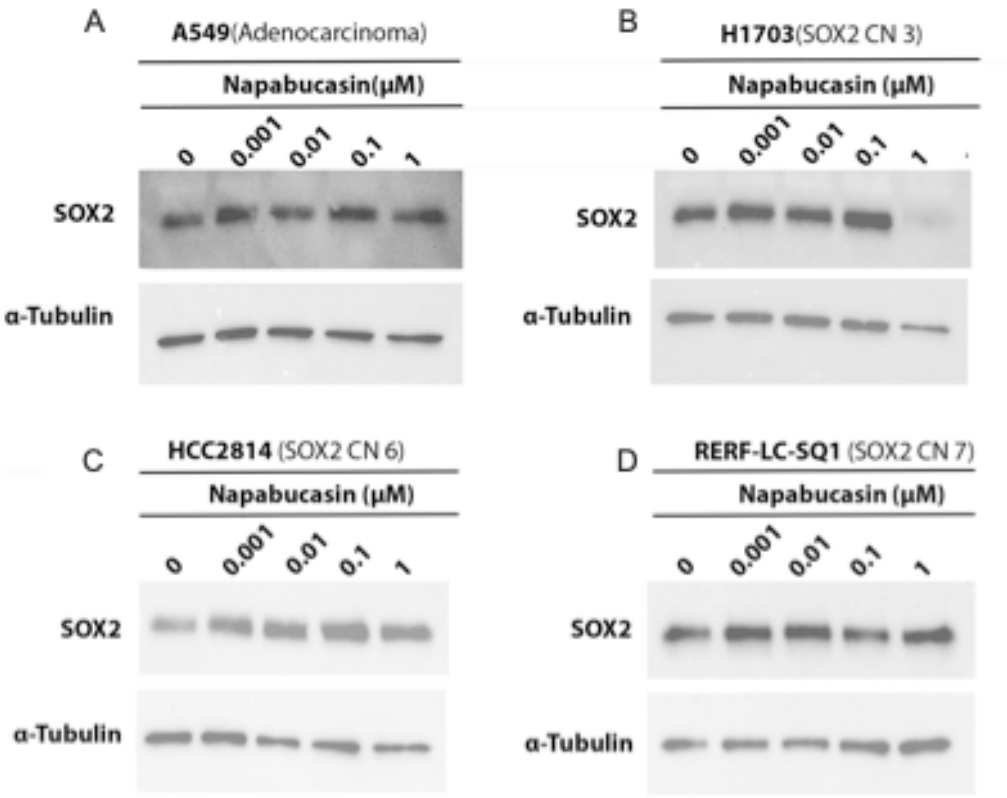

Figure 67: Impact of Napabucasin (ORY-1001) on SOX2 protein expression in lung cancer cell lines at 24 hours. A549, NCI-H1703, HCC2814 and RERF-LC-SQ1 were treated with 0 – 10 μM Napabucasin for 48 hours. Whole cell lysates were collected, and SOX2 expression was assessed using western blotting. α-Tubulin is used as a loading control (housekeeping protein). Western blots repeated at least twice, with representative blots shown. No data 10 μM as as napabucasin toxicity prevented collection of sufficient protein.

6.3.6.4 Napabucasin: summary

Napabucasin suppresses viability of squamous cell lung cancer cell lines at pharmacologically meaningful concentrations. However, there was no convincing evidence for an impact of napabucasin on SOX2 expression. Napabucasin does not show promise as a drug to modulate SOX2 expression in squamous cell lung cancer, but could still be an interest as an agent in squamous cell lung cancer as part of other therapeutic strategies.

6.4 Summary

This chapter presents a review of drugs that have been reported to modulate SOX2 expression levels in other contexts. These drugs were tested to assess their impact on viability and SOX2 expression in a panel of squamous cell lung cancer cell lines, with a focus on whether these agents reduce SOX2 expression in 3q amplified squamous cell lung cancer. Approaches that were explored were: KDM1A Inhibition; NAE Inhibition; CDK7 Inhibition; BRD4 Inhibition and STAT3 Inhibition. The most important findings of this chapter are that AZD5153 (BRD4 inhibition) and SY-5609 (CDK7 inhibition) modulate SOX2 expression across the panel of squamous cell lung cancer cell lines, including in the context of 3q amplification. AZD5153 and SY-5609 are therefore identified as important candidates for further research and development in the context of 3q amplified squamous cell lung cancer.

The remaining drugs were not promising as strategies to target SOX2 in squamous cell lung cancer. ORY-1001 (KDM1A inhibition) and napabucasin (STAT3 inhibition) did not convincingly alter SOX2 expression in any tested cell lines. Pevonedistat (NAE inhibition) reduced SOX2 expression in non-amplified NSCLC cell lines but did not reduce SOX2 expression in the two tested 3q amplified cell lines at pharmacologically translatable concentrations. However, whilst pevonedistat and napabucasin do not show promise for SOX2-directed therapies in 3q amplified squamous cell lung cancer, they do show activity in reducing viability of squamous cell lung cancer cells. Napabucasin and pevonedistat are therefore potential candidates for drug therapies as part of other therapeutic strategies.

6.5 Discussion

AZD5153

To the best of our knowledge, this is the first demonstration that pharmacologic inhibition of BRD4 reduces SOX2 expression in squamous cell lung cancer cells. These results are fully in keeping with the known roles of BRD4 (292). BRD4 preferentially upregulates genes associated with super enhancers (327), and has been shown to directly bind the SOX2 e1 enhancer, where it promotes SOX2 transcription (298). PROTAC-mediated degradation of BRD4 suppresses SOX2 expression in squamous cancer cell lines (298, 299). The potential for pharmacologic manipulation of the axis has previously been demonstrated in NUT midline carcinoma *in vitro*, where JQ1 reverses the SOX2 overexpression driven by the abnormal BRD4-NUT fusion protein (299). JQ1 was the first BET inhibitor developed, and has broader actions across multiple BET proteins, albeit with higher specificity to BRD4 (308). AZD5153 has several advantages over earlier compounds, including high potency and specificity against BRD4 (309).

Impact of AZD5153 on cell viability was tested in seven squamous cell lines, of these three had 3q amplification and four did not have 3q amplification. Absolute IC50 was less than 0.3 μM in all three amplified cell lines, whilst three out of four non-amplified lines had an IC50 exceeding 1 μM. It is possible that 3q amplification may be associated with an increase in sensitivity to AZD5153, but definitive conclusions require testing in a larger panel of cell lines. Further work will characterise the impact of AZD5153 on a wide range of cellular behaviours including colony formation, invasion, and migration in 3q amplified versus non-amplified cell lines, and will also assess the impact of AZD5153 on squamous cell lung cancer organoid models. It is acknowledged that the suppression of SOX2 expression by AZD5153 is incomplete, and further work will also assess the impact of more prolonged incubation with AZD5153 on SOX2 expression. BRD4 acts as a broad regulator of transcriptional activity (292), and therefore likely has widespread impacts on the transcriptome. Clarification of differentially expressed genes with

RNAseq in 3q amplified and non-amplified cell lines will also be a useful extension to this work. Finally, to move AZD5153 forward as a potential clinical candidate, the impact of BRD4i in more complex models of squamous cell lung cancer are needed. In particular, the option for moving AZD5153 into work in patient derived xenograft models of squamous cell lung cancer are being actively explored. This work will allow validation of the present work in models that more accurately recapitulate tumour biology and microenvironment and will allow assessment of whether AZD5153 suppresses the metastatic phenotype driven by 3q amplification.

SY-5609

The findings that SY-5609 reduces SOX2 expression in squamous cell lung cancer models is fully in keeping with published data with THZ1 (288). When considered as a whole, it is likely that SOX2 suppression is a class effect of CDK7 inhibitors. Future work will assess with ICEC0942 replicates the suppression of SOX2 seen with SY-5609. In addition, the impact of more prolonged incubation with ICEC0942 and SY-5609 on SOX2 expression will be assessed, to examine whether lower doses of CDK7 inhibition reduce SOX2 are seen at extended time points.

A key discrepancy between the analysis presented in this thesis and the published data (288), is that in the present analysis CDK7 inhibitor sensitivity was not clearly stratified based on 3q amplification status. Of note, the dose-response curves for THZ1 across both analyses are remarkably similar, suggesting that methodological differences are unlikely to be playing a major role in this discrepancy. Instead, it would seem likely that this discrepancy is due to a relatively small panel of cell lines being tested in both analyses, differences in cell line panels being analysed, and differences in criteria applied for '3q amplification' (the present analysis including more cell lines with high level amplification, whilst the previous analysis including more diploid lines). Whilst testing in a wider panel of cell lines would be of value, greater clarity would be provided by engineering 3q amplified vs non-amplified cell lines within the same genetic background and assessing whether this alters CDK7 inhibitor sensitivity. Future work will also assess the impact

of SY-5609 on colony formation, invasion, and migration in 3q amplified vs non-amplified lines, and will also assess the impact of AZD5153 on squamous cell lung cancer organoid models. Finally, options to test CDK7 inhibitors in more faithful models of squamous cell lung cancer including patient derived xenograft models are being actively explored.

The mechanism through which CDK7 inhibition alters SOX2 expression has not been studied, although transcriptional repression seems likely. CDK7 has been shown to play a role in regulating transcription at super enhancers (327), which is of particular relevance as a super enhancer element is co-amplified with SOX2 in squamous malignancies, and plays a crucial role in driving SOX2 overexpression (298). To the best of our knowledge, no studies have examined whether CDK7 plays a role at the SOX2 super enhancer. However, CDK7 is known to preferentially drive other genes associated with super enhancers (328, 329). Further work will be needed to assess the mechanism of how CDK7 downregulates SOX2. Firstly, using qPCR (quantitative Polymerase Chain Reaction) to assess the impact on SOX2 mRNA expression. If transcriptional repression of SOX2 by CDK7 inhibition is confirmed, it will be helpful to assess whether CDK7 binds SOX2 enhancers using ChIP-seq (Chromatin Immunoprecipitation Sequencing).

Combined BRD4 and CDK7 inhibition

Both BRD4 and CDK7 play a role in regulating transcription at super enhancers, and both are shown to suppress SOX2 expression in lung cancer cell lines in the present work. Interestingly, co-inhibition of BRD4 and CDK7 synergistic suppress viability and colony formation in head and neck squamous cell lung cancer *in vitro* (327), and combination treatment is efficacious in xenograft models (327). It is not known whether BRD4 inhibition and CDK7 inhibition are synergistic in squamous cell lung cancer. Likewise, it is not known whether combination treatment is more effective at suppressing SOX2 expression than monotherapies. However, clearly this is an important area for future work.

Pevonedistat

Assessment of pevonedistat (NAE inhibition) confirms previously published data that treatment can reduce SOX2 expression in NSCLC cell lines (283). However, whilst pevonedistat markedly reduced SOX2 expression in non-amplified cells, reductions in SOX2 expression were either less apparent or absent. It is possible that MSX2 plays less of a role in driving SOX2 expression in the context of 3q amplification. Whilst a larger panel of 3q amplified lines would give a more definitive picture, the failure of pevonedistat in two amplified cell lines implies this is not a promising strategy to prioritise for further testing.

ORY-1001

ORY-1001 (LSD-1 inhibition) had no noticeable impact on SOX2 expression and had no impact on cell viability except at very high concentrations. Previous investigations into LSD-1 inhibition and SOX2 expression have either been in mammosphere culture (274) or used grossly supra pharmacological drug concentrations (275). In breast cancer, ORY-1001 only demonstrated activity in the mammosphere model of cancer stem cells, with no activity in adherent culture (274). It is possible that H3K9 is only a relevant modulator of SOX2 in the context of stem cells. Alternatively, the lack of activity of ORY-1001 could be due to the limitations of 2D culture. Adherent culture was chosen as it allows for assessment of SOX2 overexpression driven by amplification without the additional complication of stem cell driven SOX2 expression that may be seen in stem cell models like sphere forming assays. In addition, sphere forming assays were attempted in initial validation experiments, but presented issues with reproducibility across the number of lines and drugs required to be screened. Therefore, whilst it remains possible that ORY-1001 could modulate SOX2 expression in the stem cell component, based on present evidence it does not seem a promising strategy to target SOX2 expression in 3q amplification. ORY-1001 has not been prioritised for further testing.

Napabucasin

Napabucasin treatment resulted in dose-dependent reductions in cell viability, and therefore remains a candidate for a general therapeutic strategy in squamous cell lung cancers. However, there was no observable impact on SOX2 expression in any tested cell line. It is important to note that published literature reporting an impact of napabucasin on SOX2 expression use either higher doses of napabucasin, longer incubation with drugs, or assess expression at the level of mRNA (or all three). In glioblastoma cells, 10 days of 5 μM napabucasin reduces SOX2 mRNA (317). In lung cancer cell lines, 1 μM napabucasin reduces SOX2 mRNA at 72 hours (319). 20 μM napabucasin reduces SOX2 protein expression in breast cancer cells (318). I cannot exclude the possibility that higher concentrations or prolonged incubation with napabucasin may have an impact on SOX2 protein expression. However, due to the degree of toxicity consistently observed at 24 and 48 hours, it seems unlikely that any delayed impact of napabucasin on SOX2 protein expression is a major mediator of napabucasin's effects. Overall, napabucasin does not seem a promising strategy to target SOX2 in 3q amplified squamous cell lung cancer. Napabucasin has not been prioritised for further testing.

6.6 Conclusions

AZD5153 (BRD4 inhibition) and SY-5609 (CDK7 inhibition) modulate SOX2 expression in squamous cell lung cancer cell lines, including in cells with 3q amplification. AZD5153 and SY-5609 are therefore of interest for further research and development.

Chapter 7: 3q Amplified Squamous Cell Lung Cancer Part 3
Unsupervised FACS-assisted Genome Wide CRISPR Screen to identify potential alternate strategies.

7.1 Introduction

In Chapter 4, it is demonstrated that *SOX2* is a critical oncogene within the 3q amplicon in squamous cell lung cancer. In Chapter 5, it is demonstrated that AZD5153 (BRD4 inhibition) and SY-5609 (CDK7 inhibition) modulate SOX2 expression in the context of 3q amplification. However, SOX2 sits at the centre of a complex network of pathways, and is regulated at a transcriptional, post-transcriptional and post-translational level (314, 330). Regulation of SOX2 is best described in the context of embryonal stem cells and neural development (313, 314, 331-333), with additional data available in some cancers, including glioblastoma (334) and breast cancer (335). There is a paucity of data exploring the network regulating SOX2 in squamous cell lung cancer or in the context of 3q amplification. No studies have examined the regulation of SOX2 in squamous cell lung cancer in an unsupervised manner. In this chapter, FACS-assisted genome wide CRISPR knockout screening will be used to identify potential candidates reduce the expression of SOX2. FACS-assisted genome wide CRISPR knockout screening combines fluorescence-activated cell sorting (FACS) and CRISPR knockout to identify proteins or pathways that regulate the expression of a protein of interest (336). This approach has been successfully used by others (337-344), including in defining a role of AKIRIN2 in the nuclear trafficking of proteasomes (339) and to identify v-ATPase as a candidate drug target to lower ataxin-2 (340).

In this screen, 3q amplified cells will be expanded and transduced with the GeCKO library and cells will be sorted into $SOX2^{HIGH}$ and $SOX2^{LOW}$ populations, sgRNA will then be sequenced to allow identification of candidates which may regulate SOX2. Potential candidates will then be validated with siRNA. This approach contrasts with that undertaken in Chapter 5, and it is hoped

that this strategy will identify additional candidates for future research, as well as provide insights into the regulation of SOX2 in 3q amplified squamous cell lung cancer cells.

7.2 Aims and Objectives

Aim:

1. To identify potential candidate pathways and proteins that negatively regulate SOX2 expression in 3q amplified squamous cell lung cancer.

Objectives

1. Optimise FACS sorting strategy for SOX2 in 3q amplified squamous cell lung cancer.
2. Perform Genome-Wide CRISPR screen to identify candidate pathways and proteins that negatively regulate SOX2 expression in 3q amplified squamous cell lung cancer.
3. Validate potential candidates with siRNA.

7.3 Results

7.3.1 Optimisation for CRISPR screen

Optimisation was completed in two 3q amplified squamous cell lung cancer cell lines: HCC2814 and RERF-LC-SQ1.

7.3.1.1 Puromycin kill curve

To avoid selecting for cells transduced with multiple lentiviral sgRNA, it is important to determine the minimum puromycin concentration required for efficient selection (200). Puromycin kill curves were performed for RERF-LC-SQ1 and HCC2814, cell viability was assessed using CellTiter-Glo after 96 hours of puromycin treatment (Figure 68). The lowest dose of puromycin which achieved < 1% cell viability relative to control (no drug) was selected for future puromycin selection: 0.50 µg/ml for RERF-LC-SQ1 and 0.75 µg/ml for HCC2814.

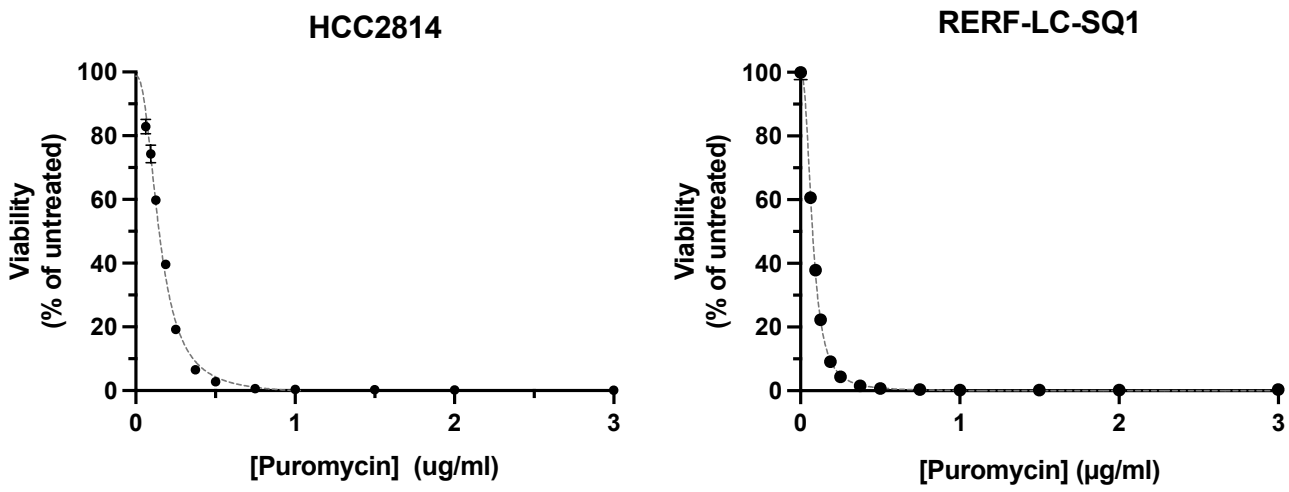

Figure 68: Puromycin kill curves for RERF-LC-SQ1 and HCC2814. Cells were seeded in 96 well plates. Cell viability was assessed with CellTiter-Glo 2.0 96 hours post treatment with puromycin (0 – 3 µg/ml). Experiment completed once for each cell line, with each condition seeded and drugged in at least triplicate. Plotted as mean ± SEM using Prsim 10, curve plotted with non-linear regression.

7.3.1.2 Moiety of Infection

Volume of virus required to achieve a Moiety of Infection (MOI) of 0.3 was defined for RERF-LC-SQ1 and HCC2814. Target MOI was 0.3 to minimise the number of cells being transduced with multiple sgRNA (200). Cells were transduced with 0 – 800 µL lentiviral supernatant in 6 well plates by spinfection, with moiety of infection determined by CellTiter-Glo 2.0. Relative viability was used to estimate moiety of infection, and plotted in Prism 10. Volume of virus required to achieve MOI of 0.3 was interpolated from the curve (6.76 µL for HCC2814 and 11.79 µL for RERF-LC-SQ1).

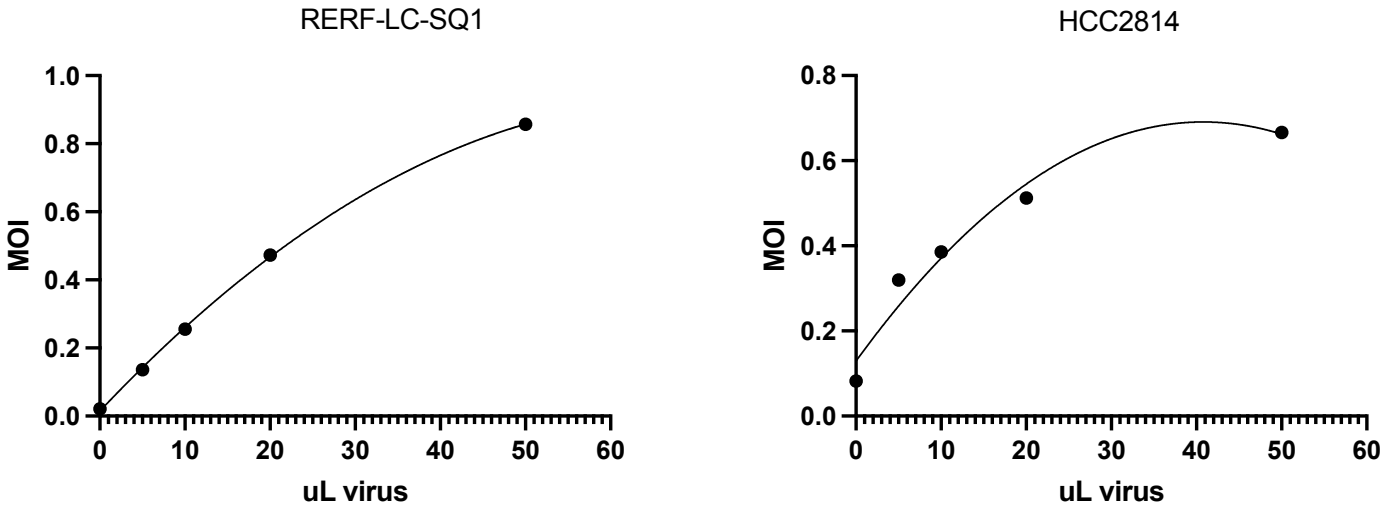

Figure 69: Determination of viral concentration required to achieve MOI of 0.3. Cells were transduced by spinfection with 0 – 800 µL lentivirus in a 6-well plate format. After overnight incubation, cells were detached and seeded in opaque-walled 96 well plates. After 4 days of puromycin selection, relative viability was calculated using CellTiter-Glo 2.0 to assess moiety of infection. Experiment conducted once for each cell line, with cells seeded in quadruplicate for each CellTiter-Glo replicate. 0 – 50 µL virus both cell lines, as above this saturation point was reached and viability started reducing, prohibiting accurate curve fitting.

7.3.1.3 Optimisation of sort strategy for SOX2

Flow Cytometry protocols for SOX2 are poorly defined with limited validation published in the literature. It was therefore necessary to define protocols for SOX2 staining for FACS. SOX2 siRNA knockdown was included as a negative control to ensure specificity of staining. Earlier in this thesis, it is shown that D6D9 anti-SOX2 Rabbit monoclonal antibody (Cell Signalling Technology, USA) show good specificity of staining on western blot analysis. The same antibody clone was therefore chosen for assessment of SOX2 expression by flow cytometry, using Alexa-Fluor 488 Conjugated SOX2 (D6D9) Rabbit mAb (#5049, Cell Signaling Technology).

Optimisation 1

As described previously, HCC2814 and RERF-LC-SQ1 were transfected with either non-targeting control siRNA (scramble) or siRNA targeting SOX2 (Silencer select, S13295) (Thermofisher, USA). After 48 hours, a proportion of cells were collected for lysates for western blotting and a proportion were stained for flow cytometry. For the cells prepared for flow cytometry, fixation and permeabilization was completed using the BD Cytofix/Cytoperm Fixation/Permeabilization kit (BD Biosciences, USA) (as per manufacturer's instructions), cells were then stained with 1:50 Alexa-Fluor 488 Conjugated SOX2 (D6D9) Rabbit mAb (#5049, Cell Signalling Technology), with analysis on the BD FACSAria Fusion Flow Cytometer (University of Birmingham Flow Cytometry Facility). Effective knockdown of SOX2 was confirmed on western blotting, with clear differentiation between SOX2-KD and SOX2-WT. However, staining performed poorly on flow cytometry: with poor differentiation between stained and unstained cells, and poor differentiation between SOX2-WT and SOX2-KD. Overall, this staining strategy was felt to be inadequate for an effective FACS-assisted genome wide CRISPR screen.

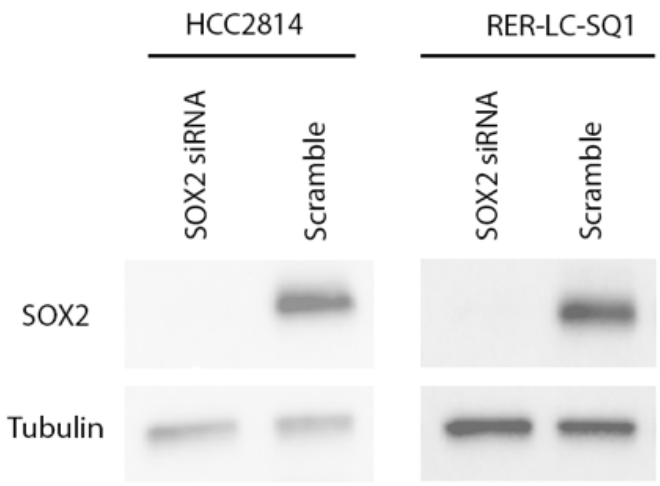

Figure 70: Confirmation of effective knockdown of SOX2 with S13295 siRNA on western blotting in RERF-LC-SQ1 and HCC2814. HCC2814 and RERF-LC-SQ1 were transfected with either negative control siRNA (scramble) or siRNA targeting SOX2 (S13295) using reverse transfection in a 6-wel plate format. Whole cell lysates were collected 48 hours post-transfection and SOX2 proteine expression was assessed with western blotting (D6D9 antibody). Tubulin included as loading control. Repeated at least three times, with representative blots shown.

Optimisation 2

It was hypothesised that the poor staining for SOX2 could be due to inadequate fixation/permeabilization. Therefore, the fixation/permeabilization kit was changed to the eBioscience™ Foxp3/Transcription Factor Staining buffer set (Thermofisher, USA). An isotype control was added as a further negative control, with protocols remaining otherwise the same as Optimisation 1. Improvement in staining was modest at best. Overall, this strategy was still judged to be inadequate.

Optimisation 3

Both antibody clone and flurophore was changed, using PE anti-SOX2 14A6A34 (Biolegend). Cells were fixed using eBioscience™ Foxp3/Transcription Factor Staining buffer set. SOX2 knockdown, isotype control and unstained cells were included as negative controls. Staining was bright, with good differentiation between stained cells and appropriate negative controls (both SOX2 knockdown with siRNA and isotype control). Furthermore, sort attempts on the on BD FACSAria Fusion Flow Cytometer resulted in pure $SOX2^{HIGH}$ and $SOX2^{LOW}$ populations. This protocol was adopted for the FACS-assisted Genome Wide CRISPR screen (Full protocol described in 2.3.6 Fluorescence-activated Cell Sorting (FACS): Sample Preparation

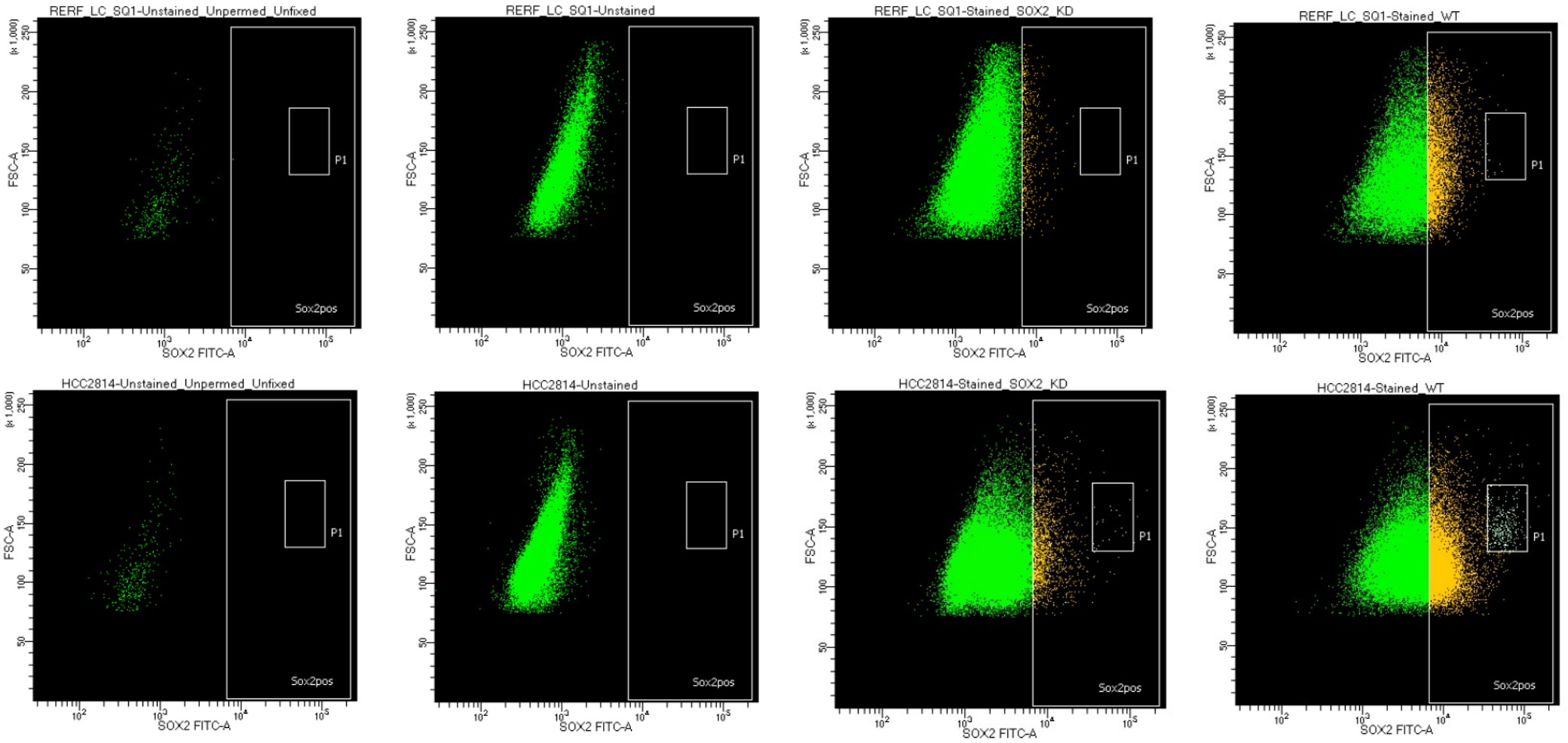

Figure 71: First optimisation of SOX2 flow cytometry. RERF-LC-SQ1 and HCC2814 were transfected with non-targeting siRNA (WT) or siRNA targeting SOX2 (KD). 48 hours post-transfection, cells were fixed and permeabilized with BD Cytofix/Cytoperm Fixation/Permeabilization kit and stained 1:50 Alexa-Fluor 488 Conjugated SOX2 (D6D9) Rabbit mAb. Unstained/Unpermed/Unfixed and unstained cells were included as further negative controls. Fluorescent staining was weak, with poor differentiation between stained cells and either unstained or SOX2 knockdown.

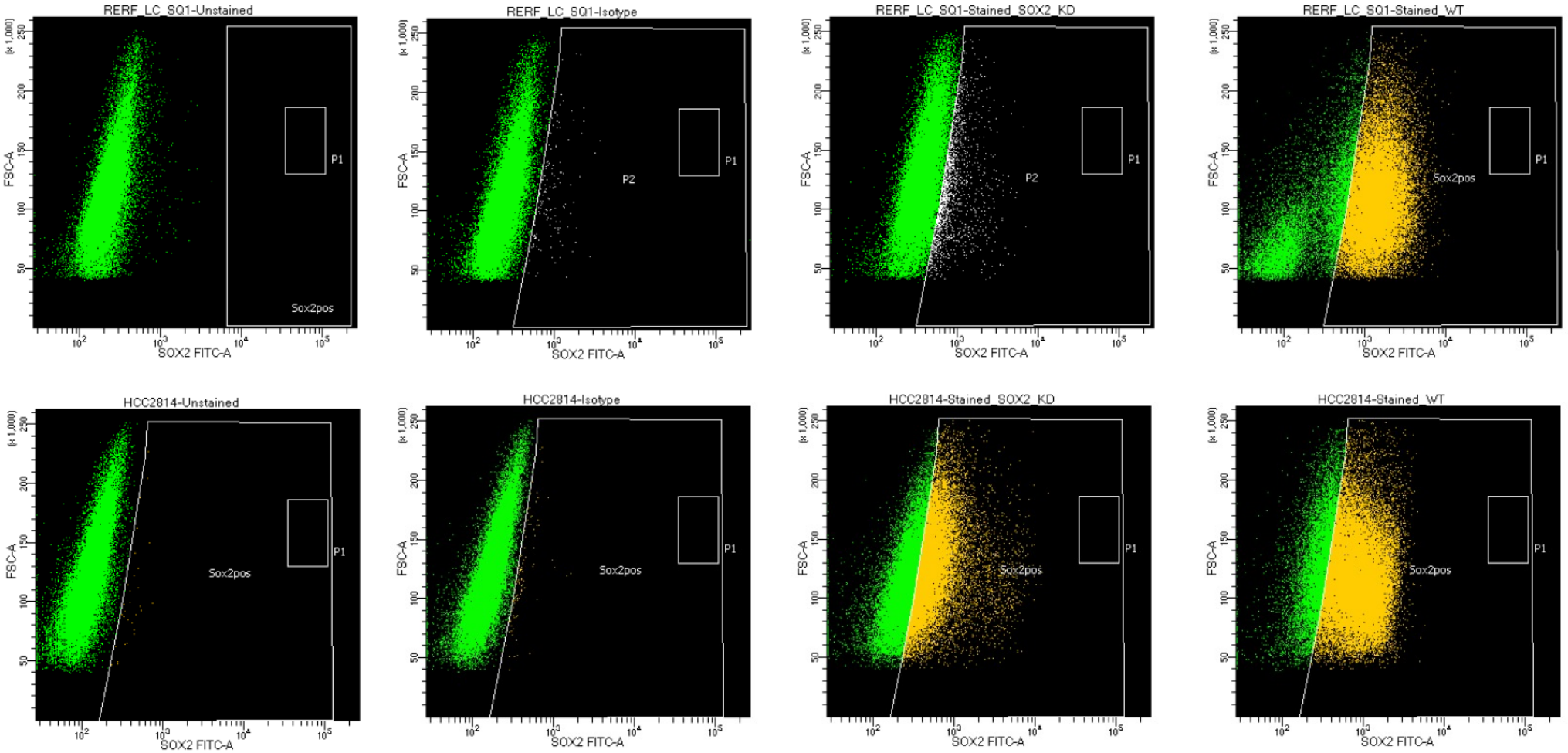

Figure 72: Second optimisation of SOX2 flow cytometry. RERF-LC-SQ1 and HCC2814 were transfected with non-targeting siRNA (WT) or siRNA targeting SOX2 (KD). 48 hours post-transfection, cells were fixed and permeabilized with eBioscience™ Foxp3/Transcription Factor Staining buffer set and stained 1:50 Alexa-Fluor 488 Conjugated SOX2 (D6D9) Rabbit mAb. Unstained/Unpermed/Unfixed (not shown), and unstained cells, and cell stained with isotype control were included as further negative controls. Fluorescent staining was weak, with poor differentiation between stained cells and either unstained or SOX2 knockdown.

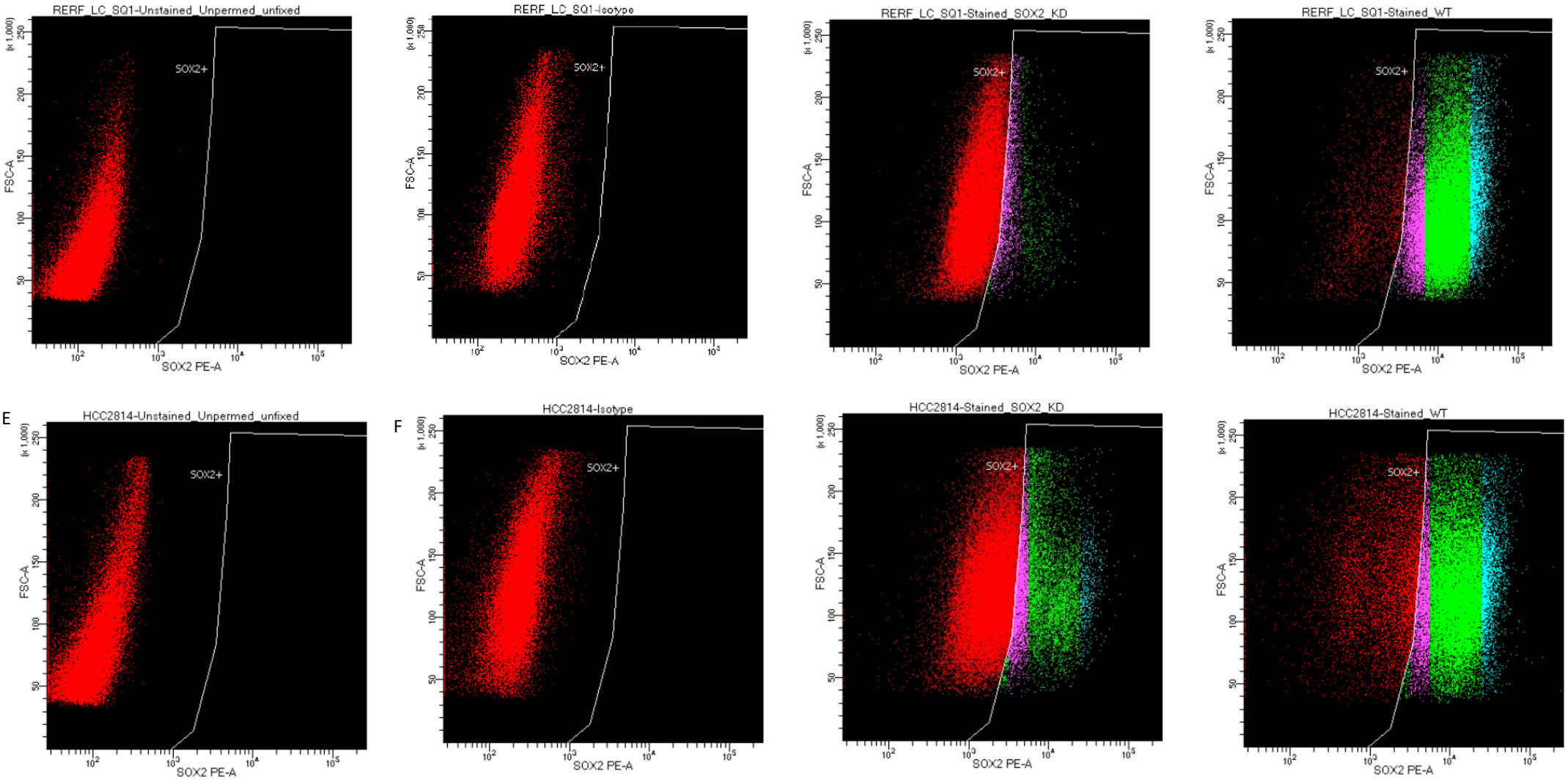

Figure 73: Final Optimisation of SOX2 Staining on Flow Cytometry: RERF-LC-SQ1 and HCC2814 were transfected with non-targeting siRNA (WT) or siRNA targeting SOX2 (KD). 48 hours post-transfection, cells were fixed and permeabilized with eBioscience™ Foxp3/Transcription Factor Staining buffer set and stained 1:50 PE anti-SOX2 14A6A34 (Biolegend). Unstained/Unpermed/Unfixed, and unstained cells, and cell stained with isotype control were included as further negative controls.

7.3.3 Genome-Wide CRISPR Screen

RERF-LC-SQ1 was selected for the CRISPR screen due to better performance on flow cytometry, and because RERF-LC-SQ1 is a more robust cell line and more suitable for the large-scale cell culture required for a genome-wide CRISPR screen.

2.8×10^8 RERF-LC-SQ1 cells were seeded in 6 well plates and transduced with the GeCKO library. After overnight incubation cells were transferred to T150 cm^2 flasks. After a further 24 hours cells 0.50 µg/ml puromycin was added, and puromycin selection was continued for 7 days. After 7 days of puromycin selection, 6.2×10^7 cells were pelleted and snap frozen and 12.4×10^7 cells were stained for with PE anti-SOX2 for FACS (with an additional 12.4×10^7 for controls).

FACS sorting was undertaken to achieve two populations: $SOX2^{HIGH}$ (the top 10% of SOX2 expressing cells) and $SOX2^{LOW}$ (the bottom 10% of SOX2 expressing cells + cells negative for SOX2). To achieve clean populations, a doubled sorting strategy was applied, with an initial enrichment sort followed by a precision sorting of the enriched population. Purity of populations was confirmed, and this strategy resulted in clean populations with less than 0.5% crossover between $SOX2^{HIGH}$ and $SOX2^{LOW}$ populations (Figure 74). Final output of FACS sorting was 1.95×10^6 in the $SOX2^{LOW}$ population and 0.75×10^6 in the $SOX2^{HIGH}$ population.

Sorted cells were pelleted by centrifugation and frozen. DNA was extracted, and library preparation was completed as per section 2.4.9. Sequencing was performed by Genomics Birmingham on Illumina Nextseq, with output in FASTQ format.

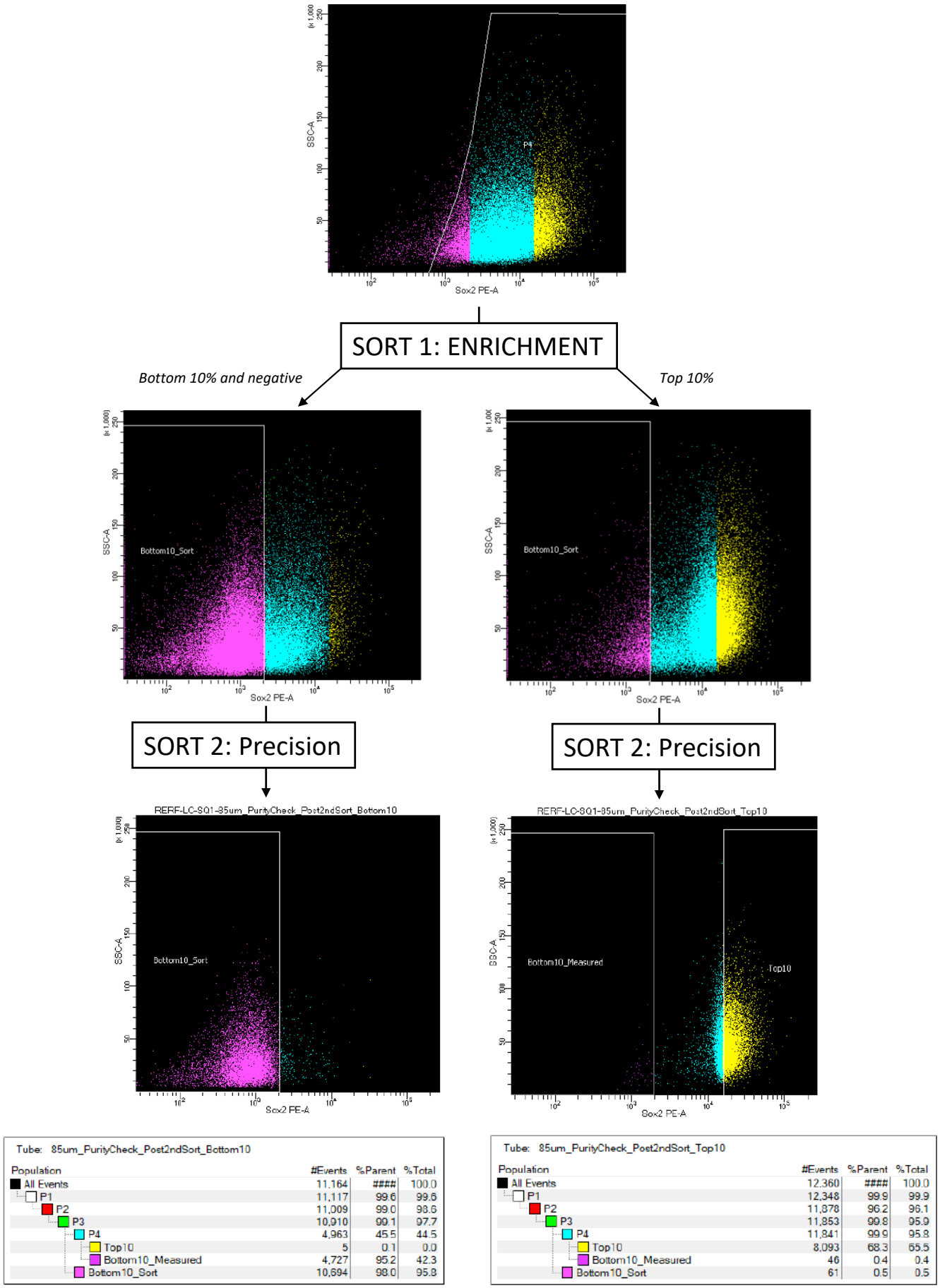

Tube: 85um_PurityCheck_Post2ndSort_Bottom10

Population	#Events	%Parent	%Total
All Events	11,164	####	100.0
P1	11,117	99.6	99.6
P2	11,009	99.0	98.6
P3	10,910	99.1	97.7
P4	4,963	45.5	44.5
Top10	5	0.1	0.0
Bottom10_Measured	4,727	95.2	42.3
Bottom10_Sort	10,694	98.0	95.8

Tube: 85um_PurityCheck_Post2ndSort_Top10

Population	#Events	%Parent	%Total
All Events	12,360	####	100.0
P1	12,348	99.9	99.9
P2	11,878	96.2	96.1
P3	11,853	99.8	95.9
P4	11,841	99.9	95.8
Top10	8,093	68.3	65.5
Bottom10_Measured	46	0.4	0.4
Bottom10_Sort	61	0.5	0.5

Figure 74: Sort strategy for Genome-wide CRISPR screen. Cell Sorting was performed by the University of Birmingham's Flow Cytometry Facility. Cells were stained for SOX2 using 1:50 PE anti-SOX2 14A6A34 (Biolegend). Dead cells were stained using Fixable Viability Dye eFluor 450, with dead cells removed from both populations. Cells were sorted using the BD FACSAria Fusion Flow Cytometer using an 85 µm nozzle, with an enrichment at Precision yield before performing a purity 16-32-0 on the 'SOX2^{LOW}' (bottom 10% and negative cells) and 'SOX2^{HIGH}' (top 10% cells). Purity of populations was confirmed with ≤ 0.5% crossover between populations

Genome Wide CRISPR Screen Analysis

Analysis of the GeCKO output was performed using Model-Based Analysis of Genome-wide CRISPR-Cas9 Knockout software (MAGeCKFlute, SourceForge, USA) (analysis completed by Professor Andrew Beggs). MAGeCKFlute is an integrative analysis pipeline for pooled CRISPR screens that combines the MAGeCK and MAGeCK-VISPR algorithm (345).

Initial results of the CRISPR screen are presented in Figure 75, which identifies sgRNA enriched in the SOX2^{LOW} population versus SOX2^{HIGH}. A β-score is generated, with a positive score indicating enrichment in SOX2^{LOW}, implying that knockout of the gene of interest may drive reduced SOX2 expression. Likewise, a negative score indicates enrichment in SOX2^{HIGH}, implying that knockout of the gene may drive increased SOX2 expression. Encouragingly, *SOX2* was enriched in the SOX2 low population (β-score 2.3512), which serves as a useful internal positive control. The most enriched genes in the SOX2^{HIGH} population were *NME8* (β-score 4.8692) and *HIST2H4B* (β-score 4.2087). The most enriched gene in the SOX2^{LOW} population were *USP17L5* (β-score -5.4586) and *PLN* (β-score -3.7311). A scatter plot which takes into account essentiality on DepMap is shown in Figure 76.

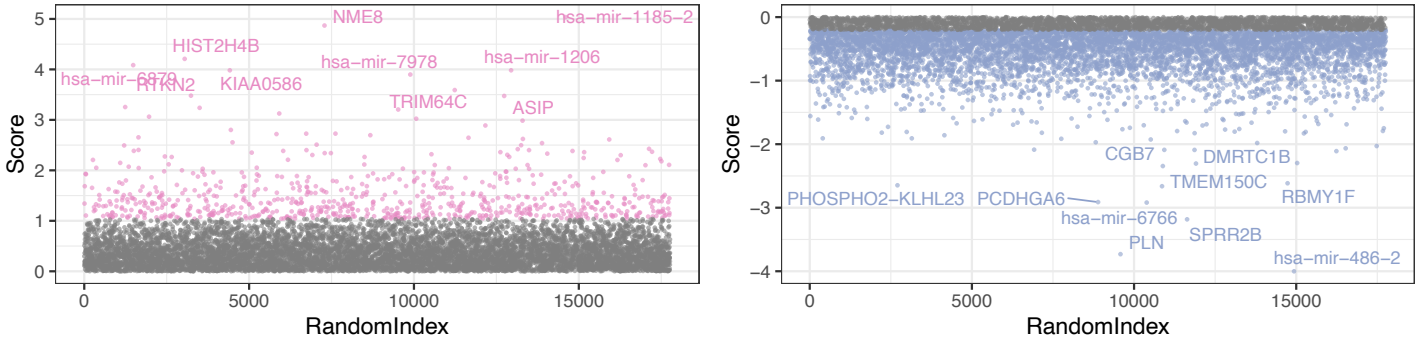

Figure 75: Dot plots of sgRNA positively and negatively selected in the SOX2^{LOW} population. Negative β scores imply enrichment in the SOX2^{HIGH} population, whilst positive β scores imply enrichment in the SOX2^{LOW} population

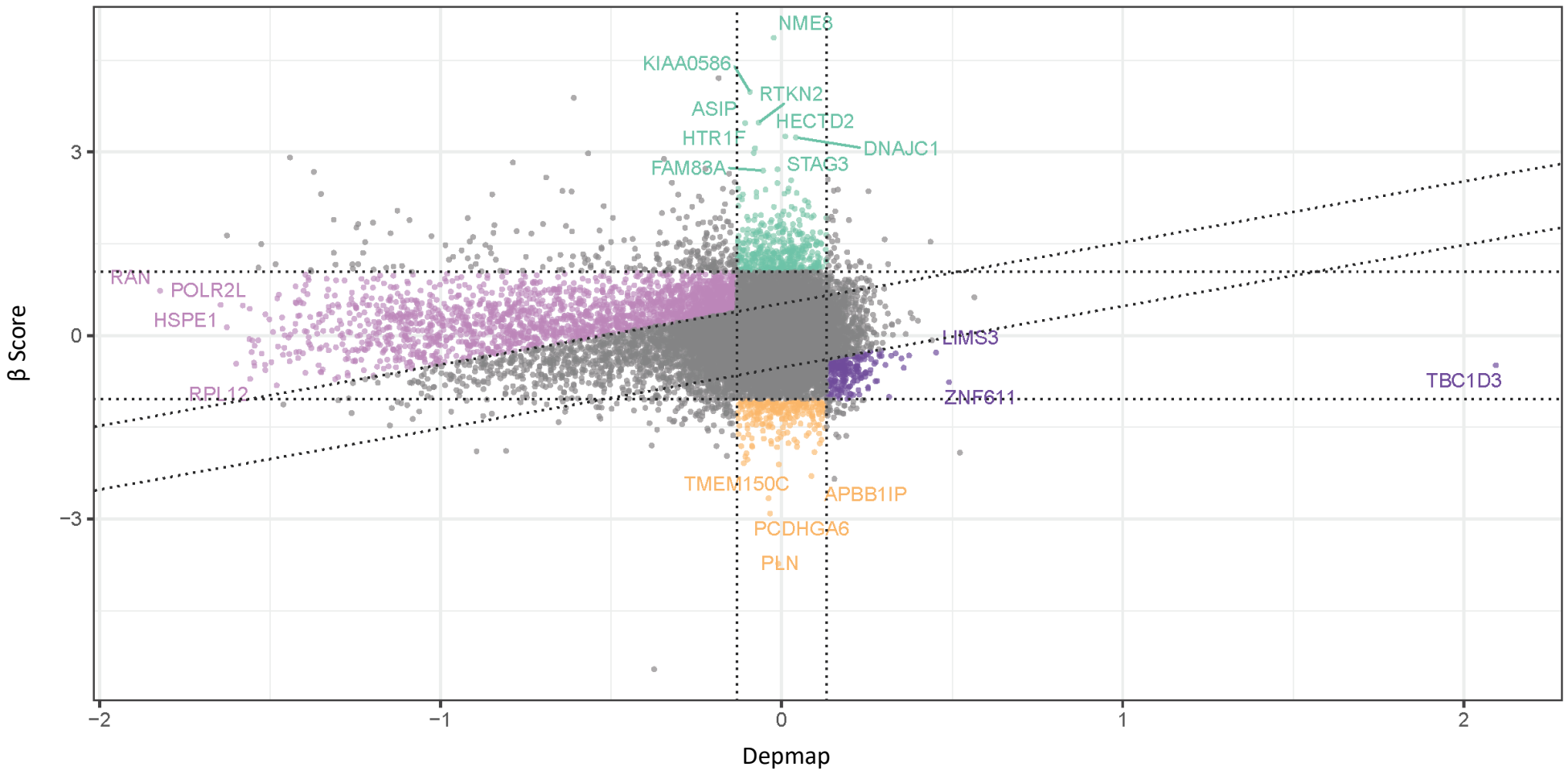

Figure 76: Scatter plot dividing genes according to β-score and Depmap dependency. Horizontal and vertical dashed lines indicate ± one standard deviation. Top middle (green) indicate genes which are strongly enriched in the SOX2^{LOW} population without being strongly dependent genes on Depmap. Bottom middle (orange) indicate genes which are strongly enriched in the SOX2^{HIGH} population without being strongly dependent genes on Depmap

Prioritisation and Validation of Candidates

Candidates were selected based on enrichment in the $SOX2^{LOW}$, with a β-score of at least 2.3512 (the β-score for SOX2). Candidates were prioritised if a pharmacological agent was available or was in development to target said candidate. miRNA hits were not pursued as miRNA currently have poor therapeutic tractability. Likewise hits were not pursued if there was no drug pipeline for the candidate protein. Candidates were preferred where there was evidence of toxicity in 3q amplified squamous cell lung cancer cells on DepMap data. Based on these criteria, five candidates were selected for validation: *PCNA* (β-score 2.912), *PGM3* (β-score 2.7269), *TTI1* (β-score 2.83), *EIF4G1* (β-score 2.3645), and *VCP* (β-score 2.675). Candidates were validated with siRNA knockdown in RERF-LC-SQ1. siRNA validation was preferred so that CRISPR results could be validated with a second modality. As the CRISPR screen was performed in a single cell line, it was important to validate in a second cell line. Therefore, if an impact on knockdown was confirmed in RERF-LC-SQ1, the candidate was validated in a second 3q amplified cell line (HCC2814).

EntrezID	Gene ID	β-Score	Dependency RERF-LC-SQ1	Dependency Amplified
51314	*NME8*	4.8692	-0.09013	-0.03383
554313	*HIST2H4B*	4.2087	NA	NA
9786	*KIAA0586*	3.9824	-0.03007	-0.04963
64946	*CENPH*	3.8878	-0.67803	-0.40874
646754	*TRIM64C*	3.5906	NA	NA
219790	*RTKN2*	3.4794	-0.19243	-0.16847
434	*ASIP*	3.4737	0.24309	0.06075
143279	*HECTD2*	3.2543	0.07674	-0.00958
64215	*DNAJC1*	3.2385	0.12251	0.00455
55224	*ETNK2*	3.0628	0.05456	-0.04948
3355	*HTR1F*	2.9847	-0.00397	-0.13556
3015	*H2AFZ*	2.9782	NA	NA
5111	*PCNA*	2.9121	-2.57881	-1.8106
387	*RHOA*	2.8887	-0.01528	-0.57485
9675	*TTI1*	2.83	-0.88184	-0.92881
100310812	*SPDYE2L*	2.8008	NA	NA
5238	*PGM3*	2.7269	-0.17581	-0.21609
10734	*STAG3*	2.7189	0.05162	0.03319
84985	*FAM83A*	2.6962	0.04193	-0.00412
7415	*VCP*	2.6753	-2.17825	-1.90252
100288695	*LIMS3L*	2.6537	NA	NA
51056	*LAP3*	2.6457	-0.04902	-0.09135
23065	*EMC1*	2.5839	-0.14782	-0.54883
53842	*CLDN22*	2.5541	NA	0.21112
317754	*POTED*	2.5393	-0.11077	-0.02177
388630	*TRABD2B*	2.5088	-0.12538	-0.06739
8362	*HIST1H4K*	2.4977	NA	NA
219402	*MTIF3*	2.4934	-0.21443	-0.15404
50650	*ARHGEF3*	2.4043	-0.07416	-0.06280
641	*BLM*	2.4007	-0.27560	-0.34471
100132396	*ZNF705B*	2.4005	NA	0.29409
51062	*ATL1*	2.386	-0.00629	-0.09205
442590	*SPDYE5*	2.3849	NA	NA
165140	*OXER1*	2.3837	0.05185	0.00815
9275	*BCL7B*	2.3682	0.05044	0.08970
1981	*EIF4G1*	2.3645	-0.91066	-0.66033
3823	*KLRC3*	2.3603	-0.13157	0.10332
6047	*RNF4*	2.3553	-0.43083	-0.71832
6657	*SOX2*	2.3512	-1.61804	-0.72144
221960	*CCZ1B*	2.3415	NA	NA
89122	*TRIM4*	2.3415	-0.17633	0.01113
4133	*MAP2*	2.331	0.39491	0.09649
114784	*CSMD2*	2.3189	-0.20896	0.00825
1642	*DDB1*	2.3144	-1.76481	-1.69285
79915	*ATAD5*	2.3073	-0.24692	-0.34903
51550	*CINP*	2.3068	-0.62751	-1.06423
51042	*ZNF593*	2.3038	-0.38272	-0.57882
23439	*ATP1B4*	2.3007	0.00389	-0.11126
54799	*MBTD1*	2.2749	-0.22155	-0.37933
147015	*DHRS13*	2.2666	-0.17875	-0.17456
170954	*PPP1R18*	2.2648	0.00603	-0.01679
1139	*CHRNA7*	2.2263	-0.02170	-0.00114
84218	*TBC1D3F*	2.2094	NA	NA
285220	*EPHA6*	2.2067	0.19402	0.13187
100885850	*PTGES3L-AARSD1*	2.2057	NA	NA
10321	*CRISP3*	2.1794	0.17852	0.14466
6602	*SMARCD1*	2.1479	-0.35249	-0.34156
2806	*GOT2*	2.1192	-0.33033	-0.41013
81557	*MAGED4B*	2.1155	NA	NA
728340	*GTF2H2C*	2.1148	NA	-0.55406

Table 46: Ranked List of Candidates from CRISPR Screen ranked according to β-score. Top 60 candidates enriched in SOX2^{LOW} population MicroRNAs are excluded. Ranked on β-score. Depmap dependency is displayed across all cell lines 'DepMap Overall' alongside dependency in RERF-LC-SQ1. Candidates explored in greater depth are highlighted.

PCNA

Proliferating Cell Nuclear Antigen (PCNA) is a multifunctional protein with roles that include the regulation of DNA synthesis, repair, and transcription. Profound knockdown of PCNA was achieved using siRNA. PCNA knockdown resulted in a time-dependent reduction in SOX2 protein expression in RERF-LC-SQ1, with greatest effects seen at extended time points (120 and 144 hours) (Figure 77). These results were validated in a second 3q amplified cell line (HCC2814). These results validate the findings of the CRISPR screen, suggesting that PCNA plays an important role in regulation of SOX2 expression in 3q amplified squamous cell lung cancer cells.

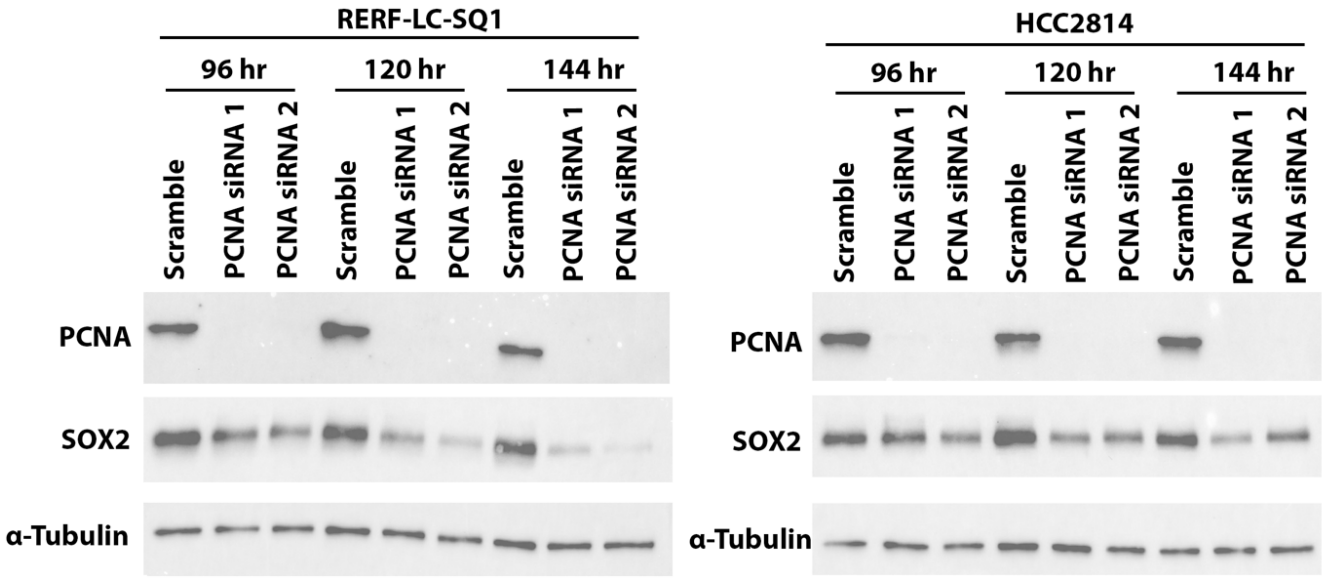

Figure 77: Western blot of impact of PCNA knockdown on SOX2 protein levels in RERF-LC-SQ1 and HCC2814. RERF-LC-SQ1 cells were transfected with 40 nM negative control siRNA 'scramble' or 40 nM of siRNA against PCNA. Protein lysates were taken at the indicated time points, protein lysates were assessed for SOX2, PCNA and Tubulin (loading control). Experiment performed in duplicate with representative blot shown

PGM3

PGM3 is an enzyme that forms part of the Hexosamine Biosynthetic Pathway (HBP). Knockdown of PGM3 was achieved using siRNA in RERF-LC-SQ1. PGM3 knockdown resulted in a time-dependent reduction in SOX2 protein expression in RERF-LC-SQ1, with greatest effects seen at extended time points (120 and 144 hours) (Figure 77). Notably, the impact of PGM3 knockdown on SOX2 expression was more marked with PGM3 siRNA 2 (s10411) than PGM3 siRNA 1 (s10409). Knockdown of PGM3 had no observable impact on SOX2 protein expression in HCC2814. PGM3 produces a strong double band in HCC2814, which may reflect alternately spliced transcripts. Whilst siRNA removes the upper band, the stronger lower band remains. It is therefore possible that PGM3 knockdown failed to remove the predominant transcript in HCC2814. Alternatively, PGM3 may not play an essential role in regulating SOX2 in HCC2814, and therefore the effects of PGM3 on SOX2 could be cell dependent.

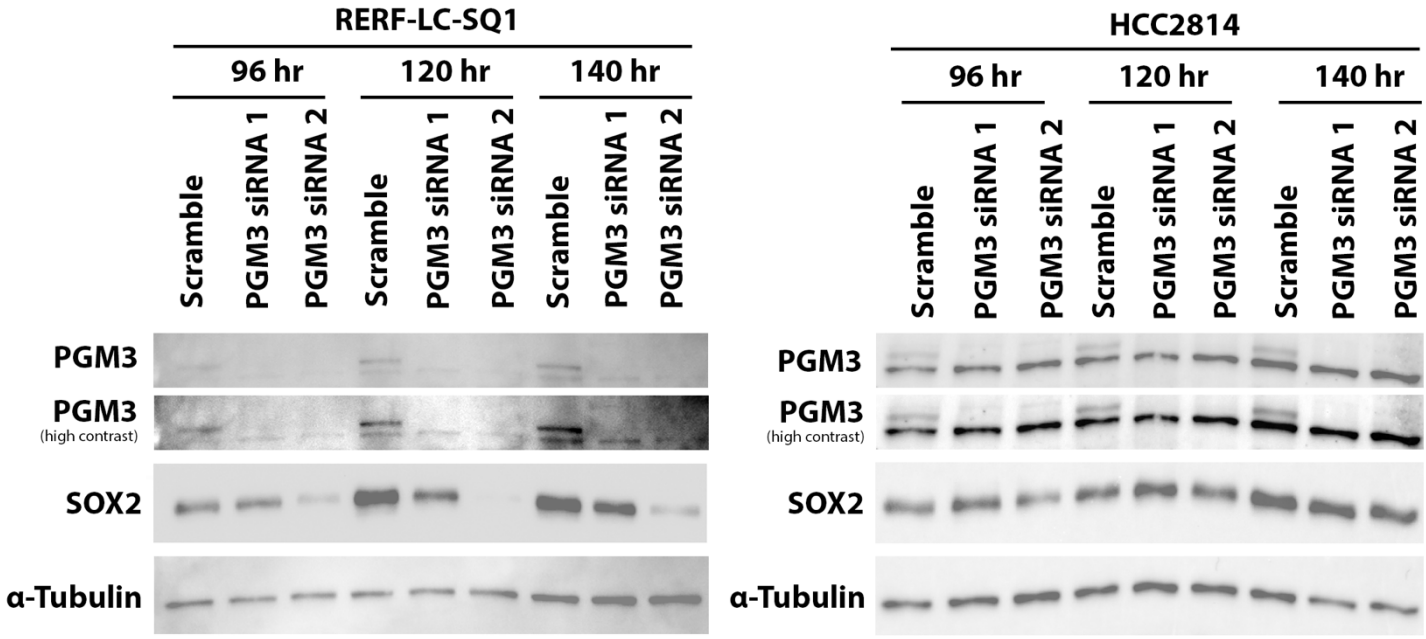

Figure 78: Western blot of impact of PGM3 knockdown on SOX2 protein levels in RERF-LC-SQ1 and HCC2814. RERF-LC-SQ1 cells were transfected with 40 nM negative control siRNA 'scramble' or 40 nM of siRNA against PCNA. Protein lysates were taken at the indicated time points, protein lysates were assessed for SOX2, PGM3 and Tubulin (loading control). Experiment performed in duplicate with representative blot shown. High contrast images generated by applying 'AutoContrast' to entire image using photoshop, with no adjustment to any individual bands or region of the image, original unadjusted image is displayed above

VCP

VCP (p97) regulates protein degradation, predominantly by regulating the release of proteins from cellular structures and protein aggregates, complexes and chromatin (346, 347). Prolonged and profound knockdown of VCP was achieved using siRNA VCP knockdown and resulted in reduction in SOX2 protein expression at 72 hours (Figure 79). Notably at more extended time points, VCP knockdown also impacts on expression of α-Tubulin (Figure 79) and β-actin (not shown), likely reflecting cellular toxicity or a more widespread impact on protein homeostasis. These results were validated in a second 3q amplified cell line (HCC2814), with similar reduction in expression of housekeeping proteins at extended timepoints. These results validate the findings of the CRISPR screen, suggesting that VCP plays a role in regulation of SOX2 expression in 3q amplified squamous cell lung cancer cells. However, these results may be relatively non-specific.

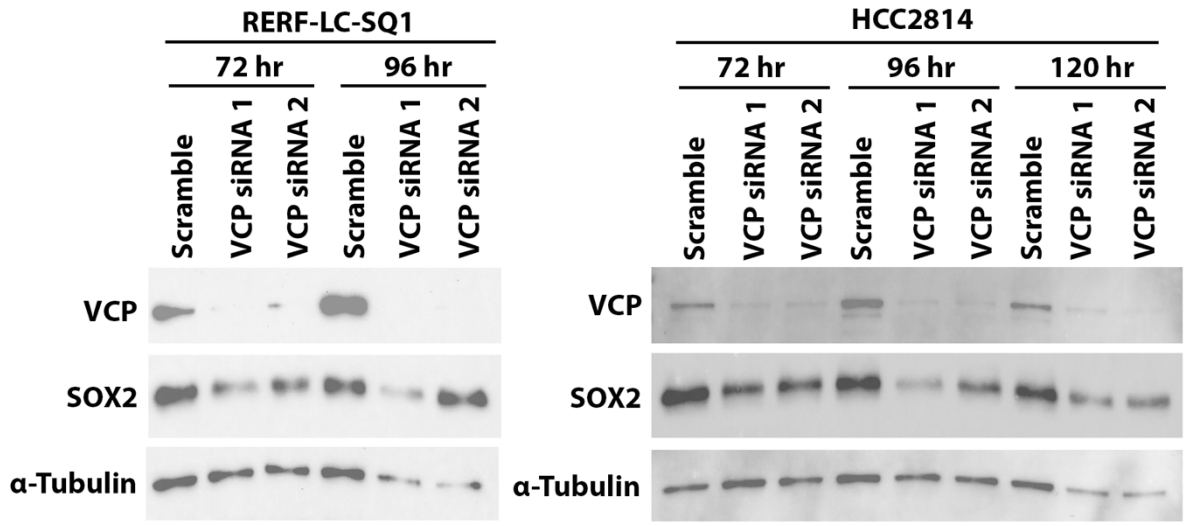

Figure 79: Western blot of impact of VCP knockdown on SOX2 protein levels in RERF-LC-SQ1 (A) and HCC2814 (B). RERF-LC-SQ1 cells were transfected with 40 nM negative control siRNA 'scramble' or 40 nM of siRNA against VCP. Protein lysates were taken at the indicated time points, protein lysates were assessed for SOX2, VCP and Tubulin (loading control). Experiment performed in duplicate with representative blot shown

TTI1

TELO-2 interacting protein (TTI1) is a component of the Triple T Complex (TTT), which comprises TEL2, TTI1 and TTI2. TTI1 interacts with and stabilizes PIKK proteins (mTOR, ATM, ATR and DNA-PKcs, SMG-1, and TRRAP (348). Prolonged and profound knockdown of TTI1 was achieved using siRNA. TTI1 knockdown had a minimal or no impact on SOX2 protein levels (Figure 80). Whilst these results suggest that TTI1 may play a role in regulation of SOX2 in the context of 3q amplification, this small effect is unlikely to be therapeutically meaningful.

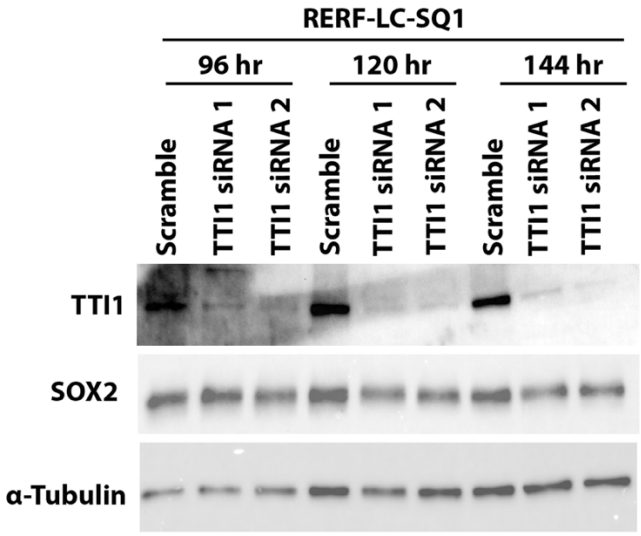

Figure 80: Western blot of impact of TTI1 knockdown on SOX2 protein levels in RERF-LC-SQ1 cell line. RERF-LC-SQ1 cells were transfected with 40 nM negative control siRNA 'scramble' or 40 nM of siRNA against TTI1 (S10133, S10134). Protein lysates were taken at the indicated time points, protein lysates were assessed for SOX2, TTI1 and Tubulin (loading control). Experiment performed in duplicate with representative blot shown

EIF4G1

EIF4G1 is an attractive candidate in targeting SOX2, as EIFG1 sits at 3q27.1 and is therefore commonly co-amplified with SOX2. Prolonged and profound knockdown of EIF4G1 was achieved using siRNA. However, even at extended time points, EIF4G1 knockdown had minimal impact on SOX2 protein levels. EIFG1 was therefore not successfully validated as a candidate target to modulate SOX2 expression in 3q amplified cell lines.

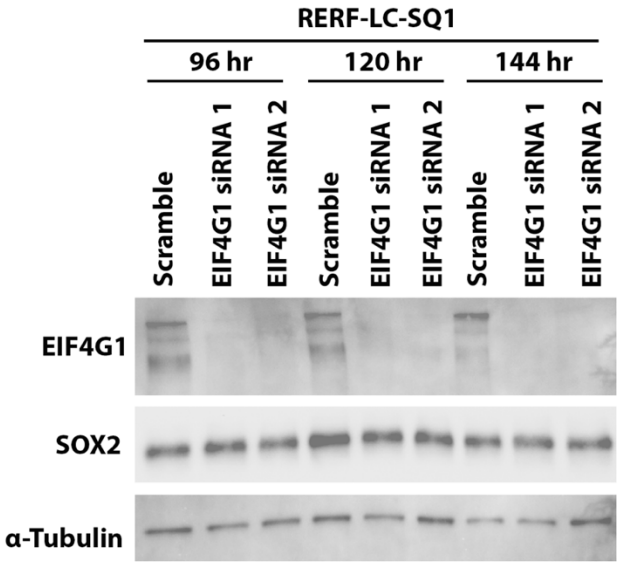

Figure 81: Western blot of impact of EIF4G1 knockdown on SOX2 protein levels in RERF-LC-SQ1 cell line. RERF-LC-SQ1 cells were transfected with 40 nM negative control siRNA 'scramble' or 40 nM of siRNA against EIF4G. Protein lysates were taken at the indicated time points, protein lysates were assessed for SOX2, EIF4G1 and Tubulin (loading control). Experiment performed in duplicate with representative blot shown

7.5 Discussion

No studies have undertaken an analysis of SOX2 regulation in 3q amplification or squamous cell lung cancer in an unsupervised manner. In this chapter, FACS-assisted genome wide CRISPR knockout screening was used to identify potential candidates to target upstream of SOX2. Based on the initial CRISPR screen, five candidates were selected for validation: PCNA, PGM3, VCP, TTI1 and EIF4G1. PCNA was the most convincing candidate on validation: PCNA demonstrated profound reduction in SOX2 expression in two tested cell lines, whilst having minimal impact on housekeeping proteins. Targeting PCNA is therefore a potential approach to reduce SOX2 in squamous cell lung cancer and is a candidate for ongoing research and development.

7.5.1 PCNA

Proliferating Cell Nuclear Antigen (PCNA) is a highly conserved multifunctional protein. PCNA is best characterised as a DNA sliding clamp: PCNA forms a homotrimer, creating a ring around DNA, facilitating recruitment of proteins to replication machinery. PCNA regulates multiple processes, including: DNA replication and repair; chromatin assembly; gene transcription and cell cycle control (349). Cytoplasmic PCNA regulates apoptosis (350), glycolysis (351), and cell signalling, including MAPK and PI3K/Akt signalling, and TLR-associated cytokine release (352). Cell-surface PCNA inhibits NK-mediated killing of cancer cells by binding NKp44 (353). PCNA is upregulated in NSCLC (354), with expression being higher in squamous cell lung cancer than adenocarcinoma (355) and expression is associated with poor prognosis (354-356). Overexpression of PCNA promotes cell growth, colony formation and inhibits apoptosis in lung adenocarcinoma cells, at least in part through activation of STAT3 (354). To the best of our knowledge, this is the first work that has demonstrated that PCNA plays a critical role in maintaining SOX2 expression. However, this is clearly in keeping with the known roles of PCNA in transcription, proliferation, and stemness. Future work will validate PCNA as a target to modulate SOX2 expression in a wider panel of cell lines as well as lung cancer organoid models.

An outstanding question is whether pharmacological inhibition of PCNA replicates the results of PCNA knockdown. Any approach to targeting PCNA in malignancy requires targeting towards malignant cells, as an unselected approach would result in substantial toxicity. One option is to take advantage of PCNA's altered substrate sensitivity in cancer cells. Under normal conditions, PCNA preferentially binds proteins containing a PIP-box motif. In conditions of cellular stress, such as cancer, post-translational modifications increase PCNA's affinity for binding to proteins with APIM motifs (357-359). Therefore, APIM-motif peptides preferentially target PCNA in cancer cells (357-359). ATX-101 is a cell-penetrating APIM-containing peptide that has demonstrated efficacy in multiple preclinical models (358, 360, 361). Of particular relevance, ATX-101 impairs stemness of glioblastoma cells, including downregulating expression of SOX2 (362). In a Phase I trial of 25 patients with solid cancers (4 with NSCLC), ATX-101 was well-tolerated, and achieved stable disease in 70% of the patients in the efficacy population (363). An alternate route to target PCNA is by targeting the cancer specific PCNA isoform (caPCNA), which differs from regular PCNA due to differential post-translational modifications (addition of methyl esthers to aspartic and glutamic acid residues) (364). caPCNA is widely expressed in cancer cells, with minimal expression in normal tissues (365-367). AOH39 and AOH1160 specifically target caPCNA, and treatment results in cycle arrest, apoptosis and accumulation of double strand breaks in cancer cells, whilst sparing normal cells (364). AOH1160 reduces growth of glioblastoma stem cells, sensitises cancer cells to cisplatin, and is active in xenograft models of breast and small-cell lung cancer (364). Further development has resulted in AOH1996, a metabolically stable compound suitable for ongoing drug development (368). Further work will test AOH1996 and ATX-101 *in vitro* to assess whether these agents replicate the results seen with siRNA knockdown across a panel of cell lines, and the impact of these agents on cell viability, colony formation and migration.

7.4.2 PGM3

PGM3 encodes phosphoglucomutase 3, an enzyme that catalyses the isomerization of N-acetylglucosamine-6-P to N-acetylglucsamine-1-P as part of the Hexosamine Biosynthetic Pathway (HBP) (369, 370). The Hexosamine Biosoynthetic Pathway is a multistep process that produces Uridine Diphosphate-N-Acetylglucosamine (UDP-GlcNAc), which is required for O-linked glycosylation, N-linked glycosylation, and O-GlcNAcylation (Figure 82).

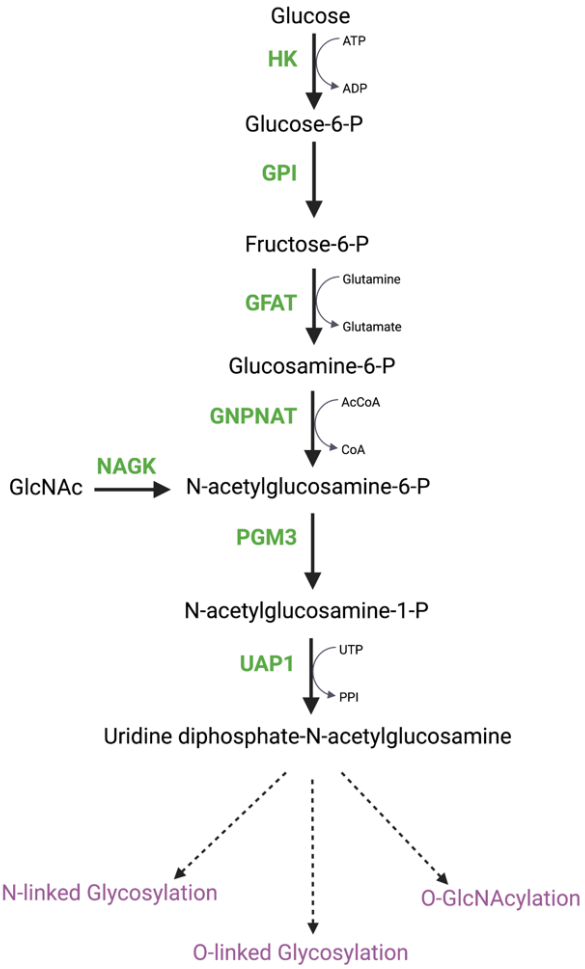

Figure 82: The Hexosamine Biosynthesis Pathway. The first two steps of the Hexosamine Biosynthesis Pathway are shared with glycolysis: Hexokinase (HK) phosphorylates glucose, producing Glucose-6-phosphate, which is then converted to fructose-6-phosphate by phosoglucose isomerase (GPI). Fructose-6-Phosphate Transaminase (GFAT) converts Fructose-6-Phosphate and Glutamine to Glucosamine-6-Phosphate and glutamate. Glucosamine-phosphate N-acetyltransferase (GNPNAT) converts Glucosamine-6-Phosphate and Acetyl-CoA to N-acetylglucosamine-6-phosphate and CoA. Glucosamine-6-Phosphate is isomerized to N-acetylglucosamine-1-phosphate by PGM3 (GlcNAc phosphomutase). The final end-product of the pathway is uridine diphosphate-N-acetylglucosamine, which is produced from N-acetylglucosamine and UTP by UDP-N-acetylglucosamine pyrophosphorylase (UAP1). N-acetylglucosamine is essential for N-linked glycosylation, O-linked glycosylation, and O-GlcNAcylation. Adapted from (215), created using Biorender.com

O-GlycNAcylation plays a role in regulating stemness and pluripotency (370). In embryonic stem cells, O-GlycNAcylation of SOX2 regulates cell renewal and cell fate (371). O-GlcNAcylation increases SOX2 transcriptional activity, increases protein stability and promotes nuclear localization in pancreatic cancer (372). In addition, O-GlycNAcylation stabilises eukaryotic initiation factor 4E (eIF4E), which binds to the 5'-untranslated region of the SOX2 transcript, promoting SOX2 translation (373). It is therefore plausible that the hexosamine biosynthesis pathway would modulate SOX2 expression in 3q amplified lung cancer. However, the siRNA validation data for PGM3 was conflicting. Whilst siRNA knockdown of PGM3 reduced SOX2 expression in RERF-LC-SQ1, the magnitude of the reduction differed between the two tested siRNAs. In addition, PGM3 knockdown had no observable impact on SOX2 expression in HCC2814. These results may reflect discrepant knockdown across alternately spliced transcripts or may reflect non-specificity of siRNA knockdown. Alternatively, the effects of PGM3 on SOX2 could be cell line dependent. Further work will explore and validate these results. Firstly, through assessment of a wider panel of cell lines. Secondly, validation with CRISPR knockout will provide clarity by reducing non-specific results. Finally, it would be interesting to explore the impact of glucose deprivation on SOX2 expression in 3q amplified cell lines.

A further area of development is exploration of crosstalk and synergy between PCNA depletion and therapeutic strategies explored in Chapter 6. Interestingly, BRD4 inhibits the unloading of PCNA from chromatin (374). BET inhibition with JQ1 reduces the amount PCNA bound to nascent DNA (374). It would therefore be interesting to explore whether co-inhibition of BRD4 and PCNA is synergistic, or a more effective strategy for downregulating SOX2 expression.

7.4.3 VCP

Valosin-containing protein (VCP) (p97) is a highly conserved 97-kDa adenosine triphosphatase (ATPase). VCP mediates protein unfolding, uncoupling from binding partners, and release from cellular structures or membranes. As a result, VCP monitors protein quality, promotes proteasomal degradation, maintains genomic stability and regulates autophagy (346, 347). VCP is overexpressed in lung cancers, where expression is associated with worse prognosis (347, 375, 376). Inhibition or knockdown of VCP reduces proliferation and induces apoptosis in lung, pancreatic, colorectal and lung cancer cell lines (376-378), and reduces migration and invasion of lung adenocarcinoma and osteosarcoma cells (376, 379). The results presented in this chapter suggest that VCP may play a role in regulating SOX2 in 3q amplified squamous cell lung cancer. In keeping with this, VCP levels have been reported to correlate with SOX2 in breast cancer cell lines, and VCP expression is enriched in breast cancer stem cell populations (380). Furthermore, VCP knockdown depletes breast cancer stem cells, impairs mammosphere formation, and reduces SOX2, OCT4 and other stemness factors (380). Overall, cancer cells appear to be more sensitive to VCP inhibition: siRNA against VCP reduce viability of cutaneous squamous cell cancer cell lines, but was non-toxic to normal keratinocytes (381), with similar findings in breast cancer cell lines versus non-cancerous breast cells (380). Future work will validate VCP as a target to modulate SOX2 expression in a wider panel of cell lines as well as squamous cell lung cancer organoid models.

Targeting VCP may modulate SOX2 expression in 3q amplified squamous cell lung cancer. N^2,N^4-dibenzylquinazoline-2,4-diamine (DBeQ), ML-240 and ML-241 were the first ATP competitive inhibitor of VCP. However, whilst these agents are useful lead compounds for *in vitro* research, they were unsuitable for in vivo studies (382). Further optimisation of ATP competitive inhibitors resulted in development of CB-5083 and CB-5539 (382). CB-5083 treatment impairs endoplasmic reticulum-associated degradation, drives accumulation of polyubiquitinated proteins,

increases accumulation of endoplasmic-reticulum-associated degradation (ERAD) substrates, promotes proteotoxic stress and is pro-apoptotic, and showed promising results in xenograft models (383). However, Phase I trials of CB-5083 were halted due to ophthalmic side effects, likely due to off-target effects on phosphodiesterase-6 (PDE6) (384). CB-5339 is a second-generation CB-5083 analogue, with reduced activity on PDE6 whilst maintaining activity against VCP (385). A Phase I Trial of CB-5339 in Acute Myeloid Leukemia or Myelodysplastic Syndrome is ongoing (NCT04402541) (386). Non-covalent, non-ATP competitive inhibitors have also been developed, of which UPCDC30245 and NM-873 are the most potent, although NMS-873 lacks in vivo efficacy (382). Crucially, any experiments with VCP inhibition would need to pay careful attention to the specificity of any effect on SOX2. Based on the siRNA experiments presented in this chapter, there may only be a narrow window where SOX2 is targeted in preference to other proteins. As a result, it is possible that VCP inhibition as an indirect 'SOX2-targeting' approach may be limited by non-specific toxicity on the wider proteome.

7.4.4 TTI1

TELO-2 interacting protein (TTI1) is a component of the Triple T Complex (TTT), which comprises TEL2, TTI1 and TTI2. TTI1 interacts with and stabilizes PIKK proteins (mTOR, ATM, ATR and DNA-PKcs, SMG-1, and TRRAP (348). TTI1 is upregulated in both lung adenocarcinoma and squamous cell lung cancer, and predicts poor prognosis (348) and reduces proliferation, migration and invasion of lung adenocarcinoma cells in vitro. To the best of our knowledge, this is the first work to show that TTI1 is within the regulatory framework of SOX2. However, the impact of TTI1 knockdown on SOX2 expression is relatively modest. Therefore, whist TTI1 activity may support SOX2 expression, it does not seem to be a critical regulator. Based on the present evidence, TTI1 directed therapy would not appear to be a particularly promising candidate to take forward in this context.

7.4.5 Other candidates for future work

Only a relatively small number of potential candidates identified within the CRISPR screen were taken forward for further validation. It is likely that other proteins enriched in the SOX2^{LOW} population would be of interest for further research, either in the context of understanding the biology of SOX2 regulation or in exploring alternate therapeutic avenues.

One further candidate for further investigation is *RHOA*, which has a comparable β-score to *PCNA*. RhoA belongs to the family of Rho GTPases, which share substantial homology to Ras. RhoA drives proliferation, invasiveness and mediates epithelial mesenchymal transition (EMT), and cancer stem cell phenotypes (387-391). RhoA was previously viewed as undruggable. However, small molecular inhibitors of RhoA have been discovered (392). Rhosin (a first-generation RhoA inhibitior) downregulates SOX2 in gastric adenocarcinoma spheroids (393). RhoA is therefore a highly attractive as a candidate for a potential modulator of SOX2 expression in 3q amplified squamous cell lung cancer.

NME8 was the gene with the highest β-score, and therefore is a potential crucial regulator of SOX2. However, this was not taken forward as a candidate for validation due to no therapeutic options for targeting. The lack of therapeutic tractability does not negate the potential biological interest. NME8 encodes Thioredoxin domain-containing protein 3 (TXNDC3) / spermatid-specific thioredoxin-2 (SPTRX-2). Notably, SOX2 and TXNDC3 both play roles in spermatogenesis (394, 395) and differentiation and maintenance of respiratory cilia (396, 397). However, any interaction between SOX2 and TXNDC3 is beyond the scope of this thesis.

7.5.6 Potential weaknesses and alternate approaches

A weakness of this current CRISPR screen is that the initial screen was conducted in a single cell line. Undertaking the CRISPR screen in multiple cell lines will strengthen the evidence and is planned for future work. However, the intention of the present work was to utilise the CRISPR screen as tool for hypothesis generation and a springboard for further work, which has proved fruitful. Validated candidates were therefore tested in a second 3q amplified cell line, with plans for validation in further cell lines in future work. In addition, any drug screens arising from this work will be conducted in a wider panel of cell lines to ensure that any identified approaches are widely applicable across 3q amplified cell lines. A further potential weakness is that any drug candidates that are identified will be targeting SOX2 indirectly and will therefore likely have more off-target and non-specific actions than direct SOX2-directed therapies. Potential alternate direct targeting strategies will be discussed in the final discussion chapter, as well as the relative merits and disadvantages of these potential approaches. Finally, due to the design of the screen, we are only able to identify candidates that impact on SOX2 protein levels. The screen will therefore miss strategies that impact on SOX2 activity without modulating SOX2 expression. A potential supplementary approach would be to perform a second CRISPR screen using a SOX2 response reporter, which may reveal alternate candidates for further work.

It is acknowledged that PCNA, TTI1, VCP and EIF4G1 are all genes that are listed as 'common essential' in either DepMap and/or CEG2 (210, 398). Common essential genes are genes that are required for all (or almost all) cell lines, and is defined in DepMap as genes ranking in the top most depleting gens in at least 90% of cell lines (210). Whether to include or exclude common essential genes in the gene list from the CRISPR screen was carefully considered, and it was decided not to exclude these genes to maintain the breadth of the screen. It is important to note that whilst a number of the genes chosen for validation are common essential, the majority of the other 'top genes' are not listed as common essential genes, including: *NME8, KIAA0586,*

TRIM64C, RTKN2, ASIP, HECTD2, DNAJC1, ETNK2, HTR1F, RHOA, STAG3, FAM83A (210). This discrepancy reflects the decision to prioritise candidates with pharmacological agents in development, and therefore reflects the current pharmacological pipeline. Nonetheless, this highlights potential challenges in pharmacological development. Whilst drugs targeting common essential genes are used current oncology practice (such as CDK4/6i, MEK1/2i) and are undergoing clinical development (such as ATMi, ATRi, CHK1i) (399), targeting pan-essential genes does present challenges. In particular, a key challenge in targetting common essential genes is a potential narrow therapeutic index *in vivo*, and such approaches require careful pre-clinical drug development (399).

SOX2 was the 39th top ranked protein coding gene enriched in the SOX2 low population. The GeCKO v2 library includes guides against 19052 protein coding genes. Therefore, SOX2 was in the top 0.2% of genes. However, it is acknowledged that *SOX2* is not the top candidate despite selecting on SOX2 expression. Technical aspects of a flow-assisted CRISPR screen may well contribute to this, including variance in guide specificity, and stochastic noise inherent in such a screen. Repeat CRISPR screen runs could mitigate the stochastic variability. However, repeat runs were not possible during the present PhD due to time limitations. It is also acknowledged that pre-apoptotic cells may be enriched in the SOX2 low population, as this population may not be effectively excluded by live/dead staining. Some of the identified hits may therefore reflect non-specific toxicity. In addition, genes that have non-specific effects on transcription and translation will also be included in the SOX2 low population. Once again, this highlights the importance of thorough validation of results from this screen, which will take place in further work.

Finally, it must be noted that candidates validated in Chapter 6 were not identified as part of the current CRISPR screen. There are several potential contributing factors. Firstly, a genome-wide

CRISPR combined with FACS sorting may lack sensitivity to identify all potential candidates targeting SOX2 in this context. In addition, there is inherent variation in the results when comparing pharmacological inhibition and CRISPR knockout, due to factors such as guide sensitivity, stochastic variability and presence or absence of redundancy. These two approaches should therefore be viewed as complementary methods to identify a range of potential strategies to target SOX2 in this context for ongoing research and development.

7.6 Conclusions

SOX2 sits at a network of multiple regulatory pathways, and this GeCKO screen sought to identify potential alternate strategies to modulate SOX2 expression in 3q amplified squamous cell lung cancer. Results suggest that PCNA may be a critical regulator of SOX2, and is a candidate for further ongoing work. In addition, VCP, TTI1 and PGM3 are also identified as additional regulators of SOX2 expression in 3q amplified squamous cell lung cancer.

Chapter 8: Discussion

8.1 Overview and Key Findings

Lung cancer is at the forefront of personalised medicine in oncology. However, current targeted therapies are largely restricted to never smokers with well characterised oncogene addiction. This thesis sought to help address this discrepancy, by focussing on common genetic aberrations in smoking related lung cancer: *STK11* mutation, *KRAS* mutation, and 3q amplification.

Chapter 3 focussed on *STK11*-mutant lung adenocarcinoma, using serial ctDNA samples to identify potential resistance mutations in *STK11*-mutant adenocarcinoma treated with mTORC1/2 inhibition (vistusertib). Reactivation of PI3K/Akt signalling following prolonged mTORC1/2 inhibition was also explored *in vitro.* Firstly, it was demonstrated that STK11 deficient cells are not exempt from relief of feedback inhibition on receptor tyrosine kinases, which drives re-activation of PI3K/Akt/FOXO signalling. This re-activation of pro-mitogenic signalling may contribute to suboptimal efficacy of mTORC1/2 inhibition. Secondly, it was noted that *FOXP1* and *SMARCA4* mutations become enriched on treatment in patients with *STK11*-mutant lung adenocarcinoma treated with vistusertib. It is possible that *FOXP1* and *SMARCA4* mutations may contribute to resistance to therapy.

Chapter 4 focussed on *KRAS* mutant lung adenocarcinoma, analysing ctDNA to identify potential sensitising and resistance mutations in KRAS-mutant adenocarcinoma treated with CDK4/6 inhibition (palbociclib). Absence of *KDR* variants, and presence of *MTOR* or *CHEK2* mutations on ctDNA may predict better prognosis in *KRAS*-mutant NSCLC treated with palbociclib. This population may reflect a new cohort of patients who may particularly benefit from CDK4/6 inhibitor therapy.

In the remaining chapters, the work focussed on 3q amplified squamous cell lung cancer. *SOX2* is one of the few genes within the amplicon where amplification correlates with increased dependency and SOX2 is therefore a potential rational target in in 3q amplified squamous cancers. Potential drug strategies that have previously been reported to modulate SOX2 expression were applied to 3q amplified squamous cell lung cancer, with CDK7 inhibition and BRD4 inhibition being potential promising approaches. In addition, a FACS-assisted genome-wide CRISPR screen was undertaken to identify potential novel strategies for targeting SOX2 in 3q amplified squamous cell lung cancer. The most convincing candidate identified from the CRISPR screen and subsequent validation was PCNA. Further work will be conducted to explore whether hits identified in the CRISPR screen are replicated when pharmacological agents are used to target the proteins of interest.

Relevance of individual results has been discussed in individual chapters, as has potential weaknesses in specific approaches taken and directions for future work. Therefore, this final chapter will take a broader approach, discussing how the work in this thesis highlights some difficulties faced in developing targeted therapies in smoking related lung cancer in the present era, as well as discussing potential options for more direct targeting of SOX2 which could be directions for research in the future.

8.2 Fighting negative feedback

As discussed elsewhere, a key issue with mTORC1/2 inhibition is relief of feedback inhibition, driving receptor tyrosine kinase mediated reactivation of PI3K/Akt/FOXO signalling (180, 181). Whilst it was hoped that this would be less relevant in the context of *STK11* loss, this proved to not be the case (Chapter 3). Targeting cell signalling at a single point risks therapy being overridden by adaptative oncogenic signalling networks. Combination therapies that target

pathways at multiple levels may be needed to overcome this issue, as exemplified by combining fulvestrant and alpelisib in *PIK3CA* mutant hormone receptor positive breast cancer (216). Indeed, such strategies are being explored in ComboMATCH (217). It remains to be seen whether platform studies based on rational combination therapies will be more fruitful, or whether such combinations will be limited by toxicity.

8.3 Co-mutations, heterogeneity, and evolution

Three large platform studies have sought to identify new targetable oncogenic drivers: NCI-MATCH, LUNG-MAP, and the National Lung Matrix Trial (127, 218, 219). Whilst these platform studies triaged patients with potential driver mutations to rational therapy, an emerging challenge is that co-mutations may contribute to therapy resistance (219). This is particularly relevant in smoking-related lung cancer: smoking-related lung cancer has a high tumour mutational burden which contrasts to the simpler genetic background seen in adenocarcinomas driven by classic oncogenic drivers in non-smokers (220-222). Intra-tumour heterogeneity and clonal evolution add further complexity: around 30% of somatic mutations in early-stage NSCLC are sub-clonal, with smoking-related lung cancer having a higher burden of both clonal and sub-clonal mutations (223). Furthermore, a surgical biopsy from the primary tumour is a poor reflection of metastatic disease: in mNSCLC 33.3% of cases have unique driver mutations in metastases that were not observed in primary tumours (224).

In Chapter 3 and 4, several co-mutations that may alter sensitivity to treatment are identified. *MTOR* mutations and *CHEK2* mutations were enriched in patients with *KRAS*-mutant lung cancer who went onto have prolonged PFS on Palbociclib. In contrast, *SMARCA4* and *FOXP1* mutations appeared to be selected for in *STK11*-mutant lung cancer patients on vistusertib treatment. Truly personalised oncology treatment needs to consider the entire genetic profile of tumours, as well as the potential clonal evolution in response to therapy. Conventional tissue-based biopsies

provide sequencing data from a single area of disease at a single point of time. As a result, conventional biopsies may miss subclonal mutations, and will not assess heterogeneity and clonal evolution. ctDNA provides an opportunity for more complete sampling of the overall disease, as well as assessment of dynamics of mutational profiles (225), albeit with some loss of sensitivity.

8.4 Germline variants

Personalised medicine in cancer has generally focussed on targeting somatic mutations. However, the cancer genome is a combination of somatic mutations and germline variants. In addition, cancer therapy occurs in the context of the patients' own genetic landscape, with well-recognised interactions between germline variants and cancer drug metabolism, exposure and toxicity (226). Germline variants have important therapeutic implications, including in the use of PARP inhibition in breast cancer patients with pathogenic or likely pathogenic germline BRCA variants (227). Likewise, *DPYD* testing is now routine for patients prior to Fluorouracil treatment, allowing for prediction of toxicity and adjustments to therapy. Other clinically relevant interactions include *ACYP2* and *WSF1* in predicting ototoxicity with cisplatin (226), *UGT1A1* predicting toxicity with irinotecan (226), and *CYP2D6* determining tamoxifen efficacy (228). In this thesis, it is found that *KDR* may be associated with worse prognosis in *KRAS*-mutant lung adenocarcinoma treated with Palbociclib. As *KDR* encodes *VEGFR2*, this may reflect increased angiogenesis (229-231). However, as *KDR* hyperactivation has been shown to drive CDK4/6 resistance in bladder cancer cells (232), this could reflect a true resistance mechanism to therapy. Further work will explore this in NSCLC in vitro. However, perhaps more pressingly, it is unknown whether these results are generalisable to patients with breast cancer treated with CDK4/6 inhibitor therapy, as this will have impact of a current therapy in routine clinical use. Overall, these results highlight the importance of assessing germline variants in clinical trials of novel therapies, as focussing solely on somatic mutations and discounting SNPs may miss important predictive or prognostic biomarkers.

8.5 Identifying oncogenic drivers within an amplicon

The PI3K/Akt pathway is a well-studied pathway in squamous cell lung cancer, and *PIK3CA* is a well-known oncogene within the 3q amplicon. However, clinical experience in targeting the PI3K/Akt pathway in 3q amplified squamous cell lung cancer has been disappointing (127, 233). In Chapter 4 it is demonstrated that 3q amplification was not associated with increased dependency on *PIK3CA* in squamous cell lines. Instead, the highest ranked gene that was selectively deleterious to 3q amplified vs non amplified cell lines was the nearby oncogene *SOX2*. The assertion that *SOX2* may be a more critical component of the amplicon is supported by published data: in an arrayed shRNA screen of 14 tested 3q genes (including *PIK3CA*), SOX2 knockdown had the greatest anti-proliferative effect in 3q amplified cell lines (191). When taken together, these results suggest that *SOX2*, and not *PIK3CA* may be the core driver in this region. However, it is possible that the relevance of oncogenes within an amplicon may evolve during oncogenesis. PIK3CA amplification appears to be important in early oncogenesis (234, 235) for example allowing tolerance of aneuploidy (236). It is therefore possible that *PI3KCA* may become less crucial in the presence of the multiple concurrent oncogenic drivers seen in established squamous cell lung cancer, alternatively *PIK3CA* may play a role in the wider multi-gene cassette.

Our findings with *SOX2* and *PIK3CA* in 3q amplification closely parallel work seeking to clarify the driver in 8p amplified squamous cell lung cancer. *FGFR1* is a well-known oncogene within the 8p11-12 amplicon, however targeting FGFR has proved disappointing in the context of amplification (188, 189). FGFR mRNA expression poorly correlates with *FGFR1* copy number, and depletion of FGFR1 has marginal impacts on xenograft growth, suggesting that *FGFR1* may not be a critical driver within the amplicon (190). Instead, the nearby H3K36 methyltransferase *NSD3* may be the more critical component of the amplicon: *NSD3* copy number strongly correlates with NSD3 expression, and depletion of NSD3 substantially impairs xenograft growth (190). Overall, these data highlight the importance of precisely defining the driver genes within

any amplicon before embarking on trials of targeted therapies. In addition, the work in this thesis demonstrates the value of publicly available data such as the Cancer Dependency Map Project (DepMap) and The Cancer Genome Atlas (TCGA) in such assessments: these data were invaluable for streamlining the assessment of potential drivers within the 3q amplicon.

8.6 Indirect targeting of SOX2

Whilst SOX2 is an attractive candidate target in squamous cell lung cancer, transcription factors remain challenging drug targets. In Chapter 5 potential strategies to target SOX2 were explored, with a focus on harnessing drugs already in development with a view to rapid clinical translation. In Chapter 6, a FACS-assisted genome wide CRISPR screen was conducted, with the most promising validated candidate being PCNA, a clear area for further research and development. However, a clear disadvantage of all the approaches explored within this thesis is that all approaches represent indirect targeting of SOX2. As SOX2 sits within a complex regulatory network, indirect targeting may result in incomplete suppression, allow potential therapeutic escape, or increased toxicity due to wider impacts on cellular processes. These indirect approaches may explain the lack of increased sensitivity of 3q amplified cell lines to therapy.

8.7 Direct targeting of SOX2: potential approaches

SOX2 could be more effectively targeted by direct approaches. Peptide or nucleic acid aptamers are one potential route for direct targeting of SOX2. Nucleic acid aptamers are short sequences of DNA or RNA that bind a target molecule (237). Likewise, peptide aptamers are peptides that bind a target molecule (237). Peptide aptamers that target SOX2 and the SOX2/CDP complex have been identified through library screening (238, 239). Targeting SOX2 or SOX2/CDP using peptide aptamers reduces proliferation, migration and invasion of 3q amplified oesophageal squamous cells in vitro, and suppresses xenograft growth and metastasis (238, 239). One potential concern with targeting SOX2 directly with aptamers or siRNA is that non-cancerous stem cells may be inadvertently targeted, which could cause significant toxicity. One emerging approach

is the use of nucleic acid aptamer-siRNA chimeras, which allows more precise targeting, by using aptamers that bind cell receptors to deliver siRNA selectively into cancerous cells (240). Theoretically, one approach could therefore be to combine SOX2 siRNA with an aptamer targeting a cell receptor highly expressed on squamous cell lung cancer cells (but not present on the stem cell population). An even more refined approach would be to combine SOX2 siRNA with an aptamer targeting a commonly coamplified protein encoded by a gene within the 3q amplicon. However, translation of aptamers to the clinic remains limited. The only FDA-approved aptamer is pepagatanib, an anti-VEGF aptamer used in age-related macular degeneration (241). Nonetheless, aptamers have entered clinical trials in cancer, with a notable example being the anti-nucleolin aptamer AS1411 which reached Phase II Trials (242).

Another potential approach is to specifically target SOX2 is Targeted Protein Degradation (TPD). Targeted Protein Degradation are therapeutic approaches that target a specific protein for degradation, generally via the ubiquitin-proteasome system (243, 244). TPD approaches include PROTAC (Proteolysis targeting Chimeras) and molecular glue degraders (243, 244). PROTACs comprise three components: the binding moiety (which binds the protein of interest), a linker, and an E3 ubiquitin ligase binding moiety (245). As a result, PROTACs promote polyubiquitination and degradation of the target protein, and therefore provide an option for targeting 'undruggable' proteins. PROTACs targeting a range of proteins including STAT3 have entered clinical trials (245), with PROTAC against the androgen receptor demonstrating clinical safety and efficacy in prostate cancer (246). Whilst no SOX2-specific PROTACs have been reported this far, this would clearly represent an alternate route to target SOX2 in 3q amplified squamous cell lung cancer.

Molecular glues are an alternate route to targeting previously 'undruggable' proteins. Molecular glues are compounds that promote colocalization of two proteins to form a ternary complex

(244). The first discovered molecular glues were cyclosporin A (CsA) and tacrolimus (FK406), which form cyclophilin-CsA-Calcineurin and FKBP12-FK406-Calcineurin complexes (244). Molecular glue degraders promote the interaction between the target protein and a ubiquitin ligase, resulting in ubiquitination of the protein of interest and its resultant degradation. Thalidomide's function as a molecular glue degrader was discovered in retrospect: thalidomide recruits the E3 ligase cereblon to various targets including the IKAROS zinc finger proteins (247). Rational discovery of molecular glues is now possible (248, 249), with a notable example being the design of a molecular glue that targets the transcription factor β-catenin for degradation (248). Therefore, molecular glue degraders represent a plausible, but unexplored, route for more direct targeting of SOX2.

Overall, whilst SOX2 currently remains a challenging drug target, it is hoped that with ongoing work and development, therapies may be developed for the future.

Appendix 1: Primer Sequencies for GECKO screen NGS

Primer	Sequence (5'-3')
Fwd-1	AATGATACGGCGACCACCGAGATCTACACTCTTTCCCTACACGACGCTCTTCCGATCTTAAGTAGAGGCTTTATATATCTTGTGGAAAGGACGAAACACC
Fwd-2	AATGATACGGCGACCACCGAGATCTACACTCTTTCCCTACACGACGCTCTTCCGATCTATCATGCTTAGCTTTATATATCTTGTGGAAAGGACGAAACACC
Fwd-3	AATGATACGGCGACCACCGAGATCTACACTCTTTCCCTACACGACGCTCTTCCGATCTGATGCACATCTGCTTTATATATCTTGTGGAAAGGACGAAACACC
Fwd-4	AATGATACGGCGACCACCGAGATCTACACTCTTTCCCTACACGACGCTCTTCCGATCTCGATTGCTCGACGCTTTATATATCTTGTGGAAAGGACGAAACACC
Fwd-5	AATGATACGGCGACCACCGAGATCTACACTCTTTCCCTACACGACGCTCTTCCGATCTTCGATAGCAATTCGCTTTATATATCTTGTGGAAAGGACGAAACACC
Fwd-6	AATGATACGGCGACCACCGAGATCTACACTCTTTCCCTACACGACGCTCTTCCGATCTATCGATAGTTGCTTGCTTTATATATCTTGTGGAAAGGACGAAACACC
Fwd-7	AATGATACGGCGACCACCGAGATCTACACTCTTTCCCTACACGACGCTCTTCCGATCTGATCGATCCAGTTAGGCTTTATATATCTTGTGGAAAGGACGAAACACC
Fwd-8	AATGATACGGCGACCACCGAGATCTACACTCTTTCCCTACACGACGCTCTTCCGATCTCGATCGATTTGAGCCTGCTTTATATATCTTGTGGAAAGGACGAAACACC
Fwd-9	AATGATACGGCGACCACCGAGATCTACACTCTTTCCCTACACGACGCTCTTCCGATCTACGATCGATACACGATCGCTTTATATATCTTGTGGAAAGGACGAAACACC
Fwd-10	AATGATACGGCGACCACCGAGATCTACACTCTTTCCCTACACGACGCTCTTCCGATCTTACGATCGATGGTCCAGAGCTTTATATATCTTGTGGAAAGGACGAAACACC

Supplementary Table 1: Forward Primer Sequences used for NGS in CRISPR Screen. Adapted from (199)

Primer	Sequence (5'-3')
Rev-1	CAAGCAGAAGACGGCATACGAGATTCGCCTTGGTGACTGGAGTTCAGACGTGTGCTCTTCCGATCTCCGACTCGGTGCCACTTTTTCAA
Rev-4	CAAGCAGAAGACGGCATACGAGATATTCTAGGGTGACTGGAGTTCAGACGTGTGCTCTTCCGATCTCCGACTCGGTGCCACTTTTTCAA
Rev-5	CAAGCAGAAGACGGCATACGAGATCGTTACCAGTGACTGGAGTTCAGACGTGTGCTCTTCCGATCTCCGACTCGGTGCCACTTTTTCAA

Supplementary Table 2: Reverse Primer Sequences used for NGS in CRISPR Screen. Barcode is highlighted in red. Unsorted cells were barcoded with Rev-1, $SOX2^{LOW}$ were barcoded with Rev-4, $SOX2^{HIGH}$ were barcoded with Rev-5. Adapted from (199)

Appendix 2: Search Strategy for Chapter 6

Literatures search performed using Pubmed (Medline)
Search performed by single reviewer (Robbins), with intent of narrative review
Not performed as formal systematic review

Initial search performed in April 2021, with repeat searches until August 2023

(SOX2) AND (cancer* OR neoplasm* OR tumo?r* OR oncolog* OR malignan* OR carcinoma*) AND (drug* OR target* OR regulat* OR therapy OR therapeutic)

Abstracts were screened, with references of relevant papers and literature reviews also searched to identify additional candidates

Drugs or drug classes in active development were prioritised

Targeting strategies with current limited therapeutic tractability (e.g. PROTACs, miRNA and lncRNA) were deprioritised

References

1. Novello S, Barlesi F, Califano R, Cufer T, Ekman S, Levra MG, et al. *Metastatic non-small-cell lung cancer: ESMO Clinical Practice Guidelines for diagnosis, treatment and follow-up.* Annals of Oncology. 2016;**27**:v1-v27.

2. Wooten DJ, Meyer CT, Lubbock AL, Quaranta V, Lopez CF. *MuSyC is a consensus framework that unifies multi-drug synergy metrics for combinatorial drug discovery.* Nature communications. 2021;**12**(1):4607.

3. Meyer CT, Wooten DJ, Paudel BB, Bauer J, Hardeman KN, Westover D, et al. *Quantifying drug combination synergy along potency and efficacy axes.* Cell systems. 2019;**8**(2):97-108. e16.

4. Middleton G, Fletcher P, Popat S, Savage J, Summers Y, Greystoke A, et al. *The National Lung Matrix Trial of personalized therapy in lung cancer.* Nature. 2020;**583**(7818):807-12.

5. Akhtar N, Bansal JG. Risk factors of Lung Cancer in nonsmoker. *Current problems in cancer.* 2017;**41**(5):328-39.

6. Travis WD, Brambilla E, Nicholson AG, Yatabe Y, Austin JH, Beasley MB, et al. *The 2015 World Health Organization classification of lung tumors: impact of genetic, clinical and radiologic advances since the 2004 classification*. Journal of thoracic oncology. 2015;**10**(9):1243-60.

7. Cruz CSD, Tanoue LT, Matthay RA. *Lung cancer: epidemiology, etiology, and prevention. Clinics in chest medicine.* 2011;**32**(4):605-44.

8. Hasse CE. Cancerous tumors in the respiratory organ. In: Swaine WE, editor. *An Anatomical Descriptrion of the Diseases of the Organs of the Circulation and Respiration.* England, London: Sydeham Society; 1984. p. 370.

9. de Groot PM, Wu CC, Carter BW, Munden RF. *The epidemiology of lung cancer.* Transl Lung Cancer Res. 2018;**7**(3):220-33.

10. Adler I. *Primary malignant growths of the lungs and bronchi: A pathological and clinical study.* New York, NH: Longmans, Green & Company; 1912.

11. Cancer Research UK. Available from: https://www.cancerresearchuk.org/health-professional/cancer-statistics/. Accessed May 2021

12. Ferlay J, Colombet M, Soerjomataram I, Dyba T, Randi G, Bettio M, et al. *Cancer incidence and mortality patterns in Europe: Estimates for 40 countries and 25 major cancers in 2018.* European journal of cancer. 2018;**103**:356-87.

13. Islami F, Ward EM, Sung H, Cronin KA, Tangka FK, Sherman RL, et al. *Annual report to the nation on the status of cancer, part 1: national cancer statistics.* JNCI: Journal of the National Cancer Institute. 2021;**113**(12):1648-69.

14. Cronin KA, Scott S, Firth AU, Sung H, Henley SJ, Sherman RL, et al. *Annual report to the nation on the status of cancer, part 1: National cancer statistics.* Cancer. 2022;**128**(24):4251-84.

15. Cancer Research UK. Available from: https://www.cancerresearchuk.org/health-professional/cancer-statistics/statistics-by-cancer-type/lung-cancer. Accessed June 2023

16. Islami F, Torre LA, Jemal A. *Global trends of lung cancer mortality and smoking prevalence.* Translational lung cancer research. 2015;**4**(4):327.

17. Pelosof L, Ahn C, Gao A, Horn L, Madrigales A, Cox J, et al. *Proportion of never-smoker non–small cell lung cancer patients at three diverse institutions*. JNCI: Journal of the National Cancer Institute. 2017;**109**(7):djw295.

18. Sun S, Schiller JH, Gazdar AF. *Lung cancer in never smokers—a different disease*. Nature Reviews Cancer. 2007;**7**(10):778-90.

19. Raaschou-Nielsen O, Andersen ZJ, Beelen R, Samoli E, Stafoggia M, Weinmayr G, et al. *Air pollution and lung cancer incidence in 17 European cohorts: prospective analyses from the European Study of Cohorts for Air Pollution Effects (ESCAPE).* The lancet oncology. 2013;**14**(9):813-22.

20. Pope Iii CA, Burnett RT, Thun MJ, Calle EE, Krewski D, Ito K, et al. *Lung cancer, cardiopulmonary mortality, and long-term exposure to fine particulate air pollution.* Jama. 2002;**287**(9):1132-41.

21. Hill W, Lim EL, Weeden CE, Lee C, Augustine M, Chen K, et al. *Lung adenocarcinoma promotion by air pollutants.* Nature. 2023;**616**(7955):159-67.

22. Öberg M, Jaakkola MS, Woodward A, Peruga A, Prüss-Ustün A. *Worldwide burden of disease from exposure to second-hand smoke: a retrospective analysis of data from 192 countries.* The lancet. 2011;**377**(9760):139-46.

23. Besaratinia A, Pfeifer GP. *Second-hand smoke and human lung cancer.* Lancet Oncol. 2008;**9**(7):657-66.

24. Asomaning K, Miller DP, Liu G, Wain JC, Lynch TJ, Su L, et al. *Second hand smoke, age of exposure and lung cancer risk.* Lung cancer. 2008;**61**(1):13-20.

25. Brennan P, Buffler PA, Reynolds P, Wu AH, Wichmann HE, Agudo A, et al. *Secondhand smoke exposure in adulthood and risk of lung cancer among never smokers: a pooled analysis of two large studies.* International journal of cancer. 2004;**109**(1):125-31.

26. Lorigan P, Radford J, Howell A, Thatcher N. *Lung cancer after treatment for Hodgkin's lymphoma: a systematic review.* Lancet Oncol. 2005;**6**(10):773-9.

27. Huang Y-J, Huang T-W, Lin F-H, Chung C-H, Tsao C-H, Chien W-C. *Radiation therapy for invasive breast cancer increases the risk of second primary lung cancer: a nationwide population-based cohort analysis.* Journal of Thoracic Oncology. 2017;**12**(5):782-90.

28. Hong S, Mok Y, Jeon C, Jee SH, Samet JM. *Tuberculosis, smoking and risk for lung cancer incidence and mortality.* International journal of cancer. 2016;**139**(11):2447-55.

29. Engels EA, Shen M, Chapman RS, Pfeiffer RM, Yu YY, He X, et al. *Tuberculosis and subsequent risk of lung cancer in Xuanwei, China.* International journal of cancer. 2009;**124**(5):1183-7.

30. Wu AH, Fontham ET, Reynolds P, Greenberg RS, Buffler P, Liff J, et al. *Previous lung disease and risk of lung cancer among lifetime nonsmoking women in the United States*. American journal of epidemiology. 1995;**141**(11):1023-32.

31. Kirk GD, Merlo C, O'Driscoll P, Mehta SH, Galai N, Vlahov D, et al. *HIV infection is associated with an increased risk for lung cancer, independent of smoking*. Clinical Infectious Diseases. 2007;**45**(1):103-10.

32. Engels EA, Brock MV, Chen J, Hooker CM, Gillison M, Moore RD. *Elevated incidence of lung cancer among HIV-infected individuals*. Journal of Clinical Oncology. 2006;**24**(9):1383-8.

33. Sigel K, Makinson A, Thaler J. *Lung cancer in persons with HIV. Current Opinion in HIV and AIDS*. 2017;**12**(1):31.

34. Tsyganov M, Pevzner A, Ibragimova M, Deryusheva I, Litviakov N. *Human papillomavirus and lung cancer: an overview and a meta-analysis.* Journal of cancer research and clinical oncology. 2019;**145**(8):1919-37.

35. Jett J, Stone E, Warren G, Cummings KM. *Cannabis use, lung cancer, and related issues.* Journal of Thoracic Oncology. 2018;**13**(4):480-7.

36. Aldington S, Harwood M, Cox B, Weatherall M, Beckert L, Hansell A, et al. *Cannabis use and risk of lung cancer: a case–control study.* European Respiratory Journal. 2008;**31**(2):280-6.

37. Mehra R, Moore BA, Crothers K, Tetrault J, Fiellin DA. *The association between marijuana smoking and lung cancer: a systematic review.* Archives of internal medicine. 2006;**166**(13):1359-67.

38. Wu T-C, Tashkin DP, Djahed B, Rose JE. *Pulmonary hazards of smoking marijuana as compared with tobacco.* New England Journal of Medicine. 1988;**318**(6):347-51.

39. Hinz B, Ramer R. *Cannabinoids as anticancer drugs: Current status of preclinical research.* British Journal of Cancer. 2022;**127**(1):1-13.

40. Lifestyles Team, NHS Digital. *Smoking, Drinking and Drug Use among Young People in England, 2021.* In: NHS Digitam, part of the Government Statistical Service. 2022.

41. Bracken-Clarke D, Kapoor D, Baird AM, Buchanan PJ, Gately K, Cuffe S, et al. *Vaping and lung cancer–A review of current data and recommendations.* Lung Cancer. 2021;**153**:11-20.

42. Tang M-S, Wu X-R, Lee H-W, Xia Y, Deng F-M, Moreira AL, et al. *Electronic-cigarette smoke induces lung adenocarcinoma and bladder urothelial hyperplasia in mice.* Proceedings of the National Academy of Sciences. 2019;**116**(43):21727-31.

43. Tellez CS, Grimes MJ, Juri DE, Do K, Willink R, Dye WW, et al. *Flavored E-cigarette product aerosols induce transformation of human bronchial epithelial cells*. Lung Cancer. 2023;**179**:107180.

44. Schaal CM, Bora-Singhal N, Kumar DM, Chellappan SP. *Regulation of Sox2 and stemness by nicotine and electronic-cigarettes in non-small cell lung cancer.* Molecular cancer. 2018;**17**:1-16.

45. Tokuhata GK, Lilienfeld A. *Familial aggregation of lung cancer in humans.* Journal of the National Cancer Institute. 1963;**30**(2):289-312.

46. Jonsson S, Thorsteinsdottir U, Gudbjartsson DF, Jonsson HH, Kristjansson K, Arnason S, et al. *Familial risk of lung carcinoma in the Icelandic population.* Jama. 2004;**292**(24):2977-83.

47. Rachtan J, Sokołowski A, Niepsuj S, Zemła B, Zwierko M. *Familial lung cancer risk among women in Poland.* Lung cancer. 2009;**65**(2):138-43.

48. Sellers TA, Chen PL, Potter JD, Bailey-Wilson JE, Rothschild H, Elston RC. *Segregation analysis of smoking-associated malignancies: Evidence for mendelian inheritance.* American journal of medical genetics. 1994;**52**(3):308-14.

49. Matakidou A, Eisen T, Houlston R. *Systematic review of the relationship between family history and lung cancer risk.* British journal of cancer. 2005;**93**(7):825-33.

50. Bermejo JL, Hemminki K. *Familial lung cancer and aggregation of smoking habits: a simulation of the effect of shared environmental factors on the familial risk of cancer.* Cancer Epidemiology and Prevention Biomarkers. 2005;**14**(7):1738-40.

51. Schwartz AG, Ruckdeschel JC. *Familial lung cancer: genetic susceptibility and relationship to chronic obstructive pulmonary disease*. Am J Respir Crit Care Med. 2006;**173**(1):16-22.

52. Kanwal M, Ding XJ, Cao Y. *Familial risk for lung cancer.* Oncology letters. 2017;**13**(2):535-42.

53. Ji X, Bossé Y, Landi MT, Gui J, Xiao X, Qian D, et al. *Identification of susceptibility pathways for the role of chromosome 15q25. 1 in modifying lung cancer risk*. Nature Communications. 2018;**9**(1):3221.

54. Bossé Y, Amos CI. *A decade of GWAS results in lung cancer.* Cancer Epidemiology and Prevention Biomarkers. 2018;**27**(4):363-79.

55. Gabrielsen ME, Romundstad P, Langhammer A, Krokan HE, Skorpen F. *Association between a 15q25 gene variant, nicotine-related habits, lung cancer and COPD among 56 307 individuals from the HUNT study in Norway.* European Journal of Human Genetics. 2013;**21**(11):1293-9.

56. Cheng Y, Wang C, Zhu M, Dai J, Wang Y, Geng L, et al. *Targeted sequencing of chromosome 15q25 identified novel variants associated with risk of lung cancer and smoking behavior in Chinese.* Carcinogenesis. 2017;**38**(5):552-8.

57. Saccone NL, Culverhouse RC, Schwantes-An T-H, Cannon DS, Chen X, Cichon S, et al. *Multiple independent loci at chromosome 15q25. 1 affect smoking quantity: a meta-analysis and comparison with lung cancer and COPD.* PLoS genetics. 2010;**6**(8):e1001053.

58. Timofeeva MN, Hung RJ, Rafnar T, Christiani DC, Field JK, Bickeböller H, et al. *Influence of common genetic variation on lung cancer risk: meta-analysis of 14 900 cases and 29 485 controls.* Human molecular genetics. 2012;**21**(22):4980-95.

59. Truong T, Hung RJ, Amos CI, Wu X, Bickeböller H, Rosenberger A, et al. *Replication of lung cancer susceptibility loci at chromosomes 15q25, 5p15, and 6p21: a pooled analysis from the International Lung Cancer Consortium.* Journal of the National Cancer Institute. 2010;**102**(13):959-71.

60. Hung RJ, McKay JD, Gaborieau V, Boffetta P, Hashibe M, Zaridze D, et al. *A susceptibility locus for lung cancer maps to nicotinic acetylcholine receptor subunit genes on 15q25.* Nature. 2008;**452**(7187):633-7.

61. Dong J, Cheng Y, Zhu M, Wen Y, Wang C, Wang Y, et al. *Fine mapping of chromosome 5p15. 33 identifies novel lung cancer susceptibility loci in Han Chinese.* International journal of cancer. 2017;**141**(3):447-56.

62. McKay JD, Hung RJ, Gaborieau V, Boffetta P, Chabrier A, Byrnes G, et al. *Lung cancer susceptibility locus at 5p15.33.* Nature genetics. 2008;**40**(12):1404-6.

63. Pande M, Spitz MR, Wu X, Gorlov IP, Chen WV, Amos CI. *Novel genetic variants in the chromosome 5p15. 33 region associate with lung cancer risk.* Carcinogenesis. 2011;**32**(10):1493-9.

64. Wang Y, Broderick P, Webb E, Wu X, Vijayakrishnan J, Matakidou A, et al. *Common 5p15. 33 and 6p21. 33 variants influence lung cancer risk*. Nature genetics. 2008;**40**(12):1407-9.

65. McKay JD, Hung RJ, Han Y, Zong X, Carreras-Torres R, Christiani DC, et al. *Large-scale association analysis identifies new lung cancer susceptibility loci and heterogeneity in genetic susceptibility across histological subtypes.* Nature genetics. 2017;**49**(7):1126-32.

66. Li W-Q, Pfeiffer RM, Hyland PL, Shi J, Gu F, Wang Z, et al. *Genetic polymorphisms in the 9p21 region associated with risk of multiple cancers.* Carcinogenesis. 2014;**35**(12):2698-705.

67. Wang Y, McKay JD, Rafnar T, Wang Z, Timofeeva MN, Broderick P, et al. *Rare variants of large effect in BRCA2 and CHEK2 affect risk of lung cancer.* Nature genetics. 2014;**46**(7):736-41.

68. Hu Z, Wu C, Shi Y, Guo H, Zhao X, Yin Z, et al. *A genome-wide association study identifies two new lung cancer susceptibility loci at 13q12. 12 and 22q12. 2 in Han Chinese.* Nature genetics. 2011;**43**(8):792-6.

69. Liu M, Niu X, Liu H, Chen J. *Germline EGFR mutations in lung cancer.* Oncology Letters. 2023;**26**(1):1-11.

70. Hearle N, Schumacher V, Menko FH, Olschwang S, Boardman LA, Gille JJ, et al. *Frequency and spectrum of cancers in the Peutz-Jeghers syndrome*. Clinical Cancer Research. 2006;**12**(10):3209-15.

71. McBride KA, Ballinger ML, Killick E, Kirk J, Tattersall MH, Eeles RA, et al. *Li-Fraumeni syndrome: cancer risk assessment and clinical management.* Nature reviews Clinical oncology. 2014;**11**(5):260-71.

72. Kerrigan K, Chan J, Vagher J, Kohlmann W, Naumer A, Anson J, et al. *Lung cancer in Li-Fraumeni syndrome.* JCO Precision Oncology. 2021;**5**:552-6.

73. Non-small Cell Lung Cancer Collaborative Group. *Chemotherapy in non-small cell lung cancer: a meta-analysis using updated data on individual patients from 52 randomised clinical trials.* Bmj. 1995;**311**(7010):899-909.

74. Bagchi S, Yuan R, Engleman EG. *Immune checkpoint inhibitors for the treatment of cancer: clinical impact and mechanisms of response and resistance.* Annual Review of Pathology: Mechanisms of Disease. 2021;**16**:223-49.

75. Huo J-L, Wang Y-T, Fu W-J, Lu N, Liu Z-S. *The promising immune checkpoint LAG-3 in cancer immunotherapy: from basic research to clinical application.* Frontiers in Immunology. 2022;**13**:956090.

76. Cha J-H, Chan L-C, Li C-W, Hsu JL, Hung M-C. Mechanisms controlling PD-L1 expression in cancer. Molecular cell. 2019;**76**(3):359-70.

77. Zhong X, Tumang JR, Gao W, Bai C, Rothstein TL. *PD-L2 expression extends beyond dendritic cells/macrophages to B1 cells enriched for VH11/VH12 and phosphatidylcholine binding.* European journal of immunology. 2007;**37**(9):2405-10.

78. Dowell AC, Munford H, Goel A, Gordon NS, James ND, Cheng K, et al. PD-L2 is constitutively expressed in normal and malignant urothelium. Frontiers in Oncology. 2021;**11**:626748.

79. Takamochi K, Hara K, Hayashi T, Kohsaka S, Takahashi F, Suehara Y, et al. *Clinical relevance of PD-L2 expression in surgically resected lung adenocarcinoma.* Lung Cancer. 2022;**168**:50-8.

80. Matsubara T, Takada K, Azuma K, Takamori S, Toyokawa G, Haro A, et al. *A clinicopathological and prognostic analysis of PD-L2 expression in surgically resected primary lung squamous cell carcinoma*. Annals of surgical oncology. 2019;**26**:1925-33.

81. da Cunha Santos G, Shepherd FA, Tsao MS. EGFR mutations and lung cancer. Annual Review of Pathology: Mechanisms of Disease. 2011;**6**:49-69.

82. Shepherd FA, Rodrigues Pereira J, Ciuleanu T, Tan EH, Hirsh V, Thongprasert S, et al. *Erlotinib in previously treated non–small-cell lung cancer*. New England Journal of Medicine. 2005;**353**(2):123-32.

83. Kris MG, Natale RB, Herbst RS, Lynch Jr TJ, Prager D, Belani CP, et al. *Efficacy of gefitinib, an inhibitor of the epidermal growth factor receptor tyrosine kinase, in symptomatic patients with non–small cell lung cancer: a randomized trial.* Jama. 2003;**290**(16):2149-58.

84. Fukuoka M, Yano S, Giaccone G, Tamura T, Nakagawa K, Douillard J-Y, et al. *Multi-institutional randomized phase II trial of gefitinib for previously treated patients with advanced non–small-cell lung cancer.* Journal of clinical oncology. 2003;**21**(12):2237-46.

85. Lynch TJ, Bell DW, Sordella R, Gurubhagavatula S, Okimoto RA, Brannigan BW, et al. *Activating mutations in the epidermal growth factor receptor underlying responsiveness of non–small-cell lung cancer to gefitinib.* New England Journal of Medicine. 2004;**350**(21):2129-39.

86. Paez JG, Jänne PA, Lee JC, Tracy S, Greulich H, Gabriel S, et al. *EGFR mutations in lung cancer: correlation with clinical response to gefitinib therapy*. Science. 2004;**304**(5676):1497-500.

87. Weinstein IB, Joe A. *Oncogene addiction.* Cancer research. 2008;**68**(9):3077-80.

88. Yun C-H, Mengwasser KE, Toms AV, Woo MS, Greulich H, Wong K-K, et al. *The T790M mutation in EGFR kinase causes drug resistance by increasing the affinity for ATP.* Proceedings of the National Academy of Sciences. 2008;**105**(6):2070-5.

89. Goss G, Tsai C-M, Shepherd FA, Bazhenova L, Lee JS, Chang G-C, et al. *Osimertinib for pretreated EGFR Thr790Met-positive advanced non-small-cell lung cancer (AURA2): a multicentre, open-label, single-arm, phase 2 study.* The lancet oncology. 2016;**17**(12):1643-52.

90. Cross DA, Ashton SE, Ghiorghiu S, Eberlein C, Nebhan CA, Spitzler PJ, et al. *AZD9291, an irreversible EGFR TKI, overcomes T790M-mediated resistance to EGFR inhibitors in lung cancer.* Cancer discovery. 2014;4(9):1046-61.

91. Lababede O, Meziane MA. *The Eighth Edition of TNM Staging of Lung Cancer: Reference Chart and Diagrams.* Oncologist. 2018 Jul;**23**(7):844-848

92. Oudkerk M, Devaraj A, Vliegenthart R, Henzler T, Prosch H, Heussel CP, et al. *European position statement on lung cancer screening.* The Lancet Oncology. 2017;**18**(12):e754-e66.

93. de Koning HJ, van der Aalst CM, de Jong PA, Scholten ET, Nackaerts K, Heuvelmans MA, et al. *Reduced lung-cancer mortality with volume CT screening in a randomized trial.* New England journal of medicine. 2020;**382**(6):503-13.

94. Kramer BS, Berg CD, Aberle DR, Prorok PC. *Lung cancer screening with low-dose helical CT: results from the National Lung Screening Trial (NLST).* Journal fo medical Screening, 18(3), 109-11.

95. Crino L, Weder W, Van Meerbeeck J, Felip E. *Early stage and locally advanced (non-metastatic) non-small-cell lung cancer: ESMO Clinical Practice Guidelines for diagnosis, treatment and follow-up*. Annals of oncology. 2010;**21**(S 5):v103-v15.

96. Cruz C, Afonso M, Oliveiros B, Pêgo A. *Recurrence and risk factors for relapse in patients with non-small cell lung cancer treated by surgery with curative intent.* Oncology. 2017;**92**(6):347-52.

97. Winton T, Livingston R, Johnson D, Rigas J, Johnston M, Butts C, et al. *Vinorelbine plus cisplatin vs. observation in resected non–small-cell lung cancer.* New England Journal of Medicine. 2005;**352**(25):2589-97.

98. Lou F, Huang J, Sima CS, Dycoco J, Rusch V, Bach PB. *Patterns of recurrence and second primary lung cancer in early-stage lung cancer survivors followed with routine computed tomography surveillance.* The Journal of thoracic and cardiovascular surgery. 2013;**145**(1):75-82.

99. Demicheli R, Fornili M, Ambrogi F, Higgins K, Boyd JA, Biganzoli E, et al. *Recurrence dynamics for non–small-cell lung cancer: effect of surgery on the development of metastases.* Journal of Thoracic Oncology. 2012;**7**(4):723-30.

100. Wu C-F, Fu J-Y, Yeh C-J, Liu Y-H, Hsieh M-J, Wu Y-C, et al. *Recurrence risk factors analysis for stage I non-small cell lung cancer.* Medicine. 2015;**94**(32).

101. Al-Kattan K, Sepsas E, Fountain SW, Townsend ER. *Disease recurrence after resection for stage I lung cancer.* European journal of cardio-thoracic surgery. 1997;**12**(3):380-4.

102. Pignon J-P, Tribodet H, Scagliotti GV, Douillard J-Y, Shepherd FA, Stephens RJ, et al. *Lung adjuvant cisplatin evaluation: a pooled analysis by the LACE Collaborative Group.* Database of Abstracts of Reviews of Effects (DARE): Quality-assessed Reviews [Internet]: Centre for Reviews and Dissemination (UK); 2008.

103. NSCLC Meta-analyses Collaborative group. *Adjuvant chemotherapy, with or without postoperative radiotherapy, in operable non-small-cell lung cancer: two meta-analyses of individual patient data.* The Lancet. 2010;**375**(9722):1267-77.

104. Cortés ÁA, Urquizu LC, Cubero JH. *Adjuvant chemotherapy in non-small cell lung cancer: state-of-the-art.* Translational lung cancer research. 2015;**4**(2):191.

105. The International Adjuvant Lung Cancer Trial Collaborative Group. *Cisplatin-based adjuvant chemotherapy in patients with completely resected non–small-cell lung cancer.* New England Journal of Medicine. 2004;**350**(4):351-60.

106. Douillard J, Rosell R, Delena M, Legroumellec A, Torres A, Carpagano F. *Adjuvant Navelbine International Trialist Association (ANITA). Phase III adjuvant vinorelbine and cisplatin versus observation in completely resected non-small–cell lung cancer patients: final results after 70-month median follow-up*. J Clin Oncol. 2005;**23**:A7013.

107. Felip E, Altorki N, Zhou C, Csőszi T, Vynnychenko I, Goloborodko O, et al. *Adjuvant atezolizumab after adjuvant chemotherapy in resected stage IB–IIIA non-small-cell lung cancer (IMpower010): A randomised, multicentre, open-label, phase 3 trial.* The Lancet. 2021;**398**(10308):1344-57.

108. O'Brien M, Paz-Ares L, Marreaud S, Dafni U, Oselin K, Havel L, et al. *Pembrolizumab versus placebo as adjuvant therapy for completely resected stage IB–IIIA non-small-cell lung cancer (PEARLS/KEYNOTE-091): an interim analysis of a randomised, triple-blind, phase 3 trial.* The Lancet Oncology. 2022;**23**(10):1274-86.

109. NSCLC Meta-analysis Collaborative Group. *Preoperative chemotherapy for non-small-cell lung cancer: a systematic review and meta-analysis of individual participant data.* The Lancet. 2014;**383**(9928):1561-71.

110. Subramanian MP, Puri V. *Neoadjuvant vs. adjuvant chemotherapy in locally advanced non-small cell lung cancer—is timing everything?* Journal of thoracic disease. 2019;**11**(12):5674.

111. Felip E, Rosell R, Maestre JA, Rodríguez-Paniagua JM, Morán T, Astudillo J, et al. *Preoperative chemotherapy plus surgery versus surgery plus adjuvant chemotherapy versus surgery alone in early-stage non–small-cell lung cancer.* Journal of clinical oncology. 2010;**28**(19):3138-45.

112. Brandt WS, Yan W, Zhou J, Tan KS, Montecalvo J, Park BJ, et al. *Outcomes after neoadjuvant or adjuvant chemotherapy for cT2-4N0-1 non–small cell lung cancer: a propensity-matched analysis.* The Journal of thoracic and cardiovascular surgery. 2019;**157**(2):743-53. e3.

113. Forde PM, Spicer J, Lu S, Provencio M, Mitsudomi T, Awad MM, et al. *Neoadjuvant nivolumab plus chemotherapy in resectable lung cancer.* New England Journal of Medicine. 2022;**386**(21):1973-85.

114. Wu Y-L, Tsuboi M, He J, John T, Grohe C, Majem M, et al. *Osimertinib in resected EGFR-mutated non–small-cell lung cancer.* New England Journal of Medicine. 2020;**383**(18):1711-23.

115. Zhong D, Liu X, Khuri FR, Sun S-Y, Vertino PM, Zhou W. *LKB1 is necessary for Akt-mediated phosphorylation of proapoptotic proteins.* Cancer research. 2008;**68**(18):7270-7.

116. Yue D, Xu S, Wang Q, Li X, Shen Y, Zhao H, et al. *Erlotinib versus vinorelbine plus cisplatin as adjuvant therapy in Chinese patients with stage IIIA EGFR mutation-positive non-small-cell lung cancer (EVAN): a randomised, open-label, phase 2 trial.* The Lancet Respiratory Medicine. 2018;**6**(11):863-73.

117. Pennell NA, Neal JW, Chaft JE, Azzoli CG, Jänne PA, Govindan R, et al. *SELECT: a phase II trial of adjuvant erlotinib in patients with resected epidermal growth factor receptor–mutant non–small-cell lung cancer.* Journal of Clinical Oncology. 2019;**37**(2):97.

118. Tsuboi M, Herbst RS, John T, Kato T, Majem M, Grohé C, et al. *Overall Survival with Osimertinib in Resected EGFR-Mutated NSCLC.* New England Journal of Medicine. 2023;**389**(2):137-147

119. Liu S-Y, Bao H, Wang Q, Mao W-M, Chen Y, Tong X, et al. *Genomic signatures define three subtypes of EGFR-mutant stage II–III non-small-cell lung cancer with distinct adjuvant therapy outcomes.* Nature communications. 2021;**12**(1):1-11.

120. Siegel RL, Miller KD, Wagle NS, Jemal A. *Cancer statistics*, 2023. Ca Cancer J Clin. 2023;**73**(1):17-48.

121. Hendriks L, Kerr K, Menis J, Mok T, Nestle U, Passaro A, et al. *Oncogene-addicted metastatic non-small-cell lung cancer: ESMO Clinical Practice Guideline for diagnosis, treatment and follow-up.* Annals of Oncology. 2023;**34**(4):339-57.

122. Wang M, Herbst RS, Boshoff C. *Toward personalized treatment approaches for non-small-cell lung cancer.* Nature medicine. 2021;**27**(8):1345-56.

123. Yu X, Ji X, Su C. *HER2-altered non-small cell lung cancer: biology, clinicopathologic features, and emerging therapies*. Frontiers in Oncology. 2022;**12**:860313.

124. Goto K, Goto Y, Kubo T, Ninomiya K, Kim S-W, Planchard D, et al. *Trastuzumab Deruxtecan in Patients With HER2-Mutant Metastatic Non-Small-Cell Lung Cancer: Primary Results From the Randomized, Phase II DESTINY-Lung02 Trial.* Journal of Clinical Oncology. 2023;**41**(31):4852-4863.

125. Ostrem JM, Peters U, Sos ML, Wells JA, Shokat KM. *K-Ras (G12C) inhibitors allosterically control GTP affinity and effector interactions.* Nature. 2013;**503**(7477):548-51.

126. de Langen AJ, Johnson ML, Mazieres J, Dingemans A-MC, Mountzios G, Pless M, et al. *Sotorasib versus docetaxel for previously treated non-small-cell lung cancer with KRASG12C mutation: a randomised, open-label, phase 3 trial.* The Lancet. 2023;**401**(10378):733-46.

127. Jänne PA, Riely GJ, Gadgeel SM, Heist RS, Ou S-HI, Pacheco JM, et al. *Adagrasib in non–small-cell lung cancer harboring a KRASG12C mutation.* New England Journal of Medicine. 2022;**387**(2):120-31.

128. Hofmann MH, Gerlach D, Misale S, Petronczki M, Kraut N. *Expanding the reach of precision oncology by drugging all KRAS mutants*. Cancer Discovery. 2022;**12**(4):924-37.

129. Zhou C, Li W, Song Z, Zhang Y, Huang D, Yang Z, et al. LBA33 *A first-in-human phase I study of a novel KRAS G12D inhibitor HRS-4642 in patients with advanced solid tumors harboring KRAS G12D mutation.* Annals of Oncology. 2023;**34**:S1273.

130. Arbour KP, S; Garrido-Laguna, I; Hong, DS; Woldpin B; Pelster MS; Barve M; Starodub, A; Sommerhalder, D; Chang, S; Zhang, Y; Salman Z; Wang, X; Gustafson, C; Spira, AI. *652O - Preliminary clinical activity of RMC-6236, a first-in-class, RAS-selective, tri-complex RAS-MULTI(ON) inhibitor in patients with KRAS mutant pancreatic ductal adenocarcinoma (PDAC) and non-small cell lung cancer (NSCLC).* Annals of Oncology. 2023;**34**:S458 - S97.

131. Douillard J, Ostoros G, Cobo M, Ciuleanu T, McCormack R, Webster A, et al. *First-line gefitinib in Caucasian EGFR mutation-positive NSCLC patients: a phase-IV, open-label, single-arm study.* British journal of cancer. 2014;**110**(1):55-62.

132. Mok TS, Wu Y-L, Thongprasert S, Yang C-H, Chu D-T, Saijo N, et al. *Gefitinib or carboplatin–paclitaxel in pulmonary adenocarcinoma.* New England Journal of Medicine. 2009;**361**(10):947-57.

133. Fukuoka M, Wu Y-L, Thongprasert S, Sunpaweravong P, Leong S-S, Sriuranpong V, et al. *Biomarker analyses and final overall survival results from a phase III, randomized, open-label, first-line study of gefitinib versus carboplatin/paclitaxel in clinically selected patients with advanced non–small-cell lung cancer in Asia (IPASS).* Journal of clinical oncology. 2011;**29**(21):2866-74.

134. Han J-Y, Park K, Kim S-W, Lee DH, Kim HY, Kim HT, et al. *First-SIGNAL: first-line single-agent iressa versus gemcitabine and cisplatin trial in never-smokers with adenocarcinoma of the lung.* Journal of clinical oncology. 2012;**30**(10):1122-8.

135. Yoshioka H, Shimokawa M, Seto T, Morita S, Yatabe Y, Okamoto I, et al. *Final overall survival results of WJTOG3405, a randomized phase III trial comparing gefitinib versus cisplatin with docetaxel as the first-line treatment for patients with stage IIIB/IV or postoperative recurrent EGFR mutation-positive non-small-cell lung cancer.* Annals of Oncology. 2019;**30**(12):1978-84.

136. Mitsudomi T, Morita S, Yatabe Y, Negoro S, Okamoto I, Tsurutani J, et al. *Gefitinib versus cisplatin plus docetaxel in patients with non-small-cell lung cancer harbouring mutations of the epidermal growth factor receptor (WJTOG3405): an open label, randomised phase 3 trial.* The lancet oncology. 2010;**11**(2):121-8.

137. Maemondo M, Inoue A, Kobayashi K, Sugawara S, Oizumi S, Isobe H, et al. *Gefitinib or chemotherapy for non–small-cell lung cancer with mutated EGFR.* New England Journal of Medicine. 2010;**362**(25):2380-8.

138. Rosell R, Carcereny E, Gervais R, Vergnenegre A, Massuti B, Felip E, et al. *Erlotinib versus standard chemotherapy as first-line treatment for European patients with advanced EGFR mutation-positive non-small-cell lung cancer (EURTAC): a multicentre, open-label, randomised phase 3 trial.* The lancet oncology. 2012;**13**(3):239-46.

139. Zhou C, Wu Y-L, Chen G, Feng J, Liu X-Q, Wang C, et al. *Erlotinib versus chemotherapy as first-line treatment for patients with advanced EGFR mutation-positive non-small-cell lung*

cancer (OPTIMAL, CTONG-0802): a multicentre, open-label, randomised, phase 3 study. The lancet oncology. 2011;**12**(8):735-42.

140. Zhou C, Wu Y, Chen G, Feng J, Liu X-Q, Wang C, et al. *Final overall survival results from a randomised, phase III study of erlotinib versus chemotherapy as first-line treatment of EGFR mutation-positive advanced non-small-cell lung cancer (OPTIMAL, CTONG-0802).* Annals of oncology. 2015;**26**(9):1877-83.

141. Yang JC-H, Wu Y-L, Schuler M, Sebastian M, Popat S, Yamamoto N, et al. *Afatinib versus cisplatin-based chemotherapy for EGFR mutation-positive lung adenocarcinoma (LUX-Lung 3 and LUX-Lung 6): analysis of overall survival data from two randomised, phase 3 trials.* The lancet oncology. 2015;**16**(2):141-51.

142. Yang JC-H, Schuler MH, Yamamoto N, O'Byrne KJ, Hirsh V, Mok T, et al. *LUX-Lung 3: A randomized, open-label, phase III study of afatinib versus pemetrexed and cisplatin as first-line treatment for patients with advanced adenocarcinoma of the lung harboring EGFR-activating mutations.* American Society of Clinical Oncology; 2012: LBA7500

143. Sequist LV, Yang JC-H, Yamamoto N, O'Byrne K, Hirsh V, Mok T, et al. *Phase III study of afatinib or cisplatin plus pemetrexed in patients with metastatic lung adenocarcinoma with EGFR mutations.* Journal of clinical oncology. 2013;**31**(27):3327-34.

144. Wu Y-L, Zhou C, Hu C-P, Feng J, Lu S, Huang Y, et al. *Afatinib versus cisplatin plus gemcitabine for first-line treatment of Asian patients with advanced non-small-cell lung cancer harbouring EGFR mutations (LUX-Lung 6): an open-label, randomised phase 3 trial.* The lancet oncology. 2014;**15**(2):213-22.

145. Park K, Tan E-H, O'Byrne K, Zhang L, Boyer M, Mok T, et al. *Afatinib versus gefitinib as first-line treatment of patients with EGFR mutation-positive non-small-cell lung cancer (LUX-Lung 7): a phase 2B, open-label, randomised controlled trial.* The Lancet Oncology. 2016;**17**(5):577-89.

146. Paz-Ares L, Tan E-H, O'Byrne K, Zhang L, Hirsh V, Boyer M, et al. *Afatinib versus gefitinib in patients with EGFR mutation-positive advanced non-small-cell lung cancer: overall survival data from the phase IIb LUX-Lung 7 trial*. Annals of Oncology. 2017;**28**(2):270-7.

147. Mok TS, Wu Y-L, Ahn M-J, Garassino MC, Kim HR, Ramalingam SS, et al. *Osimertinib or platinum–pemetrexed in EGFR T790M–positive lung cancer.* New England Journal of Medicine. 2017;**376**(7):629-40.

148. Wu Y-L, Mok T, Han J-Y, Ahn M-J, Delmonte A, Ramalingam S, et al. *Overall survival (OS) from the AURA3 phase III study: Osimertinib vs platinum-pemetrexed (plt-pem) in patients (pts) with EGFR T790M advanced non-small cell lung cancer (NSCLC) and progression on a prior EGFR-tyrosine kinase inhibitor (TKI).* Annals of Oncology. 2019;**30**:ix158.

149. Soria J-C, Ohe Y, Vansteenkiste J, Reungwetwattana T, Chewaskulyong B, Lee KH, et al. *Osimertinib in untreated EGFR-mutated advanced non–small-cell lung cancer.* New England journal of medicine. 2018;**378**(2):113-25.

150. Ramalingam SS, Vansteenkiste J, Planchard D, Cho BC, Gray JE, Ohe Y, et al. *Overall survival with osimertinib in untreated, EGFR-mutated advanced NSCLC.* New England Journal of Medicine. 2020;**382**(1):41-50.

151. Camidge DR, Bang Y-J, Kwak EL, Iafrate AJ, Varella-Garcia M, Fox SB, et al. *Activity and safety of crizotinib in patients with ALK-positive non-small-cell lung cancer: updated results from a phase 1 study.* The lancet oncology. 2012;**13**(10):1011-9.

152. Kwak EL, Bang Y-J, Camidge DR, Shaw AT, Solomon B, Maki RG, et al. *Anaplastic lymphoma kinase inhibition in non–small-cell lung cancer.* New England Journal of Medicine. 2010;**363**(18):1693-703.

153. Blackhall F, Camidge DR, Shaw AT, Soria J-C, Solomon BJ, Mok T, et al. *Final results of the large-scale multinational trial PROFILE 1005: efficacy and safety of crizotinib in previously treated patients with advanced/metastatic ALK-positive non-small-cell lung cancer.* Esmo Open. 2017;**2**(3):e000219.

154. Shaw AT, Kim D-W, Nakagawa K, Seto T, Crinó L, Ahn M-J, et al. *Crizotinib versus chemotherapy in advanced ALK-positive lung cancer*. New England Journal of Medicine. 2013;**368**(25):2385-94.

155. Kim D-W, Mehra R, Tan DS, Felip E, Chow LQ, Camidge DR, et al. *Activity and safety of ceritinib in patients with ALK-rearranged non-small-cell lung cancer (ASCEND-1): updated results from the multicentre, open-label, phase 1 trial.* The lancet oncology. 2016;**17**(4):452-63.

156. Nishio M, Felip E, Orlov S, Park K, Yu C-J, Tsai C-M, et al. *Final overall survival and other efficacy and safety results from ASCEND-3: Phase II study of ceritinib in ALKi-naive patients with ALK-rearranged NSCLC.* Journal of Thoracic Oncology. 2020;**15**(4):609-17.

157. Felip E, Orlov S, Park K, Yu C-J, Tsai C-M, Nishio M, et al. *ASCEND-3: A single-arm, open-label, multicenter phase II study of ceritinib in ALKi-naïve adult patients (pts) with ALK-rearranged (ALK+) non-small cell lung cancer (NSCLC).* American Society of Clinical Oncology; 2015. 8060

158. Felip E, Nishio M, Orlov S, Park K, Yu C-J, Tsai C-M, et al. *Overall survival results of ceritinib in ALKi-naïve patients with ALK-rearranged NSCLC (ASCEND-3).* Annals of Oncology. 2018;**29**:viii745.

159. Soria J-C, Tan DS, Chiari R, Wu Y-L, Paz-Ares L, Wolf J, et al. *First-line ceritinib versus platinum-based chemotherapy in advanced ALK-rearranged non-small-cell lung cancer (ASCEND-4): a randomised, open-label, phase 3 study.* The Lancet. 2017;**389**(10072):917-29.

160. Barlesi F, Dingemans A-M, Yang J-H, Ou S-H, Ahn J, De Petris L, et al. *Updated efficacy and safety from the global phase II NP28673 study of alectinib in patients (pts) with previously treated ALK+ non-small-cell lung cancer (NSCLC).* Annals of Oncology. 2016;**27**:vi437.

161. Ou S-HI, Ahn JS, De Petris L, Govindan R, Yang JC-H, Hughes B, et al. *Alectinib in crizotinib-refractory ALK-rearranged non–small-cell lung cancer: a phase II global study.* Journal of clinical oncology. 2016;**34**(7):661-8.

162. Seto T, Kiura K, Nishio M, Nakagawa K, Maemondo M, Inoue A, et al. *CH5424802 (RO5424802) for patients with ALK-rearranged advanced non-small-cell lung cancer (AF-001JP study): a single-arm, open-label, phase 1–2 study.* The lancet oncology. 2013;**14**(7):590-8.

163. Tamura T, Kiura K, Seto T, Nakagawa K, Maemondo M, Inoue A, et al. *Three-year follow-up of an alectinib phase I/II study in ALK-positive non–small-cell lung cancer: AF-001JP.* Journal of Clinical Oncology. 2017;**35**(14):1515.

164. Peters S, Camidge DR, Shaw AT, Gadgeel S, Ahn JS, Kim D-W, et al. *Alectinib versus crizotinib in untreated ALK-positive non–small-cell lung cancer.* New England Journal of Medicine. 2017;**377**(9):829-38.

165. Mok T, Camidge D, Gadgeel S, Rosell R, Dziadziuszko R, Kim D-W, et al. *Updated overall survival and final progression-free survival data for patients with treatment-naive advanced*

ALK-positive non-small-cell lung cancer in the ALEX study. Annals of oncology. 2020;**31**(8):1056-64.

166. Hotta K, Hida T, Nokihara H, Morise M, Kim Y, Azuma K, et al. *Final overall survival analysis from the phase III J-ALEX study of alectinib versus crizotinib in ALK inhibitor-naïve Japanese patients with ALK-positive non-small-cell lung cancer.* ESMO open. 2022;**7**(4):100527.

167. Nakagawa K, Hida T, Nokihara H, Morise M, Azuma K, Kim YH, et al. *Final progression-free survival results from the J-ALEX study of alectinib versus crizotinib in ALK-positive non-small-cell lung cancer*. Lung Cancer. 2020;**139**:195-9.

168. Hida T, Nokihara H, Kondo M, Kim YH, Azuma K, Seto T, et al. *Alectinib versus crizotinib in patients with ALK-positive non-small-cell lung cancer (J-ALEX): an open-label, randomised phase 3 trial.* The Lancet. 2017;**390**(10089):29-39.

169. Gettinger SN, Bazhenova LA, Langer CJ, Salgia R, Gold KA, Rosell R, et al. *Activity and safety of brigatinib in ALK-rearranged non-small-cell lung cancer and other malignancies: a single-arm, open-label, phase 1/2 trial.* The lancet oncology. 2016;**17**(12):1683-96.

170. Camidge DR, Kim HR, Ahn M-J, Yang JC-H, Han J-Y, Lee J-S, et al. *Brigatinib versus crizotinib in ALK-positive non–small-cell lung cancer.* New England Journal of Medicine. 2018;**379**(21):2027-39.

171. Huber RM, Hansen KH, Rodríguez LP-A, West HL, Reckamp KL, Leighl NB, et al. *Brigatinib in crizotinib-refractory ALK+ NSCLC: 2-year follow-up on systemic and intracranial outcomes in the phase 2 ALTA trial.* Journal of Thoracic Oncology. 2020;**15**(3):404-15.

172. Kim D-W, Tiseo M, Ahn M-J, Reckamp KL, Hansen KH, Kim S-W, et al. *Brigatinib in patients with crizotinib-refractory anaplastic lymphoma kinase-positive non-small-cell lung cancer: a randomized, multicenter phase II trial.* Journal of Clinical Oncology. 2017;**35**(22):2490-8.

173. Shaw AT, Bauer TM, de Marinis F, Felip E, Goto Y, Liu G, et al. *First-line lorlatinib or crizotinib in advanced ALK-positive lung cancer.* New England Journal of Medicine. 2020;**383**(21):2018-29.

174. Solomon BJ, Bauer TM, Mok TS, Liu G, Mazieres J, de Marinis F, et al. *Efficacy and safety of first-line lorlatinib versus crizotinib in patients with advanced, ALK-positive non-small-cell lung cancer: updated analysis of data from the phase 3, randomised, open-label CROWN study.* The Lancet Respiratory Medicine. 2023;**11**(4):354-66.

175. Baldacci S, Besse B, Avrillon V, Mennecier B, Mazieres J, Dubray-Longeras P, et al. *Lorlatinib for advanced anaplastic lymphoma kinase–positive non–small cell lung cancer: Results of the IFCT-1803 LORLATU cohort.* European Journal of Cancer. 2022;**166**:51-9.

176. Shaw AT, Riely GJ, Bang Y-J, Kim D-W, Camidge DR, Solomon BJ, et al. *Crizotinib in ROS1-rearranged advanced non-small-cell lung cancer (NSCLC): updated results, including overall survival, from PROFILE 1001.* Annals of Oncology. 2019;**30**(7):1121-6.

177. Shaw AT, Ou S-HI, Bang Y-J, Camidge DR, Solomon BJ, Salgia R, et al. *Crizotinib in ROS1-rearranged non–small-cell lung cancer.* New England Journal of Medicine. 2014;**371**(21):1963-71.

178. Shen L, Qiang T, Li Z, Ding D, Yu Y, Lu S*. First-line crizotinib versus platinum-pemetrexed chemotherapy in patients with advanced ROS1-rearranged non-small-cell lung cancer.* Cancer medicine. 2020;**9**(10):3310-8.

179. Wu Y-L, Yang JC-H, Kim D-W, Lu S, Zhou J, Seto T, et al*. Phase II study of crizotinib in East Asian patients with ROS1-positive advanced non–small-cell lung cancer.* Journal of Clinical Oncology. 2018;**36**(14):1405-11.

180. Wu Y-L, Lu S, Yang JC-H, Zhou J, Seto T, Ahn M-J, et al. *Final Overall Survival, Safety, and Quality of Life Results From a Phase 2 Study of Crizotinib in East Asian Patients With ROS1-Positive Advanced NSCLC.* JTO Clinical and Research Reports. 2022;**3**(10):100406.

181. Moro-Sibilot D, Cozic N, Pérol M, Mazières J, Otto J, Souquet P, et al. *Crizotinib in c-MET- or ROS1-positive NSCLC: results of the AcSé phase II trial.* Annals of Oncology. 2019;**30**(12):1985-91.

182. 182. Landi L, Chiari R, Tiseo M, D'Incà F, Dazzi C, Chella A, et al. *Crizotinib in MET-Deregulated or ROS1-Rearranged Pretreated Non–Small Cell Lung Cancer (METROS): A Phase II, Prospective, Multicenter, Two-Arms Trial.* Clinical Cancer Research. 2019;**25**(24):7312-9.

183. Shaw AT, Solomon BJ, Chiari R, Riely GJ, Besse B, Soo RA, et al. *Lorlatinib in advanced ROS1-positive non-small-cell lung cancer: a multicentre, open-label, single-arm, phase 1–2 trial.* The Lancet Oncology. 2019;**20**(12):1691-701.

184. Paz-Ares L, Doebele R, Farago A, Liu S, Chawla S, Tosi D, et al. *Entrectinib in NTRK fusion-positive non-small cell lung cancer (NSCLC): Integrated analysis of patients (pts) enrolled in STARTRK-2, STARTRK-1 and ALKA-372-001.* Annals of Oncology. 2019;**30**:ii48-ii9.

185. Doebele RC, Drilon A, Paz-Ares L, Siena S, Shaw AT, Farago AF, et al. *Entrectinib in patients with advanced or metastatic NTRK fusion-positive solid tumours: integrated analysis of three phase 1–2 trials.* The Lancet Oncology. 2020;**21**(2):271-82.

186. Lim SM, Kim HR, Lee J-S, Lee KH, Lee Y-G, Min YJ, et al. *Open-label, multicenter, phase II study of ceritinib in patients with non–small-cell lung cancer harboring ROS1 rearrangement.* Journal of clinical oncology. 2017;**35**(23):2613-8.

187. Cho BC, Doebele RC, Lin J, Nagasaka M, Baik C, Van Der Wekken A, et al. MA11. *07 phase 1/2 TRIDENT-1 study of repotrectinib in patients with ROS1+ or NTRK+ advanced solid tumors.* Journal of Thoracic Oncology. 2021;**16**(3):S174-S5.

188. Drilon A, Camidge DR, Lin JJ, Kim S-W, Solomon BJ, Dziadziuszko R, et al. *Repotrectinib in ROS1 Fusion–Positive Non–Small-Cell Lung Cancer.* New England Journal of Medicine. 2024;**390**(2):118-31.

189. Drilon A, Oxnard GR, Tan DS, Loong HH, Johnson M, Gainor J, et al. *Efficacy of selpercatinib in RET fusion–positive non–small-cell lung cancer.* New England Journal of Medicine. 2020;**383**(9):813-24.

190. Besse B, Drilon AE, Solomon BJ, Subbiah V, Tan DS-W, Park K, et al. *Updated overall efficacy and safety of selpercatinib in patients (pts) with RET fusion+ non-small cell lung cancer (NSCLC).* Journal of Clinical Oncology. 2021;**39**(15 suppl) 9065.

191. Drilon A, Subbiah V, Gautschi O, Tomasini P, De Braud F, Solomon BJ, et al. *Selpercatinib in patients with RET fusion–positive non–small-cell lung cancer: updated safety and efficacy from the registrational LIBRETTO-001 phase I/II trial.* Journal of Clinical Oncology. 2023;**41**(2):385.

192. Gainor JF, Curigliano G, Kim D-W, Lee DH, Besse B, Baik CS, et al. *Pralsetinib for RET fusion-positive non-small-cell lung cancer (ARROW): a multi-cohort, open-label, phase 1/2 study*. The lancet oncology. 2021;**22**(7):959-69.

193. Griesinger F, Curigliano G, Thomas M, Subbiah V, Baik C, Tan DS, et al. *Safety and efficacy of pralsetinib in RET fusion–positive non-small-cell lung cancer including as first-line therapy: Update from the ARROW trial.* Annals of Oncology. 2022;**33**(11):1168-78.

194. Camidge DR, Otterson GA, Clark JW, Ou S-HI, Weiss J, Ades S, et al. *Crizotinib in patients with MET-amplified NSCLC.* Journal of Thoracic Oncology. 2021;**16**(6):1017-29.

195. Drilon A, Clark JW, Weiss J, Ou S-HI, Camidge DR, Solomon BJ, et al. *Antitumor activity of crizotinib in lung cancers harboring a MET exon 14 alteration.* Nature medicine. 2020;**26**(1):47-51.

196. Wolf J, Seto T, Han J-Y, Reguart N, Garon EB, Groen HJ, et al. *Capmatinib in MET exon 14–mutated or MET-amplified non–small-cell lung cancer.* New England Journal of Medicine. 2020;**383**(10):944-57.

197. Schuler M, Berardi R, Lim W-T, de Jonge M, Bauer T, Azaro A, et al. *Molecular correlates of response to capmatinib in advanced non-small-cell lung cancer: clinical and biomarker results from a phase I trial.* Annals of Oncology. 2020;**31**(6):789-97.

198. Dagogo-Jack I, Moonsamy P, Gainor JF, Lennerz JK, Piotrowska Z, Lin JJ, et al. *A phase 2 study of capmatinib in patients with MET-altered lung cancer previously treated with a MET inhibitor.* Journal of Thoracic Oncology. 2021;**16**(5):850-9.

199. Paik PK, Felip E, Veillon R, Sakai H, Cortot AB, Garassino MC, et al. *Tepotinib in non–small-cell lung cancer with MET exon 14 skipping mutations. New* England Journal of Medicine. 2020;**383**(10):931-43.

200. Planchard D, Kim TM, Mazieres J, Quoix E, Riely G, Barlesi F, et al. *Dabrafenib in patients with BRAFV600E-positive advanced non-small-cell lung cancer: a single-arm, multicentre, open-label, phase 2 trial.* The Lancet Oncology. 2016;**17**(5):642-50.

201. Planchard D, Besse B, Groen HJ, Souquet P-J, Quoix E, Baik CS, et al. *Dabrafenib plus trametinib in patients with previously treated BRAFV600E-mutant metastatic non-small cell lung cancer: an open-label, multicentre phase 2 trial.* The Lancet Oncology. 2016;**17**(7):984-93.

202. Planchard D, Besse B, Groen HJ, Hashemi SM, Mazieres J, Kim TM, et al. *Phase 2 study of dabrafenib plus trametinib in patients with BRAF V600E-mutant metastatic NSCLC: updated 5-year survival rates and genomic analysis.* Journal of Thoracic Oncology. 2022;**17**(1):103-15.

203. Subbiah V, Gervais R, Riely G, Hollebecque A, Blay J-Y, Felip E, et al. *Efficacy of vemurafenib in patients with non–small-cell lung cancer with BRAF V600 mutation: an open-label, single-arm cohort of the histology-independent VE-BASKET study.* JCO Precision Oncology. 2019;**3**:1-9.

204. Tomasini P, Mazieres J, Cropet C, Troussard X, Malka D, Ray-Coquard I, et al. *538P Vemurafenib in non-melanoma V600 and non-V600 BRAF mutated cancers: Results of the AcSé basket trial*. Annals of Oncology. 2020;**31**:S470-S1.

205. Mazieres J, Cropet C, Montané L, Barlesi F, Souquet P, Quantin X, et al. *Vemurafenib in non-small-cell lung cancer patients with BRAFV600 and BRAFnonV600 mutations.* Annals of Oncology. 2020;**31**(2):289-94.

206. Drilon A, Tan DS, Lassen UN, Leyvraz S, Liu Y, Patel JD, et al. *Efficacy and Safety of Larotrectinib in Patients With Tropomyosin Receptor Kinase Fusion–Positive Lung Cancers.* JCO Precision Oncology. 2022;**6**:e2100418.

207. Li BT, Smit EF, Goto Y, Nakagawa K, Udagawa H, Mazières J, et al. *Trastuzumab deruxtecan in HER2-mutant non–small-cell lung cancer.* New England Journal of Medicine. 2022;**386**(3):241-51.

208. Tsurutani J, Iwata H, Krop I, Jänne PA, Doi T, Takahashi S, et al. *Targeting HER2 with trastuzumab deruxtecan: a dose-expansion, phase I study in multiple advanced solid tumors.* Cancer discovery. 2020;**10**(5):688-701.

209. Li BT, Shen R, Buonocore D, Olah ZT, Ni A, Ginsberg MS, et al. *Ado-trastuzumab emtansine for patients with HER2-mutant lung cancers: results from a phase II basket trial.* Journal of Clinical Oncology. 2018;**36**(24):2532.

210. Li BT, Shen R, Buonocore D, Olah ZT, Ni A, Ginsberg MS, et al. *Ado-trastuzumab emtansine in patients with HER2 mutant lung cancers: Results from a phase II basket trial.* American Society of Clinical Oncology; 2017.

211. Li BT, Makker V, Buonocore DJ, Offin MD, Olah ZT, Panora E, et al. *A multi-histology basket trial of ado-trastuzumab emtansine in patients with HER2 amplified cancers.* American Society of Clinical Oncology; 2018. 2502

212. Hotta K, Aoe K, Kozuki T, Ohashi K, Ninomiya K, Ichihara E, et al. *A phase II study of trastuzumab emtansine in HER2-positive non–small cell lung cancer.* Journal of Thoracic Oncology. 2018;**13**(2):273-9.

213. Stinchcombe T, Stahel RA, Bubendorf L, Bonomi P, Villegas AE, Kowalski D, et al. *Efficacy, safety, and biomarker results of trastuzumab emtansine (T-DM1) in patients (pts) with previously treated HER2-overexpressing locally advanced or metastatic non-small cell lung cancer (mNSCLC).* American Society of Clinical Oncology; 2017. 8509.

214. Peters S, Stahel R, Bubendorf L, Bonomi P, Villegas A, Kowalski DM, et al. *Trastuzumab emtansine (T-DM1) in patients with previously treated HER2-overexpressing metastatic non–small cell lung cancer: efficacy, safety, and biomarkers.* Clinical Cancer Research. 2019;**25**(1):64-72.

215. Skoulidis F, Li BT, Dy GK, Price TJ, Falchook GS, Wolf J, et al. *Sotorasib for lung cancers with KRAS p. G12C mutation.* New England Journal of Medicine. 2021;**384**(25):2371-81.

216. Dy G, Govindan R, Velcheti V, editors. *Long-term outcomes with sotorasib in pretreated KRAS p. G12C-mutated NSCLC: 2-year analysis of CodeBreaK 100.* AACR Annual Meeting; 2022.

217. Murciano-Goroff YR, Lito P. *The KRYSTAL-1 study of adagrasib—a new trial for KRASG12C-mutated non-small-cell lung cancer*. Nature Reviews Clinical Oncology. 2022;**19**:677-678

218. Reck M, Rodríguez-Abreu D, Robinson A, Hui R, Csoszi T, Fulop A, et al. *Updated analysis of KEYNOTE-024: pembrolizumab versus platinum-based chemotherapy for advanced non-small-cell lung cancer with PD-L1 tumor proportion score of 50% or greater.* 2019;**37**(7):537-546

219. Xiao H-Q, Tian R-H, Zhang Z-H, Du K-Q, Ni Y-M. *Efficacy of pemetrexed plus platinum doublet chemotherapy as first-line treatment for advanced nonsquamous non-small-cell-lung cancer: a systematic review and meta-analysis*. OncoTargets and therapy. 2016:1471-6.

220. Hendriks L, Kerr K, Menis J, Mok T, Nestle U, Passaro A, et al. *Non-oncogene-addicted metastatic non-small-cell lung cancer: ESMO Clinical Practice Guideline for diagnosis, treatment and follow-up.* Annals of Oncology. 2023;**34**(4):358-76.

221. Fossella FV. *Docetaxel in Second-Line Treatment of non-small-Cell Lung Cancer*. Clinical Lung Cancer. 2002;**3**:S23-S8.

222. Felip E, Rosell R. *Pemetrexed as second-line therapy for advanced non-small-cell lung cancer (NSCLC).* Therapeutics and Clinical Risk Management. 2008;**4**(3):579-85.

223. Reck M, Kaiser R, Mellemgaard A, Douillard J-Y, Orlov S, Krzakowski M, et al. *Docetaxel plus nintedanib versus docetaxel plus placebo in patients with previously treated non-small-cell lung cancer (LUME-Lung 1): a phase 3, double-blind, randomised controlled trial.* The lancet oncology. 2014;**15**(2):143-55.

224. Garon EB, Ciuleanu T-E, Arrieta O, Prabhash K, Syrigos KN, Goksel T, et al. *Ramucirumab plus docetaxel versus placebo plus docetaxel for second-line treatment of stage IV non-small-cell lung cancer after disease progression on platinum-based therapy (REVEL): a multicentre, double-blind, randomised phase 3 trial.* The Lancet. 2014;**384**(9944):665-73.

225. Middleton G, Robbins H, Andre F, Swanton C. *A state-of-the-art review of stratified medicine in cancer: towards a future precision medicine strategy in cancer.* Annals of Oncology. 2022;**33**(2):143-57.

226. Herbst RS, Gandara DR, Hirsch FR, Redman MW, LeBlanc M, Mack PC, et al. *Lung Master Protocol (Lung-MAP)—a biomarker-driven protocol for accelerating development of therapies for squamous cell lung cancer: SWOG S1400.* Clinical cancer research. 2015;**21**(7):1514-24.

227. Huang L, Guo Z, Wang F, Fu L. *KRAS mutation: from undruggable to druggable in cancer.* Signal transduction and targeted therapy. 2021;**6**(1):386.

228. Cancer Genome Atlas Research Network. *Comprehensive molecular profiling of lung adenocarcinoma.* Nature. 2014;**511**(7511):543.

229. Dogan S, Shen R, Ang DC, Johnson ML, D'Angelo SP, Paik PK, et al. *Molecular epidemiology of EGFR and KRAS mutations in 3,026 lung adenocarcinomas: higher susceptibility of women to smoking-related KRAS-mutant cancers*. Clinical cancer research. 2012;**18**(22):6169-77.

230. Ricciuti B, Leonardi GC, Metro G, Grignani F, Paglialunga L, Bellezza G, et al. *Targeting the KRAS variant for treatment of non-small cell lung cancer: potential therapeutic applications.* Expert Review of Respiratory Medicine. 2016;**10**(1):53-68.

231. Chen N, Fang W, Lin Z, Peng P, Wang J, Zhan J, et al. *KRAS mutation-induced upregulation of PD-L1 mediates immune escape in human lung adenocarcinoma.* Cancer Immunology, Immunotherapy. 2017;**66**:1175-87.

232. Liu C, Zheng S, Jin R, Wang X, Wang F, Zang R, et al. *The superior efficacy of anti-PD-1/PD-L1 immunotherapy in KRAS-mutant non-small cell lung cancer that correlates with an inflammatory phenotype and increased immunogenicity.* Cancer letters. 2020;**470**:95-105.

233. Cascetta P, Marinello A, Lazzari C, Gregorc V, Planchard D, Bianco R, et al. *KRAS in NSCLC: State of the Art and Future Perspectives.* Cancers. 2022;**14**(21):5430.

234. Skoulidis F, Byers LA, Diao L, Papadimitrakopoulou VA, Tong P, Izzo J, et al. *Co-occurring genomic alterations define major subsets of KRAS-mutant lung adenocarcinoma with distinct biology, immune profiles, and therapeutic vulnerabilities.* Cancer discovery. 2015;**5**(8):860-77.

235. Skoulidis F, Heymach JV. *Co-occurring genomic alterations in non-small-cell lung cancer biology and therapy*. Nature Reviews Cancer. 2019;**19**(9):495-509.

236. Downward J. *Targeting RAS signalling pathways in cancer therapy.* Nature reviews cancer. 2003;**3**(1):11-22.

237. Zhou K, Lin C, Tseng C-L, Ramnath N, Dowell J, Kelley M. P2. *09-15 Real World Efficacy and Safety of Sotorasib in US Veterans with KRAS G12C Mutated Non-Small Cell Lung Cancer.* Journal of Thoracic Oncology. 2023;**18**(11):S337-S8.

238. Julve M, Kennedy O, Lindsay C, Walters-Davies R, Button M, Steele N, et al. *1116P United Kingdom real-world experience of sotorasib in KRAS G12C mutant non-small cell lung cancer: A British thoracic oncology group review.* Annals of Oncology. 2022;**33**:S1061-S2.

239. Garcia BNC, van Kempen LC, Kuijpers CC, Schuuring E, Willems SM, van der Wekken AJ. *Prevalence of KRAS p.(G12C) in stage IV NSCLC patients in the Netherlands; a nation-wide retrospective cohort study.* Lung Cancer. 2022;**167**:1-7.

240. Puyol M, Martín A, Dubus P, Mulero F, Pizcueta P, Khan G, et al. *A synthetic lethal interaction between K-Ras oncogenes and Cdk4 unveils a therapeutic strategy for non-small cell lung carcinoma*. Cancer cell. 2010;**18**(1):63-73.

241. Patnaik A, Rosen LS, Tolaney SM, Tolcher AW, Goldman JW, Gandhi L, et al. *Efficacy and safety of abemaciclib, an inhibitor of CDK4 and CDK6, for patients with breast cancer, non–small cell lung cancer, and other solid tumors.* Cancer discovery. 2016;**6**(7):740-53.

242. Son K-H, Kim M-Y, Shin J-Y, Kim J-O, Kang J-H. *Synergistic antitumor effect of taxanes and CDK4/6 inhibitor in lung cancer cells and mice harboring KRAS mutations.* Anticancer Research. 2021;**41**(10):4807-20.

243. Morrison L, Loibl S, Turner NC. *The CDK4/6 inhibitor revolution—a game-changing era for breast cancer treatment.* Nature Reviews Clinical Oncology. 2023:1-17.

244. Rubin SM, Sage J, Skotheim JM. *Integrating old and new paradigms of G1/S control.* Molecular cell. 2020;**80**(2):183-92.

245. Hume S, Dianov GL, Ramadan K. *A unified model for the G1/S cell cycle transition.* Nucleic acids research. 2020;**48**(22):12483-501.

246. Qie S, Diehl JA. *Cyclin D1, cancer progression, and opportunities in cancer treatment.* Journal of molecular medicine. 2016;**94**:1313-26.

247. Alao JP. *The regulation of cyclin D1 degradation: roles in cancer development and the potential for therapeutic invention.* Molecular cancer. 2007;**6**:1-16.

248. Luangdilok S, Wanchaijiraboon P, Chantranuwatana P, Teerapakpinyo C, Shuangshoti S, Sriuranpong V. *Cyclin D1 expression as a potential prognostic factor in advanced KRAS-mutant non-small cell lung cancer.* Translational Lung Cancer Research. 2019;**8**(6):959.

249. Dragoj M, Milosevic Z, Bankovic J, Dinic J, Pesic M, Tanic N, et al. *Association of CCND1 overexpression with KRAS and PTEN alterations in specific subtypes of non-small cell lung carcinoma and its influence on patients' outcome.* Tumor Biology. 2015;**36**:8773-80.

250. Goldman JW, Mazieres J, Barlesi F, Dragnev KH, Koczywas M, Göskel T, et al. *A randomized phase III study of abemaciclib versus erlotinib in patients with stage IV non-small cell lung cancer with a detectable KRAS mutation who failed prior platinum-based therapy: JUNIPER*. Frontiers in Oncology. 2020;**10**:578756.

251. Haines E, Chen T, Kommajosyula N, Chen Z, Herter-Sprie GS, Cornell L, et al. *Palbociclib resistance confers dependence on an FGFR-MAP kinase-mTOR-driven pathway in KRAS-mutant non-small cell lung cancer.* Oncotarget. 2018;**9**(60):31572.

252. Raimondi L, Raimondi FM, Pietranera M, Di Rocco A, Di Benedetto L, Miele E, et al. *Assessment of resistance mechanisms and clinical implications in patients with KRAS mutated-metastatic breast cancer and resistance to CDK4/6 inhibitors*. Cancers. 2021;**13**(8):1928.

253. Dahmani R, Just P, Delay A, Canal F, Finzi L, Prip-Buus C, et al. *A novel LKB1 isoform enhances AMPK metabolic activity and displays oncogenic properties.* Oncogene. 2015;**34**(18):2337-46.

254. Karuman P, Gozani O, Odze RD, Zhou XC, Zhu H, Shaw R, et al. *The Peutz-Jegher gene product LKB1 is a mediator of p53-dependent cell death.* Molecular cell. 2001;**7**(6):1307-19.

255. Faubert B, Vincent EE, Griss T, Samborska B, Izreig S, Svensson RU, et al*. Loss of the tumor suppressor LKB1 promotes metabolic reprogramming of cancer cells via HIF-1α.* Proceedings of the National Academy of Sciences. 2014;**111**(7):2554-9.

256. Sanchez-Cespedes M. *A role for LKB1 gene in human cancer beyond the Peutz–Jeghers syndrome.* Oncogene. 2007;**26**(57):7825-32.

257. Matsumoto S, Iwakawa R, Takahashi K, Kohno T, Nakanishi Y, Matsuno Y, et al. *Prevalence and specificity of LKB1 genetic alterations in lung cancers*. Oncogene. 2007;**26**(40):5911-8.

258. Sanchez-Cespedes M, Parrella P, Esteller M, Nomoto S, Trink B, Engles JM, et al. *Inactivation of LKB1/STK11 is a common event in adenocarcinomas of the lung. Cancer research.* 2002;**62**(13):3659-62.

259. Calles A, Sholl LM, Rodig SJ, Pelton AK, Hornick JL, Butaney M, et al. *Immunohistochemical loss of LKB1 is a biomarker for more aggressive biology in KRAS-mutant lung adenocarcinoma.* Clinical Cancer Research. 2015;**21**(12):2851-60.

260. Schabath MB, Welsh EA, Fulp WJ, Chen L, Teer JK, Thompson ZJ, et al. *Differential association of STK11 and TP53 with KRAS mutation-associated gene expression, proliferation and immune surveillance in lung adenocarcinoma.* Oncogene. 2016;**35**(24):3209-16.

261. Mahoney C, Choudhury B, Davies H, Edkins S, Greenman C, Van Haaften G, et al. *LKB1/KRAS mutant lung cancers constitute a genetic subset of NSCLC with increased sensitivity to MAPK and mTOR signalling inhibition*. British journal of cancer. 2009;**100**(2):370-5.

262. La Fleur L, Falk-Sörqvist E, Smeds P, Berglund A, Sundström M, Mattsson JS, et al. *Mutation patterns in a population-based non-small cell lung cancer cohort and prognostic impact of concomitant mutations in KRAS and TP53 or STK11.* Lung Cancer. 2019;**130**:50-8.

263. Bange E, Marmarelis ME, Hwang W-T, Yang Y-X, Thompson JC, Rosenbaum J, et al. *Impact of kras and tp53 co-mutations on outcomes after first-line systemic therapy among patients with stk11-mutated advanced non–small-cell lung cancer.* JCO precision oncology. 2019;**3**:1-11.

264. Aredo JV, Padda SK, Kunder CA, Han SS, Neal JW, Shrager JB, et al. *Impact of KRAS mutation subtype and concurrent pathogenic mutations on non-small cell lung cancer outcomes.* Lung Cancer. 2019;**133**:144-50.

265. El Osta B, Behera M, Kim S, Berry LD, Sica G, Pillai RN, et al. *Characteristics and outcomes of patients with metastatic KRAS-mutant lung adenocarcinomas: the lung cancer mutation consortium experience.* Journal of Thoracic Oncology. 2019;**14**(5):876-89.

266. Shire NJ, Klein AB, Golozar A, Collins JM, Fraeman KH, Nordstrom BL, et al. *STK11 (LKB1) mutations in metastatic NSCLC: Prognostic value in the real world.* Plos one. 2020;**15**(9):e0238358.

267. Koyama S, Akbay EA, Li YY, Aref AR, Skoulidis F, Herter-Sprie GS, et al. *STK11/LKB1 deficiency promotes neutrophil recruitment and proinflammatory cytokine production to suppress T-cell activity in the lung tumor microenvironment.* Cancer research. 2016;**76**(5):999-1008.

268. Gillette MA, Satpathy S, Cao S, Dhanasekaran SM, Vasaikar SV, Krug K, et al. *Proteogenomic characterization reveals therapeutic vulnerabilities in lung adenocarcinoma.* Cell. 2020;**182**(1):200-25. e35.

269. Skoulidis F, Hellman M, Awad M, Gainor J, Rizvi H, Carter B, et al. *LKB1 loss is a novel genomic predictor of de novo resistance to PD-1/PD-L1 axis blockade in KRAS-mutant lung adenocarcinoma.* Annals of Oncology. 2017;**28**:v467.

270. Shang X, Li Z, Sun J, Zhao C, Lin J, Wang H. *Survival analysis for non-squamous NSCLC patients harbored STK11 or KEAP1 mutation receiving atezolizumab.* Lung Cancer. 2021;**154**:105-12.

271. Kottakis F, Bardeesy N. *LKB1-AMPK axis revisited.* Cell research. 2012;**22**(12):1617-20.

272. Gwinn DM, Shackelford DB, Egan DF, Mihaylova MM, Mery A, Vasquez DS, et al. *AMPK phosphorylation of raptor mediates a metabolic checkpoint.* Molecular cell. 2008;**30**(2):214-26.

273. Eichner LJ, Brun SN, Herzig S, Young NP, Curtis SD, Shackelford DB, et al. *Genetic analysis reveals AMPK is required to support tumor growth in murine Kras-dependent lung cancer models.* Cell metabolism. 2019;**29**(2):285-302. e7.

274. Hollstein PE, Eichner LJ, Brun SN, Kamireddy A, Svensson RU, Vera LI, et al. *The AMPK-related kinases SIK1 and SIK3 mediate key tumor-suppressive effects of LKB1 in NSCLC. Cancer discovery*. 2019;**9**(11):1606-27.

275. Kottakis F, Nicolay BN, Roumane A, Karnik R, Gu H, Nagle JM, et al. *LKB1 loss links serine metabolism to DNA methylation and tumorigenesis.* Nature. 2016;**539**(7629):390-5.

276. Liu W, Monahan KB, Pfefferle AD, Shimamura T, Sorrentino J, Chan KT, et al. *LKB1/STK11 inactivation leads to expansion of a prometastatic tumor subpopulation in melanoma.* Cancer cell. 2012;**21**(6):751-64.

277. Ji H, Ramsey MR, Hayes DN, Fan C, McNamara K, Kozlowski P, et al. *LKB1 modulates lung cancer differentiation and metastasis.* Nature. 2007;**448**(7155):807-10.

278. Carretero J, Shimamura T, Rikova K, Jackson AL, Wilkerson MD, Borgman CL, et al. *Integrative genomic and proteomic analyses identify targets for Lkb1-deficient metastatic lung tumors.* Cancer cell. 2010;**17**(6):547-59.

279. Kim J, Lee HM, Cai F, Ko B, Yang C, Lieu EL, et al. *The hexosamine biosynthesis pathway is a targetable liability in KRAS/LKB1 mutant lung cancer.* Nature metabolism. 2020:1-12.

280. Chen Z, Cheng K, Walton Z, Wang Y, Ebi H, Shimamura T, et al. *A murine lung cancer co-clinical trial identifies genetic modifiers of therapeutic response.* Nature. 2012;**483**(7391):613-7.

281. Masui K, Tanaka K, Akhavan D, Babic I, Gini B, Matsutani T, et al. *mTOR complex 2 controls glycolytic metabolism in glioblastoma through FoxO acetylation and upregulation of c-Myc.* Cell metabolism. 2013;**18**(5):726-39.

282. Momcilovic M, McMickle R, Abt E, Seki A, Simko SA, Magyar C, et al. *Heightening energetic stress selectively targets LKB1-deficient non–small cell lung cancers.* Cancer research. 2015;**75**(22):4910-22.

283. Powles T, Wheater M, Din O, Geldart T, Boleti E, Stockdale A, et al. *A randomised phase 2 study of AZD2014 versus everolimus in patients with VEGF-refractory metastatic clear cell renal cancer.* European urology. 2016;**69**(3):450-6.

284. Schmid P, Zaiss M, Harper-Wynne C, Ferreira M, Dubey S, Chan S, et al. *MANTA-a randomized phase II study of fulvestrant in combination with the dual mTOR inhibitor AZD2014 or everolimus or fulvestrant alone in estrogen receptor-positive advanced or metastatic breast cancer.* Cancer Research. 2018;**78**(4). GS2-07

285. O'Reilly KE, Rojo F, She Q-B, Solit D, Mills GB, Smith D, et al. *mTOR inhibition induces upstream receptor tyrosine kinase signaling and activates Akt.* Cancer research. 2006;**66**(3):1500-8.

286. Rodrik-Outmezguine VS, Chandarlapaty S, Pagano NC, Poulikakos PI, Scaltriti M, Moskatel E, et al. *mTOR kinase inhibition causes feedback-dependent biphasic regulation of AKT signaling.* Cancer discovery. 2011;**1**(3):248-59.

287. Shtivelman E, Hensing T, Simon GR, Dennis PA, Otterson GA, Bueno R, et al. *Molecular pathways and therapeutic targets in lung cancer.* Oncotarget. 2014;**5**(6):1392.

288. Cancer Genome Atlas Research Network. *Comprehensive genomic characterization of squamous cell lung cancers.* Nature. 2012;**489**(7417):519.

289. Paz-Ares LG, Luft A, Tafreshi A, Gumus M, Mazieres J, Hermes B, et al. *Phase 3 study of carboplatin-paclitaxel/nab-paclitaxel (Chemo) with or without pembrolizumab (Pembro) for patients (Pts) with metastatic squamous (Sq) non-small cell lung cancer (NSCLC).* American Society of Clinical Oncology; 2018. 105

290. Novello S, Kowalski DM, Luft A, Gümüş M, Vicente D, Mazières J, et al. *Pembrolizumab plus chemotherapy in squamous non–small-cell lung cancer: 5-year update of the phase III KEYNOTE-407 study.* Journal of Clinical Oncology. 2023;**41**(11):1999.

291. Li S, de Camargo Correia GS, Wang J, Manochakian R, Zhao Y, Lou Y. *Emerging Targeted Therapies in Advanced Non-Small-Cell Lung Cancer.* Cancers. 2023;**15**(11):2899.

292. Riess J, Frankel P, Massarelli E, Nieva J, Lai W-C, Koczywas M, et al. *Ma13. 08 a phase 1 trial of sapanisertib and telaglenastat (Cb-839) in patients with advanced nsclc (Nci 10327): Results from dose escalation.* Journal of Thoracic Oncology. 2022;17(9):S91-S2.

293. Chae YK, Hong F, Vaklavas C, Cheng HH, Hammerman P, Mitchell EP, et al. *Phase II study of AZD4547 in patients with tumors harboring aberrations in the FGFR pathway: results from the NCI-MATCH trial (EAY131) subprotocol W.* Journal of Clinical Oncology. 2020;**38**(21):2407.

294. Aggarwal C, Redman MW, Lara Jr PN, Borghaei H, Hoffman P, Bradley JD, et al. *SWOG S1400D (NCT02965378), a phase II study of the fibroblast growth factor receptor inhibitor AZD4547 in previously treated patients with fibroblast growth factor pathway–activated stage IV squamous cell lung cancer (Lung-MAP Substudy).* Journal of Thoracic Oncology. 2019;**14**(10):1847-52.

295. Yuan G, Flores NM, Hausmann S, Lofgren SM, Kharchenko V, Angulo-Ibanez M, et al. *Elevated NSD3 histone methylation activity drives squamous cell lung cancer*. Nature. 2021;**590**(7846):504-8.

296. Bass AJ, Watanabe H, Mermel CH, Yu S, Perner S, Verhaak RG, et al. *SOX2 is an amplified lineage-survival oncogene in lung and esophageal squamous cell carcinomas.* Nature genetics. 2009;**41**(11):1238-42.

297. Redon R, Hussenet T, Bour G, Caulee K, Jost B, Muller D, et al. *Amplicon mapping and transcriptional analysis pinpoint cyclin L as a candidate oncogene in head and neck cancer.* Cancer research. 2002;**62**(21):6211-7.

298. McCaughan F, Pole JC, Bankier AT, Konfortov BA, Carroll B, Falzon M, et al. *Progressive 3q amplification consistently targets SOX2 in preinvasive squamous lung cancer.* American journal of respiratory and critical care medicine. 2010;**182**(1):83-91.

299. Tan AC. *Targeting the PI3K/Akt/mTOR pathway in non-small cell lung cancer (NSCLC). Thoracic cancer.* 2020;**11**(3):511-8.

300. Martini M, De Santis MC, Braccini L, Gulluni F, Hirsch E. *PI3K/AKT signaling pathway and cancer: an updated review.* Annals of medicine. 2014;**46**(6):372-83.

301. Fumarola C, Bonelli MA, Petronini PG, Alfieri RR. *Targeting PI3K/AKT/mTOR pathway in non small cell lung cancer.* Biochemical pharmacology. 2014;**90**(3):197-207.

302. Robbins HL, Hague A. *The PI3K/Akt pathway in tumors of endocrine tissues.* Frontiers in endocrinology. 2016;**6**:188.

303. Lim WT, Zhang W, Miller C, Watters J, Gao F, Viswanathan A, et al. *PTEN and phosphorylated AKT expression and prognosis in early-and late-stage non-small cell lung cancer.* Oncology reports. 2007;**17**(4):853-7.

304. Balsara BR, Pei J, Mitsuuchi Y, Page R, Klein-Szanto A, Wang H, et al. *Frequent activation of AKT in non-small cell lung carcinomas and preneoplastic bronchial lesions.* Carcinogenesis. 2004;**25**(11):2053-9.

305. Tsao AS, McDonnell T, Lam S, Putnam JB, Bekele N, Hong WK, et al. *Increased phospho-AKT (Ser473) expression in bronchial dysplasia: implications for lung cancer prevention studies.* Cancer Epidemiology and Prevention Biomarkers. 2003;**12**(7):660-4.

306. Tsurutani J, Fukuoka J, Tsurutani H, Shih JH, Hewitt SM, Travis WD, et al. *Evaluation of two phosphorylation sites improves the prognostic significance of Akt activation in non–small-cell lung cancer tumors.* Journal of clinical oncology. 2006;**24**(2):306-14.

307. Scrima M, De Marco C, Fabiani F, Franco R, Pirozzi G, Rocco G, et al. *Signaling networks associated with AKT activation in non-small cell lung cancer (NSCLC): new insights on the role of phosphatydil-inositol-3 kinase.* PloS one. 2012;**7**(2):e30427.

308. Yamamoto H, Shigematsu H, Nomura M, Lockwood WW, Sato M, Okumura N, et al. *PIK3CA mutations and copy number gains in human lung cancers*. Cancer research. 2008;**68**(17):6913-21.

309. Angulo B, Suarez-Gauthier A, Lopez-Rios F, Medina P, Conde E, Tang M, et al. *Expression signatures in lung cancer reveal a profile for EGFR-mutant tumours and identify selective PIK3CA overexpression by gene amplification.* The Journal of pathology. 2008;**214**(3):347-56.

310. Ji M, Guan H, Gao C, Shi B, Hou P. *Highly frequent promoter methylation and PIK3CA amplification in non-small cell lung cancer (NSCLC).* BMC cancer. 2011;**11**(1):1-11.

311. Scheffler M, Bos M, Gardizi M, König K, Michels S, Fassunke J, et al. *PIK3CA mutations in non-small cell lung cancer (NSCLC): genetic heterogeneity, prognostic impact and incidence of prior malignancies.* Oncotarget. 2015;**6**(2):1315.

312. Kim BR, Van de Laar E, Cabanero M, Tarumi S, Hasenoeder S, Wang D, et al. *SOX2 and PI3K cooperate to induce and stabilize a squamous-committed stem cell injury state during lung squamous cell carcinoma pathogenesis.* PLoS biology. 2016;**14**(11):e1002581.

313. Shinohara S, Ichiki Y, Fukuichi Y, Honda Y, Kanayama M, Taira A, et al. *Squamous cell carcinoma transformation from adenocarcinoma as an acquired resistance after the EGFR TKI therapy in (EGFR-mutated) non-small cell lung cancer*. Journal of thoracic disease. 2018;**10**(7):E526.

314. Park S, Shim JH, Lee B, Cho I, Park W-Y, Kim Y, et al. *Paired genomic analysis of squamous cell carcinoma transformed from EGFR-mutated lung adenocarcinoma.* Lung Cancer. 2019;**134**:7-15.

315. Bonelli MA, Cavazzoni A, Saccani F, Alfieri RR, Quaini F, La Monica S, et al. *Inhibition of PI3K pathway reduces invasiveness and epithelial-to-mesenchymal transition in squamous lung cancer cell lines harboring PIK3CA gene alterations.* Molecular cancer therapeutics. 2015;**14**(8):1916-27.

316. Engelman JA, Chen L, Tan X, Crosby K, Guimaraes AR, Upadhyay R, et al. *Effective use of PI3K and MEK inhibitors to treat mutant Kras G12D and PIK3CA H1047R murine lung cancers*. Nature medicine. 2008;**14**(12):1351-6.

317. Brognard J, Clark AS, Ni Y, Dennis PA. *Akt/protein kinase B is constitutively active in non-small cell lung cancer cells and promotes cellular survival and resistance to chemotherapy and radiation.* Cancer research. 2001;**61**(10):3986-97.

318. Vansteenkiste JF, Canon J-L, De Braud F, Grossi F, De Pas T, Gray JE, et al. *Safety and efficacy of buparlisib (BKM120) in patients with PI3K pathway-activated non-small cell lung cancer: results from the phase II BASALT-1 study.* Journal of Thoracic Oncology. 2015;**10**(9):1319-27.

319. André F, Ciruelos E, Rubovszky G, Campone M, Loibl S, Rugo HS, et al. *Alpelisib for PIK3CA-mutated, hormone receptor–positive advanced breast cancer.* New England Journal of Medicine. 2019;**380**(20):1929-40.

320. Novak D, Hüser L, Elton JJ, Umansky V, Altevogt P, Utikal J, editors. *SOX2 in development and cancer biology.* Seminars in cancer biology.2020 Vol 67, pp74-82: Academic Press.

321. Stark Z, Storen R, Bennetts B, Savarirayan R, Jamieson RV. *Isolated hypogonadotropic hypogonadism with SOX2 mutation and anophthalmia/microphthalmia in offspring.* European journal of human genetics. 2011;**19**(7):753-6.

322. Mihelec M, Abraham P, Gibson K, Krowka R, Susman R, Storen R, et al. Novel SOX2 partner-factor domain mutation in a four-generation family. European journal of human genetics. 2009;17(11):1417-22.

323. Kelberman D, Rizzoti K, Avilion A, Bitner-Glindzicz M, Cianfarani S, Collins J, et al. *Mutations within Sox2/SOX2 are associated with abnormalities in the hypothalamo-pituitary-gonadal axis in mice and humans.* The Journal of clinical investigation. 2006;**116**(9):2442-55.

324. Avilion AA, Nicolis SK, Pevny LH, Perez L, Vivian N, Lovell-Badge R. *Multipotent cell lineages in early mouse development depend on SOX2 function. Genes & development.* 2003;**17**(1):126-40.

325. Keramari M, Razavi J, Ingman KA, Patsch C, Edenhofer F, Ward CM, et al. *Sox2 is essential for formation of trophectoderm in the preimplantation embryo.* PloS one. 2010;**5**(11):e13952.

326. Wicklow E, Blij S, Frum T, Hirate Y, Lang RA, Sasaki H, et al. *HIPPO pathway members restrict SOX2 to the inner cell mass where it promotes ICM fates in the mouse blastocyst.* PLoS genetics. 2014;**10**(10):e1004618.

327. Gontan C, de Munck A, Vermeij M, Grosveld F, Tibboel D, Rottier R. *Sox2 is important for two crucial processes in lung development: branching morphogenesis and epithelial cell differentiation.* Developmental biology. 2008;**317**(1):296-309.

328. Tompkins DH, Besnard V, Lange AW, Wert SE, Keiser AR, Smith AN, et al. *Sox2 is required for maintenance and differentiation of bronchiolar Clara, ciliated, and goblet cells.* PloS one. 2009;**4**(12):e8248.

329. Wuebben EL, Rizzino A. *The dark side of SOX2: cancer-a comprehensive overview*. Oncotarget. 2017;**8**(27):44917.

330. Metz EP, Rizzino A. *Sox2 dosage: A critical determinant in the functions of Sox2 in both normal and tumor cells. Journal of cellular physiology*. 2019;**234**(11):19298-306.

331. Wilbertz T, Wagner P, Petersen K, Stiedl A-C, Scheble VJ, Maier S, et al. *SOX2 gene amplification and protein overexpression are associated with better outcome in squamous cell lung cancer.* Modern pathology. 2011;**24**(7):944-53.

332. Lu Y, Futtner C, Rock JR, Xu X, Whitworth W, Hogan BL, et al. *Evidence that SOX2 overexpression is oncogenic in the lung*. PloS one. 2010;**5**(6):e11022.

333. Mukhopadhyay A, Berrett KC, Kc U, Clair PM, Pop SM, Carr SR, et al. *Sox2 cooperates with Lkb1 loss in a mouse model of squamous cell lung cancer*. Cell reports. 2014;**8**(1):40-9.

334. Ferone G, Song J-Y, Sutherland KD, Bhaskaran R, Monkhorst K, Lambooij J-P, et al. *SOX2 is the determining oncogenic switch in promoting lung squamous cell carcinoma from different cells of origin*. Cancer cell. 2016;**30**(4):519-32.

335. Liu Y, Yin N, Wang X, Khoor A, Sambandam V, Ghosh AB, et al. *Chromosome 3q26 gain is an early event driving coordinated overexpression of the PRKCI, SOX2, and ECT2 oncogenes in lung squamous cell carcinoma.* Cell reports. 2020;**30**(3):771-82. e6.

336. Porter L, McCaughan F, editors. *SOX2 and squamous cancers*. Seminars in Cancer Biology; 2020: Elsevier.

337. Boumahdi S, Driessens G, Lapouge G, Rorive S, Nassar D, Le Mercier M, et al. *SOX2 controls tumour initiation and cancer stem-cell functions in squamous-cell carcinoma.* Nature. 2014;**511**(7508):246-50.

338. Fukazawa T, Guo M, Ishida N, Yamatsuji T, Takaoka M, Yokota E, et al. *SOX2 suppresses CDKN1A to sustain growth of lung squamous cell carcinoma.* Scientific reports. 2016;**6**(1):1-12.

339. Stroun M, Anker P, Maurice P, Lyautey J, Lederrey C, Beljanski M. *Neoplastic characteristics of the DNA found in the plasma of cancer patients*. Oncology. 1989;**46**(5):318-22.

340. Zhou Q, Li W, Leng B, Zheng W, He Z, Zuo M, et al. *Circulating cell free DNA as the diagnostic marker for ovarian cancer: a systematic review and meta-analysis.* PloS one. 2016;**11**(6):e0155495.

341. Wang X, Shi X-Q, Zeng P-W, Mo F-M, Chen Z-H. *Circulating cell free DNA as the diagnostic marker for colorectal cancer: a systematic review and meta-analysis.* Oncotarget. 2018;**9**(36):24514.

342. Dang DK, Park BH. *Circulating tumor DNA: Current challenges for clinical utility.* The Journal of Clinical Investigation. 2022;**132**(12).

343. Rolfo C, Mack P, Scagliotti GV, Aggarwal C, Arcila ME, Barlesi F, et al. *Liquid biopsy for advanced NSCLC: a consensus statement from the international association for the study of lung cancer.* Journal of Thoracic Oncology. 2021;**16**(10):1647-62.

344. Abbosh C, Birkbak NJ, Wilson GA, Jamal-Hanjani M, Constantin T, Salari R, et al. *Phylogenetic ctDNA analysis depicts early-stage lung cancer evolution*. Nature. 2017;**545**(7655):446-51.

345. Cohen JD, Li L, Wang Y, Thoburn C, Afsari B, Danilova L, et al. *Detection and localization of surgically resectable cancers with a multi-analyte blood test.* Science. 2018;**359**(6378):926-30.

346. Chen X, Gole J, Gore A, He Q, Lu M, Min J, et al. *Non-invasive early detection of cancer four years before conventional diagnosis using a blood test.* Nature communications. 2020;**11**(1):3475.

347. Klein EA, Richards D, Cohn A, Tummala M, Lapham R, Cosgrove D, et al. *Clinical validation of a targeted methylation-based multi-cancer early detection test using an independent validation set.* Annals of Oncology. 2021;**32**(9):1167-77.

348. Lennon AM, Buchanan AH, Kinde I, Warren A, Honushefsky A, Cohain AT, et al. *Feasibility of blood testing combined with PET-CT to screen for cancer and guide intervention*. Science. 2020;**369**(6499):eabb9601.

349. Liu MC, Oxnard G, Klein E, Swanton C, Seiden M, Liu MC, et al. *Sensitive and specific multi-cancer detection and localization using methylation signatures in cell-free DNA.* Annals of Oncology. 2020;**31**(6):745-59.

350. Aggarwal C, Marmarelis ME, Hwang W-T, Scholes DG, McWilliams TL, Singh AP, et al. *Association Between Availability of Molecular Genotyping Results and Overall Survival in Patients With Advanced Nonsquamous Non–Small-Cell Lung Cancer.* JCO Precision Oncology. 2023;**7**:e2300191.

351. Lim C, Tsao M, Le L, Shepherd F, Feld R, Burkes R, et al. *Biomarker testing and time to treatment decision in patients with advanced nonsmall-cell lung cancer.* Annals of Oncology. 2015;26(**7**):1415-21.

352. Zugazagoitia J, Ramos I, Trigo JM, Palka M, Gómez-Rueda A, Jantus-Lewintre E, et al. *Clinical utility of plasma-based digital next-generation sequencing in patients with advance-stage lung adenocarcinomas with insufficient tumor samples for tissue genotyping.* Annals of Oncology. 2019;**30**(2):290-6.

353. Palmero R, Taus A, Viteri S, Majem M, Carcereny E, Garde-Noguera J, et al. *Biomarker discovery and outcomes for comprehensive cell-free circulating tumor DNA versus standard-of-care tissue testing in advanced non–small-cell lung cancer.* JCO Precision Oncology. 2021;**5**:93-102.

354. Raez LE, Brice K, Dumais K, Lopez-Cohen A, Wietecha D, Izquierdo PA, et al. *Liquid Biopsy Versus Tissue Biopsy to Determine Front Line Therapy in Metastatic Non-Small Cell Lung Cancer (NSCLC).* Clinical Lung Cancer. 2023;**24**(2):120-9.

355. Park S, Olsen S, Ku BM, Lee MS, Jung HA, Sun JM, et al. *High concordance of actionable genomic alterations identified between circulating tumor DNA–based and tissue-based next-generation sequencing testing in advanced non–small cell lung cancer: The Korean Lung Liquid Versus Invasive Biopsy Program.* Cancer. 2021;**127**(16):3019-28.

356. Leighl NB, Page RD, Raymond VM, Daniel DB, Divers SG, Reckamp KL, et al. *Clinical utility of comprehensive cell-free DNA analysis to identify genomic biomarkers in patients with newly diagnosed metastatic non–small cell lung cancer.* Clinical cancer research. 2019;**25**(15):4691-700.

357. Dziadziuszko R, Mok T, Peters S, Han J-Y, Alatorre-Alexander J, Leighl N, et al. *Blood first assay screening trial (BFAST) in treatment-naive advanced or metastatic NSCLC: initial results of the phase 2 ALK-positive cohort*. Journal of Thoracic Oncology. 2021;**16**(12):2040-50.

358. Le X, Sakai H, Felip E, Veillon R, Garassino MC, Raskin J, et al. *Tepotinib efficacy and safety in patients with MET exon 14 skipping NSCLC: outcomes in patient subgroups from the*

VISION study with relevance for clinical practice. Clinical Cancer Research. 2022;**28**(6):1117-26.

359. Gale D, Heider K, Ruiz-Valdepenas A, Hackinger S, Perry M, Marsico G, et al. *Residual ctDNA after treatment predicts early relapse in patients with early-stage non-small cell lung cancer.* Annals of Oncology. 2022;**33**(5):500-10.

360. Peng M, Huang Q, Yin W, Tan S, Chen C, Liu W, et al. *Circulating tumor DNA as a prognostic biomarker in localized non-small cell lung cancer.* Frontiers in oncology. 2020;**10**:561598.

361. Xia L, Mei J, Kang R, Deng S, Chen Y, Yang Y, et al. *Perioperative ctDNA-based molecular residual disease detection for non–small cell lung cancer: a prospective multicenter cohort study (LUNGCA-1).* Clinical Cancer Research. 2022;**28**(15):3308-17.

362. Abbosh C, Frankell AM, Harrison T, Kisistok J, Garnett A, Johnson L, et al. *Tracking early lung cancer metastatic dissemination in TRACERx using ctDNA.* Nature. 2023;**616**(7957):553-62.

363. Gray JE, Okamoto I, Sriuranpong V, Vansteenkiste J, Imamura F, Lee JS, et al. *Tissue and plasma EGFR mutation analysis in the FLAURA trial: Osimertinib versus Comparator EGFR tyrosine kinase inhibitor as first-line treatment in patients with EGFR-mutated advanced non–small cell lung cancer.* Clinical cancer research. 2019;**25**(22):6644-52.

364. Shepherd FA, Papadimitrakopoulou V, Mok T, Wu Y-L, Han J-Y, Ahn M-J, et al. *Early clearance of plasma EGFR mutations as a predictor of response to osimertinib in the AURA3 trial.* American Society of Clinical Oncology; 2018. 9027

365. Chmielecki J, Mok T, Wu Y-L, Han J-Y, Ahn M-J, Ramalingam SS, et al. *Analysis of acquired resistance mechanisms to osimertinib in patients with EGFR-mutated advanced non-small cell lung cancer from the AURA3 trial.* Nature communications. 2023;**14**(1):1071.

366. Doudna JA, Charpentier E. *The new frontier of genome engineering with CRISPR-Cas9. Science.* 2014;**346**(6213):1258096.

367. Joung J, Konermann S, Gootenberg JS, Abudayyeh OO, Platt RJ, Brigham MD, et al. *Genome-scale CRISPR-Cas9 knockout and transcriptional activation screening. Nature protocols*. 2017;**12**(4):828-63.

368. Evers B, Jastrzebski K, Heijmans JP, Grernrum W, Beijersbergen RL, Bernards R. *CRISPR knockout screening outperforms shRNA and CRISPRi in identifying essential genes. Nature biotechnology.* 2016;**34**(6):631-3.

369. Jason S, Yusa K. *Genome-wide CRISPR-Cas9 screening in mammalian cells.* Methods. 2019;**164**:29-35.

370. Ianevski A, Giri AK, Aittokallio T. *SynergyFinder 2.0: visual analytics of multi-drug combination synergies.* Nucleic acids research. 2020;**48**(W1):W488-W93.

371. Chen S, Sanjana NE, Zheng K, Shalem O, Lee K, Shi X, et al. *Genome-wide CRISPR screen in a mouse model of tumor growth and metastasis.* Cell. 2015;**160**(6):1246-60.

372. Kandoth C. mskcc/vcf2maf: vcf2maf v1.6.18. (2020). Doi:10.5281/zenodo.593251

373. Mayakonda A, Lin D-C, Assenov Y, Plass C, Koeffler HP. *Maftools: efficient and comprehensive analysis of somatic variants in cancer.* Genome research. 2018;**28**(11):1747-56.

374. Gentleman RC, Carey VJ, Bates DM, Bolstad B, Dettling M, Dudoit S, et al. *Bioconductor: open software development for computational biology and bioinformatics.* Genome biology. 2004;**5**(10):1-16.

375. Kent WJ, Sugnet CW, Furey TS, Roskin KM, Pringle TH, Zahler AM, et al. *The human genome browser at UCSC.* Genome research. 2002;**12**(6):996-1006.

376. UCSC Genome Browser. Available from: http://genome.ucsc.edu.

377. Nassar LR, Barber GP, Benet-Pagès A, Casper J, Clawson H, Diekhans M, et al. *The UCSC genome browser database: 2023 update*. Nucleic acids research. 2023;**51**(D1):D1188-D95.

378. Weinstein JN, Collisson EA, Mills GB, Shaw KR, Ozenberger BA, Ellrott K, et al. *The cancer genome atlas pan-cancer analysis project.* Nature genetics. 2013;**45**(10):1113-20.

379. Gao J, Aksoy BA, Dogrusoz U, Dresdner G, Gross B, Sumer SO, et al. *Integrative analysis of complex cancer genomics and clinical profiles using the cBioPortal.* Science signaling. 2013;**6**(269):pl1-pl.

380. Cerami E, Gao J, Dogrusoz U, Gross BE, Sumer SO, Aksoy BA, et al. *The cBio cancer genomics portal: an open platform for exploring multidimensional cancer genomics data.* AACR; 2012.

381. The Cancer Dependency Map Project, DepMap. Available from: https://depmap.org/portal/. Last Accessed July 2024

382. Meyers RM, Bryan JG, McFarland JM, Weir BA, Sizemore AE, Xu H, et al. *Computational correction of copy number effect improves specificity of CRISPR–Cas9 essentiality screens in cancer cells.* Nature genetics. 2017;**49**(12):1779-84.

383. Wickham H, Averick M, Bryan J, Chang W, McGowan LDA, François R, et al. *Welcome to the Tidyverse.* Journal of open source software. 2019;**4**(43):1686.

384. R Core Team. R: *A language and environment for statistical computing*. R Foundation for Statistical Computing, Vienna, Austria. Available from: https://www.R-project.org/. Accessed July 2024

385. Basu B, Krebs MG, Sundar R, Wilson RH, Spicer J, Jones R, et al. *Vistusertib (dual m-TORC1/2 inhibitor) in combination with paclitaxel in patients with high-grade serous ovarian and squamous non-small-cell lung cancer.* Annals of Oncology. 2018;**29**(9):1918-25.

386. Verheijen RB, Atrafi F, Schellens JH, Beijnen JH, Huitema AD, Mathijssen RH, et al. *Pharmacokinetic optimization of everolimus dosing in oncology: a randomized crossover trial.* Clinical pharmacokinetics. 2018;**57**(5):637-44.

387. Hientz K, Mohr A, Bhakta-Guha D, Efferth T. *The role of p53 in cancer drug resistance and targeted chemotherapy.* Oncotarget. 2017;**8**(5):8921.

388. Tian Y, Xu L, Li X, Li H, Zhao M. *SMARCA4: current status and future perspectives in non-small-cell lung cancer.* Cancer Letters. 2023;**554**:216022.

389. Schoenfeld AJ, Bandlamudi C, Lavery JA, Montecalvo J, Namakydoust A, Rizvi H, et al. *The genomic landscape of SMARCA4 alterations and associations with outcomes in patients with lung cancer*. Clinical Cancer Research. 2020;**26**(21):5701-8.

390. Negrao MV, Araujo HA, Lamberti G, Cooper AJ, Akhave NS, Zhou T, et al. *Comutations and KRASG12C Inhibitor Efficacy in Advanced NSCLC.* Cancer Discovery. 2023:OF1-OF16.

391. Chmielecki J, Gray JE, Cheng Y, Ohe Y, Imamura F, Cho BC, et al. *Candidate mechanisms of acquired resistance to first-line osimertinib in EGFR-mutated advanced non-small cell lung cancer*. Nature Communications. 2023;**14**(1):1070.

392. Sheng H, Li X, Xu Y. *Knockdown of FOXP1 promotes the development of lung adenocarcinoma.* Cancer biology & therapy. 2019;**20**(4):537-45.

393. Hieronymus H, Iaquinta PJ, Wongvipat J, Gopalan A, Murali R, Mao N, et al. *Deletion of 3p13-14 locus spanning FOXP1 to SHQ1 cooperates with PTEN loss in prostate oncogenesis*. Nature communications. 2017;**8**(1):1081.

394. Wei H, Geng J, Shi B, Liu Z, Wang Y-H, Stevens AC, et al. *Cutting edge: Foxp1 controls naive CD8+ T cell quiescence by simultaneously repressing key pathways in cellular metabolism and cell cycle progression.* The Journal of Immunology. 2016;**196**(9):3537-41.

395. Sclafani F, Chau I, Cunningham D, Hahne JC, Vlachogiannis G, Eltahir Z, et al. *KRAS and BRAF mutations in circulating tumour DNA from locally advanced rectal cancer. Scientific reports.* 2018;**8**(1):1445.

396. Bick AG, Weinstock JS, Nandakumar SK, Fulco CP, Leventhal MJ, Bao EL, et al*. Inherited causes of clonal hematopoiesis of indeterminate potential in TOPMed whole genomes.* BioRxiv. 2019:782748.

397. Stout LA, Kassem N, Hunter C, Philips S, Radovich M, Schneider BP. *Identification of germline cancer predisposition variants during clinical ctDNA testing.* Scientific Reports. 2021;**11**(1):13624.

398. Glubb DM, Cerri E, Giese A, Zhang W, Mirza O, Thompson EE, et al. *Novel functional germline variants in the VEGF receptor 2 gene and their effect on gene expression and microvessel density in lung cancer.* Clinical Cancer Research. 2011;**17**(16):5257-67.

399. EMBL-EBI. ProtVar 2024. Available from: *https://www.ebi.ac.uk/ProtVar/*.

400. Apellániz-Ruiz M, Diekstra MH, Roldán JM, Boven E, Castellano D, Gelderblom H, et al. *Evaluation of KDR rs34231037 as a predictor of sunitinib efficacy in patients with metastatic renal cell carcinoma.* Pharmacogenetics and Genomics. 2017;**27**(6):227-31.

401. Masago K, Fujita S, Muraki M, Hata A, Okuda C, Otsuka K, et al. *Next-generation sequencing of tyrosine kinase inhibitor-resistant non-small-cell lung cancers in patients harboring epidermal growth factor-activating mutations.* BMC cancer. 2015;**15**(1):1-8.

402. Zaman N, Dass SS, Du Parcq P, Macmahon S, Gallagher L, Thompson L, et al. *The KDR (VEGFR-2) genetic polymorphism Q472H and c-KIT polymorphism M541L are associated with more aggressive behaviour in astrocytic gliomas.* Cancer Genomics & Proteomics. 2020;**17**(6):715-27.

403. Chou M, Giles KM, Illa-Bochaca I, Mastroianni J, Vega-Saenz de Miera E, Krogsgaard M, et al. *Association of pathogenic germline variant KDR Q472H with angiogenesis and resistance to treatment in melanoma.* American Society of Clinical Oncology; 2020.

404. Zhu X, Wang Y, Xue W, Wang R, Wang L, Zhu M-L, et al. *The VEGFR-2 protein and the VEGFR-2 rs1870377 A> T genetic polymorphism are prognostic factors for gastric cancer.* Cancer Biology & Therapy. 2019;**20**(4):497-504.

405. Silva IP, Salhi A, Giles KM, Vogelsang M, Han SW, Ismaili N, et al. *Identification of a novel pathogenic germline KDR variant in melanoma.* Clinical Cancer Research. 2016;**22**(10):2377-85.

406. Tinhofer I, Stenzinger A, Eder T, Konschak R, Niehr F, Endris V, et al. *Targeted next-generation sequencing identifies molecular subgroups in squamous cell carcinoma of the head*

and neck with distinct outcome after concurrent chemoradiation. Annals of Oncology. 2016;**27**(12):2262-8.

407. Song Z-Z, Zhao L-F, Zuo J, Fan Z-S, Wang L, Wang Y-D. *Clinical outcomes and safety of apatinib mesylate in the treatment of advanced non-squamous non-small cell lung cancer in patients who progressed after standard therapy and analysis of the KDR gene polymorphism.* OncoTargets and therapy. 2020:603-13.

408. Geng N, Su J, Liu Z, Ding C, Xie S, Hu W. *The influence of KDR genetic variation on the efficacy and safety of patients with advanced NSCLC receiving first-line bevacizumab plus chemotherapy regimen.* Technology in Cancer Research & Treatment. 2021;20:15330338211019433.

409. Tong Z, Sathe A, Ebner B, Qi P, Veltkamp C, Gschwend JE, et al. *Functional genomics identifies predictive markers and clinically actionable resistance mechanisms to CDK4/6 inhibition in bladder cancer.* Journal of Experimental & Clinical Cancer Research. 2019;**38**(1):1-14.

410. Cho S, Hwang ES. *Status of mTOR activity may phenotypically differentiate senescence and quiescence.* Molecules and cells. 2012;**33**:597-604.

411. Xu S, Cai Y, Wei Y. *mTOR signaling from cellular senescence to organismal aging*. Aging and disease. 2014;**5**(4):263.

412. Maskey RS, Wang F, Lehman E, Wang Y, Emmanuel N, Zhong W, et al. *Sustained mTORC1 activity during palbociclib-induced growth arrest triggers senescence in ER+ breast cancer cells.* Cell Cycle. 2021;**20**(1):65-80.

413. Bruno L, Ostinelli A, Waisberg F, Enrico D, Ponce C, Rivero S, et al. *Cyclin-dependent kinase 4/6 inhibitor outcomes in patients with advanced breast cancer carrying germline pathogenic variants in DNA repair–related genes.* JCO Precision Oncology. 2022;**6**:e2100140.

414. Haricharan S, Punturi N, Singh P, Holloway KR, Anurag M, Schmelz J, et al. *Loss of MutL disrupts CHK2-dependent cell-cycle control through CDK4/6 to promote intrinsic endocrine therapy resistance in primary breast cancer.* Cancer discovery. 2017;**7**(10):1168-83

415. Bea S, Zettl A, Wright G, Salaverria I, Jehn P, Moreno V, et al. *Diffuse large B-cell lymphoma subgroups have distinct genetic profiles that influence tumor biology and improve gene-expression-based survival prediction.* Blood. 2005;**106**(9):3183-90.

416. Yi M, Tan Y, Wang L, Cai J, Li X, Zeng Z, et al. *TP63 links chromatin remodeling and enhancer reprogramming to epidermal differentiation and squamous cell carcinoma development.* Cellular and Molecular Life Sciences. 2020;**77**:4325-46.

417. Li P-Y, Wang P, Gao S-G, Dong D-Y. *Long noncoding RNA SOX2-OT: regulations, functions, and roles on mental illnesses, cancers, and diabetic complications.* BioMed Research International. 2020;2020.

418. Shahryari A, Jazi MS, Samaei NM, Mowla SJ. *Long non-coding RNA SOX2OT: expression signature, splicing patterns, and emerging roles in pluripotency and tumorigenesis.* Frontiers in genetics. 2015;**6**:196.

419. Arun G, Diermeier SD, Spector DL. *Therapeutic targeting of long non-coding RNAs in cancer. Trends in molecular medicine*. 2018;**24**(3):257-77.

420. Thompson NA, Ranzani M, van der Weyden L, Iyer V, Offord V, Droop A, et al. *Combinatorial CRISPR screen identifies fitness effects of gene paralogues.* Nature communications. 2021;**12**(1):1302.

421. Hsieh M-H, Choe JH, Gadhvi J, Kim YJ, Arguez MA, Palmer M, et al. *p63 and SOX2 dictate glucose reliance and metabolic vulnerabilities in squamous cell carcinomas*. Cell reports. 2019;**28**(7):1860-78. e9.

422. Wu D, Pang Y, Wilkerson M, Wang D, Hammerman P, Liu J. *Gene-expression data integration to squamous cell lung cancer subtypes reveals drug sensitivity.* British journal of cancer. 2013;**109**(6):1599-608.

423. Gonçalves E, Poulos RC, Cai Z, Barthorpe S, Manda SS, Lucas N, et al. *Pan-cancer proteomic map of 949 human cell lines.* Cancer Cell. 2022;**40**(8):835-49. e8.

424. Tatsumori T, Tsuta K, Masai K, Kinno T, Taniyama T, Yoshida A, et al. *p40 is the best marker for diagnosing pulmonary squamous cell carcinoma: comparison with p63, cytokeratin 5/6, desmocollin-3, and sox2.* Applied Immunohistochemistry & Molecular Morphology. 2014;**22**(5):377-82.

425. Hüser L, Novak D, Umansky V, Altevogt P, Utikal J. *Targeting SOX2 in anticancer therapy.* Expert opinion on therapeutic targets. 2018;**22**(12):983-91.

426. Fang Y, Liao G, Yu B. *LSD1/KDM1A inhibitors in clinical trials: advances and prospects*. Journal of hematology & oncology. 2019;**12**(1):1-14.

427. Noce B, Di Bello E, Fioravanti R, Mai A. *LSD1 inhibitors for cancer treatment: Focus on multi-target agents and compounds in clinical trials.* Frontiers in Pharmacology. 2023;**14**:1120911.

428. Salamero O, Montesinos P, Willekens C, Pérez-Simón JA, Pigneux A, Récher C, et al. *First-in-human phase I study of Iadademstat (ORY-1001): a first-in-class lysine-specific histone demethylase 1A inhibitor, in relapsed or refractory acute myeloid leukemia*. Journal of Clinical Oncology.2020 **38**(36) 4260.

429. Cuyàs E, Gumuzio J, Verdura S, Brunet J, Bosch-Barrera J, Martin-Castillo B, et al. *The LSD1 inhibitor iadademstat (ORY-1001) targets SOX2-driven breast cancer stem cells: a potential epigenetic therapy in luminal-B and HER2-positive breast cancer subtypes*. Aging (Albany NY). 2020;**12**(6):4794.

430. Zhang X, Lu F, Wang J, Yin F, Xu Z, Qi D, et al*. Pluripotent stem cell protein Sox2 confers sensitivity to LSD1 inhibition in cancer cells.* Cell reports. 2013;**5**(2):445-57.

431. Soucy TA, Dick LR, Smith PG, Milhollen MA, Brownell JE. *The NEDD8 conjugation pathway and its relevance in cancer biology and therapy.* Genes & cancer. 2010;**1**(7):708-16.

432. Foster JH, Barbieri E, Zhang L, Scorsone KA, Moreno-Smith M, Zage P, et al. *The Anti-Tumor Activity of the NEDD8 Inhibitor Pevonedistat in Neuroblastoma.* International Journal of Molecular Sciences. 2021;**22**(12):6565.

433. Ferris J, Espona-Fiedler M, Hamilton C, Holohan C, Crawford N, McIntyre AJ, et al. *Pevonedistat (MLN4924): mechanism of cell death induction and therapeutic potential in colorectal cancer.* Cell death discovery. 2020;**6**(1):1-14.

434. Xu J, Li Z, Zhuo Q, Ye Z, Fan G, Gao H, et al. *Pevonedistat Suppresses Pancreatic Cancer Growth via Inactivation of the Neddylation Pathway.* Frontiers in Oncology. 2022;**12**:822039

435. Sekeres MA, Watts J, Radinoff A, Sangerman MA, Cerrano M, Lopez PF, et al. *Randomized phase 2 trial of pevonedistat plus azacitidine versus azacitidine for higher-risk MDS/CMML or low-blast AML*. Leukemia. 2021;**35**(7):2119-24.

436. Swords RT, Coutre S, Maris MB, Zeidner JF, Foran JM, Cruz J, et al. *Pevonedistat, a first-in-class NEDD8-activating enzyme inhibitor, combined with azacitidine in patients with AML*. Blood, The Journal of the American Society of Hematology. 2018;**131**(13):1415-24.

437. Bauer TM, Harvey RD, Lee CB, Aggarwal C, Cohen RB, Sedarati F, et al. *Investigational NEDD8-activating enzyme inhibitor pevonedistat (Pev) plus chemotherapy in patients (Pts) with solid tumors (Phase 1b study): Antitumor activity of pev plus carboplatin (Carbo)/paclitaxel (Pac).* American Society of Clinical Oncology; 2016: 2580

438. Yin Y, Xie C-M, Li H, Tan M, Chen G, Schiff R, et al. *The FBXW2–MSX2–SOX2 axis regulates stem cell property and drug resistance of cancer cells.* Proceedings of the National Academy of Sciences. 2019;**116**(41):20528-38.

439. Sava GP, Fan H, Coombes RC, Buluwela L, Ali S. *CDK7 inhibitors as anticancer drugs.* Cancer and Metastasis Reviews. 2020;**39**(3):805-23.

440. Olson CM, Liang Y, Leggett A, Park WD, Li L, Mills CE, et al. *Development of a selective CDK7 covalent inhibitor reveals predominant cell-cycle phenotype.* Cell chemical biology. 2019;**26**(6):792-803. e10.

441. Cheng Z-J, Miao D-L, Su Q-Y, Tang X-L, Wang X-L, Deng L-B, et al. *THZ1 suppresses human non-small-cell lung cancer cells in vitro through interference with cancer metabolism.* Acta Pharmacologica Sinica. 2019;**40**(6):814-22.

442. Wang J, Zhang R, Lin Z, Zhang S, Chen Y, Tang J, et al. *CDK7 inhibitor THZ1 enhances antiPD-1 therapy efficacy via the p38α/MYC/PD-L1 signaling in non-small cell lung cancer.* Journal of hematology & oncology. 2020;**13**(1):1-16.

443. Hur JY, Kim HR, Lee JY, Park S, Hwang JA, Kim WS, et al. *CDK7 inhibition as a promising therapeutic strategy for lung squamous cell carcinomas with a SOX2 amplification*. Cellular Oncology. 2019;**42**(4):449-58.

444. Coombes RC, Howell S, Lord SR, Kenny L, Mansi J, Mitri Z, et al. *Dose escalation and expansion cohorts in patients with advanced breast cancer in a Phase I study of the CDK7-inhibitor samuraciclib.* Nature communications. 2023;**14**(1):4444.

445. Bashir B, Sharma M, Juric D, Papadopoulos KP, Hamilton EP, Richardson DL, et al. *Phase 1/1b study of SY-5609, a selective and potent CDK7 inhibitor, in advanced solid tumors and in 2L/3L pancreatic ductal adenocarcinoma (PDAC) in combination with gemcitabine+/-nab-paclitaxel*. American Society of Clinical Oncology; 2023:3080

446. Juric D, Richardson DL, Bashir B, Sharma M, Papadopoulos KP, Mathews S, et al. *Tolerability and preliminary activity of the potent, selective, oral CDK7 inhibitor SY-5609 in combination with fulvestrant in patients with advanced hormone receptor-positive (HR+), HER2-breast cancer (BC).* American Society of Clinical Oncology; 2023:3081

447. Donati B, Lorenzini E, Ciarrocchi A. *BRD4 and Cancer: going beyond transcriptional regulation.* Molecular cancer. 2018;**17**(1):164.

448. Liu W, Stein P, Cheng X, Yang W, Shao N, Morrisey E, et al. *BRD4 regulates Nanog expression in mouse embryonic stem cells and preimplantation embryos.* Cell Death & Differentiation. 2014;**21**(12):1950-60.

449. Wu T, Pinto HB, Kamikawa YF, Donohoe ME. *The BET family member BRD4 interacts with OCT4 and regulates pluripotency gene expression.* Stem cell reports. 2015;**4**(3):390-403.

450. Im JH, Hwang SI, Kim J-W, Park S-J, Kang K-r, You JS, et al. *Inhibition of BET selectively eliminates undifferentiated pluripotent stem cells*. Science Bulletin. 2018;**63**(8):477-87.

451. Alghamdi S, Khan I, Beeravolu N, McKee C, Thibodeau B, Wilson G, et al. *BET protein inhibitor JQ1 inhibits growth and modulates WNT signaling in mesenchymal stem cells.* Stem Cell Research & Therapy. 2016;**7**(1):1-16.

452. Horne GA, Stewart HJ, Dickson J, Knapp S, Ramsahoye B, Chevassut T. *Nanog requires BRD4 to maintain murine embryonic stem cell pluripotency and is suppressed by bromodomain inhibitor JQ1 together with Lefty1.* Stem Cells and Development. 2015;**24**(7):879-91.

453. Liu Y, Wu Z, Zhou J, Ramadurai DK, Mortenson KL, Aguilera-Jimenez E, et al. *A predominant enhancer co-amplified with the SOX2 oncogene is necessary and sufficient for its expression in squamous cancer*. Nature Communications. 2021;**12**(1):7139.

454. Wang R, Liu W, Helfer CM, Bradner JE, Hornick JL, Janicki SM, et al. *Activation of SOX2 expression by BRD4-NUT oncogenic fusion drives neoplastic transformation in NUT midline carcinoma.* Cancer research. 2014;**74**(12):3332-43.

455. Kasiri S, Shao C, Chen B, Wilson AN, Yenerall P, Timmons BC, et al. *GLI1 blockade potentiates the antitumor activity of PI3K antagonists in lung squamous cell carcinoma.* Cancer research. 2017;**77**(16):4448-59.

456. Bora-Singhal N, Perumal D, Nguyen J, Chellappan S. *Gli1-mediated regulation of Sox2 facilitates self-renewal of stem-like cells and confers resistance to EGFR inhibitors in non–small cell lung cancer.* Neoplasia. 2015;**17**(7):538-51.

457. Pietrobono S, Gaudio E, Gagliardi S, Zitani M, Carrassa L, Migliorini F, et al. *Targeting non-canonical activation of GLI1 by the SOX2-BRD4 transcriptional complex improves the efficacy of HEDGEHOG pathway inhibition in melanoma.* Oncogene. 2021;**40**(22):3799-814.

458. Pietrobono S, Anichini G, Sala C, Manetti F, Almada LL, Pepe S, et al. *ST3GAL1 is a target of the SOX2-GLI1 transcriptional complex and promotes melanoma metastasis through AXL.* Nature communications. 2020;**11**(1):1-18.

459. Kar S, Sengupta D, Deb M, Pradhan N, Patra SK. *SOX2 function and Hedgehog signaling pathway are co-conspirators in promoting androgen independent prostate cancer*. Biochimica et Biophysica Acta (BBA)-Molecular Basis of Disease. 2017;**1863**(1):253-65.

460. Beauchamp EM, Ringer L, Bulut G, Sajwan KP, Hall MD, Lee Y-C, et al. *Arsenic trioxide inhibits human cancer cell growth and tumor development in mice by blocking Hedgehog/GLI pathway*. The Journal of clinical investigation. 2011;**121**(1):148-60.

461. Kim J, Lee JJ, Kim J, Gardner D, Beachy PA. *Arsenic antagonizes the Hedgehog pathway by preventing ciliary accumulation and reducing stability of the Gli2 transcriptional effector.* Proceedings of the National Academy of Sciences. 2010;**107**(30):13432-7.

462. Tang Y, Gholamin S, Schubert S, Willardson MI, Lee A, Bandopadhayay P, et al. *Epigenetic targeting of Hedgehog pathway transcriptional output through BET bromodomain inhibition*. Nature medicine. 2014;**20**(7):732-40.

463. Shorstova T, Foulkes WD, Witcher M. *Achieving clinical success with BET inhibitors as anti-cancer agents.* British journal of cancer. 2021;**124**(9):1478-90.

464. Rhyasen GW, Hattersley MM, Yao Y, Dulak A, Wang W, Petteruti P, et al. *AZD5153: a novel bivalent BET bromodomain inhibitor highly active against hematologic malignancies. Molecular cancer therapeutics*. 2016;**15**(11):2563-74.

465. Xu K, Chen D, Qian D, Zhang S, Zhang Y, Guo S, et al. *AZD5153, a novel BRD4 inhibitor, suppresses human thyroid carcinoma cell growth in vitro and in vivo. Biochemical and biophysical research communications*. 2018;**499**(3):531-7.

466. Shen G, Chen J, Zhou Y, Wang Z, Ma Z, Xu C, et al. *AZD5153 inhibits prostate cancer cell growth in vitro and in vivo.* Cellular Physiology and Biochemistry. 2018;**50**(2):798-809.

467. Wang JS-Z, De Vita S, Karlix JL, Cook C, Littlewood GM, Hattersley MM, et al. *First-in-human study of AZD5153, a small molecule inhibitor of bromodomain protein 4 (BRD4), in patients (pts) with relapsed/refractory (RR) malignant solid tumor and lymphoma: Preliminary data*. American Society of Clinical Oncology; 2019: 3085

468. Foshay KM, Gallicano GI. *Regulation of Sox2 by STAT3 initiates commitment to the neural precursor cell fate. Stem cells and development*. 2008;**17**(2):269-78.

469. Zhang S, Xiong X, Sun Y. *Functional characterization of SOX2 as an anticancer target. Signal transduction and targeted therapy.* 2020;**5**(1):135.

470. Wang H, Deng J, Ren H-Y, Jia P, Zhang W, Li MQ, et al. *STAT3 influences the characteristics of stem cells in cervical carcinoma.* Oncology letters. 2017;**14**(2):2131-6.

471. Chung SS, Giehl N, Wu Y, Vadgama JV. *STAT3 activation in HER2-overexpressing breast cancer promotes epithelial-mesenchymal transition and cancer stem cell traits. International journal of oncology.* 2014;**44**(2):403-11.

472. Han D, Yu T, Dong N, Wang B, Sun F, Jiang D. *Napabucasin, a novel STAT3 inhibitor suppresses proliferation, invasion and stemness of glioblastoma cells.* Journal of Experimental & Clinical Cancer Research. 2019;**38**(1):1-12.

473. Liu X, Huang J, Xie Y, Zhou Y, Wang R, Lou J. *Napabucasin attenuates resistance of breast cancer cells to tamoxifen by reducing stem cell-like properties*. Medical Science Monitor: International Medical Journal of Experimental and Clinical Research. 2019;**25**:8905.

474. MacDonagh L, Gray SG, Breen E, Cuffe S, Finn SP, O'Byrne KJ, et al. *BBI608 inhibits cancer stemness and reverses cisplatin resistance in NSCLC*. Cancer Letters. 2018;**428**:117-26.

475. Liu K, Jiang M, Lu Y, Chen H, Sun J, Wu S, et al. *Sox2 cooperates with inflammation-mediated Stat3 activation in the malignant transformation of foregut basal progenitor cells.* Cell stem cell. 2013;**12**(3):304-15

476. Marineau JJ, Hamman KB, Hu S, Alnemy S, Mihalich J, Kabro A, et al. Discovery of SY-5609: a selective, noncovalent inhibitor of CDK7. Journal of Medicinal Chemistry. 2021;65(2):1458-80.

477. Hamilton EP, Wang JS, Oza AM, Patel MR, Ulahannan SV, Bauer T, et al. *First-in-human Study of AZD5153, A Small-molecule Inhibitor of Bromodomain Protein 4, in Patients with Relapsed/Refractory Malignant Solid Tumors and Lymphoma.* Molecular Cancer Therapeutics. 2023;**22**(10):1154-65.

478. Fritsch C, Huang A, Chatenay-Rivauday C, Schnell C, Reddy A, Liu M, et al. *Characterization of the novel and specific PI3Kα inhibitor NVP-BYL719 and development of the patient stratification strategy for clinical trials.* Molecular cancer therapeutics. 2014;**13**(5):1117-29.

479. Davies BR, Greenwood H, Dudley P, Crafter C, Yu D-H, Zhang J, et al. *Preclinical pharmacology of AZD5363, an inhibitor of AKT: pharmacodynamics, antitumor activity, and correlation of monotherapy activity with genetic background.* Molecular cancer therapeutics. 2012;**11**(4):873-87.

480. Okusaka T, Morimoto M, Eguchi Y, Nakamura S, Iino S, Kageyama R. *A Phase I Study to Investigate the Safety, Tolerability and Pharmacokinetics of Napabucasin Combined with Sorafenib in Japanese Patients with Unresectable Hepatocellular Carcinoma.* Drugs in R&D. 2023:1-9.

481. Zhang W, Ge H, Jiang Y, Huang R, Wu Y, Wang D, et al. *Combinational therapeutic targeting of BRD4 and CDK7 synergistically induces anticancer effects in head and neck squamous cell carcinoma.* Cancer Letters. 2020;**469**:510-23.

482. Lovén J, Hoke HA, Lin CY, Lau A, Orlando DA, Vakoc CR, et al. *Selective inhibition of tumor oncogenes by disruption of super-enhancers.* Cell. 2013;**153**(2):320-34.

483. Chipumuro E, Marco E, Christensen CL, Kwiatkowski N, Zhang T, Hatheway CM, et al. *CDK7 inhibition suppresses super-enhancer-linked oncogenic transcription in MYCN-driven cancer*. Cell. 2014;**159**(5):1126-39.

484. Ormsbee Golden BD, Wuebben EL, Rizzino A. *Sox2 expression is regulated by a negative feedback loop in embryonic stem cells that involves AKT signaling and FoxO1*. PloS one. 2013;**8**(10):e76345.

485. Gao Z, Cox JL, Gilmore JM, Ormsbee BD, Mallanna SK, Washburn MP, et al. *Determination of protein interactome of transcription factor Sox2 in embryonic stem cells engineered for inducible expression of four reprogramming factors.* Journal of Biological Chemistry. 2012;**287**(14):11384-97.

486. Julian LM, Vandenbosch R, Pakenham CA, Andrusiak MG, Nguyen AP, McClellan KA, et al*. Opposing regulation of Sox2 by cell-cycle effectors E2f3a and E2f3b in neural stem cells.* Cell stem cell. 2013;**12**(4):440-52.

487. Garros-Regulez L, Garcia I, Carrasco-Garcia E, Lantero A, Aldaz P, Moreno-Cugnon L, et al. *Targeting SOX2 as a therapeutic strategy in glioblastoma.* Frontiers in oncology. 2016;**6**:222.

488. Dey A, Kundu M, Das S, Jena BC, Mandal M. *Understanding the function and regulation of Sox2 for its therapeutic potential in breast cancer.* Biochimica et Biophysica Acta (BBA)-Reviews on Cancer. 2022;**1877**(2):188692.

489. Genolet O, Ravid Lustig L, Schulz EG. *Dissecting molecular phenotypes through FACS-based pooled CRISPR screens.* Embryonic Stem Cell Protocols: Springer; 2022. p. 1-24.

490. Fomicheva M, Macara IG. *Genome-wide CRISPR screen identifies noncanonical NF-κB signaling as a regulator of density-dependent proliferation*. Elife. 2020;**9:**e63603.

491. Gu SS, Zhang W, Wang X, Jiang P, Traugh N, Li Z, et al. *Therapeutically increasing MHC-I expression potentiates immune checkpoint blockade.* Cancer discovery. 2021;**11**(6):1524-41.

492. de Almeida M, Hinterndorfer M, Brunner H, Grishkovskaya I, Singh K, Schleiffer A, et al. *AKIRIN2 controls the nuclear import of proteasomes in vertebrates*. Nature. 2021;**599**(7885):491-6.

493. Kim G, Nakayama L, Blum JA, Akiyama T, Boeynaems S, Chakraborty M, et al. *Genome-wide CRISPR screen reveals v-ATPase as a drug target to lower levels of ALS protein ataxin-2.* Cell reports. 2022;**41**(4).

494. Menasche BL, Crisman L, Gulbranson DR, Davis EM, Yu H, Shen J. *Fluorescence activated cell sorting (FACS) in genome-wide genetic screening of membrane trafficking.* Current protocols in cell biology. 2019;**82**(1):e68.

495. Park JS, Helble JD, Lazarus JE, Yang G, Blondel CJ, Doench JG, et al. *A FACS-based genome-wide CRISPR screen reveals a requirement for COPI in Chlamydia trachomatis invasion.* IScience. 2019;**11**:71-84.

496. Wu T, Wang Y, Xiao T, Ai Y, Li J, Zeng YA, et al. *Lentiviral CRISPR-guided RNA library screening identified Adam17 as an upstream negative regulator of Procr in mammary epithelium.* BMC biotechnology. 2021;**21**(1):1-8.

497. Condon KJ, Orozco JM, Adelmann CH, Spinelli JB, van der Helm PW, Roberts JM, et al. *Genome-wide CRISPR screens reveal multitiered mechanisms through which mTORC1 senses mitochondrial dysfunction.* Proceedings of the National Academy of Sciences. 2021;**118**(4):e2022120118.

498. Wang B, Wang M, Zhang W, Xiao T, Chen C-H, Wu A, et al. *Integrative analysis of pooled CRISPR genetic screens using MAGeCKFlute.* Nature protocols. 2019;**14**(3):756-80.

499. van den Boom J, Meyer H. *VCP/p97-mediated unfolding as a principle in protein homeostasis and signaling.* Molecular cell. 2018;**69**(2):182-94.

500. Costantini S, Capone F, Polo A, Bagnara P, Budillon A. *Valosin-Containing protein (VCP)/p97: a prognostic biomarker and therapeutic target in cancer*. International journal of molecular sciences. 2021;**22**(18):10177.

501. Zhang LX, Yang X, Wu ZB, Liao ZM, Wang DG, Chen SW, et al. *TTI1 promotes non-small-cell lung cancer progression by regulating the mTOR signaling pathway.* Cancer Science. 2023; **11**(3):855

502. Wang S-C. *PCNA: a silent housekeeper or a potential therapeutic target? Trends in pharmacological sciences*. 2014;**35**(4):178-86.

503. Witko-Sarsat V, Mocek J, Bouayad D, Tamassia N, Ribeil J-A, Candalh C, et al. *Proliferating cell nuclear antigen acts as a cytoplasmic platform controlling human neutrophil survival.* Journal of Experimental Medicine. 2010;**207**(12):2631-45.

504. Naryzhny SN, Lee H. *Proliferating cell nuclear antigen in the cytoplasm interacts with components of glycolysis and cancer.* FEBS letters. 2010;**584**(20):4292-8.

505. Olaisen C, Müller R, Nedal A, Otterlei M. *PCNA-interacting peptides reduce Akt phosphorylation and TLR-mediated cytokine secretion suggesting a role of PCNA in cellular signaling.* Cellular Signalling. 2015;**27**(7):1478-87.

506. Rosental B, Brusilovsky M, Hadad U, Oz D, Appel MY, Afergan F, et al. *Proliferating cell nuclear antigen is a novel inhibitory ligand for the natural cytotoxicity receptor NKp44.* The Journal of Immunology. 2011;**187**(11):5693-702.

507. Wang L, Kong W, Liu B, Zhang X. *Proliferating cell nuclear antigen promotes cell proliferation and tumorigenesis by up-regulating STAT3 in non-small cell lung cancer.* Biomedicine & Pharmacotherapy. 2018;**104**:595-602.

508. Fan J, Zhou X, Huang J, Wang X, Che G. *Prognostic roles of PCNA expressions in non-small cell lung cancer: a meta-analysis.* Int J Clin Exp Med. 2016;**9**(3):5655-65.

509. Fujii M, Motoi M, Saeki H, Aoe K, Moriwaki S. *Prognostic significance of proliferating cell nuclear antigen (PCNA) expression in non-small cell lung cancer.* Acta Medica Okayama. 1993;**47**(2):103-8.

510. Gilljam KM, Feyzi E, Aas PA, Sousa MM, Müller R, Vågbø CB, et al. *Identification of a novel, widespread, and functionally important PCNA-binding motif.* Journal of Cell Biology. 2009;**186**(5):645-54.

511. Müller R, Misund K, Holien T, Bachke S, Gilljam KM, Våtsveen TK, et al. *Targeting proliferating cell nuclear antigen and its protein interactions induces apoptosis in multiple myeloma cells.* PloS one. 2013;**8**(7):e70430.

512. Søgaard CK, Blindheim A, Røst LM, Petrović V, Nepal A, Bachke S, et al. *"Two hits-one stone"; increased efficacy of cisplatin-based therapies by targeting PCNA's role in both DNA repair and cellular signaling*. Oncotarget. 2018;**9**(65):32448.

513. Søgaard CK, Moestue SA, Rye MB, Kim J, Nepal A, Liabakk N-B, et al. *APIM-peptide targeting PCNA improves the efficacy of docetaxel treatment in the TRAMP mouse model of prostate cancer.* Oncotarget. 2018;**9**(14):11752.

514. Gederaas OA, Søgaard CD, Viset T, Bachke S, Bruheim P, Arum C-J, et al. *Increased anticancer efficacy of intravesical mitomycin C therapy when combined with a PCNA targeting peptide*. Translational Oncology. 2014;**7**(6):812-23.

515. Gravina GL, Colapietro A, Mancini A, Rossetti A, Martellucci S, Ventura L, et al. *ATX-101, a peptide targeting PCNA, has antitumor efficacy alone or in combination with radiotherapy in murine models of human glioblastoma.* Cancers. 2022;**14**(2):289.

516. Lemech CR, Kichenadasse G, Marschner J-P, Alevizopoulos K, Otterlei M, Millward M. *ATX-101, a cell-penetrating protein targeting PCNA, can be safely administered as intravenous infusion in patients and shows clinical activity in a Phase 1 study.* Oncogene. 2023;**42**(7):541-4.

517. Gu L, Lingeman R, Yakushijin F, Sun E, Cui Q, Chao J, et al. *The Anticancer Activity of a First-in-Class Small-Molecule Targeting PCNA*. Clinical Cancer Research. 2018;**24**(23):6053-65.

518. Shen F, Hickey R, Kamran J, Phipps EA, Malkas LH. *Expression of caPCNA and antineoplastic action of caPeptides in pancreatic cancer cells.* Cancer Research. 2010;70(8_Supplement):1597

519. Malkas LH, Herbert BS, Abdel-Aziz W, Dobrolecki LE, Liu Y, Agarwal B, et al. *A cancer-associated PCNA expressed in breast cancer has implications as a potential biomarker*. Proceedings of the National Academy of Sciences. 2006;**103**(51):19472-7.

520. Wang X, Hickey RJ, Malkas LH, Koch MO, Li L, Zhang S, et al. *Elevated expression of cancer-associated proliferating cell nuclear antigen in high-grade prostatic intraepithelial neoplasia and prostate cancer.* The Prostate. 2011;**71**(7):748-54.

521. Gu L, Li M, Li CM, Haratipour P, Lingeman R, Jossart J, et al. *Small molecule targeting of transcription-replication conflict for selective chemotherapy.* Cell chemical biology. 2023;**30**(10):1235-47. e6.

522. Chiaradonna F, Ricciardiello F, Palorini R. *The nutrient-sensing hexosamine biosynthetic pathway as the hub of cancer metabolic rewiring.* Cells. 2018;**7**(6):53.

523. Akella NM, Ciraku L, Reginato MJ. *Fueling the fire: emerging role of the hexosamine biosynthetic pathway in cancer.* BMC biology. 2019;**17**(1):1-14.

524. Kim DK, Lee J-S, Lee EY, Jang H, Han S, Kim HY, et al. *O-GlcNAcylation of Sox2 at threonine 258 regulates the self-renewal and early cell fate of embryonic stem cells*. Experimental & Molecular Medicine. 2021;**53**(11):1759-68.

525. Sharma NS, Gupta VK, Dauer P, Kesh K, Hadad R, Giri B, et al. *O-GlcNAc modification of Sox2 regulates self-renewal in pancreatic cancer by promoting its stability.* Theranostics. 2019;**9**(12):3410.

526. Cao B, Duan M, Xing Y, Liu C, Yang F, Li Y, et al. *O-GlcNAc transferase activates stem-like cell potential in hepatocarcinoma through O-GlcNAcylation of eukaryotic initiation factor 4E.* Journal of Cellular and Molecular Medicine. 2019;**23**(4):2384-98.

527. Kang M-S, Kim J, Ryu E, Ha NY, Hwang S, Kim B-G, et al. *PCNA unloading is negatively regulated by BET proteins.* Cell reports. 2019;**29**(13):4632-45. e5.

528. Yamamoto S, Tomita Y, Hoshida Y, Iizuka N, Monden M, Yamamoto S, et al. *Expression level of valosin-containing protein (p97) is correlated with progression and prognosis of non-small-cell lung carcinoma.* Annals of surgical oncology. 2004;**11**:697-704.

529. Valle CW, Min T, Bodas M, Mazur S, Begum S, Tang D, et al. *Critical role of VCP/p97 in the pathogenesis and progression of non-small cell lung carcinoma.* PloS one. 2011;**6**(12):e29073.

530. Fu Q, Jiang Y, Zhang D, Liu X, Guo J, Zhao J. *Valosin-containing protein (VCP) promotes the growth, invasion, and metastasis of colorectal cancer through activation of STAT3 signaling.* Molecular and cellular biochemistry. 2016;**418**:189-98.

531. Lee YS, Klomp JE, Stalnecker CA, Goodwin CM, Gao Y, Droby GN, et al. *VCP/p97, a pleiotropic protein regulator of the DNA damage response and proteostasis, is a potential therapeutic target in KRAS-mutant pancreatic cancer.* Genes & Cancer. 2023;**14**:30.

532. Li AA, Zhang Y, Li F, Zhou Y, Liu ZL, Long XH. *The mechanism of VCP-mediated metastasis of osteosarcoma based on cell autophagy and the EMT pathway*. Clinical and Translational Oncology. 2023;**25**(3):653-61.

533. Li C, Huang Y, Fan Q, Quan H, Dong Y, Nie M, et al. *p97/VCP is highly expressed in the stem-like cells of breast cancer and controls cancer stemness partly through the unfolded protein response.* Cell Death & Disease. 2021;**12**(4):286.

534. McHugh A, Fernandes K, Chinner N, Ibrahim AF, Garg AK, Boag G, et al. *The identification of potential therapeutic targets for cutaneous squamous cell carcinoma.* Journal of Investigative Dermatology. 2020;**140**(6):1154-65. e5.

535. Kilgas S, Ramadan K. *Inhibitors of the ATPase p97/VCP: From basic research to clinical applications.* Cell Chemical Biology. 2023.

536. Anderson DJ, Le Moigne R, Djakovic S, Kumar B, Rice J, Wong S, et al. *Targeting the AAA ATPase p97 as an approach to treat cancer through disruption of protein homeostasis*. Cancer cell. 2015;**28**(5):653-65

537. Leinonen H, Cheng C, Pitkänen M, Sander CL, Zhang J, Saeid S, et al. *A p97/valosin-containing protein inhibitor drug CB-5083 has a potent but reversible off-target effect on phosphodiesterase-6.* Journal of Pharmacology and Experimental Therapeutics. 2021;**378**(1):31-41.

538. Roux B, Vaganay C, Vargas JD, Alexe G, Benaksas C, Pardieu B, et al. *Targeting acute myeloid leukemia dependency on VCP-mediated DNA repair through a selective second-generation small-molecule inhibitor.* Science translational medicine. 2021;**13**(587):eabg1168.

539. Benajiba L, Carraway HE, Hamad N, Stein EM, Yannakou CK, Burroughs A, et al. *Trials in Progress: A Phase I Study to Evaluate the Safety and Pharmacokinetic Profiles of CB-5339 in Participants with Relapsed/Refractory Acute Myeloid Leukemia or Relapsed/Refractory Intermediate or High-Risk Myelodysplastic Syndrome*. Blood. 2020;**136**:21.

540. Sahai E, Marshall CJ. *RHO–GTPases and cancer*. Nature Reviews Cancer. 2002;**2**(2):133-42.

541. Yoon C, Cho S-J, Aksoy BA, Park DJ, Schultz N, Ryeom SW, et al. *Chemotherapy resistance in diffuse-type gastric adenocarcinoma is mediated by RhoA activation in cancer stem-like cells.* Clinical cancer research. 2016;**22**(4):971-83.

542. Liu X, Chen D, Liu G. *Overexpression of RhoA promotes the proliferation and migration of cervical cancer cells.* Bioscience, biotechnology, and biochemistry. 2014;**78**(11):1895-901.

543. Wu M, Wu Zf, Rosenthal DT, Rhee EM, Merajver SD. *Characterization of the roles of RHOC and RHOA GTPases in invasion, motility, and matrix adhesion in inflammatory and aggressive breast cancers.* Cancer. 2010;**116**(S11):2768-82.

544. Yang X, Zheng F, Zhang S, Lu J. *Loss of RhoA expression prevents proliferation and metastasis of SPCA1 lung cancer cells in vitro.* Biomedicine & Pharmacotherapy. 2015;**69**:361-6.

545. Beak M, Park S, Kim J-H, Eom HJ, Lee H-Y, Kim YH, et al. *Second-Generation JK-206 Targets the Oncogenic Signal Mediator RHOA in Gastric Cancer*. Cancers. 2022;**14**(7):1604.

546. Yoon C, Cho S-J, Aksoy BA, Park DJ, Schultz N, Ryeom SW, et al. *Chemotherapy Resistance in Diffuse-Type Gastric Adenocarcinoma Is Mediated by RhoA Activation in Cancer Stem-Like CellsRhoA in Diffuse Gastric Cancer Stem-Like Cells.* Clinical cancer research. 2016;**22**(4):971-83.

547. Sadek CM, Damdimopoulos AE, Pelto-Huikko M, Gustafsson JÅ, Spyrou G, Miranda-Vizuete A. *Sptrx-2, a fusion protein composed of one thioredoxin and three tandemly repeated NDP-kinase domains is expressed in human testis germ cells.* Genes to Cells. 2001;**6**(12):1077-90.

548. Reza E, Azizi H, Skutella T. *Sox2 localization during spermatogenesis and its association with other spermatogenesis markers using protein-protein network analysis*. Journal of Reproduction & Infertility. 2023;**24**(3):171.

549. Karikalan B, Chakravarthi S. *Primary Ciliary Dyskinesia-An Update on the Genetics of Underlying Pathological Mechanisms. Current Respiratory Medicine Reviews.* 2023;**19**(3):190-201.

550. Hart T, Tong AHY, Chan K, Van Leeuwen J, Seetharaman A, Aregger M, et al. *Evaluation and design of genome-wide CRISPR/SpCas9 knockout screens.* G3: Genes, Genomes, Genetics. 2017;**7**(8):2719-27.

551. Chang L, Ruiz P, Ito T, Sellers WR. *Targeting pan-essential genes in cancer: challenges and opportunities*. Cancer cell. 2021;**39**(4):466-79.

552. Meric-Bernstam F, Ford JM, O'Dwyer PJ, Shapiro GI, McShane LM, Freidlin B, et al. *National Cancer Institute Combination Therapy Platform Trial with Molecular Analysis for Therapy Choice (ComboMATCH).* Clinical Cancer Research. 2023;**29**(8):1412-22.

553. O'Dwyer PJ, Gray RJ, Flaherty KT, Chen AP, Li S, Wang V, et al. *The NCI-MATCH trial: lessons for precision oncology*. Nature Medicine. 2023:1-9.

554. Wang X, Ricciuti B, Nguyen T, Li X, Rabin MS, Awad MM, et al. *Association between smoking history and tumor mutation burden in advanced non–small cell lung cancer*. Cancer research. 2021;**81**(9):2566-73.

555. Singal G, Miller PG, Agarwala V, Li G, Kaushik G, Backenroth D, et al. *Association of patient characteristics and tumor genomics with clinical outcomes among patients with non–small cell lung cancer using a clinicogenomic database.* Jama. 2019;**321**(14):1391-9.

556. Willis C, Fiander M, Tran D, Korytowsky B, Thomas J-M, Calderon F, et al. *Tumor mutational burden in lung cancer: a systematic literature review.* Oncotarget. 2019;**10**(61):6604.

557. Jamal-Hanjani M, Wilson GA, McGranahan N, Birkbak NJ, Watkins TB, Veeriah S, et al. *Tracking the evolution of non–small-cell lung cancer.* New England Journal of Medicine. 2017;**376**(22):2109-21.

558. Al Bakir M, Huebner A, Martínez-Ruiz C, Grigoriadis K, Watkins TB, Pich O, et al. *The evolution of non-small cell lung cancer metastases in TRACERx*. Nature. 2023:1-10.

559. Reizine NM, O'Donnell PH. *Modern developments in germline pharmacogenomics for oncology prescribing.* CA: A Cancer Journal for Clinicians. 2022;**72**(4):315-32.

560. Tutt AN, Garber JE, Kaufman B, Viale G, Fumagalli D, Rastogi P, et al. *Adjuvant olaparib for patients with BRCA1-or BRCA2-mutated breast cancer.* New England Journal of Medicine. 2021;**384**(25):2394-405.

561. Hoskins JM, Carey LA, McLeod HL. *CYP2D6 and tamoxifen: DNA matters in breast cancer.* Nature Reviews Cancer. 2009;**9**(8):576-86.

562. Berenjeno IM, Piñeiro R, Castillo SD, Pearce W, McGranahan N, Dewhurst SM, et al. *Oncogenic PIK3CA induces centrosome amplification and tolerance to genome doubling.* Nature communications. 2017;**8**(1):1773.

563. Mascini M, Palchetti I, Tombelli S. *Nucleic acid and peptide aptamers: fundamentals and bioanalytical aspects*. Angewandte Chemie International Edition. 2012;**51**(6):1316-32.

564. Liu K, Xie F, Zhao T, Zhang R, Gao A, Chen Y, et al. *Targeting SOX2 protein with peptide aptamers for therapeutic gains against esophageal squamous cell carcinoma.* Molecular therapy. 2020;**28**(3):901-13.

565. Chen Y, Zhang K, Zhang R, Wang Z, Yang L, Zhao T, et al. *Targeting the SOX2/CDP protein complex with a peptide suppresses the malignant progression of esophageal squamous cell carcinoma.* Cell Death Discovery. 2023;**9**(1):399.

566. Zhang Y, Xie X, Yeganeh PN, Lee D-J, Valle-Garcia D, Meza-Sosa KF, et al. *Immunotherapy for breast cancer using EpCAM aptamer tumor-targeted gene knockdown.* Proceedings of the National Academy of Sciences. 2021;**118**(9):e2022830118.

567. Ng EW, Shima DT, Calias P, Cunningham Jr ET, Guyer DR, Adamis AP. *Pegaptanib, a targeted anti-VEGF aptamer for ocular vascular disease.* Nature reviews drug discovery. 2006;**5**(2):123-32.

568. Bates PJ, Laber DA, Miller DM, Thomas SD, Trent JO. *Discovery and development of the G-rich oligonucleotide AS1411 as a novel treatment for cancer.* Experimental and molecular pathology. 2009;**86**(3):151-64.

569. Fang Y, Wang S, Han S, Zhao Y, Yu C, Liu H, et al. *Targeted protein degrader development for cancer: advances, challenges, and opportunities.* Trends in Pharmacological Sciences. 2023;**44**(5):303-17.

570. Zhao L, Zhao J, Zhong K, Tong A, Jia D. *Targeted protein degradation: mechanisms, strategies and application.* Signal Transduction and Targeted Therapy. 2022;**7**(1):113.

571. Liu Z, Hu M, Yang Y, Du C, Zhou H, Liu C, et al. *An overview of PROTACs: a promising drug discovery paradigm.* Molecular Biomedicine. 2022;**3**(1):46.

572. Gao X, Burris III HA, Vuky J, Dreicer R, Sartor AO, Sternberg CN, et al. *Phase 1/2 study of ARV-110, an androgen receptor (AR) PROTAC degrader, in metastatic castration-resistant prostate cancer (mCRPC).* American Society of Clinical Oncology; 2022.17

573. Sasso JM, Tenchov R, Wang D, Johnson LS, Wang X, Zhou QA. *Molecular glues: The adhesive connecting targeted protein degradation to the clinic.* Biochemistry. 2022;**62**(3):601-23.

574. Simonetta KR, Taygerly J, Boyle K, Basham SE, Padovani C, Lou Y, et al. *Prospective discovery of small molecule enhancers of an E3 ligase-substrate interaction.* Nature communications. 2019;**10**(1):1402.

575. Toriki ES, Papatzimas JW, Nishikawa K, Dovala D, Frank AO, Hesse MJ, et al. *Rational chemical design of molecular glue degraders.* ACS Central Science. 2023;**9**(5):915-26.

1. Novello S, Barlesi F, Califano R, Cufer T, Ekman S, Levra MG, et al. Metastatic non-small-cell lung cancer: ESMO Clinical Practice Guidelines for diagnosis, treatment and follow-up. Annals of Oncology. 2016;27:v1-v27.
2. Wooten DJ, Meyer CT, Lubbock AL, Quaranta V, Lopez CF. MuSyC is a consensus framework that unifies multi-drug synergy metrics for combinatorial drug discovery. Nature communications. 2021;12(1):4607.
3. Meyer CT, Wooten DJ, Paudel BB, Bauer J, Hardeman KN, Westover D, et al. Quantifying drug combination synergy along potency and efficacy axes. Cell systems. 2019;8(2):97-108. e16.
4. Brierley JD, Gospodarowicz MK, Wittekind C. TNM classification of malignant tumours: John Wiley & Sons; 2017.
5. Oudkerk M, Devaraj A, Vliegenthart R, Henzler T, Prosch H, Heussel CP, et al. European position statement on lung cancer screening. The Lancet Oncology. 2017;18(12):e754-e66.
6. de Koning HJ, van der Aalst CM, de Jong PA, Scholten ET, Nackaerts K, Heuvelmans MA, et al. Reduced lung-cancer mortality with volume CT screening in a randomized trial. New England journal of medicine. 2020;382(6):503-13.
7. Kramer BS, Berg CD, Aberle DR, Prorok PC. Lung cancer screening with low-dose helical CT: results from the National Lung Screening Trial (NLST). SAGE Publications Sage UK: London, England; 2011. p. 109-11.
8. Crino L, Weder W, Van Meerbeeck J, Felip E. Early stage and locally advanced (non-metastatic) non-small-cell lung cancer: ESMO Clinical Practice Guidelines for diagnosis, treatment and follow-up. Annals of oncology. 2010;21(S 5):v103-v15.
9. Cruz C, Afonso M, Oliveiros B, Pêgo A. Recurrence and risk factors for relapse in patients with non-small cell lung cancer treated by surgery with curative intent. Oncology. 2017;92(6):347-52.
10. Winton T, Livingston R, Johnson D, Rigas J, Johnston M, Butts C, et al. Vinorelbine plus cisplatin vs. observation in resected non–small-cell lung cancer. New England Journal of Medicine. 2005;352(25):2589-97.
11. Lou F, Huang J, Sima CS, Dycoco J, Rusch V, Bach PB. Patterns of recurrence and second primary lung cancer in early-stage lung cancer survivors followed with routine

computed tomography surveillance. The Journal of thoracic and cardiovascular surgery. 2013;145(1):75-82.
12. Demicheli R, Fornili M, Ambrogi F, Higgins K, Boyd JA, Biganzoli E, et al. Recurrence dynamics for non–small-cell lung cancer: effect of surgery on the development of metastases. Journal of Thoracic Oncology. 2012;7(4):723-30.
13. Wu C-F, Fu J-Y, Yeh C-J, Liu Y-H, Hsieh M-J, Wu Y-C, et al. Recurrence risk factors analysis for stage I non-small cell lung cancer. Medicine. 2015;94(32).
14. Al-Kattan K, Sepsas E, Fountain SW, Townsend ER. Disease recurrence after resection for stage I lung cancer. European journal of cardio-thoracic surgery. 1997;12(3):380-4.
15. Pignon J-P, Tribodet H, Scagliotti GV, Douillard J-Y, Shepherd FA, Stephens RJ, et al. Lung adjuvant cisplatin evaluation: a pooled analysis by the LACE Collaborative Group. Database of Abstracts of Reviews of Effects (DARE): Quality-assessed Reviews [Internet]: Centre for Reviews and Dissemination (UK); 2008.
16. Group NM-aC. Adjuvant chemotherapy, with or without postoperative radiotherapy, in operable non-small-cell lung cancer: two meta-analyses of individual patient data. The Lancet. 2010;375(9722):1267-77.
17. Cortés ÁA, Urquizu LC, Cubero JH. Adjuvant chemotherapy in non-small cell lung cancer: state-of-the-art. Translational lung cancer research. 2015;4(2):191.
18. Group IALCTC. Cisplatin-based adjuvant chemotherapy in patients with completely resected non–small-cell lung cancer. New England Journal of Medicine. 2004;350(4):351-60.
19. Douillard J, Rosell R, Delena M, Legroumellec A, Torres A, Carpagano F. Adjuvant Navelbine International Trialist Association (ANITA). Phase III adjuvant vinorelbine and cisplatin versus observation in completely resected non-small–cell lung cancer patients: final results after 70-month median follow-up. J Clin Oncol. 2005;23:A7013.
20. Felip E, Altorki N, Zhou C, Csőszi T, Vynnychenko I, Goloborodko O, et al. Adjuvant atezolizumab after adjuvant chemotherapy in resected stage IB–IIIA non-small-cell lung cancer (IMpower010): A randomised, multicentre, open-label, phase 3 trial. The Lancet. 2021;398(10308):1344-57.
21. O'Brien M, Paz-Ares L, Marreaud S, Dafni U, Oselin K, Havel L, et al. Pembrolizumab versus placebo as adjuvant therapy for completely resected stage IB–IIIA non-small-cell lung cancer (PEARLS/KEYNOTE-091): an interim analysis of a randomised, triple-blind, phase 3 trial. The Lancet Oncology. 2022;23(10):1274-86.
22. Group NM-aC. Preoperative chemotherapy for non-small-cell lung cancer: a systematic review and meta-analysis of individual participant data. The Lancet. 2014;383(9928):1561-71.
23. Subramanian MP, Puri V. Neoadjuvant vs. adjuvant chemotherapy in locally advanced non-small cell lung cancer—is timing everything? Journal of thoracic disease. 2019;11(12):5674.
24. Felip E, Rosell R, Maestre JA, Rodríguez-Paniagua JM, Morán T, Astudillo J, et al. Preoperative chemotherapy plus surgery versus surgery plus adjuvant chemotherapy versus surgery alone in early-stage non–small-cell lung cancer. Journal of clinical oncology. 2010;28(19):3138-45.
25. Brandt WS, Yan W, Zhou J, Tan KS, Montecalvo J, Park BJ, et al. Outcomes after neoadjuvant or adjuvant chemotherapy for cT2-4N0-1 non–small cell lung cancer: a propensity-matched analysis. The Journal of thoracic and cardiovascular surgery. 2019;157(2):743-53. e3.

26. Forde PM, Spicer J, Lu S, Provencio M, Mitsudomi T, Awad MM, et al. Neoadjuvant nivolumab plus chemotherapy in resectable lung cancer. New England Journal of Medicine. 2022;386(21):1973-85.
27. Wu Y-L, Tsuboi M, He J, John T, Grohe C, Majem M, et al. Osimertinib in resected EGFR-mutated non–small-cell lung cancer. New England Journal of Medicine. 2020;383(18):1711-23.
28. Zhong D, Liu X, Khuri FR, Sun S-Y, Vertino PM, Zhou W. LKB1 is necessary for Akt-mediated phosphorylation of proapoptotic proteins. Cancer research. 2008;68(18):7270-7.
29. Yue D, Xu S, Wang Q, Li X, Shen Y, Zhao H, et al. Erlotinib versus vinorelbine plus cisplatin as adjuvant therapy in Chinese patients with stage IIIA EGFR mutation-positive non-small-cell lung cancer (EVAN): a randomised, open-label, phase 2 trial. The Lancet Respiratory Medicine. 2018;6(11):863-73.
30. Pennell NA, Neal JW, Chaft JE, Azzoli CG, Jänne PA, Govindan R, et al. SELECT: a phase II trial of adjuvant erlotinib in patients with resected epidermal growth factor receptor–mutant non–small-cell lung cancer. Journal of Clinical Oncology. 2019;37(2):97.
31. Tsuboi M, Herbst RS, John T, Kato T, Majem M, Grohé C, et al. Overall Survival with Osimertinib in Resected EGFR-Mutated NSCLC. New England Journal of Medicine. 2023.
32. Liu S-Y, Bao H, Wang Q, Mao W-M, Chen Y, Tong X, et al. Genomic signatures define three subtypes of EGFR-mutant stage II–III non-small-cell lung cancer with distinct adjuvant therapy outcomes. Nature communications. 2021;12(1):1-11.
33. Siegel RL, Miller KD, Wagle NS, Jemal A. Cancer statistics, 2023. Ca Cancer J Clin. 2023;73(1):17-48.
34. Hendriks L, Kerr K, Menis J, Mok T, Nestle U, Passaro A, et al. Oncogene-addicted metastatic non-small-cell lung cancer: ESMO Clinical Practice Guideline for diagnosis, treatment and follow-up☆. Annals of Oncology. 2023;34(4):339-57.
35. Wang M, Herbst RS, Boshoff C. Toward personalized treatment approaches for non-small-cell lung cancer. Nature medicine. 2021;27(8):1345-56.
36. Goto K, Goto Y, Kubo T, Ninomiya K, Kim S-W, Planchard D, et al. Trastuzumab Deruxtecan in Patients With HER2-Mutant Metastatic Non-Small-Cell Lung Cancer: Primary Results From the Randomized, Phase II DESTINY-Lung02 Trial. Journal of Clinical Oncology. 2023:1-12.
37. Douillard J, Ostoros G, Cobo M, Ciuleanu T, McCormack R, Webster A, et al. First-line gefitinib in Caucasian EGFR mutation-positive NSCLC patients: a phase-IV, open-label, single-arm study. British journal of cancer. 2014;110(1):55-62.
38. Mok TS, Wu Y-L, Thongprasert S, Yang C-H, Chu D-T, Saijo N, et al. Gefitinib or carboplatin–paclitaxel in pulmonary adenocarcinoma. New England Journal of Medicine. 2009;361(10):947-57.
39. Fukuoka M, Wu Y-L, Thongprasert S, Sunpaweravong P, Leong S-S, Sriuranpong V, et al. Biomarker analyses and final overall survival results from a phase III, randomized, open-label, first-line study of gefitinib versus carboplatin/paclitaxel in clinically selected patients with advanced non–small-cell lung cancer in Asia (IPASS). Journal of clinical oncology. 2011;29(21):2866-74.
40. Han J-Y, Park K, Kim S-W, Lee DH, Kim HY, Kim HT, et al. First-SIGNAL: first-line single-agent iressa versus gemcitabine and cisplatin trial in never-smokers with adenocarcinoma of the lung. Journal of clinical oncology. 2012;30(10):1122-8.
41. Yoshioka H, Shimokawa M, Seto T, Morita S, Yatabe Y, Okamoto I, et al. Final overall survival results of WJTOG3405, a randomized phase III trial comparing gefitinib versus

cisplatin with docetaxel as the first-line treatment for patients with stage IIIB/IV or postoperative recurrent EGFR mutation-positive non-small-cell lung cancer. Annals of Oncology. 2019;30(12):1978-84.
42. Mitsudomi T, Morita S, Yatabe Y, Negoro S, Okamoto I, Tsurutani J, et al. Gefitinib versus cisplatin plus docetaxel in patients with non-small-cell lung cancer harbouring mutations of the epidermal growth factor receptor (WJTOG3405): an open label, randomised phase 3 trial. The lancet oncology. 2010;11(2):121-8.
43. Maemondo M, Inoue A, Kobayashi K, Sugawara S, Oizumi S, Isobe H, et al. Gefitinib or chemotherapy for non–small-cell lung cancer with mutated EGFR. New England Journal of Medicine. 2010;362(25):2380-8.
44. Rosell R, Carcereny E, Gervais R, Vergnenegre A, Massuti B, Felip E, et al. Erlotinib versus standard chemotherapy as first-line treatment for European patients with advanced EGFR mutation-positive non-small-cell lung cancer (EURTAC): a multicentre, open-label, randomised phase 3 trial. The lancet oncology. 2012;13(3):239-46.
45. Zhou C, Wu Y-L, Chen G, Feng J, Liu X-Q, Wang C, et al. Erlotinib versus chemotherapy as first-line treatment for patients with advanced EGFR mutation-positive non-small-cell lung cancer (OPTIMAL, CTONG-0802): a multicentre, open-label, randomised, phase 3 study. The lancet oncology. 2011;12(8):735-42.
46. Zhou C, Wu Y, Chen G, Feng J, Liu X-Q, Wang C, et al. Final overall survival results from a randomised, phase III study of erlotinib versus chemotherapy as first-line treatment of EGFR mutation-positive advanced non-small-cell lung cancer (OPTIMAL, CTONG-0802). Annals of oncology. 2015;26(9):1877-83.
47. Yang JC-H, Wu Y-L, Schuler M, Sebastian M, Popat S, Yamamoto N, et al. Afatinib versus cisplatin-based chemotherapy for EGFR mutation-positive lung adenocarcinoma (LUX-Lung 3 and LUX-Lung 6): analysis of overall survival data from two randomised, phase 3 trials. The lancet oncology. 2015;16(2):141-51.
48. Yang JC-H, Schuler MH, Yamamoto N, O'Byrne KJ, Hirsh V, Mok T, et al. LUX-Lung 3: A randomized, open-label, phase III study of afatinib versus pemetrexed and cisplatin as first-line treatment for patients with advanced adenocarcinoma of the lung harboring EGFR-activating mutations. American Society of Clinical Oncology; 2012.
49. Sequist LV, Yang JC-H, Yamamoto N, O'Byrne K, Hirsh V, Mok T, et al. Phase III study of afatinib or cisplatin plus pemetrexed in patients with metastatic lung adenocarcinoma with EGFR mutations. Journal of clinical oncology. 2013;31(27):3327-34.
50. Wu Y-L, Zhou C, Hu C-P, Feng J, Lu S, Huang Y, et al. Afatinib versus cisplatin plus gemcitabine for first-line treatment of Asian patients with advanced non-small-cell lung cancer harbouring EGFR mutations (LUX-Lung 6): an open-label, randomised phase 3 trial. The lancet oncology. 2014;15(2):213-22.
51. Park K, Tan E-H, O'Byrne K, Zhang L, Boyer M, Mok T, et al. Afatinib versus gefitinib as first-line treatment of patients with EGFR mutation-positive non-small-cell lung cancer (LUX-Lung 7): a phase 2B, open-label, randomised controlled trial. The Lancet Oncology. 2016;17(5):577-89.
52. Paz-Ares L, Tan E-H, O'Byrne K, Zhang L, Hirsh V, Boyer M, et al. Afatinib versus gefitinib in patients with EGFR mutation-positive advanced non-small-cell lung cancer: overall survival data from the phase IIb LUX-Lung 7 trial. Annals of Oncology. 2017;28(2):270-7.
53. Goss G, Tsai C-M, Shepherd FA, Bazhenova L, Lee JS, Chang G-C, et al. Osimertinib for pretreated EGFR Thr790Met-positive advanced non-small-cell lung cancer (AURA2): a

multicentre, open-label, single-arm, phase 2 study. The lancet oncology. 2016;17(12):1643-52.
54. Mok TS, Wu Y-L, Ahn M-J, Garassino MC, Kim HR, Ramalingam SS, et al. Osimertinib or platinum–pemetrexed in EGFR T790M–positive lung cancer. New England Journal of Medicine. 2017;376(7):629-40.
55. Wu Y-L, Mok T, Han J-Y, Ahn M-J, Delmonte A, Ramalingam S, et al. Overall survival (OS) from the AURA3 phase III study: Osimertinib vs platinum-pemetrexed (plt-pem) in patients (pts) with EGFR T790M advanced non-small cell lung cancer (NSCLC) and progression on a prior EGFR-tyrosine kinase inhibitor (TKI). Annals of Oncology. 2019;30:ix158.
56. Soria J-C, Ohe Y, Vansteenkiste J, Reungwetwattana T, Chewaskulyong B, Lee KH, et al. Osimertinib in untreated EGFR-mutated advanced non–small-cell lung cancer. New England journal of medicine. 2018;378(2):113-25.
57. Ramalingam SS, Vansteenkiste J, Planchard D, Cho BC, Gray JE, Ohe Y, et al. Overall survival with osimertinib in untreated, EGFR-mutated advanced NSCLC. New England Journal of Medicine. 2020;382(1):41-50.
58. Camidge DR, Bang Y-J, Kwak EL, Iafrate AJ, Varella-Garcia M, Fox SB, et al. Activity and safety of crizotinib in patients with ALK-positive non-small-cell lung cancer: updated results from a phase 1 study. The lancet oncology. 2012;13(10):1011-9.
59. Kwak EL, Bang Y-J, Camidge DR, Shaw AT, Solomon B, Maki RG, et al. Anaplastic lymphoma kinase inhibition in non–small-cell lung cancer. New England Journal of Medicine. 2010;363(18):1693-703.
60. Blackhall F, Camidge DR, Shaw AT, Soria J-C, Solomon BJ, Mok T, et al. Final results of the large-scale multinational trial PROFILE 1005: efficacy and safety of crizotinib in previously treated patients with advanced/metastatic ALK-positive non-small-cell lung cancer. Esmo Open. 2017;2(3):e000219.
61. Shaw AT, Kim D-W, Nakagawa K, Seto T, Crinó L, Ahn M-J, et al. Crizotinib versus chemotherapy in advanced ALK-positive lung cancer. New England Journal of Medicine. 2013;368(25):2385-94.
62. Kim D-W, Mehra R, Tan DS, Felip E, Chow LQ, Camidge DR, et al. Activity and safety of ceritinib in patients with ALK-rearranged non-small-cell lung cancer (ASCEND-1): updated results from the multicentre, open-label, phase 1 trial. The lancet oncology. 2016;17(4):452-63.
63. Nishio M, Felip E, Orlov S, Park K, Yu C-J, Tsai C-M, et al. Final overall survival and other efficacy and safety results from ASCEND-3: Phase II study of ceritinib in ALKi-naive patients with ALK-rearranged NSCLC. Journal of Thoracic Oncology. 2020;15(4):609-17.
64. Felip E, Orlov S, Park K, Yu C-J, Tsai C-M, Nishio M, et al. ASCEND-3: A single-arm, open-label, multicenter phase II study of ceritinib in ALKi-naïve adult patients (pts) with ALK-rearranged (ALK+) non-small cell lung cancer (NSCLC). American Society of Clinical Oncology; 2015.
65. Felip E, Nishio M, Orlov S, Park K, Yu C-J, Tsai C-M, et al. Overall survival results of ceritinib in ALKi-naïve patients with ALK-rearranged NSCLC (ASCEND-3). Annals of Oncology. 2018;29:viii745.
66. Soria J-C, Tan DS, Chiari R, Wu Y-L, Paz-Ares L, Wolf J, et al. First-line ceritinib versus platinum-based chemotherapy in advanced ALK-rearranged non-small-cell lung cancer (ASCEND-4): a randomised, open-label, phase 3 study. The Lancet. 2017;389(10072):917-29.

67. Barlesi F, Dingemans A-M, Yang J-H, Ou S-H, Ahn J, De Petris L, et al. Updated efficacy and safety from the global phase II NP28673 study of alectinib in patients (pts) with previously treated ALK+ non-small-cell lung cancer (NSCLC). Annals of Oncology. 2016;27:vi437.
68. Ou S-HI, Ahn JS, De Petris L, Govindan R, Yang JC-H, Hughes B, et al. Alectinib in crizotinib-refractory ALK-rearranged non–small-cell lung cancer: a phase II global study. Journal of clinical oncology. 2016;34(7):661-8.
69. Seto T, Kiura K, Nishio M, Nakagawa K, Maemondo M, Inoue A, et al. CH5424802 (RO5424802) for patients with ALK-rearranged advanced non-small-cell lung cancer (AF-001JP study): a single-arm, open-label, phase 1–2 study. The lancet oncology. 2013;14(7):590-8.
70. Tamura T, Kiura K, Seto T, Nakagawa K, Maemondo M, Inoue A, et al. Three-year follow-up of an alectinib phase I/II study in ALK-positive non–small-cell lung cancer: AF-001JP. Journal of Clinical Oncology. 2017;35(14):1515.
71. Peters S, Camidge DR, Shaw AT, Gadgeel S, Ahn JS, Kim D-W, et al. Alectinib versus crizotinib in untreated ALK-positive non–small-cell lung cancer. New England Journal of Medicine. 2017;377(9):829-38.
72. Mok T, Camidge D, Gadgeel S, Rosell R, Dziadziuszko R, Kim D-W, et al. Updated overall survival and final progression-free survival data for patients with treatment-naive advanced ALK-positive non-small-cell lung cancer in the ALEX study. Annals of oncology. 2020;31(8):1056-64.
73. Hotta K, Hida T, Nokihara H, Morise M, Kim Y, Azuma K, et al. Final overall survival analysis from the phase III J-ALEX study of alectinib versus crizotinib in ALK inhibitor-naïve Japanese patients with ALK-positive non-small-cell lung cancer. ESMO open. 2022;7(4):100527.
74. Nakagawa K, Hida T, Nokihara H, Morise M, Azuma K, Kim YH, et al. Final progression-free survival results from the J-ALEX study of alectinib versus crizotinib in ALK-positive non-small-cell lung cancer. Lung Cancer. 2020;139:195-9.
75. Hida T, Nokihara H, Kondo M, Kim YH, Azuma K, Seto T, et al. Alectinib versus crizotinib in patients with ALK-positive non-small-cell lung cancer (J-ALEX): an open-label, randomised phase 3 trial. The Lancet. 2017;390(10089):29-39.
76. Gettinger SN, Bazhenova LA, Langer CJ, Salgia R, Gold KA, Rosell R, et al. Activity and safety of brigatinib in ALK-rearranged non-small-cell lung cancer and other malignancies: a single-arm, open-label, phase 1/2 trial. The lancet oncology. 2016;17(12):1683-96.
77. Camidge DR, Kim HR, Ahn M-J, Yang JC-H, Han J-Y, Lee J-S, et al. Brigatinib versus crizotinib in ALK-positive non–small-cell lung cancer. New England Journal of Medicine. 2018;379(21):2027-39.
78. Huber RM, Hansen KH, Rodríguez LP-A, West HL, Reckamp KL, Leighl NB, et al. Brigatinib in crizotinib-refractory ALK+ NSCLC: 2-year follow-up on systemic and intracranial outcomes in the phase 2 ALTA trial. Journal of Thoracic Oncology. 2020;15(3):404-15.
79. Kim D-W, Tiseo M, Ahn M-J, Reckamp KL, Hansen KH, Kim S-W, et al. Brigatinib in patients with crizotinib-refractory anaplastic lymphoma kinase-positive non-small-cell lung cancer: a randomized, multicenter phase II trial. Journal of Clinical Oncology. 2017;35(22):2490-8.
80. Shaw AT, Bauer TM, de Marinis F, Felip E, Goto Y, Liu G, et al. First-line lorlatinib or crizotinib in advanced ALK-positive lung cancer. New England Journal of Medicine. 2020;383(21):2018-29.

81. Solomon BJ, Bauer TM, Mok TS, Liu G, Mazieres J, de Marinis F, et al. Efficacy and safety of first-line lorlatinib versus crizotinib in patients with advanced, ALK-positive non-small-cell lung cancer: updated analysis of data from the phase 3, randomised, open-label CROWN study. The Lancet Respiratory Medicine. 2023;11(4):354-66.
82. Baldacci S, Besse B, Avrillon V, Mennecier B, Mazieres J, Dubray-Longeras P, et al. Lorlatinib for advanced anaplastic lymphoma kinase–positive non–small cell lung cancer: Results of the IFCT-1803 LORLATU cohort. European Journal of Cancer. 2022;166:51-9.
83. Shaw AT, Riely GJ, Bang Y-J, Kim D-W, Camidge DR, Solomon BJ, et al. Crizotinib in ROS1-rearranged advanced non-small-cell lung cancer (NSCLC): updated results, including overall survival, from PROFILE 1001. Annals of Oncology. 2019;30(7):1121-6.
84. Shaw AT, Ou S-HI, Bang Y-J, Camidge DR, Solomon BJ, Salgia R, et al. Crizotinib in ROS1-rearranged non–small-cell lung cancer. New England Journal of Medicine. 2014;371(21):1963-71.
85. Shen L, Qiang T, Li Z, Ding D, Yu Y, Lu S. First-line crizotinib versus platinum-pemetrexed chemotherapy in patients with advanced ROS1-rearranged non-small-cell lung cancer. Cancer medicine. 2020;9(10):3310-8.
86. Wu Y-L, Yang JC-H, Kim D-W, Lu S, Zhou J, Seto T, et al. Phase II study of crizotinib in East Asian patients with ROS1-positive advanced non–small-cell lung cancer. Journal of Clinical Oncology. 2018;36(14):1405-11.
87. Wu Y-L, Lu S, Yang JC-H, Zhou J, Seto T, Ahn M-J, et al. Final Overall Survival, Safety, and Quality of Life Results From a Phase 2 Study of Crizotinib in East Asian Patients With ROS1-Positive Advanced NSCLC. JTO Clinical and Research Reports. 2022;3(10):100406.
88. Moro-Sibilot D, Cozic N, Pérol M, Mazières J, Otto J, Souquet P, et al. Crizotinib in c-MET-or ROS1-positive NSCLC: results of the AcSé phase II trial. Annals of Oncology. 2019;30(12):1985-91.
89. Landi L, Chiari R, Tiseo M, D'Incà F, Dazzi C, Chella A, et al. Crizotinib in MET-Deregulated or ROS1-Rearranged Pretreated Non–Small Cell Lung Cancer (METROS): A Phase II, Prospective, Multicenter, Two-Arms TrialCrizotinib in ROS1-and MET-Deregulated NSCLC. Clinical Cancer Research. 2019;25(24):7312-9.
90. Shaw AT, Solomon BJ, Chiari R, Riely GJ, Besse B, Soo RA, et al. Lorlatinib in advanced ROS1-positive non-small-cell lung cancer: a multicentre, open-label, single-arm, phase 1–2 trial. The Lancet Oncology. 2019;20(12):1691-701.
91. Paz-Ares L, Doebele R, Farago A, Liu S, Chawla S, Tosi D, et al. Entrectinib in NTRK fusion-positive non-small cell lung cancer (NSCLC): Integrated analysis of patients (pts) enrolled in STARTRK-2, STARTRK-1 and ALKA-372-001. Annals of Oncology. 2019;30:ii48-ii9.
92. Doebele RC, Drilon A, Paz-Ares L, Siena S, Shaw AT, Farago AF, et al. Entrectinib in patients with advanced or metastatic NTRK fusion-positive solid tumours: integrated analysis of three phase 1–2 trials. The Lancet Oncology. 2020;21(2):271-82.
93. Lim SM, Kim HR, Lee J-S, Lee KH, Lee Y-G, Min YJ, et al. Open-label, multicenter, phase II study of ceritinib in patients with non–small-cell lung cancer harboring ROS1 rearrangement. Journal of clinical oncology. 2017;35(23):2613-8.
94. Cho BC, Doebele RC, Lin J, Nagasaka M, Baik C, Van Der Wekken A, et al. MA11. 07 phase 1/2 TRIDENT-1 study of repotrectinib in patients with ROS1+ or NTRK+ advanced solid tumors. Journal of Thoracic Oncology. 2021;16(3):S174-S5.
95. Drilon A, Camidge DR, Lin JJ, Kim S-W, Solomon BJ, Dziadziuszko R, et al. Repotrectinib in ROS1 Fusion–Positive Non–Small-Cell Lung Cancer. New England Journal of Medicine. 2024;390(2):118-31.

96. Drilon A, Oxnard GR, Tan DS, Loong HH, Johnson M, Gainor J, et al. Efficacy of selpercatinib in RET fusion–positive non–small-cell lung cancer. New England Journal of Medicine. 2020;383(9):813-24.
97. Besse B, Drilon AE, Solomon BJ, Subbiah V, Tan DS-W, Park K, et al. Updated overall efficacy and safety of selpercatinib in patients (pts) with RET fusion+ non-small cell lung cancer (NSCLC). Wolters Kluwer Health; 2021.
98. Drilon A, Subbiah V, Gautschi O, Tomasini P, De Braud F, Solomon BJ, et al. Selpercatinib in patients with RET fusion–positive non–small-cell lung cancer: updated safety and efficacy from the registrational LIBRETTO-001 phase I/II trial. Journal of Clinical Oncology. 2023;41(2):385.
99. Gainor JF, Curigliano G, Kim D-W, Lee DH, Besse B, Baik CS, et al. Pralsetinib for RET fusion-positive non-small-cell lung cancer (ARROW): a multi-cohort, open-label, phase 1/2 study. The lancet oncology. 2021;22(7):959-69.
100. Griesinger F, Curigliano G, Thomas M, Subbiah V, Baik C, Tan DS, et al. Safety and efficacy of pralsetinib in RET fusion–positive non-small-cell lung cancer including as first-line therapy: Update from the ARROW trial. Annals of Oncology. 2022;33(11):1168-78.
101. Camidge DR, Otterson GA, Clark JW, Ou S-HI, Weiss J, Ades S, et al. Crizotinib in patients with MET-amplified NSCLC. Journal of Thoracic Oncology. 2021;16(6):1017-29.
102. Drilon A, Clark JW, Weiss J, Ou S-HI, Camidge DR, Solomon BJ, et al. Antitumor activity of crizotinib in lung cancers harboring a MET exon 14 alteration. Nature medicine. 2020;26(1):47-51.
103. Wolf J, Seto T, Han J-Y, Reguart N, Garon EB, Groen HJ, et al. Capmatinib in MET exon 14–mutated or MET-amplified non–small-cell lung cancer. New England Journal of Medicine. 2020;383(10):944-57.
104. Schuler M, Berardi R, Lim W-T, de Jonge M, Bauer T, Azaro A, et al. Molecular correlates of response to capmatinib in advanced non-small-cell lung cancer: clinical and biomarker results from a phase I trial. Annals of Oncology. 2020;31(6):789-97.
105. Dagogo-Jack I, Moonsamy P, Gainor JF, Lennerz JK, Piotrowska Z, Lin JJ, et al. A phase 2 study of capmatinib in patients with MET-altered lung cancer previously treated with a MET inhibitor. Journal of Thoracic Oncology. 2021;16(5):850-9.
106. Paik PK, Felip E, Veillon R, Sakai H, Cortot AB, Garassino MC, et al. Tepotinib in non–small-cell lung cancer with MET exon 14 skipping mutations. New England Journal of Medicine. 2020;383(10):931-43.
107. Planchard D, Kim TM, Mazieres J, Quoix E, Riely G, Barlesi F, et al. Dabrafenib in patients with BRAFV600E-positive advanced non-small-cell lung cancer: a single-arm, multicentre, open-label, phase 2 trial. The Lancet Oncology. 2016;17(5):642-50.
108. Planchard D, Besse B, Groen HJ, Souquet P-J, Quoix E, Baik CS, et al. Dabrafenib plus trametinib in patients with previously treated BRAFV600E-mutant metastatic non-small cell lung cancer: an open-label, multicentre phase 2 trial. The Lancet Oncology. 2016;17(7):984-93.
109. Planchard D, Besse B, Groen HJ, Hashemi SM, Mazieres J, Kim TM, et al. Phase 2 study of dabrafenib plus trametinib in patients with BRAF V600E-mutant metastatic NSCLC: updated 5-year survival rates and genomic analysis. Journal of Thoracic Oncology. 2022;17(1):103-15.
110. Subbiah V, Gervais R, Riely G, Hollebecque A, Blay J-Y, Felip E, et al. Efficacy of vemurafenib in patients with non–small-cell lung cancer with BRAF V600 mutation: an open-

label, single-arm cohort of the histology-independent VE-BASKET study. JCO Precision Oncology. 2019;3:1-9.
111. Tomasini P, Mazieres J, Cropet C, Troussard X, Malka D, Ray-Coquard I, et al. 538P Vemurafenib in non-melanoma V600 and non-V600 BRAF mutated cancers: Results of the AcSé basket trial. Annals of Oncology. 2020;31:S470-S1.
112. Mazieres J, Cropet C, Montané L, Barlesi F, Souquet P, Quantin X, et al. Vemurafenib in non-small-cell lung cancer patients with BRAFV600 and BRAFnonV600 mutations. Annals of Oncology. 2020;31(2):289-94.
113. Drilon A, Tan DS, Lassen UN, Leyvraz S, Liu Y, Patel JD, et al. Efficacy and Safety of Larotrectinib in Patients With Tropomyosin Receptor Kinase Fusion–Positive Lung Cancers. JCO Precision Oncology. 2022;6:e2100418.
114. Li BT, Smit EF, Goto Y, Nakagawa K, Udagawa H, Mazières J, et al. Trastuzumab deruxtecan in HER2-mutant non–small-cell lung cancer. New England Journal of Medicine. 2022;386(3):241-51.
115. Tsurutani J, Iwata H, Krop I, Jänne PA, Doi T, Takahashi S, et al. Targeting HER2 with trastuzumab deruxtecan: a dose-expansion, phase I study in multiple advanced solid tumors. Cancer discovery. 2020;10(5):688-701.
116. Li BT, Shen R, Buonocore D, Olah ZT, Ni A, Ginsberg MS, et al. Ado-trastuzumab emtansine for patients with HER2-mutant lung cancers: results from a phase II basket trial. Journal of Clinical Oncology. 2018;36(24):2532.
117. Li BT, Shen R, Buonocore D, Olah ZT, Ni A, Ginsberg MS, et al. Ado-trastuzumab emtansine in patients with HER2 mutant lung cancers: Results from a phase II basket trial. American Society of Clinical Oncology; 2017.
118. Li BT, Makker V, Buonocore DJ, Offin MD, Olah ZT, Panora E, et al. A multi-histology basket trial of ado-trastuzumab emtansine in patients with HER2 amplified cancers. American Society of Clinical Oncology; 2018.
119. Hotta K, Aoe K, Kozuki T, Ohashi K, Ninomiya K, Ichihara E, et al. A phase II study of trastuzumab emtansine in HER2-positive non–small cell lung cancer. Journal of Thoracic Oncology. 2018;13(2):273-9.
120. Stinchcombe T, Stahel RA, Bubendorf L, Bonomi P, Villegas AE, Kowalski D, et al. Efficacy, safety, and biomarker results of trastuzumab emtansine (T-DM1) in patients (pts) with previously treated HER2-overexpressing locally advanced or metastatic non-small cell lung cancer (mNSCLC). American Society of Clinical Oncology; 2017.
121. Peters S, Stahel R, Bubendorf L, Bonomi P, Villegas A, Kowalski DM, et al. Trastuzumab emtansine (T-DM1) in patients with previously treated HER2-overexpressing metastatic non–small cell lung cancer: efficacy, safety, and biomarkers. Clinical Cancer Research. 2019;25(1):64-72.
122. Skoulidis F, Li BT, Dy GK, Price TJ, Falchook GS, Wolf J, et al. Sotorasib for lung cancers with KRAS p. G12C mutation. New England Journal of Medicine. 2021;384(25):2371-81.
123. Dy G, Govindan R, Velcheti V, editors. Long-term outcomes with sotorasib in pretreated KRAS p. G12C-mutated NSCLC: 2-year analysis of CodeBreaK 100. AACR Annual Meeting; 2022.
124. de Langen AJ, Johnson ML, Mazieres J, Dingemans A-MC, Mountzios G, Pless M, et al. Sotorasib versus docetaxel for previously treated non-small-cell lung cancer with KRASG12C mutation: a randomised, open-label, phase 3 trial. The Lancet. 2023;401(10378):733-46.

125. Murciano-Goroff YR, Lito P. The KRYSTAL-1 study of adagrasib—a new trial for KRASG12C-mutated non-small-cell lung cancer. Nature Reviews Clinical Oncology. 2022:1-2.
126. Jänne PA, Riely GJ, Gadgeel SM, Heist RS, Ou S-HI, Pacheco JM, et al. Adagrasib in non–small-cell lung cancer harboring a KRASG12C mutation. New England Journal of Medicine. 2022;387(2):120-31.
127. Middleton G, Fletcher P, Popat S, Savage J, Summers Y, Greystoke A, et al. The National Lung Matrix Trial of personalized therapy in lung cancer. Nature. 2020;583(7818):807-12.
128. Zhou K, Lin C, Tseng C-L, Ramnath N, Dowell J, Kelley M. P2. 09-15 Real World Efficacy and Safety of Sotorasib in US Veterans with KRAS G12C Mutated Non-Small Cell Lung Cancer. Journal of Thoracic Oncology. 2023;18(11):S337-S8.
129. Julve M, Kennedy O, Lindsay C, Walters-Davies R, Button M, Steele N, et al. 1116P United Kingdom real-world experience of sotorasib in KRAS G12C mutant non-small cell lung cancer: A British thoracic oncology group review. Annals of Oncology. 2022;33:S1061-S2.
130. Garcia BNC, van Kempen LC, Kuijpers CC, Schuuring E, Willems SM, van der Wekken AJ. Prevalence of KRAS p.(G12C) in stage IV NSCLC patients in the Netherlands; a nation-wide retrospective cohort study. Lung Cancer. 2022;167:1-7.
131. Network CGAR. Comprehensive molecular profiling of lung adenocarcinoma. Nature. 2014;511(7511):543.
132. Zhou C, Li W, Song Z, Zhang Y, Huang D, Yang Z, et al. LBA33 A first-in-human phase I study of a novel KRAS G12D inhibitor HRS-4642 in patients with advanced solid tumors harboring KRAS G12D mutation. Annals of Oncology. 2023;34:S1273.
133. Arbour KP, S; Garrido-Laguna, I; Hong, DS; Woldpin B; Pelster MS; Barve M; Starodub, A; Sommerhalder, D; Chang, S; Zhang, Y; Salman Z; Wang, X; Gustafson, C; Spira, AI. 652O - Preliminary clinical activity of RMC-6236, a first-in-class, RAS-selective, tri-complex RAS-MULTI(ON) inhibitor in patients with KRAS mutant pancreatic ductal adenocarcinoma (PDAC) and non-small cell lung cancer (NSCLC). Annals of Oncology. 2023;34:S458 - S97.
134. Puyol M, Martín A, Dubus P, Mulero F, Pizcueta P, Khan G, et al. A synthetic lethal interaction between K-Ras oncogenes and Cdk4 unveils a therapeutic strategy for non-small cell lung carcinoma. Cancer cell. 2010;18(1):63-73.
135. Patnaik A, Rosen LS, Tolaney SM, Tolcher AW, Goldman JW, Gandhi L, et al. Efficacy and safety of abemaciclib, an inhibitor of CDK4 and CDK6, for patients with breast cancer, non–small cell lung cancer, and other solid tumors. Cancer discovery. 2016;6(7):740-53.
136. Son K-H, Kim M-Y, Shin J-Y, Kim J-O, Kang J-H. Synergistic antitumor effect of taxanes and CDK4/6 inhibitor in lung cancer cells and mice harboring KRAS mutations. Anticancer Research. 2021;41(10):4807-20.
137. Morrison L, Loibl S, Turner NC. The CDK4/6 inhibitor revolution—a game-changing era for breast cancer treatment. Nature Reviews Clinical Oncology. 2023:1-17.
138. Rubin SM, Sage J, Skotheim JM. Integrating old and new paradigms of G1/S control. Molecular cell. 2020;80(2):183-92.
139. Hume S, Dianov GL, Ramadan K. A unified model for the G1/S cell cycle transition. Nucleic acids research. 2020;48(22):12483-501.
140. Qie S, Diehl JA. Cyclin D1, cancer progression, and opportunities in cancer treatment. Journal of molecular medicine. 2016;94:1313-26.
141. Alao JP. The regulation of cyclin D1 degradation: roles in cancer development and the potential for therapeutic invention. Molecular cancer. 2007;6:1-16.

142. Luangdilok S, Wanchaijiraboon P, Chantranuwatana P, Teerapakpinyo C, Shuangshoti S, Sriuranpong V. Cyclin D1 expression as a potential prognostic factor in advanced KRAS-mutant non-small cell lung cancer. Translational Lung Cancer Research. 2019;8(6):959.
143. Dragoj M, Milosevic Z, Bankovic J, Dinic J, Pesic M, Tanic N, et al. Association of CCND1 overexpression with KRAS and PTEN alterations in specific subtypes of non-small cell lung carcinoma and its influence on patients' outcome. Tumor Biology. 2015;36:8773-80.
144. Goldman JW, Mazieres J, Barlesi F, Dragnev KH, Koczywas M, Göskel T, et al. A randomized phase III study of abemaciclib versus erlotinib in patients with stage IV non-small cell lung cancer with a detectable KRAS mutation who failed prior platinum-based therapy: JUNIPER. Frontiers in Oncology. 2020;10:578756.
145. Haines E, Chen T, Kommajosyula N, Chen Z, Herter-Sprie GS, Cornell L, et al. Palbociclib resistance confers dependence on an FGFR-MAP kinase-mTOR-driven pathway in KRAS-mutant non-small cell lung cancer. Oncotarget. 2018;9(60):31572.
146. Raimondi L, Raimondi FM, Pietranera M, Di Rocco A, Di Benedetto L, Miele E, et al. Assessment of resistance mechanisms and clinical implications in patients with KRAS mutated-metastatic breast cancer and resistance to CDK4/6 inhibitors. Cancers. 2021;13(8):1928.
147. Dahmani R, Just P, Delay A, Canal F, Finzi L, Prip-Buus C, et al. A novel LKB1 isoform enhances AMPK metabolic activity and displays oncogenic properties. Oncogene. 2015;34(18):2337-46.
148. Karuman P, Gozani O, Odze RD, Zhou XC, Zhu H, Shaw R, et al. The Peutz-Jegher gene product LKB1 is a mediator of p53-dependent cell death. Molecular cell. 2001;7(6):1307-19.
149. Faubert B, Vincent EE, Griss T, Samborska B, Izreig S, Svensson RU, et al. Loss of the tumor suppressor LKB1 promotes metabolic reprogramming of cancer cells via HIF-1α. Proceedings of the National Academy of Sciences. 2014;111(7):2554-9.
150. Sanchez-Cespedes M. A role for LKB1 gene in human cancer beyond the Peutz–Jeghers syndrome. Oncogene. 2007;26(57):7825-32.
151. Matsumoto S, Iwakawa R, Takahashi K, Kohno T, Nakanishi Y, Matsuno Y, et al. Prevalence and specificity of LKB1 genetic alterations in lung cancers. Oncogene. 2007;26(40):5911-8.
152. Sanchez-Cespedes M, Parrella P, Esteller M, Nomoto S, Trink B, Engles JM, et al. Inactivation of LKB1/STK11 is a common event in adenocarcinomas of the lung. Cancer research. 2002;62(13):3659-62.
153. Calles A, Sholl LM, Rodig SJ, Pelton AK, Hornick JL, Butaney M, et al. Immunohistochemical loss of LKB1 is a biomarker for more aggressive biology in KRAS-mutant lung adenocarcinoma. Clinical Cancer Research. 2015;21(12):2851-60.
154. Skoulidis F, Byers LA, Diao L, Papadimitrakopoulou VA, Tong P, Izzo J, et al. Co-occurring genomic alterations define major subsets of KRAS-mutant lung adenocarcinoma with distinct biology, immune profiles, and therapeutic vulnerabilities. Cancer discovery. 2015;5(8):860-77.
155. Schabath MB, Welsh EA, Fulp WJ, Chen L, Teer JK, Thompson ZJ, et al. Differential association of STK11 and TP53 with KRAS mutation-associated gene expression, proliferation and immune surveillance in lung adenocarcinoma. Oncogene. 2016;35(24):3209-16.
156. Mahoney C, Choudhury B, Davies H, Edkins S, Greenman C, Van Haaften G, et al. LKB1/KRAS mutant lung cancers constitute a genetic subset of NSCLC with increased

sensitivity to MAPK and mTOR signalling inhibition. British journal of cancer. 2009;100(2):370-5.
157. La Fleur L, Falk-Sörqvist E, Smeds P, Berglund A, Sundström M, Mattsson JS, et al. Mutation patterns in a population-based non-small cell lung cancer cohort and prognostic impact of concomitant mutations in KRAS and TP53 or STK11. Lung Cancer. 2019;130:50-8.
158. Bange E, Marmarelis ME, Hwang W-T, Yang Y-X, Thompson JC, Rosenbaum J, et al. Impact of kras and tp53 co-mutations on outcomes after first-line systemic therapy among patients with stk11-mutated advanced non–small-cell lung cancer. JCO precision oncology. 2019;3:1-11.
159. Aredo JV, Padda SK, Kunder CA, Han SS, Neal JW, Shrager JB, et al. Impact of KRAS mutation subtype and concurrent pathogenic mutations on non-small cell lung cancer outcomes. Lung Cancer. 2019;133:144-50.
160. El Osta B, Behera M, Kim S, Berry LD, Sica G, Pillai RN, et al. Characteristics and outcomes of patients with metastatic KRAS-mutant lung adenocarcinomas: the lung cancer mutation consortium experience. Journal of Thoracic Oncology. 2019;14(5):876-89.
161. Shire NJ, Klein AB, Golozar A, Collins JM, Fraeman KH, Nordstrom BL, et al. STK11 (LKB1) mutations in metastatic NSCLC: Prognostic value in the real world. Plos one. 2020;15(9):e0238358.
162. Koyama S, Akbay EA, Li YY, Aref AR, Skoulidis F, Herter-Sprie GS, et al. STK11/LKB1 deficiency promotes neutrophil recruitment and proinflammatory cytokine production to suppress T-cell activity in the lung tumor microenvironment. Cancer research. 2016;76(5):999-1008.
163. Gillette MA, Satpathy S, Cao S, Dhanasekaran SM, Vasaikar SV, Krug K, et al. Proteogenomic characterization reveals therapeutic vulnerabilities in lung adenocarcinoma. Cell. 2020;182(1):200-25. e35.
164. Skoulidis F, Hellman M, Awad M, Gainor J, Rizvi H, Carter B, et al. LKB1 loss is a novel genomic predictor of de novo resistance to PD-1/PD-L1 axis blockade in KRAS-mutant lung adenocarcinoma. Annals of Oncology. 2017;28:v467.
165. Shang X, Li Z, Sun J, Zhao C, Lin J, Wang H. Survival analysis for non-squamous NSCLC patients harbored STK11 or KEAP1 mutation receiving atezolizumab. Lung Cancer. 2021;154:105-12.
166. Kottakis F, Bardeesy N. LKB1-AMPK axis revisited. Cell research. 2012;22(12):1617-20.
167. Gwinn DM, Shackelford DB, Egan DF, Mihaylova MM, Mery A, Vasquez DS, et al. AMPK phosphorylation of raptor mediates a metabolic checkpoint. Molecular cell. 2008;30(2):214-26.
168. Eichner LJ, Brun SN, Herzig S, Young NP, Curtis SD, Shackelford DB, et al. Genetic analysis reveals AMPK is required to support tumor growth in murine Kras-dependent lung cancer models. Cell metabolism. 2019;29(2):285-302. e7.
169. Hollstein PE, Eichner LJ, Brun SN, Kamireddy A, Svensson RU, Vera LI, et al. The AMPK-related kinases SIK1 and SIK3 mediate key tumor-suppressive effects of LKB1 in NSCLC. Cancer discovery. 2019;9(11):1606-27.
170. Kottakis F, Nicolay BN, Roumane A, Karnik R, Gu H, Nagle JM, et al. LKB1 loss links serine metabolism to DNA methylation and tumorigenesis. Nature. 2016;539(7629):390-5.
171. Liu W, Monahan KB, Pfefferle AD, Shimamura T, Sorrentino J, Chan KT, et al. LKB1/STK11 inactivation leads to expansion of a prometastatic tumor subpopulation in melanoma. Cancer cell. 2012;21(6):751-64.

172. Ji H, Ramsey MR, Hayes DN, Fan C, McNamara K, Kozlowski P, et al. LKB1 modulates lung cancer differentiation and metastasis. Nature. 2007;448(7155):807-10.
173. Carretero J, Shimamura T, Rikova K, Jackson AL, Wilkerson MD, Borgman CL, et al. Integrative genomic and proteomic analyses identify targets for Lkb1-deficient metastatic lung tumors. Cancer cell. 2010;17(6):547-59.
174. Kim J, Lee HM, Cai F, Ko B, Yang C, Lieu EL, et al. The hexosamine biosynthesis pathway is a targetable liability in KRAS/LKB1 mutant lung cancer. Nature metabolism. 2020:1-12.
175. Chen Z, Cheng K, Walton Z, Wang Y, Ebi H, Shimamura T, et al. A murine lung cancer co-clinical trial identifies genetic modifiers of therapeutic response. Nature. 2012;483(7391):613-7.
176. Masui K, Tanaka K, Akhavan D, Babic I, Gini B, Matsutani T, et al. mTOR complex 2 controls glycolytic metabolism in glioblastoma through FoxO acetylation and upregulation of c-Myc. Cell metabolism. 2013;18(5):726-39.
177. Momcilovic M, McMickle R, Abt E, Seki A, Simko SA, Magyar C, et al. Heightening energetic stress selectively targets LKB1-deficient non–small cell lung cancers. Cancer research. 2015;75(22):4910-22.
178. Powles T, Wheater M, Din O, Geldart T, Boleti E, Stockdale A, et al. A randomised phase 2 study of AZD2014 versus everolimus in patients with VEGF-refractory metastatic clear cell renal cancer. European urology. 2016;69(3):450-6.
179. Schmid P, Zaiss M, Harper-Wynne C, Ferreira M, Dubey S, Chan S, et al. MANTA-a randomized phase II study of fulvestrant in combination with the dual mTOR inhibitor AZD2014 or everolimus or fulvestrant alone in estrogen receptor-positive advanced or metastatic breast cancer. CANCER RESEARCH. 2018;78(4).
180. O'Reilly KE, Rojo F, She Q-B, Solit D, Mills GB, Smith D, et al. mTOR inhibition induces upstream receptor tyrosine kinase signaling and activates Akt. Cancer research. 2006;66(3):1500-8.
181. Rodrik-Outmezguine VS, Chandarlapaty S, Pagano NC, Poulikakos PI, Scaltriti M, Moskatel E, et al. mTOR kinase inhibition causes feedback-dependent biphasic regulation of AKT signaling. Cancer discovery. 2011;1(3):248-59.
182. Shtivelman E, Hensing T, Simon GR, Dennis PA, Otterson GA, Bueno R, et al. Molecular pathways and therapeutic targets in lung cancer. Oncotarget. 2014;5(6):1392.
183. Network CGAR. Comprehensive genomic characterization of squamous cell lung cancers. Nature. 2012;489(7417):519.
184. Paz-Ares LG, Luft A, Tafreshi A, Gumus M, Mazieres J, Hermes B, et al. Phase 3 study of carboplatin-paclitaxel/nab-paclitaxel (Chemo) with or without pembrolizumab (Pembro) for patients (Pts) with metastatic squamous (Sq) non-small cell lung cancer (NSCLC). American Society of Clinical Oncology; 2018.
185. Novello S, Kowalski DM, Luft A, Gümüş M, Vicente D, Mazières J, et al. Pembrolizumab plus chemotherapy in squamous non–small-cell lung cancer: 5-year update of the phase III KEYNOTE-407 study. Journal of Clinical Oncology. 2023;41(11):1999.
186. Li S, de Camargo Correia GS, Wang J, Manochakian R, Zhao Y, Lou Y. Emerging Targeted Therapies in Advanced Non-Small-Cell Lung Cancer. Cancers. 2023;15(11):2899.
187. Riess J, Frankel P, Massarelli E, Nieva J, Lai W-C, Koczywas M, et al. Ma13. 08 a phase 1 trial of sapanisertib and telaglenastat (Cb-839) in patients with advanced nsclc (Nci 10327): Results from dose escalation. Journal of Thoracic Oncology. 2022;17(9):S91-S2.

188. Chae YK, Hong F, Vaklavas C, Cheng HH, Hammerman P, Mitchell EP, et al. Phase II study of AZD4547 in patients with tumors harboring aberrations in the FGFR pathway: results from the NCI-MATCH trial (EAY131) subprotocol W. Journal of Clinical Oncology. 2020;38(21):2407.
189. Aggarwal C, Redman MW, Lara Jr PN, Borghaei H, Hoffman P, Bradley JD, et al. SWOG S1400D (NCT02965378), a phase II study of the fibroblast growth factor receptor inhibitor AZD4547 in previously treated patients with fibroblast growth factor pathway–activated stage IV squamous cell lung cancer (Lung-MAP Substudy). Journal of Thoracic Oncology. 2019;14(10):1847-52.
190. Yuan G, Flores NM, Hausmann S, Lofgren SM, Kharchenko V, Angulo-Ibanez M, et al. Elevated NSD3 histone methylation activity drives squamous cell lung cancer. Nature. 2021;590(7846):504-8.
191. Bass AJ, Watanabe H, Mermel CH, Yu S, Perner S, Verhaak RG, et al. SOX2 is an amplified lineage-survival oncogene in lung and esophageal squamous cell carcinomas. Nature genetics. 2009;41(11):1238-42.
192. Redon R, Hussenet T, Bour G, Caulee K, Jost B, Muller D, et al. Amplicon mapping and transcriptional analysis pinpoint cyclin L as a candidate oncogene in head and neck cancer. Cancer research. 2002;62(21):6211-7.
193. McCaughan F, Pole JC, Bankier AT, Konfortov BA, Carroll B, Falzon M, et al. Progressive 3q amplification consistently targets SOX2 in preinvasive squamous lung cancer. American journal of respiratory and critical care medicine. 2010;182(1):83-91.
194. Robbins HL, Hague A. The PI3K/Akt pathway in tumors of endocrine tissues. Frontiers in endocrinology. 2016;6:188.
195. Aggarwal C, Marmarelis ME, Hwang W-T, Scholes DG, McWilliams TL, Singh AP, et al. Association Between Availability of Molecular Genotyping Results and Overall Survival in Patients With Advanced Nonsquamous Non–Small-Cell Lung Cancer. JCO Precision Oncology. 2023;7:e2300191.
196. Zugazagoitia J, Ramos I, Trigo JM, Palka M, Gómez-Rueda A, Jantus-Lewintre E, et al. Clinical utility of plasma-based digital next-generation sequencing in patients with advance-stage lung adenocarcinomas with insufficient tumor samples for tissue genotyping. Annals of Oncology. 2019;30(2):290-6.
197. Palmero R, Taus A, Viteri S, Majem M, Carcereny E, Garde-Noguera J, et al. Biomarker discovery and outcomes for comprehensive cell-free circulating tumor DNA versus standard-of-care tissue testing in advanced non–small-cell lung cancer. JCO Precision Oncology. 2021;5:93-102.
198. Raez LE, Brice K, Dumais K, Lopez-Cohen A, Wietecha D, Izquierdo PA, et al. Liquid Biopsy Versus Tissue Biopsy to Determine Front Line Therapy in Metastatic Non-Small Cell Lung Cancer (NSCLC). Clinical Lung Cancer. 2023;24(2):120-9.
199. Joung J, Konermann S, Gootenberg JS, Abudayyeh OO, Platt RJ, Brigham MD, et al. Genome-scale CRISPR-Cas9 knockout and transcriptional activation screening. Nature protocols. 2017;12(4):828-63.
200. Gao J, Aksoy BA, Dogrusoz U, Dresdner G, Gross B, Sumer SO, et al. Integrative analysis of complex cancer genomics and clinical profiles using the cBioPortal. Science signaling. 2013;6(269):pl1-pl.
201. Cerami E, Gao J, Dogrusoz U, Gross BE, Sumer SO, Aksoy BA, et al. The cBio cancer genomics portal: an open platform for exploring multidimensional cancer genomics data. AACR; 2012.

202. Basu B, Krebs MG, Sundar R, Wilson RH, Spicer J, Jones R, et al. Vistusertib (dual m-TORC1/2 inhibitor) in combination with paclitaxel in patients with high-grade serous ovarian and squamous non-small-cell lung cancer. Annals of Oncology. 2018;29(9):1918-25.
203. Verheijen RB, Atrafi F, Schellens JH, Beijnen JH, Huitema AD, Mathijssen RH, et al. Pharmacokinetic optimization of everolimus dosing in oncology: a randomized crossover trial. Clinical pharmacokinetics. 2018;57(5):637-44.
204. [Available from: https://depmap.org/portal/.
205. Yin Y, Xie C-M, Li H, Tan M, Chen G, Schiff R, et al. The FBXW2–MSX2–SOX2 axis regulates stem cell property and drug resistance of cancer cells. Proceedings of the National Academy of Sciences. 2019;116(41):20528-38.
206. Sava GP, Fan H, Coombes RC, Buluwela L, Ali S. CDK7 inhibitors as anticancer drugs. Cancer and Metastasis Reviews. 2020;39(3):805-23.
207. Rhyasen GW, Hattersley MM, Yao Y, Dulak A, Wang W, Petteruti P, et al. AZD5153: a novel bivalent BET bromodomain inhibitor highly active against hematologic malignancies. Molecular cancer therapeutics. 2016;15(11):2563-74.
208. Xu K, Chen D, Qian D, Zhang S, Zhang Y, Guo S, et al. AZD5153, a novel BRD4 inhibitor, suppresses human thyroid carcinoma cell growth in vitro and in vivo. Biochemical and biophysical research communications. 2018;499(3):531-7.
209. Shen G, Chen J, Zhou Y, Wang Z, Ma Z, Xu C, et al. AZD5153 inhibits prostate cancer cell growth in vitro and in vivo. Cellular Physiology and Biochemistry. 2018;50(2):798-809.
210. Liu W, Stein P, Cheng X, Yang W, Shao N, Morrisey E, et al. BRD4 regulates Nanog expression in mouse embryonic stem cells and preimplantation embryos. Cell Death & Differentiation. 2014;21(12):1950-60.
211. Wu T, Pinto HB, Kamikawa YF, Donohoe ME. The BET family member BRD4 interacts with OCT4 and regulates pluripotency gene expression. Stem cell reports. 2015;4(3):390-403.
212. Liu Y, Wu Z, Zhou J, Ramadurai DK, Mortenson KL, Aguilera-Jimenez E, et al. A predominant enhancer co-amplified with the SOX2 oncogene is necessary and sufficient for its expression in squamous cancer. Nature Communications. 2021;12(1):7139.
213. Im JH, Hwang SI, Kim J-W, Park S-J, Kang K-r, You JS, et al. Inhibition of BET selectively eliminates undifferentiated pluripotent stem cells. Science Bulletin. 2018;63(8):477-87.
214. Alghamdi S, Khan I, Beeravolu N, McKee C, Thibodeau B, Wilson G, et al. BET protein inhibitor JQ1 inhibits growth and modulates WNT signaling in mesenchymal stem cells. Stem Cell Research & Therapy. 2016;7(1):1-16.
215. Chiaradonna F, Ricciardiello F, Palorini R. The nutrient-sensing hexosamine biosynthetic pathway as the hub of cancer metabolic rewiring. Cells. 2018;7(6):53.
216. André F, Ciruelos E, Rubovszky G, Campone M, Loibl S, Rugo HS, et al. Alpelisib for PIK3CA-mutated, hormone receptor–positive advanced breast cancer. New England Journal of Medicine. 2019;380(20):1929-40.
217. Meric-Bernstam F, Ford JM, O'Dwyer PJ, Shapiro GI, McShane LM, Freidlin B, et al. National Cancer Institute Combination Therapy Platform Trial with Molecular Analysis for Therapy Choice (ComboMATCH). Clinical Cancer Research. 2023;29(8):1412-22.
218. Herbst RS, Gandara DR, Hirsch FR, Redman MW, LeBlanc M, Mack PC, et al. Lung Master Protocol (Lung-MAP)—a biomarker-driven protocol for accelerating development of therapies for squamous cell lung cancer: SWOG S1400. Clinical cancer research. 2015;21(7):1514-24.

219. O'Dwyer PJ, Gray RJ, Flaherty KT, Chen AP, Li S, Wang V, et al. The NCI-MATCH trial: lessons for precision oncology. Nature Medicine. 2023:1-9.
220. Wang X, Ricciuti B, Nguyen T, Li X, Rabin MS, Awad MM, et al. Association between smoking history and tumor mutation burden in advanced non–small cell lung cancer. Cancer research. 2021;81(9):2566-73.
221. Singal G, Miller PG, Agarwala V, Li G, Kaushik G, Backenroth D, et al. Association of patient characteristics and tumor genomics with clinical outcomes among patients with non–small cell lung cancer using a clinicogenomic database. Jama. 2019;321(14):1391-9.
222. Willis C, Fiander M, Tran D, Korytowsky B, Thomas J-M, Calderon F, et al. Tumor mutational burden in lung cancer: a systematic literature review. Oncotarget. 2019;10(61):6604.
223. Jamal-Hanjani M, Wilson GA, McGranahan N, Birkbak NJ, Watkins TB, Veeriah S, et al. Tracking the evolution of non–small-cell lung cancer. New England Journal of Medicine. 2017;376(22):2109-21.
224. Al Bakir M, Huebner A, Martínez-Ruiz C, Grigoriadis K, Watkins TB, Pich O, et al. The evolution of non-small cell lung cancer metastases in TRACERx. Nature. 2023:1-10.
225. Abbosh C, Frankell AM, Harrison T, Kisistok J, Garnett A, Johnson L, et al. Tracking early lung cancer metastatic dissemination in TRACERx using ctDNA. Nature. 2023;616(7957):553-62.
226. Reizine NM, O'Donnell PH. Modern developments in germline pharmacogenomics for oncology prescribing. CA: A Cancer Journal for Clinicians. 2022;72(4):315-32.
227. Tutt AN, Garber JE, Kaufman B, Viale G, Fumagalli D, Rastogi P, et al. Adjuvant olaparib for patients with BRCA1-or BRCA2-mutated breast cancer. New England Journal of Medicine. 2021;384(25):2394-405.
228. Hoskins JM, Carey LA, McLeod HL. CYP2D6 and tamoxifen: DNA matters in breast cancer. Nature Reviews Cancer. 2009;9(8):576-86.
229. Glubb DM, Cerri E, Giese A, Zhang W, Mirza O, Thompson EE, et al. Novel functional germline variants in the VEGF receptor 2 gene and their effect on gene expression and microvessel density in lung cancer. Clinical Cancer Research. 2011;17(16):5257-67.
230. Silva IP, Salhi A, Giles KM, Vogelsang M, Han SW, Ismaili N, et al. Identification of a novel pathogenic germline KDR variant in melanoma. Clinical Cancer Research. 2016;22(10):2377-85.
231. Zaman N, Dass SS, Du Parcq P, Macmahon S, Gallagher L, Thompson L, et al. The KDR (VEGFR-2) genetic polymorphism Q472H and c-KIT polymorphism M541L are associated with more aggressive behaviour in astrocytic gliomas. Cancer Genomics & Proteomics. 2020;17(6):715-27.
232. Tong Z, Sathe A, Ebner B, Qi P, Veltkamp C, Gschwend JE, et al. Functional genomics identifies predictive markers and clinically actionable resistance mechanisms to CDK4/6 inhibition in bladder cancer. Journal of Experimental & Clinical Cancer Research. 2019;38(1):1-14.
233. Vansteenkiste JF, Canon J-L, De Braud F, Grossi F, De Pas T, Gray JE, et al. Safety and efficacy of buparlisib (BKM120) in patients with PI3K pathway-activated non-small cell lung cancer: results from the phase II BASALT-1 study. Journal of Thoracic Oncology. 2015;10(9):1319-27.
234. Kim BR, Van de Laar E, Cabanero M, Tarumi S, Hasenoeder S, Wang D, et al. SOX2 and PI3K cooperate to induce and stabilize a squamous-committed stem cell injury state during lung squamous cell carcinoma pathogenesis. PLoS biology. 2016;14(11):e1002581.

235. Balsara BR, Pei J, Mitsuuchi Y, Page R, Klein-Szanto A, Wang H, et al. Frequent activation of AKT in non-small cell lung carcinomas and preneoplastic bronchial lesions. Carcinogenesis. 2004;25(11):2053-9.
236. Berenjeno IM, Piñeiro R, Castillo SD, Pearce W, McGranahan N, Dewhurst SM, et al. Oncogenic PIK3CA induces centrosome amplification and tolerance to genome doubling. Nature communications. 2017;8(1):1773.
237. Mascini M, Palchetti I, Tombelli S. Nucleic acid and peptide aptamers: fundamentals and bioanalytical aspects. Angewandte Chemie International Edition. 2012;51(6):1316-32.
238. Liu K, Xie F, Zhao T, Zhang R, Gao A, Chen Y, et al. Targeting SOX2 protein with peptide aptamers for therapeutic gains against esophageal squamous cell carcinoma. Molecular therapy. 2020;28(3):901-13.
239. Chen Y, Zhang K, Zhang R, Wang Z, Yang L, Zhao T, et al. Targeting the SOX2/CDP protein complex with a peptide suppresses the malignant progression of esophageal squamous cell carcinoma. Cell Death Discovery. 2023;9(1):399.
240. Zhang Y, Xie X, Yeganeh PN, Lee D-J, Valle-Garcia D, Meza-Sosa KF, et al. Immunotherapy for breast cancer using EpCAM aptamer tumor-targeted gene knockdown. Proceedings of the National Academy of Sciences. 2021;118(9):e2022830118.
241. Ng EW, Shima DT, Calias P, Cunningham Jr ET, Guyer DR, Adamis AP. Pegaptanib, a targeted anti-VEGF aptamer for ocular vascular disease. Nature reviews drug discovery. 2006;5(2):123-32.
242. Bates PJ, Laber DA, Miller DM, Thomas SD, Trent JO. Discovery and development of the G-rich oligonucleotide AS1411 as a novel treatment for cancer. Experimental and molecular pathology. 2009;86(3):151-64.
243. Fang Y, Wang S, Han S, Zhao Y, Yu C, Liu H, et al. Targeted protein degrader development for cancer: advances, challenges, and opportunities. Trends in Pharmacological Sciences. 2023;44(5):303-17.
244. Zhao L, Zhao J, Zhong K, Tong A, Jia D. Targeted protein degradation: mechanisms, strategies and application. Signal Transduction and Targeted Therapy. 2022;7(1):113.
245. Liu Z, Hu M, Yang Y, Du C, Zhou H, Liu C, et al. An overview of PROTACs: a promising drug discovery paradigm. Molecular Biomedicine. 2022;3(1):46.
246. Gao X, Burris III HA, Vuky J, Dreicer R, Sartor AO, Sternberg CN, et al. Phase 1/2 study of ARV-110, an androgen receptor (AR) PROTAC degrader, in metastatic castration-resistant prostate cancer (mCRPC). American Society of Clinical Oncology; 2022.
247. Sasso JM, Tenchov R, Wang D, Johnson LS, Wang X, Zhou QA. Molecular glues: The adhesive connecting targeted protein degradation to the clinic. Biochemistry. 2022;62(3):601-23.
248. Simonetta KR, Taygerly J, Boyle K, Basham SE, Padovani C, Lou Y, et al. Prospective discovery of small molecule enhancers of an E3 ligase-substrate interaction. Nature communications. 2019;10(1):1402.
249. Toriki ES, Papatzimas JW, Nishikawa K, Dovala D, Frank AO, Hesse MJ, et al. Rational chemical design of molecular glue degraders. ACS Central Science. 2023;9(5):915-26.